

**TECTONO-SEDIMENTARY EVOLUTION  
OF A PASSIVE MARGIN:  
THE PINDOS ZONE OF THE NW  
PELOPONNESE, GREECE**

**PAUL J. DEGNAN**

**THESIS SUBMITTED FOR THE DEGREE OF  
DOCTOR OF PHILOSOPHY**

**UNIVERSITY OF EDINBURGH  
1992**



## **DECLARATION**

**I declare that this thesis has been written by myself and is the result of my own research, except where contributions have been stated and duly acknowledged.**



## ABSTRACT

An integrated sedimentological, structural and geochemical study has been used to elucidate the tectono-sedimentary evolution of the Pindos Zone in the NW Peloponnese. The study area is interpreted as part of the Apulian passive margin which was bordered to the east by a small Neotethyan basin, the Pindos Ocean. The Pindos Zone is an elongate north-south trending imbricated terrane consisting of deep-water sedimentary rocks (the Pindos Group) that were deposited in the Pindos Ocean. The sedimentary rocks range in age from the Late Triassic to the Eocene. These sediments were deposited on a volcanic substratum that is sparsely preserved as blocks within melange at the base of Pindos thrust sheets. cursory analysis suggests that the extrusive igneous rocks exhibit geochemical signatures comparable with island arc tholeiite (IAT). However, further geochemical study indicates that parental members of the suites represent transitional within plate basalt (WPB) to mid-ocean ridge basalt (MORB) lava. The recognition of spatial and temporal facies trends within the over lying sedimentary rocks, augmented by laboratory analysis, allows the sedimentary evolution of the passive margin to be documented from rifting to final suturing. Earliest recorded sediments consist of Late Triassic sandstones, derived mainly from a metamorphic source terrane, intercalated with *Halobia*-bearing limestones. Thereafter, a proximal to distal facies distinction is recognised in the sedimentary sequence. Late Triassic to Liassic facies consist of coarse calcirudites and nodular limestones in the west, while to the east, distal calciturbidite, micrite and chert facies are present. During Aalenian times, sedimentation underwent a fundamental change from calcareous to siliceous deposition, via an argillaceous interval. The Middle and Late Jurassic is dominated by radiolarian-rich, ribbon-bedded, cherts. The passive margin period was interrupted in the Late Jurassic by a short period of localised faulting and volcanic activity. The evidence for this event is from dated radiolarian cherts, with substantial manganese enrichment and syn-sedimentary deformation, deposited above a contemporary basaltic basement. The manganese component of the sub-CCD sediment was supplied primarily from a hydrothermal source, with additional hydrogenous trace element scavenging away from discharge sites. The resumption of calcareous deposition dates from the Tithonian, with coarse-grained platform and slope derived carbonate deposited in the west, while thinner hemipelagic and calciturbidite sediments characterise easterly outcrops. This sedimentation pattern was disturbed at the Cretaceous/Tertiary boundary by the gradual transition from calcareous to dominantly terrigenous sedimentation. The change occurred due to a sea level fall and/or Early Tertiary closure of the Pindos ocean. As the Pindos oceanic plate between Apulia and the Pelagonian micro-continent was consumed, an accretionary complex developed above an eastward-dipping subducting slab during the Eocene. The sedimentary cover of the down going oceanic crust was off-scraped to form a folded and imbricated thrust wedge that was finally emplaced onto the adjacent carbonate platform to the west (the Gavrovo-Tripolitza), as the Apulian continental margin approached the site of subduction during the Upper Oligocene. The configuration of the continental margin and the sea floor topography influenced passive margin sediment distribution patterns. These factors also affected structuration during Tertiary compression. Emplacement of the Pindos thrust sheets onto the platform was facilitated by the collapse of the margin to form a foredeep ahead of the orogenic wedge, followed by folding and thrust development within the neritic sequences, due to footwall collapse. There was little "out-of-sequence" thrusting in the Pindos thrust stack, as evidenced by the preservation of "proximal" sedimentary facies at a structurally low level in the west, while more "distal" facies occur in structurally higher thrust slices further east. Minor post-emplacement compression is indicated by north-verging folds and minor east-west striking reverse faults. Timing is poorly constrained between the Oligocene and the beginning of extensional neotectonics. Reactivation of thrust related transverse faults, in addition to widespread normal faulting, occurred from Pliocene times onward and this is related to the uplift of the Peloponnese and extensional stresses locally centred on the Gulf of Corinth.

## ACKNOWLEDGEMENTS

This thesis has been completed with the aid of several people to whom I owe thanks. Firstly, I am indebted to my three supervisors. I am especially obliged to Dr Alastair Robertson who provided me with a tremendous project and enthusiastically supplied continuous advice and support. In particular, I am grateful for all the field supervision, unstintingly given, in Greece, Oman and India. Dr John Dixon has provided advice and critically read earlier versions of this work. Dr Soteris Varnavas of Patras University kindly gave valuable time to resolve logistical problems and expertly reviewed the section on manganese metallogenesis.

I have benefited from constructive discussions with many geo-scientists, too numerous to mention, and I am extremely grateful to each one of them. Special thanks are due to the geological staff at Edinburgh University, also Drs Jan Alexander, Wes Gibbons, David Piper, Georgia Pe-Piper and Mike Searle.

In France, guidance, advice and helpful discussion was given by Profs. Olivier Monod, Jean-Jacques Fleury, Patrick De Wever and Francois Thiebault. The staff and students of the Laboratoire de Science de la Terre, Universit e de Paris-Sud, Orsay are thanked for their hospitality during my visit as part of the ERASMUS program.

The dating of faunal specimens was kindly provided by H.G. Owen (Natural History Museum), C. Betzler (Cologne University) and G. Rose (University College London).

Technical assistance at Edinburgh University was expertly and amiably supplied by Geoff Angel, Peder Aspen, Diane Baty, Yvonne Cooper, Jane Foster, Dodie James and Stuart Kearns. They are thanked, as are the secretaries, Helena, Heather and Denise. Cups of tea and gossip were provided by Jimmy Paterson.

The National Environmental Research Council provided the grant for this project and are thanked for fieldwork and conference support. Contributions were also received from the European Community (ERASMUS), the International Association of Sedimentologists, Shell Petroleum, the Royal Society of London and the University of Edinburgh. This assistance is gratefully acknowledged.

During my field work I had the pleasure of getting to know many people in Greece including Themis, Vassilis, George and Fredrik of Themis Bar, Acro Corinth. I am especially grateful to Charlie, Tazos, Olga and Will in Patras, for friendship and somewhere congenial to stay on days off. In the mountains, two villages in particular will always be remembered for their hospitality and beautiful setting, Livardzi and Aroania.

I have especially enjoyed the past years in geology. Friends and colleagues have provided stimulating discussion and advice on matters Tethyan and non-Tethyan. Thanks are due to the Eastern Med Tethyan Crew (past and present), consisting of Pete Clift, Greg Jones, Steve Batty, Ian Sharp, Nana Kolokotroni, Timur Ustaomer, Tony Morris, Fotini Liakopolou, Andy Poole and Ed Follows; also, Stuart Kearns, Dave Whitmarsh, Seb Leigh, Mark Seger and Angus Maxwell. I would like to especially thank Jillian Thompson for field assistance and much support.

Finally, I wish to dedicate this thesis to my mother and father, Agnes and Peter Degnan. Without their considerable support and understanding, over all the years, this work and many other things would not have been possible. Thank you.

# CONTENTS

## SECTION A: INTRODUCTION

Declaration	I
Abstract	II
Acknowledgements	III

### CHAPTER 1: INTRODUCTION

1.1 The Pindos Zone of the Peloponnese: Introduction	1
1.2 The Hellenides & the Isopic Zones of Greece.	5
1.2.1 Hellenides	5
1.2.2 Pre-Apulian Zone	9
1.2.3 Ionian Zone	9
1.2.4 Gavrovo-Tripolitza Zone	11
1.2.5 Pindos Zone	11
1.2.6 Vardoussia Zone	12
1.2.7 Parnassos Zone	12
1.2.8 Beotian Zone	13
1.2.9 Othris Zone	13
1.2.10 Pelagonian Zone	14
1.3 Mesozoic Tethys	14
1.4 History of Previous Research	17
1.4.1 Early Work	17
1.4.2 Recent Work	18
1.5 Objectives and Methodology	20

### CHAPTER 2: STRATIGRAPHY OF THE PINDOS GROUP

2.1 Introduction	22
2.2 Previous Stratigraphic Schemes	24
2.3 Formal Stratigraphy	24
2.3.1 Pindos Group	24
2.3.2 Priolithos Formation	26
2.3.3 Drimos Formation	27
2.3.4 Lesteena Formation	29
2.3.4.1 Kakotari Member	29
2.3.4.2 Kastelli Mudstone Member	30
2.3.4.3 Aroania Chert Member	31
2.3.5 Lambia Formation	33
2.3.5.1 Paos Limestone Member	33
2.3.5.2 Klitoria Sandstone Member	35
2.3.5.3 Erymanthos Limestone Member	36
2.3.5.4 Kataraktis Passage Member	37
2.3.6 Pindos Flysch Formation	39
2.3.7 Other Lithologic Units	40
2.4 Summary of the Stratigraphy of the Pindos Group	40

<b>SECTION B: SEDIMENTOLOGY &amp; STRUCTURE OF THE PINDOS ZONE</b>
--

Introduction	43
--------------	----

### CHAPTER 3: PRIOLITHOS & DRIMOS FORMATIONS

3.1 Introduction	50
3.2 Priolithos Formation	51
3.2.1 Lithological Description	51
3.2.2 Distribution and Depositional Environment	55
3.2.3 Discussion	58
3.2.4 Ancient Comparisons	59
3.2.5 Modern Comparisons	60
3.3 Drimos Formation	60
3.3.1 Lithological Description	60
3.3.2 Distribution and Depositional Environment	68
3.3.3 Discussion	73
3.3.4 Ancient and Modern Comparisons	79
3.4 Conclusions	80
Plates	

### CHAPTER 4: LESTEENA FORMATION

4.1 Introduction	91
4.2 Kakotari Member	93
4.2.1 Lithological Description	93
4.2.2 Discussion	93
4.3 Kastelli Mudstone Member	96
4.3.1 Lithological Description and Diagenesis	96
4.3.2 Distribution and Depositional Environment	99
4.3.3 Discussion	101
4.3.4 Summary	104
4.4 Aroania Chert Member	105
4.4.1 Introduction	105
4.4.2 Lithological Description	106
4.4.3 Distribution and Depositional Environment	109
4.4.4 Silica Diagenesis	113
4.4.5 Ancient Comparisons	115
4.4.6 Modern Comparisons	115
4.4.7 Discussion	116
4.4.8 Summary	119
4.5 Manganese Enrichment of the Aroania Chert Member	120
4.5.1 Introduction	120
4.5.2 Field Relations	120
4.5.3 Mineralogy	123
4.5.4 Whole Rock Geochemistry	125
4.5.5 Electron Microprobe Study	128
4.5.6 Interpretations	131
4.5.7 Discussion	139
4.5.8 Ancient Comparisons	145
4.5.9 Modern Comparisons	146
4.5.10 Summary	147
4.6 Conclusions	148
Plates	

## CHAPTER 5: LAMBIA & PINDOS FLYSCH FORMATIONS

5.1 Introduction	159
5.2 <b>Lambia Formation</b>	161
5.2.1 Paos Limestone Member	161
5.2.2 Klitoria Sandstone Member	165
5.2.3 Erymanthos Limestone Member	168
5.2.4 Kataraktis Passage Member	174
5.2.5 Ancient Comparisons	178
5.2.6 Modern Comparisons	178
5.3 <b>Pindos Flysch Formation</b>	179
5.3.1 Lithological Description	179
5.3.2 Distribution and Depositional Environment	183
5.3.3 Discussion	184
5.3.4 Ancient Comparisons	188
5.3.5 Modern Comparisons	189
5.4 <b>Conclusions</b>	189
<b>Plates</b>	

## CHAPTER 6: STRUCTURAL ANALYSIS OF THE PINDOS ZONE

6.1 <b>Introduction</b>	199
6.1.1 Structural Terminology	200
6.2 <b>Regional Structural Descriptions</b>	202
6.2.1 The Frontal Imbricates	202
6.2.2 The Central Imbricates	206
6.2.3 The Eastern Imbricates	210
6.3 <b>Analysis of Pindos Zone Deformation</b>	214
6.3.1 Introduction to Fold Analysis	214
6.3.2 Meso-scale Folding	216
6.3.3 Macro-scale Folding	222
6.3.4 The Relative Timing of Folding	227
6.3.5 Thrust Surface Geometries	229
6.3.6 Timing of Deformation	230
6.3.7 Estimates of Orogenic Shortening	230
6.4 <b>Ancillary Structures</b>	234
6.4.1 Coeval Transverse Faulting	234
6.4.2 Rock Cleavage	237
6.4.3 Joints and Veining	238
6.4.4 Palaeomagnetic Study	239
6.5 <b>Compressional Deformation Model</b>	241
6.5.1 Regional Setting	241
6.5.2 Earliest Deformation	242
6.5.3 Later Pre-emplacment Deformation	243
6.5.4 Emplacement	247
6.6 <b>Post Emplacement Tectonics</b>	247
6.6.1 Compressional Tectonics	247
6.6.2 Extensional Neotectonics	249
6.7 <b>Conclusions</b>	251
<b>Plates</b>	

## SECTION C: ADDITIONAL TECTONO-SEDIMENTARY COMPONENTS

### CHAPTER 7: THE GAVROVO-TRIPOLITZA ZONE

7.1 Introduction	262
7.2 GTZ Basement	263
7.2.1 Introduction	263
7.2.2 GTZ Volcanics: Petrography	265
7.2.3 GTZ Volcanics: Electron Probe Analysis	266
7.2.4 Geochemistry	268
7.2.5 Interpretation	270
7.3 Tripolitza Zone Stratigraphy & Sedimentology	273
7.3.1 Tripolitza Platform	273
7.3.2 Early Tertiary Syn-Orogenic Sediments	276
7.4 Depositional Environment	280
7.4.1 GTZ Carbonates	280
7.4.2 GTZ Flysch	281
7.5 GTZ Structure	282
7.5.1 Intra-Platform Deformation	282
7.5.2 Foreland Deformation	288
7.6 Discussion	288
7.6.1 Foreland Basin Model	288
7.6.2 Interpretation of Field Data: Platform Collapse	289
7.6.3 Migration of the Foreland Basin	291
7.6.4 Palaeocurrent Orientation	292
7.7 Conclusions	292
Plates	

### CHAPTER 8: TECTONO-SEDIMENTARY MELANGE

8.1 Introduction	299
8.2 TSM Geological Setting	301
8.2.1 Drakovouni	301
8.2.2 Central Peloponnese	304
8.2.3 Southern Peloponnese	306
8.2.4 Eastern Peloponnese	307
8.2.5 Other Localities	308
8.2.6 Jurassic Chert Association	309
8.3 TSM Fabric Studies	310
8.3.1 Fabric Descriptions	310
8.3.2 A Model for Fabric Development	311
8.3.3 Melange Formation in the Pindos Overthrust Terrane	313
8.4 Igneous Lithologies	317
8.4.1 Petrography	317
8.4.2 Geochemistry	321
8.4.3 Tectono-Magmatic Discrimination Diagrams	323
8.4.4 Discussion	327
8.4.5 Interpretation of the Geochemical Results	331
8.4.6 A Proposed Model for Pindos Zone Magmatism	339
8.5 Conclusions	341
Plates	

## SECTION D: SYNTHESIS

### CHAPTER 9: TECTONO-SEDIMENTARY EVOLUTION OF THE PINDOS ZONE

9.1 Introduction	349
9.2 Basin Evolution	349
9.2.1 Basin Formation	349
9.2.2 Sedimentary Evolution	354
9.2.3 The Pindos Basin as a Neotethyan Ocean	359
9.3 Basin Closure and Deformation	362
9.3.1 Initiation of Basin Closure	362
9.3.2 Pindos Subduction-Accretion	364
9.3.3 Platform Collapse and Transition to a Foreland Basin	366
9.3.4 Emplacement of the Pindos Thrust Stack	367
9.3.5 Post Emplacement Tectonics	367
9.4 Epilogue	368

### REFERENCES

- APPENDIX 1: Graphic Sedimentary Logs**
- APPENDIX 2: Analytical Techniques**
- APPENDIX 3: Sedimentary Geochemical results**
- APPENDIX 4: Localities of Geochemically Analysed Sedimentary Rocks**
- APPENDIX 5: Igneous Geochemical Results**
- APPENDIX 6: Thin-section Catalogue**

- ENCLOSURE 1: Geological Map**
- ENCLOSURE 2: Cross Section**

## **SECTION A: INTRODUCTION**

### **CHAPTER 1: INTRODUCTION**

### **CHAPTER 2: STRATIGRAPHY OF THE PINDOS GROUP**



## CHAPTER 1 INTRODUCTION

### 1.1 THE PINDOS ZONE OF THE PELOPONNESE: INTRODUCTION

The Pindos Mountains, as a geographic entity, extend from the Albanian border in the north, south to approximately the region of Karpenision. From there, south to the Gulf of Patras, the continuation of the mountain range is known as Panetolikon, and on the other side of the Gulf, as Panakhaion and Erymanthos. The geology of the mountain chain varies along its length. In the north, a variety of lithologies are exposed, including structurally complex ophiolites (Jones 1990), while further south a more regular series of sedimentary thrust sheets are found. In the classical literature (Renz 1955, Brunn 1956), the term "Pindos nappes" has meant the Pindos ophiolite of northern Greece. The Mesozoic sedimentary sequences studied in this work have been attributed to the "Pindos-Olonos" series (corresponding to the mountains of Pindos in the north and Olonos, the ancient Greek for Erymanthos, in the south). Both the ophiolites and the sedimentary succession are located within a tectonostratigraphic terrane known as the Pindos Zone. In this work, the "Pindos Zone" corresponds to the Pindos-Olonos series of earlier authors. Where reference is made to the ophiolites of the Pindos in northern Greece, this will be stated.

The main study area is a mountainous region of the NW Peloponnese that roughly extends from the mountains of Erymanthos in the west, to Chelmos in the east (Figure 1.1). The terrain is generally rugged with steep sided valleys that cut through the mountains, both north-south parallel to the dominant structural strike, and east-west. Maximum elevations are 2224m on Erymanthos and 2340m on Chelmos. In the central area, topographic expression is slightly less pronounced. The dominant relief-forming lithology of the Pindos Zone is the Cretaceous limestone of the Lambia Formation (Section 5.2.3). Access is reasonable, with an increasing number of good quality metalled roads and less impressive but adequate tracks. There are also footpaths of poor quality that are used by shepherds, or tracks formed by generations of goats. Thanks to the large goat population, combined with occasional forest fires, the quality of exposure is very good. Many mountain tops are devoid of vegetation. Where vegetation is present, it consists of scrubby grassland with Mediterranean holly (*Ilex aquifolium*) or pine forest in less accessible areas, as found for example in the south of the study area and around Chelmos. Apart from goat and sheep rearing, agriculture is important, although in decline, as the country

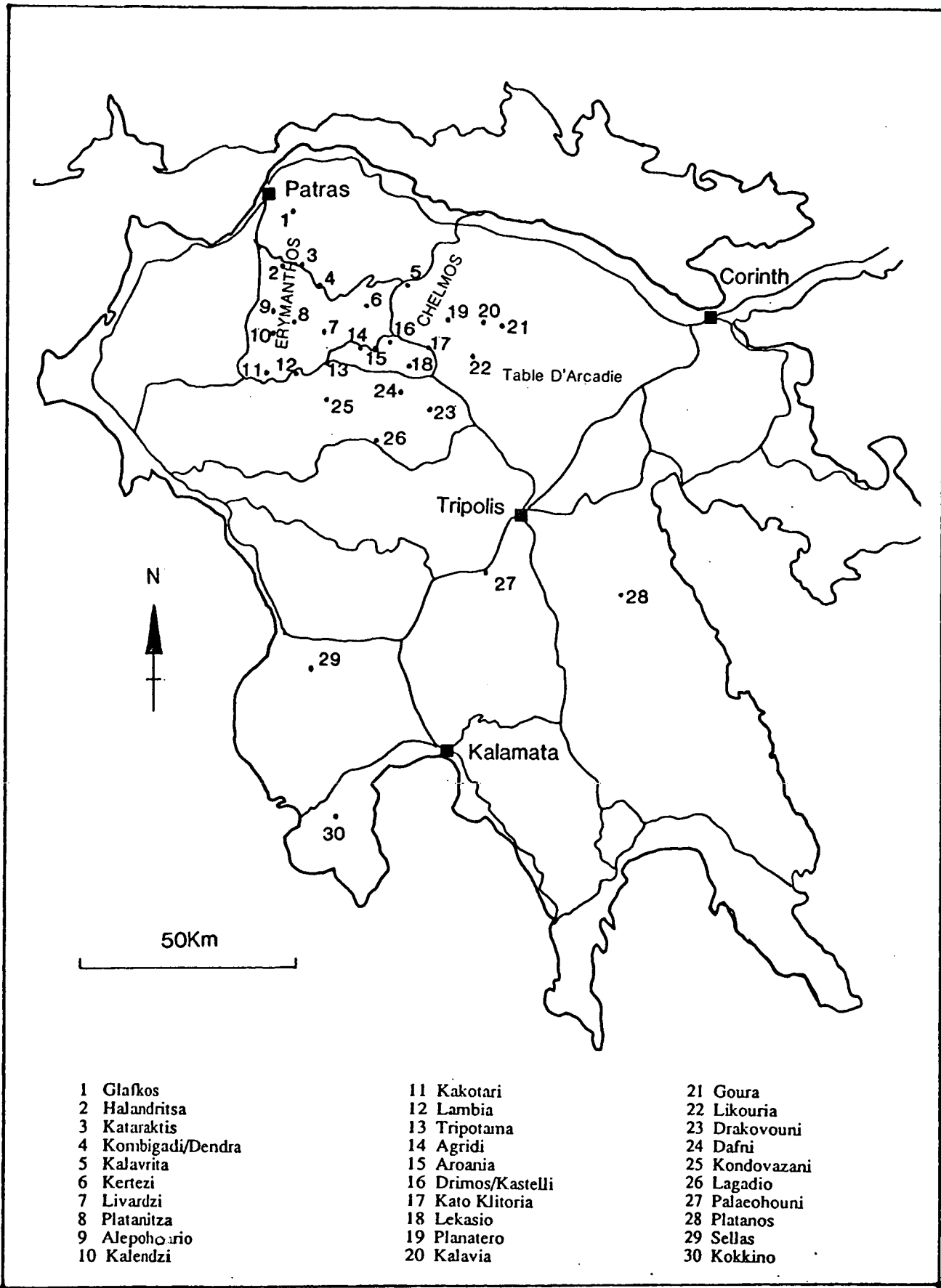


**Fig. 1.1** Locality map of the towns and villages mentioned in the text.

population diminishes due to migration to the cities. The main crops grown are maize and straw for the winter feeding of livestock.

Figure 1.2 schematically shows the main structural features of the NW Peloponnese. To the west of the Pindos thrust front, the topography flattens out over a short distance to become a frontal plain where fertile soils, supplied with water from the mountains, allow the cultivation of grains and fruit crops. This area corresponds to an area of flysch deposited in a foredeep ahead of the Pindos nappes.

To the north and south, neotectonic half-grabens have formed from the Pliocene onwards (Sebrier 1977, M. Seger, pers. comm. 1990). The Gulf of Corinth, separating the Peloponnese from continental Greece, is one such feature. The basin fill is dominantly lacustrine marl and coarse alluvial clastics, largely derived from the Pindos nappes. These neotectonic faults have a WNW-ESE orientation.

To the east of the Chelmos massif are a series of plains and mountains consisting of Cretaceous Pindos limestone and neritic limestones of the Tripolitza Zone. Deep fertile depressions (e.g. Stymphalia, Fenou and the Nemea plains) existed as lakes in historical times, but have since been naturally drained. Well developed former shore lines are observed.

Structurally, the Pindos Zone west of Chelmos defines an imbricate fan of steeply eastward-dipping folded and thrust strata that were transported towards the west. A number of transverse faults, many of which are demonstrably coeval with the main phase of compressional tectonics, are well exposed in the study area. Other faults, orthogonal to the main tectonic strike, as well as some north-south trending structures, are of neotectonic origin.

The Pindos Zone sediments to the east of the Chelmos Mountain are generally gently dipping Cretaceous limestones, with occasional outcrops of Jurassic radiolarite. Deformation is often intense, with observable thrust faulting and folding. However the monotony and homogeneity of outcrop make the large scale identification and correlation of structures extremely difficult. This area was termed the "Table d'Arcadie" by Dercourt (1964).

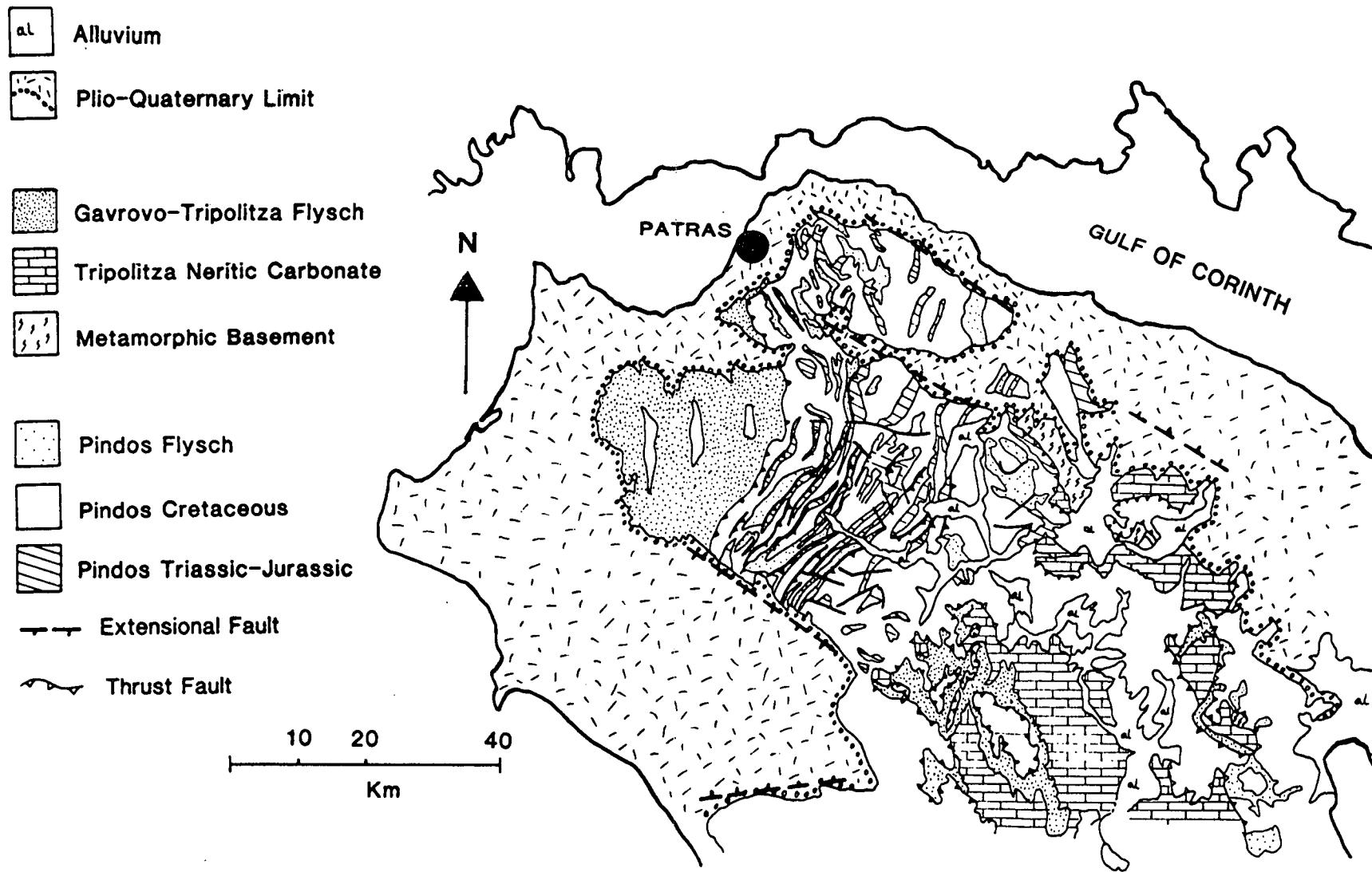


Fig. 1.2 Generalised geological map of the northern Peloponnese showing the dominant structural trends (Eocene-Oligocene N-S thrusts, Quaternary NW-SE extensional faults) and the relative disposition of the Pindos and Gavrovo-Tripolitza Zones.

## 1.2 THE HELLENIDES AND THE ISOPIC ZONES OF GREECE

### 1.2.1 The Hellenides

The Hellenides are part of the arcuate Alpine mountain belt in Europe (Kober 1929, Smith & Moores 1974, Jacobshagen 1978b). They are the Greek extension of the Dinarides in Yugoslavia and also include a portion of the Albanian mountains south of the Scutari-Pec lineament. The western limit to the Hellenides has been considered as the 1000m Ionian Sea submarine contour, or alternatively, the probable limit to Early Tertiary thrust faulting as observed on the islands of Zakynthos and Kephallonia; the eastern Hellenide limit is loosely taken as the western boundary to the Rhodope Zone (Smith & Moores 1974), beyond which lies the Balkan chain and the Pontides of Turkey.

Greece has traditionally been sub-divided into a number of tectono-stratigraphic belts that contain stratigraphic successions markedly different from those of adjacent zones (Figure 1.3). Boundaries between neighbouring zones are significant regional structural lineaments. Each tectono-stratigraphic unit can therefore be considered as a terrane in the sense of Howell (1989). These terranes are known as "isopic zones" in older literature, an idiom locally applied to Greece and first coined by Kossmatt (1924). The term is well established in early Greek geological literature and came into common usage through the work and definitions of Renz (1955) and Aubouin (1959). The zones trend approximately north-south on mainland Greece and the Peloponnese, but are considered to have an arcuate tendency parallel to the Hellenic trench, basically east-west, in the Aegean Sea (Aubouin *et al.* 1976, Fleury 1980).

A division of the Hellenides into "internal" and "external" domains was introduced by Brunn (1956) to distinguish those areas affected by both Late Jurassic-Early Cretaceous and Cenozoic deformation, from those affected solely by the effects of Early Tertiary orogenesis. However, different definitions exist as to what criteria should be used to define the internal or external zones (c.f. Aubouin 1974, Underhill 1985), further complicated by the addition of the term "intermediate zones" (Fleury 1980). A distinction is therefore made here, between the Pelagonian Zone and those to the east (internal) and those to the west of the Pelagonian Zone (external) (Figure 1.3). This adopted terminology is geographical and essentially the same as Brunn's subdivision, but does not necessarily involve any tectonic connotation.

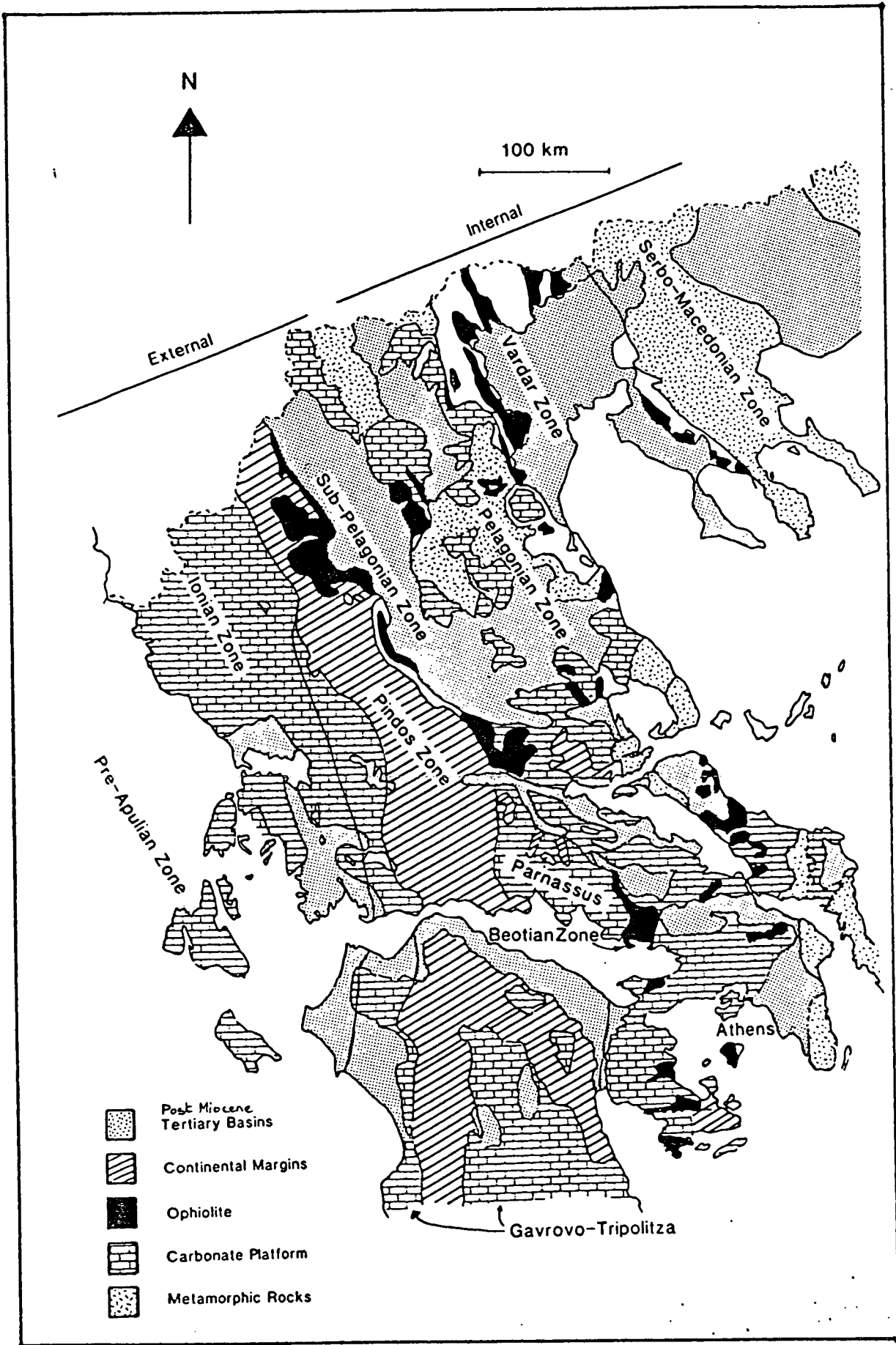


**Fig. 1.3** Simplified map indicating the tectono-stratigraphic zones ("Isopic zones") of Greece.

Plate tectonic reconstructions for the Hellenide terranes are contentious (c.f. Robertson & Dixon 1984, Dercourt *et al.* 1986). Following careful work by several international research groups, the general biostratigraphy and lithological successions of sedimentary sequences from each zone have now been established. Consequently, there is little controversy concerning the age of sedimentary sequences, or the broad timing of Alpine deformational events. Controversies do persist, however, concerning palaeogeographic and tectonic reconstructions of these zones. One particular question relevant to this study concerns the origin of ophiolite thrust sheets (Pindos, Vourinos and Othris ophiolites), that were emplaced within the Hellenides during the Mesozoic (Late Jurassic) event. There are two schools of thought regarding the genesis and emplacement of these oceanic crustal units. One school considers that they were derived from a Vardar Ocean that lay to the east of the Pelagonian Zone (Aubouin *et al.* 1970, Laubscher 1971, Zimmerman 1971, Vergely 1976). In this scenario emplacement involved thrusting of ophiolites over the Pelagonian Zone with large-scale folding and partial erosion (Bernoulli & Laubscher 1972). Other authors (Vergely 1984) consider that the Pindos and Othris ophiolites originated from an external domain (the Maliac Zone) while the Vourinos had an internal, Vardarian, origin. There is a growing body of evidence which suggests that the origin was the same for each ophiolite, namely, from a Pindos Ocean that lay to the west of the Pelagonian Zone. A number of different lines of evidence support a west to east emplacement direction (Smith *et al.* 1975, Green 1982, Jones 1990, Jones & Robertson 1991, Clift & Robertson 1990, Robertson *et al.* 1991). These include high temperature fabrics, folds and brittle structures within the ophiolite; and facies trends and sedimentary structures in the underlying basinal and continental margin successions. Further reference will be made to these, and other, lines of evidence in later chapters.

Notwithstanding the above complications, which relate to the inferred extent of Neotethyan oceanic areas, the preserved tectonostratigraphic zones can be viewed in the context of distinct palaeogeographic provinces. The westerly terranes essentially comprise either neritic, redeposited or pelagic carbonate sequences (loosely corresponding to sedimentary platform, slope and basin environments respectively), that developed on the Apulian promontory of Gondwanaland (Fleury 1980). In addition, important horizons of detrital sediment are present, as well as basement lithologies.

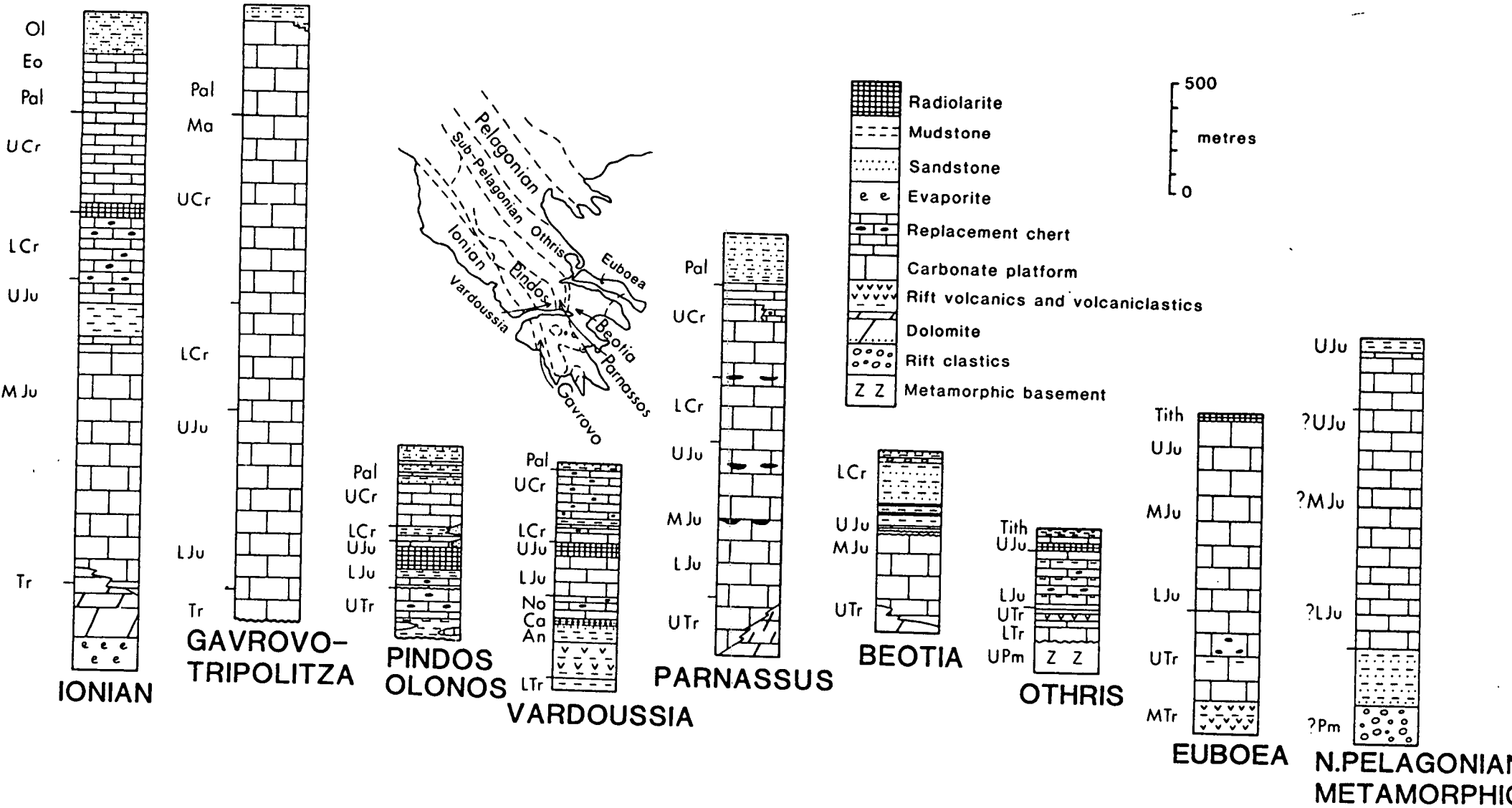


**Fig. 1.4** Representative logs summarising the stratigraphy of the tectono-stratigraphic zones and sub-units related to the Pindos ocean.



This work mainly concerns the Pindos Zone and its relationship to the Gavrovo-Tripolitza Zone which are both exposed in the study area. Neither zone was subject to the compressional deformation that affected areas further to the east during the Mesozoic. Consequently detailed reconstructions for this part of the Mesozoic Apulian passive margin are possible. It is appropriate to include a brief description of each of the tectono-stratigraphic zones mentioned. Generalized stratigraphic columns are shown in Figure 1.4 and a palaeogeographic interpretation (after Robertson *et al.* 1991) is shown in Figure 1.5.

### 1.2.2 The Pre-Apulian Zone

This is the most westerly of the tectonostratigraphic zones and is exposed only on the Ionian islands of Paxos, Lefkas, Kephallonia and Zakynthos. It has been described in terms of two sub-zones (Thiebault 1982). Essentially, Jurassic carbonates and evaporites pass up into Cretaceous dolomites which, in turn are overlain by a thick sequence of neritic carbonates of Middle Cretaceous to Eocene age. These are subsequently overlain by Oligo-Miocene marls and limestones. The total thickness is greater than 4000m (B.P. 1971). The zone is considered as the stable eastern margin to the Apulian micro-continent. Work has shown however, that compressive structures are to be found which indicate that a deformation front was active at a period transitional between the Hellenide orogeny and the onset of subduction around the Hellenic arc (Underhill 1985).

### 1.2.3 The Ionian Zone

This zone crops out along the western margin of mainland Greece and on parts of the Ionian islands. The basal lithology is evaporitic (Triassic) overlain by Upper Triassic to Liassic neritic carbonates (Thiebault 1982, Underhill 1985, Clews 1989). A significant phase of extensional tectonics is reflected in the deposition of pelagic and reworked carbonates during the subsidence of the Ionian trough in the Middle Jurassic. Deep-water carbonates, with accessory chert intervals, continued through to the base of the Oligocene when flysch sedimentation became established and continued until Lower Miocene times (Fleury 1980). The carbonates are 3000-3500m thick and the flysch is estimated to be up to 6000m in thickness (Institut Francais du Petrole (IFP) 1966). The Ionian Zone was overthrust from the east by the Gavrovo-Tripolitza Zone during the Miocene (Underhill 1985). The principle decollement horizon was the Triassic basal evaporites, which later became mobilized

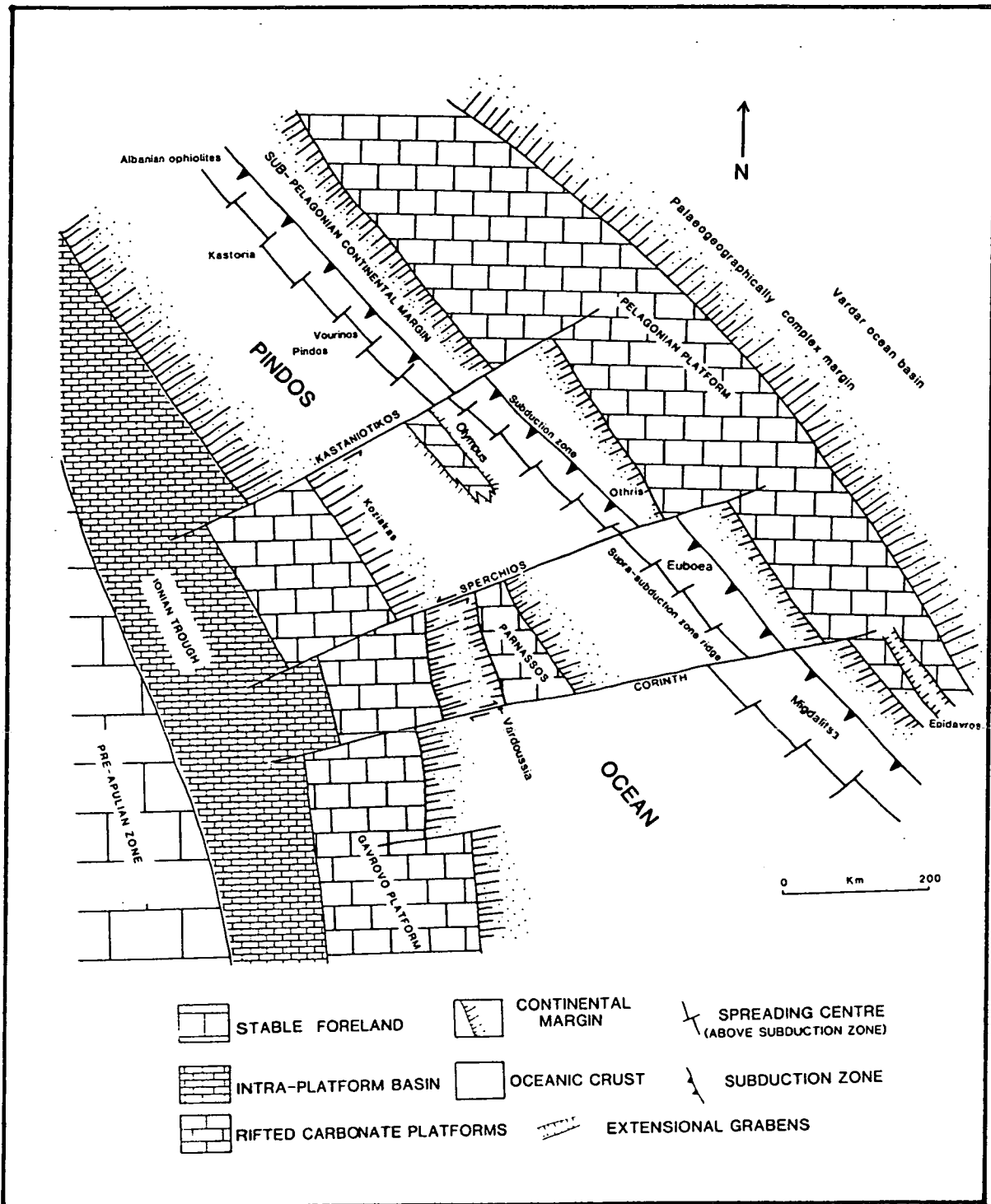


**Fig. 1.5** Palaeogeographic reconstruction of the Pindos ocean in the Mid-Jurassic. Spreading in the Late Triassic-Early Jurassic was followed by the cessation of the spreading ridge. Regional compression, related to the opening of the North Atlantic then initiated a west dipping intra-oceanic subduction zone near the former spreading axis. Ophiolites were generated above the subduction zone and were emplaced in pre-Tithonian time following collision of the trench with the western margin of the Pelagonian microcontinent (After Robertson et al. 1991).

and formed salt domes, possibly due to the effects of overpressuring from overlying Gavrovo-Tripolitza thrust sheets (Underhill 1988, 1989).

#### 1.2.4 The Gavrovo-Tripolitza Zone

The stratigraphy and sedimentology of this zone will be more fully described in Chapter 7 as it forms part of the study area. The zone comprises two sub-zones. The Gavrovo sub-zone, which displays neritic sedimentation from the Upper Jurassic to the Upper Eocene, is overlain by flysch deposits of dominantly Oligo-Miocene age. This sub-zone was partially overthrust by the Pindos thrust sheets from the east. The other sub-zone, the Tripolitza, has been completely overthrust by the Pindos thrust sheets. It is exposed through a series of tectonic windows within the Pindos mountains of the Peloponnese. A metamorphic basement and volcanics, of unknown age, comprise the Zaroukla Group of De Wever (1975). The metamorphics have been correlated with the "Phyllite series" of Jacobshagen *et al.* (1978a), which are thought to be meta-sediments of Carboniferous and Permian age. There is an overlying horizon of gypsiferous evaporites, which appear to have facilitated decollement, although the overlying thrust sheets have an unknown displacement. Above these strata lie Triassic to Upper Eocene neritic carbonates. A cover of Tertiary flysch is present, however, the carbonate-flysch horizon generally represents the detachment surface to the over-riding Pindos thrust sheets in the study area. Further south, thick outcrops of Tripolitza flysch are preserved. The total thickness is approximately 3000m.

The present location of the Tripolitza and Gavrovo sub-zones, with respect to one another, appear to reflect the palaeogeographic positioning of distinct domains. Differences in stratigraphy and inferred depositional environment suggest that although both domains were part of a contiguous carbonate platform of great extent, the Gavrovo was the more inboard with respect to Apulia, while the Tripolitza sub-zone extended outboard to the periphery of the continental shelf (Thiebault 1982).

#### 1.2.5 The Pindos Zone

The greater part of this thesis concerns the Pindos Zone. It is dominantly a series of deep-water sediments, consisting of hemipelagic and redeposited carbonates, radiolarian cherts and turbiditic siliciclastics that range from the Upper Triassic to Upper Eocene in age. The zone represents continental margin sedimentation in a

Neotethyan basin adjacent to Apulia. The sedimentary cover to a volcanic substratum, with oceanic affinities (Section 8.4), was completely detached and obducted towards the west onto the Gavrovo-Tripolitza platform. Lithological thickness is variable and is considered to reflect variations in basin-floor topography and proximity to the continental margin of Apulia.

### 1.2.6 The Vardoussia Zone

The Vardoussia Zone is considered to be palaeogeographically intermediate to that of the Pindos Zone and the Parnassos Zone (Celet 1962). The sedimentary facies indicate a slope environment comprising redeposited neritic and hemipelagic sediments which, near the base are intercalated with pillow lavas and pyroclastics. The lithological sequence is interpreted as reflecting Triassic rifting, and the subsequent establishment of a western passive margin to the Parnassos carbonate platform. The zone is exposed north of the Gulf of Corinth. Interleaved Tertiary thrust sheets include ophiolitic rocks (e.g. harzburgite, pillow lavas) (Beck 1980, Robertson & Degnan 1992a). The total sedimentary thickness is approximately 1000m (Ardaens 1978).

### 1.2.7 The Parnassos Zone

This zone is also found to the north of the Gulf of Corinth, although isolated limestone blocks to the south of the Gulf (e.g. Acro-Corinth) are thought to be of Parnassos Zone affinity (Giellisch, pers. comm. 1990). The zone essentially represents an area of shallow-water deposition of Triassic to Upper Cretaceous age, after which Campanian-Maastrichtian pelagic carbonates were laid down. These sediments are between 1500-2000m thick (Celet 1962). In the Palaeocene distinctive red pelites mark the transition to Eocene flysch. Within the platform sequence there are three main horizons of bauxite which probably correspond to periods of emergence between the Middle Jurassic and the Upper Cretaceous (Fleury 1980). The zone is interpreted as a continental block rifted from the Apulian margin with minor intervening oceanic crustal units (Robertson *et al.* 1991, Robertson & Degnan 1992a). It lay to the west of the inferred main Pindos ocean spreading centre.

### 1.2.8 The Beotian Zone

This zone was defined by the presence of a considerable area of dominantly Lower Cretaceous turbiditic sandstone and debris-flow deposits containing ophiolitic material. The ophiolite-derived clastics were overlain by Cretaceous to Eocene pelagic sediments (Celet *et al.* 1976). The position of the zone between the Parnassos and Pelagonian platformal domains would appear to be of considerable palaeogeographic significance. The Tithonian-Berriasian "flysch" is underlain by Triassic to Middle Jurassic platformal limestones. These have been considered as "indistinguishable from those of the Parnassos zone" (Green 1982). However, field evidence suggests that the inferred thrust contact separating the Beotian Zone from the Pelagonian Zone is a neotectonic extensional fault, related to the Gulf of Corinth graben system (e.g. at Aliko and Elopia; AHF Robertson & PJ Degnan, unpublished data). This, combined with the deformation history and similarity to Pelagonian sections, lead Robertson & Degnan to correlate the platformal limestones with Pelagonian Zone carbonates. Papanikolaou & Sideris (1979) argued that the Beotian Zone does not constitute an isopic zone as it is not strictly proven to be a distinctive long-lived palaeogeographic entity. Rather, it appears that the Beotian Zone is better considered as a peripheral area to the Pelagonian Zone that underwent a different subsidence history to the rest of that province.

### 1.2.9 The Othris Zone

The Othris Zone (Smith *et al.* 1975 & 1979) is essentially synonymous with the Sub-Pelagonian Zone of Aubouin (1959) and the Maliac Zone of Vergely (1984). It consists of a pre-Permian basement unconformably overlain by Upper Permian to Lower Triassic shallow-marine conglomerates, sandstones and shales. Thereafter there is a divergence in facies between easterly and westerly areas until the Late Jurassic. Easterly exposures preserve platformal limestones, while to the west, Middle Triassic volcanics are overlain by a sequence of continental margin sediments which become progressively more distal towards the west. Prior to the Late Jurassic ophiolitic obduction event that affected this region, a continuous cover of deep-water radiolarian cherts and shales was deposited across each of the above mentioned units. Ophiolite emplacement from the west is recorded (Smith *et al.* 1979) as occurring in Late Jurassic to Early Cretaceous times, with subsequent thrusting and imbrication of the underlying deep marine sediments over the platformal sequences. After ophiolite emplacement, a transgressive Late Cretaceous

shallow-marine carbonate was deposited, which itself is overlain by Cenozoic terrigenous flysch.

### 1.2.10 The Pelagonian Zone

In the Pelagonian Zone, Palaeozoic and Lower Mesozoic clastic sediments are seen to have been deposited on a Palaeozoic granite and metamorphic basement. These are in turn overlain by Triassic-Jurassic platformal limestones that were deposited after final continental break-up and subsidence. During the Upper Jurassic, ophiolites were obducted from a Pindos basin that lay to the west (Robertson *et al.* 1991). The ophiolites were partially eroded and a transgressive series of Late Jurassic to Late Cretaceous cover sediments (platformal) were deposited (Brunn 1956).

## 1.3 MESOZOIC NEOTETHYS

Many attempts have been made to correlate the stratigraphic successions of the various zones with domains from outside the immediate area. For example, similar facies to the Pindos sequences, and of comparable ages, are found throughout the Eastern Mediterranean and Middle East. These include the Lagonegro zone of southern Italy (Scandone 1967), Antalya nappes of Turkey (Dumont *et al.* 1972, Robertson & Woodcock 1982), the Pichakun Zone of Iran (Ricou 1976), and the Hawasina thrust sheets of Oman (Cooper 1986, 1990, Robertson & Searle 1990). Fleury (1980) speculated on the possible connections between various platformal/pelagic couplets through the Aegean and through the Peri-Adriatic. The present day location of the major eastern Mediterranean tectono-stratigraphic domains is shown on Figure 1.6.

Alpine continent-continent collision led to the closure of major sedimentary basins and the emplacement of remnant oceanic crust onto adjacent land-masses. On-land regions that are now represented by deep-marine sediments, as well as suture zones of ophiolitic material, define relatively narrow belts of widespread occurrence, leading workers to postulate the existence of several small Neotethyan ocean basins of which the Pindos Zone is just one strand (Robertson & Dixon 1984, c.f. Dercourt *et al.* 1986), (Figure 1.7).

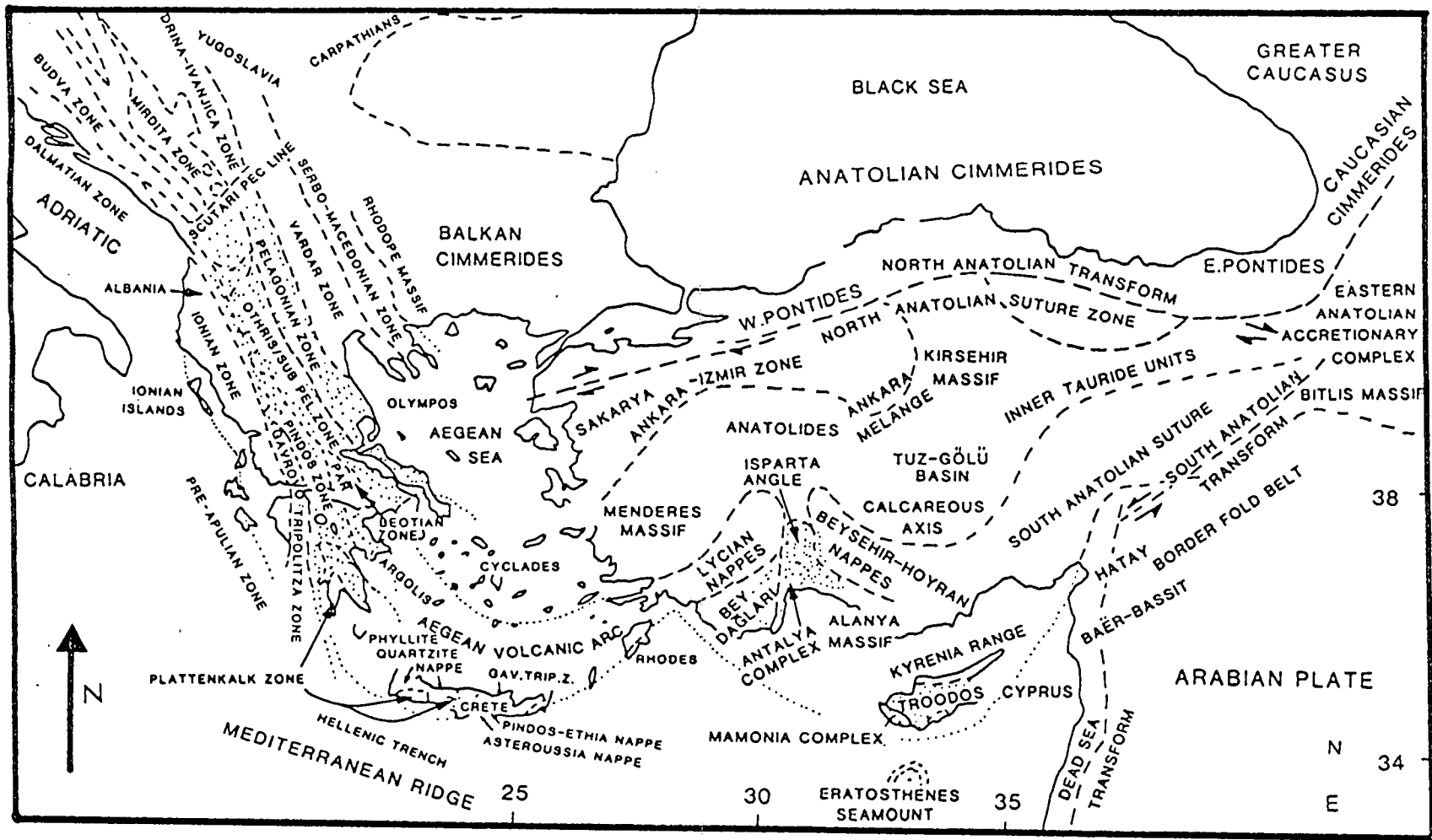
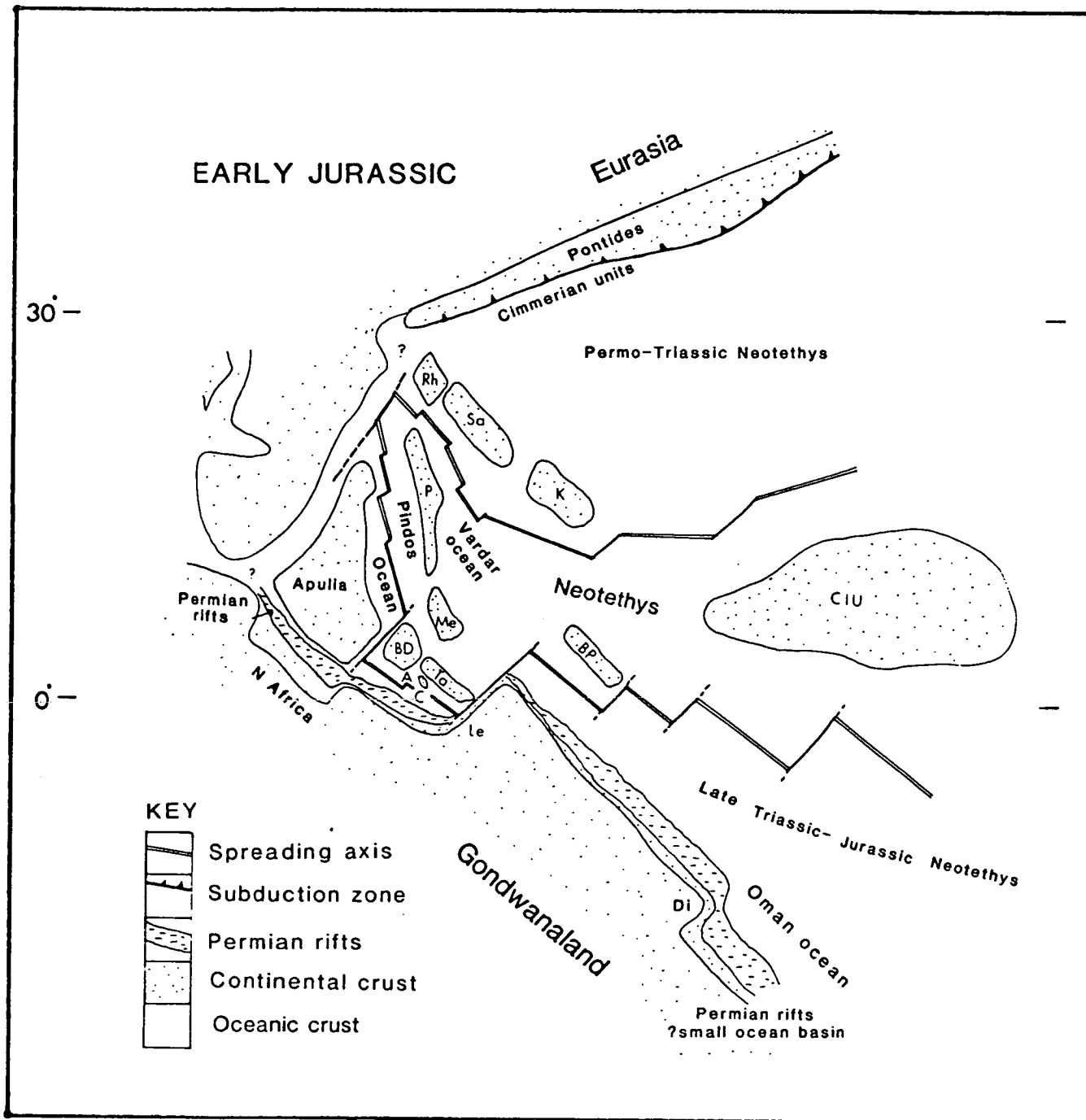


Fig. 1.6 The principle tectonic units of the Eastern Mediterranean and Near East region. Note the proposed continuation of Greek terranes northwards and around the Aegean Arc into Turkey. (From Robertson et al. 1991)



**Fig. 1.7** Palaeogeographic reconstruction of the Eastern Mediterranean in the Mid-Jurassic based on field evidence and palaeomagnetic data (After Robertson et al. 1991).

Rh=Rhodope Zone, Sa=Sakarya unit, K=Kirsehir unit, P=Pelagonnian Zone, Me=Menderes Massif, BD=Bey Daglari platform, BP=Bitlis-Puturge Massifs, Ta=Tauride carbonate platforms, A=Antalya ocean, C=Cyprus ocean, Le=Levant passive margin, D=Dibba Zone, Oman, CIU=Central Iran unit.



Present day exposures of Neotethyan terranes are often fragmentary in nature, thus any palaeogeographic reconstructions are speculative. Despite the severe limitations imposed by incomplete sequences and partial outcrops in structurally complex terranes, attempts have been made by numerous authors to visualize the Neotethyan domain at various times. Tools utilized include field based studies, geochemistry, biostratigraphy and palaeomagnetism. A comprehensive review of work pertaining to the wider regional setting of the Hellenide zones in a Mesozoic Neotethyan context, is beyond the scope of this work. However, important contributions have been provided by Smith (1971), Dewey *et al.* (1973), Smith & Woodcock (1982), Robertson & Dixon (1984), Sengor (1984), Dercourt *et al.* (1986) and Le Pichon *et al.* (1988). A concise and recent summary of views concerning the plate tectonic evolution of Tethys is provided by Clews (1989), while Robertson *et al.* (1991), specifically consider Eastern Mediterranean Tethyan evolution.

## 1.4 HISTORY OF PREVIOUS RESEARCH

### 1.4.1 Early Work

The earliest mention of coherent geological subdivisions in the Peloponnese is credited to the work of Phillipson (1892). He described an "Ionian Zone" (comprising the Pre-Apulian, Ionian and Gavrovo-Tripolitza of today), and a "Pindos Zone". The fold and thrust nature of the Pindos Zone was also first identified by Phillipson. Negris (1908) dated the basal turbiditic sandstone lithology of the Pindos (Priolithos Formation, this study) as being Triassic. This dating appears to have been forgotten in the literature until the age of the lithofacies was "re-discovered" by Terry (1969) in northern Greece. In 1955 a 1:500,000 scale geological map of Greece, based largely on the work of Renz, was published posthumously. During the first half of the 20<sup>th</sup> century, his stratigraphical research refined and increased the understanding of the zones of Greece. The 1950s saw the first activity of the "French school of geology" in Greece. This culminated in the seminal works of Brunn (1956), Aubouin (1959) and Celet (1962) in the external zones of continental Greece, and Dercourt (1964) in the northern Peloponnese.

Aubouin (1959) formulated the first stratigraphic scheme for the Pindos Zone and also suggested a palaeogeographic relationship between the Pindos and Gavrovo-Tripolitza Zones, in which the Gavrovo-Tripolitza platform was located west of the Pindos basin.

The thesis of Dercourt, the result of twelve years of extensive study, has become the foundation upon which later work has been based in the region of the north Peloponnese. He identified the stratigraphic subdivisions, as defined by Aubouin in continental Greece, and extended the known biostratigraphic correlations. In addition he identified the extent and significance of many of the major structural features present.

#### 1.4.2 Recent Work

An attempt was made by Temple (1968) to describe the mechanism of thrusting in the Pindos Zone in terms of large-scale gravity sliding. As he observed, a 2-3° slope is necessary to induce gravity driven sliding, this would require uplift in the east of some 3-5 km. As an alternative to such uplift, Temple appeals to an unrealistic "undulatory wave" mechanism to provide impetus, where-by folds in the autochthon are timed so as to provide successive slopes that propel the allochthon westwards.

Tsoflias (1969a) discovered and dated, as Upper Triassic, ammonites from the frontal region of the Pindos Zone near to the city of Patras. These were within a disrupted outcrop of sediments and volcanics that included an Ammonitico Rosso-type facies and tuffs. Tsoflias argued that the rocks represented the western margin to the Pindos basin, which existed in the Triassic as a "flexure" (horst?) between the Pindos Zone deep water sediments and the neritic carbonates of the Gavrovo-Tripolitza Zone.

During the early to mid 1970s, a series of geological maps and theses were produced under the direction of Dercourt (Meilliez 1971, Flament 1973, De Wever 1975 and Izart 1976). This work included much biostratigraphic detail that allowed greater resolution of the stratigraphy, particularly the Pindos Zone Triassic sediments (Flament 1973) and the Gavrovo-Tripolitza Zone platform carbonates (De Wever 1975). De Wever (1976a, b) also described a "Formation a Blocs", comprising a tectono-sedimentary melange of volcanics and sediments situated between the Pindos and Tripolitza units. A synthesis of the four theses with additional observations and interpretations was provided by Fleury (1980). In addition to research from the North Peloponnese, Fleury also described the Pindos Zone of southern continental Greece. A major portion of his monograph is concerned with the identification and dating of Cretaceous and Early Tertiary foraminifers from the Pindos and Gavrovo-Tripolitza Zones.

A description of the geology of the external zones of the southern Peloponnese was provided by Thiebault (1982). This included sections on the local stratigraphy of the Pindos Zone and an evolutionary model of the basin with conjecture as to relationships with adjacent zones.

A number of papers have been published, mostly in French journals, detailing the results of the biostratigraphic research pertaining to the Pindos Zone. These are further referred to in Chapter 2.

De Wever *et al.* (1986) consider that the end of Jurassic radiolarian deposition coincides with wide-spread changes in oceanic circulation within the Neotethys. They suggest that the establishment of a latitudinal current led to the cessation of local upwellings of nutrient rich waters. Thiebault *et al.* (1986) further state that there is a change in sediment composition observed in southern Greece at this time, with an increase in smectite, chlorite, serpentine and certain elemental ratios up-section. This they also ascribe to changing oceanic circulation patterns.

Green (1982) described the sedimentology and structure of the Pindos Zone north of the Gulf of Corinth. His study concentrated on sedimentological descriptions from north of the present study area. A structural chapter clearly describes and explains the development of meso-scale chevron folds. A concluding chapter details a preferred evolutionary model for the Pindos Zone that strongly supports the existence of a Pindos ocean. A conscious effort has been made in this study not to duplicate aspects of Greens work in the present area.

The volcanic rocks of the Pindos Zone of the Peloponnese have been studied by Richter & Lensch (1977, 1989). These papers are mostly of a petrological nature and concern extrusives found in the tectono-sedimentary melange at a number of locations. The authors believe there to be two volcanic suites, one of mid-ocean ridge or ophiolitic affinity, the other typical of island arc volcanics.

Geochemical analyses of the volcanic rocks were undertaken by Pe-Piper & Piper (1984, 1990). The results of their work are interpreted to show a significant subduction zone signature in extrusive rocks exposed below the Pindos thrust sheets. This they consider to reflect active subduction of Palaeotethys beneath Apulia although they concur with the views of Robertson & Degnan (*pers. comm.* 1988,

1989) that the extensive andesites may alternatively represent partial melting of older subduction modified material.

Piper and Pe-Piper (1980) suggest that there may have been a western source for the terrigenous sediments found within the Pindos Group. This is based on palaeocurrents and facies analysis, although the extent of the data set is not provided. The geochemistry and sedimentary setting of manganese-rich cherts are described by Pe-Piper & Piper (1989).

## **1.5 OBJECTIVES AND METHODOLOGY**

Although previous research has been undertaken in the Pindos and Gavrovo-Tripolitza Zones, the work has generally been concerned with precise stratigraphic correlations based on faunal identification and the location of lithologic boundaries for mapping purposes on a 1:50,000 scale. There is an obvious gap in the literature with respect to detailed sedimentological studies. In addition, previous attempts at describing the structural evolution of the Pindos Zone are inadequate and based upon out-dated concepts of compressional tectonics. There is on-going debate concerning the nature of the basement to deep water sediments exemplified by the Pindos Zone of Greece and the Hawasina sequences of Oman. A geologically integrated study is considered a valid and necessary approach in order to resolve fundamental questions regarding the early evolution of such basins. The main objectives of this present work were as follows:-

Firstly, to arrive at an understanding of the basin evolution. An assessment of the sedimentary depositional environment was made through a description of spatial and temporal variations in sedimentary facies. Sections were measured and key lithological horizons correlated. Field observations were augmented by laboratory based techniques. This approach was supplemented by comparisons with similar facies from present day oceanic areas and other well studied Tethyan regions. By using these tools of basin analysis the first detailed palaeogeographic reconstruction of the Apulian passive continental margin has been accomplished.

The second main objective was to establish the nature of the basal sub-stratum of the Pindos Basin, in particular, to determine whether this was continental or oceanic in character. Geochemical analysis of volcanic rocks, adjacent to and within, the

Pindos Zone was undertaken. By using established methods to discriminate tectonic environments using immobile trace elements (e.g. Pearce & Cann 1973), allied with petrographic observation and geological field relations, the early history of the Pindos Basin can be better defined.

A major aim of the study was to describe and interpret the structural style and the sequence of deformation affecting the Pindos Zone. Closure of the Pindos Basin led to the complete detachment of the deep-sea sediments from their volcanic basement. The deformational history of these sediments is recorded in the structures present and the study seeks to explain the Tertiary tectonic history of the Pindos Zone and its emplacement relationship with the Gavrovo-Tripolitza Zone.

To achieve these objectives, field work was undertaken over three seasons. This was concentrated in the main study area, but also included extensive reconnaissance work throughout the Peloponnese and continental Greece. In addition, Tethyan continental margin sequences were studied in Oman (Hawasina basin sediments) and the Ladakh Himalaya (Lamayuru Complex of the Indus Suture Zone), for comparisons.

A number of geological maps covering most of Greece have been produced by the Greek Institute of Geology and Mineral Exploration (IGME) and several of these were used in the course of this study. In addition, topographic maps and aerial photographs were obtained from the Greek Military Geographical Service.

In Britain a number of laboratory-based techniques were utilised to provide supplementary information. These include X-ray fluorescence spectroscopy (XRF), X-ray diffraction (XRD), cathodoluminescence (CL), electron microprobe analysis (EMPA), scanning electron microscopy (SEM) and microfossil extraction techniques. Descriptions of the methods used are given in Appendix 2.

The rationale of the project, therefore, was to use a variety of methods to describe the Mesozoic and Early Tertiary sedimentary and tectonic history of the Pindos Zone as exposed in the NW Peloponnese, and to document the geodynamic evolution of the basin in relation to adjacent domains. The integrated nature of the project, drawing on diverse aspects of current geological research, allows direct comparisons to be made with modern day processes currently operating in passive and active margin settings.

## CHAPTER 2 STRATIGRAPHY OF THE PINDOS GROUP

### 2.1 INTRODUCTION

It is widely appreciated that some form of stratigraphic framework is an essential prerequisite to a full understanding of the development of sedimentary basins. It is especially important to document the stratigraphic successions from regions, such as the Pindos Zone, where strata have been severely disrupted and original, pre-deformational, contacts are not always preserved. Without the development of an adequate stratigraphic template a complete understanding of subsequent deformation is impossible.

The purpose of this chapter is to define the characteristics of the lithostratigraphic sequences of the Pindos Group (i.e. the sedimentary succession of the Pindos Zone, Section 2.3) in a formal context, and to relate these lithostratigraphic sections to the biostratigraphic data obtained by earlier workers. Type sections are described for each formation from localities where structural complications are minimal and, where possible, there are clear stratigraphic contacts with over- and under-lying formations.

The complex task of unravelling the relative disposition of strata, based on their fossil contents, is a major endeavour which fortunately to a large extent has already been accomplished by earlier workers (Dercourt 1964, Tsoflias 1969a,b, Flament 1973, Dercourt *et al.* 1973, De Wever 1975, Fleury 1980). Dating has mostly been based on microfaunal identification, the results of which are summarised here.

In order to develop the overall chronostratigraphy of the Pindos Group, it is necessary to integrate observed lithostratigraphic and biostratigraphic features. Previous stratigraphic schemes for the NW Peloponnese have concentrated on the biostratigraphic aspect of correlations. In this study the stratigraphy is perceived from the viewpoint of lithological character. For the purpose of this work it was felt necessary to formally define stratigraphic sections on lithostratigraphic grounds, as mappable units. This is in accordance with the internationally accepted rules of stratigraphic nomenclature (Hedberg 1976, Harland *et al.* 1989, Whittaker *et al.* 1991), which do not depend solely on biostratigraphy.


		AUBOUIN 1959	DERCOURT et al. 1973 FLEURY 1980	GREEN 1982		DEGNAN (This Study)			
CENOZOIC		Flysch du Pinde		Pindos Flysch Group		Pindos Flysch Fm			
CRETACEOUS	U	Couches de Passage		Stephani Mbr	Evrítania Fm	Kataraktis Passage Mbr		PINDOS GROUP	
		Calcaires en Plaquettes		Frangista Lst Mbr		Erymanthos Lst Mbr			
	L	Premier Flysch de Pinde	Marnes Rouges	Green Sst Mbr	Platanos Fm	Paos Lst Mbr			
						Klitoria Sst Mbr			
JURASSIC	U	Les Jaspes	Calcaires a Calpionelles	Aspro Lst Mbr	Trikorton Lst Mbr	Kakotari Lst Mbr	Aroania Chert Mbr	Lesteena Fm	
	M	a Radiolarites	Radiolarites	Stenoma Shale Mbr			Trikhonis Fm		Kastelli Mdst Mbr
			Pelites de Kasteli	Riganon Chert Mbr					
	L			Voutiron Shale Mbr					
TRIASSIC	U	Les Jaspes et	Calcaires de Drimos	Karitsa Lst Mbr		Karpenision Fm	Drimos Fm		
				Proussos Shale Mbr					
		Calcaires a Halobia		Petroto Lst Mbr					
		Le Detrique Triassique		Navpaktos Sst Mbr			Priolithos Fm		
 TECTONIC BASE									

Table 2.1 Previous stratigraphic schemes for the Pindos Zone and their relation to the stratigraphy presented in this work.

## 2.2 PREVIOUS STRATIGRAPHIC SCHEMES

Brunn (1956) and Aubouin (1959) were the first to propose a complete stratigraphic column for the Pindos Zone. Dercourt *et al.* (1973) adapted and extended this scheme, specifically for the sediments of the NW Peloponnese. This is the system that was adopted by Fleury in his own work (1980) and was used as a basis for the geological maps of the Greek Geological Survey (IGME). Due to the extent of lithological variations between other areas and the NW Peloponnese, and the essentially biostratigraphic nature of earlier schemes which are not in accordance with recommended international stratigraphical guidelines, it was felt necessary to construct a new stratigraphy. Table 2.1 details previous stratigraphic schemes applicable to the Pindos Zone of the NW Peloponnese, and correlates them to the formal stratigraphy presented in this study.

## 2.3 FORMAL STRATIGRAPHY

### 2.3.1 The Pindos Group

The Pindos Group is defined as the sedimentary succession of the Pindos Zone. It consists of the following five formations; Priolithos Formation, Drimos Formation, Lesteena Formation, Lambia Formation and the Pindos Flysch Formation. The Lesteena Formation is further sub-divided into three members. These are the Kastelli Mudstone Member, the Aroania Chert Member and the Kakotari Member. The Lambia Formation is similarly sub-divided<sup>but</sup> into four members; the Paos Limestone Member, the Klitoria Sandstone Member, the Erymanthos Limestone Member and the Kataraktis Passage Member. This stratigraphic sub-division reflects either local lithological characteristics (e.g. Kakotari Member), or the difficulty in drawing specific intra-formational boundaries on a regional basis (e.g. Kataraktis Passage Member). Thus this scheme confirms and emphasizes the established definition of a formation, a clearly mappable unit distinguishable from surrounding lithologies, as the principle division for stratigraphic description (Hedberg 1976, Holland *et al.* 1978, Harland *et al.* 1989).



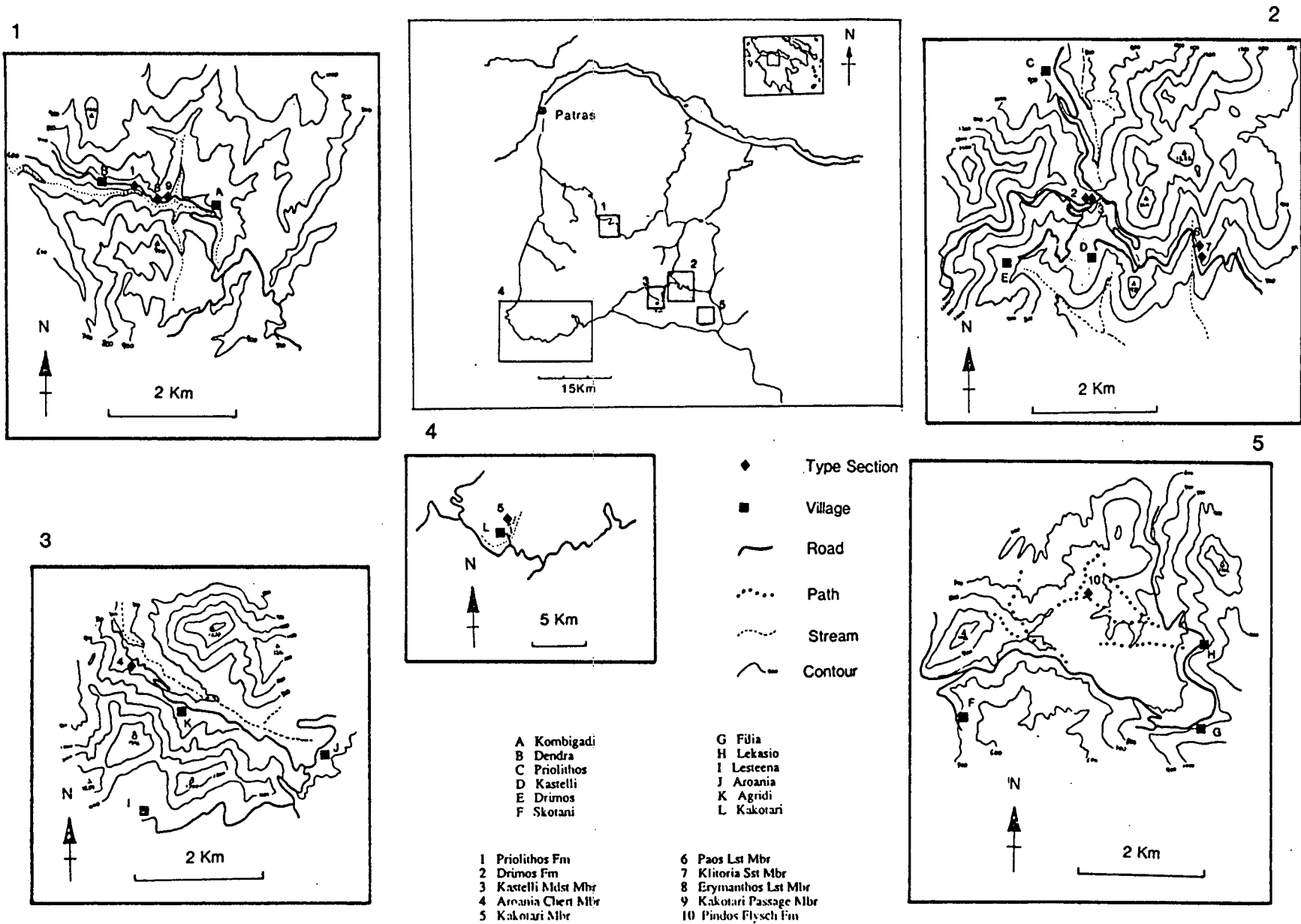


Fig. 2.1. Locality map of the stratigraphic type sections.

### 2.3.2 Priolithos Formation

#### Synonymy

Le Detrique Triassique (Dercourt *et al.* 1973), Navpactos Sandstone Member of the Karpenision Formation (Green 1982).

#### Type section

The type section is located on the main Halandritsa to Kalavrita road, (Figure 2.1) approximately 1.5km west of the village of Kombigadi. It is exposed in a stream about 20m below the road. The type section is tectonically contorted by many folds and small faults. A section of 14m was measured (Log A2, Appendix 1) which represents a continuous intact thickness, although it is likely that up to 40m of section may be present.

#### Lithology

The Formation is dominantly turbiditic terrigenous sandstone, with interbedded argillaceous beds. Arenite beds are between 2-15cm thick and occasionally show normal grading with parallel laminated tops. Grain size is fine to medium, with moderate to poor sorting of dominantly sub-rounded to sub-angular clasts. In the field, the Priolithos Formation can be identified by the presence of intercalated limestone beds. These are dark, very well cemented 10-20cm thick beds of micrite, sometimes containing *Halobia* sp. pelagic bivalves.

#### Boundaries

The thickness of this Formation is unknown as the base is always a tectonic surface. The upper boundary is transitional to the overlying Drimos Formation as the proportion of limestone increases.

#### Distribution and Environment

Within the study area, exposures of the Priolithos Formation are found from the western-most limit of the Pindos Group outcrop (the Pindos front), to as far east as Kato Klitoria (Figure 1.1). Successions are generally incomplete since the formation occurs only at the base of major thrust sheets and is often structurally disrupted. The Priolithos Formation appears to be missing from many areas in the central and southern Peloponnese. Although the proportion of argillite/limestone/arenite varies in different localities, no meaningful deductions can be made from this variation in the study area because of the sparse outcrop.

### Biostratigraphy

In addition to pelagic bivalves of the *Halobia* genus, a conodont fauna is also reported, this includes the following species; *Epigondolella abneptis* (Huckriede), *Prioniodella decrescens* (Tatge) and *Ozarkodina tortilis* (Tatge), (Flament 1973). These indicate an Upper Triassic (Carnian-Norian) age for the Priolithos Formation.

### 2.3.3 Drimos Formation

#### Synonymy

Les Jaspes et Calcaires a Halobia (Aubouin 1959), Calcaires de Drimos (Dercourt *et al.* 1973), Petrote Limestone Member, Proussos Shale Member and Karitsa Limestone Member of the Karpenision Formation (Green 1982).

#### Type section

The type section (Log B3, Appendix 1) is located on the Aroania to Kalavrita road; it begins approximately 500m before the col and the junction with the Kato Klitoria to Kalavrita road (Figure 2.1). The thickness of the measured section is 103m.

#### Lithology

The succession is dominantly interbedded hemipelagic calcilitite and very fine grained calciturbidite. Near the base of the section an interval of siliceous mudstone and chert is found. In addition, in the lower part of the section are hemipelagic carbonates containing "filaments" (shell fragments of the pelagic bivalve *Halobia*), and beds of oolitic limestone. There is a subtle colour change in the carbonate through the section, from dominantly pale green at the base to grey at the top. Replacement chert nodules are found at irregular intervals. Bed thicknesses are generally 2-8cm but increases upwards to 5-15cm.

#### Boundaries

The base of the Formation is stratigraphically conformable with the Priolithos Formation. The Formation passes conformably upwards into the Kastelli Mudstone Member of the Leestena Formation.

#### Distribution and Environment

Lithostratigraphic equivalents are found throughout the study area, although to the east of Chelmos no rock below the radiolarite of the Leestena Formation has been

recognized. There is a very marked change in the sedimentary characteristics from the west towards the east within the Drimos Formation. This is inferred to reflect proximity to a continental margin. In the west, deposits interpreted as rockfall deposits and debris flows are present, as well as calcirudites derived from high density turbidity currents. Further east, as in the type section, deposition is considered to reflect deposition from distal turbidity currents and hemipelagic settling. Consequently there is a great deal of spatial variation in the thickness of the Formation. The bed morphology of the more distal beds is considered to be essentially tabular, although it is likely that there has been some small scale channelisation, as evidenced by the presence of intraformational erosion surfaces.

### Biostratigraphy

The Formation has been dated as Upper Carnian to Liassic on the basis of conodont and pelagic bivalve age determinations. In the lowermost beds *Halobia cassiana* and *H. styriaca* have been identified (Dercourt 1964). In addition, several conodont species have been identified by Flament (1973) including; *Epigondolella abneptis* (Huckriede), *E. primitia* (Mosher), *Paragondolella polygnathiformis* (Budurov & Stefanov) and *E. bidentata* (Mosher). These span the Upper Carnian to the Upper Norian. Fleury (1980) considers the shale and chert interval of the Drimos Formation to represent the Rhaetic to Liassic period as it coincides approximately with the disappearance of *Halobia* sp. This is confirmed by De Wever & Origlia-Devos (1982b). They report that only Liassic radiolaria were recognized in specimens taken from cherts of the type section, however the limestone beds below the fossiliferous chert horizon most probably represents the Rhaetic.

The limestones above the chert interval are considered to represent the greater part of the Liassic. They are certainly post-Norian but pre-Pliensbachian (Fleury 1980) as the presence of fossil algae *Labrynthina* confirms. The upper age limit is believed to be Toarcian or possibly Aalenian, as the algae *Thaumatoporella* sp, *Glomospira* sp, *Haurania* sp and *Cayeuxia* sp have all been identified below the overlying Kastelli Mudstone Member (Fleury 1980).

## 2.3.4 Lesteena Formation

### 2.3.4.1 Kakotari Member

#### Synonymy

None. New name.

#### Type Section

The type section is found approximately 2km north of the village of Kakotari, along a track that follows the river towards Kryovrissi (Figure 2.1). The section (Log C1, Appendix 1) is in a stream bed located to the west of the track, on a prominent bend. The locality has been dated as Upper Triassic to Upper Cretaceous (Izart 1976). No new age determinations for this locality have been attempted because of the similarity of facies from throughout the section, and the fact that the rocks are mostly redeposited limestones. However, a section was logged above a yellow-grey dolomitic carbonate rudite horizon, and below beds where *Globo truncana* sp. was identified. This is considered to correspond as closely as practicable to the Liassic to Lower Cretaceous interval. The thickness of the section is 127m.

#### Lithology

The beds are almost exclusively calcirudites, ranging in clast size from gravel to cobble grade. The conglomerates are mostly clast-supported, monomict, with beds up to 2m thick. Clasts are mostly micrites and oolitic packstones. In addition, some gravel-grade conglomerate beds, up to 1.5m thick, are entirely made up of coralline material. Similar channelised beds are found within the Aroania Chert Member further towards the east.

#### Boundaries

The boundaries are somewhat arbitrary, in that the lithofacies in the immediate area are very similar, but have been shown to span the Upper Triassic to Palaeocene interval (Izart 1976). The lower boundary is taken as an area where the rock colour changes from a buff-grey to a darker grey. This corresponds to an increase in the calcium carbonate component in the rock. The upper boundary, similarly, is arbitrary in that it is the first bed where Cretaceous pelagic foraminifera (*Globo truncana* sp.) were observed.

## Distribution and Environment

The member is only found in the extreme frontal thrust sheets in the south of the study area. Reefal calcirudites were found a further 2km north of the type section but, due to tectonic complexity, the facies transition to the more regular, thinner-bedded and siliceous cherts as found in the frontal thrust sheets further north, was not observed. The character of the sediment, and the possibility of an original sharp facies change, suggests an upper fan (Mutti & Ricci Lucchi 1972, Normark 1978) or even canyon environment. For the reasons given above, the age is poorly constrained but is considered to be at least in part synchronous with the Kastelli Mudstone and Aroania Chert Members.

### 2.3.4.2 Kastelli Mudstone Member

#### Synonymy

Les Jaspes a Radiolarites (Aubouin 1959), Pelites de Kastelli (Dercourt *et al.* 1973), Voutirion Shale Member of the Trikonis Formation (Green 1982).

#### Type Section

The type section (Log D6, Appendix 1) is a continuation of the underlying Drimos Formation, i.e. on the Aroania to Kalavrita road (Figure 2.1). The succession is 38m thick.

#### Lithology

At this locality the Kastelli Mudstone Member is a series of intercalated mudstones and limestones. Unlike the pelites of the Drimos Formation, the mudstones are noticeably thicker, in the order of 2-6cm thick. The siliceous content of the mudstone increases upwards. The muds include variegated greens and yellow, but are dominantly red-brown in colour. Some of the limestones are oolitic or very fine calcarenites and/or siltstones.

#### Boundaries

The base of the succession conformably overlies the Drimos Formation, where there is a distinct increase in the ratio and thickness of mudstones to limestone upwards. There is a gradual transition conformably upwards into the overlying radiolaria rich cherts of the Aroania Chert Member.

### Distribution and Environment

The Kastelli Mudstone Member has acted as a major decollement horizon for the thrust faults that cut the Pindos Group. The Member is situated between the more competent Drimos Formation limestones and the Aroania Chert Member. Due to the great lithological contrast, the member is often sheared and cut-out from a number of successions. It is preserved, however, where thrust sheet detachments have utilized other suitable horizons in which rheological differences are maximised. The Kastelli Mudstone Member is found in most parts of the study area, from the very frontal sheets where the thickness is greatly reduced (less than 2m) as far east as Kalavrita. The member is not present in the frontal sheet at Kakotari, described in Section 2.3.4.1. The deposition of the mudstone reflects a major change in sedimentary environment, corresponding to the raising of the calcite compensation depth (CCD) and a decrease in the supply of calcareous sediment.

### Biostratigraphy

The member is dated as Aalenian (Fleury 1980) based on the presence of the algae *Meyendorffina cayeuxi* (Lucas), considered by Flament (1973) to span the Aalenian-Bajocian, and *Lucasella cayeuxi* (Lucas). Flament (1973) also reports the presence of the foraminifer *Ataxiophragmidiides* sp. Comparisons with similar mudstones, dated as Upper Pleinsbachian to Toarcian from the Alps du Vincetin, have led Lyberis *et al* (1980) to suggest an older age. This is not considered valid for the Peloponnese as several other microfaunal species have been described (De Wever & Origlia-Devos, 1982a), including *Mesoendothyra croatia* (Gusic), *Thaumatoporella parvovesiculifera* (Raineri), *Lucasella* sp. and *Lenticulina* sp.

### 2.3.4.3 Aroania Chert Member

#### Synonymy

Les Jaspes a Radiolarites (Aubouin 1959), Radiolarites (Dercourt *et al.* 1973), Stenoma Shale Member and Riganon Chert Member of the Trikonis Formation (Green 1982).

#### Type Section

This is located on the Aroania to Tripotama road, ca. 2km NW of Agridi. The type section (Log E9, Appendix 1) is found 1km before a hairpin bend which rises up towards Agridi village (Figure 2.1). The section is 99m thick.

### Lithology

The type section is entirely free of bedded limestone. It comprises varying proportions of vitreous and argillaceous radiolarian chert, with interbedded mudstones. The mudstones increase in proportion towards the top. There are two prominent manganiferous chert horizons, although diagenetic manganese is also present throughout the member. Some chert horizons have a "pinch and swell" aspect, others contain parallel laminations.

### Boundaries

The lower contact is defined as the first continuous occurrence of bedded chert above the underlying Kastelli Mudstone Member. The upper contact is a minor reverse fault with overlying limestone of the Paos Limestone Member, however, the chert sequence is considered to be essentially complete.

### Distribution and Environment

The Aroania Chert Member is found throughout the study area and also in some localities to the east of Chelmos within the "Table d'Arcadie". The thickness of the member is extremely variable, from less than 1m at Kakotari to possibly greater than 100m. In the west there is a greater degree of variability in the beds that make up the member, in texture, grain size and colour. Intraformational conglomerates and breccias containing reefal material are sometimes found. These differences reflect the inferred proximity to the Apulian margin and the channelisation of high density turbidity currents. The member was certainly deposited below the contemporaneous CCD.

### Biostratigraphy

The Member has been dated as Bajocian to Tithonian (De Wever 1989). This is based on the identification of seventeen diagnostic radiolarian assemblages found mainly in the Karpenision area of continental Greece, but including some samples from the Peloponnese (De Wever & Oriliglia-Devos 1982a, De Wever & Cordey 1986).



## 2.3.5 Lambia Formation

### 2.3.5.1 Paos Limestone Member

#### Synonymy

The lower-most horizons of both the Calcaires en Plaquettes (Aubouin 1959), the "Niveaux de Transition" and Calcaires Rose sub-division of Fleury (1980) and the Frangista Limestone Member of the Evritania Formation (Green 1982).

#### Type Section

This is found on the Kato Klitoria to Kalavrita road via Kastelli, approximately 1km east of the Kastelli junction (Figure 2.1). The type section is 70m thick (Log F1, Appendix 1).

#### Lithology

The succession comprises pink micrite and siltstone, thin bedded cherts, shales and calcarenite, both with and without nodular chert. Within the Paos Limestone Member is the Klitoria Sandstone Member. The proportion of replacement chert is observed to increase towards the top of the section.

#### Boundaries

The lower boundary is taken to be the top of the uppermost chert and mudstone of the Aroania Chert Member, below a series of 2-5cm thick pink limestones. The upper boundary is where the proportion of light-blue and grey limestones of the Erymanthos Limestone Member comprises greater than 50% of the bed thickness over a five metre interval.

#### Distribution and Environment

The Paos Limestone Member is distinctive because of its position above the cherts and its pink colouration. The pink colouration of beds occurs over a thicker interval in the eastern Klitoria area than in the more proximal areas. However, the member is recognized in all sections which preserve strata between the Aroania Chert Member and Erymanthos Member limestones. In the most proximal sheets at Alepohorio, a white porcellaneous limestone, lithologically identical to a *Calpionellid* sp. bearing limestone from Solinari in the southern Peloponnese (Figure 1.1), is considered as the local base to the Paos Limestone Member. In addition, in the more proximal sheets, channelised calcirudites are present, as well as channelised pink siltstones.

The calcirudites are often light grey, with large replacement chert nodules. These lie stratigraphically below finer-grained micrites and calciturbidites of the Erymanthos Limestone Member.

#### Biostratigraphy

Calpionellid limestone from north of the Gulf of Corinth has been dated as Upper Tithonian to Berriasian, or possibly Lower Valanginian in age (Fleury 1980). Among the species identified are; *Calpionella alpina* and *Calpionella elliptica* (Upper Tithonian); *Stomiosphaera molucanna* and *Nannoconus* sp. (Lower to Middle Berriasian); *Calpionella oblonga*, *Calpionellopsis* sp. and *Tintinopsella* sp. (Upper Berriasian). Lyberis (1978) reported *Calpionellites darderi*, dated as Lower Valanginian. In other parts of the Pindos Zone, north of the Gulf of Corinth, an additional member, the "Marnes Rouge" (Fleury 1980) was deposited above the calpionellid-bearing limestones. This interval was not identified in the proximal thrust sheets of Alepohorio, where the porcellanous Calpionellid bearing limestones were found. Instead it probably corresponds to the increased quantity of mudstone found at the top of the Aroania Chert Member, transitional into the Paos Limestone Member of the more distal locations. In the "Marnes Rouges" of continental Greece, the following microfossils are reported (Fleury 1980); *Praeglobotruncana stephani*, *Rotalipora appenninica* and *Favusella washitensis*. These correspond to a Lower Cenomanian to lower Middle Cenomanian interval. Above these *Praeglobotruncana stephani*, *Broeckina balcanica* and *Rotalipora cushmani* were found, along with *Orbitolina* debris. This assemblage confirms a Middle to Upper Cenomanian age. The youngest beds include *Globotruncana coronata* which became established in the Turonian.

The upper part of the Paos Limestone Member is considered equivalent to the "Niveaux de Transition" and Calcaires Rose of Fleury (1980), which has been dated as Lower Turonian to the Lower Santonian. This interval is characterized within the Pindos Group by *Globotruncana helvetica* (Turonian) and *Globotruncana "renzi"* (Turonian to base Santonian). However, Fleury states that only one sample yielded a datable foraminifer (of *Gt. "renzi"*) from the uppermost beds.

The member is therefore of Tithonian to Coniacian or possibly Santonian age.

### 2.3.5.2 Klitoria Sandstone Member

#### Synonymy

Premier Flysch de Pinde (Aubouin 1959, Fleury 1980), Green Sandstone Member (Green 1982).

#### Type Section

The member is best exposed as two sandstone units within, and separated by, limestones and mudstones of the Paos Limestone Member type section on the Kato Klitoria to Kalavrita road (Figure 2.1). The member type section is 20m thick (Log F1, Appendix 1).

#### Lithology

The Klitoria Sandstone Member is a terrigenous fine-to coarse-grained arenite, with interbedded mudstone and occasional thin limestones. The beds are often graded, with ripple cross-lamination and parallel-lamination. Bedding contacts are sometimes irregular erosional scours and there are flute and groove casts on the bases of some beds. Clasts are sub-angular to sub-rounded and moderately to well sorted. The clast composition includes detrital quartz, carbonate, feldspar and lithic fragments, including shale rip-up clasts and chert.

#### Boundaries

The base of the member is a clear contact between the underlying pink limestones of the Paos Member and green lith arenite. A series of sandstone beds, isolated from other sandstone units, is sometimes informally termed a "package". The type section consists of two packages, the first (oldest) is 14m thick. This is separated from the second package by 4.5m of pink limestone. The second package is 6m thick, the upper boundary of which is a clearly conformable contact with overlying pink limestones.

#### Distribution and Environment

The Klitoria Sandstone Member is somewhat enigmatic in that its distribution is very erratic in the study area. Apart from rare 2-5cm-thick terrigenous beds found on Erymanthos Mountain, there is no evidence for deposition of the sandstones west of Tripotama (Figure 1.1). Many sedimentary features suggest a turbidity current mechanism of deposition. The member thickness, even over short distances, is

highly variable. Palaeocurrent indicators show a current orientation that is highly variable.

### Biostratigraphy

Dercourt (1964) discovered several examples of *Orbitolina concava* (Cenomanian) in the Pindos Zone of the north Peloponnese, from pelites and sandstones which were correlated with the Klitoria Sandstone Member. Flament (1973) dated a section in the area of Kato Klitoria (which may be the same as the above type section) as Turonian. This is based on the diagnostic presence of *Aedissacus* sp. and *Moncharmontia* sp. (Lower Cenomanian to Turonian) below the first sandstone package, and *Globotruncana helvetica* (Turonian) from an interbedded limestone within the two sandstone packages.

### 2.3.5.3 Erymanthos Limestone Member

#### Synonymy

Calcaire en Plaquettes (Aubouin 1959, Fleury 1980), Frangista Limestone Member of the Evritania Formation (Green 1982).

#### Type Section

The type section (Log G1, Appendix 1) is located on the main Halandritsa to Kalavrita road about 800m west of the village of Kombigadi. It is part of the same sequence from which the Priolithos Formation type section was taken (Figure 2.1). The type section is 182m thick.

#### Lithology

Internally the member is relatively homogenous, being composed of grey to blue-grey micrites, silt to fine arenite grade calciturbidite, gravel to pebble grade conglomerate and thin shale partings. There are three distinct intervals where abundant pelagic foraminifers (*Globotruncana* sp) are observed, although they can be found less concentrated throughout the member.

#### Boundaries

The lower boundary is taken to be where the proportion of grey-blue limestone is 50% or more, by thickness, relative to the underlying pink limestone of the Paos

Limestone Member over a five metre interval. The upper boundary is taken from the first occurrence of black replacement chert horizons within the limestone.

#### Distribution and Environment

The Erymanthos Limestone Member is the dominant relief-forming lithology of the Pindos Group. It is found throughout the Pindos Zone. Ascertaining the thickness from many localities is probably impossible because of the degree of folding and the lack of marker horizons. It is, however, not believed to be constant, varying between 150m in the west to possibly 400-500m on the Table d'Arcadie in the east. There is a marked change in grain-size and bed thickness in some areas. Near to the Pindos front, clast-supported breccio-conglomerates and gravel-grade conglomerates are commonly recorded. Further east, the composition of the member becomes more constantly micritic, to silt grade, with faint parallel laminations near the tops of individual beds. The differences reflect a proximal to distal style of deposition.

#### Biostratigraphy

Dating the base of the unit is problematic because of uncertainty concerning the age of the uppermost Paos Limestone Member beds, compounded by a lack of diagnostic microfauna within the lowermost Erymanthos Limestone Member beds. The oldest definite age assigned to the member occurs where *Globotruncana asymetrica* and *Globotruncana elevata* are found together in the same horizon. This corresponds to the Upper Santonian to Lower Campanian interval (Fleury 1980). The upper boundary is defined as the first occurrence of black replacement cherts. This is a characteristic marker horizon (discussed in section 2.3.5.4), which straddles the Mesozoic/Cenozoic boundary. The period of time represented by the deposition of the Erymanthos Limestone member is considered as Coniacian to Upper Maastrichtian.

#### 2.3.5.4 Kataraktis Passage Member

##### Synonymy

Couches de Passage (Aubouin 1959, Fleury 1980), Stephani Member of the Evritania Formation (Green 1982).

### Type Section

The type section (Log H1, Appendix 1) is a continuation of the underlying Erymanthos Limestone Member (Figure 2.1). The type section is 177m thick.

### Lithology

The member is a transitional series that illustrates the change from dominantly carbonate deposition to more terrigenous clastics. Consequently, it contains lithologies typical of both the underlying and the overlying stratigraphic units, namely intercalated limestones, mudstones and sandstones. The base of the succession comprises blue-grey micrites and silt grade limestones with black cherts. The proportion of argillite and sandstone increases upwards.

### Boundaries

The lower boundary of the type section is taken as the first occurrence of a black replacement chert horizon. The upper boundary is where the ratio of terrigenous sandstone beds to limestone exceeds 50% over a ten metre interval.

### Distribution and Environment

The transitional beds of the Kataraktis Passage Member are found throughout the Pindos Group. They are interpreted as representing the earliest sedimentary response to an advancing orogenic front from the east, but, there may also be a eustatic control influencing the nature of the sediment. Limestone beds of the Kataraktis Passage Member display a wider range of sedimentary structures in the west compared to more easterly localities, e.g. extensive convolute bedding, debris flows and rock falls are present. ⊗

### Biostratigraphy

The black cherts have been dated as straddling the Mesozoic/Cenozoic boundary (Flament 1973, Fleury 1980). In the region of Kato Klitoria, Flament (1973) identified several microfossil species, including; *Globotruncana arca*, *Gt. contusa*, *Gt. stuarti* and *Gt. stuartiformis* (Upper Maastrichtian). These are in a section immediately below black cherts, above which a sample was attributed to the Lower Palaeocene based on the presence of *Globorotalia compressa* and *Globorotalia pseudobulloides*. The black cherts are considered a temporal marker horizon throughout the study area. At the type section black cherts are found below the lowermost terrigenous deposits. In other places however, e.g. Aroania, the cherts are intercalated within a series of beds, including terrigenous siltstones. The lowermost

⊗ The change in sedimentation indicates that the inferred rise and abyssal plain depositional environment, adjacent to the Apulian margin, gradually filled with siliciclastic debris supplied from the north (as a result of tectonic activity).

beds of the Pindos Flysch Formation are Palaeocene, Therefore the Kataraktis Passage member is dated as Maastrichtian to Palaeocene.

### 2.3.6 Pindos Flysch Formation

#### Synonymy

Flysch du Pinde (Aubouin 1959, Dercourt 1964, Fleury 1980), Pindos Flysch Group (Green 1982).

#### Type Section

The type section (Log I1, Appendix 1) is located 1600m to the west of the Lekasio to Kato Klitoria road, along a track found 1km south of the village (Figure 2.1). The section does not exhibit lower, or upper stratigraphic contacts. However, it is a representative section which over a small interval shows many of the features found in the Pindos Flysch Formation. The type section is 36m thick.

#### Lithology

The formation is a series of massive and graded sandstones with interbedded shales and mudstones. Sedimentary structures indicate deposition by turbidity currents. Clast sizes range from very fine-grained to gravel grade. Many of the gravel grade deposits are composed almost entirely of quartzose sediment. Metamorphic, volcanic and sedimentary clasts are common. The section also contains interbedded red and blue-grey mudstones.

#### Boundaries

Stratigraphic boundaries for the section are not exposed. However, for other localities the lower boundary is taken as the position where the terrigenous sandstone component exceeds 50%, by thickness, of the sediment over a five metre interval. The upper boundaries are everywhere tectonic or erosional.

#### Distribution and Environment

The Pindos Flysch Formation is generally preserved in structural synforms, or directly below overlying thrust sheets. It is potentially present throughout the Pindos Zone. The sediment is interpreted to initially represent the passive infilling of the Pindos Basin, supplied with sediment from a collision zone to the north. The sediment evolved into a trench deposit, incorporated into an accretionary wedge as

the Pindos oceanic crust was subducted. With time, as the Apulian margin was downwarped, a foreland basin developed on the continental crust of the Gavrovo-Tripolitza Zone with the diachronous migration of terrigenous sedimentation from an oceanic setting to that of a classical foredeep.

### Biostratigraphy

The earliest Pindos flysch sediments are dated as Palaeocene (Fleury 1980). Dercourt and Magne (1973) have dated lowermost Pindos flysch from the NE Peloponnese as Upper Palaeocene, based on the identification of *Globorotalia pseudomenardii*, *Globigerina primitiva* and *Truncorotalia velascoensis*. The formation is considered to extend into the Eocene (Tsoflias 1984).

### 2.3.7 Other Lithologic Units

In addition to the observed sedimentary succession, volcanic rocks were seen to be in direct stratigraphic contact with overlying limestones of the Drimos Formation (at Kokkino, southern Peloponnese, Figure 1.1). These volcanic rocks have geochemical affinities with extrusives incorporated into a tectono-sedimentary melange found at the base of some thrust slices at a number of locations throughout the Peloponnese (De Wever 1975, 1976a,b, Richter & Lensch 1977, 1989, Pe-Piper & Piper 1990). The igneous rocks and other components of the tectono-sedimentary melange are considered more fully in Chapter 8.

## 2.4 SUMMARY OF THE STRATIGRAPHY OF THE PINDOS GROUP

The sedimentary fill of the Pindos Basin, in the region of the NW Peloponnese, was deposited over approximately 170 million years, from the Upper Carnian to the Upper Eocene. Several distinct mappable units were identified on a regional scale, and these lithostratigraphic units are the essence of the formalised stratigraphy presented here. Each formation has its own lithological characteristics which are clearly different to adjacent formations. Within individual formations there is a degree of lateral and vertical facies variation. This is expressed by thickness and compositional changes, reflected in the stratigraphy by the assignment of informal member status to certain sedimentary successions. Previously published biostratigraphical data have been used, after recognition of described lithologies, to date the above formations. The lithostratigraphic formations and members described



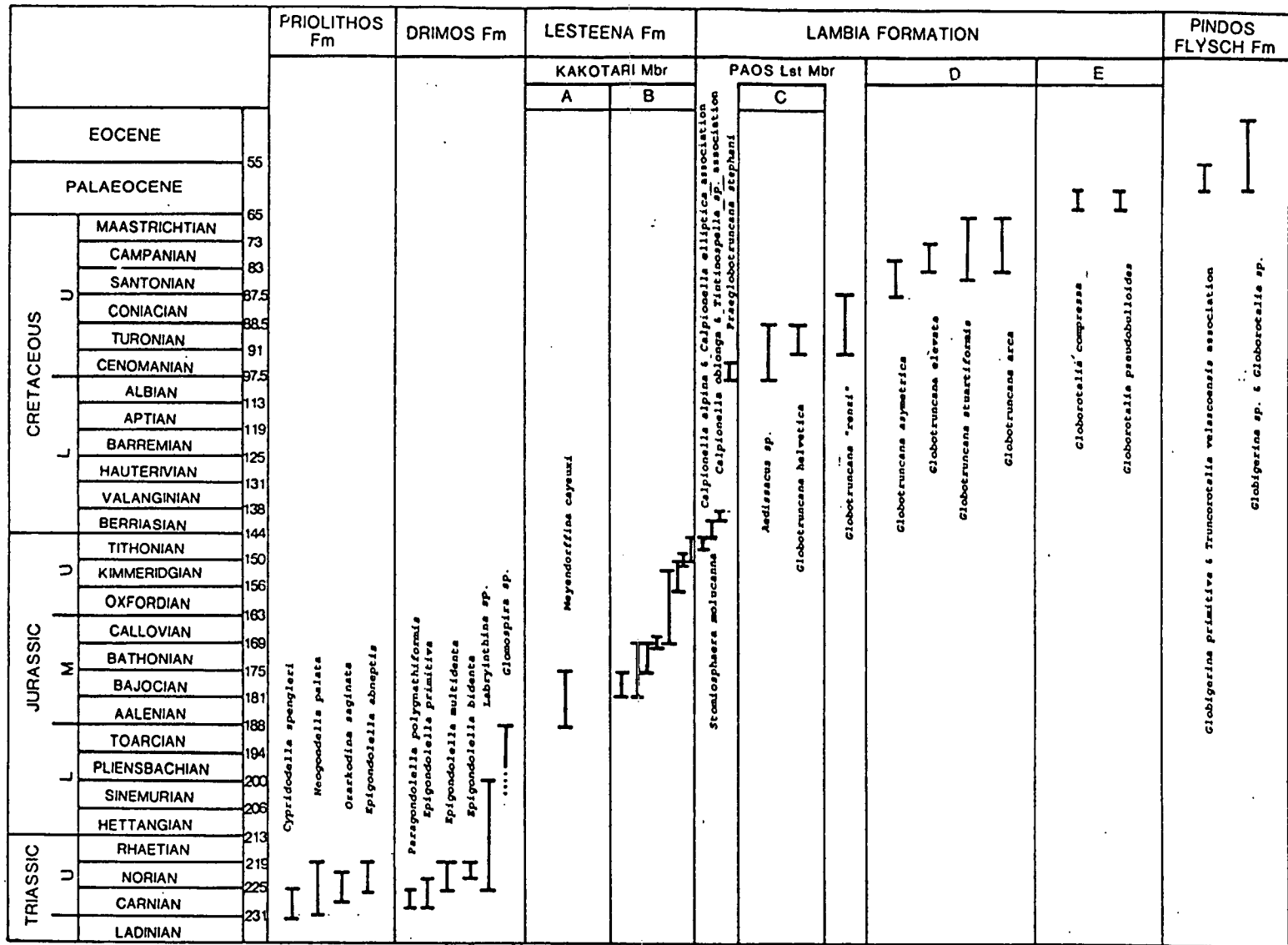


Fig. 2.2 Biostratigraphic compilation diagram indicating the biozonation of some of the species used by previous workers to date the Pindos Group (references in the text).

above can be correlated with relative ease in most cases, to the earlier biostratigraphic divisions of the "French school". Figure 2.2 is a diagrammatic representation of the faunal contents used by earlier workers to date the preceding stratigraphic units. This biostratigraphic compilation is taken from several sources; Fleury 1980 (Cretaceous and Early Tertiary foraminifera and summaries); Dercourt 1964 (Pindos Group); Flament 1973 (Upper Triassic conodonts); De Wever 1975, 1989 (Jurassic radiolarians); and Tsoflias 1979, 1984 (Triassic ammonites and Eocene foraminifera). Additional age determinations for selected samples utilized in this work and found by the author, have been identified and dated. These are referred to in later sections.

**SECTION B: SEDIMENTOLOGY & STRUCTURE OF  
THE PINDOS ZONE**

**CHAPTER 3: PRIOLITHOS & DRIMOS FORMATIONS**

**CHAPTER 4: LESTEENA FORMATION**

**CHAPTER 5: LAMBIA & PINDOS FLYSCH FORMATIONS**

**CHAPTER 6: STRUCTURAL ANALYSIS OF THE PINDOS  
ZONE**

## SECTION B: SEDIMENTOLOGY & STRUCTURE OF THE PINDOS ZONE

### INTRODUCTION

The following four chapters comprise the essential history of the Pindos Zone. They follow in a chronological sequence, rather than being organised on a facies or palaeoenvironmental basis. This layout is intended to clarify the temporal development of the basin. The sedimentology of the Pindos Group is described, as are the effects of Early Tertiary compressional tectonics. The purpose of this introduction is to discuss the gross depositional environment of the Pindos Group and to state some of the sedimentological methods and terminology that have been used in the construction of the following chapters.

#### Sedimentary Depositional Environments and Processes

The Pindos Group sediments are inferred to represent deep water continental margin deposits, based on the observed sedimentary structures and facies distribution. The large scale geomorphological features of a continental margin comprise the shelf, shelf-break, slope, rise and abyssal plain (Figure B1). In the case of the Pindos Zone, reworked sediments were largely derived from off the adjacent Gavrovo-Tripolitza platform, and transported to slope and rise settings by mass transport mechanisms, with hemipelagic sediment settling on the abyssal plain. The entire Pindos Group sequence, representing some 170 million years of continuous sedimentation, reaches a maximum preserved thickness of only 500-1000m. The inferred morphology of the Pindos margin is further described in Section 3.3.3.2.

Table B1 provides a guide to mass transport processes with their distinctive resultant sedimentary structures and characteristic transport mechanisms (after Nardin *et al.* 1979). Inferred mass transport processes include rock falls, debris flows, liquified flows and turbidity currents. The essential characteristics of each mass flow process is summarised here (partially after Nardin *et al.* 1979 and Lowe, 1979).

**Rock fall:-** This can result from mass movement processes or as the aggregate result of individually dislodged clasts. Rock fall sediment bodies comprise poorly sorted, angular to sub-angular clasts. They can be polymict, but are more generally monomict. Rock fall deposits are clast supported and have been variously termed

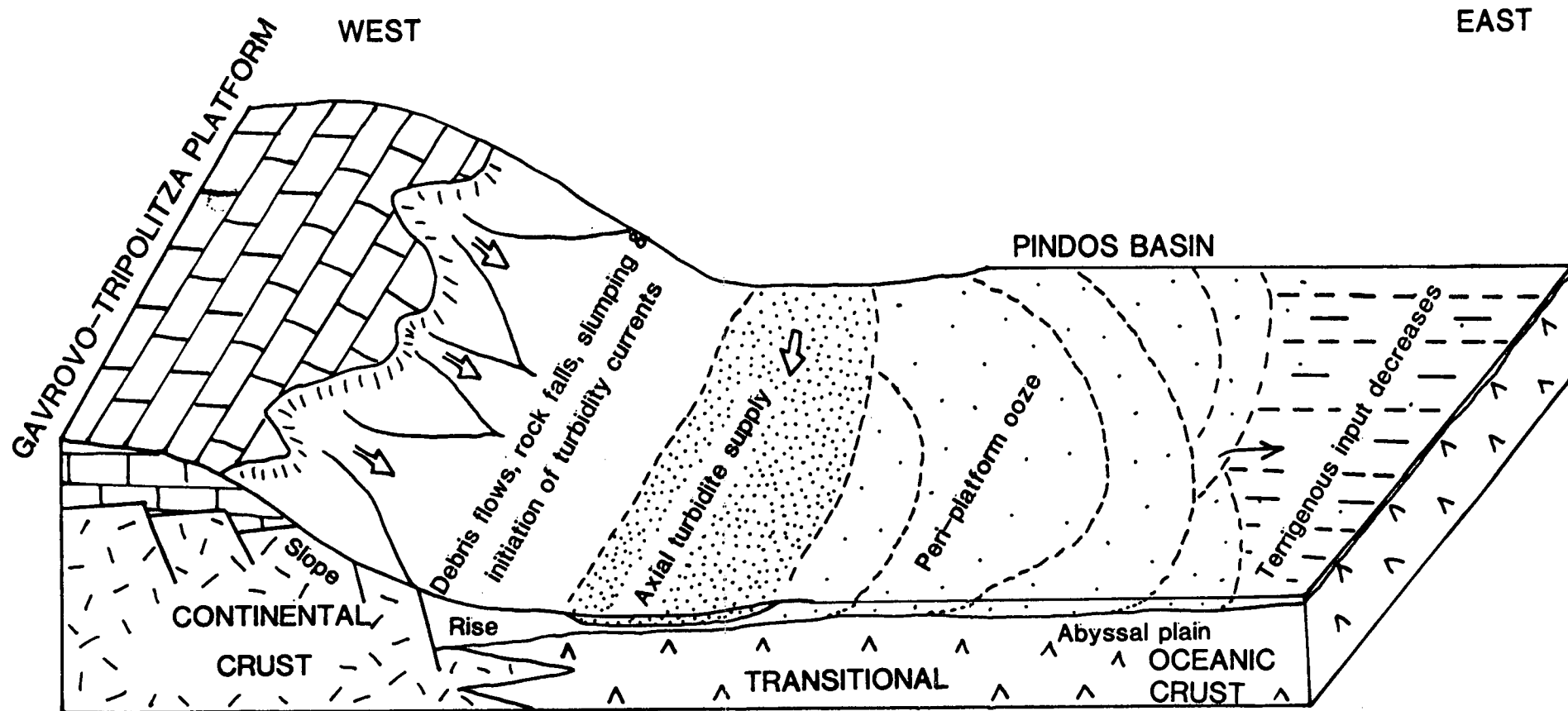


Fig B.1 Schematic diagram indicating the principle physiographic elements of a passive margin.

Mass Transport Process		Mech. Behaviour	Sedimentary Structures	Transport Mechanism & Sediment Support
ROCK FALL		ELASTIC	Grain supported conglomerates, disorganized, open network, variable matrix.	Freefall & rolling of individual blocks or clasts along steep slopes.
SLIDE	GLIDE		Essentially undeformed, continuous bedding although possibly some plastic deformation particularly at toe. Folds, tensional faults, joints, slickensides, rotational blocks if slumped.	Shear failure along discrete planes with little internal deformation or rotation.
	SLUMP			Shear failure accompanied by rotation along discrete surfaces with little internal deformation.
SEDIMENT GRAVITY FLOW	MASS FLOW	DEBRIS FLOW MUD FLOW GRAIN FLOW	PLASTIC	Matrix supported, random fabric, clast size variable. Rip-ups, rafts, inverse grading & flow structures possible.
				Shear distributed through the sediment mass. Strength is principally from cohesion due to clay content. Additional matrix support may come from buoyancy. Cohesionless sediment supported by dispersive pressure. Flow may be inertial (high concentration) or viscous (low concentration) regime. Usually requires steep slopes.
	FLUIDAL FLOW	LIQUIFIED FLOW FLUIDIZED FLOW TURBIDITY CURRENT	VISCIOUS FLUID	Massive, A-axis parallel to flow and imbrication, inverse grading near base.
				Dewatering structures, sandstone dykes, load structures, convolute bedding, homogenized sediment.
				Cohesionless sediment supported by upward displacement of fluid as loosely packed structure collapses, settling into more tightly packed framework.
			Cohesionless sediment supported by the forced upward movement of escaping pore fluid.	
			Bouma series.	Supported by fluid turbulence.

Table B.1 The mass transport processes, sedimentary structures, transport mechanisms and sediment support mechanisms in sediment gravity flows (modified after Nardin et al. 1979).

marine talus (Friedman & Sanders 1978), subaqueous talus (Johns 1978) and peri-platform talus (McIlreath & James 1979).

**Debris flows:-** Massive beds of chaotic, matrix supported conglomerate comprising an admixture of components, are often considered to result from debris flow mechanisms. Debris flows are supported by matrix strength, principally from the cohesion of clays and buoyancy forces. Shear is irregularly distributed through the transporting medium and may locally lead to weakly defined fabrics such as the imbrication of clasts, flow structures and inverse grading.

**Liquified flows:-** Liquified flow deposits are characterised by dewatering structures and convolute bedding. The sediment body is supported by the displacement of intergranular fluid, from areas of relative high pressure to lower pressure, usually upwards. Such movement typically results in fluid escape structures (e.g. sand volcanoes; dish and pillar structures) with ensuing tighter packing of grains. Shearing of semi-lithified sediment leads to convolute bedding, or beds with a preferred vergence as indicated by syn-sedimentary folds.

**Turbidity currents:-** Sediment transported in a turbulent flow, carried in suspension and supported by fluid turbulence. The sedimentary structures of turbidity current deposits are classically considered as the "Bouma sequence" (Bouma 1962) with additional structures such as tool and current sole markings. The basic Bouma sequence consists of five divisions, each corresponding to an individual facies, present alone, or in combination within a turbidite bed. The divisions are:-

Te- Muds.

Td- Parallel-laminated silt and mud (lower-flow regime).

Tc- Ripple cross-laminated fine sandstone.

Tb- Parallel-laminated sandstone (upper-flow regime).

Ta- Graded or massive sandstone.

In addition to the above mass transport processes, pelagic deposition is a significant mechanism in the deposition of Pindos Group sediments. Pelagic deposition, as a process, involves the settling out from suspension of sediments that are descending through the water column in an open-sea setting. A distinction is made between pelagic and hemipelagic sediments although both are laid down by pelagic depositional processes. Berger (1974) defines a pelagic sediment as having less than

25% of the >5 $\mu$ m fraction being made-up of neritically derived material, terrigenous mud and volcanic dust, the remainder being composed of pelagic organisms. A hemi-pelagic sediment, is considered to have greater than 25% of the above constituents in the >5 $\mu$ m fraction. This is in accord with the current definitions as used on DSDP and ODP projects. Alternatively, Pickering *et al.* (1989) state that pelagic sediments comprise organic debris, wind blown dust, volcanic ejecta and rafted material that enters the marine environment beyond the shelf-slope break, or is created by open-ocean organisms. Hemipelagic sediments, on the other hand, contain up to 75% pelagic component, with the remainder being terrigenous mud derived from coastal erosion, or river plumes. Mudstone deposits that were deposited through turbidity current mechanisms are not included. Piper (1978) describes the criteria for distinguishing between fine grained sediments deposited from turbid flows and those from pelagic settling. Hemipelagic sedimentation is likely to be episodic, while pelagic deposits represent the background continuous rain of fine-grained marine sediment.

### Facies

A facies is the totality of properties that characterise a specified rock unit. In this work, lithofacies refers specifically to a rock, rather than simply features of that rock. If two rock units have very similar physical, chemical and/or biological attributes, then they can be considered to be of the same facies. The term facies does not here have any generic connotation, i.e. it does not imply a particular sedimentary mechanism (e.g. debris flow), nor a particular environment (e.g. base of slope). Generally, however, the same facies repeated in a vertical sequence indicates similar processes and/or environments of deposition. When the characteristics of a set of facies are known, deductions, based upon their spatial and temporal relationships, can lead to the recognition of possible depositional environments and sedimentary processes. This leads to the concept of a facies association, defined as a grouping of facies that suggest a certain environmental interpretation based upon the vertical and lateral progression of lithofacies. A simplified outline of the Pindos Group facies and environments of deposition is provided in Table B2 while a fuller consideration of the facies concept is provided by Walker (1979) and Reading (1989).



AGE		STRATIGRAPHY		LITHOLOGY/ENVIRONMENT								
CENOZOIC		PINDOS FLYSCH Fm		Turbiditic sst & pelite. Trench/foreland basin deposit.								
CRETACEOUS	UPPER	KATARRAKTIS PASSAGE Mbr		Interbedded calc-turbidite, sst and pelagic lst.								
		ERYMANTHOS LST Mbr		LAMBIA Fm	<table border="1"> <tr> <th>PROXIMAL</th> <th>DISTAL</th> </tr> <tr> <td>Calc-rudite, calc-arenite &amp; pelagic lst. Base of slope.</td> <td>Fine grained calc-turbidite &amp; pelagic lst. Abyssal.</td> </tr> <tr> <td rowspan="3">Calc-rudite &amp; calc-arenite.</td> <td>Pink pelagic lst.</td> </tr> <tr> <td>Turbiditic sst interbeds.</td> </tr> <tr> <td>Pink marls &amp; pelagic lst.</td> </tr> </table>	PROXIMAL	DISTAL	Calc-rudite, calc-arenite & pelagic lst. Base of slope.	Fine grained calc-turbidite & pelagic lst. Abyssal.	Calc-rudite & calc-arenite.	Pink pelagic lst.	Turbiditic sst interbeds.
	PROXIMAL	DISTAL										
	Calc-rudite, calc-arenite & pelagic lst. Base of slope.	Fine grained calc-turbidite & pelagic lst. Abyssal.										
Calc-rudite & calc-arenite.	Pink pelagic lst.											
	Turbiditic sst interbeds.											
	Pink marls & pelagic lst.											
LOWER	PAOS LST Mbr		Calc-rudite & calc-arenite.	Pink pelagic lst.								
	KLITORIA SST Mbr			Turbiditic sst interbeds.								
JURASSIC	MALM	KAKOTARI LST Mbr	AROANIA CHERT Mbr	LESTEENA Fm	<table border="1"> <tr> <td>Massive reefal calc-rudite.</td> <td>Silicified calc-turbidite &amp; cherts. Sub CCD continental rise.</td> <td>Radiolarian cherts.</td> </tr> <tr> <td>Proximal fan deposit</td> <td colspan="2">Argillaceous mdst and shale.</td> </tr> </table>	Massive reefal calc-rudite.	Silicified calc-turbidite & cherts. Sub CCD continental rise.	Radiolarian cherts.	Proximal fan deposit	Argillaceous mdst and shale.		
	Massive reefal calc-rudite.		Silicified calc-turbidite & cherts. Sub CCD continental rise.		Radiolarian cherts.							
	Proximal fan deposit	Argillaceous mdst and shale.										
	DOGGER	KASTELLI MDST Mbr	LESTEENA Fm	Proximal fan deposit	Argillaceous mdst and shale.							
LIAS	DRIMOS Fm					Calc-turbidite, debris flows and volcaniclastics.	Fine grained calc-turbidite and pelagic lst.					
TRIASSIC	UPPER	DRIMOS Fm		Calc-turbidite, debris flows and volcaniclastics.	Fine grained calc-turbidite and pelagic lst.							
		PRIOLITHOS Fm		Turbiditic sst & pelite.								

**Table B.2** Simplified relationship between the stratigraphy presented here, the principle rock types and the inferred environment of deposition.

### Flysch

A debate persists as to the use of the term flysch. Flysch was first used in the 19<sup>th</sup> century to describe deep marine alternations of sandstone and shale found in the Swiss Alps. Some geologists maintain that the term should be only used to describe the syn-orogenic deposits of the Swiss "Flysch Zone". Others (e.g. Mitchell & Reading 1989), argue for more general usage. This author agrees that the term "flysch" is useful in that it succinctly summarizes a number of characteristics that can be applied to a rock type given that name, encompassing (loosely) facies, environment and depositional process. Specifically, the common perception is of a thick sequence of alternating coarse and fine clastic sediment, primarily deposited by turbidity currents ahead of a tectonically active orogenic belt, in a deep marine setting.

### Palaeocurrent Methodology

Where palaeocurrent indicators were observed, their orientation and polarity were recorded. Most indicators are found in turbiditic sandstones and limestones; they include flutes, groove casts, trough and planar cross lamination, the preferential orientation of organic debris ("tea leaf lineation") and soft sediment fold vergence. The orientation of the long axis of pebble and cobble grade clasts were measured in conglomerates. The palaeocurrents presented are as accurate as the outcrop permits, particular difficulties were met in ascertaining flow directions from trough cross laminae exposed in only two dimensions. Tectonic dips varied widely. Where the bedding dip was less than 30° no adjustment was made. For dips greater than 30°, beds were rotated back to horizontal (Ragan 1985).

## CHAPTER 3: PRIOLITHOS & DRIMOS FORMATIONS

### 3.1 INTRODUCTION

In this chapter the facies, petrology and diagenetic history of the Priolithos and Drimos Formations are presented. In addition, the distribution of the facies and proposed palaeoenvironments are established. The sediments studied are then considered, in a broader context, in terms of the larger scale influences affecting the patterns of sedimentation observed in the NW Peloponnese, particularly with respect to the morphologies of continental margins. Finally, analogies are provided from other Tethyan areas and present-day regions where similar processes were, or are, operative.

The stratigraphically lowermost sediments of the Pindos Group are represented by the Priolithos Formation, of Camian to Norian age. In the study area, the Priolithos Formation is poorly exposed and found only occasionally above major thrust faults, at the base of sedimentary sequences. The formation is often highly folded and faulted, making even local correlations difficult. A terrigenous facies of turbiditic sandstones and siltstone/shale is dominant, but intercalated dark, fine-grained limestones are also present, often with pelagic bivalve debris.

In places, the base of the overlying Drimos Formation is a thrust plane, while in other areas the base is conformably above the Priolithos Formation. The Drimos Formation is widely observed, dominated by reworked carbonate and hemipelagic calcareous sediments, fine grained in distal (easterly) localities, but coarse grained in more westerly (proximal) outcrops. Other lithologies present within the formation include nodular limestone, bedded and nodular chert, shale and, in proximal locations, calcarenite with a significant volcanoclastic component. Within the Pindos Group this formation displays a great degree of variability, both in thickness and composition. Secondary dolomite is found in certain horizons, particularly in calciturbidites of peloidal and skeletal material. Various models for deep-sea dolomitization are presented, along with a preferred mechanism of dolomitization. The distribution of the various facies in the Drimos Formation allows comparisons to be made with present day sediment distribution patterns adjacent to carbonate platforms.

## 3.2 PRIOLITHOS FORMATION

### 3.2.1 Lithological Description

#### 3.2.1.1 Facies

There are three major facies within the Priolithos Formation, litharenite, shale/siltstone and dark grey (sometimes bioclastic) siliceous micrite.

#### Litharenite

Litharenite (Plate 3.2) is the dominant facies of the Priolithos Formation. It is well-bedded with variable bed thicknesses of between 3 and 40cm. Grains are sub-rounded to sub-angular, moderately sorted and dominantly fine-grained, although coarser grade material is present, especially in the thicker beds. The weathered rock often appears blue-grey, or green, while freshly exposed surfaces are pale brown. Bed morphology appears to be tabular, with planar and sometimes erosive, bedding contacts. No channel margins are observed. Slight grading can be present, but more usually the beds are massive. Few palaeocurrents were recorded and these were restricted to measurements from rare sole structures and low angle trough cross-lamination, observed on single faces only, and recognised by the slight alternations of coarse and fine grains. Planar, bedding-parallel laminations, mica and carbonaceous fragments are common. A Priolithos Formation outcrop north of Lambia (Figure 1.1), yielded a very poorly preserved fossil of the Order Ammonoidea (Plate 3.1). It has been tentatively identified as either a *Meekoceratinid sp.* (Scythian) or a *Noritid sp.* (Anisian) by Dr H.G. Owen (pers. comm. 1989). Given the poor condition of the specimen and the known age of the formation (i.e. Carnian/Norian), from pelagic bivalve and Conodont species (Flament 1973), the identification is suspect. Alternatively the sediment containing the specimen has been reworked.

#### Siltstone/shale

Intercalated within the sandstones are blue to dark grey organic and mica-rich siltstone and shale beds up to 30cm thick. The pelites have a friable texture, but are otherwise structureless. The siltstones are also structureless and homogenous, although bedding parallel laminated siltstones are occasionally observed. The siltstones usually form individually distinct beds, rather than the graded tops of thicker, coarser-grained beds; however, they are sometimes capped by a thin pelite interval. Where the upper bedding surfaces are visible they are often rich in muscovite flakes.



## Limestone

The third facies found within the Priolithos Formation is a well-cemented dark, almost black, partially silicified limestone. The limestone generally occurs as isolated beds, of between 10 and 20cm thickness (and rarely up to 42cm), within the sandstone and shale facies. Most of the limestones are featureless in hand specimen, although some contain *Halobia* sp. (Section 3.3.1.6). The presence of the dark limestone lithology within the sandstones is the clearest indicator which, in the field, can help to distinguish the formation from otherwise similar sandstones of Tertiary age. Such dark and compact limestone beds are unique in the Pindos Group. The only other lithologically similar samples are found within intensely sheared mudstones along thrust planes between Drimos and Livardzi (Figure 1.1).

## Carbonate Debris Flow Facies

An additional facies of a carbonate debris flow deposit is found immediately below the Drimos Formation at Alephorio (Figure 1.1), above the Pindos frontal thrust. It consists of resedimented irregularly shaped concretions. These are composed of micrite and some contain benthic foraminifera (of platform derivation). They are of a similar composition and shape as overlying nodules of the Drimos Formation described in Section 3.3.1.2.

### 3.2.1.2 Petrography

The dominantly fine-grained litharenite samples are petrographically variable. For example, although most display closely-packed grain supported fabrics, matrix supported fabrics (i.e. wackestone) are also present. A wide variation in the proportion of carbonate components is also noted, with more carbonate allochems generally present in specimens from westerly outcrops. Some samples show extensive iron oxide staining along grain rims, except where there are grain-to-grain tangential contacts. Others have stringers of insoluble residues, while the majority of samples have little iron oxide at all. 300 points were counted on each of three thin sections of fine-medium grained sandstone. The following results (%) were obtained:-

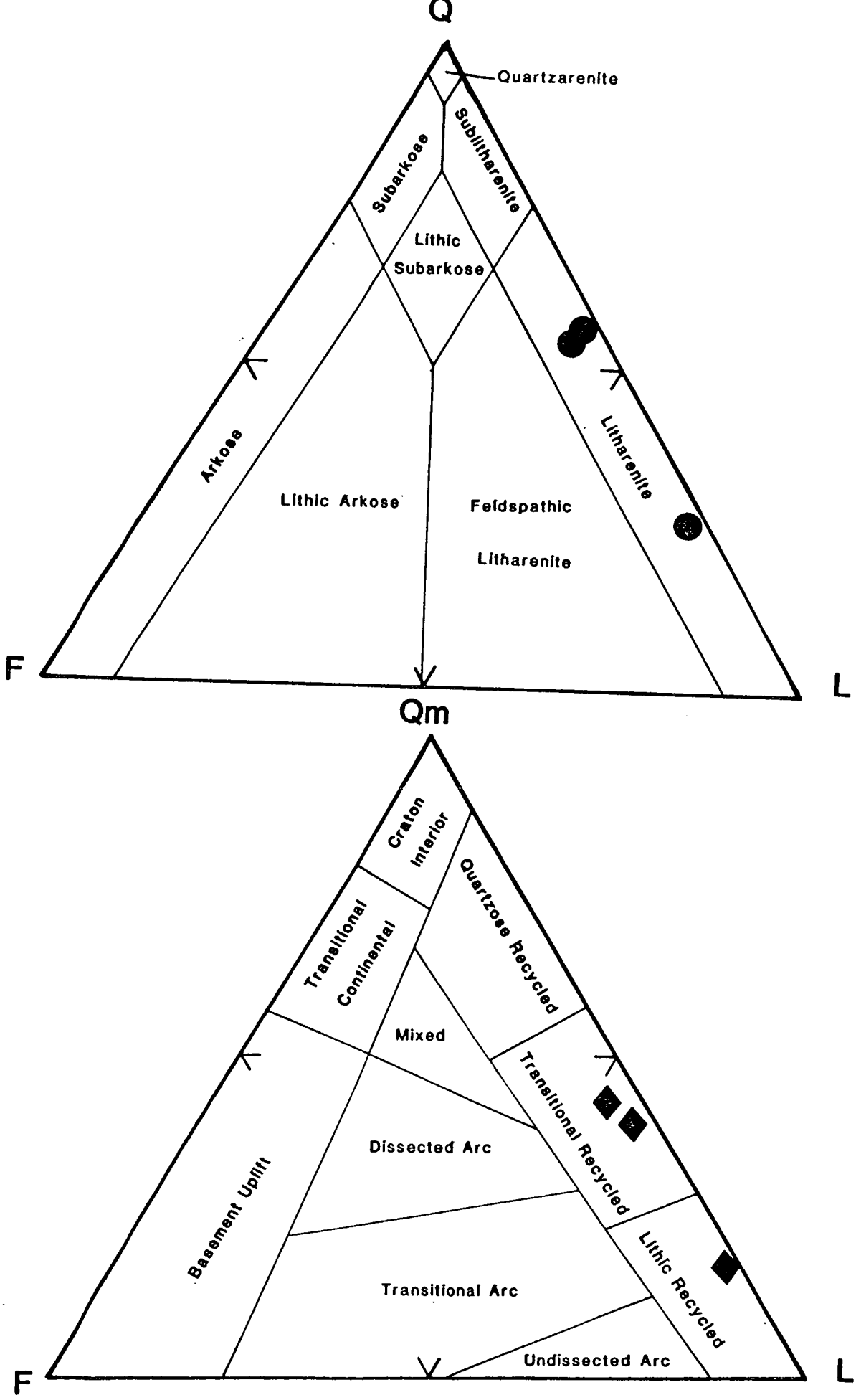


Fig. 3.1 Arenites of the Priolithos Formation plotted on the QFL diagram of McBride (1963) and the QmFL diagram of Dickinson & Suczek (1979).

	PD/88/37	PD/90/744	PD/90/749
Monocrystalline quartz (Qm)	40	18	43
Polycrystalline quartz (Qp)	16	9	11
Feldspar (F)	3	2	5
Metamorphic lithic fragments (Lm)	6	1	2
Volcanic lithic fragments (Lv)	2	1	1
Sedimentary lithic fragments (Ls)	33	69	38

Total quartz (Q) = (Qm) + (Qp)

Total feldspar (F) = Plagioclase and alkaline feldspar

Total lithic fragments (L) = (Lm) + (Lv) + (Ls)

The results of the framework point counting were plotted on a standard Q:F:L diagram (McBride 1963) and a Qm:F:L diagram to reflect provenance (Dickinson & Suczek 1979). The results (Figure 3.1) indicate that the sandstones plot in the litharenite (McBride 1963, Folk 1966) and recycled orogen fields (Dickinson *et al.* 1983), respectively. The characteristics of the three main constituents can be summarized as follows:-

### Quartz

The quartz present includes both strained monocrystalline quartz with undulose extinction, often with fluid inclusions, and polycrystalline quartz with internally sutured contacts. Some quartz clasts are intermediate, in that they show incipient polycrystalline zonation from a strained monocrystalline grain. Cathodoluminescence produces mainly red/brown luminescence from the quartz, typical of a metamorphic origin (Miller 1988), with subsidiary blue fluorescing clasts, indicative of a plutonic origin.

### Feldspar

Feldspar is a very minor constituent of the Priolithos Formation sandstone. Alkali feldspar and smaller quantities of plagioclase are present.

### Lithic fragments

Lithic fragments seen in thin section comprise clasts of metamorphic, sedimentary and, rarely, volcanic origin. The metamorphic lithic fragments identified include mica, quartz-mica aggregates and other schist fragments. Sedimentary lithic fragments are dominantly skeletal particles of carbonate consisting primarily of echinoderm, molluscan and foraminiferal fragments; however, highly variable proportions of oolite and peloids are seen. Sample 749 has carbonate fragments

consisting mostly of non-orientated *Halobia sp.* shell debris dispersed in the rock. Also present are rounded clasts of clays and reworked siltstone. The volcanic fragments identified are clasts of highly altered chlorite and trachybasalt.

### 3.2.1.3 Diagenesis

A succession of diagenetic effects are seen. The effects of litharenite compaction are recognised in the close packing of grains, sometimes with sutured, concavo-convex (not stylolitized), grain to grain contacts. Elongate flakes of muscovite are observed to be bent and fractured between quartz grains.

Clasts stained with iron oxides were coated during early diagenesis, before carbonate rim cementation, but after grain to grain juxtapositioning through compaction. It is envisaged that the iron oxides were introduced through iron rich fluids in the porewaters, possibly leached from clay minerals in pelite beds during compaction.

Little fine grained, original clay matrix is preserved; rather, original voids and matrix material have largely been infilled and/or altered with a succession of carbonate cements. Many of the quartz clasts have authigenic silica syntaxial overgrowths which are only visible by the use of cathodoluminescence examination. They also display varying amounts of an authigenic overgrowth of amorphous calcite. Skeletal carbonate grains display evidence of the replacement of aragonite and original calcite by calcite spar. A fine to relatively coarse mosaic of ferroan calcite spar cement is commonly observed to have neomorphosed original matrix material and infilled pore spaces.

## **3.2.2 Distribution and Depositional Environment**

### 3.2.2.1 Distribution

The occurrence of the Triassic Priolithos Formation is generally fragmentary despite several sedimentary sections being observed in the study area, from localities close to the Pindos front to as far east as Kato Klitoria (Figure 1.1). Four Priolithos Formation sections were logged (Figure 3.2, Appendix 1, Logs A1-A4) although the lack of intact sections makes meaningful spatial correlations impossible and it is not known if facies variability is a palaeoenvironmental effect, or a consequence of stratigraphic position. The distribution of the Priolithos Formation facies did not yield any interpretable pattern in the NW Peloponnese, except that the proportion of



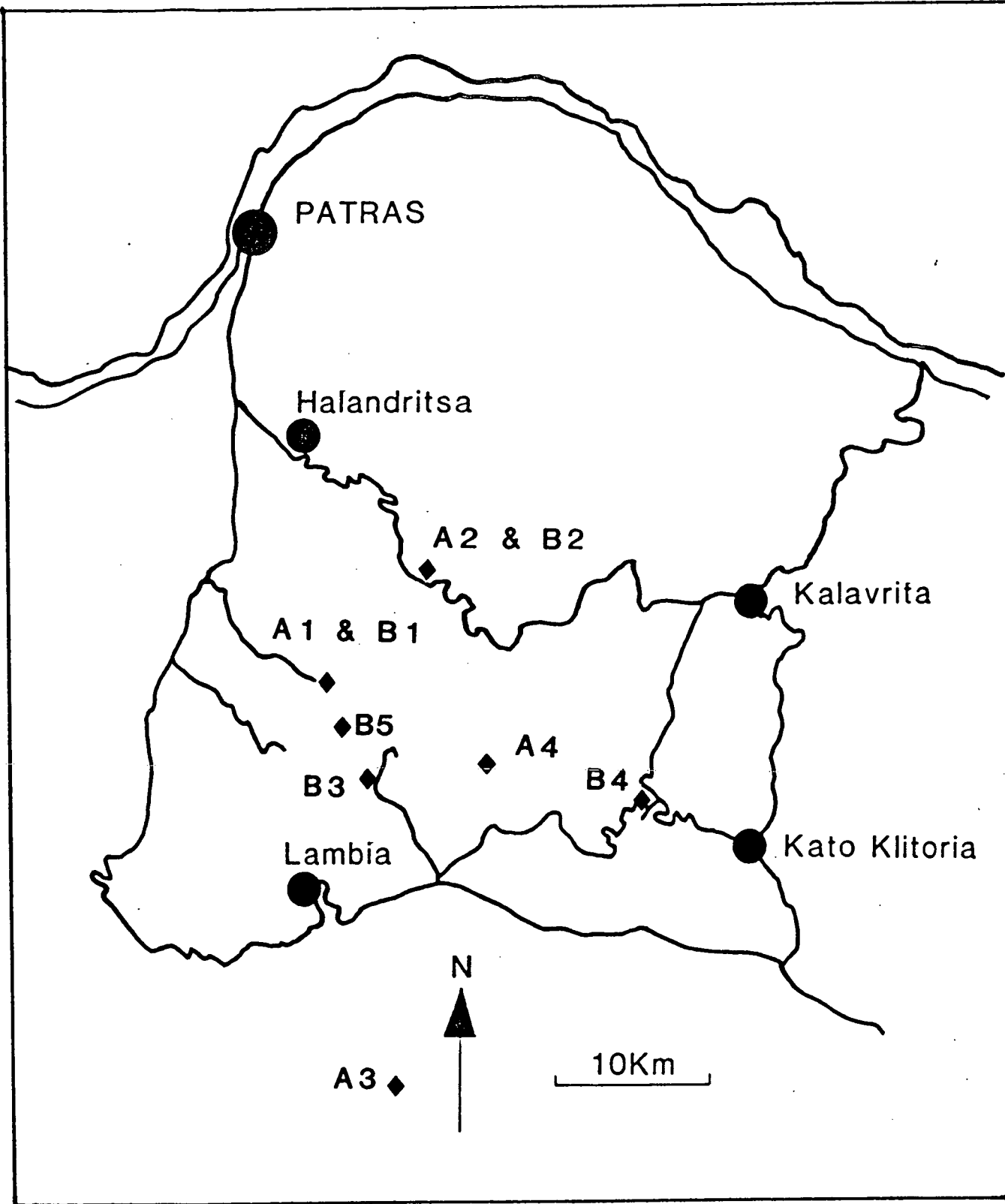


**Fig. 3.2** Map indicating the locations of the sedimentary log sites of the Priolithos and Drimos Formations.

platform derived components appears to be greater in the west <sup>eg. A1</sup> (Alephorio) than in more easterly localities (e.g. Klitoria).

### 3.2.2.2 Depositional Environment

The sandstones of the Priolithos Formation are litharenites (Mc Bride 1963, Folk 1966), with terrigenous clastic components indicative of composite derivation from a dominantly metamorphic provenance, but also including rare clasts from volcanic centres. Additionally, carbonate clasts reflect the admixture of platform and slope material.

The partial Bouma sequences (Ta & Tb, Ta & Tc and Td & Te intervals), erosive bases and the presence of groove marks in sandstone beds, indicate that the sandstones and siltstones were deposited from turbidity flows. Structureless and graded beds (Bouma interval Ta) represent rapid deposition followed by burial, while planar laminae and trough cross-lamination (Bouma intervals Tb & Tc) indicate the tractional transport of bed load in a waning current, from upper-flow to lower-flow regimes. Shales and siltstones are probably the finer-grained equivalents of the sandstones, representing the less energetic tail of a turbid flow or the further travelled flows of more dilute turbidity currents. The turbidity currents were most probably initiated on the continental slope, allowing variable quantities of platform and upper slope detritus to be incorporated. Sparse palaeocurrent data suggest supply from the north and north-west.

Relatively quiescent periods allowed the settling of hemipelagic carbonate ooze, with a low diversity faunal assemblage of radiolarians evenly distributed within these hemipelagic beds. The siliceous micro-organisms probably provided the SiO<sub>2</sub> necessary for the partial silicification of limestone beds (c.f. Chapter 4). Limestones with laminae of densely packed pelagic bivalve debris are similar in fabric to those of the overlying Drimos Formation (Section 3.3.1.6). These have been interpreted as shelf and slope derived reworked sediment, probably transported by low density turbidity currents originating on the continental slope.

Given the highly variable proportions of pelite to arenite and the higher concentration of platform derived detritus in proximal locations, the Priolithos Formation may largely represent small, base-of-slope, coalescing, fans of mainly terrigenous sediment transported over the developing Gavrovo-Tripolitza platform. Additional carbonate allochems become incorporated there prior to off-slope

transport by turbidity currents. Such a scenario would be in agreement with the model proposed by Fleury (1980) who uses data from a much larger area of continental Greece to suggest that terrigenous sediments were derived from the west.

The sediment distribution inferred above implies that the Late Triassic facies patterns of the Priolithos Formation were controlled by distance from the Apulian margin. However, this interpretation cannot be demonstrated by consideration of facies in the NW Peloponnese alone. The coarse-grained terrigenous facies of the Late Triassic in the Tethys, e.g. Cyprus, Antalya, Oman, are commonly regarded as predominantly rift related deposits reflecting the opening of the Neotethys (Robertson *et al.* 1991).

### 3.2.3 Discussion

As no lithologies are exposed beneath the Priolithos Formation, due to underlying major thrust detachments, the composition of the immediate basement is unknown. In the southern Peloponnese, at Kokkino, *Halobia* sp.-bearing limestones of the Drimos Formation conformably overlie volcanoclastic sediment, itself deposited upon pillow lavas. Thus, the Priolithos Formation is locally missing. This may be due to volcanic activity prior to limestone deposition, but after dispersal of the terrigenous sediment, or as preferred, sites such as Kokkino represent locally elevated volcanic areas around which the sandstones were deposited. Evidence from the tectono-sedimentary melange in the NW Peloponnese (Chapter 8) suggests that the Pindos basal thrust may have detached along a volcanic sediment-siliciclastic interface. The question which arises is whether the Priolithos Formation is (a) sediment onlapping rift shoulders of attenuated continental crust, or, (b) does the siliciclastic sediment represent the first phase of sediment deposited onto juvenile transitional or oceanic crust? Evidence is summarized in Section 9.2.3, detailing the arguments for an oceanic Pindos Basin, where it is considered that the gross palaeogeography of the Pindos Basin, between the Apulian and Pelagonian microcontinents, was probably established during the Middle Triassic. It is proposed that extensional tectonics during the rift phase led to the establishment of a faulted margin with localised fault controlled volcanic activity (Section 8.4.6). Thus, the main source area for the Priolithos Formation is considered as most probably associated with the erosion of uplifted rift shoulders of metamorphic basement located inboard, along the Apulian margin. It is possible that the deposits were derived from the Pelagonian micro-continent, however, the petrological similarity of

clasts within the Priolithos Formation litharenite and clasts comprising the Klitoria Sandstone Formation, probably derived from westerly source areas, (Section 5.2.2.2), and the distribution of Priolithos Formation facies seen in continental Greece (Fleury 1980), suggest that the terrigenous source of the sandstones was located within the Apulian microcontinent. In contrast, Thiebault (1982) has suggested a derivation from as far away as the North African province of Gondwana.

Fleury (1980) reports Triassic sandstones, equivalent to the Priolithos Formation, from north of the Gulf of Corinth near Megdhovas, containing granitic clasts (including boulder grade blocks). Recently, Pe-Piper & Koukouvelas (1990) report granitic and porphyritic rhyolite clasts within Pliocene conglomerate deposits on the outskirts of Patras. They are unsure of the origin but suggest that they may be derived from igneous rocks of the tectono-sedimentary melange at the base of the Pindos thrust sheets (Section 8.4). No granitic samples were discovered in the tectono-sedimentary melange by this author. It is probable that the Patras granitic clasts may be reworked clasts from the most proximal deposits of the Priolithos Formation, no longer preserved in the Peloponnese, and therefore analogous to those found in the Triassic sandstones at Megdhovas. Furthermore, a rhyolitic lava olistolith was discovered within the Drimos Formation volcanoclastic sandstone and is discussed in Section 3.3.1.3.

### 3.2.4 Ancient Comparisons

The Late Triassic Hatip Sandstones of the Alakir Cay Group in the Antalya Complex of Turkey (Robertson & Woodcock 1981) are very closely analogous to the sediments of the Priolithos Formation. The Hatip Sandstone outcrops are fragmentary and are interpreted as turbidity current deposits, derived from a low-grade metamorphic terrane with minor constituents from igneous intrusions. Other lithologically similar Triassic rocks are found in Oman. A Camian/Norian age has been established for the fine grained quartzose sandstones of Unit II of the Zulla Formation in the Hamrat Duru Group (Cooper 1986). Thin shales, siltstones and sandstones are considered to have been derived from a pre-Permian basement and a Permo-Triassic platform. The Priolithos Formation is also comparable with the Lower Jurassic turbiditic "quartz-arenites" and peloidal calcarenites of the Guweyza Formation in the Hamrat Duru Group (Cooper 1986). In the Aghios Photios Group, outcropping in SW Cyprus, Swarbrick & Robertson (1980) describe Late Triassic

sandstones of the Vlambouros Formation. These consist of quartzose sandstones, siltstone and mudstone; also subordinate calcareous rocks.

### **3.2.5 Modern Comparisons**

The Priolithos Formation is considered as a rift-related sedimentary sequence deposited on juvenile oceanic/transitional crust. Therefore, present day regions under-going extensional tectonism, leading to the incipient development of passive margins, may be expected to provide analogies to the rift related environment of the Pindos basin. Such modern-day regions are best exemplified by the Gulf of Aden and Red Sea basins (Ball 1979).

## **3.3 DRIMOS FORMATION**

### **3.3.1 Lithological Description**

The Drimos Formation displays a wide variety of facies. In the simplest terms, the type of deposit can be related to distance from the Apulian shelf. Thus, "proximal" sediments are characterized by abundant, more shallow water type facies and/or coarser grade clasts. More "distal" deposits, typically found in the greater part of the study area, are deeper water facies, i.e. dominantly pelagic finer grade sediments. Despite the diversity of the formation, no individual facies is considered as a distinctly mappable lithostratigraphic unit, due to facies intercalation, or a locally restricted distribution. Sedimentary sections have been logged (B1 to B5, Appendix 1) and the outcrop localities are shown on Figure 3.2. Eight distinct facies types have been observed and their characteristics are listed below.

#### **3.3.1.1 Facies 1: Rudite**

The rudaceous facies are principally confined to the most westerly locations, where they predominate. They are also found as thinner beds intercalated within other facies as far east as Livardzi. Outcrops located further outboard (e.g. Aroania and Drimos), do not contain rudite grade sediment. Because of the wide geographic spread, inferred to be controlled by proximity to the continental margin (Section 3.3.3.2), there are no typical bedding thicknesses, but rather a range from a few centimetres to greater than 3m.

Along the greater part of the Pindos front, as between Kakotari and Kalendzi (Figure 1.1), 1 to 3m thick beds of matrix and clast-supported material was observed as the typical Drimos Formation facies. Clasts are sub-rounded, cobble grade, up to 12 x 8cm, and are of platform and slope origin with many beds containing neritic forams, megalodonts (Plate 3.6) and clasts of reworked micrite. At Alepohorio (Figure 1.1), a rudite is found immediately above the Priolithos Formation, where it occurs as isolated gravel grade, and occasionally pebble grade, matrix-supported conglomerate, with a maximum bed thickness of 52cm. Isolated beds also occur further up-section (Log B1). Further east, between Agrambela and Kryovrissi, a 70m thick Drimos Formation sequence was measured (Log B5). This contains, near the top, a 7m thick, matrix-supported conglomerate with sub-angular carbonate clasts of pebble grade, within a coarse arenite grade matrix. The unit is poorly graded and appears to represent several depositional events. It is erosive into the underlying finer grade calciturbidite. Just 130m to the north of the logged section, is more than 50m thickness of the same rudite facies that erosively cut a channel through the greater part of the underlying Drimos Formation.

A second rudite sub-facies is also recognised from proximal localities around Erymanthos. It is a clast-supported facies composed of pink micrite, unlike the grey micrite of the above rudite (Plate 3.5). The clasts are rounded and generally of pebble grade. Contacts are often stylolitic. Discrete clasts of slightly varying composition are clearly observed and a conglomerate fabric is obvious. The rock is not therefore a stylobreccia (pseudo-breccia).

### 3.3.1.2 Facies 2: Nodular Limestone

There are two types of nodular limestone observed. These can be compared with two distinct types of nodular limestone described by Tucker (1974), Cephalopodenkalk facies and Ammonitico Rosso. The characteristics of the first Pindos nodular limestone facies are comparable with the Cephalopodenkalk-type facies. The rock contains irregular concretions with a range of sizes from 0.5 to 5cm long. The length:height ratio is approximately 3:2. The concretions are hard, well lithified, buff to grey micrite that sometimes contain a partially preserved neritic fauna. The calcareous nodules are sometimes isolated between irregular, anastomosing marl seams, but more generally a partially continuous bedding is preserved. The facies is well exposed at Alepohorio where discrete, resedimented irregularly shaped concretions are present in debris flow horizons of the Priolithos Formation (below

the development of the nodular facies locally, Section 3.2.1.1) and these provide evidence for the early lithification of limestone nodules.

At two localities close to the Pindos front, the second nodular limestone facies (Ammonitico Rosso), was observed. Strictly it does not belong to the Drimos Formation, being Ladinian-Carnian in age (Tsoflias 1969a, b) and it is not in depositional contact with other Pindos Group sediments. The facies is, however, included here as it forms an integral part of the study area. The outcrops are found at Glafkos in the Peloponnese, first described by Tsoflias, and at Megdhovas in continental Greece, first described by Fleury (1980). In addition, blocks were found within the tectono-sedimentary melange at Alepohorio. The facies is a micritic pink limestone with a lower matrix content than the above, Cephalopodenkalk limestone. Concretions are observed in contact with adjacent nodules, sometimes giving a stylobreccia texture. No ammonites were found, although Tsoflias (1969a, b) reported ammonites of the *Trachyceras aon* bio-zone (Ladinian-Lower Carnian) at Glafkos. Thus, deposition of this facies was possibly in part synchronous with the Priolithos Formation sedimentation.

In association with Ammonitico Rosso which was found at the base of a thrust sheet at Alepohorio, a single block of a distinctive lithology, not found elsewhere, was discovered. It is included here because of its potential palaeogeographic importance and possible relationship with the pink nodular limestone (Section 3.3.2.2). The rock is a red, very argillaceous chert with angular, elongate, variously oriented clasts of pistachio green coloured schist. In thin section (Plate 3.5) the schist has been almost totally replaced by carbonate except for thin mica stringers. The mudstone contains radiolaria, which on extraction were seen to be totally replaced by quartz, and therefore undatable.

### 3.3.1.3 Facies 3: Volcaniclastic Sandstone

#### Field Relations

The volcaniclastic sandstone is oligomict, comprising mostly carbonate grains and up to 20% by volume, of volcanic debris. The outcrop is found at the head of the Alepohorio valley (Figure 1.1). It is an overturned, fining-up sequence, which near the base contains a massive block of lava, measuring 20x10x20m, with well formed columnar cooling joints (Plate 3.4). The vertical(?) cooling joints are not congruent with the vertical plane of the surrounding sandstones. The lava is melanocratic and is mostly non-vesicular, although there are areas with concentrations of oblate vesicles.

The margins of the block are sharp, but without obvious tectonic features, e.g. slickensides or fault breccia. Thus, it appears that the block is an olistolith, rather than being faulted into position. It is certain that the lava block was in place prior to the deposition of the surrounding sediment, as beds of coarse to gravel grade volcanoclastic sandstone, with a few cobble-sized lava clasts, have mantled the lava block. The volcanoclastic sandstone sequence has been overthrust by right-way-up upper Drimos Formation pink rudite, Lesteena Formation cherts and Cretaceous limestones (Plate 6.1).

From the base to the top of the volcanoclastic sandstone overturned sequence there is a definite fining-up trend. Bed thickness ranges in size from 2 to 40cm and appears to be positively correlated to clast size, which ranges from silt to gravel grade. Some beds appear graded, but there are no sole structures. In hand specimen the presence of lava clasts is clear, as is the presence of clastic carbonate. There are also sparse carbonaceous fragments and mica present. A pelagic bivalve (*Halobia sp.*) was found in a few lowermost beds and the section was continued unbroken into an 8 to 20m thick, channelised calcirudite, itself conformably below the Lesteena Chert Member (Log E3). Thus, the volcanoclastic sediment is considered as contemporaneous with the Drimos Formation limestones. An alternative explanation would require the deep erosion of 80-100m of Drimos Formation limestone into an underlying Priolithos Formation. This is not impossible, but is considered unlikely, given the thickness of sediment necessarily missing through such erosion.

### Petrology

Thin section observation and the results of XRF (samples PD/90/764 & 765) indicate that the volcanic rocks of the lava flow block are rhyolite. An igneous hand specimen (PD/90/761) from low in the volcanoclastic flysch stratigraphy is also rhyolite. In thin section, 90% of the rock consists of a non-aligned fine groundmass of feldspar and iron oxide, admixed with microquartz of a similar grain size. Isolated porphyroclasts of simply twinned alkali feldspar (sanidine) are found in the groundmass. Volcanic clasts are abundant in the sandstone, but have generally undergone varying degrees of chloritisation. Most of the grains are coarse arenite grade and composed of rhyolite.



PD/90/762 & 763 were seen to comprise the following constituents (in %):

	<u>PD/90/762</u>	<u>PD/90/763</u>
Peloidal limestone	40	35
Free ooids	5	5
Micrite/peloids	10	20
Skeletal carbonate	15	10
Monocrystalline quartz	10	10
Polycrystalline quartz	5	5
Lava	10	15
Glauconite & mica	5	5

One of the samples is a clast supported, gravel grade conglomerate, with moderate to good sorting and sub-angular to rounded grains. Some ooids are seen to have nucleated around quartz grains (Plate 3.7) and echinoid grains often have syntaxial overgrowths (Plate 3.7). Around many grains a remnant (aragonite ?) accicular fringing cement is seen. The grains are now cemented by a calcite spar, which comprises approximately 30% of the thin section surface area.

Another sample is broadly similar in composition. There is more matrix and the poorly sorted, sub-rounded grains exhibit a wackestone fabric. All grains have an early iron oxide rim cement. This pre-dates compaction as some grains are indented into neighbouring clasts with concavo-convex boundaries and these junctures are also iron-stained. The main cement is a coarse calcite spar mosaic.

#### 3.3.1.4 Facies 4: Calcarenite/Calcsiltite

##### Field Relations

This facies comprises sediment with a range of clast sizes, composition, sorting and bedding thicknesses. The facies is recognised by a clastic fabric and because of the frequent incorporation of reworked and fresh sediment, graded bedding and the presence of parallel and trough-cross lamination. No unequivocal sole marks were ever recognised. In the field there is a gradation from the rudite facies into calcarenite facies. They both contain a similar admixture of carbonate components, the main constituents being micrite, peloids, ooids, neritic skeletal fragments (thick walled bivalves, echinoderms & algae), pelagic biota (*Halobia* shells and radiolarians) and additionally, occasional fine, monocrystalline, quartz grains. It is

perhaps significant that although oolites were found at all stratigraphic levels, oolite bearing beds were mostly concentrated in the upper 30m of logged sections.

The proximal calcarenite sediment often contains light coloured, replacement chert nodules. These are generally isolated, but occur at discrete intervals within a bed. A particularly distinctive type of nodule is found only in the proximal Drimos Formation calcarenite, being spherical, from 5 to 15cm in diameter and composed of white, coarse, chalcedonic silica (Plate 3.3). Chert nodules in the more distal calcisiltites are similar to those found in the micrites (Section 3.3.1.5), i.e. they are generally elongate, red-brown or grey and finely crystalline.

#### Petrology

In thin section the more proximal calcarenites are often dolomitised to varying degrees. The dolomite occurs as discrete euhedral rhombs, scattered in the host rock and of an undisputed secondary origin, as there are no signs indicative of transportation observed (e.g. crystal abrasion or fracturing). An important observation is that where calcarenite and micrite beds are in depositional contact, the dolomite appears to have preferentially nucleated in the calcarenite horizons (Plate 3.8). Certain beds have undergone almost complete dolomitization with interpenetrating crystallization and it is not possible to determine the original texture of the rock.

Individual peloids in the arenite are uniform, dark micrite pellets while oolites often show a distinct concentric zonation. Some, however, have a radial pattern. This is probably due to the replacement, by neomorphic calcite, of original radial aragonite crystallites. The texture of the calciturbidite is packstone to grainstone. The cement is always a coarse calcite spar, occasionally poikilitically enclosing several grains.

#### 3.3.1.5 Facies 5: Micrites

##### Field Relations

The micrite facies is usually thin-bedded, from 2 to 10cm thick, although higher in the section, above the chert interval, beds thicken up to 10 to 20cm. The colour of the micrite varies from olive green to grey to pink but is generally the same colour as surrounding mudstone beds. While the rock is often a pure, homogenous, micrite, biomicrite is also present with radiolarian and *Halobia* sp. allochems (see 3.3.1.6). Possible bioturbation is suggested by broad, burrow-like inhomogeneities in the cryptocrystalline calcite. Well developed pyrite cubes are seen in several beds.

Irregular, bedding parallel chert nodules are sometimes present, although not as frequently as in the calcarenite/calcsiltite.

### Petrology

In thin section, remnant "ghosts" of radiolarians and thin bivalve shells are seen to be replaced by a slightly coarser calcite than in the background micrite. Discrete euhedral dolomite rhombs are seen in some of the micrite thin sections, although in much lesser concentrations than in the calcarenite (Plate 3.8).

#### 3.3.1.6 Facies Group 6: Halobia Limestone

The pelagic bivalve *Halobia* is a thin-shelled pelycepod of the Order *Pterioida* (Family *Posidoniidae*). Several species are recognised, although in thin section it is difficult to assign specific species status. The bivalve is a widespread component of deep water Triassic Tethyan facies. The *Halobia*-bearing limestone is a special facies group comprising pelagic bivalve-bearing limestones of both the calcarenite/calcsiltite and micrite facies. A great many beds in the lower section, generally below the chert interval, contain extensive concentrations of thin shelled bivalve debris. Consequently bedding occurs on a variety of scales with thin (0.5cm) to thick (10cm plus) *Halobia*-rich horizons.

In micritic *Halobia* limestone, bedding is thin and shell fragments are unorientated and often mixed with radiolarians (Plate 3.8). The shells are replaced by micrite or calcite spar to varying degrees. In the more obvious biomicrite, *Halobia* shells sometimes display a geopetal structure, with the "way-up" defined by a fabric selective shelter porosity, infilled by coarse calcite spar (Plate 3.4). Where there has been extensive silicification of a *Halobia*-bearing micrite, cryptocrystalline quartz selectively replaces the micrite, leaving diffuse calcitized *Halobia* lumachelles (Plate 3.8).

In coarser grained beds, the shells are often tightly packed together and orientated parallel to bedding (Plate 3.4). They form a variable proportion of a bed, from a few percent to c.a. 80%. The shells are sometimes a prismatic calcite, or otherwise totally replaced by calcite spar.

#### Halobia Shell Morphology

Two types of thin shelled bivalve, within the Drimos Formation, were observed on bedding planes. The first is a large, flat, strongly radially ribbed shell, up to 5cm in

length (Plate 3.6). Poor preservation meant that the umbonal region was not observed. The second shell type is much smaller, 0.5 to 1cm in length and arcuate in shape. Ribbing is well developed (radial) and the umbonal region is strongly rounded (Plate 3.6).

In thin section, the shells are generally disarticulated, although a few intact valves were observed in the micrite. The majority of fragments are less than 0.5cm in length. Individual filaments can be straight (probably corresponding to the first shell type above) or arcuate (corresponding to the second type). Small undulations are observed on well preserved shells, and probably represent ribbing.

#### 3.3.1.7 Facies 7: Mudstone

Very thin, millimetre-scale, intercalations of mudstone are present throughout the Formation. In addition, horizons of thicker, fissile mudstone are present, especially towards the top of the formation. The colour varies from olive green to brown, but especially pink in proximity to the intraformational chert interval and near to the top of the sequence. The chief minerals present are illite and quartz. The proportion of quartz probably increases towards the chert horizon (facies 8) although specific analyses were not made.

#### 3.3.1.8 Facies 8: Bedded Chert

Isolated beds of radiolarian cherts are found throughout the formation. Additionally, there is a particular horizon found at the more outboard localities, approximately a third of the way up from the base of the formation. This is best exemplified at Drimos (Log B3, Appendix 1) where a chert package is 6m thick, above an intercalated series of cherts and limestones. The bedding is 2 to 5cm thick and the chert is dark red to brown in colour, with thin siliceous mudstone intercalations. Near the village of Platanitza (Figure 1.1), 18m of orange to pink, argillaceous, chertified limestone was observed. The section occurs above thin bedded micrite and calciturbidite, and below a thick interval of matrix-supported rudite. It is not considered a stratigraphic equivalent to the extensively observed chert interval above. This distinctive lithology was not seen elsewhere, and no radiolarian species were extractable.

### 3.3.2 Distribution and Depositional Environment

#### 3.3.2.1 Distribution

##### Facies 1: Rudite

The lithology is restricted to the west of the study area, where there is the greatest concentration of rudite beds, thicker individual beds and the largest clast sizes. Thick, laterally extensive beds of calcirudite are notable near Kakotari and are also well developed along the Pindos front as far as Kalendzi. The sedimentary logs show that stratigraphically, coarser beds are more common near the base and top of the sequence in slightly more distal (eastern) areas.

##### Facies 2: Nodular Limestone

The nodular limestone facies were only well exposed at Glafkos (Ammonitico Rosso-type) and Alepohorio (Cephalopodenkalc-type). In addition nodular limestones are found in the tectono-sedimentary melange and north of the Gulf of Corinth, at Megdovas.

##### Facies 3: Volcaniclastic Sandstone

The volcaniclastic facies was observed at one location only, at the head of the Alepohorio valley, deeply incised into Erymanthos Mountain. The area is structurally complicated (Section 6.2) and the facies is exposed due to the dissection of a frontal imbricate. Thus the facies could be present in other areas, but not exposed. A small number of thin, pebble grade, volcaniclastic debris flows are found intercalated within the Drimos Formation, as recorded at the Agrambela monastery (Log B1).

##### Facies 4, 5, 6 & 7

These facies are found throughout the study area as either proximal deposits or, more commonly, the dominant facies of distal environments. *Halobia* limestone is found only in the lower third of the Drimos Formation. The other facies vary in their stratigraphic position and importance. The presence of dolomite in the more proximal outcrops of micrite, and more especially calcarenite, is considered in Section 3.3.3.1. Shimmield & Price (1984) studied hemipelagic sediments from off Baja, California. They found dolomite in deposits between the shelf break and continental rise, but little or none on the shelf, nor on the oceanic plain. This is possibly significant in further confirming the proposed proximity of the margin.

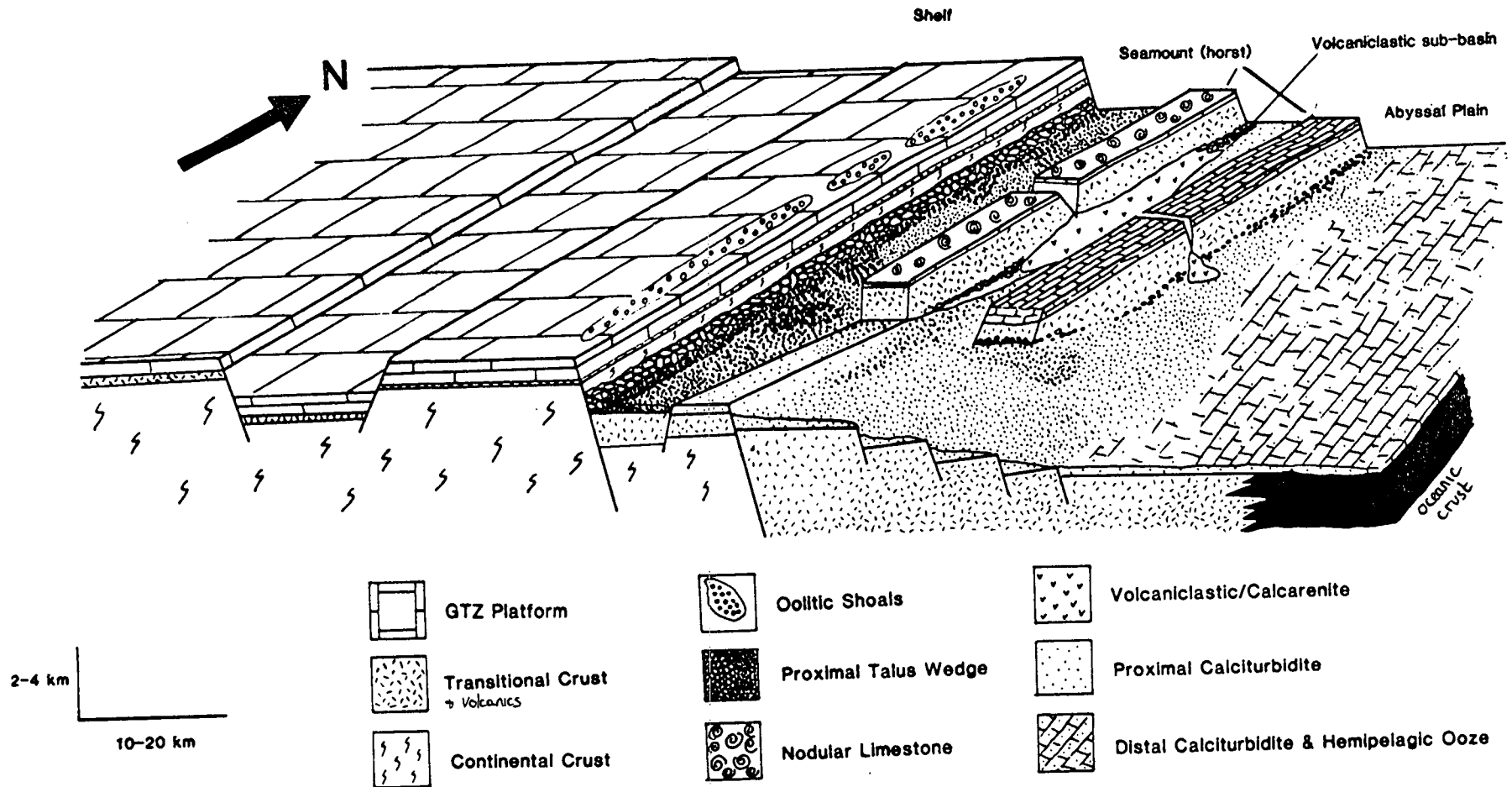


**Fig. 3.3** Schematic interpretation of the Apulian margin during the Upper Triassic/Liassic based on the palinspastic reconstruction of the sedimentary facies of the Drimos Formation.

### Facies 8: Chert

Bedded radiolarian chert is found in more distal localities and concentrated horizons are restricted to a distinct interval, roughly coeval with the disappearance of widespread *Halobia*-bearing limestone.

#### 3.3.2.2 Depositional Environment

There are three major depositional environments inferred for the Drimos Formation: slope-rise apron; a silled (possibly perched) volcanoclastic sub-basin and abyssal plain. The proposed palaeoenvironment is schematically shown in Figure 3.3 .

#### Proximal Facies Environments

The rudite (facies 1) depositional setting is inferred to represent the most proximal environment. The widely distributed calcirudite along almost all of the Pindos front is best envisaged as a base-of-slope talus wedge, derived from a line source along the shelf break. There is no evidence for a carbonate fan, rather, an apron morphology rapidly thinning to the east, is envisaged. It is clear that deeply incised channels extended from the apron, cutting through more distal deposits. This facilitated the transport of conglomerate further outboard, as seen between Agrambela and Kryovrissi, although these deposits also thin rapidly eastward. Restoration of the thrust sheets indicates that the preserved talus wedge was no wider than 5 km. The rudite is both matrix and clast supported. Based on the criteria outlined in the introduction to Section B, itself derived from several sources, the rudite is considered to have been deposited principally through debris flow and rockfall depositional mechanisms. Rockfall deposits require a steep slope. Furthermore, the very localised concentration of rudite, rapidly fining to the east, strongly suggests a distinct change in the angle of slope, from relatively steep in the west, to a much shallower angle of repose. There appears to be a genetic link between the rudite facies and the calcarenite, both especially occurring near the top of the formation and with similar compositions. Similar associations have been noted from other areas in Greece (e.g. Othris, Price 1977).

The second, pink rudite, facies is found only in the upper section of the Drimos Formation. It appears to be tabular on the scale observed, but is probably channelised. No individual bed could be continued for any distance. The well rounded, homogenous, pink limestone clasts may indicate that the deposits represent reworked debris flow sediment from off a proposed narrow shelf of seamounts, using established routes from these specific sources.

In the proximal areas of Alepohorio and Glafkos, the rudite appears to be largely missing. Instead, nodular limestones (Cephalopodenkalk and Ammonitico Rosso, facies 2), typical of Tethyan pelagic sequences on submarine highs (Tucker 1974, Jenkyns 1974), are present. The Ammonitico Rosso sediment found at Glafkos is not located on the structurally lowermost thrust sheet, and therefore, as no large scale out of sequence thrusting is obvious (Chapter 6), this cannot have been the most proximal environment. This contention is supported by the presence of Ammonitico Rosso-type sediment in the tectono-sedimentary melange. Glafkos was therefore outboard of the Apulian shelf break. Such near-margin edifices may have been isolated volcanic seamounts or basement fault blocks (horsts) capped by extrusive rocks close to the continental margin. At Megdhovas, the Ammonitico Rosso facies was overstepped by shallow water carbonates (Fleury 1980, AHF Robertson & PJ Degnan, unpublished data). Palaeogeographically, the area was probably located on the margin, close to the shelf break proper and was thus in a position where Lower Jurassic progradation of the platform could take place.

The nodular nature, the shape of the concretions and the composition of the Cephalopodenkalk-type sediment, suggests the preferential cementation of irregular burrow systems in a mixed clay/carbonate substrate. It is likely that the texture was further enhanced by diagenetic segregation as proposed by Jenkyns (1974). It is probable that the locations exemplified by Alepohorio were palaeo-topographic highs, possibly horsts adjacent to the slope, and conglomeratic debris-flows and rockfalls by-passed this relatively elevated environment. After a period of nodular limestone formation, Log B4 indicates that the sediment deposited at Alepohorio became more typical of slightly more outboard environments. It is probable that with time the area subsided (thermal relaxation?) and was swamped by finer grained calciturbidite.

The single argillaceous chert sample (PD/90/758), with calcitised schist allochems, is undatable. However, the association with the nodular limestone suggests a speculative depositional scenario. The schist certainly underwent replacement by carbonate prior to redeposition. This was possibly the result of percolation by hydrothermal fluids, rich in carbonate, through the continental basement. The hydrothermalism was probably coeval with the basement uplift and volcanism inferred in Section 3.2.3 (see also Section 9.2.1). During the Late Triassic/Lower Jurassic the basement was exposed, either actually on a slope or on a faulted block. The lack of any other clastic component other than schist, and the concentration of



the schist clasts, attests to the proximity of the basement source. Possibly a basement olistolith was detached, in the same manner proposed for the rhyolite block within facies 3. Fragmented schist may have been deposited in pink calcareous ooze on the slopes of a horst, capped by Ammonitico Rosso-type facies. Radiolarian debris provided the silica for later transformation to chert.

The rhyolite in the volcanoclastic sediment (facies 3) is best considered as an olistolith, derived from exposed basement, and this would indicate the proximity of a steep slope. The presence of this large lava block, the reasonably well preserved volcanic component in the sandstone and the apparently restricted setting suggest the presence of a silled sub-basin receiving locally shed debris, probably off a volcanic seamount or faulted igneous basement. Very little of the volcanic sediment escaped for more widespread distribution (c.f. Log B.1). Coarser grained, probably time equivalent, calciturbidite and rudite facies are found further east. Thus the proposed environment must have been by-passed by the base of slope talus wedge until immediately before the deposition of a channeled rudite found below the radiolarite facies of the Lesteena Formation. A suggested environment for such volcanoclastic sediment would be a restricted trough, dammed to the west and east (also north & south?), and possibly topographically elevated with respect to more outboard localities (Figure 3.3).

The carbonate allochems seen in the volcanoclastic sandstone samples provide an interesting depositional and diagenetic history. It is envisaged that there was deposition of a polymict coarse arenite to gravel grade sediment on the shelf, including mica and quartz derived from a metamorphic terrane. This was a well sorted "clean" sediment with little lime mud. Ooids nucleated, some on quartz grains, in an energetic shoal setting. An early, remnant (aragonite ?) accicular rim cement suggests that some grains were immobile for long enough for a fringe of aragonite needles to form, as proposed by Ball (1967) for ooids in the troughs of megaripples. Off shelf transport, by turbidity currents, mixed the shoal and skeletal detritus, and incorporated volcanic debris (possibly off steep fault scarp walls). The sediment was deposited in a basinal setting where circulating pore waters gave a hematite rim to certain horizons during early diagenesis. Compaction fractured ooids followed by the development of concavo-convex boundaries. Continued burial led to syntaxial overgrowths and a final pore-filling coarse spar calcite cement.

### Distal Facies Environment

The greater part of the Drimos Formation is representative of the more "distal" facies, being composed of finer grained calcarenite/calcsiltite and hemipelagic micrite. The allochems are mostly carbonate, comprising fresh skeletal fragments, ooids and reworked, lithified sediment. The variation of section thicknesses, even over relatively small distances, is considered indicative of an irregular topography. The apparent generic relationship of calcarenite to the rudite facies has been noted above. Sedimentary structures in the calcarenite/calcsiltite, although lacking sole structures, indicate deposition from turbulent currents. The facies is considered equivalent to calciturbidite. Thus debris flows initiated on the shelf margin and slope are suitable precursors to the more distal, finer grained calciturbidites.

Distinct concentrations of *Halobia* shell fragments in the calcarenite are noted. Rather than representing "*Halobia* blooms" with pelagic settling through the water column, it is suggested that the *Halobia* lumachelles were mainly deposited by the same turbidity currents as the surrounding sediment. Due to the high surface area to density ratio of the bivalve, the shells are considered as the hydraulic equivalents to much finer grained debris. Thus, in a turbidity flow they would settle out more gradually than denser, but similarly sized material, with the preferential alignment of lumachelles on top of coarser beds. A pelagic mode of life is indicated by the presence of *Halobia*-bearing hemipelagic micrites. However, the concentrations can be contrasted with the proportions of *Halobia* found in the calciturbidite. This indicates that the *Halobia* habitat was largely to be found on the shelf and shelf edge, rather than in open sea conditions.

### 3.3.3 Discussion

#### 3.3.3.1 Deep Sea Dolomite

The presence of authigenic rhombohedral dolomite in the deep water carbonates of the Drimos Formation is of interest. In the field, dolostones were sometimes identified, but there was no extensive dolomite development recognised. The deep sea depositional environment does not fit into any of the depositional or diagenetic settings traditionally proposed for dolomitization, which are all related to burial in shallow water environments. Reviews of dolomite formation include Morrow (1982), Mackel & Mountjoy (1986) and Hardie (1987).

It was noted that the proportion of dolomite varies widely in the thin sections examined, from nil to almost total replacement. Micrites are generally deficient in dolomite, while calciturbidites, rich in peloids and skeletal debris, have undergone greater dolomitization, with larger rhombs present relative to adjacent micrite beds (Plate 3.8).

There are a number of possible models to account for the dolomite found in the Drimos Formation. Of the various mechanisms of dolomitization, models involving continental margin deposits are considered here. Most importantly, a potential source for magnesium (Mg) must be established, as the supply is most probably the principle limiting factor in dolomite formation. There are a number of possible sources of Mg:-

- 1) Mg derived from the crystal lattices of clay.
- 2) Mg adsorbed onto the surface of clays or organic particles.
- 3) The oxidation of organic material.
- 4) The circulation of Mg-rich sea water, buried with the sediment.
- 5) Diffusion of Mg from over-lying sea water.
- 6) Mg derived from an igneous basement
- 7) Mg derived from high Mg-calcite

The conversion of smectite to illite has been considered as a possible reaction that would release Mg (Perry & Hower 1972). This reaction occurs at elevated temperatures and the diagenesis of mudstones, rich in illite, is considered in Section 4.3.1.4. The literature indicates that marine dolomite, formed in deep sea sediments, is the result of near surface processes (as discussed further below) so that a late stage clay transformation is not considered applicable. In addition, there is insufficient evidence to suggest that dolomitization is more prevalent adjacent to intercalated mudstones in the Drimos Formation, nor is it found in more mudstone rich horizons.

Baker & Burns (1985) state that the magnesium content of organic particles is insignificant in the formation of marine dolomite. They consider that the proportion of Mg present in plankton, deposited in hemipelagic sediment, is insufficient to cause extensive dolomitization. Similarly they discount an origin of Mg from buried sea water by calculating the total flux of dissolved magnesium possible by advection.

By a process of elimination, Baker & Burns (1985) propose that diffusion from overlying sea water is the most important source of magnesium in deep water dolomite. They suggest that dolomite will form close to the sea water/sediment interface within the zone of microbial sulphate reduction. Compton & Siever (1985) also postulated that diffusion of Mg from sea water can account for dolomite in the calcareous sediments of the Monterey Formation, western USA. They emphasise that the magnitude of the Mg flux through the sediment is proportional to the rate of dolomite formation and inversely proportional to the rate of sediment accumulation.

Pliocene dolomitic sediment, from ODP leg 107 in the Tyrrhenian Sea, was analysed by Robertson (1990a). The sediments are brightly coloured, manganiferous and ferruginous dolomitic sediments, overlain by siltstone and clay rich nanofossil ooze. Early stage dolomitization is indicated from isotopic evidence (McKenzie *et al.* 1990). It was suggested that the supply of Mg was largely provided by talc, derived from the erosion of peridotites and modified by sea water. Additional Mg was possibly supplied from the ultramafic substratum directly. The sediments described from the Tyrrhenian Sea are deep water deposits, but otherwise there are no other similarities with the facies of the Drimos Formation. It has been shown that there were contemporaneous sandstones with a volcanic component (Facies Group 3) in the Drimos Formation. However, the extent of the exposed extrusives is not known. Mass balance calculations would be necessary to estimate the potential of such a source, unfortunately not possible due to a lack of exposure. A potentially important mechanism, derivation of Mg from an igneous basement is possible in the dolomitization of the Lower Jurassic sediments of the Pindos Group. However, given that the volcanic substratum was largely sediment covered, the mechanism is not considered applicable in the dolomitization of the sediments studied here.

The proposed model to account for the development of dolomite in the Drimos Formation is based on the observations and suggestions of Mullins *et al.* (1984) who found extensive protodolomite (defined by Graf & Goldsmith 1956) in the upper slope sediments of the Little Bahama Banks. Piston cores revealed that carbonate sediment is dominated by aragonite and Mg-calcite. The deposits indicate the rapid deposition of predominantly platform derived material during the present sea level high stand. Furthermore, radiocarbon dating indicates very rapid deposition rates of c.a. 640cm/1000y. Oxygen and carbon stable isotope data indicate that the diagenetic formation of protodolomite occurred at or near the sea floor. In addition, the protodolomite (10-20% volume) appears at 120cm below the sediment surface,

corresponding to the disappearance of aragonite and Mg-calcite, with only calcite (80-90% volume) remaining. This zone is also characterized by an increase in sand sized carbonate particles. Mullins *et al.* (1984) proposed that protodolomite precipitated by the dissolution of aragonite and the exsolution of Mg-calcite under anoxic conditions, following sulphate depletion by microbial activity (sulphate ions are found to inhibit dolomitization, thus, dolomitization must occur below the sulphate reduction zone [Baker & Kastner 1981]).

The genesis of dolomite, in the Drimos Formation, by a similar mechanism to that outlined above is attractive for several reasons. Firstly, normal peri-platform ooze and carbonate platform sediments, contain a mix of aragonite, Mg-calcite and calcite (Bathurst 1976). Several experiments (Friedman 1964, Land 1967, Schroeder & Siegel 1969) show that Mg-calcite dissolution occurs in sea water and on burial at pressures similar to those for aragonite dissolution. Thus, where turbidity currents sweep shelf derived debris to base of slope environments, there is a ready supply of Mg. Secondly, the fabric of a carbonate calciturbidite, especially of skeletal debris, oolite and peloids, is initially a loose framework with high porosity, thus facilitating (Mg-bearing) pore fluid flow. This may be particularly relevant to the observation that dolomite is less well developed in micrite. Thirdly, the same observation is in contrast to the premise of Baker & Burns (1985) and Compton & Siever (1985) who state that the greatest rate of dolomite formation in hemipelagic sediments occurs principally in slowly accumulating sediment. In the Drimos Formation limestone, dolomitization occurs principally in sediment with the greatest rates of accumulation, viz. calciturbidite.

Considering the shallow burial origin proposed for authigenic dolomite found in hemipelagic sediment, and in keeping with experimental studies (Kushnir & Kastner 1982), the dolomite of the Drimos Formation limestone is considered as an early diagenetic *in-situ* phase, derived from the dissolution of Mg-calcite. There is obviously a great deal of further research to be undertaken in this field.

### 3.3.3.2 The Morphology of Continental Margins

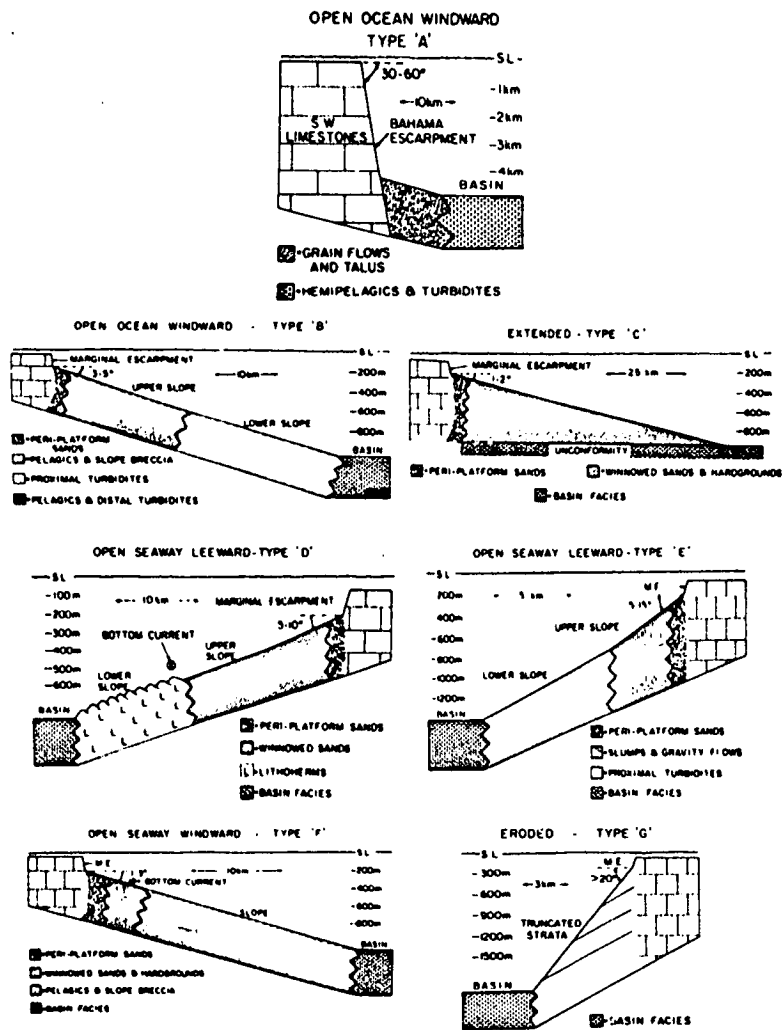
This section briefly describes work detailing the present day morphology of continental margins, and the way in which this affects the distribution of sedimentary facies in the slope to continental rise environment. By comparing facies distributions observed in the rock record with the sediment patterns of present day

environments, it is possible to make statements regarding the nature of the sediment source, the approximate angle of slope and the depositional mechanisms operative.

Ginsburg & James (1974) divided carbonate platforms into two types, rimmed, which are high energy shelf break areas, and open (or ramp) platforms where the shelf gently deepens oceanward. Mullins & Neumann (1979) further extended this classification to include seven main types of deep carbonate bank margin. They are illustrated in Figure 3.4 with brief descriptions of typical sedimentary facies and depositional controls alongside. Appraisal of the Drimos Formation sediment pattern conforms most closely with the "Type A" margin of Mullins & Neumann, or the "by-pass escarpment" type model of Read (1984). The main characteristics of these escarpment models are a steep (usually fault controlled) slope of up to 60° and high relief of up to 5000m. Sediment supply is from off both the shelf and the slope. Transport mechanisms in this slope environment are rockfalls, slides, debris flows and turbidity currents. The base of slope reveals a thin talus apron, grading rapidly into hemipelagic and finer grained basinal sediments.

It is emphasised here that the most proximal deposits of the Pindos Group probably represent the more outboard part of a base of slope (continental rise) environment and not the slope proper. Evidence to support this includes the lack of intraformational truncation surfaces or other extensive slump or slide structures. There are no boulder-size, or greater, talus deposits such as would be expected at the most proximal parts of the slope rise, as found for example in Oman (Sumeini Group, Watts & Garrison 1986). Instead, the presence of extensive, cobble grade rudite, confined to a narrow band and which apparently does not prograde significantly into the basin, implies a rapid change in the angle of deposition, such as found at the base of a steep slope, but outboard of the base proper.

It is noticeable that the Pindos basin, throughout its history, was largely starved of sediment, in comparison to many parts of the eastern USA passive margin for example. The adjacent Gavrovo-Tripolitza platform was productive throughout its history (Section 7.3.1), and any fine grained platform sediment must have by-passed the slope to drift as hemipelagic ooze. The base of slope was instead supplied with reworked sediment or oolitic and skeletal calciturbidites. Such sediment dispersal implies a by-pass margin (McIlreath & James 1984), with a shelf-break rimmed by oolitic shoals. By-pass margins are characterised by the rapid vertical aggradation of



Bank Margin Type	Down-to-Basin Slopes	Seismic Facies	Processes and Controls	Sedimentary Facies
Type 'A'—Open Ocean Windward—East of LBB	Very narrow; steep (30–60 degrees).	—	Basement faulting; carbonate buildup; submarine erosion; grain flows; rock falls; pelagic sedimentation; turbidity currents	Outcrops of shallow-water limestones along slope; wedge of thick massive to inversely graded bioclastic grain flows and talus blocks at base of slope which grade rapidly seaward into pelagic and hemipelagic muds.
Type 'B'—Open Ocean Windward—North of LBB	Broad (up to 50 km wide); gentle (2–5 degrees).	Even parallel continuous to transparent on upper slope; discontinuous to chaotic on lower slope.	On-bank transport of back-reef sediments; downslope transport of fore-reef material; pelagic sedimentation; debris flows; turbidity currents.	Peri-platform facies adjacent to bank; upper slope pelagic oozes and slope breccia; lower slope peri-reef biolithoclastic turbidites.
Type 'C'—Extended—Northwest of LBB and GBB	Very broad (up to 100 km and more); very gentle (< 1 degree).	Oblique progradational; divergent to even parallel continuous.	Pelagic sedimentation; sediment winnowing, reworking and deposition by bottom currents; submarine cementation.	Peri-platform facies adjacent to bank; massive current winnowed sands; strata form a thick wedge which thickens toward the bank.
Type 'D'—Open Seaway Leeward—West of LBB and GBB	Moderate width (< 25 km); moderate steepness (5–10 degrees).	Discontinuous-chaotic on upper slope; mounded chaotic on lower slope.	Off-bank transport; bottom current flow; biological buildups; pelagic sedimentation, turbidity currents; submarine cementation.	Peri-platform facies adjacent to bank; massive submarine cemented current winnowed sands and turbidites on upper slope; linear band(s) of current oriented submarine lithified bioherms on lower slope; hardgrounds.
Type 'E'—Open Seaway Leeward—South of LBB	Narrow (5–15 km wide); steep (6–20 degrees)	Chaotic to mounded chaotic on upper slope; discontinuous on lower slope.	Off-bank transport; slumps and gravity flows; turbidity currents; pelagic sedimentation.	Peri-platform facies adjacent to bank; mixed gravity flow deposits and slumps on upper slope; biolithoclastic turbidites on lower slope.
Type 'F'—Open Seaway Windward—North of GBB	Broad (25 km wide or more); Gentle (< 2 degrees).	Even parallel continuous; minor wavy subparallel chaotic.	On-bank transport; pelagic sedimentation; debris flows; submarine cementation, bottom currents.	Peri-platform facies adjacent to bank; slope consists of pelagic oozes and muddy slope breccia with hardgrounds and current winnowed sands on uppermost slope minor turbidites.
Type 'G'—Eroding Mouth of NWPC Basin	Very narrow (< 5 km wide); very steep (> 20 degrees).	—	Submarine erosion.	Slope facies thin or absent; truncated strata.
Basin	—	Even parallel continuous	Pelagic sedimentation; turbidity currents; reworking by bottom currents.	Pelagic oozes interbedded with thin distal turbidites.

Fig. 3.4 Depositional models and summary of recognition criteria for deep carbonate bank margins in the Northern Bahamas (after Mullins et al. 1979).

shallow water sediment on the shelf, enabling the platform to keep pace with rising sea level, but not providing sufficient sediment for lateral accretion.

### 3.3.4 Ancient and Modern Comparisons

There are a number of possible analogues in the literature which are comparable to the proposed base of slope to abyssal environment outlined in this chapter. In the Tethyan region, the uppermost sections of the Zulla Formation and the Guweyza Limestone Formation of the Dibba Zone, Oman (Cooper 1986, 1989), comprises Late Triassic and Lower Jurassic sediments. *Halobia*-bearing limestones are conformably overlain by oolitic calcarenites with shale partings. Minor pebble conglomerates, silicified limestones and chert are also present. The sequence is capped by a regional conglomeratic horizon.

In the Antalya complex, Turkey, the Bozyer Formation of the Kumluca Zone, is a Late Triassic example of an imbricated Tethyan margin (Robertson & Woodcock 1981). Lithologies are principally calcilutites with *Halobia* fragments, although there are strong variations in facies, notably to the south where intercalations of calcirudite and calcarenite are found. The more distal part of the margin is represented by hemipelagic limestone and shale of the Gokdere Formation in the Godene Zone of the Antalya Complex.

The Drimos Formation is the time equivalent of the Marona Formation and the lower parts of the Episkopi Formation of the Mamonia Complex, SW Cyprus. Lithologies present include *Halobia*-bearing limestones, siltstone, mudstone, calcilutite, calcarenite and calcirudite. The stratigraphy of these units is described by Swarbrick & Robertson (1980).

Outwith the Tethyan realm, the Cathedral escarpment of the Canadian Rocky Mountains preserves a Middle Cambrian steep slope capped by a platform and *in-situ* base of slope basinal deposits (McIlreath 1977). The escarpment is only up to 300m high and was formed by the rapid up-building of a reef. It is therefore on a much smaller scale than proposed for the Pindos margin. Nevertheless, the facies patterns seen along the base of slope are comparable with those proposed for the Pindos continental rise.



Present day carbonate margin morphologies have been described in Section 3.3.3.2 where it was concluded that steep by-pass margins provide the facies patterns which are the closest analogues to those found in the sediments of the Drimos Formation. In particular many of the Bahama slopes and rises appear analogous to the inferred Apulian margin. The Bahama Escarpment to the east of the Little Bahama Banks, has a slope of 28 to 40° which drops to abyssal depths (4500m). The prevailing wind leads to the onshore transport of material on to the platform with only storm induced water agitation leading to the off margin deposition of hemipelagic sediment. Mullins & Lynts (1977) suggest that the escarpment was controlled by basement faults formed during rifting and that the slope may mark the continent-ocean transition.

### 3.4 CONCLUSIONS

The terrigenous sediments of the Priolithos Formation are interpreted as deposits derived from metamorphic and volcanic centres along the rifted Apulian margin. The detritus was mixed with carbonate allochems on a Triassic platform and slope, and transported by turbidity currents to a base-of-slope environment. The turbidity currents may have been initiated by tectonic activity related to continental extension and volcanism. Intervening, relatively quiescent, periods are represented by intercalated, hemipelagic, siliceous limestones.

The variety of sediments present in the Drimos Formation dominantly reflects the distance of the depositional site from the continental margin. Eight distinct facies are recognised. Proximal deposits are represented by thick accumulations of rudite that formed a base-of-slope talus apron, with detritus supplied from the slope and platform. The continental rise talus wedge thinned rapidly eastwards although deep submarine channels selectively directed coarser sediment to more distal depositional sites. Nodular limestones formed on submarine highs that were largely by-passed by debris flows and rock falls. Volcaniclastic sandstones are unique in the study area and appear to be derived from a volcanic edifice, possibly faulted igneous basement. Further outboard, an irregular sea floor topography was blanketed in hemipelagic micrite and chert, and distal calciturbidite sediment. Dolomite is especially enriched in certain calciturbidite horizons and is here considered to be chiefly derived from the dissolution of Mg-calcite and an early diagenetic origin is proposed.

## PLATES

### PLATE 3.1: Priolithos Formation

(A) Intercalated sandstone and limestone of the Priolithos Formation type-section. Note the folded and faulted nature of the outcrop. The face is approximately 3m high. (B) The transition from the Priolithos Formation to the Drimos Formation at Alephorio. At the level of the hammer a debris flow is present, comprising irregularly shaped clasts of nodular limestone. (C) Poorly preserved, Triassic ammonoid found in Priolithos Formation sandstone near Lambia. (D) Thinly bedded pelite, sandstone and limestone of the Priolithos Formation at Livardzi.

### PLATE 3.2: Priolithos Formation - Petrography

(A) Moderately sorted litharenite. Clasts are mainly mono- and polycrystalline quartz and lithic fragments cemented by a fine calcite spar. XP, Scale bar = 0.7mm  
 (B) Peloidal grainstone with subsidiary quartz and terrigenous lithic fragments, admixed with *Halobia* sp shell fragments. XP, Scale bar = 0.5mm  
 (C) Mixed source arenite with calcareous components mixed with quartz and lithic fragments, passing-up into a pelitic horizon dominated by *Halobia* sp. XP, Scale bar = 0.5mm

### PLATE 3.3: Drimos Formation

(A) Pseudo-nodular limestones. To the left of the photograph is a channelised mud-dominated debris flow containing large clasts (to cobble grade) of basalt. Hammer for scale. (B) Medium bedded calciturbidites. Hammer for scale to left of photograph. (C) Thick bedded calciturbidite with an angular rudite base grading upwards into medium-grained top. Spherical chert nodules are developed, often linking-up parallel to bedding. Hammer for scale. (D) Cobble grade debris flow rudite comprising elongate sub-rounded carbonate clasts in a pink, siliceous mudstone matrix. Hammer for scale.

### PLATE 3.4: Drimos Formation

(A) Well developed columnar jointing in rhyolite olistolith found within the volcanoclastic sandstone facies. Note that the joints are not vertical but inclined into the page and the surrounding sandstone beds are discordant with respect to this orientation. The olistolith is approximately 6m high in the photograph. (B) Trough-cross lamination developed in calciturbidite. Ruler for scale. (C) Closely packed *Halobia* sp shells in calciturbidite. XP, Scale bar = 0.3mm  
 (D) Rounded pelagic bivalve shells in a micrite matrix. Note the coarse calcite spar filling an original shelter porosity and defining the way-up. XP, Scale bar = 0.3mm

### PLATE 3.5: Drimos Formation

(A) Clast-supported, sub-rounded, conglomerate with stylolitic clast boundaries. Clasts exclusively comprise pink pelagic limestones. (B) Angular schist fragments, totally replaced by carbonate except for remnant stringers of muscovite (musc). The isolated clasts are supported in a siliceous mudstone matrix containing poorly preserved radiolarians (r). PPL, Scale bar = 0.2mm

### PLATE 3.6: Drimos Formation - Bivalves

(A) Well preserved Triassic *Megalodont* sp, from the Ammonitico Rosso sediment (laterally equivalent to the Drimos Formation) north of the Gulf of Corinth. Hammer handle for scale. (B) Cross-section of a *Megalodont* sp bivalve from calciturbidite in the frontal Pindos thrust sheets. Pen for scale. (C) Moderately well preserved impression of flat *Halobia* sp shells on micrite bedding plane. Scale bar = 5cm. (D) Rounded pelagic bivalve shell in gravel grade calciturbidite. Lens cap for scale.

**PLATE 3.7: Drimos Formation - Petrography**

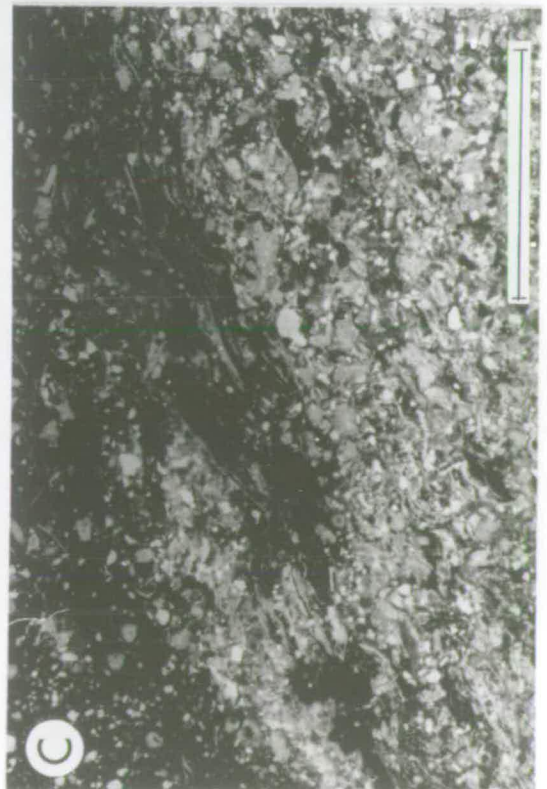
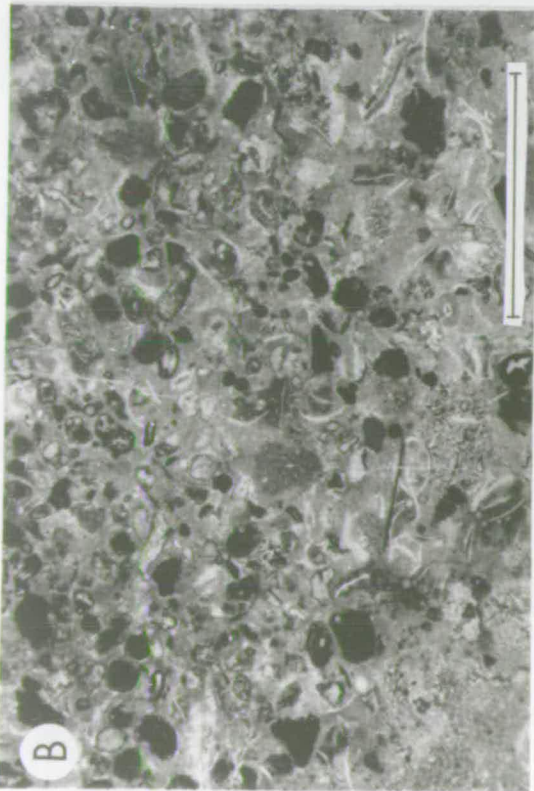
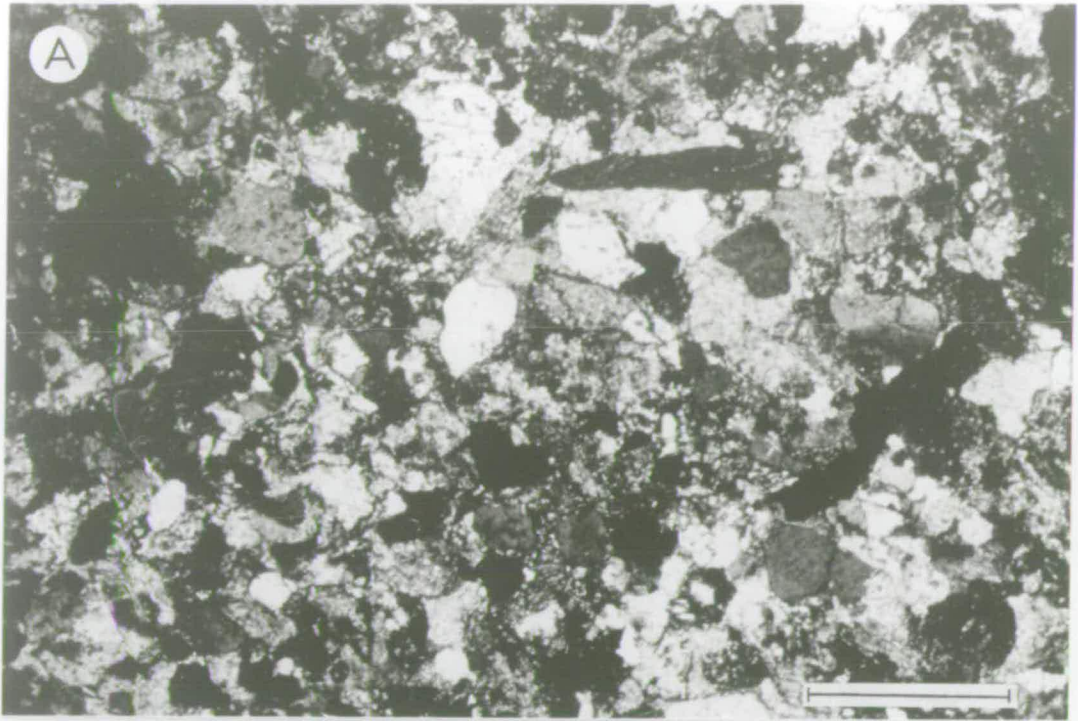
(A) Syntaxial calcite overgrowth on an echinoderm fragment in a well sorted packstone calciturbidite. XP, Scale bar = 0.2mm (B) Well sorted packstone calciturbidite. Note the fragmented oolite which has nucleated around a quartz grain. The oolite rim has an early fibrous calcite rim (after aragonite?), the pore-filling cement is a mosaic of coarse spar. PPL, Scale bar = 0.2mm (C) Well sorted packstone calciturbidite. Clasts are micrite peloids neomorphosed to a fine calcite spar, patchy relict micrite is still visible. The cement is a coarser calcite spar which grew into voids from grain boundaries, forming triple junctions at the interstices. PPL, Scale bar = 0.2mm (D) Packstone calciturbidite comprising micrite and platformal allochems. Some clasts are neomorphosed to spar and further replaced by chalcedony. Note the ferruginous grain boundaries which are also present where clasts have been sutured, indicating that rim cements were generated prior to compaction. PPL, Scale bar = 0.2mm

**PLATE 3.8: Drimos Formation - Petrography**

(A) Bioclastic micritic limestone containing randomly orientated thin-shelled *Halobia* sp fragments and radiolarians. Euhedral dolomite crystals are present. PPL, Scale bar = 0.2mm (B) Calciturbidite. Lower half of the photograph is a bioclastic peloidal packstone with large euhedral dolomite rhombs present. Upper half is a graded siltstone/micrite. The crystals are markedly smaller than in the packstone but, also note how the concentration and size of the dolomite rhombs decreases away from the siltstone base. PPL, Scale bar = 0.2mm (C) Chertification of a *Halobia*-rich bioclastic micrite. A mosaic of microcrystalline chert has totally replaced the micrite groundmass and only patchy areas of remnant calcite preserve the outline of the *Halobia* shells. XP, Scale bar = 0.2mm (D) Chertification of a calciturbidite packstone. Note that the groundmass is totally replaced by a cryptocrystalline chert with only partial replacement of the carbonate clasts, which are fringed by an early microcrystalline chert. Isolated unreplaced dolomite rhombs are present. XP, Scale bar = 0.2mm

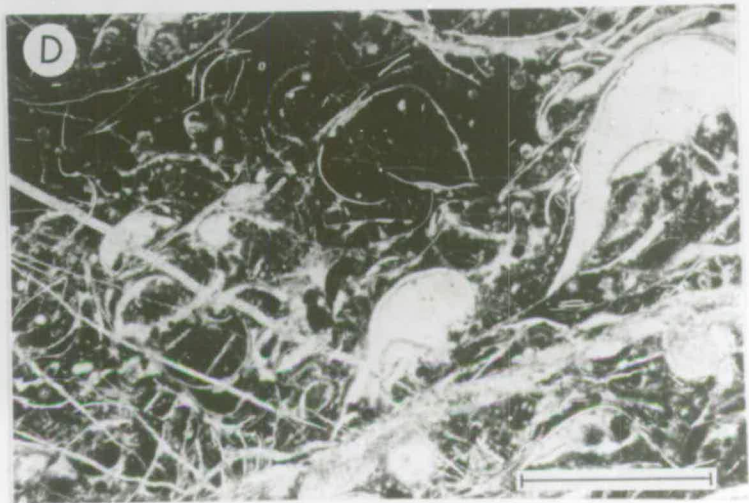
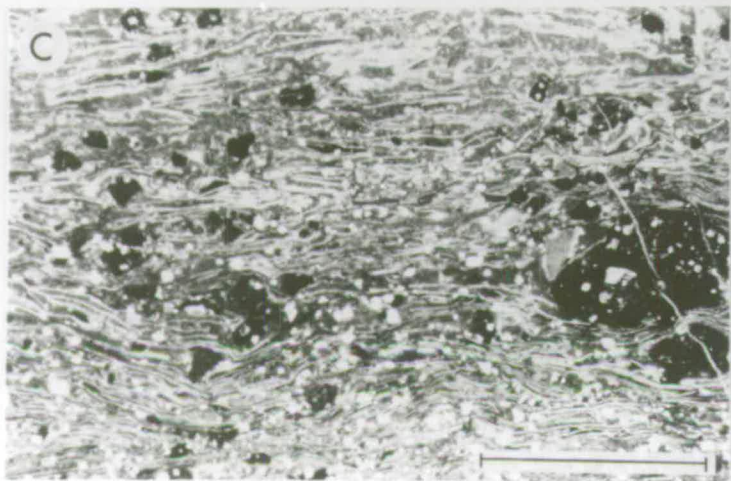






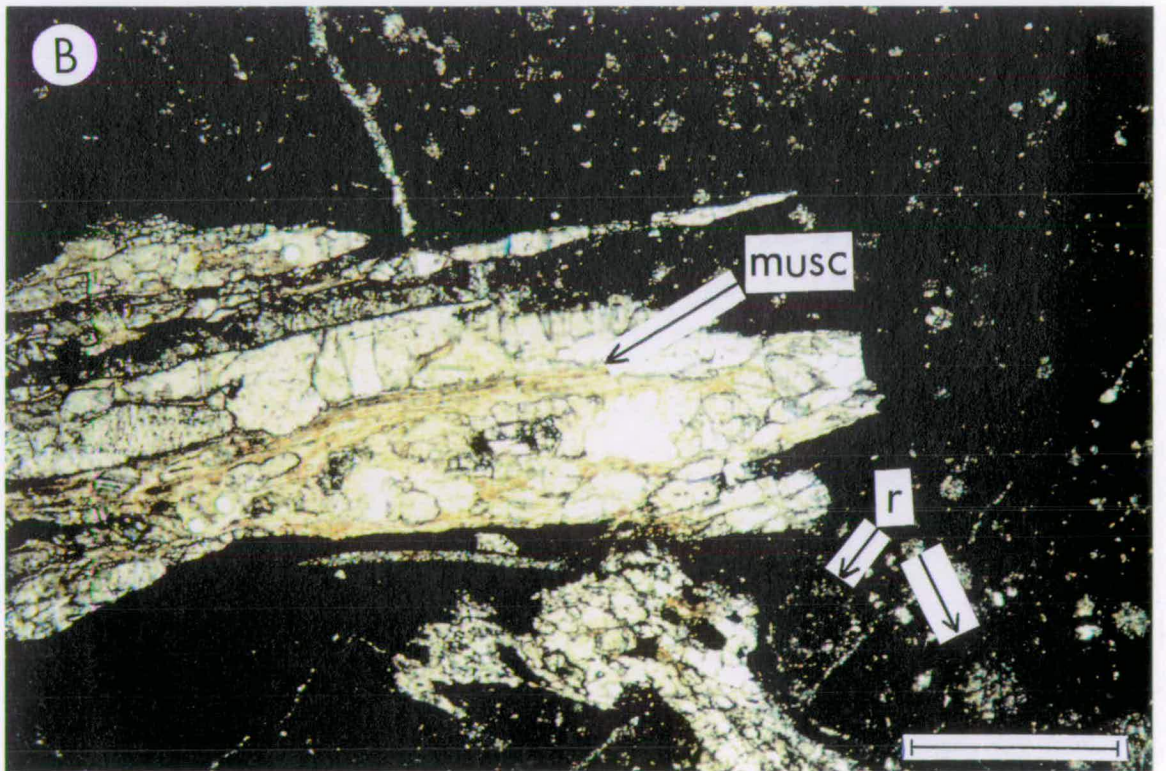








# PLATE 3.5





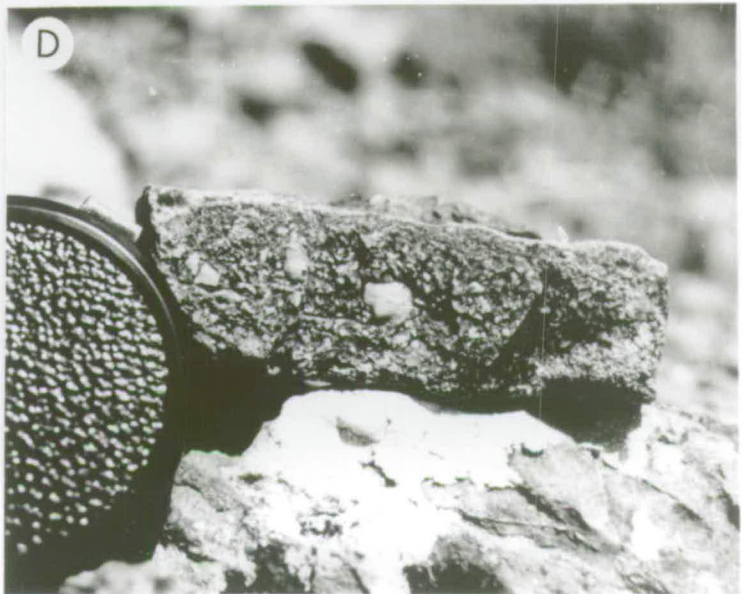
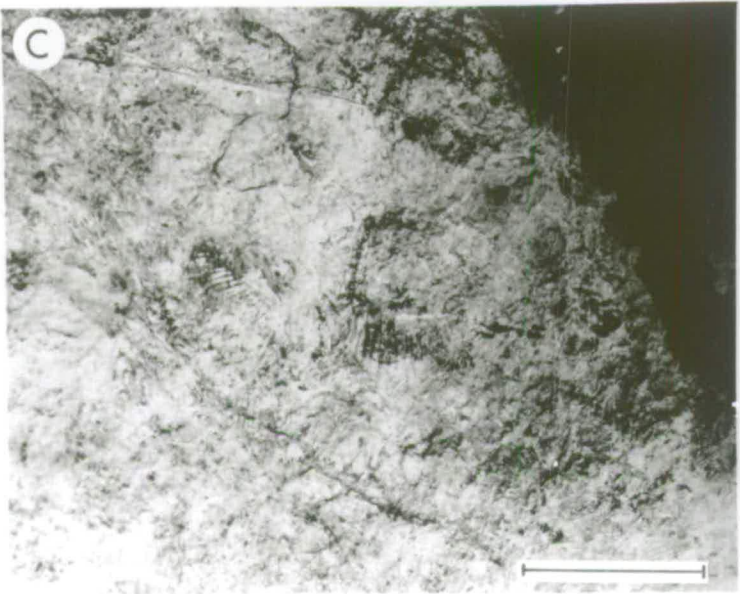




# PLATE 3.7

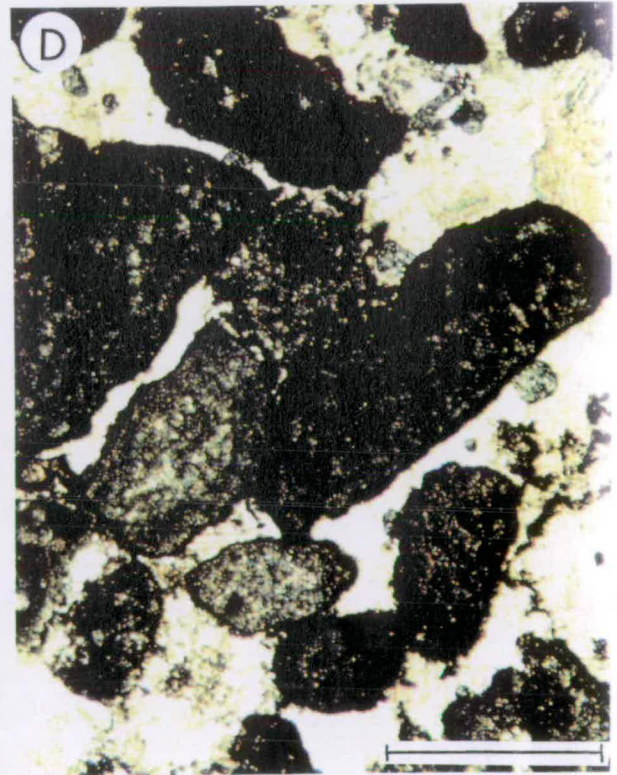
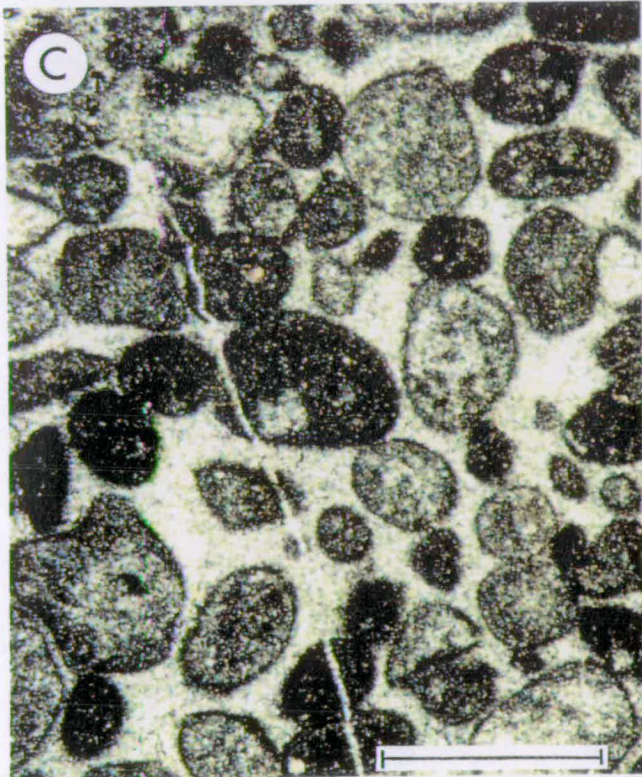
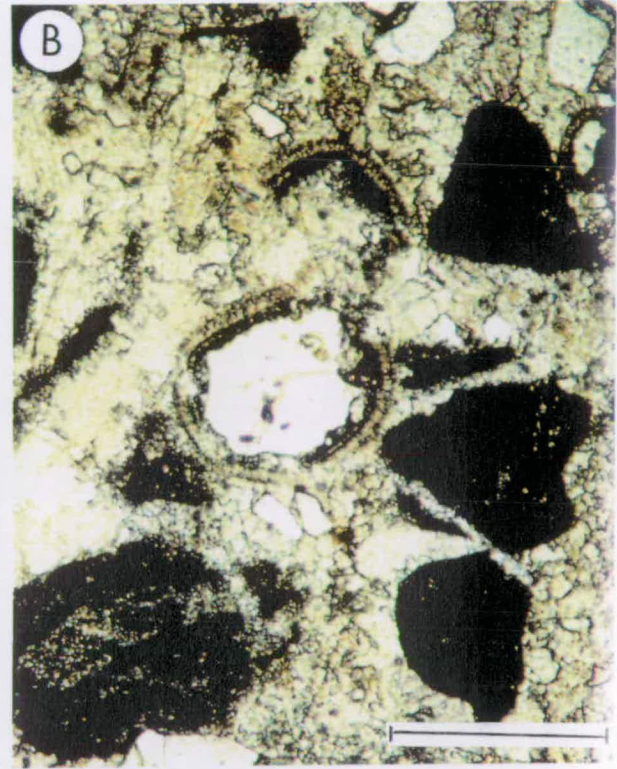
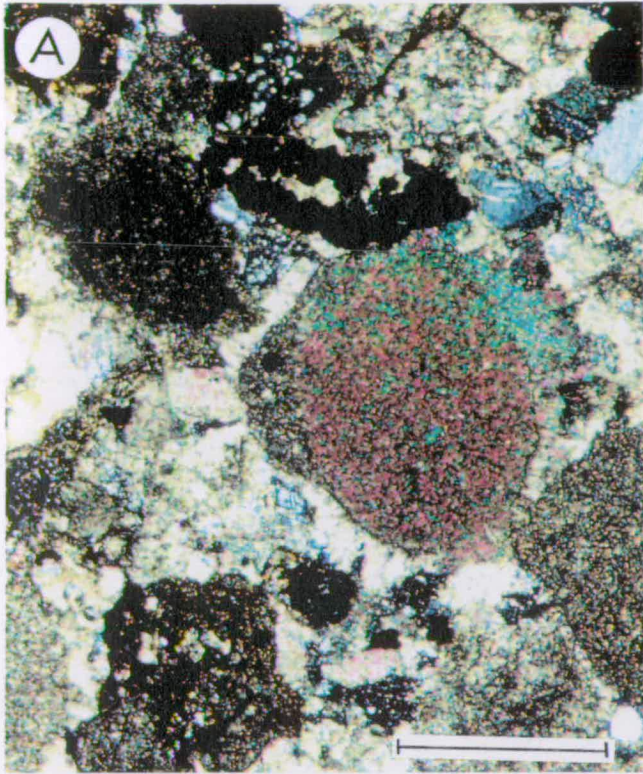
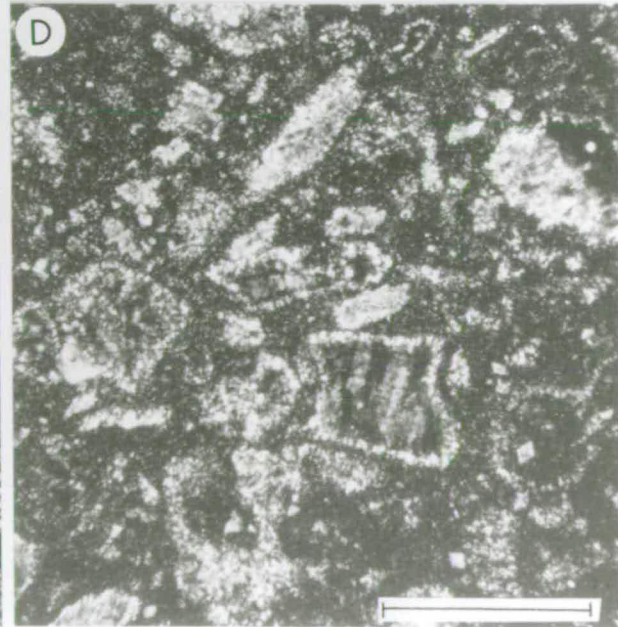
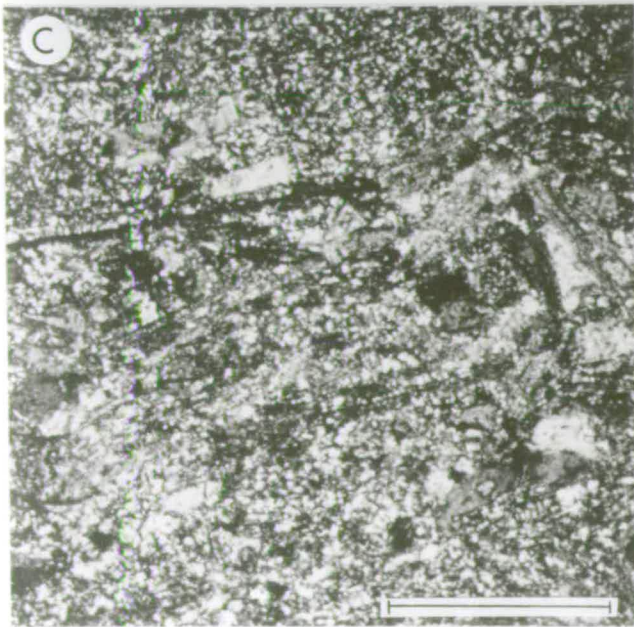
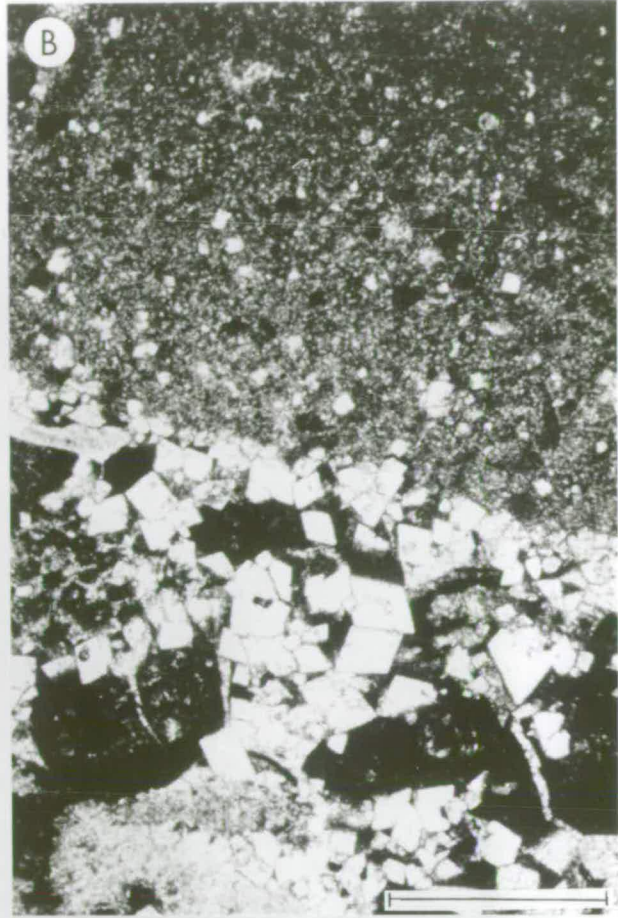
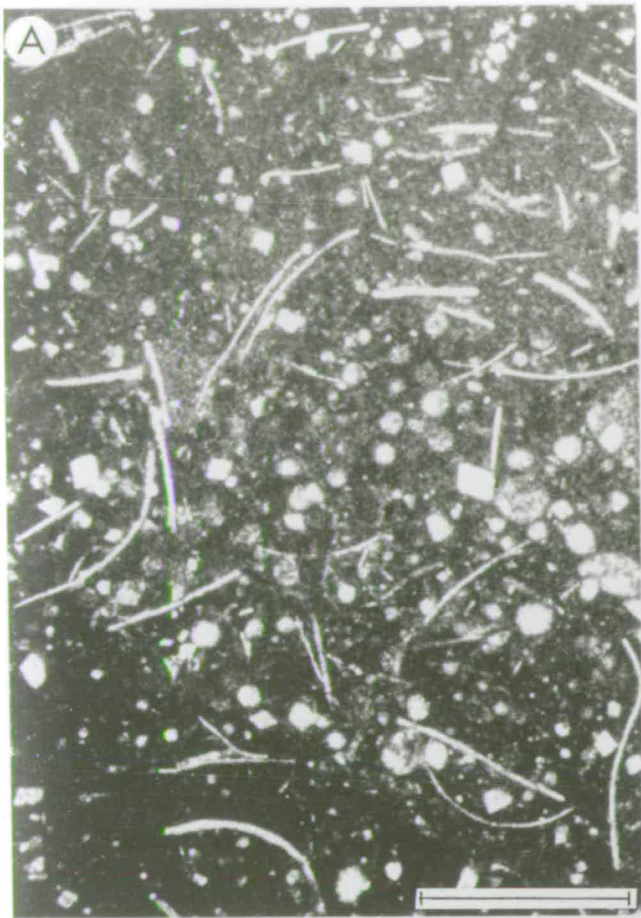




# PLATE 3.8



## CHAPTER 4 THE LESTEENA FORMATION

### 4.1 INTRODUCTION

The Lesteena Formation exhibits facies and thickness variations which reflect a variety of external influences on the depositional system. The result is a diverse stratigraphic unit consisting dominantly of radiolarian cherts, but also including replacement silica, siliceous mudstones, hemipelagic limestones and channelised breccias and conglomerates. The formation spans the Aalenian to Tithonian and comprises three members.

The Kakotari Member is restricted to the SW of the study area and consists almost entirely of megabreccias and conglomerates. The member represents a distinctive variation in lithological facies, laterally equivalent to, and coeval with, the deposition of the two other Lesteena Formation members. The composition of the dominant lithology is similar to channelised breccia deposits of the Aroania Chert Member. The member was difficult to study because of the absence of distinguishing lithologies and poor exposure, making correlations difficult.

The Kastelli Mudstone Member is an argillaceous facies that records the transition from the dominantly carbonate sediments of the underlying Drimos Formation, to more siliceous sedimentation as represented by the Aroania Chert Member. The Kastelli Mudstone Member is a rheologically weak horizon that deforms readily with respect to adjacent lithologies. Consequently, strain is often concentrated at this level and results in the development of major decollement planes. It is clear that in many localities the Kastelli Mudstone Member has been tectonically attenuated and is sometimes now completely absent. Notwithstanding this, a number of intact sections are present and have been studied.

Overlying the Kastelli Mudstone Member is a siliceous sequence of variable thickness, the Aroania Chert Member. At the base, and especially in more westerly locations, a green vitreous chert is found, above which a variable thickness of ribbon-bedded, often radiolarian bearing, red chert was deposited. Channelised conglomerates and breccias are present and are observed to thin towards the east. The member exhibits a mid-member carbonate interval which outcrops in more proximal localities.

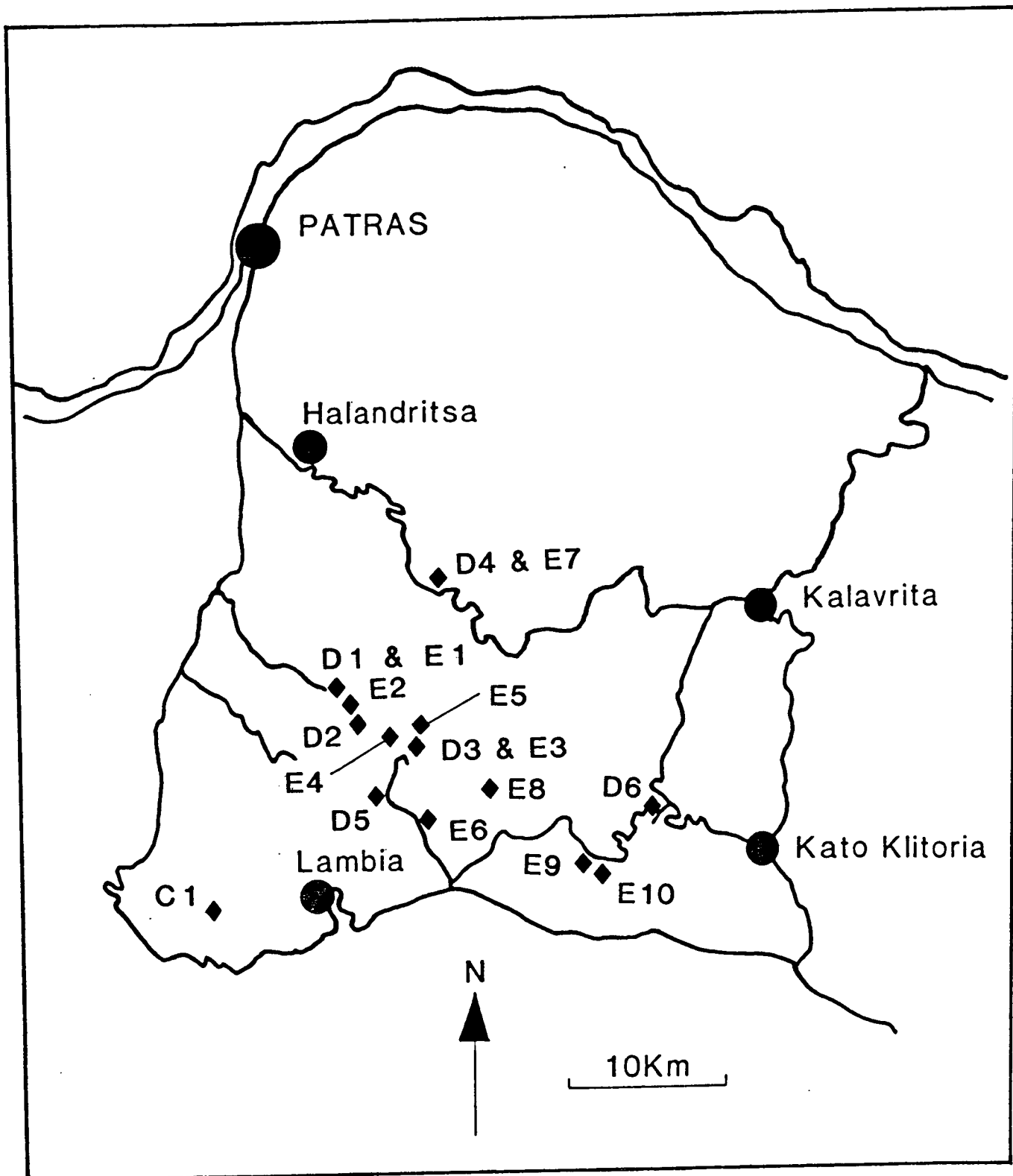


**Fig. 4.1** Map indicating the locations of the sedimentary log sites of the Lesteena Formation.

## 4.2 THE KAKOTARI MEMBER

### 4.2.1 Lithological Description

The Kakotari Member is observed in only one region of the study area. The lithology merits member status within the Lesteena Formation as it is lithologically distinct and appears to be the lateral equivalent of both the Kastelli Mudstone Member and the Aroania Chert Member. The general area was first described by Izart (1976) who dated a section from the Upper Triassic to Lower Cretaceous. Due to the monotony of the sequence and difficulties encountered in measuring a section, data were scanty and only one graphic log was constructed (Log C1, Appendix 1).

A description of the type-section was given in Section 2.3.4.1. The sequence is characterised by the presence of thick beds, between 50cm and 2m, of cobble grade to gravel grade breccia and conglomerate. Bedding contacts are mostly planar on the scale observed, however thick scrub makes the lateral correlation of beds difficult. The upper and lower sequence boundaries are arbitrary. The lowermost bed is above a yellow-grey dolomitic limestone bed containing large white spherical chert nodules (observed in the Drimos Formation 15km along strike). The uppermost bed is below a micrite containing a recrystallised *Globotrunca* sp. that could not be identified. The rudite is generally a sub-rounded to sub-angular, clast supported, monomict conglomerate with varying amounts of matrix material, mostly of arenite grade carbonate. Many of the clasts contain platform derived fauna, although the majority are featureless micrite.

Certain horizons contain clast-supported breccias that contain poorly sorted reefal debris (such as coral, algae, belemnites, bivalves, echinoid fragments, ooids and peloids) similar to that found in Aroania Chert Member interbeds to the E and NE (Section 4.4.2.6). These beds are massive, up to 2m thick and contain varying amounts of matrix carbonate. The beds are not graded. The only other evidence for lithologies comparable to other Lesteena Formation members is a 10cm red siliceous mudstone intercalated within a series of coarse-grained calciturbidites.

### 4.2.2 Discussion

The facies of the Kakotari Member can be recognised several kilometers to the north. Unfortunately, due to tectonic complexity and the difficulty in tracing contacts, a definite boundary for the Kakotari Member could not be established with certainty. It appears that the transition back into the Kastelli Mudstone and Aroania

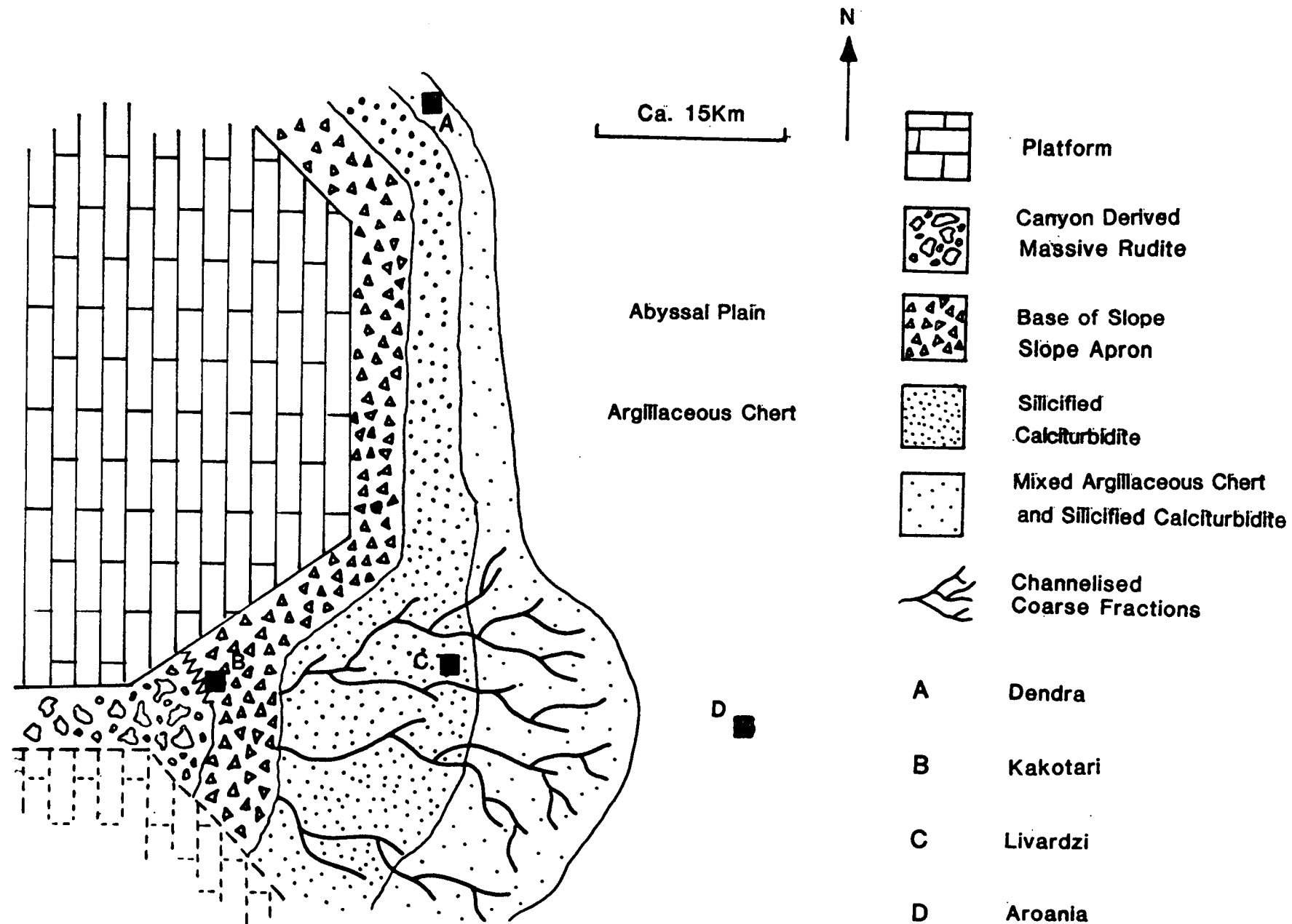


Fig. 4.2 Schematic interpretation of the depositional setting of the Kakotari Member, at Kakotari, in relation to the more outboard positions of the coeval Kastelli Mudstone and Aroania Chert Members.

Chert Members is marked either by (1) faulting, (2) a depositional transition, or (3) an original geomorphological boundary. Despite the paucity of data and the lack of lateral continuity, a tentative environmental model can be constructed.

In the thrust sheet immediately to the east of the section (Aghios Kyriaki), Izart (1976) mentions that equivalent breccias are covered by red chert. Tectonically disrupted sequences were observed in the mountains around Aghios Kyriaki, comprising interbedded breccias, coarse calciturbidite and vitreous and argillaceous red chert. Further east and north, measured sections (north of Lambia, Platanitza, Agrambela) and isolated fault bounded outcrops have channelised breccia of reefal material identical to the breccia of Kakotari, interbedded within the Aroania Chert Member.

The proximal nature of the Kakotari locality is beyond doubt. It is suggested that the outcrop represents an upper-fan environment, rich in rock fall and debris-flow material derived from the platform and upper-slope environment and transported through a submarine canyon system. A canyon point source is preferred, as the base of slope talus-apron morphology inferred for the more proximal deposits of the Drimos Formation and Erymanthos Limestone Member is not observed at Kakotari. Also, the reef provenance of many breccia clasts indicates an origin from within the platform rather than from the slope or fringing ooid shoals, as suggested for clasts in the talus apron. The slope apron areas along strike from Kakotari were covered in siliceous sediment during the Upper Jurassic while cherts are not present at Kakotari. In addition, beds are thinner and the clast-size is generally smaller than found at Kakotari. Thus, the Kakotari breccia represents either a shallower part of the basin and/or it was being supplied by a regular supply of debris from highly unstable areas transported down-slope to the Kakotari locality via a canyon. The apparent radial pattern of reef derived coarse deposits within the Aroania Chert Member indicates an extensive fan morphology for a period of the Upper Jurassic (Figure 4.2). The fact that there is no observed contact between the Kakotari Member and the Kastelli Mudstone and Aroania Chert Members further north, suggests that there may be the subtle intercalation of fan lobes, becoming more distal northwards as well as to the east. Lack of an identifiable sharp boundary suggests that high angle faulting or a canyon wall boundary is not appropriate. These, however, cannot be discounted.

Canyon systems can develop due to fault propagation at high angles to a margin. They can originate during initial rifting (Carter 1988) and remain operative from a



few, through to tens of millions of years. It is possibly significant that a large neotectonic fault has down-thrown the Olympia region immediately to the south by several hundred metres. The relevance of palaeogeographic control on compressional deformation during the Early Tertiary, and on neotectonics, is discussed in Chapter 6. Above the measured section, the Upper (?) Cretaceous is represented by conglomerate, finer grained calciturbidite and micrite.

### 4.3 KASTELLI MUDSTONE MEMBER

#### 4.3.1 Lithological Description and Diagenesis

The type section from near the village of Drimos, on the Aroania to Kalavrita road (Figure 2.1), was described in Section 2.3.4.2. At this locality the Kastelli Mudstone Member shales are seen to lie with stratigraphic continuity upon the uppermost limestones of the Drimos Formation.

##### 4.3.1.1 Facies

The succession is dominantly red-coloured mudstone (Plate 4.1) with intercalated limestones, although local variations are known. SEM analyses from several samples indicate that the mudstone is, in fact, a very fine-grained siltstone containing<sup>in</sup> clasts of up to 50µm in diameter. In the more proximal areas of Erymanthos (Figure 1.1), the Kastelli Mudstone Member is represented by a sequence consisting almost entirely of red mudstones. Individual beds are rarely greater than 5cm thick and are distinguished from one another by slight textural variations, fine chert intercalations or colour changes. A blocky or fissile texture is typically observed.

Commonly inter-bedded within the mudstones of more distal localities are thin beds of limestone, both pelagic micrites as well as siltstone to medium-arenite grade, distal calciturbidite, with occasional lutite tops. Beds are generally 3-10cm thick and contain sub-rounded allochems of micrite, recrystallised limestone, peloids and ooids, both as individual grains and as aggregates. The ooids have poorly preserved concentric structures that have undergone partial micritization (Plate 4.1). The member contains dark grey replacement chert nodules at lower stratigraphic intervals, while higher up, bedded chert horizons, up to 2-3cm thick, increase in frequency. Towards the top of the member, optical microscope examination reveals that some beds of calciturbidite have undergone almost complete dissolution of carbonate. Individual clasts are identifiable as oolites or sub-rounded limestone

clasts, but are now mostly composed of microcrystalline quartz. Within many sequences, including those studied at Dendra and Klitoria, a fragile rock composed of decalcified clasts is found. These form beds of 5-10cm thickness and have a dusty texture, they are extremely susceptible to weathering.

Both the proximal and more distal shales have locally developed green horizons that take the form of thin (less than 1cm), bedding-parallel planes following jointing. In addition, at a number of localities the coloured bands are seen to be sinuous in the horizontal plane and most probably represent the chemical reduction of sediment within burrows (*Chondrites*). This style of bioturbation is similar to that found in many of the intra-member limestones of the Aroania Chert Member.

No sediment hiatuses are visible in the member, nor are there sedimentary structures present which might be indicative of current deposition, although clay diagenesis may have obscured any primary features.

#### 4.3.1.2 Mineralogy

The mineral content of the Kastelli Mudstone Member samples was analysed by XRD. The dominant clay constituent is illite. The basal beds contain carbonate, this diminishes up-section as the mudstones become increasingly more siliceous. Hematite is present. Detrital quartz and feldspar was recognised from SEM examination, as were overgrowths of the same minerals (Plate 4.1). It was not possible to optically resolve the clay minerals.

#### 4.3.1.3 Geochemistry

Selected mudstone samples were analysed by XRF and the results are tabulated in Appendix 3. The mudstones are all siliceous with SiO<sub>2</sub> content ranging between 58% and 78%. Al<sub>2</sub>O<sub>3</sub> contents range between 8.22% and 16.39% while Fe<sub>2</sub>O<sub>3</sub> contents range between 3.27% and 7.54%. After Barratt (1981), the Fe<sub>2</sub>O<sub>3</sub> present as hematite can be approximated as an average pelagic clay has an Fe<sub>2</sub>O<sub>3</sub> contribution from detrital silicates which is reflected in the Fe<sub>2</sub>O<sub>3</sub>/Al<sub>2</sub>O<sub>3</sub> ratio of 0.38:1 (Cronan 1976). Subtraction of this ratio from the calculated ratios of Appendix 2 gives the ratio of Fe<sub>2</sub>O<sub>3</sub> from hematite to Al<sub>2</sub>O<sub>3</sub>.

CaO has higher values at the base of the Kastelli Mudstone Member, e.g. 2.65%, while immediately below the Aroania Chert Member the content is 0.47%. The

$K_2O$  is significant, between 2.6% and 6.7%, and this reflects the composition of the illite present in the samples. The  $MgO$  content varies between 1.6% to 3%.

The trace element concentrations are all fairly consistent with no unexpected values or marked peaks through the member.

#### 4.3.1.4 Diagenesis

Illite can be purely detrital but is more usually authigenic, resulting from the transformation of smectite with burial at 1-2km depth. The exact mechanism and geochemical pathway of the illite formation has not been ascertained in this study.

The hematite present in the Kastelli Mudstone Member can similarly be detrital or authigenic. Non-detrital hematite forms by dehydration-reprecipitation reactions from Fe-oxyhydroxides by way of a goethite precursor. The transition from goethite to hematite requires temperatures of 115-130°C and is therefore formed only after considerable burial. Such conditions were probably reached through overburden pressure and tectonic stacking. It is probable that some of the hematite was of terrigenous derivation as statistical analysis of illite clay rich in hematite, from the overlying Aroania Chert Member, shows a positive correlation between  $Al_2O_3$  and  $Fe_2O_3$  with a ratio in excess of that normal for pelagic clays (see geochemistry above). This suggests that both were derived from the same terrigenous source.

The mudstones are texturally homogenous despite colour variation. It is probable that the prevalent hematite imparts the characteristic red colour to the shales. Mineralogically and geochemically (e.g. Samples PD89/311-314, 536-9, 569-573), there is little apparent difference between the red, green and yellow mudstones found within the member. Green colouration in sediments has sometimes been ascribed to minute concentrations of certain minerals, e.g. chlorite and stilpnomelane (Barrett 1979, 1981). However, due to the lack of such minerals in XRD traces, the various colours are considered to reflect local REDOX conditions affecting the oxidation state of the mudstone early in the diagenetic history. Much of the early sediment diagenesis occurs close to the sediment/water interface and is driven by the degradation of organic debris (Lyle 1983), leading in turn to a colour change across the  $Fe^{2+}/Fe^{3+}$  Redox boundary. The reduced areas are not related to pore-water circulation and reduction during tectonic activity as they certainly formed prior to the development of cleavage (Plate 4.1).

In another attempt to explain the colour variation in shale, Torrent and Schwertmann (1986) postulated that the changes depend on the presence or absence of clusters of hematite crystals. They suggested that individual crystal dispersion is more likely to produce yellow and orange hues, whereas clustered hematite has different optical properties which induce red and purple hues. A further factor influencing colour may be the isomorphous substitution by Ti or Al, for Fe in the hematite crystal lattice.

Much of the SiO<sub>2</sub> in the shale has undergone diagenesis to cryptocrystalline quartz. The major source of the silica is thought to have been derived from an increase in radiolarian abundance, as reflected in the greater frequency of chert intercalations upsection. A discussion of silica diagenesis is given in Section 4.4.4 .

The dusty textured, easily weathered and fragile rock described in Section 4.3.1.1 has undergone aggressive dissolution without diagenetic replacement. The rock appears to have originally been calciturbidite and it is probable that there has been complete dissolution of the original carbonate matrix and partial decalcification of individual clasts. These beds do not contain pore filling silica and it is possible that the surrounding mudstones provided largely impermeable horizons to later, silica rich, circulating fluids. This would hinder diagenetic replacement and pore filling by quartz.

#### **4.3.2 Distribution and Depositional Environment.**

##### **4.3.2.1 Distribution**

The thickness of the Kastelli Mudstone Member is variable, from less than 5m to greater than 20m in proximal locations while the thickness is more constant at approximately 35-40m in more distal areas. Although pelagic deposition is considered the main depositional mechanism, the thickness variations are in part due to the intercalation of non-mudstone beds in distal settings. The mudstone accumulation itself, however, is in part dependant upon ponding from low velocity currents (low density turbidity currents or nepheloid currents) and/or local erosion or non-deposition. Because of these uncertainties, accurate mean sedimentation rates cannot be calculated.

Figures 4.1 & Appendix 1 (Logs D1-D6) show the geographic distribution of logged sections and the thickness changes found in the Kastelli Mudstone Member. From these diagrams it can be seen that the member is thinnest in the west, i.e. palaeogeographically closer to the Apulian margin. In addition, the member in these areas is seen to consist almost entirely of mudstones with a high illite content and little of the interbedded limestones found further east. It is important to note that the transition to argillaceous sedimentation is especially abrupt in proximal areas, the fine sediment being laid down upon coarse channelised conglomerates of the Drimos Fm.

#### 4.3.2.2 Depositional Environment

There are two possible interpretations for the depositional environment of the shales of the proximal outcrops: (a) they represent the channel abandonment of fan deposits, or (b) they reflect background sedimentation after the complete termination in clastic supply to a particular area.

The underlying calcirudite/calcarenite lithologies of the Drimos Formation are interpreted as dominantly continental rise sheet-turbidites (Section 3.3.2.2). The lithological boundary between these coarse-grained deposits and the overlying Kastelli Mudstone Member is sharply defined with a transitional zone restricted to a few metres at most. Channel abandonment successions are frequently recognized by fining-up sequences. Fan lobe switching results in channelised and over-bank deposits being found at adjacent localities for the same time interval. Additionally, overbank deposits usually have characteristics which indicate a similar provenance to the channelised material (e.g. they are composed of a similar lithology but have different grain-sizes, or they are different lithologies with a known association, such as a common metamorphic history or a shared depositional environment prior to reworking and redeposition). Apart from infrequent, thin interbeds (2-20cm) of calcarenite, the mudstones are clearly not lithologically related to the Drimos Formation calciturbidites, neither compositionally nor texturally.

A turbidity current mechanism is not considered a likely mode of deposition for the mudstones. Rupke (1975) and Piper (1978) discuss the various features which can be used to distinguish fine grained turbidites and overbank deposits from pelagic and hemipelagic deposits. The red mudstones/siltstones are unrelated to the carbonate sediments that were being produced on the adjacent Gavrovo-Tripolitza platform and it is likely that they represent wind-blown particles or terrigenous suspension particulates that accumulated continuously on the sea floor through pelagic

deposition. The member is considered to represent an interval without significant coarse clastic input.

The more distal locations exhibit the facies association of mudstones, argillaceous cherts and limestones. The mudstones are geochemically and mineralogically identical to their proximal equivalents and are likewise considered as suspension deposits or aeolian in origin. Intercalations of limestone are common in the lower part of the sequence, while an association of chert and mudstone dominates the upper part of the section. The limestones are similar in composition to those of the underlying Drimos Formation, with packstone and grainstone fabrics being produced by the distal deposition of slope and platform derived carbonates from turbidity currents. An explanation of their presence within the member is dependent upon accurate age relations with proximal localities, which cannot be obtained due to the paucity of microfauna. The shale/limestone/chert facies association of distal localities, most probably largely represents the period of time when conglomerates were being deposited adjacent to the Apulian margin to the west, prior to the thick mudstones interval. Alternatively, the complete distal sequence is coeval with the "pure" mudstone proximal facies, suggesting that calcareous debris by-passed the continental rise.

#### 4.3.3 Discussion

In this section the various factors that could account for the calcareous/siliceous transition at the end Liassic in the Pindos basin are considered. There are a number of important facts that are relevant:-

- 1) The absolute water depth of the Pindos Basin is unknown, however the transitional nature of the Kastelli Mudstone Member facies indicates that the sediment/water interface went through the critical CCD in, or around, Aalenian times. This presupposes that the position of the CCD was the main factor controlling the change from calcareous to siliceous deposition. The CCD is defined as the depth at which the rate of dissolution of calcium carbonate equals the rate of supply, and below which calcite does not accumulate (Bramlette 1961). The absolute level of the CCD is the result of dynamic equilibrium between accumulation and dissolution, influenced by three variables. These are; temperature (lower temperatures facilitate dissolution), water pressure, i.e. depth (increased pressure increases the rate of dissolution) and the chemistry of the oceanic water, particularly with respect to the

level of calcium carbonate already present in the water column. As these factors vary in different localities, it is not unexpected that absolute CCD values will vary in different basins at any given time (c.f. present-day Pacific and Atlantic CCD levels). These factors are themselves variably limited by three allocyclic controls, namely, eustatic sea level changes, biogenic productivity and tectonics.

### Eustatic Effects

Eustatic sea level changes will have an obvious affect on the position of the CCD as a multitude of inter-related factors will be affected. For example, a sea level rise will lead to a subsequent increase in pressure for any particular point in the water column, relative to a low-stand situation. This pressure increase is reflected in an absolute shallowing of the CCD, although with respect to the depth below sea level there will be no change, other things being equal. The level of the CCD rises towards the continental land mass and any sea level fluctuations, in combination with the local bathymetry, will modify the level of the CCD.

Eustatic sea level changes are induced by (a) oceanic water volume fluctuations due to glaciation, (b) ocean basin volume changes due to mid-ocean ridge activity and net changes in sediment supply, primarily through orogenesis. A number of sea level curves have been produced (Vail *et al.* 1977, Vail & Mitchum 1979, Vail & Todd 1981, Haq *et al.* 1987, 1988) although they are of debateable validity (Miall 1986, Underhill 1991). Sea level curves are cyclic on three scales which represent different periodicities:-

First-order, 200-300 m.y. cycles.

Second-order, 10-80 m.y. cycles

Third-order, 1-10 m.y. cycles.

Pitman (1979) considers that first and most second-order cycles are the result of changes in the volume of mid-ocean ridges, with estimated maximum rates of sea level change of 6.7mm/1000 years. Most third-order cycles have rates of sea level change of at least 10cm/1000 years and these are considered to result from glacio-eustatic changes. The period from the Aalenian to the resumption of carbonate deposition in the Lower Cretaceous is seen to coincide with a first order highstand (apart from a sea level fall in the Bathonian).

### Biogenic Effects

The balance between carbonate supply and extraction is critical and is largely dependant upon biogenic activity. Dissolution of calcareous sediment is possible when sea water is undersaturated with respect to carbonate. An increased supply lowers the level of the CCD until equilibrium is reached. Conversely, an increase in the degree of carbonate extraction causes a CCD rise. Increased extraction can come about through the intensification of calcareous biogenic productivity. Such an increase is likely where there is a diversification of ecological niches and where geographic dispersal facilitates an increase in population.

### Tectonic Effects

The absolute depth of the sediment/water interface below mean sea level will vary with any pronounced uplift or subsidence within a basin. This will not necessarily affect the absolute level of the CCD, only the apparent level relative to the sediment/water interface (although it may indirectly be affected as the CCD rises towards land). However, changes in the depth of a basin, whether through continental margin tectonics or due to the thermal subsidence of oceanic crust (Berger & Winterer 1974, Lancelot 1978), will leave an apparent trace in the geological record which might be interpreted as a fluctuating CCD.

The circulation of cold water bottom currents will alter with time as the configuration of continental masses change due to continental drift. De Wever & Thiebault (1981) postulated the progressive development of a southerly oceanic current into Tethyan domains during the Upper Jurassic. They believe such an equatorial water mass mixed with boreal currents and had the effect of increasing the upwelling of oxygenated water. Bottom currents, from depth and/or high latitudes, are generally nutrient rich cold waters that upwell and encourage high phytoplankton productivity with a subsequent increase in radiolarian productivity. Thus siliceous sediment may become the dominant form of pelagic deposit if the effects of tectonic activity and biogenic activity are combined.

A number of authors have attempted to define the palaeodepth of the CCD for various times at various locations (Van Andel *et al.* 1977, Berger & Winterer 1974). The Pindos basin was at sub-tropical latitudes (0 to 30°N) throughout most of the Mesozoic (Dewey *et al.* 1973, Robertson & Dixon 1984, Dercourt *et al.* 1986) and the estimated depth for the Neotethyan CCD during Oxfordian-Kimmeridgian times



is variably given as 2 to 2.5km (Hsu 1976, Bosellini & Winterer 1975, Winterer & Bosellini 1981).

2) The development of Late Jurassic cherts, although diachronous, is a common occurrence in the deeper water Tethys (e.g. Ligurian Alps, Lagonegro basin, Austrian Alps, Baer Bassit, Hawasina, Marmouonia, Antalya [De Wever 1989]). Any controlling factors must have been widespread, if not global. Radiolarian productivity undoubtedly increased throughout the Middle to Upper Jurassic in the Tethyan realm.

3) Reworked carbonates are scarce and this implies either that normal supply routes had been cut-off, either through flooding or the establishment of a physical barrier, or that the source area itself was no longer productive. However, on the Gavrovo-Tripolitza platform, carbonate sedimentation was continuous throughout the Mesozoic (Section 7.3.1).

There is no obvious mechanism to prevent the transport of fine-grained calcareous sediment away from the Apulian shelf, which was certainly productive at this time, over an extended period of time as represented by the depositional interval of the Kastelli Mudstone Member. Nor is there evidence for large scale coarse-grained sediment trapping. Consequently, the diminished supply of fine-grained carbonate is attributed to the shallowing of the CCD while a decrease in the volume of calciturbidite deposits and the increasingly siliceous nature of the member through time suggests a contemporaneous reduction in off-margin redeposition.

#### 4.3.4 Summary

The Aalenian calcareous/siliceous transition was caused by the termination of coarse clastic sediment supply, coupled with a shallowing of the CCD due partly to a gradual increase in biogenically supplied silica. Furthermore, a sea level rise is proposed to account for the reduction in fine- and coarse-grained carbonate sedimentation, as observed in the Pindos Basin, as both the supply of coarse sediment and the level of the CCD are affected.

During a (sea level) highstand the strandline recedes inland, as does the locus of coarse grained clastic sediment deposition. Upper slope areas may subside below storm wave base and thus a major influence on the initiation of gravitational slumps,

slides and debris flows is negated. Furthermore, in the event of a sea level rise previous land areas are transgressed and become the sites for colonisation by neritic organisms. Additionally, in tropical epeiric seas prolific planktonic blooms may occur, resulting in the extraction of copious amounts of calcium carbonate from seawater. Successful siliceous pelagic organisms are better able to extract nutrients and may exploit niches to the exclusion of calcareous biota (De Wever 1989). In the pelagic realm this would result in a decrease in the dilutant effects of carbonate producing plankton, while the CCD would rise due to the net extraction of calcium carbonate from sea water by neritic organisms. Any postulated sea level rise cannot have drowned the Gavrovo-Tripolitza platform.

Although it is not proved that there was tectonic activity within the Pindos Basin at the end of the Liassic, there may have been some subsidence related to the vigorous Liassic deepening of the Ionian trough (Underhill 1985, Clews 1989) and the Pelagonian Zone platform collapse seen in the Argolis peninsula (Clift & Robertson 1990). Thus local tectonics may also have been a factor in the relative rise of the CCD, although an increase in sediment transport from uplifted fault blocks would be expected, this is not observed.

#### **4.4 AROANIA CHERT MEMBER**

##### **4.4.1 Introduction**

The Aroania Chert Member consists almost entirely of radiolarian-bearing argillaceous cherts, vitreous cherts and siliceous mudstones. In addition, there is a mid-member pink bioturbated micrite present in proximal locations, while channelised conglomerates and breccias of reef derived material are found at Kryovrissi, Platanitza and Livardzi. In this section, the member is sub-divided into the various facies identified. Lithological and petrographic descriptions are provided, along with facies distributions and interpretations of the environment of deposition. A brief discussion on silica diagenesis is also included. Study of manganese-enriched cherts includes geochemical and mineralogical analysis, which leads to the conclusion that manganese concentration is primarily derived from hydrothermal exhalations.

#### 4.4.2 Lithological Description

The cherts of the Aroania Chert Member are siliceous rocks, largely devoid of carbonate and containing a restricted range of faunal debris, comprising radiolarians and scarce sponge spicules. The cherts are regarded as deep sea pelagic sediments, deposited below the CCD primarily from biogenic precursors (Wise & Weaver 1974, Robertson 1977, Jenkyns & Winterer 1982). Several chert facies have been recognised within the Aroania Chert Member. Some of the facies characteristics are local in nature, although it is possible to correlate others over large distances. The following descriptions are based on field observation and thin-section examination.

##### 4.4.2.1 Facies 1: Green Chert

The green chert facies is a distinct interval present at the base of most of the more proximal outcrops. It consists of regularly bedded, pale green, "vitreous" siliceous sediment. A relict granular texture is identified in hand-specimen based on the faint presence of arenite-grade particles. In thin-section these particles consist of microcrystalline and cryptocrystalline quartz, as does the matrix. Thus clast/matrix boundaries are difficult to recognise in thin-section. Bedding thicknesses range from 2 to 20cm with individual beds often traceable for several metres before gradually pinching out. Bedding contacts usually appear irregular, but are essentially planar. Although some radiolarian "ghosts" have been observed, these are not abundant. In hand-specimen the cherts have a hackly/conchoidal fracture. Long intervals have been measured and consist almost entirely of vitreous green chert with very minor green shale intercalations. Black, thinly-bedded cherts are present infrequently within the green chert facies. At many localities (e.g. Dendra & Erymanthos) small-scale, planar- and cross-lamination were clearly observed. At Tripotama and Platanitza (Figure 1.1), inter-bedded, 20-40cm-thick beds of silicified coarse-grained calciturbidites are preserved within the green chert facies (Plate 4.2). A laminated white chalcedonic quartz, parallel to bedding, is present in some green chert beds. The chalcedony is of the non-orientated fibrous variety. This white replacement chert is a relatively early diagenetic (possibly compaction related) manifestation as it is cut by later quartz veins, themselves cut by ubiquitous calcite veining.

##### 4.4.2.2 Facies 2: Vitreous Red Chert

The over all texture of this facies is similar to that of the green chert facies, although relict allochems are not observed. The vitreous red cherts have a brittle, conchoidal fracture and in thin section are seen to consist of crypto- and microcrystalline quartz. Distinct laminations are not observed and there are few radiolarian pseudomorphs

present. Vitreous red cherts are volumetrically important, but subordinate to, and found within, the more typical argillaceous cherts (facies 3) of the member. Bed thicknesses of 2 to 25cm are typical, although they are generally less than 10cm. One characteristic that has been described from Tethyan cherts of a similar age from other areas (Jenkyns 1974) is variously described as a "pinch and swell" or "knobbly" aspect. This results from undulose bedding surfaces that cause the attenuation or thickening of individual beds over very small distances. For example, one bed was found to thicken and thin from 4cm to 42cm to 4cm over 1.2 metres. These pinch and swell-type cherts always have siliceous mudstone intercalations that thicken where the bulbous chert is thinning. The fissility of the shale is less intense in the thinned chert areas giving the impression that compaction effects were more pronounced where the nodule is thickest.

#### 4.4.2.3 Facies 3: Argillaceous Chert

This is the dominant facies of the member. It is recognised in the field by an earthy texture, and although the rock is very hard and dense, it is less brittle than the vitreous cherts. The beds range in colour from salmon pink to red-brown. Bedding is generally in the range 2-10 cm and is often separated by thin siliceous mudstone partings, leading to rhythmic interlayering (Plate 4.2). Furthermore, the cherts are found in packages within which beds have similar textural, thickness and colour characteristics. Such packages can vary from less than 1m in thickness to greater than 20m. In the field most beds appear featureless, sedimentary structures being restricted to vague bedding-parallel laminations. In many hand specimens individual radiolarians are visible with a hand lens. In thin section these radiolarian-rich samples display a wackestone/packstone texture. Radiolarians in other samples are less abundant. Generally, there is little difference in microfossil concentration through an individual bed, however some samples show a micro-lamination which is recognized by the normal grading of radiolarian tests, a feature suggestive of current influence.

The chert groundmass is cryptocrystalline quartz. Radiolarian preservation is generally poor due to recrystallization, although radiolarian outlines are still distinct. Ornamentation (e.g. spines and pore structures) is often missing or obscured due to breakage, pressure solution and diagenesis. Most commonly, individual radiolarian moulds are composed of microcrystalline quartz. Some, however, have microcrystalline borders with length-fast chalcedonic cores (Plate 4.2). Some radiolarian tests examined in thin-section have carbonate overgrowths, whilst the

groundmass itself is unaffected. In some specimens the radiolarians are round, attesting to early cementation, while in others they are oblate with long axis parallel to bedding (Plate 4.2) indicating that compaction has variably affected the radiolarian-bearing lithologies.

Mixed iron oxide and clay seams are seen in thin-section (Plate 4.2). These represent insoluble residues resulting from pressure solution. These pressure solution seams are not stylolitic because the matrix is relatively incompetent. Rather they are anastomosing, wavy or parallel, with seams developing and terminating in unstrained areas. Baltuck (1983) stated that many chert samples, from the equivalent formation, were found north of the Gulf of Corinth with seams perpendicular to bedding. These, she suggests, were formed during Alpine tectonism. This observation is not confirmed in the NW Peloponnese, where the seams are parallel to bedding and appear to be solely related to vertical load-induced stresses.

#### 4.4.2.4 Facies 4: Manganiferous Chert

Manganiferous cherts are found at two main stratigraphic intervals near the top of the member. Individual beds have similar characteristics to the argillaceous chert facies apart from their Mn-enrichment. This facies is considered in greater detail in Section 4.5

#### 4.4.2.5 Facies 5: Siliceous Mudstone

The siliceous mudstone facies generally has a weak fissility and is coloured orange to brown, but more usually dark red. The most common occurrence of this facies is as thin partings, less than 1cm thick, between argillaceous chert beds. The facies does, however, attain thicknesses in excess of 20cm in many locations. The mudstone contains 65-81% SiO<sub>2</sub>, as quartz. The remainder of the sample is represented by Al<sub>2</sub>O<sub>3</sub>, Fe<sub>2</sub>O<sub>3</sub>, K<sub>2</sub>O and MgO derived from the clay mineral illite, minor hematite and albite. The mineralogy is broadly similar to that of the Kastelli Mudstone Member. In addition, trace quantities of several other minerals have been recorded. Chlorite is recorded from siliceous mudstones near the top of the formation, as is birnessite (a manganese oxide), sericite, paragonite, nontronite and muscovite.

#### 4.4.2.6 Associated Facies: Limestones and Reef Derived Rudite

In the most proximal outcrops, a limestone interval of variable thickness is found within the Aroania Chert Member. This is pink micrite, up to 16m thick, which in

places has undergone partial silicification leading to the development of red-brown replacement chert nodules. At the base, micrite beds are uniform and approximately 1cm thick, passing up into 5-10cm-thick beds of pink bioturbated micrite (Plate 4.2), with thin interbeds of red chert. Stylolitic pressure solution is prevalent. On Erymanthos Mountain the limestone interval is only 3m thick, appearing as a pink fine-grained calcarenite, rather than micrite, and this is channelled into the underlying chert. Laterally there are matrix-supported, pink pebble-grade conglomerates that are channelled and up to 8m thick.

The above limestone deposits are distinct from the clast-supported channelised limestone breccias of reefal material which are also found within the Aroania Chert Member. The breccias are rich in reefal material and have bed thicknesses between 1.5 and 4m, as seen at Agrambela (Log E6) and Livardzi (Log E8b). The clasts are partially recrystallised, sub-angular limestone measuring up to 3cm x 5cm. Angular red mudstone rip-up clasts and elongate, rounded red chert clasts up to 5cm x 9cm are also present. There is slight grading present. Coral polyps, bivalve fragments and belemnites have been observed. Also at Agrambela, pink, matrix-supported conglomerates were observed above the reefal breccias. Clasts within this conglomerate are micritic and identical to those seen on Erymanthos.

#### 4.4.2.7 Geochemistry

Whole rock geochemical analysis and the X-ray diffraction examination of typical (non-metalliferous) radiolarian cherts was undertaken for three argillaceous chert samples only (samples PD/88/53, PD/89/309 & 481). These typical chert components of the Aroania Chert Member have SiO<sub>2</sub> contents greater than 90%, while other oxides, dominated by CaO and Fe<sub>2</sub>O<sub>3</sub>, comprise less than 1% by weight. Siliceous mudstones from within the member have also been analysed by XRF and these results are given in Appendix 3. For a thorough account of the mineralogy and geochemistry of similar Jurassic radiolarian cherts (of Liguria, Italy) the reader is referred to Barrett (1979, 1981).

### **4.4.3 Distribution and Depositional Environments**

#### 4.4.3.1 Distribution

There is clearly a great deal of variability within the Aroania Chert Member. This is expressed in the total member thickness, individual facies thicknesses, facies

distribution and facies associations. The logs of Appendix 1 (Logs E1-E10) illustrate the lithological variability of the member and the distribution is consistent with the contention that the Pindos Zone of the Peloponnese represents a basin which extended distally eastwards. For example, the breccia deposits found within the Aroania Chert Member occur at a similar stratigraphic interval and can, therefore, be correlated across the proximal part of the basin, although they thin drastically towards the east and are not found east of Drimos. Each of the facies identified within the member suggests a differing depositional environment. The generally non-calcareous nature of the chert facies indicates deposition below the CCD throughout the basin.

#### 4.4.3.2 Depositional Environment

**Facies 1:** Green chert. This shows features such as relict carbonate allochems, parallel and trough-cross lamination and a close association with partially silicified coarse grained, thick-bedded calciturbidites. The facies is thickest in the west and thins eastwards, both in mean bed thickness and in overall facies thickness. The green cherts are interpreted as calciturbidite beds that have undergone carbonate dissolution and subsequent silicification. This is in agreement with Green (1982) who drew the same conclusion for green vitreous cherts north of the Gulf of Corinth. The beds are considered to have originally been similar to the thin calciturbidites of the upper Drimos Formation and also to the Kastelli Mudstone Member calciturbidites which have undergone carbonate dissolution, but not pervasive silicification. The dominant green colour probably reflects Redox conditions early in the depositional history, possibly due to reducing organic material derived from the platform.

**Facies 2:** Vitreous red chert. These have very few diagnostic features and are lacking in sedimentary structures indicative of current deposition. Preserved radiolarians are sparse, but silicification is intense. This facies perhaps represents periods when sedimentation consisted mainly of pelagic biogenic debris, with minor clay deposition. Radiolarian blooms could provide sediment relatively undiluted by clays, which upon burial would provide abundant free silica at certain horizons (Section 4.4.4). The facies is found throughout the study area above the green cherts and within the argillaceous chert facies, but is otherwise impossible to correlate from section to section.

**Facies 3:** Argillaceous chert. This facies is rich in siliceous microfossils and clay. Certain features, such as vague parallel laminations and the weak grading of radiolarian tests, suggest that there may have been limited reworking of a radiolarian rich sediment by nepheloid currents or redeposition from very weak turbidity currents. There are, however, no structures such as flute and load casts, convolute bedding or cross lamination, which are found at some other chert localities (e.g. Othris), and which are interpreted to indicate radiolarian deposition by turbidity currents (Nisbet & Price 1974, Price 1977, Barrett 1981). Furthermore, Folk & McBride (1978) found a correlation in the thicknesses of shale partings and the underlying beds of chert in the Ligurian Alps. This they interpreted as providing evidence that bedded cherts were deposited from turbidity currents. There is no such correlation observed in any of the measured sections from the Pindos Zone of the NW Peloponnese. Iijima *et al.* (1978) similarly found no shale/chert correlation in Triassic cherts of Japan, and suggested that radiolarian supply was constant while muds were deposited from fluctuating currents. A turbidity current mechanism cannot be proved nor disproved for the Pindos cherts, however, a simpler explanation would be the periodic deposition of radiolarian tests from blooms with more or less constant background quantities of clay and possibly rare, weak, current reworking. This periodicity is considered further in Section 4.4.7.

**Facies 4:** The manganiferous cherts are described in Section 4.5, where it is concluded that they indicate contemporaneous hydrothermal and volcanic activity that may have exploited reactivated continental margin faults. It is notable that the Upper Jurassic depositional environment locally included a volcanic substratum, as exposed at Kombigadi, Ano Vlasia and Aroania.

**Facies 5:** Siliceous mudstone. This is the consistent background facies throughout the Lesteena Formation. Illite is the major clay component, with minor quantities of the associated muscovite clay group minerals, sericite and paragonite. These are believed to be terrigenous (Baltuck 1982). Nontronite is a Fe-rich volcanogenic clay identified within a siliceous mudstone interval and its deposition was probably coeval with the volcanism seen in other areas. Chlorite was probably derived from the seafloor weathering of basalts as there is no correlation between the presence of chlorite and illite; also, detrital chlorite is found almost exclusively in non-tropical climates (Lisitzyn 1972). Similarly, birnessite occurring in the same stratigraphic interval as the chlorite may be related to a volcanic episode as a result of hydrothermal exhalations.



## Radiolarite Depositional Model

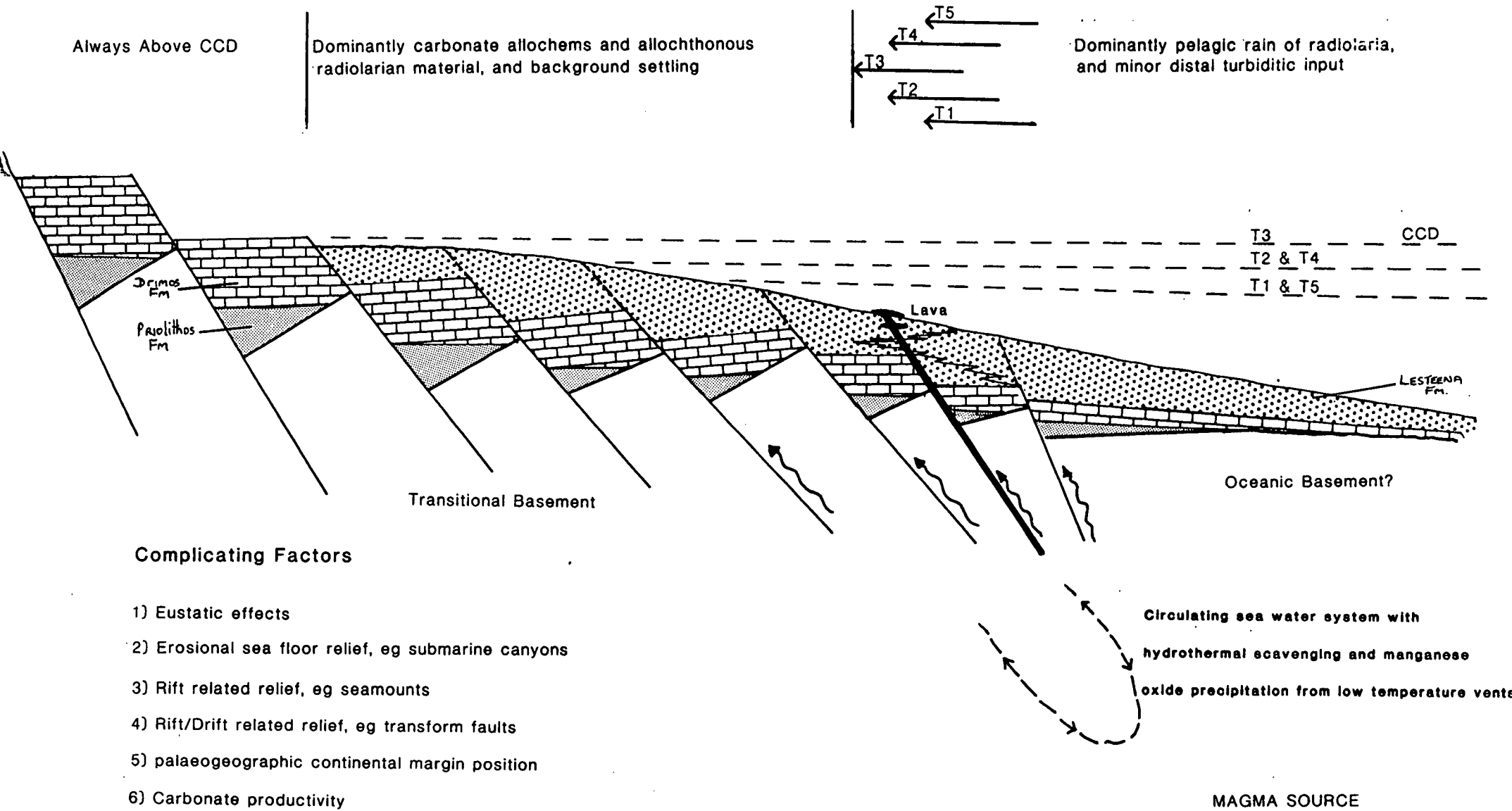


Fig. 4.3 Depositional model for the radiolarian rich cherts of the Aroania Chert Member. Explanation in text.

Of the additional facies, reef derived rudite has close similarities to the dominant facies of the contemporaneous Kakotari Member. The beds are channelised and thin towards the east. It is suggested that they represent deposits derived from a point source located near Kakotari, as described in Section 4.2. The pink micrites are found only in the most proximal outcrops. They are bioturbated and of a variable thickness. The restricted setting of these deposits in the west of the study area suggests that the CCD was lowered during the limestone interval and allowed the deposition of fine-grained limestones on the continental rise and lower slope. In addition, the existence of intra-formational monomict conglomerates suggests slope instability. A tentative explanation might involve a sealevel fall (Bathonian/Callovian ?) leading to the redeposition of slope carbonate, followed by the deposition of micrite limestones in more proximal areas, above the contemporary CCD.

Lateral thickness changes are a feature of the Aroania Chert Member stratigraphic interval. It is envisaged that there was local ponding of sediment in depressions on the sea floor, with winnowing and transport off local highs. Although there is channelisation of the inter-member rudites due to high energy transport, this is not true for the thickness changes of the Aroania Chert Member as a whole.

A radiolarite depositional model is shown on Figure 4.3 illustrating the diachronous inboard establishment of chert facies from time intervals T1 to T3 as the CCD is raised. This also affects the chertification of calciturbidite deposits closer to the slope and rise in the lower parts of proximal Aroania Chert Member logs. Areas permanently above the CCD (Kakotari?) have no significant siliceous sedimentation and the process is reversed from T3 to T5 as the CCD is lowered.

#### 4.4.4 Silica Diagenesis

The transformation of newly deposited siliceous sediment to dense chert has been extensively described in the literature and, as no new work has been attempted here, currently accepted views are presented.

It is widely recognized that much of the quartz within chert was derived from biogenic precursors (Garrison 1974, Wise & Weaver 1974, Folk & McBride 1978, Iijima *et al.* 1983). In the Mesozoic, radiolarians (zooplankton) were the primary producers of silica, while in the Tertiary they have been overtaken in volume by

diatoms (phytoplankton). Such siliceous micro-organisms precipitate amorphous silica (opal-A) in the formation of tests and frustules. Upon death, the skeletal material falls through the water column to accumulate on the sea floor. There then follows a diagenetic sequence of events, the rate of which depends upon temperature, host sediment composition and time. Initially a precipitate of inorganic amorphous silica (Opal-A') can form on the tests (Hein *et al.* 1978). Further solution-precipitation reactions follow, the kinetics of which have been studied by Kastner & Gieskes (1983), leading to the formation of Opal-CT (disordered cristobalite and tridymite). This can occur relatively soon after burial with overburden thicknesses of a few hundred metres and temperatures of 35-50°C (Muratta *et al.* 1977). XRD has revealed that the lattice ordering of Opal-CT increases with increasing diagenesis as the  $d[101]$ -spacing decreases from 4.11 to 4.04 Å (Muratta & Larson 1975). Further solution followed by recrystallisation results in the formation of less soluble quartz and chalcedonic quartz as described by Robertson (1977). Siever (1983) considers the likely burial/time conditions necessary for silica transformations within different tectonic settings. The Pindos Basin geothermal gradient is not known, but Jurassic volcanic activity may well have accentuated any burial effects. It is certain that the Pindos chert formed prior to Alpine orogenesis as deformational structures and late stage veining appear to post-date the development of the brittle cherts. The observed shale textures associated with the "pinch and swell" of the vitreous chert facies possibly indicate that silicification was a relatively early process that accompanied compaction from overlying strata, leading to the pseudo-boudinage of semi-lithified, pure siliceous sediment within more argillaceous horizons. X-ray analysis and petrography of the Pindos Zone cherts and siliceous mudstones have shown that chalcedonic quartz, cryptocrystalline and microcrystalline quartz are the only silica phases present.

The different degrees of silicification found in the siliceous mudstone, vitreous and argillaceous chert facies most probably reflect the relative concentrations of the original sedimentary components. It is proposed here that the mobilisation of silica phases is the principle consideration and that this depends on the initial ratio of silica and clay present. It was observed that there are few preserved radiolarians in the vitreous cherts. This may reflect the degree of diagenetic alteration and the "purity" (i.e. low level of clay present) of the sediment rather than being indicative of the original faunal abundance within the rock. This hypothesis is supported by the observation that the preservation of radiolarian test ornamentation appears to be better where more clay is present in samples within the argillaceous chert facies.

This may be interpreted as indicating that the mobilisation of silica is in some way inhibited where clays are present, as documented by Robertson (1977).

Williams *et al.* (1985) state that silica solubility and diagenetic pathways vary with surface free energy and surface area. Where clay concentration is low, as in the proposed packstone/wackestone texture of a radiolarian rich calciturbidite or a radiolarian-rich "pure" pelagic sediment, the open fabric and high porosity due to grain-to-grain tangential contacts would provide large surface areas and ready conduits for silica mobility. In addition, Williams & Crerar (1985) have shown that clays are able to incorporate silica from solution with a ratio dependent on the surface area of the adsorbing solid. Thus, the presence of clay can reduce the amount of free silica available in a system as well as impeding pore fluid movement.

It is concluded that in a clay-free horizon, silica transformations through solution/reprecipitation reactions are accompanied by greater solute movement, leading to a decrease in the preservation of original features such as radiolarian tests and ornament. This postulate could be tested by further sampling and geochemical enquiry.

#### 4.4.5 Ancient Comparisons

There are many Mesozoic Tethyan areas which contain siliceous formations similar to the Pindos Zone cherts. Geographically they range from the Sub-Betics of Spain (Ruiz-Ortiz *et al.* 1989) to Japan (Iijima & Utada 1983), and span Permian to Cretaceous times. Specifically within the eastern Mediterranean region, well studied series include the Hawasina nappes of Oman (Cooper 1986), the Turkish Antalya Nappes (Poisson 1977, Robertson & Woodcock 1981), Upper Jurassic cherts of Ligurian Apennines, Italy (Folk & McBride 1978, Barrett 1979, 1981), the Austrian Alps (Vecsei *et al.* 1989), the Othris Zone of Greece (Nisbett & Price 1974, Price 1977) and Upper Cretaceous to Lower Tertiary cherts of the Troodos Massif, Cyprus (Robertson 1977).

#### 4.4.6 Modern Comparisons

The maximum width of the Pindos Basin cannot be ascertained due to two periods of crustal subduction. Structural restoration of the Pindos sediments suggests a post-Jurassic width of 300km (Section 6.3.7). Some authors prefer comparisons of onland

regions containing radiolarian chert facies with narrow basins, as they tend to have shallower CCDs and are characterised by high planktonic productivity, e.g. Steinberg *et al.* (1977) compared the chemical compositions of recent North Pacific and Sea of Japan siliceous sediments with Jurassic Tethyan Cherts. They concluded that the Sea of Japan (DSDP sites 303 & 304) approximated the palaeoceanographic conditions likely in Tethyan Jurassic domains. Hein & Karl (1983) studied cores from DSDP legs 62 (Hess Rise, Pacific) and 69 (Costa Rica Rift). They compared samples which were obtained from open ocean and continental margin environments, with on-land specimens. They concluded that ribbon bedded cherts of orogenic belts are not comparable with cherts formed in open ocean settings but suggested deposition along rifted continental margins, silled basins and back arc basins. Present day analogues of the Pindos Basin are most probably represented by deep, relatively narrow oceanic basins such as the Gulf of California (DSDP site 480).

#### 4.4.7 Discussion

The rhythmically interbedded nature of facies 3 (argillaceous chert) and facies 5 (siliceous shale) has often been debated in the literature. McBride & Folk (1979) and Cooper (1986) list four main hypotheses to account for the regularly interbedded sediment. These are:-

- a) The diagenetic development of alternating siliceous mudstone and chert horizons from an originally homogenous radiolarian rich clay.
- b) Punctuated periods of ubiquitous radiolarian fauna (blooms), superimposed on background clay deposits.
- c) Periodic turbidity currents containing radiolarian-rich silt, superimposed on background clay deposits.
- d) Periodic clay sedimentation from currents, with background radiolarian deposition.

Although it is generally accepted that diagenesis plays a role in the development of chert/shale couplets, the significance attached to diagenesis is debatable. Siliceous ooze has an initial porosity of at least 70-80% prior to compaction (Steinberg *et al.* 1983). Silica solution due to overburden pressure may be accompanied by pore fluid movements prior to reprecipitation and cementation. Such fluid movement could lead to silica segregation in planes parallel to bedding and be accompanied by the

migration of other elements. Davis (1918) first proposed this mechanism, but later authors have shown that chert/shale interbeds were deposited separately, with a gradual non-diagenetic variation in elemental concentrations across bedding (Steinberg *et al.* 1983, Baltuck 1983).

This study suggests that the chert/shale layering is primarily dependent upon pelagic sedimentation with a periodic increase in radiolarian productivity, rather than being caused by diagenesis. It is therefore necessary to account for the cyclical nature of such radiolarian enriched horizons. De Wever (1987) has suggested that Milankovitch cyclicity could control the periodic proliferation of siliceous plankton. He has measured a 60m thick radiolarite section at Karpension, north of the Gulf of Corinth, which has been dated from Bajocian to Tithonian times, a period of approximately 32 million years, giving an average sedimentation rate of 1.875cm/1000y. Bed thicknesses average 4cm and lithological boundaries correspond to 1500 bed alternations of shale and chert. De Wever states that this conforms to a 21,000 year periodicity, which is in accord with the second order precessional climatic cycle of Milankovitch (1941).

The thickness of the radiolarian chert sequence varies widely in the NW Peloponnese. As stated previously, this probably corresponds to local sediment ponding and transport off local highs. Due to such variability and the lack of accurate biostratigraphic control, the Milankovitch theory cannot be tested for this area. Such a climatic control does appear to provide a feasible solution to the shale/chert interbed quandary and has been cited as causing the alternation of sedimentary cycles in other Tethyan pelagic deposits (Schwarzacher & Fischer 1982, De Boer & Wonders 1984).

While reasons were given in section 4.3.3 to account for the onset of siliceous sedimentation within the Pindos Basin, the decline in radiolarian-rich deposits will be considered here. The possible controls essentially fall into three categories, each of which would cause a fall in the level of the CCD:-

#### 1) A change in oceanic circulation.

De Wever *et al.* (1986) and De Wever (1989) state that there was a synchronous decline in radiolarian deposits throughout the Tethyan realm. There are exceptions to this, e.g. Oman, but generally radiolarians were at their acme during the Oxfordian and were finished as major sediment producers by Tithonian times.

Palaeogeographical reconstructions (Smith 1971, Dercourt *et al.* 1986) picture a westward narrowing Tethys which, by the Upper Jurassic, had connected with the Central Atlantic. Pindell (1985) provides evidence for a connection through to the Pacific between the Yucatan block and Mexico during the Tithonian or Berriasian. An equatorial latitudinal current is therefore envisaged which from the Lower Cretaceous drastically affected sedimentation by decreasing radiolarian productivity due to reduced upwelling in the Tethys.

### 2) An increase in calcareous nannoplankton.

There was a well established increase in calcareous nannofossils, primarily coccoliths, in the Early Cretaceous which accompanied the world-wide fall in the CCD (Bosellini & Winterer 1975).

### 3) A sea level fall

There are two observations in the Pindos Zone that cannot be accounted for by the two previous hypotheses. Firstly, there is a synchronous change in the grain-size as well as type of sediment recorded after the Aroania Chert Member. The overlying Paos Limestone and Erymanthos Limestone Members are rich in coarse-grained arenite-rudite grade carbonate in proximal areas. This must be a response to an influence other than a simple change in bioproductivity. Secondly, radiolarian deposition continued through to the Upper Cretaceous, not only in Oman and Turkey but also in the Pindos Zone of the southern Peloponnese (Thiebault 1982, Jones *et al.* in press). De Wever (1989) suggests that such areas may have existed as isolated sub-basins.

Although the global sea level trend indicates a sea level rise for the Cretaceous, there is a Neocomian low stand (Haq *et al.* 1988). Furthermore, there is evidence (Section 4.5.6) that local tectonics may have led to renewed extensional tectonics in the Pindos Basin during the Upper Jurassic, as shown by volcanism and syn-sedimentary deformation. Such Late Jurassic tectonic activity is widespread throughout the continental margins of Tethys (Robertson & Boyle 1983). The Lower Cretaceous style of sedimentation supports the idea of continental margin instability in the Pindos Basin and margin flanks may have been uplifted, leading to a localised relative sea level fall. Several reasons to account for the Late Jurassic activity recorded within Tethyan basins are possible, they include the following:-

- 1) There was widespread ophiolite obduction along Tethyan margins at this time. In the Pindos basin, the preferred tectonic model for ophiolite obduction involves supra-subduction zone spreading above an oceanic slab subducting with a westward polarity (Jones 1990, Jones & Robertson 1991, Robertson *et al.* 1991): In Late Jurassic times oceanic crust of Pindos Ocean origin was emplaced onto the subsided Pelagonian micro-continent. Sub-aerial erosion caused backshedding of sediment into the Pindos basin (AHF Robertson & PJ Degnan, unpublished data) which had remained open. There is no petrographic evidence that ophiolitic detritus contributed to the sediments preserved in the Pindos Zone of the NW Peloponnese. Sandstones are devoid of ophiolite debris (Section 5.2.2) although Thiebault & Fleury (1991) state that there is mineralogical evidence for ophiolite derived clay in the Pindos Zone Upper Jurassic and Cretaceous shales. There is no recorded volcanic arc development along the Apulian margin, but extensional back-arc basin stresses may have been set-up above a Benioff zone.
- 2) The opening of Mesogea and the Central Atlantic involved a major reorganisation of tectonic plates. Locally there may have been transtensional/transpressive strain above already severely weakened transitional crust.
- 3) Mantle plumes, i.e. hot spots, may have become established in certain areas. This is not considered likely, given the evidence that only limited areas were affected.

#### 4.4.8 Summary

The Aroania Chert Member is of variable thickness and lithologies record a distinct proximal-distal relationship. The silicification of calciturbidites is apparent at the base of the sequence in proximal localities, passing-up into regularly-bedded ribbon radiolarite with a thin inter-member limestone horizon. More distal localities are composed almost entirely of featureless argillaceous cherts that were deposited by the gradual accumulation of siliceous microfossils and clay below the CCD. Just as there was a degree of interdependence between factors contributing to the transition to siliceous sedimentation (Section 4.3.3), viz. eustatic and biogenic effects; the transition back to calcareous sedimentation was probably caused by several factors in combination, most importantly the ascendancy of calcareous nannofossils and the corresponding decline in the dominance of radiolarians. This may have been caused by a change in global oceanic circulation patterns. In addition, there was a possible eustatic sea level fall and increased tectonic activity along continental margins (Robertson & Boyle 1983), potentially causing renewed basin subsidence and flank uplift, resulting in the resumption of coarse-grained and terrigenous sedimentation in several basins.



## 4.5 MANGANESE ENRICHMENT OF THE AROANIA CHERT MEMBER

### 4.5.1 Introduction

Substantial manganese (Mn) enrichment occurs primarily near the top of measured sections within the Aroania Chert Member (Appendix 1, Logs E1-E10). Mn is also present to a lesser degree throughout the formation. Field observations have been combined with petrological and geochemical techniques to determine the possible origins of this enrichment.

Two types of Mn enrichment have been identified in the field. The following section largely concentrates on the likely paragenesis of sedimentary hosted ores, which are characterised by the concentration of Mn in distinct sedimentary layers, parallel to bedding, either as lenses, or as continuous horizons. In such occurrences the Mn characteristically imparts a distinctive black colour to the chert. In extremely concentrated intervals a metallic lustre is observed on fresh surfaces. Mn concentrations in analysed samples vary from 1.56% to 69.54%. Sedimentary rocks with the above characteristics are considered as ore grade lithologies. In the study area two mines (at Aroania and Drimos) produced economic quantities of ore up to the late 1950's (Galanopolous 1982).

The second occurrence of chert, with only minor enrichment in Mn, is commonly observed and is characterised by patchy areas of Mn oxides. These are irregularly distributed, diffuse disseminations that tarnish the rock but do not obscure the principal colour of the host chert. Generally the dissemination is irregular and discordant with respect to individual chert beds. There are also fracture surfaces covered by Mn oxide crystals with a radiating acicular habit (pyrolusite, Plate 4.6) developed at an angle to bedding. Both types of enrichment are clearly of a secondary origin and are considered to be exclusively related to the diagenetic remobilisation of Mn mineral phases.

### 4.5.2 Field Relations

Ore grade horizons of manganiferous chert have been found at a number of localities. In several cases, the lithostratigraphic position of analysed manganiferous chert is known from measured sections. Other samples have been taken for geochemical analysis where the exact stratigraphic position is not known. A locality

index is provided for all the analysed samples compiled in Appendix 4. Manganiferous ores from the Aroania mine are especially important and interesting. A geological map of the area and graphic log are shown in Figure 4.4 . The outcrop is fault bounded, the sequence forming an imbricate slice in the hangingwall to a major thrust which places Drimos Formation limestone over Pindos Flysch Formation deposits. The chert and manganiferous sediments are dated as Upper Jurassic (G. Rose pers. comm. 1992) based on several diagnostic radiolarian species (Plate 4.3). The outcrop cannot be traced laterally for more than 20m in any direction. The outcrop appears to be a fault bounded horse of Upper Jurassic sediment imbricated between Tertiary and Triassic sediments along a major decollement. The Aroania locality cannot be restored palinspastically due to its unique structural position.

The base of the sequence is represented by lapilli-tuff with rounded blocks of basaltic rock and volcanoclastic breccia. The geochemical affinity of this igneous rock is analogous to the volcanic specimens of the tectono-sedimentary melange (TSM) and this is described in detail in Chapter 8. In places, the pyroclastic material is well cemented and forms upstanding columnar structures (Plate 4.6). Thin-section examination (Plate 4.6) indicates that the rock originally contained some carbonate and later underwent induration by silica-rich pore fluids, as evidenced by successive phases of coarse silica cement. There is a slightly sheared, but nevertheless conformable contact between the pyroclastics and overlying sediments, which comprise thinly-bedded argillaceous cherts and concordant Mn-rich cherts. Mn-rich intervals occur as millimetre-to centimetre-thick laminations within a bed, alternating with orange-pink argillaceous chert with well defined contacts. Within the sedimentary sequence, tuffaceous beds have been identified. A number of sedimentary features indicate syn-depositional tectonic activity and slope instability. Some beds thicken in the hanging wall to small-scale normal faults and are demonstrably syn-tectonic. Generally, throws range from a few millimetres, to two or three centimetres. The orientation of the faults was not measurable due to their small size and the two dimensional outcrop, and thus accurate stress tensors could not be obtained from fault planes. The presence of a 12cm thick bed of breccia comprising locally derived dark manganiferous chert within an orange argillaceous matrix further exemplifies local sea floor instability and also has implications concerning the origin of Mn enrichment (Section 4.5.6.1) as it demonstrates that Mn enrichment occurred prior to brecciation. In addition to small scale fault structures,

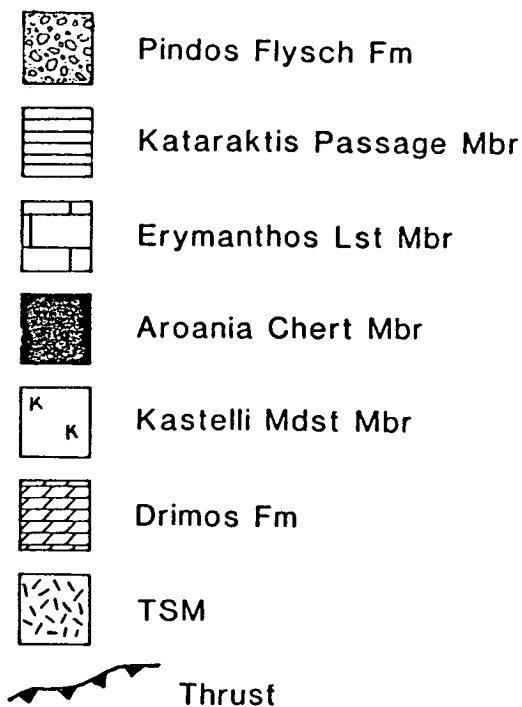
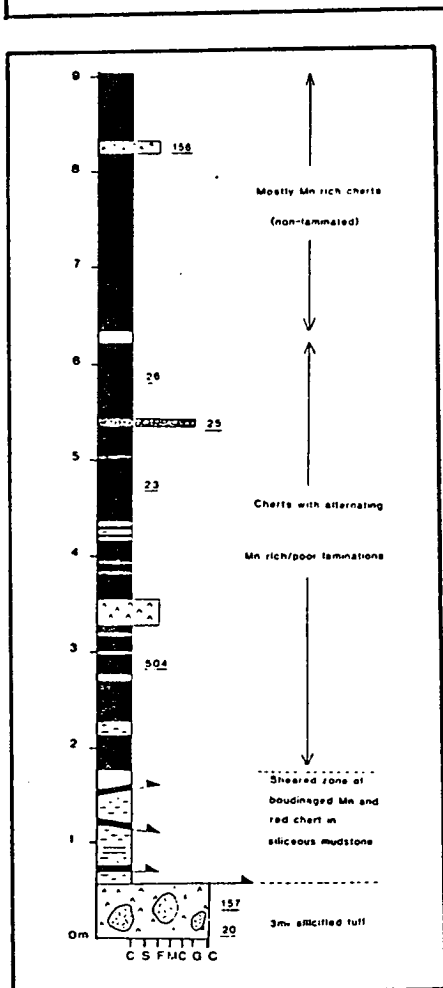
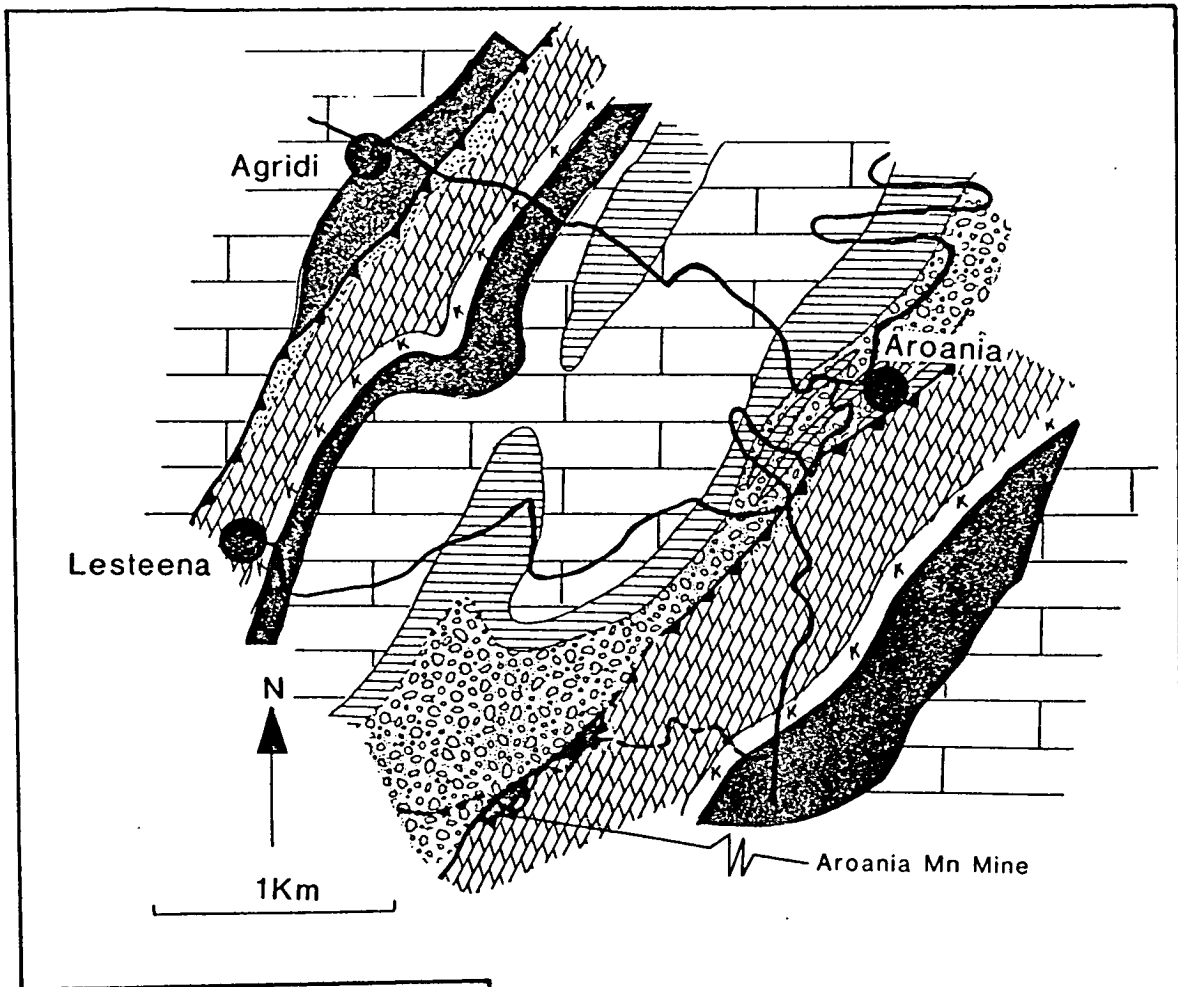


**Fig. 4.4** Geological map of the area surrounding the Aroania Mine locality and a sedimentary log of the manganese rich cherts (numbers to the right are for sample identification).

common soft sedimentary deformation, in the form of growth folds and dewatering structures, is observed (Plate 4.5).

Within a sheared mudstone matrix, lithologies found near the bounding thrust (but with obscured contacts) include lava, jasper (with 20% Fe<sub>2</sub>O<sub>3</sub>) and limestone conglomerate with *Posidonia sp.* and stylolitized clast contacts. A localised melange zone is thus inferred to be present below the coherent Aroania Mn sequence (Plate 4.6).

Ore grade material was also mined at Drimos (Figure 1.1), approximately 5km north-east of the Aroania mine. The Mn-rich horizons at Drimos occur within an undeformed chert sequence where stratigraphically over- and underlying formations are recognisable. Although Drimos is located within a structurally higher thrust slice than Aroania, the style of deposit, geochemistry and present day proximity suggest that the two locations were originally close.

In addition to the igneous rocks found at Aroania, pillow lavas and volcanoclastic sediment were also found at Kombigadi, near to Dendra (Figure 1.1). The petrology and geochemistry of the volcanic rocks is provided in Chapter 8. The lava and volcanoclastic sediment occurs at the base of a thrust sheet, below a radiolarian chert section. Way-up indicators are unclear, but it is suspected that the sequence is, at least partly, overturned. The thrust sheet was thrust faulted onto underlying turbiditic sandstone of the Pindos Flysch Formation. Radiolarian species have been extracted from interpillow sediment and successfully dated as Upper Jurassic (pers. comm. G. Rose 1992, Plate 4.4) and although only minor Mn mineralisation was found locally, the outcrop nevertheless conclusively proves the existence of igneous activity contemporaneous with deposition of the Aroania Chert Member.

#### 4.5.3 Mineralogy

The mineralogical composition of several manganiferous cherts was investigated by XRD analysis and the operating conditions and methodology are described in Appendix 2. The dominant manganese mineral identified is pyrolusite (MnO<sub>2</sub>). This is often formed as an early diagenetic mineral by the transformation of amorphous MnO<sub>2</sub> following mobilization of Mn cations (Bonatti *et al.* 1972). Electron probe and SEM analysis suggest that there is an amorphous manganese oxide phase present in some samples. This is inferred because at the scale of resolution, no distinct

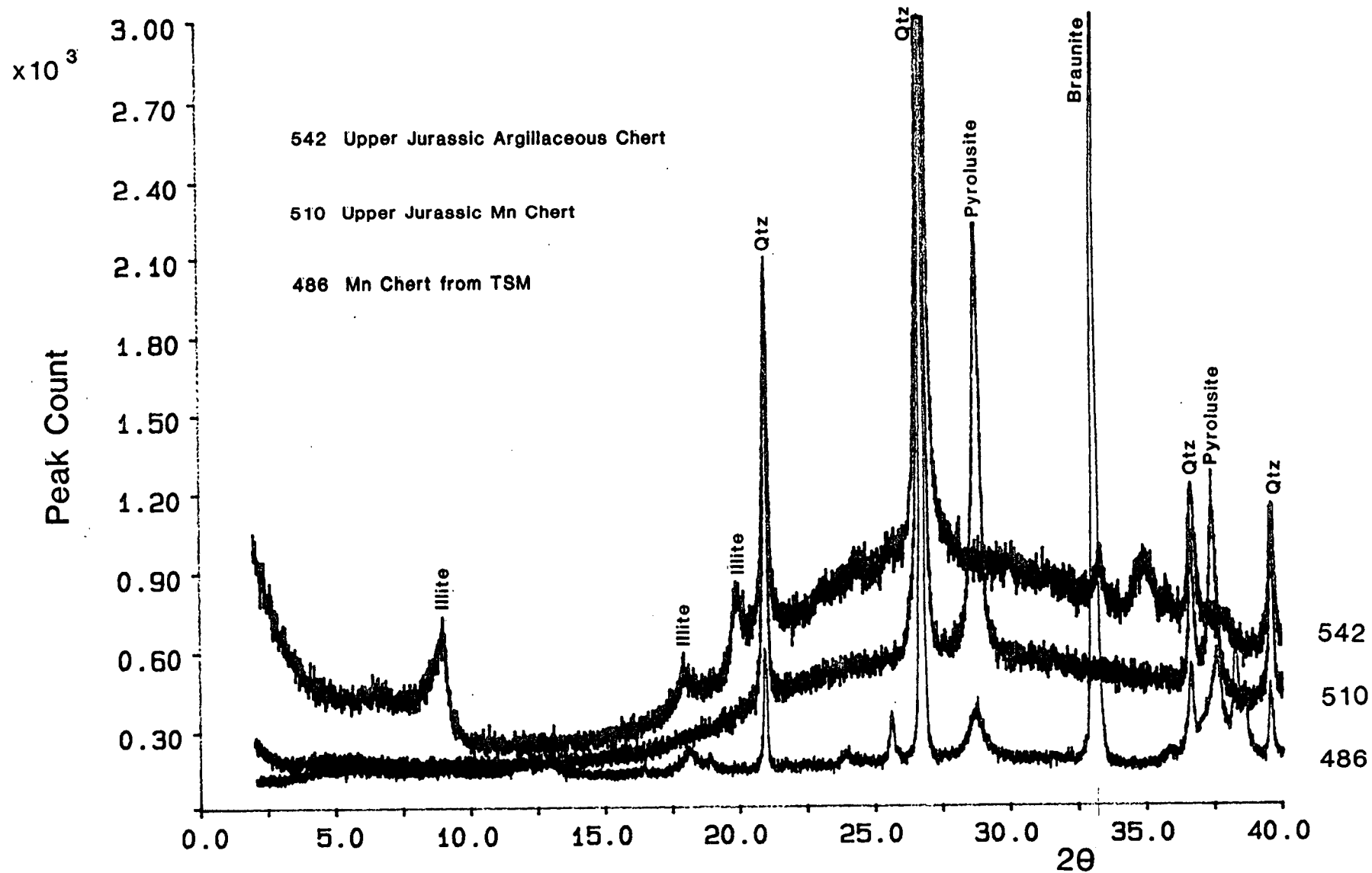


Fig. 4.5 Representative X-Ray diffraction traces for normal argillaceous chert (quartz & illite), Mn-rich chert from the Aroania Chert Member (pyrolusite, quartz) and the tectono-sedimentary melange (TSM:- quartz, braunite, pyrolusite, illite).

crystalline features were visible within colloform Mn microparticles (Section 4.5.5). The amorphous oxide may be  $\delta\text{MnO}_2$  (weak peaks at 1.42 Å and 2.40 Å), which is considered by some authors to be disordered birnessite ( $[\text{Ca,Na}] \text{Mn}_7\text{O}_{13} \cdot 3\text{H}_2\text{O}$ ) (Woo 1973, Burns & Burns 1977). Braunite ( $\text{Mn}^{2+}\text{Mn}^{3+}_6\text{O}_8[\text{SiO}_4]$ ) was also found in samples from cherts within the tectono-sedimentary melange. This manganese oxide requires higher pressure/temperature conditions for formation than pyrolusite (Burns & Burns 1977). Selected XRD plots are illustrated in Figure 4.5.

Crystalline  $\text{SiO}_2$  is abundant in all samples. SEM and petrological microscopy indicates that this is present both as chalcedonic quartz and cryptocrystalline quartz. Quartz is the primary background mineral in all metalliferous sediment samples studied. It is considered to be chiefly derived from biogenic sources (Section 4.4.4). Hydrothermal/authigenic silica may also be present, particularly within the pyroclastic material beneath Mn cherts at the Aroania mine. As will be discussed, this area is considered to represent a site of local hydrothermal activity with emanations of solutions rich in metallic cations and silica.

Hematite was identified in a number of samples. It is likely that this was originally detrital. Goethite is recorded in two samples (PD/89/207 & 174). The diagenetic formation of hematite from goethite has been discussed in section 4.3.1.4.

The dominant clay mineral present is illite, which is thought to be a background detrital phase representing continuous pelagic fallout during episodes of Mn-enrichment. Other minerals recorded are albite, calcite and apatite, which are similarly considered to be terrigenous, although they can form from hydrothermal precipitates.

#### 4.5.4 Whole Rock Geochemistry

Twenty-nine manganiferous chert samples from various localities have been analysed by XRF for major element oxides and seventeen trace elements (Appendix 3). The operating conditions and methodology are set out in Appendix 2. A correlation coefficient matrix has been constructed for all the major element oxides and the trace elements analysed (Table 4.1). Oxides and elements with the highest correlation to  $\text{MnO}$ ,  $\text{SiO}_2$  and  $\text{Al}_2\text{O}_3$  are also shown.

### Mn Chert Correlation Matrix

	SiO2	Al2O3	Fe2O3	MgO	CaO	Na2O	K2O	TiO2	MnO	P2O5	V	Ba	Sc	La	Nd	Ce	Cr	Ni	Cu	Zn	Pb	Th	Rb	Sr	Y	Zr	
Al2O3	0.282																										
Fe2O3	0.147	0.459																									
MgO	-0.182	0.327	0.238																								
CaO	-0.167	-0.233	0.095	0.076																							
Na2O	0.312	0.69	0.227	0.134	0.002																						
K2O	-0.44	0.467	0.24	0.176	-0.01	0.549																					
TiO2	0.102	0.949	0.471	0.308	-0.229	0.71	0.614																				
MnO	-0.967	-0.345	-0.248	0.034	0.067	-0.342	0.391	-0.172																			
P2O5	-0.234	-0.072	0.206	-0.064	0.879	0.146	0.264	-0.048	0.185																		
V	-0.531	-0.257	-0.233	0.495	0.117	-0.344	0.026	-0.215	0.41	-0.041																	
Ba	-0.496	-0.204	0.014	0.468	0.168	-0.316	0.103	-0.126	0.327	0.011	0.889																
Sc	0.291	0.782	0.195	0.154	-0.058	0.78	0.443	0.779	-0.335	0.1	-0.194	-0.211															
La	0.203	0.394	0.831	0.123	0.409	0.236	0.171	0.381	-0.31	0.529	-0.25	-0.045	0.37														
Nd	-0.231	-0.022	0.469	0.382	0.376	-0.218	0.11	0.026	0.029	0.245	0.53	0.776	-0.12	0.435													
Ce	-0.136	0.147	0.473	0.229	0.648	0.085	0.238	0.14	0.002	0.651	0.268	0.373	0.124	0.579	0.719												
Cr	0.156	0.01	0.173	0.06	-0.175	0.222	-0.096	0.024	-0.148	-0.161	-0.009	-0.051	0.042	-0.065	-0.098	-0.1											
Ni	-0.189	-0.154	-0.054	0.414	-0.074	-0.273	-0.248	-0.233	0.141	-0.2	0.599	0.366	-0.232	-0.207	0.103	-0.019	0.416										
Cu	-0.574	-0.115	-0.068	-0.043	0.073	-0.164	0.336	-0.079	0.604	0.308	0.491	0.4	-0.099	-0.08	0.191	0.39	0.007	0.239									
Zn	-0.406	0.012	-0.065	0.267	-0.109	-0.382	-0.042	-0.063	0.368	-0.045	0.627	0.429	-0.104	-0.089	0.216	0.168	0.066	0.728	0.596								
Pb	-0.183	-0.072	0.081	0.172	0.235	-0.096	0.08	0.015	0.039	0.055	0.37	0.458	-0.097	0.04	0.62	0.509	-0.052	0.014	0.045	0.088							
Th	0.162	0.734	0.149	0.219	-0.124	0.735	0.42	0.779	-0.185	0.022	-0.153	-0.199	0.932	0.255	-0.188	-0.001	0.046	-0.208	-0.097	-0.109	-0.116						
Rb	0.134	0.917	0.354	0.212	-0.186	0.745	0.66	0.914	-0.158	0.065	-0.221	-0.221	0.8	0.302	-0.09	0.197	0.033	-0.168	0.117	0.028	-0.105	0.744					
Sr	-0.319	-0.212	-0.147	0.398	0.177	-0.212	0.02	-0.113	0.136	-0.094	0.757	0.863	-0.131	-0.168	0.685	0.235	-0.07	0.18	0.038	0.156	0.625	-0.11	-0.267				
Y	-0.468	-0.24	-0.036	0.046	0.301	-0.24	0.236	-0.167	0.407	0.302	0.247	0.32	-0.164	0.059	0.294	0.202	-0.219	-0.017	0.271	0.125	0.182	-0.198	-0.186	0.256			
Zr	-0.166	0.115	-0.001	0.571	0.063	0.072	0.194	0.14	0.047	-0.062	0.447	0.54	0.143	-0.035	0.32	-0.007	-0.077	0.141	-0.045	0.051	-0.166	0.155	0.1	0.525	0.14		
Nb	0.188	0.769	0.508	0.196	-0.113	0.532	0.332	0.706	-0.2	0.108	-0.183	-0.174	0.575	0.396	-0.023	0.307	0.291	0.074	0.271	0.213	-0.093	0.55	0.791	-0.369	-0.301	-0.056	

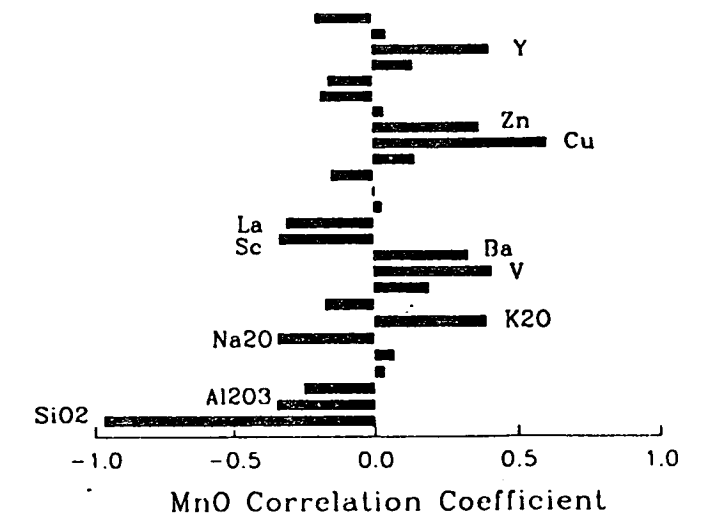
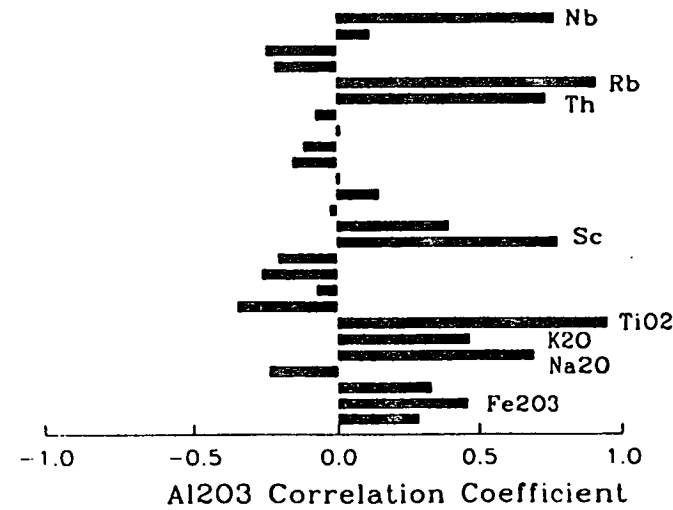
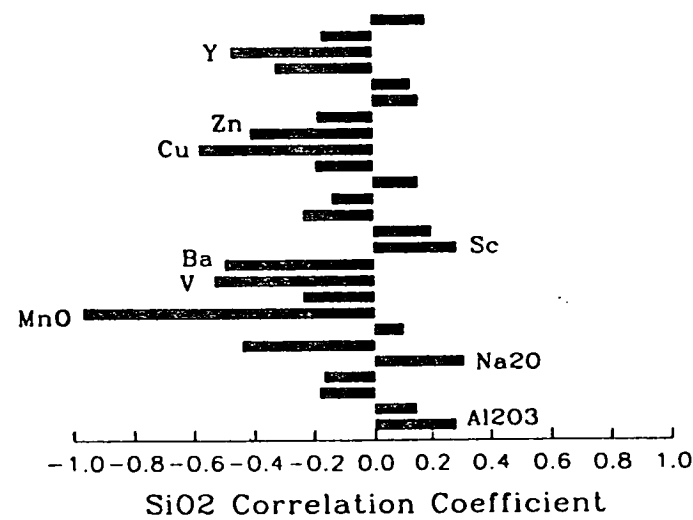


**Table 4.1** Correlation coefficient matrix for the major oxides and trace elements of the Mn-rich cherts (obtained by X-Ray fluorescence). The underlying graphs indicate those elements that correlate most (positively and negatively) with SiO<sub>2</sub>, Al<sub>2</sub>O<sub>3</sub> and MnO. The confidence level is 95% for a sample size of 29.

## MnO

The manganese oxide content varies from 1.56% to 69.54%. The most manganeseiferous are cherts found associated with tectono-sedimentary melange zones at Chelmos and Drakovouni. The average MnO concentration from the Aroania and Drimos mines is 17.5%. These values are much greater than the average of 0.7-1.7% observed today for non-carbonate pelagic sediment (Cronan 1969). MnO correlates positively with K<sub>2</sub>O, V, Ba, Cu, Zn and Y. Conversely, there is a negative correlation with SiO<sub>2</sub> (the other major phase present), Al<sub>2</sub>O<sub>3</sub>, Na<sub>2</sub>O, Sc and La.

## SiO<sub>2</sub>

The total SiO<sub>2</sub> varies inversely with the concentration of MnO present, as this is the principal component of the Lesteena Formation and the SiO<sub>2</sub> was diluted to varying degrees by enrichment in MnO. As described in Section 4.4.4 most of the silica was derived from biogenic opal-A.

## Fe<sub>2</sub>O<sub>3</sub>

Fe<sub>2</sub>O<sub>3</sub> appears to be strongly subordinate to Mn in most of the analysed samples and rarely exceeds 1% of the major oxides, although an exception to this is sample PD/89/452, where the content is 4.91%. The average Fe<sub>2</sub>O<sub>3</sub> concentration of all other Mn chert samples is 0.39%. The Fe<sub>2</sub>O<sub>3</sub> exhibits a positive correlation with Al<sub>2</sub>O<sub>3</sub> and TiO<sub>2</sub>.

## Al<sub>2</sub>O<sub>3</sub>

Al<sub>2</sub>O<sub>3</sub> is not strongly correlated with SiO<sub>2</sub> or MnO. It does, however, show a positive relationship with TiO<sub>2</sub>. Both are essentially immobile oxides, long recognised as reliable indicators of detrital sedimentation (Arrhenius *et al.* 1951). The aluminium oxide content of the cherts is, therefore, considered primarily to reflect the composition of clays settling out from the water column as background sedimentation. There are also strong positive correlations with the following; Na<sub>2</sub>O, K<sub>2</sub>O, Sc, Th, Rb and Nb.

## CaO

CaO content is low, rarely greater than 1%. This is believed to reflect the deep, sub-CCD deposition of the chert (Section 4.4.3.2).

Of the trace elements, there are obvious high concentrations of Ba, Sr, Zn and Cu in the manganese-enriched cherts, relative to cherts lacking metallic oxide phases. The



Ba content is particularly noteworthy, being consistently high and reaching an extreme value of 21055ppm (>2%).

#### 4.5.5 Electron Microprobe Study of Aroania Mn Chert

An electron microprobe study has been undertaken on sample PD/89/504 from Aroania. The operating conditions and methodology are described in Appendix 2. This specimen was chosen as it is representative of the manganese rich sediments present. The sample consists of well defined millimetre-scale alternations of metal impregnated, black, Mn-rich laminations and Mn-poor argillaceous chert (Plate 4.8). Twenty six analyses (Table 4.2) were undertaken to establish elemental variations across the laminations, and to identify detrital particles. In addition, high definition scanning electron microscopy was used to observe textural variations.

Plate 4.7 shows a false colour backscattered electron image (different colours reflect variations in atomic number) of part of the specimen analysed. Figure 4.6 is a line drawing showing the position of some of the analysis points along a transect across a lamination boundary, with SiO<sub>2</sub>, MnO and Al<sub>2</sub>O<sub>3</sub> totals also shown. The illustrated transect passes from a radiolarian test (504/1) with 96% SiO<sub>2</sub>, to the clay matrix material (504/2-3) with higher MgO, Al<sub>2</sub>O<sub>3</sub>, K<sub>2</sub>O, TiO<sub>2</sub> and FeO, reflecting the composition of detrital illite and hematite. The transect continues into the Mn-rich lamination. Points 504/5-9, are from a lamination boundary. Plate 4.8 (C) shows a SEM photomicrograph of this area. It is seen to consist of roughly spherical, manganese-enriched bodies, which have an internally zoned, colloform fabric with a bladed mineral fringe. These spheres are two orders of magnitude smaller than the radiolarian tests in the sample. Analysis points 504/5, 504/8 and 504/23 were from the cores of three spheres. 504/6, 504/9 and 504/21 were from corresponding sphere-intermediate zones, while points 504/7 and 504/22 were from the outermost zone which has a bladed fabric. The analyses indicate that the spheres have a SiO<sub>2</sub> rich core with some MnO, becoming progressively more MnO-rich outwards with a corresponding decrease in SiO<sub>2</sub>. The Mn increase is accompanied by minor, but distinct, additional CaO, TiO<sub>2</sub> (not correlated with Al<sub>2</sub>O<sub>3</sub>) and FeO.

Plate 4.8 (D) is a photomicrograph of the central, Mn-rich area of a lamination. This region is dominated by a bladed Mn mineral with very scarce small nuclei visible.

Sample PD/89/504

Electron Microprobe Results

	504/1	504/2	504/3	504/4	505/5	504/6	504/7	504/8	504/9	504/10	504/11	504/12	504/13
NA2O	0.034	0.162	0.104	0.624	0.14	0.159	0.295	0.217	0.278	0.717	0.158	0.105	0.257
MGO	0.015	0.405	1.995	0.274	0.071	0.065	0.098	0.091	0.129	0.166	1.766	0.098	0.083
AL2O3	0.144	2.74	4.47	1.374	0.287	0.161	0.531	0.372	0.642	0.414	17.81	0.896	0.697
SIO2	96.302	90.308	83.618	14.669	93.5	87.007	78.279	84.172	80.711	5.941	73.335	31.353	53.735
K2O	0.028	0.761	1.225	0.208	0.043	0.048	0.086	0.083	0.123	0.039	4.858	0.205	0.113
CAO	0.027	0.115	0.141	4.157	0.424	0.723	1.223	0.86	1.028	4.34	0.168	1.494	1.119
TIO2	0.012	0.272	0.045	0.771	0.12	0.182	0.274	0.198	0.239	0.534	0.123	0.185	0.145
MNO	0	0.212	0.156	55.614	6.02	9.725	16.705	11.221	13.566	61.084	0.457	18.152	13.115
FEO	0.042	1.513	2.759	1.365	0.151	0.188	0.279	0.247	0.275	0.979	2.506	0.418	0.268
NIO	0.029	0.029	0.043	0.053	0.028	0.001	0.028	0.024	0.025	0.071	0.043	0.019	0.025
TOTAL	96.632	96.516	94.558	79.109	100.784	98.259	97.796	97.487	97.017	74.284	101.224	52.925	69.558
	504/14	504/15	504/16	504/17	504/18	504/19	504/20	504/21	504/22	504/23	504/24	504/25	504/26
NA2O	0.356	0.057	0.225	0.278	0.716	0.515	0.137	0.182	0.332	0.082	0.042	9.328	0.276
MGO	0.124	0.681	0.118	0.088	0.245	0.327	1.078	0.066	0.09	0.06	0.09	0.133	0.121
AL2O3	0.544	4.544	0.595	0.316	0.903	2.906	8.797	0.614	0.435	0.962	1.298	12.884	0.45
SIO2	58.334	6.204	85.471	66.234	11.447	10.322	81.575	87.967	68.205	96.422	0.965	68.267	58.905
K2O	0.167	0.076	0.129	0.035	0.193	0.043	2.572	0.082	0.089	0.234	0	0.278	0.687
CAO	2.125	43.777	0.708	1.714	4.228	4.391	0.154	0.47	1.559	0.084	0.434	0.083	1.599
TIO2	0.27	0.02	0.122	0.197	0.595	0.801	0.108	0.14	0.16	0.025	0.02	0.033	0.202
MNO	28.031	0.085	10.068	24.005	58.309	58.221	0.26	5.867	21.873	0.733	78.736	0.035	28.988
FEO	0.524	0.054	0.282	0.43	1.149	0.906	2.285	0.17	0.436	0.094	0.223	0.271	0.659
NIO	0.014	0.005	0.018	0.029	0.01	0.045	0.052	0	0.02	0.013	0.015	0.009	0.018
TOTAL	90.49	55.504	97.735	93.325	77.796	78.475	97.018	95.559	93.198	98.708	81.822	91.321	89.904

Table 4.2 The results of electron microprobe analysis on Mn-rich chert sample PD/89/504 from the Aroania Mine.



The mineral particle size is similar to that of the colloform spheres, and the bladed fabric is similar to, but more developed than, the Mn-rich fringe of the boundary zone spheres. The colloform banding is absent. Several analyses were made in this area. Unfortunately, the beam diameter (4 $\mu$ m) was unable to resolve the nucleus from fringe, except for points 504/16 and 17. The analysis of point 504/16 indicates that the nucleus in the centre of the lamination is mostly SiO<sub>2</sub>, although some Mn is present. This is similar to the nuclei of spheres in the boundary areas, while the composition of 504/17 is similar to that of the outermost bladed areas of the boundary zone.

Analyses of points 504/4, 18 and 19 are anomalous in that they have a very low oxide total, but include significant CaO in addition to MnO and SiO<sub>2</sub>. Also, Na<sub>2</sub>O is higher than found at other analysed points. At the highest magnification, it was possible to image these data points as anhedral microparticles, with a very narrow bladed fringe.

Detrital feldspar and apatite were identified using the electron probe. It is possible to demonstrate that the radiolarian tests, sponge spicules and background clay were deposited from what was apparently a rain of constant composition, as the density of this material is uniform and, apart from the observed sharp increase in MnO content within the dark bands, there are no other lithological nor diagenetic differences across the Mn laminations. Baltuck (1982) concluded that the non-biogenic component of Pindos Zone cherts that she studied was derived from continental sources. The observed mineralogy and geochemistry of the clay component is in accord with this conclusion.

#### 4.5.6 Interpretations

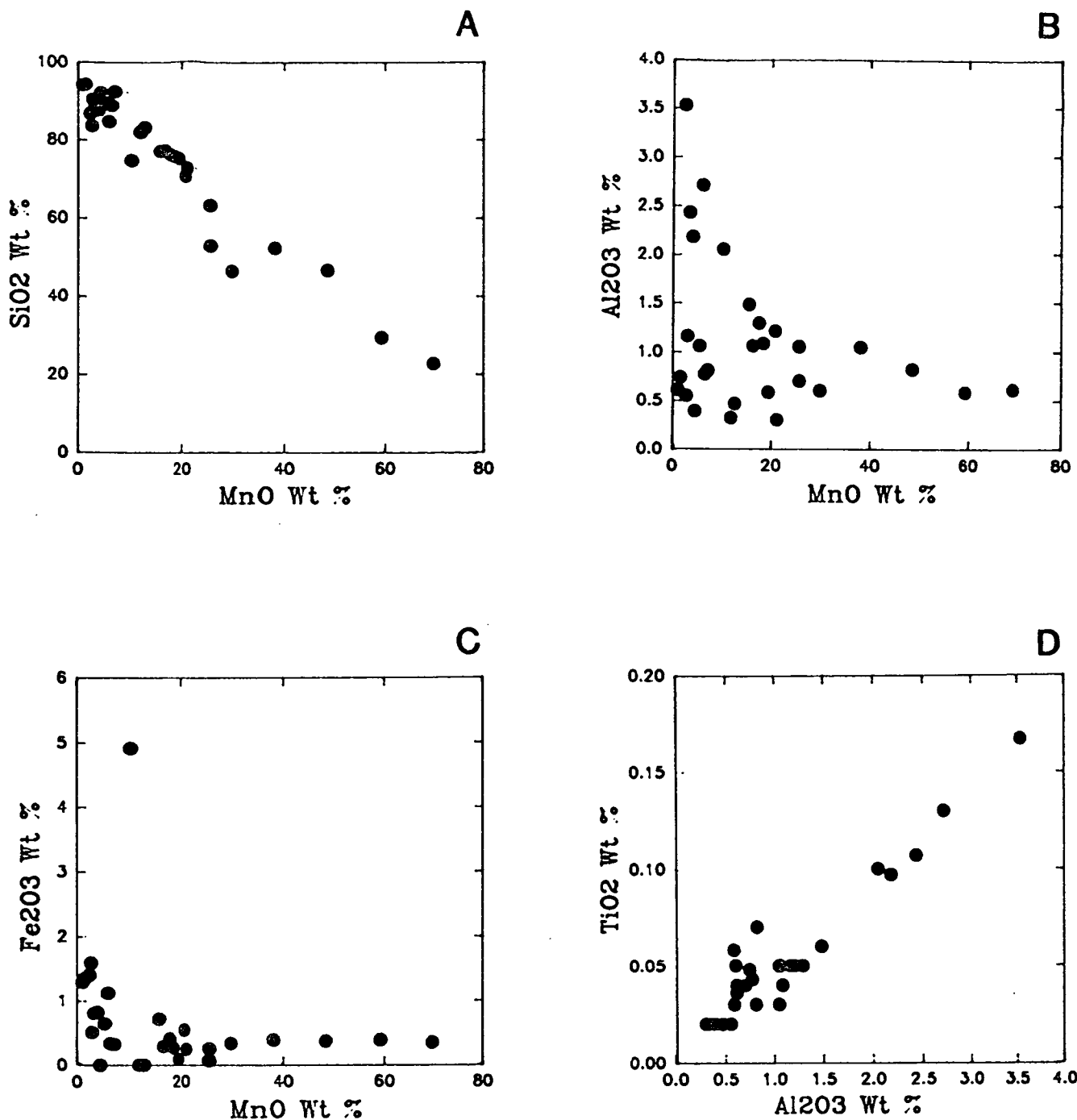
##### 4.5.6.1 Interpretation of Field & Petrological Data from Aroania

- 1) At the base of the sequence there is pyroclastic material containing remnant carbonate. This has been impregnated with pore filling macro-quartz and unorientated chalcedonic quartz that almost totally obscures the primary texture in thin-section. This fabric, and the field setting imply that the silica could be primarily of hydrothermal origin.
- 2) Deposition of Mn-rich cherts directly upon an igneous sub-stratum supports a hydrothermal origin for the Mn.

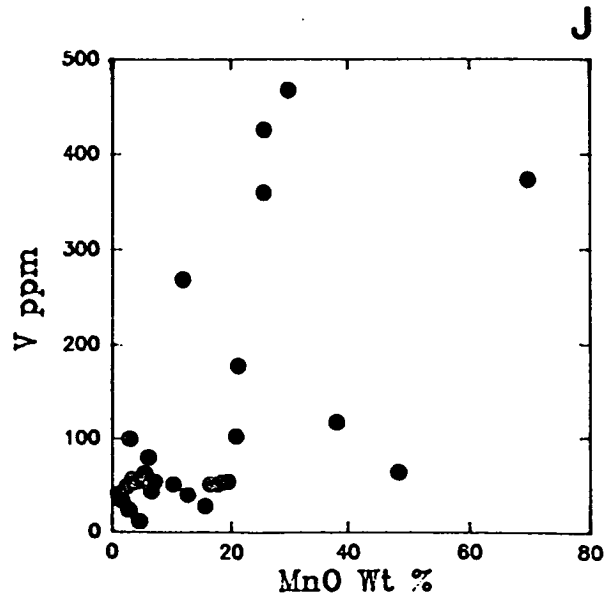
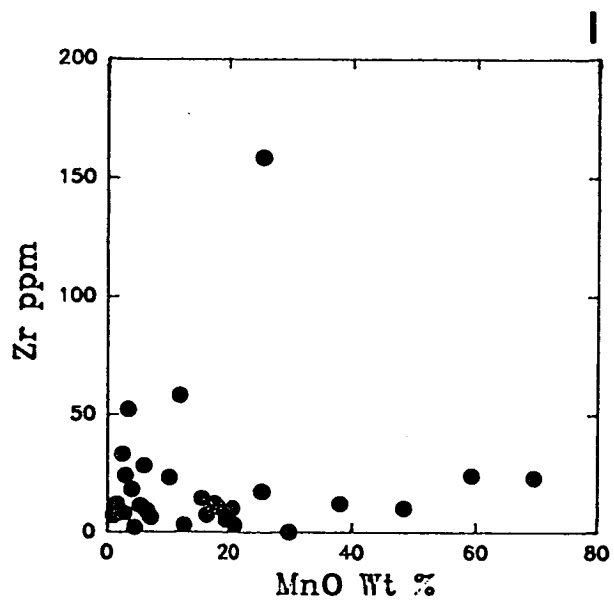
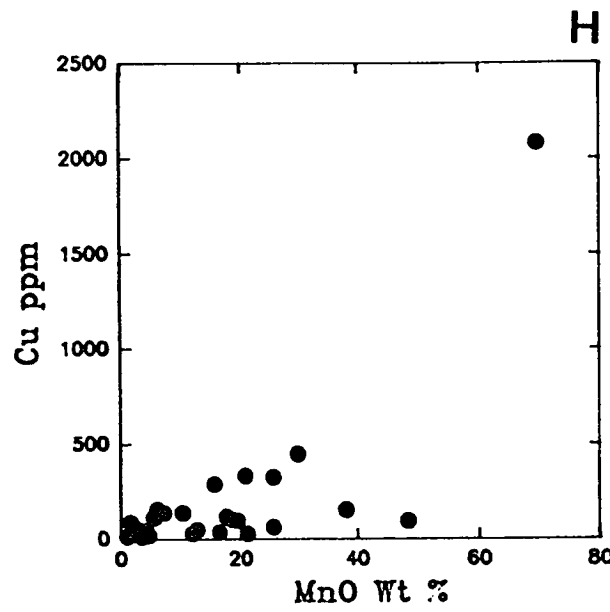
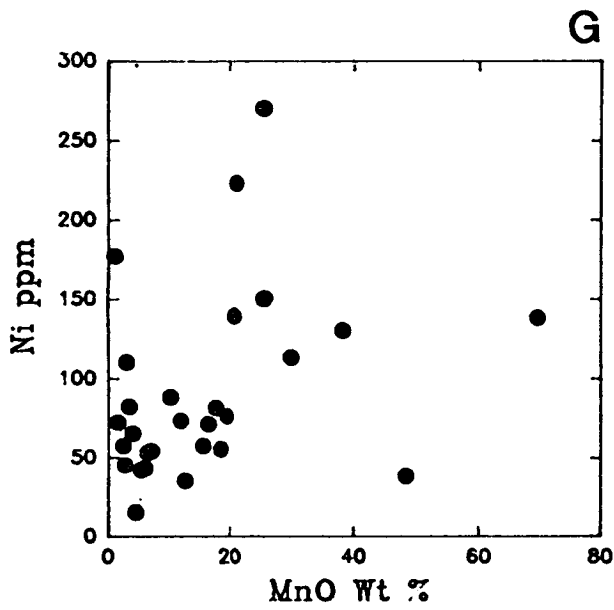
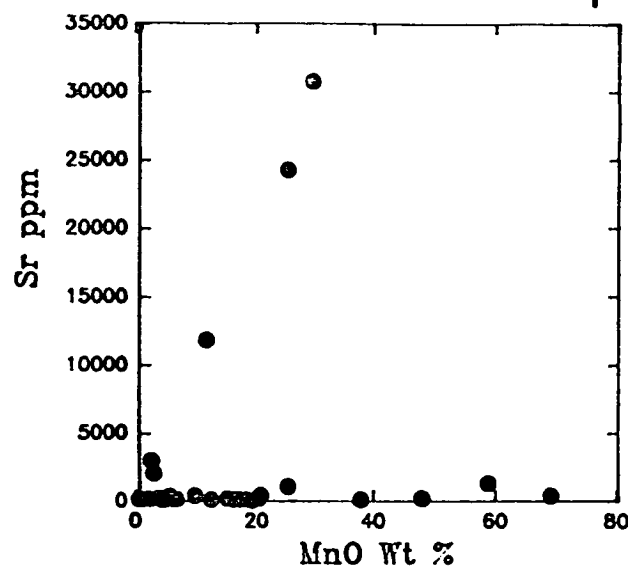
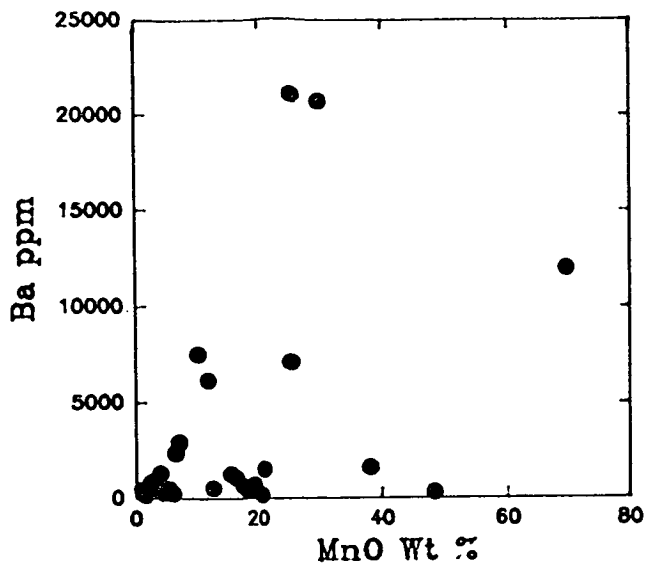
- 3) Intercalated pyroclastic material within the cherts indicates contemporaneous volcanism.
- 4) The Mn-rich laminations are considered to represent successive hydrothermal exhalations interspersed with periods of quiescence, with each Mn lamination being deposited at the sediment-water interface. This supposition is strongly supported by the fact that detrital and biogenous component concentrations are continuous through the sample, indicating that the Mn enrichment, although pulsed, was coeval with background chert deposition.
- 5) A primary origin for the Mn is supported by the observation that radiolarian tests, including ornament, are extremely well preserved within the Mn-rich laminations. This is in contrast to the compaction and test dissolution features seen in adjacent Mn-poor laminations (thin-section PD/89/504).
- 6) Bedded breccia of dark, Mn enriched clasts within an argillaceous chert matrix further indicates that Mn enrichment is not diagenetic, in the sense that it involves large scale redistribution of phases, but is of primary origin, occurring prior to what was essentially syn-tectonic brecciation.
- 7) Soft-sedimentary and brittle deformation (Plate 4.5) indicate coeval slope instability and tectonism. A reasonable supposition, given present day observations, is that volcanic emanations have exploited fundamental basement weaknesses, i.e. faults.
- 8) An absence of carbonate indicates deposition below the CCD.
- 9) Samples of chert, rich in Fe but lacking in Mn, are found in the tectono-sedimentary melange (TSM). These specimens, e.g. PD/89/481 with 20% Fe<sub>2</sub>O<sub>3</sub>, may represent sediment within a hydrothermal mound where the Fe was fractionated from Mn (Figure 4.9). Sample PD/89/429 is such a chert from Aroania.

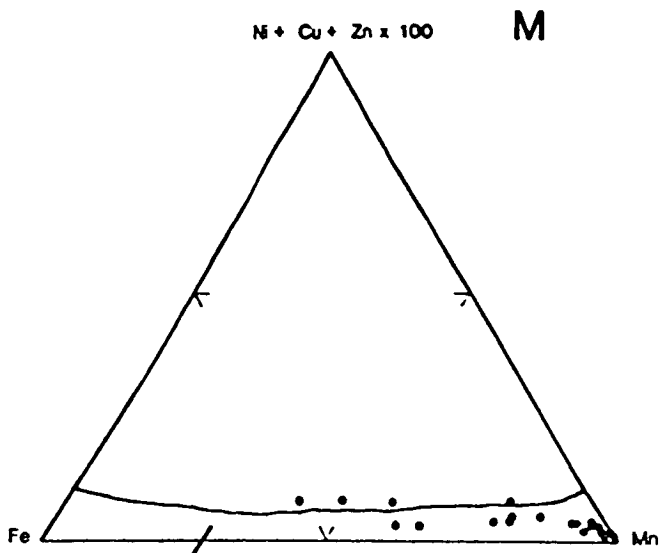
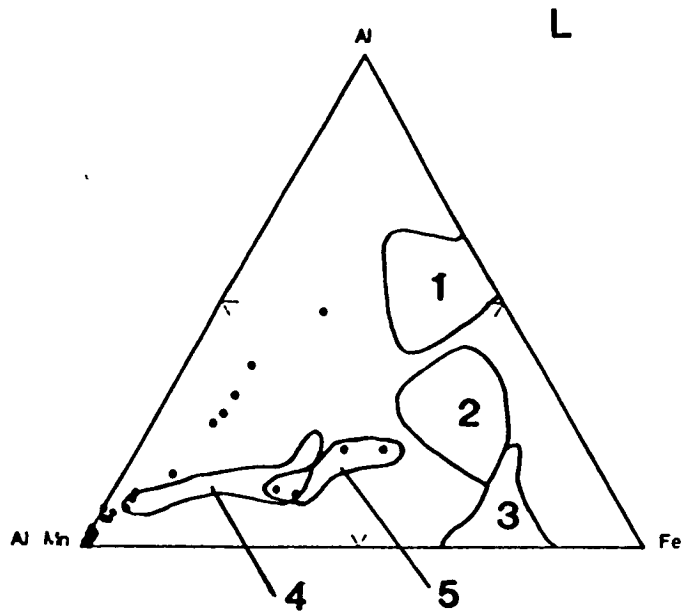
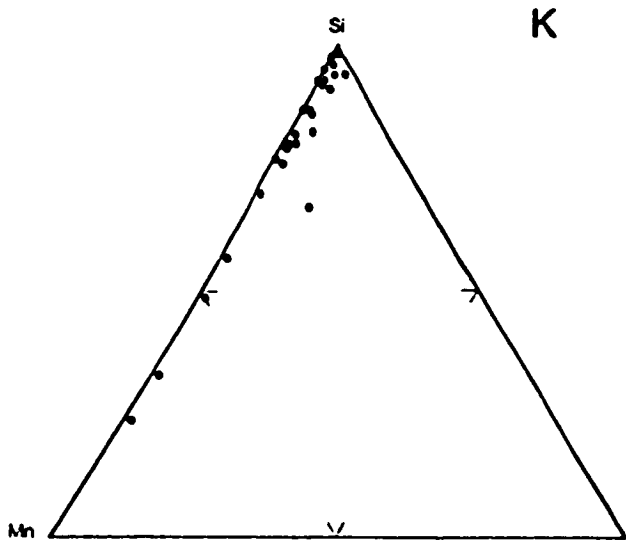
#### 4.5.6.2 Interpretation of Geochemical Patterns

Figure 4.7 [A] to [N] shows variation diagrams for selected oxides and trace elements. [A] graphically illustrates the varying ratio of SiO<sub>2</sub> and MnO present; there is a strong negative correlation as these oxides are the two principle components. [B] and [C] show a wide range of scatter and this confirms that MnO is not correlated with either Al<sub>2</sub>O<sub>3</sub> or Fe<sub>2</sub>O<sub>3</sub>. Inspection of the correlation matrix indicates that Al<sub>2</sub>O<sub>3</sub> and Fe<sub>2</sub>O<sub>3</sub> can both be correlated with one another. [D] illustrates the well known interdependence between Al<sub>2</sub>O<sub>3</sub> and TiO<sub>2</sub> found in continentally derived clays (Arrhenius *et al.* 1951).

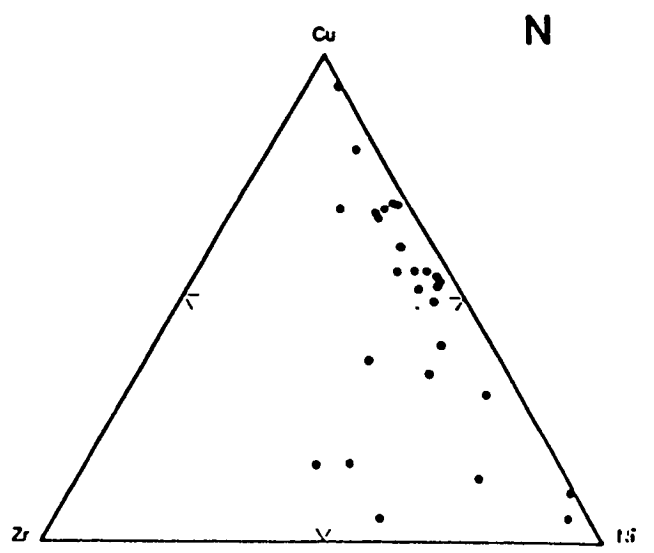


**Fig. 4.7** Variation diagrams. (A) Well defined negative correlation between SiO<sub>2</sub> and MnO. (B & C) Al<sub>2</sub>O<sub>3</sub> and Fe<sub>2</sub>O<sub>3</sub> show almost no correlation with MnO. (D) TiO<sub>2</sub>/Al<sub>2</sub>O<sub>3</sub> exemplifies the well established positive correlation between these oxides due to their presence in terrestrially derived clays. Graphs (E) to (J) indicate little correlation between trace elements and MnO, although there are sub-sets of samples with a positive correlation. Explanation in text. (K) shows the dominance of Si and Mn in the samples in relation to Al, while (L) compares the Mn chert data against published fields for:- (1) normal Pacific sediments, (2) Bauer Deep sediments, (3) East Pacific Rise sediments and (4) Mn nodules. (5) is the sub-set of Mn-rich chert with a more hydrogenous signature. The ternary diagram (M) indicates that the samples plot within or close to the hydrothermal sediment field (adapted from Bonatti 1972). (N) shows the relative concentrations of Cu, Zr and Ni; explanation in text.





Hydrothermal Field





[E] to [J] appear to indicate that there is little correlation of trace elements with Mn. However, for samples with elevated Ba, Y, Cu, Zn and V concentrations, there is a positive correlation as shown in Table 4.1. Furthermore, closer inspection of the data shows that there are two distinct trends where these elements are concerned. Most of the samples exhibit little, or no, correlation with MnO. Samples obtained principally from Aroania and Drimos, however, show secondary correlation trends (e.g. [E] MnO/Ba, [F] MnO/Sr and [H] MnO/Cu) that are masked in the matrix by the dominant lack of interdependence shown by samples from other areas.

In the ternary diagrams, [K] illustrates the bulk importance of silica, with important Mn but negligible Al<sub>2</sub>O<sub>3</sub>. [L] shows the degree of Mn/Fe fractionation and the noteworthy linear trend to Mn enrichment from a normal pelagic sediment. Due to the extremely low Fe/Mn ratio from most metalliferous sediment samples, no significant quantities of hydrothermal Fe<sub>2</sub>O<sub>3</sub> are considered to have been present in the water column and the Fe is believed to have precipitated below the ocean floor. This view is supported by the ratio of Fe<sub>2</sub>O<sub>3</sub>/Al<sub>2</sub>O<sub>3</sub> (Appendix 3), as an average value of 0.38 has been obtained for pelagic clays in which the iron oxide constituent is considered to represent the detrital Fe-silicate component (Cronan 1976, Bischoff & Rosenbauer 1977). The Pindos Mn cherts have values only slightly above this figure, and therefore most, if not all the Fe appears to have been derived from terrigenous sources. In addition, the Fe<sub>2</sub>O<sub>3</sub>/Al<sub>2</sub>O<sub>3</sub> ratios are similar to those for the Kastelli Mudstone Member (Section 4.3.1.3), which has no indication of hydrothermal activity. The positive correlation and the gradual increase in Fe<sub>2</sub>O<sub>3</sub> content with increasing Al<sub>2</sub>O<sub>3</sub> as MnO diminishes further illustrates the detrital origin of the hematite found in most samples.

In [L] a secondary field of samples with relatively high Fe/Mn ratios is present. This indicates that four samples have a distinctly more hydrogenous signature (PD/88/124, PD/89/174,452, PD/90/702). [M] attempts to discriminate hydrothermal and hydrogenous element enrichment as Ni, Cu and Zn are all elements that are readily sorbed onto Mn particulates during hydrogenous precipitation. They can also be derived from hydrothermal emanations, but in such cases the totals are an order of magnitude lower. It is seen that most of the analysed samples fall into the hydrothermal field for this plot. [N] illustrates the relative concentration of Cu and Ni in relation to Zr which is considered to be of detrital origin.

Sea water is readily able to leach many elements (e.g. Mn and Fe) from basalts under reducing conditions associated with acidic hydrothermal systems (Seyfried & Bischoff 1977, Robertson 1978). The relative concentration of REE in marine hydrothermal deposits, on the other hand, is not markedly dissimilar to that found in normal sea water (Robertson & Fleet 1976). In a sea water-basalt experiment, Menzies *et al.* (1979) showed how REE can remain essentially immobile at temperatures up to 350°C. Because of the relative speed that manganese oxides precipitate from hydrothermal exhalations compared to hydrogenous deposition, less adsorption of trace elements from sea water will normally take place. Crerar *et al.* (1980) state, however, that freshly precipitated Mn oxides have extraordinarily high surface energies and should readily scavenge and co-precipitate trace metals. Murray (1974) has located the isoelectric point of hydrous manganese dioxide at a pH of 2.25. For greater pH values the mineral has a negative charge, this may account for the initiation of electropositive trace element scavenging. The observation that some of the Mn cherts are relatively rich in elements such as Sr, Cu and Ba may be a reflection of this scavenging mechanism, but this appears unlikely. Such concentrations probably represent the initial composition of the igneous source, for example as envisaged for copper rich deposits in the Red Sea (Bischoff 1969).

The high concentration in Ba for the Pindos Mn cherts has been noted. Barium is considered to be an element introduced principally through hydrothermal activity (Bonatti *et al.* 1972, Bostrom *et al.* 1973, Bonatti 1975), although low concentrations in pelagic sediments can be derived from biogenic sources. Significant Ba enrichment was reported in hydrothermal Mn crusts described from the seamount Lametino in the Tyrrhenian Sea (Rossi *et al.* 1980), from the Eratosthenes seamount in the eastern Mediterranean Sea (Varnavas *et al.* 1988) and from the Galapagos hydrothermal mounds (Varnavas 1987). A direct positive correlation has been shown between Ba and hydrothermal Mn deposits in the Afar rift, with a corresponding negative correlation between Ba and Fe (Bonatti *et al.* 1972). No Fe/Ba correlation is shown by the Pindos Zone Mn-rich deposits, but there is a strong Mn/Ba correlation (Table 4.1). The implication is that in the Pindos Zone rocks analysed, Ba co-precipitates with Mn rich phases, in this case from hydrothermal systems.

A hydrothermal mechanism is further strongly indicated, especially for the Mn sediment from Aroania, where elevated Sr and V contents are an order of magnitude greater than can be accounted for by contributions from biogenic or hydrogenous

sources. The hydrothermal origin of Sr and V in areas where seawater-rock interaction presently takes place in hydrothermal fields has been shown by Varnavas & Cronan (1991). Ni, Zr and Cu are generally low, but are positively correlated with what are considered to be hydrothermal elements in the Aroania sediment. An exception is the high Cu value of sample PD/89/486 from Drakovouni. This sample contains braunite rather than pyrolusite and it is possible that there has been some higher temperature/pressure mobilization and subsequent concentration of Cu.

Consideration of the data indicates that there was a gradation in the form of Mn enrichment, from hydrothermal towards more hydrogenous processes, presumably reflecting the distance from hydrothermal source.

#### 4.5.6.3 Interpretation of Electron Probe Data

The electron probe study of Aroania sample PD/89/504 has led to the following interpretations:-

- 1) The colloform texture of the MnO and SiO<sub>2</sub> bands in the boundary zone suggests precipitation from a Mn-enriched solution, providing alternate Mn-rich and Mn-poor layers. The decrease in SiO<sub>2</sub> outwards with a corresponding increase in MnO, indicates that they have an intimate inverse relationship. This, along with the presence of some MnO with SiO<sub>2</sub> in the nucleus, suggests that the quartz may be authigenic rather than biogenic or detrital. This is considered a valid interpretation as the nucleation and precipitation kinetics of silica are slow (with respect to Fe) and a large fraction of Si in solution from a hydrothermal source can be expected to pass up to the sediment-water interface where it will precipitate out (Crerar *et al.* 1982).
  
- 2) The Mn appears to have existed initially as an amorphous Mn oxyhydroxide which nucleated around dominantly (authigenic) silica cores. The analysis of microparticles shown by points 504/4, 18 and 19, show increased Na and Ca, but low oxide totals. It is possible that there may be trace quantities of birnessite ([Ca,Na]Mn<sub>7</sub>O<sub>13</sub>.3H<sub>2</sub>O) present, not detectable by XRD. SEM studies on recent hydrothermal Mn crusts has shown the presence of birnessite in the form of spherules (Lalou *et al.* 1983, Moorby *et al.* 1984, Varnavas *et al.* 1988). This mineral contains both Ca and Na and the low oxide totals obtained in this study are readily explainable due to H<sub>2</sub>O within the crystal lattice (pers. comm. S. Kearns 1991). The well developed fringing bladed manganese oxide has the crystal habit of pyrolusite which is confirmed by XRD.

3) The colloform fabric of the boundary zone spheres gives way to a more crystalline material of almost pure MnO (with a radiating bladed habit) in the centres of the laminations showing the richest impregnation of manganese ore. Given that both the boundary zone and the Mn-rich lamination crystals nucleated around SiO<sub>2</sub> areas, and that the sphere fringes are morphologically and geochemically the same as the well developed Mn mineral crystals, there is undoubtedly a diagenetic time/pressure/temperature mechanism operating *in-situ* to develop pyrolusite from an originally amorphous Mn oxyhydroxide such as  $\delta\text{MnO}_2$ . Sorem & Fewkes (1977) state that birnessite and todorokite appear to form largely by ionic crystallisation from solution in the deep sea. They emphasise, however, that both colloidal deposition and direct crystallisation of MnO<sub>2</sub> can occur. The colloform texture and the amorphous MnO in the specimen boundary zone suggests colloidal deposition. Pyrolusite from the centre of manganiferous laminations may result from ionic crystallisation, although mineral transformation from an originally colloform fabric would appear to be more likely, as this would simply be an amplification of the mechanism producing the pyrolusite fringe to the colloform spheres.

#### 4.5.6.4 Additional interpretations

Other localities provide circumstantial evidence for a hydrothermal origin to the Mn enriched cherts. High grade ore at Drimos appears to form a lens that may represent the proximity of an unexposed hydrothermal vent. The degree of Mn-enrichment in the Chelmos cherts and the fact that they are found above a TSM zone which includes igneous rocks, argues for these being deposited on a volcanic substratum rather than the Drimos Formation. Whether these volcanics represent Upper Jurassic sea floor basement or extrusives overlying Triassic sediment is not known. The fact that deposits below the Aroania Chert Member are not found east of Chelmos suggests that Upper Jurassic seafloor spreading is a distinct possibility and is supported by the geochemical composition of associated basalts. This is more fully discussed in Chapter 8.

#### **4.5.7 Discussion**

##### 4.5.7.1 Alternative Mn-enrichment Processes

The Mn enrichment of deep sea sediments can be attributed to one or more of four major mechanisms. These are:-

### 1) Detrital Deposition

The deposition of terrigenous Mn-rich detrital clasts derived from continental sources is not considered applicable in the Pindos Zone as there is no evidence, either in hand specimen or from microscopic observation, that clasts with a significant metallic content have been deposited in this deep sea setting. The background continuous fallout of clay on the one hand, and the concordant nature of the banded manganese ore, on the other, also allows one to discount a primary detrital origin.

### 2) Hydrogenous Enrichment Process

Hydrogenous processes include the direct precipitation of metallic oxides from oceanic seawater and the adsorption of metal cations on to negatively charged molecules in the water column. The concentration of any given metal in seawater attempts to reach a state of dynamic equilibrium. This is usually attained by the introduction of cations into an open-system through normal weathering and transport processes; e.g. continental run-off, with extraction through biogenic uptake and sedimentation. Supersaturation with any particular element, with respect to normal seawater, may be due to local conditions, such as proximity to the low-temperature weathering of submarine igneous rocks (i.e. halmyrolysis, Bonatti & Nayudu 1965) or continental margins. Hydrogenous precipitation of manganese often results in characteristic deep sea nodules and crusts with distinctive geochemical signatures (e.g. positive Ce anomaly and general enrichment in REE compared to normal pelagic sediments, Boyle 1984, 1990). The trace metal concentrations of deep sea nodules are often enriched in elements such as Ni, Co, Cr, Cu and Zn, relative to normal pelagic sediment. This is because hydrogenous ferro-manganese hydroxides are extremely powerful scavengers of certain metallic cations due to high surface charges and the long periods of time that nodules are in contact with seawater due to slow sedimentation rates, e.g. 1mm/1000 yrs (Crerar *et al.* 1980). Consequently manganese nodules have concentrations of the above elements an order of magnitude greater than hydrothermal deposits. The Fe/Mn ratio of hydrogenous deposits usually averages about unity (Bonatti *et al.* 1972); however, there has been a strong degree of fractionation of these elements in the Pindos Mn cherts, reflected in the extremely low Fe/Mn ratios (Appendix 3).

### 3) Diagenetic Enrichment Process

The diagenetic mobilisation of metallic cations results in post-depositional redistribution of elements with the subsequent possibility of concentration or

dilution depending on local conditions. This mechanism implies substantial movement as well as mineral transformation. Post-depositional diagenetic mobilization has been suggested to account for thick accumulations of Mn oxide crusts in some pelagic sediments (Price & Calvert 1970, Bonatti *et al.* 1972). Mn migration can be induced by locally reducing conditions upon burial, with distribution by pore filling solutions. Diffusion to an overlying oxidised interface would lead to the reprecipitation of Mn phases (Lynn & Bonatti 1965). Such a mechanism would successfully fractionate Fe from Mn due to their different responses to Eh and pH (Figure 4.8). Pe-Piper & Piper (1989) state that the distribution of Mn within the cherts of the Peloponnese is due to diagenetic concentration. They cite an association with calciturbidites from stratigraphic positions that are equivalent to the Paos Limestone Member. The rocks that they studied have only minor Mn-enrichment (0.01-1.09%) and show positive correlations of Mn with Fe and Ca. These rocks are not considered similar to the much more Mn-enriched specimens detailed here and the mechanism they present is not applicable to the Pindos Mn cherts of this study.

Diagenetic concentration requires, as a necessary prerequisite for Mn dissolution, a reducing medium developed below the sediment/water interface (Price & Calvert 1970). All the host cherts bearing Mn are hematite-rich, red-coloured sediments which show no evidence of reduction. Muller & Mangini (1980) found that the organic carbon content of present day Pacific ocean siliceous facies was around 0.1-0.2% a few centimetres below the sediment/water interface and only 1% at the sediment surface. Furthermore, the Pindos Zone enriched horizons are perfectly concordant with bedding and there are no indications of diagenetic pathways cutting through the sediment.

#### 4) Hydrothermal Enrichment Process

Hydrothermal activity can lead to increased concentrations of certain elements in the water column by the establishment of sea water convection cells, circulating through crust with high heat flow and typically associated with sea-floor volcanism. Convective systems debouch the mineral-enriched hydrothermal waters into the overlying water column. It has been argued that the chemical composition of deep sea sediments enriched in metals varies with the mechanism causing that enrichment (Bostrom 1973, Bonatti *et al.* 1972, Glasby 1977, Cronan 1980, Robertson & Boyle 1983, Varnavas & Panagos 1986).

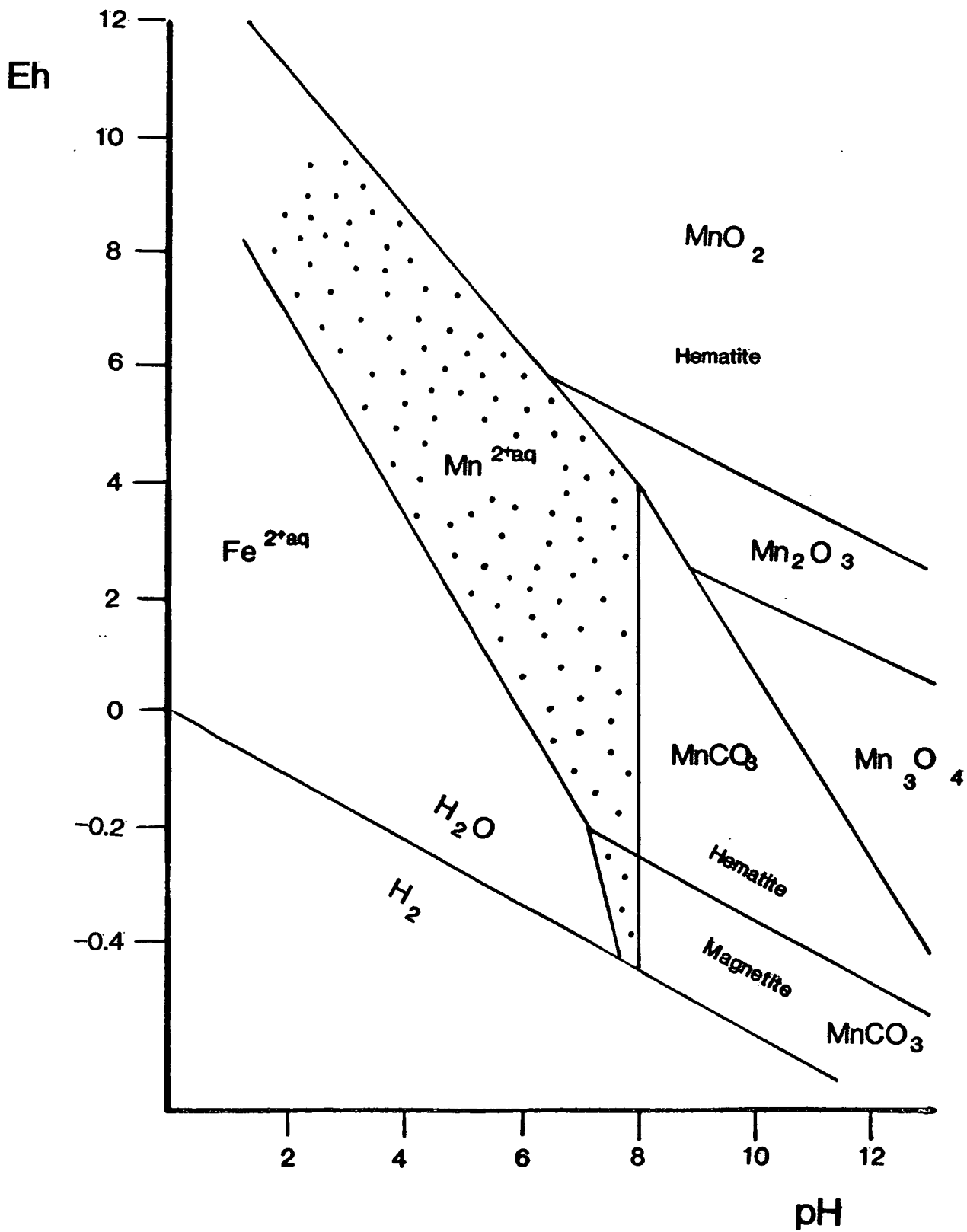


**Fig. 4.8** The stability fields for selected Mn and Fe compounds at 25°C and 1 atm pressure (after Barrett 1979).

#### 4.5.7.2 Suggested Model for Mn Enrichment

The combined evidence presented here strongly suggests that the Mn-enrichment of Upper Jurassic chert in the Pindos Zone was primarily through the precipitation of Mn-rich phases from hydrothermal fluid emanations. Due to the high degree of fractionation of Mn from Fe in the analysed samples and the absence of sulphide deposits, high temperature fluid emanations are not considered appropriate. Rather, an exhalative system based on lower temperature Mn-venting is preferred. A postulated scenario for fractionation is as follows:-

In the ascending portion of a convective cell, temperature will slowly decrease towards the overlying water column. In addition, dilution, as seawater and hydrothermal fluids mix, leads to an increase in alkalinity and subsequent oxidation of metallic phases. An Eh/pH gradient is present and this provides a ready mechanism for the separation of Mn and Fe cations (Figure 4.8) as for any given pH and Eh,  $\text{Fe}_2\text{O}_3$  is more insoluble than  $\text{MnO}_2$  (Krauskopf 1957). Thus, in regions where there is relatively slow percolation of fluids and/or low Eh/pH gradients (e.g. Galapagos mounds, Corliss *et al.* 1978, Varnavas & Cronan 1981, Varnavas *et al.* 1983), Mn is often enriched in overlying sediments, while greater concentrations of  $\text{Fe}_2\text{O}_3$  and sulphides are separated and expected at lower levels. Due to the greater solubility of Mn oxides, plumes of water can be exhaled into the overlying water column where the Mn cations can be expected to eventually precipitate. Advection by bottom currents might then lead to the Mn-enriched plumes drifting for considerable distances away from the sites of hydrothermal activity (Toth 1980). As demonstrated by Boyle (1984, 1990) in the Troodos Ophiolite (Cyprus), spatially concentrated Mn indicates localised precipitation rather than the wide dispersion of metalliferous sediment. In the Pindos Zone of the Peloponnese, localised concentrations over vertical sections measured in metres at Aroania and Drimos suggest that precipitation of the manganese was centred around a hydrothermal source in the near vicinity. Manganese may precipitate locally rather than drifting in bottom currents for one of two reasons. (1) It is known that a critical threshold in Eh/pH conditions is necessary for Mn precipitation. If the threshold is reached slowly due to gradual dilution in the water column, the Mn can be expected to drift considerable distances prior to precipitation. This may be the case for isolated beds of Mn-enriched material from other localities within the Aroania Chert Member, and probably represents more distal precipitation with a mixed hydrothermal/hydrogenous signature. Such intermediate deposits have been described by Toth (1980) and Corliss *et al.* (1978). Mn precipitation without a



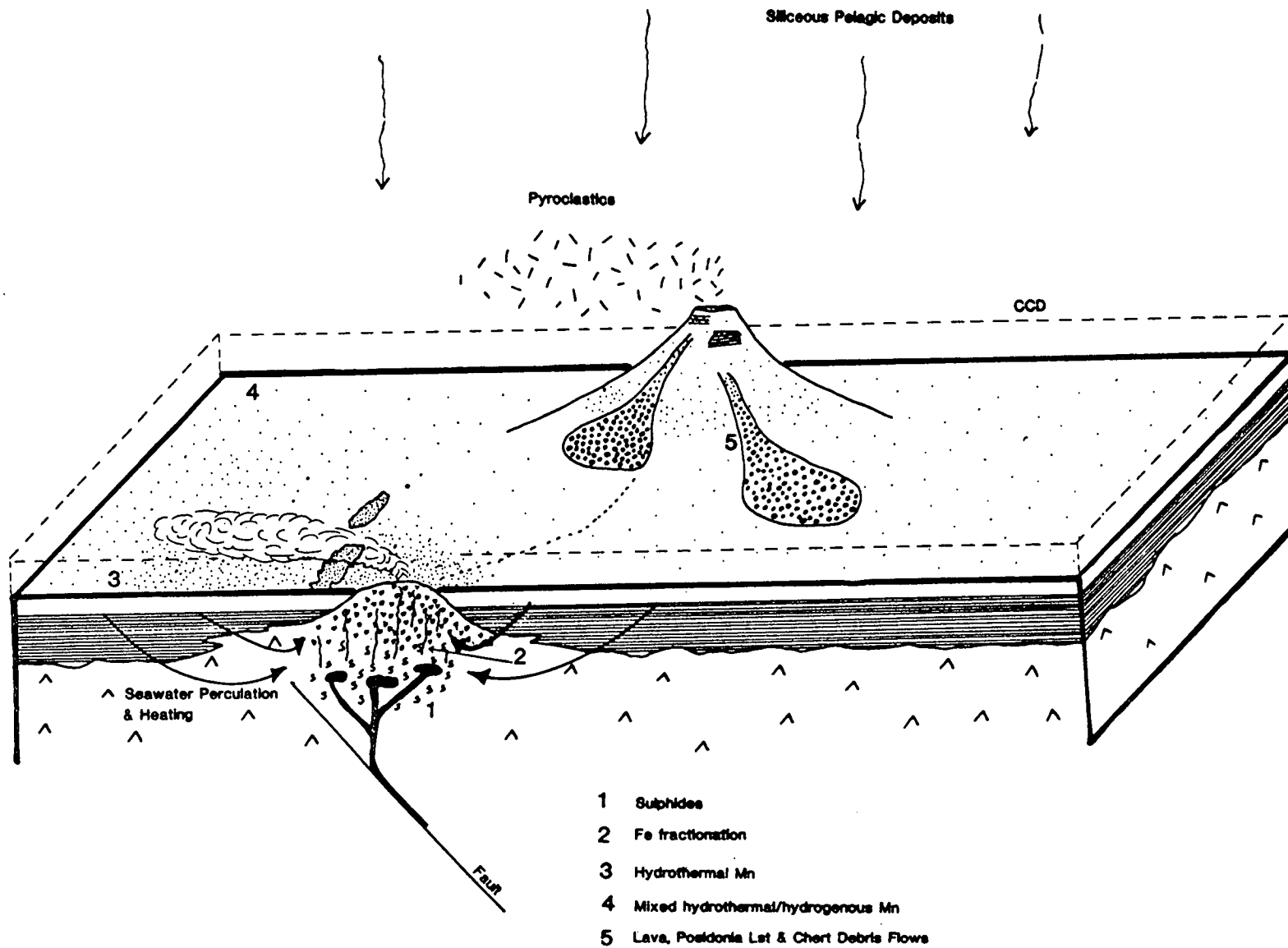


Fig. 4.9 Proposed model for the Mn-enrichment of the radiolarian cherts of the Aroania Chert Member. Explanation in text.

hydrogenous signature may reflect an already fractionated solution that attains the required Eh/pH for precipitation immediately upon expulsion from low temperature vents. (2) When  $Mn^{2+}$  starts precipitating from the water column, it acts as an autocatalyst (Krauskopf 1957), speeding up the reaction as the Mn cations are oxidised to a valence of +4 where they can be precipitated as oxides and hydroxides, primarily as birnessite, todorokite and amorphous oxyhydroxides (Crerar *et al.* 1982). The preferred model for Mn enrichment is schematically shown in Figure 4.9.

#### 4.5.8 Ancient Comparisons

There are many Tethyan passive margin sequences which exhibit Mesozoic metalliferous sedimentation associated with volcanism. Mn-enriched sediment has been studied from other areas in Greece. Panagos & Varnavas (1984) describe the geochemistry of Jurassic Mn-enriched rocks from the Othris Zone. They propose Mn precipitation sourced from hydrothermal solutions. Sulphide and oxide deposits from the Argolis Peninsula, including Mn-rich chert were analysed and described by Robertson *et al.* (1987). The sediment directly overlies MORB type lava and a mechanism involving the fractionation of Mn from Fe through a hydrothermal system with eventual low temperature venting was proposed.

Within the Antalya Complex, Robertson (1981) describes strongly fractionated Mn-rich deposits that were deposited above Upper Triassic lavas. Geochemically they show low REE patterns and enrichment in certain trace elements such as Ba, Cu and V. They appear to have formed via the same processes as the Pindos Mn-rich chert studied here.

Swarbrick (1979), Boyle (1984, 1990) and Robertson & Boyle (1983) describe manganese cherts from the Troodos Mountains, Cyprus which have geochemical signatures and field settings suggesting that Mn-enrichment was due to contemporary hydrothermal activity.

The Pindos Mn-rich cherts can also be compared with metalliferous sediment found in the Ligurian Appenines (Bonatti *et al.* 1976, Barrett 1979, 1981). The enrichment is interpreted to have been derived from hydrothermal emanations. These sediments were deposited above lavas and the Mn phase is braunite rather than pyrolusite. This most probably reflects the P/T conditions of subsequent metamorphism.

In the Wahrah Formation (Oman), Kickmaier & Peters (1991) have studied sediments that are geochemically analogous to those analysed here. The authors suggest a model whereby continentally derived Mn was deposited in sediment on the continental slope, then underwent low level diagenesis and Fe fractionation. The Mn was released into the water column where it drifted through the oxygen-minimum zone to the open ocean and sank to abyssal depths, scavenging trace elements. Finally hydrodynamic sorting led to laminations of enriched Mn chert. It appears that the sole reason for discounting a hydrothermal origin is that there is no obvious hydrothermal source for the Mn in the Wahrah Formation, although Robertson & Searle (1990) point out that there was an active spreading centre to the east during much of the Cretaceous. There are only minor geochemical differences with the Pindos Mn-rich cherts and in view of the overwhelming evidence suggestive of an alternative origin for the cherts studied here, the above mechanism is not considered valid.

Robertson & Boyle (1983) detail the tectonic setting of the various metalliferous oxide and sulphide sediments found throughout the Tethyan realm. In addition to an extensive overview they note that Upper Jurassic to Lower Cretaceous manganiferous intercalations reflect renewed volcanism along the passive continental margins of Turkey (Antalya Complex), Oman (Hawasina), Cyprus (Mamonia) and Syria (Baer-Bassit).

#### 4.5.9 Modern Comparisons

Numerous observations have been made on present day hydrothermal systems from a variety of tectonic settings including recent spreading centres, established mid-ocean ridges, hot spots, back-arc basins and island arcs (Bonatti *et al.* 1972, Moore & Vogt 1976, Lonsdale 1977, Corliss *et al.* 1978, 1979, Cann *et al.* 1977, Rona 1978, Varnavas & Cronan 1988, 1991, Varnavas *et al.* 1990). Despite the extensive use of variation diagrams it is not possible to accurately differentiate the tectonic setting of hydrothermally Mn-enriched rock by geochemical means alone.

The recognition of black and white smoker systems and the isotopic analysis of exhalations in areas of high heat flow has confirmed the long held belief that sea water percolates through fracture systems which develop in sea floor consisting of recently extruded igneous rock. Deep convection cells are set up involving the continuous circulation of sea water through hot rocks. The hydrothermal solutions

are acidic and strongly reducing (Robertson 1978), consequently they are enriched in elements such as Mn, Fe, Si, Ba, Ca, K, Li, Rb and certain trace metals such as Zn, Pb and Cu, leached from magmatic rocks. Mn and Fe are both leached from basalt as divalent ions in approximately equal proportions (Seyfried & Bischoff 1977). Fluid temperatures on exhalation can reach 350°C as estimated from the Galapagos system (Edmond *et al* 1979). Such high temperature systems are the sites of hydrothermal sulphide deposition (Robertson *et al.* 1987).

Field observations from the East Pacific provide the following description of a modern-day hydrothermal field (Crerar *et al.* 1982); "The Galapagos field includes numerous 1-20m high conical mounds and ridges underlain by 30m of siliceous-calcareous ooze; the mounds occur in 1-2km long rows sub-parallel to, and 18-30km from, the rift axis within an area of observed high heat flow. These linear rows are associated with what appear to be minor fault scarps suggesting a structural control with faults focussing hydrothermal activity". There are obvious similarities between this location and the environment as inferred for Aroania. Hydrothermal systems need not be actually on spreading ridges. Cann *et al.* (1977) describes deposits which are also similar to those found at Aroania, 30km from the spreading axis in the Gulf of Aden and Mn crusts are described by Varnavas *et al.* (1988) from the Eratosthenes seamount in the eastern Mediterranean Sea

#### 4.5.10 Summary

Field observations, whole rock geochemistry and the results of electron probe analysis confirm that Pindos Zone Mn-enriched chert has a hydrothermal origin. The data presented here indicates that hydrothermal fluids precipitated Mn with a distinctive hydrothermal signature close to sites of volcanic activity, while far travelled plumes contained Mn-microparticles which became more enriched in sorbed trace elements. This study provides the first evidence of hydrothermal mounds within the Pindos Zone, at Aroania. There are possible analogues in the geological record from other Tethyan areas and from the sites of present-day hydrothermal activity.

#### 4.6 CONCLUSIONS

The Kastelli Mudstone Member is an important transitional facies recording the change from calcareous to siliceous sedimentation at the beginning of the Middle Jurassic. There was a reduction in the supply of coarse material from the adjacent carbonate platform. This allowed the undiluted deposition of clay minerals, wind blown detrital grains and iron oxides. The argillaceous sediments of the Kastelli Mudstone Member are dominated by illite, cryptocrystalline quartz and hematite. Shales of variable thickness were deposited in westerly proximal locations, with sharp contacts above slope derived conglomerates. More distal shale outcrops are characterised by the association of thin calciturbidites, hemipelagic limestones and chert partings. At the end of the Liassic there were several factors influencing the style of sedimentation. Through time there was a reduction in the amount of carbonate present as the member became more siliceous. This was caused by 1) the significant increase in biogenic silica and 2) a sea level rise. Both factors contributed to a shallowing in the level of the CCD. The increase in radiolarian productivity may have been due to the increased upwelling of oxygenated water resulting from the mixing of oceanic equatorial and boreal currents. Direct evidence for this appears lacking and the hypothesis is therefore considered of secondary importance to the main influence of a relative sea level rise, possibly associated with basin subsidence. Recognition of the spatial and temporal distribution of the various facies within the Aroania Chert Member conforms to the model of a passive margin with a basin deepening to the east. The background deposit was a siliceous mudstone, periodically augmented by additional sediment derived from pelagic deposition of radiolarian tests. Closer to the margin, calciturbidites were silicified and a mid-member interval of limestone illustrates the effect of fluctuation of the contemporary CCD. Channelised breccia was derived from the slope and platform, reefal material being derived from an upper-fan or canyon environment, as represented by the Kakotari Member. Mn-enrichment in the Upper Jurassic is dominantly hydrothermal in origin, although sites further away from the discharge zones include manganiferous sediment with a mixed hydrothermal/hydrogenous geochemical signature. Dated radiolarian species from Kombigadi and Aroania indicate that there was active volcanism within the basin in the Upper Jurassic. The resumption of carbonate deposition and the decline in the importance of cherts was due mainly to a relative sea level fall, the ascendancy of calcareous nannofossils and the demise of siliceous radiolarians (possibly because of a change in global oceanic circulation).

## PLATES

### PLATE 4.1: Kastelli Mudstone Member

(A) Typical Kastelli Mudstone Member facies. Note the pale (green) reduced bands parallel to bedding, and later cleavage cutting across the bedding. Lens cap for scale. (B) Oolitic packstone, found interbedded with mudstones. Note the arrowed aggregate clast composed of three individual oolites, suggesting early cementation on the platform prior to redeposition. PPL, Scale bar = 5mm (C) Kastelli Mudstone section from Erymanthos Mountain. Note the isolated beds of calciturbidite, which are often oolitic. At the top of the section are found vitreous green cherts of the over-lying Aroania Member. Section c.a. 17m high. (D) SEM photomicrograph of the siltstone fabric in the Kastelli Mudstone Member. Scale bar = 400 $\mu$ m (E) SEM photomicrograph of authigenic feldspar developed in pelite of the Kastelli Mudstone Member. Scale bar = 100 $\mu$ m (F) SEM photomicrograph of authigenic quartz crystals developed in Kastelli Mudstone. Scale bar = 4 $\mu$ m (G) SEM photomicrograph of authigenic quartz (?) crystals developed in the Kastelli Mudstone. Scale bar = 10 $\mu$ m

### PLATE 4.2: Aroania Chert Member

(A) Basal facies of vitreous green chert with intercalated beds of thick chertified calciturbidite. Section c.a. 2.5m high (B) Typical "ribbon-bedded" radiolarian chert of the red argillaceous chert facies. 1m ruler for scale to the right of photograph. (C) Thin section photomicrograph of argillaceous chert with radiolarians compacted parallel to bedding. Compaction has also resulted in the development of stringers of insoluble residues. PPL, Scale bar = 0.3mm (D) Well preserved radiolarian microfossils in an argillaceous chert matrix. Note the possible effects of current winnowing to concentrate clasts in lower half of photograph. PPL, Scale bar = 0.3mm (E) Radiolarian microfossils totally replaced by chalcedonic quartz. Note the microcrystalline quartz fringe. XP, Scale bar = 0.2mm (F) Intraformational bioturbated pink pelagic limestone. Ruler is 20cm long.

### PLATE 4.3: Aroania Chert Member - Radiolarians

Upper Jurassic radiolarians extracted from Mn-bearing cherts, Aroania mine.

Specimens (A) magnification  $\times$  175, (B)  $\times$  200, (C)  $\times$  300, (D)  $\times$  275, (E)  $\times$  200, (F)  $\times$  140, (G)  $\times$  120, (I)  $\times$  300, (N)  $\times$  250, (O)  $\times$  300, all not identified. (H) *Paronella* sp. ( $\times$  200) (J) *Xiphostylus* sp. or *Acaeniotyle* sp. ( $\times$  250) (K) *Tritrabs* sp. ( $\times$  100) (L) *Archaeospongoprimum* sp. ( $\times$  300) (M) *Katroma* sp. or *Podobursa* sp. ( $\times$  140) (P) *Hsuum* cf. *mclaughlini* ( $\times$  325)

### PLATE 4.4: Aroania Chert Member - Radiolarians

Upper Jurassic radiolarians extracted from cherts deposited above extrusive rocks at Kombigadi.

Specimens (C) magnification  $\times$  300, (D)  $\times$  400, (F)  $\times$  200, (H)  $\times$  300, (J)  $\times$  300, (K)  $\times$  300, (L)  $\times$  300, all not identified. (A) *Holocryptocanium* (?) sp. ( $\times$  300). (B) *Praeconocaryomma* (?) sp. ( $\times$  150). (E) *Acanthocircus* sp. ( $\times$  180). (G) *Dictyomitrella* sp. or *Parvicingula* sp. ( $\times$  300). (I) *Pseudodictyomitra* sp. ( $\times$  300). (M) *Thanarla conica* ( $\times$  350). (N) *Thanarla* sp. ( $\times$  210). (O) *Unoma* sp. ( $\times$  275).

### PLATE 4.5: Aroania Chert Member - Soft Sedimentary Deformation

Photograph and explanatory line drawing indicating soft sedimentary deformation with dewatering structures, seen in the Mn-enriched cherts from the Aroania mine locality. Discussion in text. Lens cap for scale.

**PLATE 4.6: Aroania Chert Member - The Aroania Mine**

(A) Hand specimen of alternating Mn-rich and Mn-poor laminated chert. The illustrated face is a joint plane with well developed radiating pyrolusite crystals. Scale bar = 8cm. (B) Mn-rich cherts beneath (but depositionally over-lying) silica indurated tuffs and agglomerate. (C) Blocks found in the mixed tuff and pelite at the base of the thrust sheet include silica indurated agglomerate (left) and basalt (right). Hammer for scale. (D) Several generations of quartz veins indurating the silica cemented tuff. XP, Scale bar = 0.2mm

**PLATE 4.7: Aroania Chert Member - Electron Image**

A false colour backscattered electron image of the boundary area between, and including, Mn-enriched and Mn-poor laminations (sample PD/89/504). The large round shapes are radiolarians. Explanation and discussion in text. Scale bar = 0.1mm

**PLATE 4.8: Aroania Chert Member - Manganese Enrichment**

(A) Hand specimen of sample PD/89/504 with alternating Mn-rich and Mn-poor laminations. Note the small scale normal fault. (B) Mn-crust on the base of a chert bed. The Mn is mainly of an hydrogenous origin (PD/88/124). Explanation in text. (C) Backscattered electron image of Mn crystallization in the boundary zone of Plate 4.7. The sub-spherical colloform mineralisation consists of alternations of authigenic  $\text{SiO}_2$  and disordered MnO with a thin fringe of Pyrolusite crystals. Explanation in text. Scale bar = 50 $\mu\text{m}$  (D) Backscattered electron image of radiating accicular crystals of pyrolusite from the Mn-enriched horizon of Plate 4.7. The cores contain small amounts of authigenic  $\text{SiO}_2$ . Scale bar = 50 $\mu\text{m}$



# PLATE 4.1

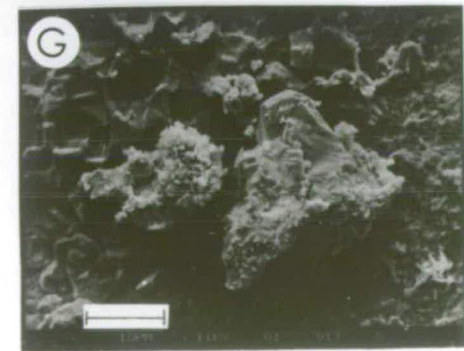
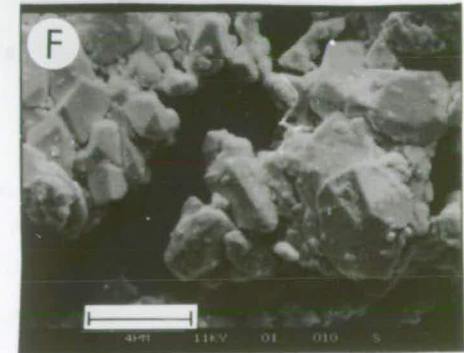
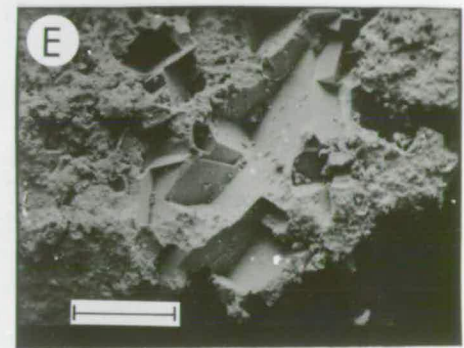
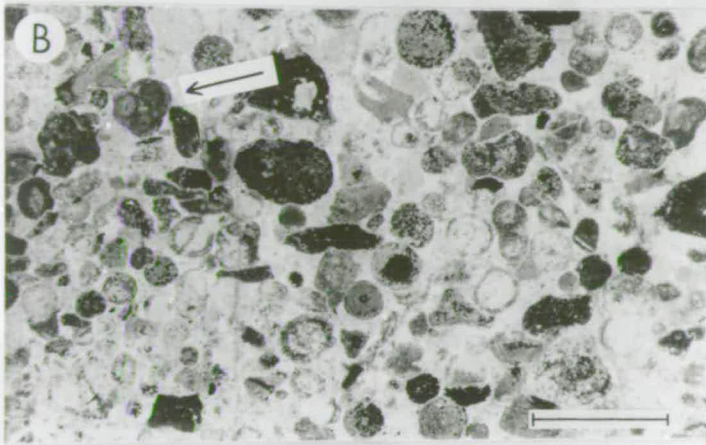
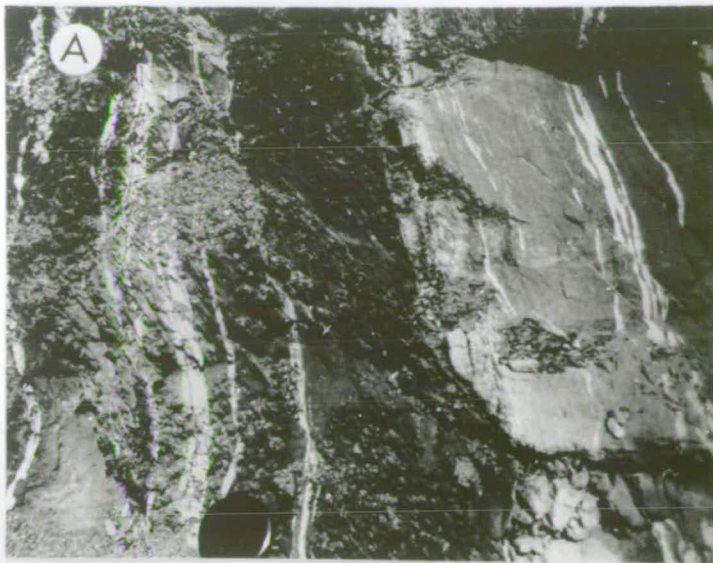




PLATE 4.2

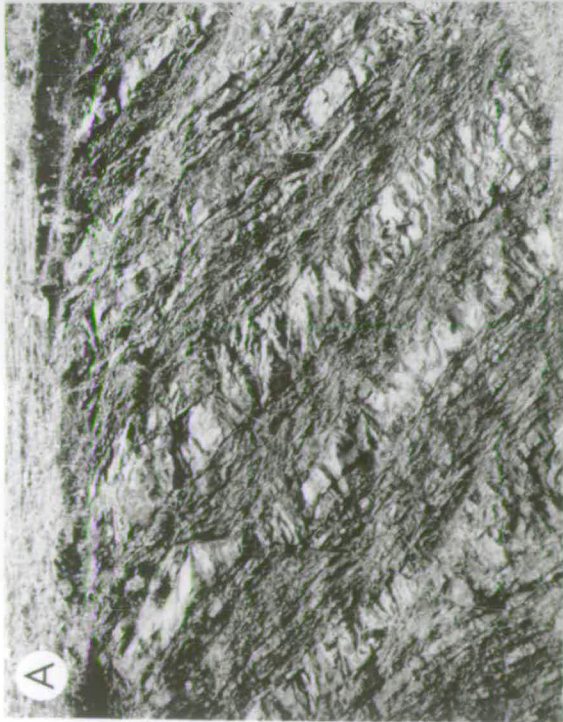
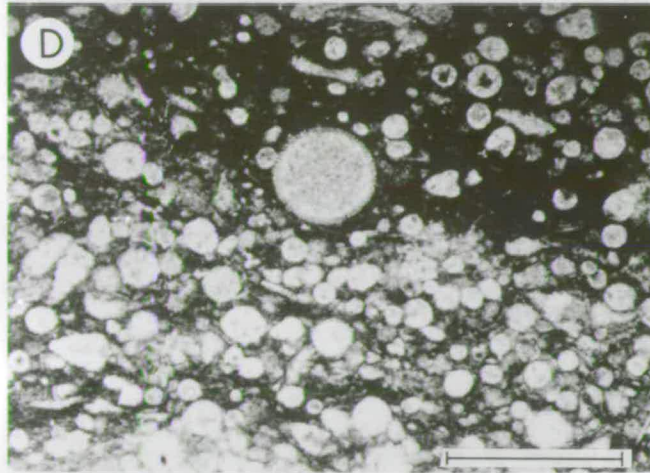
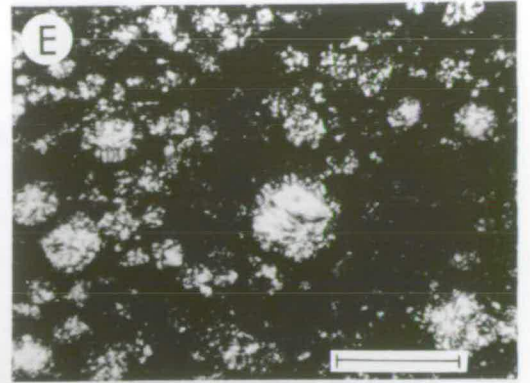
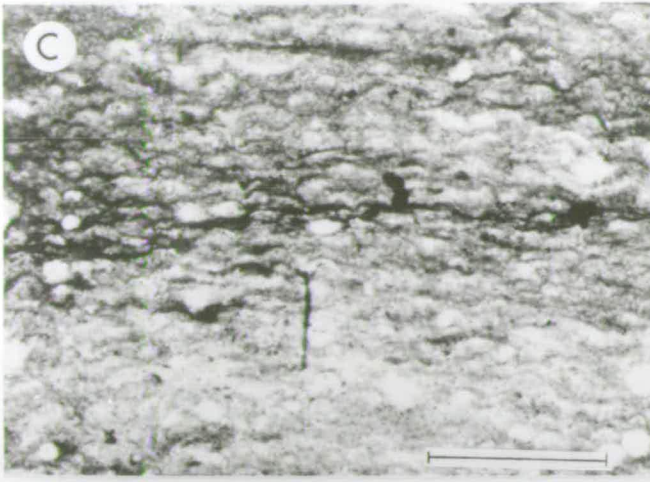




PLATE 4.3

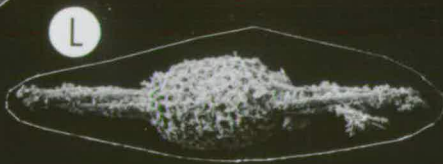
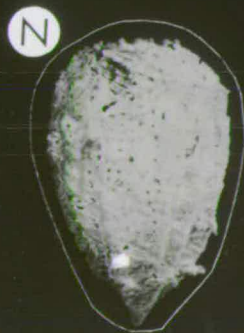
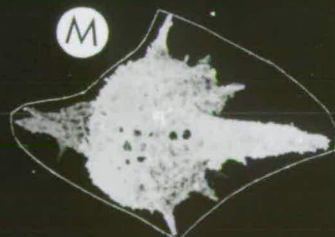
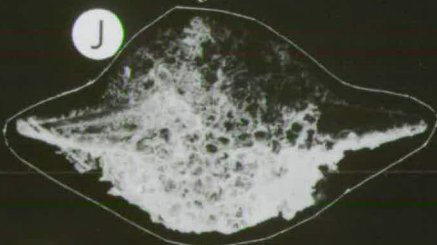
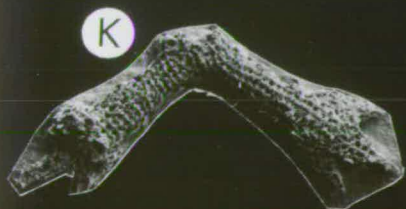
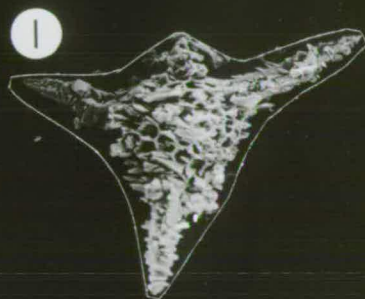
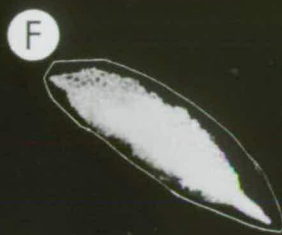
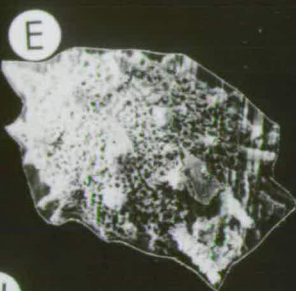
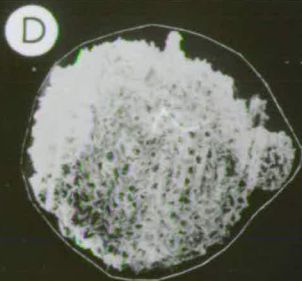
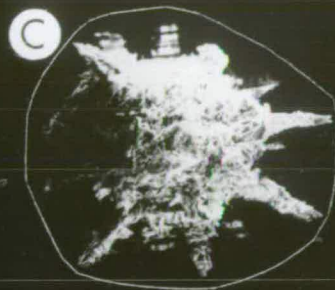
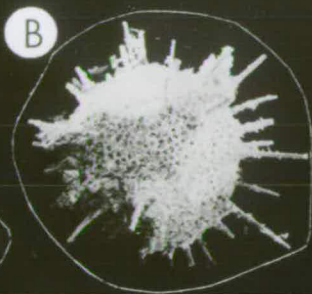
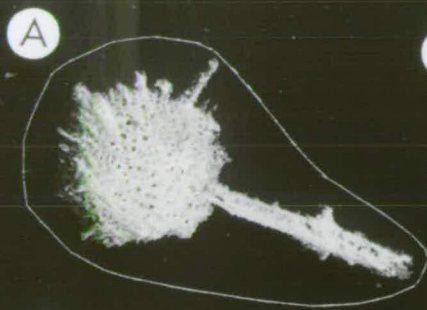
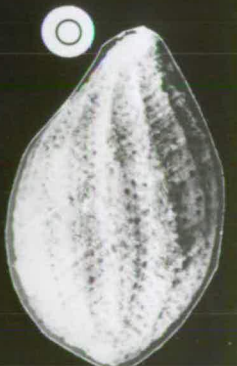
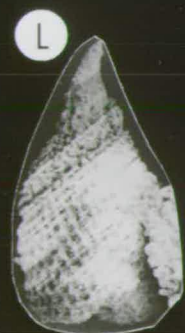
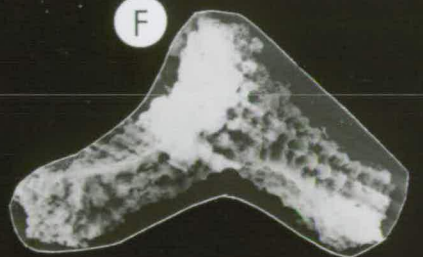
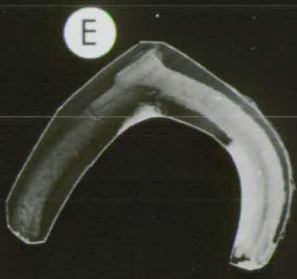
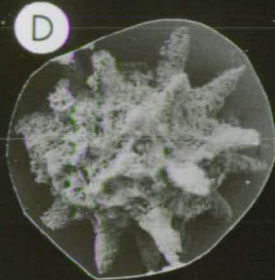
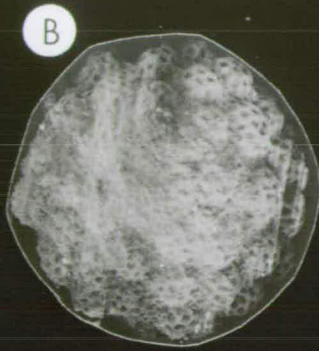
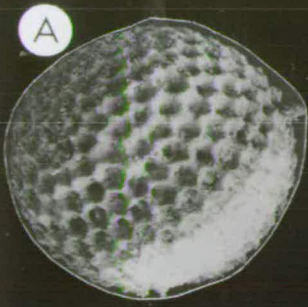
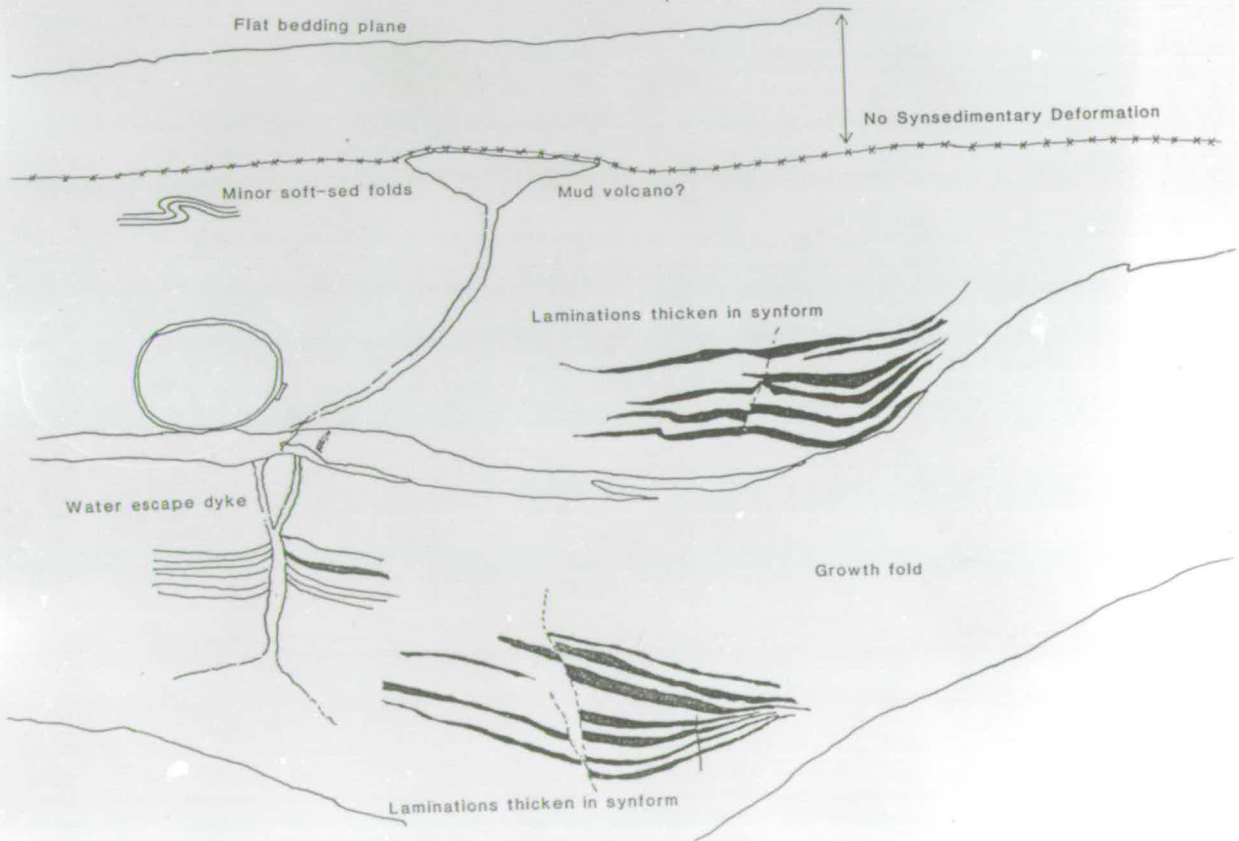


PLATE 4.4



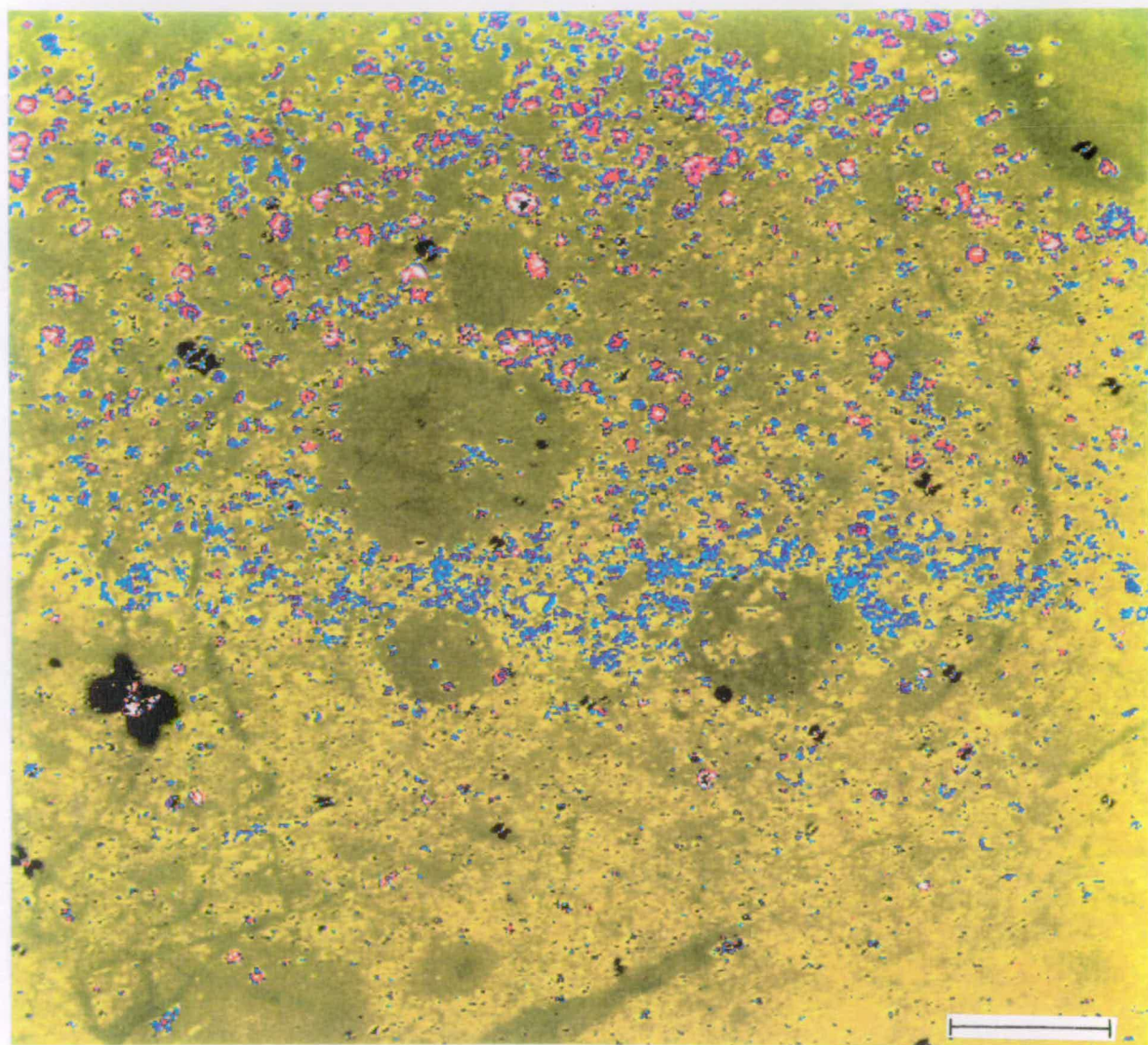








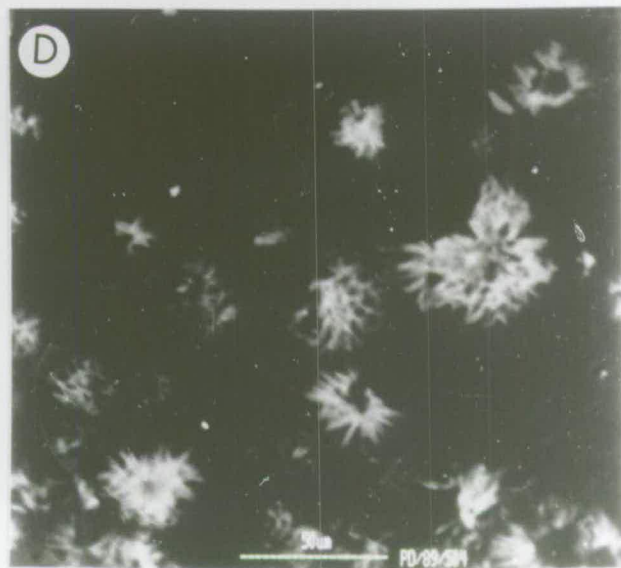
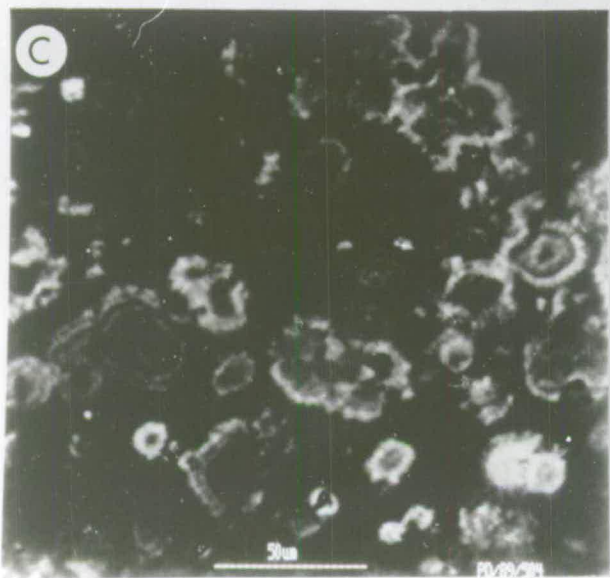
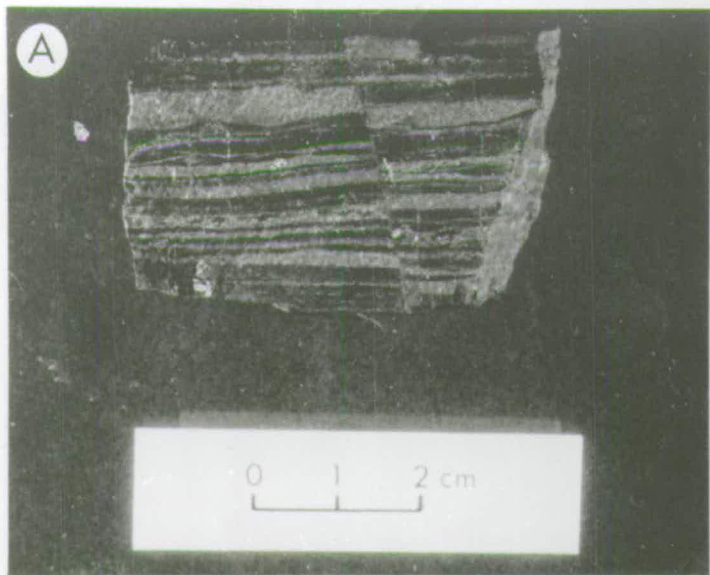
# PLATE 4.7



A: Manganese Enriched Horizon

B: Boundary Zone

C: Manganese Poor Horizon





## CHAPTER 5: THE LAMBIA & PINDOS FLYSCH FORMATIONS

### 5.1 INTRODUCTION

In this chapter the facies and sedimentary characteristics of each of the lithostratigraphic units comprising the *Lambia* and *Pindos Flysch* Formations are described. The present day distribution of the various facies is also indicated, as are proposed depositional environments.

The Cretaceous *Lambia* Formation consists of four members, three of which preserve the proximal/distal relationships established in Chapters 3 and 4. The *Paos Limestone* Member was deposited with stratigraphic continuity above the *Aroania Chert* Member (*Lesteena* Formation), from Tithonian through to Santonian(?) times. It is dominantly a pink, calcareous sequence with subordinate cherts and mudstones. Intercalated within the *Paos Limestone* Member at the type section (Section 2.3.5.1), are two distinct packages of thick bedded, carbonate-rich, quartzose turbiditic sandstone. This unit is sometimes present elsewhere as a single sandstone package. Due to the significance of the siliciclastic unit and despite a highly variable distribution, it has been given informal lithostratigraphic status and is termed the *Klitoria Sandstone* Member. Above the uppermost beds of the *Paos Limestone* Member, the *Erymanthos Limestone* Member was deposited between Coniacian/Santonian and Maastrichtian times. This unit is the most widespread lithology found throughout the *Pindos Zone* and is composed of a thick sequence of calcisiltite and micritic limestones, with subordinate chert and pelite. The member constitutes the dominant mountain-forming relief of the region. Due to frequent structural complications and the lack of suitable marker horizons, complete sequences are rarely recognised, an exception being the type section of Section 2.3.5.3. The *Erymanthos Limestone* Member passes upwards into a transitional sedimentary unit termed the *Kataraktis Passage* Member which is also of variable thickness. The transitional nature is well expressed by a gradational change from calcareous to siliciclastic sedimentation.

The *Pindos Flysch* Formation is the youngest lithostratigraphic unit preserved in the *Pindos Zone* (Palaeocene to Upper Eocene) and is a sequence of intercalated pelites and sandstones that display sedimentary characteristics indicative of deposition from turbidity currents. Due to extensive erosion, preserved thicknesses of the formation are, at most, estimated at 100m and commonly only a few tens of metres.



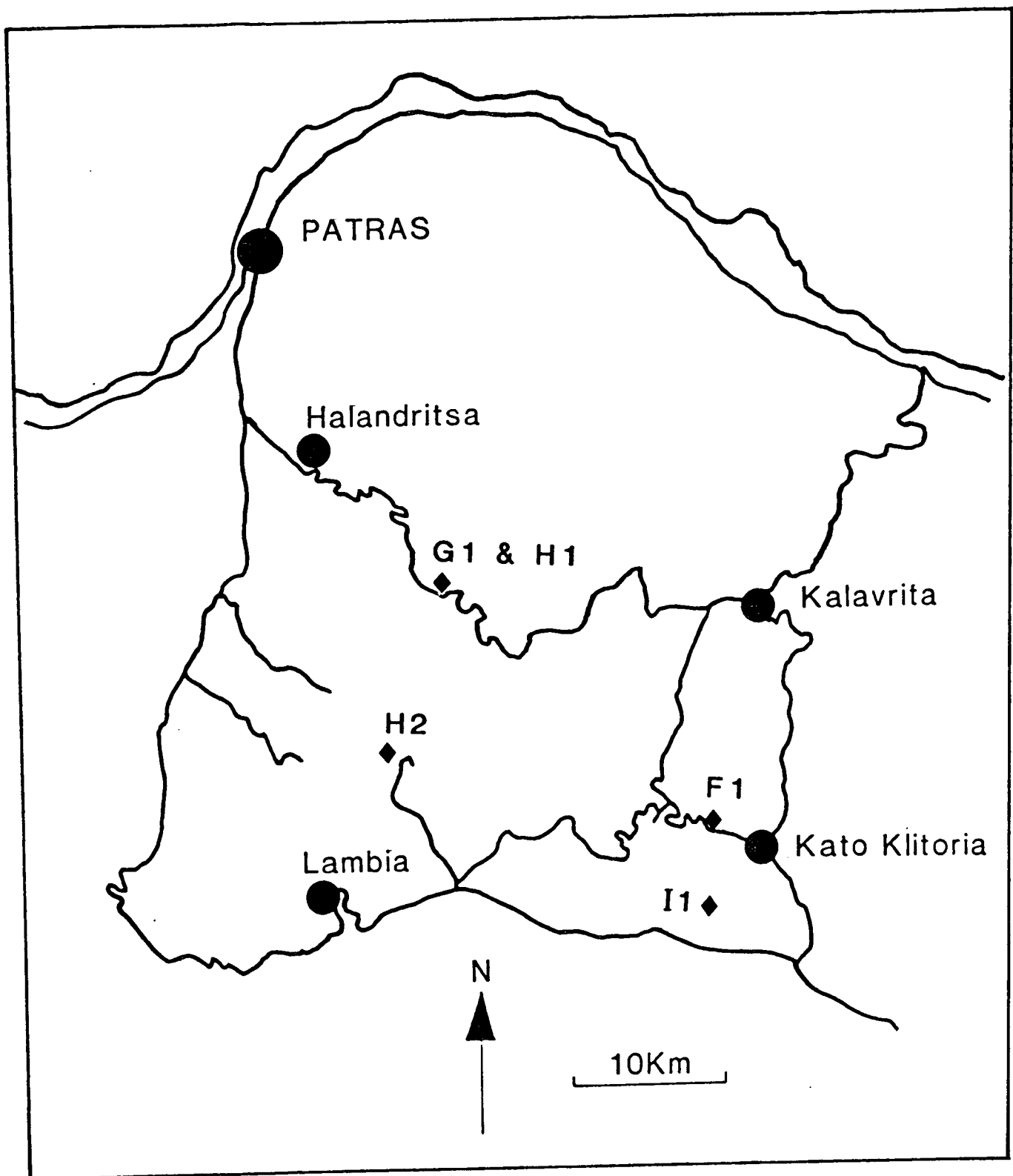


Fig. 5.1 Map indicating the locations of the sedimentary log sites of the Lambia and Pindos Flysch Formations.

## 5.2 THE LAMBIA FORMATION

### 5.2.1 The Paos Limestone Member

#### 5.2.1.1 Lithological Description

##### **Pink Calcisiltite and Micrite**

Although infrequent limestone beds are found intercalated with chert at the top of the underlying Aroania Chert Member, the Paos Limestone Member is easily recognised by the dominant presence of pink limestones. The distinguishing facies of the member, as exposed at distal localities, is a pink thinly bedded (average 5-10cm thick) and laterally continuous micritic to silt grade limestone (Plate 5.1). These fine-grained limestones are generally impure, with variable amounts of red clay present. They grade into red marls which display varying degrees of lithification. There is an occasional, but not uncommon, occurrence of a pink to red argillaceous limestone/highly calcareous mudstone with irregular green reduction bands, streaked-out parallel to bedding (Plate 5.1). These beds are up to 40cm thick and do not appear to be confined to any specific interval within the pink limestones. This facies was observed from Erymanthos to areas as far east as Klitoria.

##### **Pink Calcarenite and Conglomerate**

At the more proximal localities, pink calcarenite and, more infrequently, gravel and pebble grade pink limestone are often present, although in minor quantities when compared to the abundance of micrite and calcisiltite. Variable proportions of pink argillite matrix are present. No sedimentary features such as grading or solemarks are observed, but parallel lamination is sometimes seen in the fine-grained arenite. At localities along the Pindos front, slope derived grey calcirudite dominates the inferred Paos Limestone interval, being present above, and within, pink calcarenite and micrite. Notably, south of Agrambela in the frontal imbricate region (Section 6.2.1), several thick, pink calcareous grainstone beds are channelised. One such channel is 8m wide and filled with matrix supported, gravel grade sediment up to 65cm thick. In thin section, sand grade grainstone is seen to comprise clasts of pink and grey micrite (including bioclastic micrite with radiolarians) which display highly sutured grain boundaries (Plate 5.3). Insoluble residues have been leached from the areas of stylolitic contact and concentrated as anastomosing intergranular stringers. The grains are also preferentially elongated parallel to bedding.

### Additional Facies

Intercalated within the pink limestones are subordinate beds of grey micritic limestone, similar to those of the overlying Erymanthos Limestone Member (Section 5.2.3) and frequent beds of less calcareous, finely laminated shale (sometimes with manganese coatings) and bedded chert to 10cm thick, similar to observed lithologies within the Aroania Chert Member. Chert is also present as grey or red replacement nodules, generally elongated in bedding parallel horizons with undulatory upper and lower bounding surfaces.

At Alepohorio only (Pindos Front, Figure 1.1), a 3m thick sequence of very thinly bedded (2-5cm) white porcellaneous limestone was observed directly above the uppermost chert beds of the Aroania Chert Member (Plate 5.1). Overlying this distinctive limestone facies, the more common Paos Limestone Member facies are present. Several samples of the porcellaneous limestone were taken for thin-sectioning. Most were found to be monotonous, extremely fine-grained micrite with low concentrations of small (50-200 $\mu$ m) calcitic spheres distributed throughout the sample. It is likely that these are calcitised radiolarians. Also present are small ovoid areas (maximum 2x3cm) of partial chertification which in hand specimen have a similar texture to the background micrite and are only recognisable by a subtle grey colour variation. A thin section of a "nodule" in the micrite shows that the centre is a chertified area containing abundant radiolarians replaced by chalcedony, set in a cryptocrystalline quartz matrix. Towards the border of the nodule the silicification front becomes less intense with only chalcedonic radiolarians present in a micrite matrix. Immediately outside the silicification boundary, the nodule is surrounded by calcite containing slightly oblate fine sparry calcite crystals. These grains are all aligned in the same bedding parallel direction. The porcellaneous limestone rocks are lithologically identical to beds observed at approximately the same stratigraphic interval in the southern Peloponnese at Solinari where a section has been described by Thiebault (1982). At this locality the rocks yielded a number of *Calpionellid* species of Tithonian age.

#### 5.2.1.2 Distribution and Depositional Environment

##### Distribution

The Paos Limestone Member is considered to have been deposited throughout the region studied. This statement is qualified as it is not presently exposed everywhere, although this may be due to tectonic omission because the facies occurs at the interface between two lithostratigraphic units of strongly differing rheological

properties. The measured type section (Section 2.3.5.1, Appendix 1, Log F1) is 70m thick (including the Klitoria Sandstone Member) and, while many distal localities have sequences of comparable thickness, in some areas the sequence is very much reduced in thickness, to less than 30m. While it is probable that in many cases there has been tectonic attenuation as described above, this is often not obvious. A conclusion reached in the field is that there are rapid lateral changes in facies thickness which suggest the presence of a pronounced sea floor palaeobathymetry. Due to the long time interval inferred for the deposition of the member (possibly 65 m.y.), and the highly variable thicknesses preserved, it is postulated that there are major sedimentary hiatuses present. These are presumably due to non-deposition and/or the erosive power of bottom currents. The lateral thickness changes are especially obvious in the central imbricate region (Section 6.2.3) where channelised grainstones are present in some places (expanding the sequence), but laterally absent in others, greatly reducing the total thickness.

#### Depositional Environment

The dominant lithology of the member is pink micrite with a variable argillite contribution. It is likely that the pink pigment is hematite and, along with the clay (probably illite), is derived from terrestrial sources; in the same manner as that proposed for the Kastelli Mudstone Member and the argillaceous chert of the Aroania Chert Member (Chapter 4). Thus, the facies can be considered as being formed by background (possibly wind borne) clay and hematite mixing in the water column with the pelagic settling-out of variable quantities of shelf-derived carbonate. The member is considered a transitional lithology, between the underlying red siliceous mudstones and cherts of the Aroania Chert Member and the overlying grey limestones of the Erymanthos Limestone Member.

The pink grainstones and siltstones of proximal areas are relatively homogenous (monomict) with only a weak bedding-parallel lamination; although erosive bases and channels are common. Some of the grainstones contain clasts derived from a neritic environment, but these are relatively rare. There are no sedimentary structures which confirm deposition from turbidity currents, although strong current action is certainly necessary to form the channels observed. Turbidity currents have been suggested as the transport medium for coarse-grained lithologies of other formations (Priolithos Formation, Klitoria Sandstone Member, Pindos Flysch Formation and certain Drimos and Erymanthos Limestone beds), and they probably played a significant role in transporting some platform and slope material into the

deep water environment of the continental rise and onto the abyssal plain. The pink calcisiltite and calcarenite is therefore probably analogous to the grey calcisiltite and calcarenite of the overlying Erymanthos Limestone Member (Section 5.2.3), except that in this member there is a significantly greater inclusion of terrestrially derived argillite with hematite pigment. The presence of rounded pink micrite clasts suggests the reworking of intrabasinal deposits from higher up the slope, admixed in variable proportions with platform-derived carbonate material.

The isolated chert beds may indicate the effects of either particularly intense radiolarian productivity, or short term fluctuations in the level of the CCD. Similarly, thin shale beds may reflect the position of the coeval CCD with respect to the sediment/water interface. Alternatively, the mudstone facies may reflect temporary periods where carbonate supply from the shelf was reduced, allowing the concentration of (wind blown?) fines. Some of the chert and shale beds have thin manganese coatings which are probably of diagenetic origin (Pe-Piper & Piper 1989).

The porcellanous limestones observed at Alepohorio (absent elsewhere in the study area) and deposited prior to pink micrites, suggests that the CCD was at, or below, the sediment/water interface in more inboard locations at an earlier time than in more outboard locations. This allowed a phase of carbonate and radiolarian sediment mixing and accumulation, without the contamination of non-calcareous fines. The chert nodules in the porcellaneous limestones probably formed during early diagenesis, prior to the compaction of less competent surrounding limestone. Geeslin & Chaetz (1972) and Rio (1982) have established that silicification can occur before the complete lithification of carbonate. The abundant calcispheres in the micrite are considered to represent remnant calcitised radiolarians and they are the probable source of silica that was transported, as pore fluid, to nodule nucleation sites.

The base of the member is dated as Tithonian based on the presence of radiolarians in the underlying Aroania Chert Member (Plates 4.3<sup>4.4</sup>) and the presence of Tithonian porcellaneous limestone at Alepohorio. There is a general absence of microfauna within the member (although the morphology of the green reduction bands, in red marl, have the appearance of compacted burrow systems Plate 5.1); this may indicate deposition close to the level of the CCD, resulting in the dissolution of pelagic foraminifera and some of the hemi-pelagic sediment.

## 5.2.2 The Klitoria Sandstone Member

### 5.2.2.1 Lithological Description

The Klitoria Sandstone Member is found conformably within the Paos Limestone Member as two distinct sandstone packages in the type section (Section 2.3.5.2). The principle lithologies present in the member are sandstones, siltstones and mudstones which weather to a green colour. Sandstone beds are up to 160cm thick, but more usually 20-50cm. Siltstone beds are generally  $\frac{up}{\Delta}$  to 20cm, while pelites are at most 3-5cm. Many of the sandstone beds have erosive bases with a preserved coarse basal lag. Grading is very common, with medium-grained sandstone passing up into fine-grained sandstone or siltstone. Parallel laminations are present and the grain-size distribution and sedimentary features frequently indicate Ta & Tb or Ta & Tc Bouma sequences, sometimes with Td or Te units above. There are palaeocurrent indicators present in the beds, such as trough cross-lamination and abundant groove casts; while flute casts were also occasionally noted. On an upper bedding surface, abundant sub-parallel, undulose lineations are composed of slightly coarser sand than in the adjacent areas and these are considered to define ripple crest axes, perpendicular to the current direction.

The sandstones are fine- to medium-grained, moderately to well sorted and comprise sub-angular to sub-rounded clasts. Clast composition is dominantly carbonate, with components derived from both neritic and pelagic environments. Poly- and monocrystalline quartz and lithic fragments are present in variable proportions (Plate 5.3) and the sandstones are classified as litharenites (McBride 1963). The lithics are most frequently black and red chert (Plate 5.3), mica and mudstone rip-up clasts. A few variably altered clasts of volcanic origin are observed in thin section with chloritic replacement. Adjacent limestone beds were found to contain sparse quartz grains admixed with carbonate clasts, or sometimes floating in micrite.

### 5.2.2.2 Distribution and Depositional Environment

#### Distribution

The presence of this lithology is highly variable, and locally totally absent. In the most proximal areas no quartzose sandstone beds were recognised. The only possible evidence of the member west of Livardzi (Figure 1.1) is as rare, thin, discontinuous terrigenous siltstone beds, up to 3cm thick, found intercalated within silt-grade calciturbidite attributed to the Erymanthos Limestone Member. The most widespread occurrence of the Klitoria Sandstone Member is in an area parallel to the

KLITORIA SST MEMBER PALAEOCURRENTS

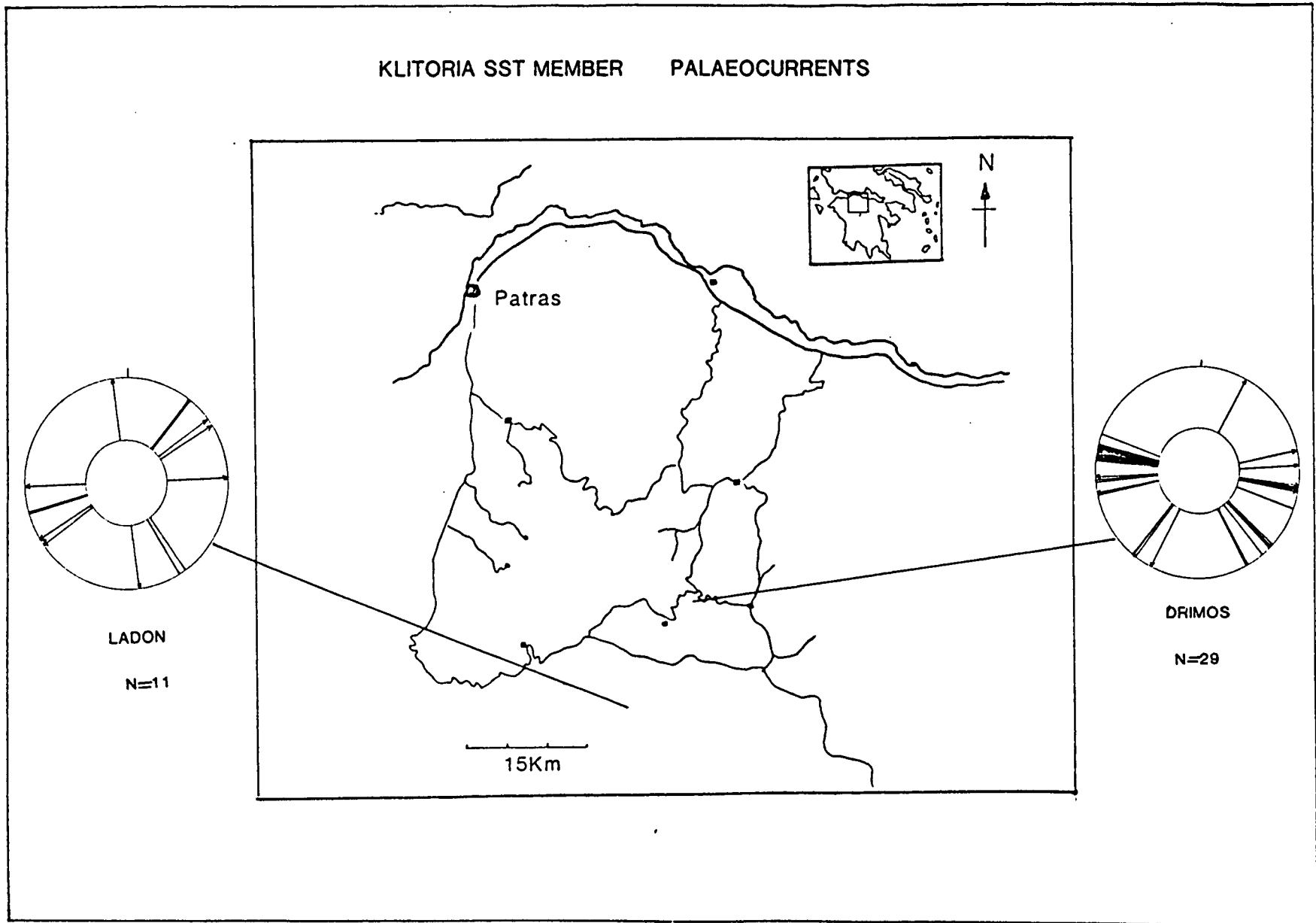


Fig. 5.2 Palaeocurrent directions from the Klitoria Sandstone Member. Arrowed indicators are bi-directional from e.g. groove casts. Other indicators are uni-directional.

mountain front, east of Livardzi and between Kalavrita in the north, to Lake Ladon in the south of the study area (Figure 1.1). The sandstones were not found to the east of Chelmos, but may be present as this region was not studied exhaustively. Even along strike the member is not present everywhere. The presence of the Klitoria Sandstone Member was also noted in the central and southern Peloponnese.

#### Depositional Environment

The sandstones and siltstones are graded, contain Bouma sequences, groove casts, flute casts and ripple laminations. They were without doubt deposited from turbidity currents. Intercalated mudstones were also probably derived from turbidity current flows (Te interval). The palaeocurrent indicators (Figure 5.2) are not consistent, even within a single package, and show current directions to both the east and west and also towards the SW at Drimos. A north-south bidirectional flow was also recorded at Ladon. Given the lack of palaeocurrent data from a wide area it is difficult to interpret this pattern. A possible explanation may be that turbid flows entered the Pindos Basin from a variety of point sources along the western margin. Alternatively, the dominant indicators might reflect a sinuous depression within the Pindos Basin, with the palaeocurrents indicating turbidity flow in meandering channels. It is possible that reflected currents could also cause the wide range of transport directions recorded.

There are no serpentinite or other ultramafic clasts present which might suggest derivation from an eroding ophiolitic terrane to the east, as proposed by Aubouin (1959) and Green (1982). However, Thiebault and Fleury (1991) have analysed contemporaneous mudstones from the Peloponnese and they state that an ophiolite-derived mineralogy is present in Lower Cretaceous mudstones. The sparse volcanic clasts present in the member appear similar to those found in the TSM volcanoclastic rocks (derived from the west, Section 8.4) and the Pindos Flysch Formation (derived from the east, Section 5.3) although in lower concentrations. The sediment source of the Klitoria Sandstone Member is considered to be located within the Apulian hinterland, given that the metamorphic quartz and volcanic fragments are mixed with carbonate clasts which were probably derived from the Apulian margin. However, an eastern provenance is not excluded.



## 5.2.3 The Erymanthos Limestone Member

### 5.2.3.1 Lithological Description

The Erymanthos Limestone Member is notable for the thick, monotonous sequence of micrite and calciturbidite that makes-up the high, mountainous terrain of the study area. The transition from the underlying Paos Limestone Member is gradational and marked by a reduction in the occurrence of pink micrite and siltite. The transition to the overlying Kataraktis Passage Member is lithologically gradational but is formally marked by the first occurrence of siliciclastic sediment, or the presence of a distinctive horizon of black replacement chert. There are four distinctive facies recognised in the Erymanthos Limestone Member:-

#### Calcirudite

In the west of the study area, at Kalendsi, calcirudite interbedded with calcarenite and micrite characterises the stratigraphically lowermost (60-80m) and also the uppermost (30m?) beds of the more proximal thrust sheets. Additionally, beds of calcirudite occur sporadically in the middle of the member. Bedding is thick, between 30cm-2m, moderately sorted and with clast sizes up to 10x15cm. Channelisation is not obvious at the scale of observation and although channel morphology is not apparent, calcirudite bases are often clearly erosive into underlying beds. Clast-supported monomict and oligomict conglomerates predominate, but matrix-supported fabrics are also common (Plate 5.2). Clasts are sub-rounded and are mostly composed of micrite. Other clasts present are reworked limestone containing peloids, ooids and neritic fauna including benthic foraminifera and rudist fragments, also algae and *Globotruncana* (a planktonic foraminifera, Plate 5.2).

The rudite-dominated outcrop is not continuous along strike, e.g. at Kalendzi, rudite comprises c.a. 60-80m thickness, while at Alepohorio rudite is intercalated with, and subordinate to, approximately 40m of arenite grade calciturbidite which passes imperceptibly into the upper stratigraphic section of the member, comprising calcisiltite and micrite. Superb, but inaccessible, exposures north of the Alepohorio valley, reveal that the calcirudite beds are channelised on a very large scale. Channel widths are estimated at between 300-500m, and width to height ratios are high (estimated at 50:1 to 100:1).

### Calcarenite

Intercalated beds of sand-grade carbonate (to 50cm thick) make-up approximately 20% of the inferred 60-80m total thickness of rudite-dominated sediment at Kalendsi. A weak grading is often present in the calcarenite. Grains are mostly sub-rounded and include neritic bioclastic debris (bryozoan, algal, rudist and echinoderm fragments), also abundant *Globotruncana* and micrite, including reworked bioclastic micrite containing Tithonian *Calpionellid* species (Plate 5.2). The allochems are closely packed to form packstone, or sometimes grainstone fabrics and the clasts are cemented by calcite spar. The type section at Dendra (Section 2.3.5.3 Appendix 1, Log G1) is considered to represent a depositionally intermediate position between proximal and distal extremes and therefore contains a mixture of facies. Notably, beds of *Globotruncana*-bearing calcarenite are more frequent than found further east, and gravel-grade conglomerate is sometimes also present, but generally finer-grained facies predominate. Calcarenite bedding at Dendra and Livardzi is thinner than in the more proximal sheets, generally up to 15cm, but is everywhere considered to be tabular.

### Calcsiltite and Micrite

Almost the complete sequence of the Erymanthos Limestone Member, east of Livardzi, consists of interbedded micrite and siltgrade carbonate with occasional fine-grained calcarenite. The middle and upper stratigraphic sections of the Erymanthos Limestone Member in proximal areas is also dominated by calcsiltite and micrite. The facies are found in approximately equal proportions in the east (distal), while calcsiltite is more frequent in the west (proximal). These facies comprise most of the total member thickness in both proximal and distal settings.

Micrite bedding is generally up to 10cm thick and laterally continuous with planar bedding contacts (Plate 5.1 and 5.2). The dominant colour is internally grey (creamy-white on exposed surfaces), or seldomly pink (similar to those described in Section 5.2.1.) or grey-green. Thin section examination reveals an homogenous rock composed of microcrystalline calcite. Horizons of concentrated accumulations of *Globotruncana* are sometimes observed in bioclastic micrite (Plate 5.2), as are faint calcitic spheres, possibly representing calcitised radiolarians or pelagic foraminiferal chambers.

Many silt-grade limestone beds of the frontal and central regions (west of Livardzi, Figure 1.1) show horizons of trough cross-lamination, parallel lamination and

occasionally convolution. The sedimentary structures are not usually particular to a complete bed, but rather to a portion of a bed (usually the upper third of the bed thickness). The convolutions are generally unorientated and indicate soft-sediment deformation. In distal locations sedimentary structures are not usually present in hand specimen, although the silt-grade grainstone fabric is clear. In thin section, calcisiltite beds, that appeared homogenous in hand specimen, were often seen to have graded bedding (Ta interval) and sometimes a sharply defined boundary with overlying lutite grade material which includes sparse grains of silt grade sediment (Plate 5.3).

#### Other Facies

Intercalated beds of dark coloured shale are usually less than 1cm thick and are often present only as bedding partings. Grey or red replacement cherts are often present as nodular horizons, but also as laterally continuous beds to 10cm thick. Replacement cherts are far less frequent in upper parts than lower in the stratigraphy. It is possible to recognise remnant carbonate allochems in some chert beds.

#### 5.2.3.2 Distribution and Depositional Environment

##### Distribution

The member is the dominant relief forming lithology of the Pindos Zone (e.g. Plate 6.1) and is found throughout the study area. Because of the paucity of marker horizons and the often intense deformation, the member does not usually exhibit continuous sections which allow an accurate appraisal of thickness. An exception is the type section (Section 2.3.5.3, Appendix 1, Log G1) located at Dendra, where a total thickness of 183m is recorded. Flament (1973), using age diagnostic *Globotrunca* species, constructed a composite section from two localities near to Kato Klitoria, which measures 248m. It is probable that thick rudite, found lower in the stratigraphy of the frontal region, has locally expanded the sequence in those areas. There is a distinct west to east proximal-distal depositional pattern present, as established for other formations and this is expressed in the facies distribution of the Erymanthos Limestone Member.

##### Depositional Environment

###### Calcirudite

The calcirudite is spatially associated with westerly localities. The presence of both clast- and matrix-supported fabrics, and the clast composition, indicates derivation from platform and slope environments by rock fall and debris flow mechanisms.

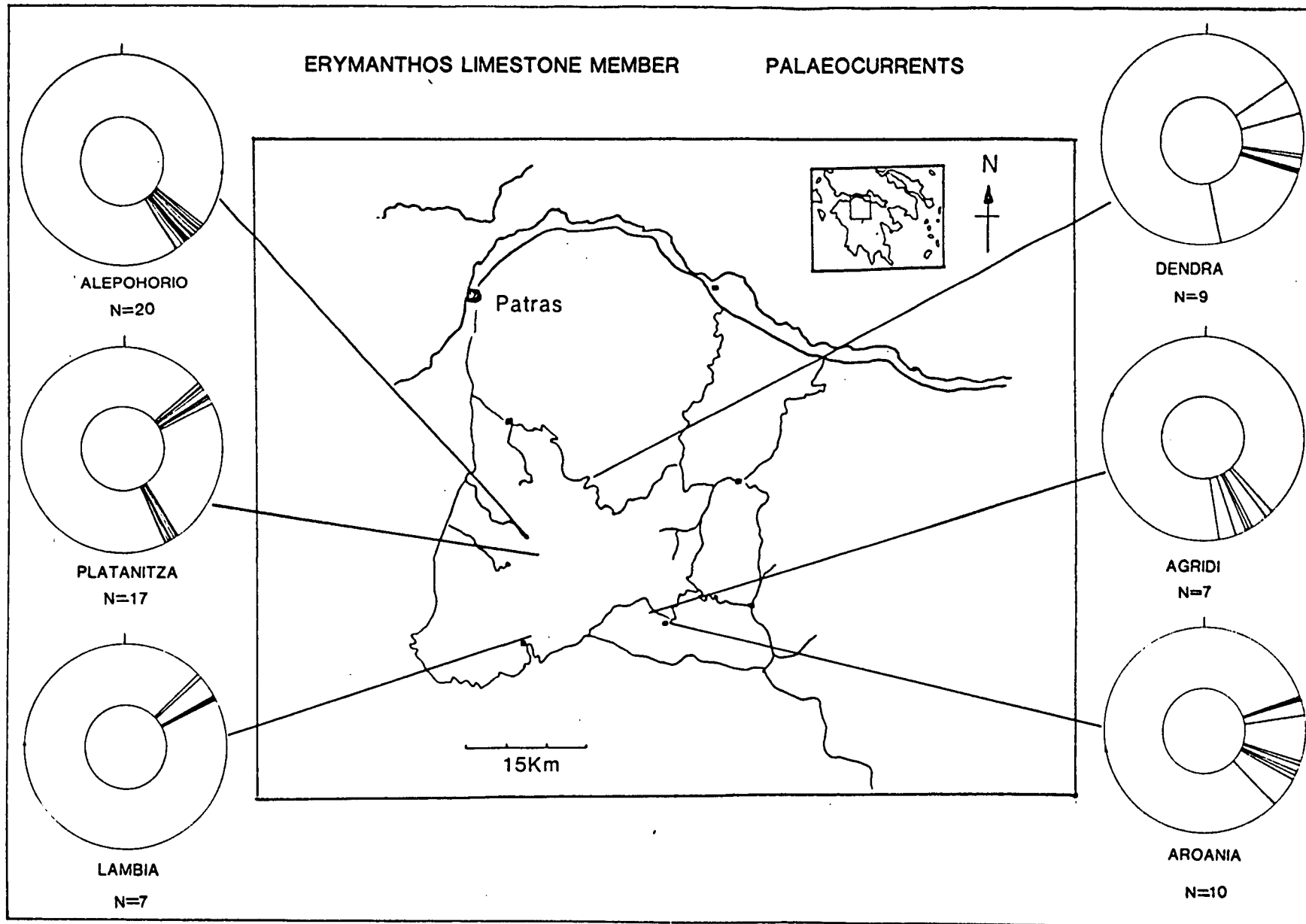


**Fig. 5.3** Palaeocurrent directions from the Erymanthos Limestone Member.

Poorly sorted matrix-supported rudite are considered to represent debris flows (Kalendsi). Such calcirudite deposits probably grade outboard into channelised turbidity flows which preserve only the Bouma Ta interval in calcarenite (Alephorio). No distinctive grading was observed in the cobble and pebble grade rudite beds, but Lowe (1982) has proposed that there may be a continuum of coarse-grained facies from disorganised matrix-supported rudite to normally graded rudite, reflecting the change in depositional mechanism from debris flows (where sediment is supported by cohesive and bouyancy forces) to high density turbulent flow (where the sediment is supported by turbulent fluid forces). The lack of grading in proximal Pindos Group sediment may simply reflect the fact that only part of the Ta interval is locally preserved. This might occur where the development of a graded bedding is inhibited by the rapid deceleration of a high density turbidity current mass flow, such that the critical flow strength is no longer sufficient to support any rudite grade sediment by turbulent fluid forces, thus "dumping" the coarsest grained sediment *en-mass* (Lowe 1982). The rudite facies of the Erymanthos Limestone Member is considered to represent a similar depositional environment to that inferred for the base of slope talus apron formed by proximal carbonate deposits of the Drimos Formation (Section 3.3.2.2).

#### Calcarenite

Packstone/grainstone calcarenite is also particularly associated with proximal localities, where the bedding is thickest. The facies is also present further east where it is likely that the sediment was unconfined by narrow channels, giving rise to sheet deposits with a tabular bed morphology. The presence of abundant neritic debris, especially rudist fragments and algae, in the calcarenites and calcirudites indicates the presence of substantial reef build-ups along the Gavrovo-Tripolitza platform (Section 7.3.1). Rudists were important reef-building organisms in the Tethyan realm during the Upper Cretaceous and algae are common to reef environments, where they help to bind loose sediment. The weak grading in calcarenite suggests an interpretation as turbidity current deposits that preserved only the Ta division. The calcarenite may be the lower density components of gravity flows which include the debris flows preserved in proximal locations as postulated above and in Section 3.3.2.2.

#### Calcsiltite

The calcsiltite facies shows definite characteristics indicative of derivation from turbidity currents and the calcsiltite is therefore equivalent to calciturbidite. Usually

only Ta intervals of low density deposits are preserved (equivalent to far travelled Te intervals of higher density flows?), but Ta-Tb, Ta-Tc and Ta-Te intervals are also present, especially in more proximal locations. Thin section examination indicates that lutite grade material, deposited above calcisiltite and with a sharp boundary dividing the intervals, was derived from the same turbidity current. The evidence for this is the inclusion of silt grade clasts in the micrite, especially near the base, which decrease in frequency upwards (Plate 5.3). Soft sediment convolutions are suggestive of liquified or fluidised flow mechanisms (Table B1), which indicate post-depositional movement while the sediment was still soft. This itself suggests deposition on a slope (liquified flow), but may alternatively be due to overpressuring by loading from the traction of overlying sediment (fluidised flow). The individual Bouma intervals are well sorted, although larger redeposited *Globotruncana* are also sometimes present. Palaeocurrent directions, chiefly obtained from trough cross-lamination in the Tc interval of calciturbidites, show a dominant flow direction to the SE, although at Platanitza and Lambia palaeoflows towards the NE were also recorded (Figure 5.3).

#### Micrite

The finest grained carbonate consists of micron-sized calcite with sparse inclusions of calcitised radiolaria and *Globotruncana*. The apparent absence of bioturbation probably reflects the homogeneity of the sediment rather than the lack of coeval infauna. The complete lack of flow-induced sedimentary structures, the generally thin bedding and the presence of thin shale partings (often found separating micrite from calcisiltite or other micritic beds), indicates that the sediment was probably a peri-platform ooze deposited through pelagic settling. There is no evidence for derivation from turbid flows or reworking by bottom currents. However, lutite of turbiditic and pelagic origin can be difficult to distinguish (Rupke 1975, Piper 1978). A turbidite origin is thus not discounted for some, or most, of the micrite beds. Very thin partings of argillite are probably illite-rich, wind blown fines, that may represent either short time periods (where a concentrated interval of off-shore storms could supply large quantities of aeolian sediment), or longer time periods when carbonate supply off the platform was restricted.

## 5.2.4 The Kataraktis Passage Member

### 5.2.4.1 Lithological Description

The Kataraktis Passage Member is transitional between the under- and overlying lithostratigraphic units. The boundaries of the unit are defined in Section 2.3.5.4. Up section, there is a gradual increase in the proportion of siliciclastic material present, until carbonate beds are extremely infrequent. The member contains facies components common to both the Erymanthos Limestone Member and the Pindos Flysch Formation. Consequently, the micrite, calcisiltite, calcarenite and calcirudite descriptions of the Erymanthos Limestone Member (Section 5.2.3) and lithological descriptions of the siliciclastic facies in the Pindos Flysch Formation (Section 5.3.1), are equally valid here. This section will mainly concentrate on field descriptions of the transition. There is also one additional facies found in the Kataraktis Passage Member, not generally present in the surrounding units:-

#### Black Chert

Individual beds of black chert are found in the Kataraktis Passage Member. Significantly, a distinctive 0.5 to 5m thick interval of black chert is also present at, or near, the base of the member. This has been dated as straddling the Mesozoic/Cenozoic boundary as it corresponds to the disappearance of *Globotruncana* sp. and the appearance of *Globigerina* sp. and *Globorotalia* sp. (Flament 1973, Fleury 1980). The lithology occurs as discrete horizons of chert within carbonate beds, with sub-bedding-parallel undulose contacts. Some beds are completely silicified, while other beds containing chert are interbedded with micrite and chert free calcisiltite beds. The black chert is usually laterally continuous, comprising 2-10cm thick beds. Elongate, bedding-parallel nodules are also sometimes present. The distinctive cherts were recognised almost everywhere and formally mark the base of the member where underlying terrigenous sediment is not present.

#### Field Descriptions

At the base of Erymanthos Mountain, outside the village of Platanitza (Figure 1.1), the transition from the Erymanthos Limestone Member to flysch is well exposed over a short (40m) interval (Log H2, Appendix 1). Turbiditic calcarenites, calcisiltites and micrites give way to coarser carbonate debris flow deposits, up to 1.4m thick and containing platform derived clasts up to 14x4cm, and thin intercalations of calcisiltite, muddy micrite and black cherts. Green pelite and

terrigenous arenite are present near the base of the member and increase in dominance upsection.

Immediately north of Livardzi, a transition is recorded in an incomplete sequence which comprises thick beds of calcirudite, of debris flow and/or high density turbidite origin, and intercalated calcisiltite and black chert. This section is significant because a relatively outboard palaeo-position is inferred for the site, based on the presence of more distal facies in other formations.

The Kataraktis Passage Member type section at Dendra (Section 2.3.5.4 Appendix 1, Log H1) is a continuation of the Erymanthos Limestone Member type section. The location has been inferred to represent a depositional site that was intermediate between Platanitza and Livardzi with respect to their inferred palaeogeographic positions. The facies present, however, suggests sediment deposition of a more distal character than at Livardzi. The occurrence of coarse lithologies is more restricted and the gradual transition to siliciclastic rocks is accompanied by the dominance of silt grade lithologies.

At Aroania, the calcareous sediment is of a more distal nature (calcisiltite and micrite only). Thin beds of fine to medium grained sandstone and pelite intercalated with carbonate are observed approximately 20m below the black chert interval.

From localities around Kato Klitoria and Chelmos (i.e. the most distal localities), and some sections examined along the flanks of the Erymanthos Mountain (i.e. at relatively proximal sites) black chert is found intercalated with calcisiltite, followed by a gradual diminution in calcareous sediment (often with trough cross-laminations and occasional convolutions) as overlying terrigenous pelite, siltite and arenite increase over an interval generally in the range of 100m. There is little or no calcirudite present.

#### 5.2.4.2 Distribution and Depositional Environment

##### **Distribution**

The total thickness of the member varies considerably as two criteria are used to delimit the base (black chert or the first occurrence of flysch) and the upper limit is where flysch dominates carbonate over a 10m interval. The member is recognised everywhere where sufficient exposure allows the transition from the Erymanthos Limestone Member to the Pindos Flysch to be recorded.



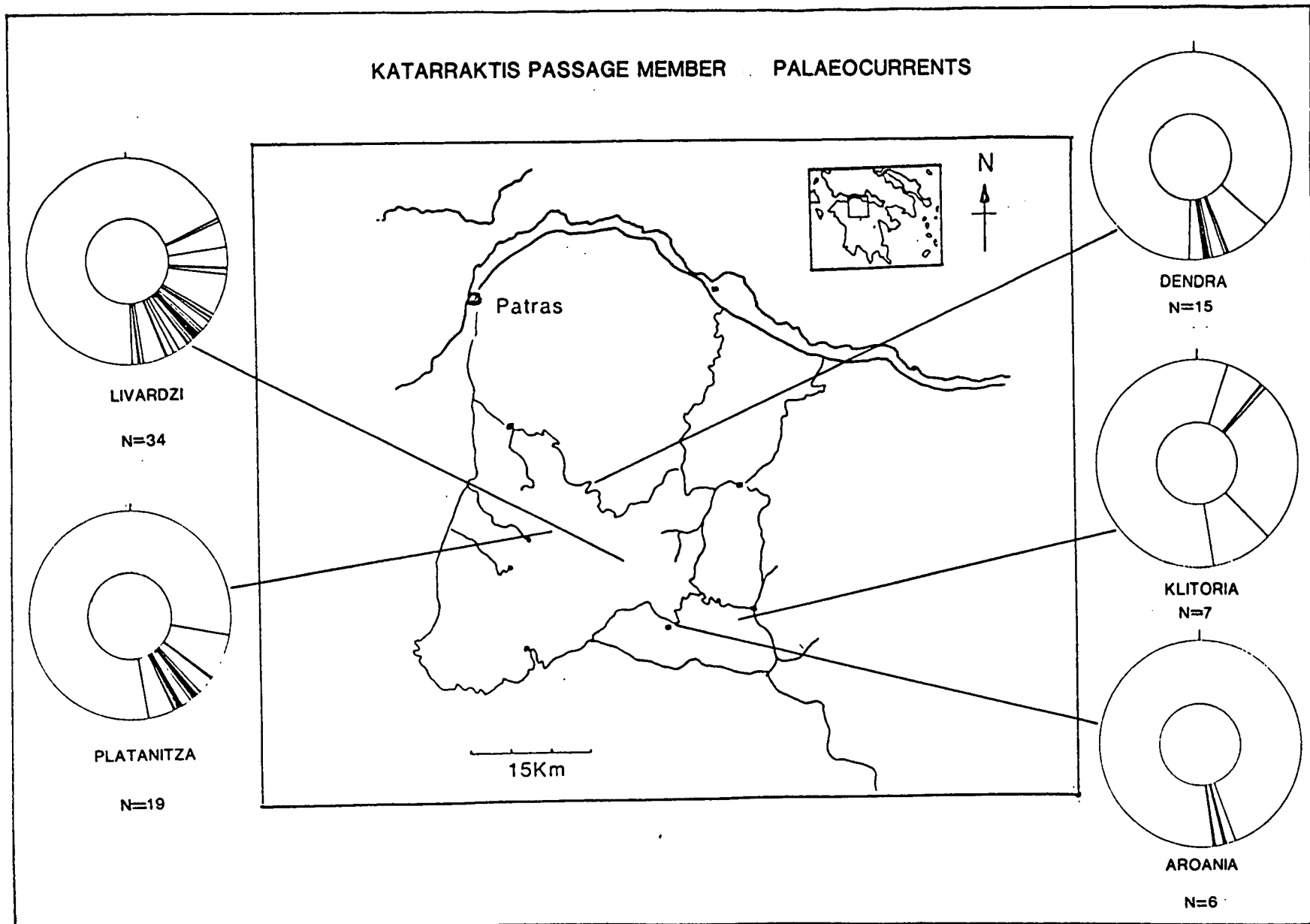


**Fig 5.4** Palaeocurrent directions from the Kataraktis Passage Member.

### Depositional Environment

A proximal to distal (eastwards) character is once again recognised in the distribution of the carbonate facies which comprise the Kataraktis Passage Member. Along the Pindos front, calcirudite was observed at the top of the Erymanthos Limestone Member (30m), overlain by flysch. It is not certain if the contact is tectonic or depositional, due to structural complications and inaccessibility. The onset of rudite-grade carbonate at Platanitza is relatively rapid, occurring immediately prior to the first fine-grained flysch beds. Dendra represents a site where occasional channeled gravel-grade conglomerate and calcarenite was deposited from platform/slope derived turbidity currents. Further outboard, fine-grained lithologies only are present. An exception is the incomplete Kataraktis Passage Member observed at Livardzi, which indicates that coarse, rudite-grade lithologies were transported to such relatively outboard localities, although no other rudite sites were found so far east. The fact that some proximal localities are devoid of calcirudite suggests that the upper reaches of channels most have originated close to the continental rise. The palaeocurrent pattern obtained from calciturbidite trough cross-lamination supports sediment derivation from the NW at Platanitza and Livardzi, while flows to the south are indicated at Dendra and Aroania (Figure 5.4). The earliest deposited flysch sediment is fine-grained arenite and pelite and few palaeocurrents were obtained. Comparisons with palaeocurrents found higher in the Pindos Flysch Formation stratigraphy would indicate a northern provenance.

The black chert present in micrite and calcisiltite is a useful time horizon. It is undoubtedly of a replacement origin, occurring as it does within discrete beds of carbonate. No geochemical analysis was performed on this facies, but it is likely that the black colour reflects an originally high organic carbon component. The fact that this facies occurs throughout the study area during the same time interval (Fleury 1980) implies that a regional factor controlled deposition and/or diagenesis. It is considered likely that the probable source of silica, to form the chert, would have been the periodic proliferation of siliceous micro-organisms, rather than a fall in the CCD.

The changing environment of the member, reflected in the increase in redeposited carbonate grain size in proximal settings, indicates the sudden (in geological terms) shedding of large quantities of carbonate sediment off an eroding Gavrovo-Tripolitza platform to the west. This event was shortly followed by the transition from carbonate to terrigenous facies, with axial(?) turbidity currents transporting

terrigenous sediment from the north which, with time, swamped carbonate sedimentation. However, the presence of the black chert "time horizon" indicates that terrigenous sediment was not deposited coevally in the study area, as in some places the earliest terrigenous sediment is older than the black chert, while in others it is younger. The possible reasons for these changes are discussed in Section 5.3.5.

### 5.2.5 Ancient Comparisons

The Lamba Formation encompasses almost all the Tithonian to end of Maastrichtian times (Late Jurassic-Cretaceous). It is dominantly a calcareous lithostratigraphic unit. The Paos Limestone Member was transitional between the underlying cherts and the Erymanthos Limestone Member. Intercalated siliciclastic deposition (Klitoria Sandstone Member) records a brief input of terrigenous sediment. Siliceous to carbonate lithological intervals are found in the largely time equivalent Derekoy Formation of the Antalya Complex, Turkey (Robertson & Woodcock 1981b) and the Episkopi Formation of the Mamonía Complex, Cyprus (Swarbrick & Robertson 1980). The Derekoy Formation also records the deposition of thin terrigenous silt and sandstone beds and the sedimentology has been used to provide evidence for Late Jurassic/Lower Cretaceous fault activity that is postulated along several Tethyan margins (Robertson & Boyle 1983). The dominance of Late Cretaceous deep water carbonate lithologies, comprising both pelagic and fine-grained turbiditic sediment in the Pindos Zone, can be compared with deposits found in other basins of the Tethyan realm, for example, the Taskaya Tepe Formation (Bilelyeri Group) of the Antalya Complex, Turkey (Robertson & Woodcock 1981b); the Monte Antola flysch of the Apennines (Scholle 1971) and the Episkopi Formation of the Mamonía Complex, Cyprus (Swarbrick & Robertson 1980).

### 5.2.6 Modern Comparisons

There is essentially no difference in the geological setting proposed for sediment deposition in the Pindos Basin between the Upper Triassic/Liassic (deposition of the Drimos Formation) and the Cretaceous period (the Lamba Formation). The depositional setting of both periods is inferred to have been similar, with a productive platform (the Gavrovo-Tripolitza) capped by reef complexes and oolitic shoals, flanking the deep water Pindos Basin that lay to the east. Thus, the by-pass margin setting proposed in Section 3.3.3.2, with the modern day Bahaman analogues are considered equally applicable here.

## 5.3 THE PINDOS FLYSCH FORMATION

### 5.3.1 Lithological Descriptions

The lithologies of the Pindos Flysch Formation are dominated by alternations of sandstone and siltstone with additional pelite and infrequent pink marls present.

#### 5.3.1.1 Sandstone

##### Field Description

The arenite grade beds are laterally continuous and range in thickness from 5cm to in excess of 1.5m. Some channelisation is apparent, with lateral thickness changes and the scouring of underlying beds. The sandstones are light brown, to olive green, depending on the degree of weathering. Constituent clasts are moderately sorted, vary from fine to very coarse-grained and are angular to sub-rounded. Most sandstone beds display at least some degree of normal grading. Particles of organic debris, including abundant wood fragments (to 1x3cm), are frequently seen in hand specimen where they can occasionally be observed to form concentrations on upper bedding surfaces. Flakes of muscovite mica are also found concentrated on upper bedding surfaces.

##### Sedimentary Structures

The sandstones of the Pindos Flysch Formation are particularly rich in sedimentary structures, of biogenic, depositional and post-depositional origin. Biogenic structures are trace fossils which belong to the *Nereites* ichnofacies, indicative of abyssal depths (Seilacher 1964, Frey 1975, Plate 5.4). This assemblage includes *Palaeodictyon*, *Chondrites*, *Helminthopsis* and *Diplocraterion* of which horizontal *Chondrites*-type grazing trails are most commonly observed.

Apart from graded bedding and planar bedding-parallel lamination, many depositional sedimentary structures are found to be potentially useful as palaeocurrent indicators (Plates 5.5 and 5.6). The structures include various types of ripple cross-lamination (planar, trough and climbing), primary current lineations, flute and groove casts and "tea-leaf" lineation (the preferred orientation of organic debris).

In common with other studies of turbidity flow deposits exhibiting palaeocurrent indicators (e.g. Leigh 1991), the bottom structures (flute and groove casts, forming parallel to the palaeoflow direction in the Bouma Ta interval) do not always

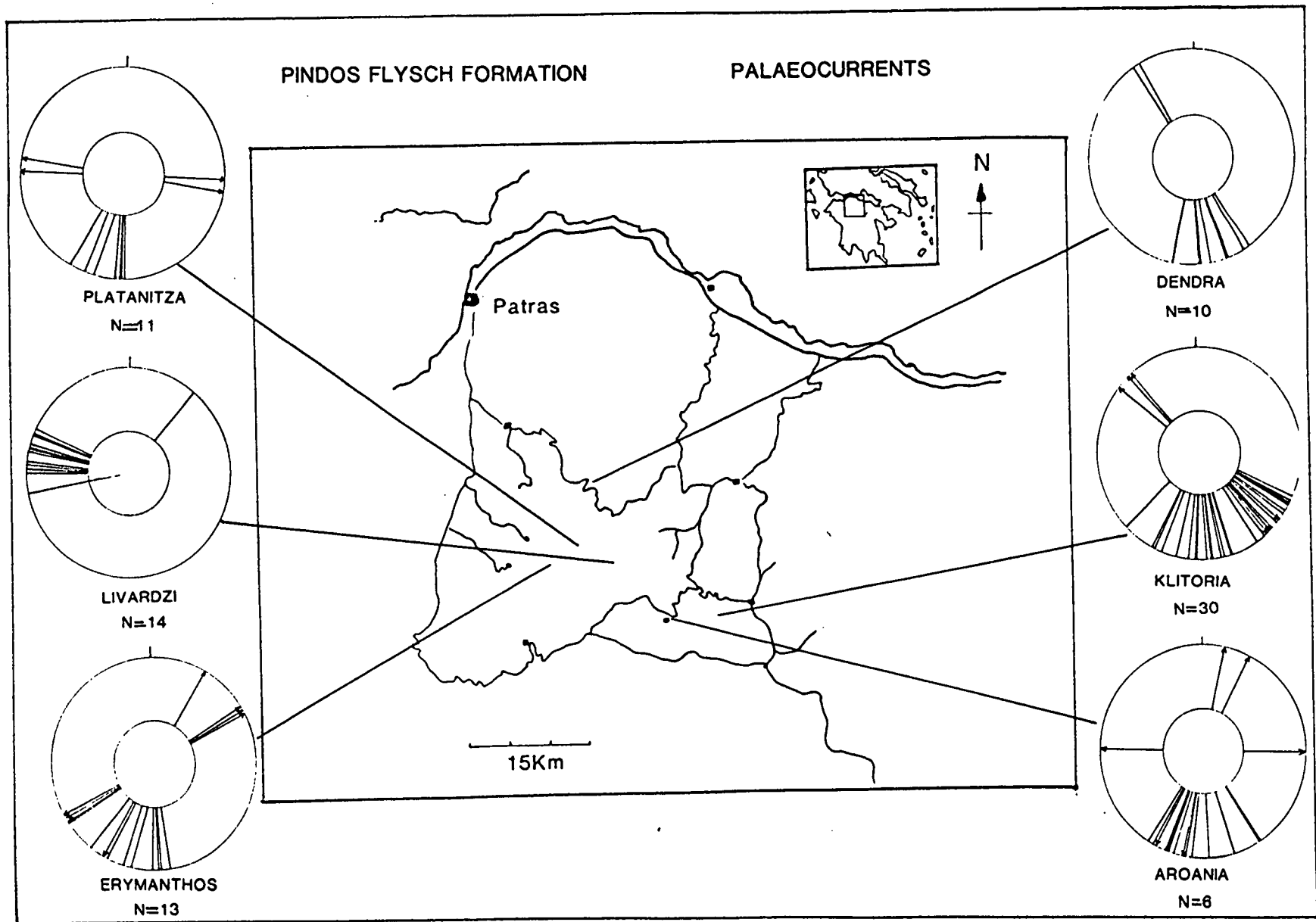


**Fig. 5.5** Palaeocurrent directions from the Pindos Flysch Formation. Arrowed indicators are bi-directional from e.g. groove casts. Other indicators are uni-directional.

correspond to orientations derived from ripple cross-lamination (forming perpendicular to the palaeoflow in the Tc interval). Various reasons have been cited to account for such discrepancies including flow reflection off channel margins or around obstacles, and internal current surges within the flow. Other reasons might include: (1) flow meandering in a waning current; (2) the differing hydraulic responses of different grain sizes to currents spreading laterally as well as forward; (3) the synchronous superimposition of currents derived from two different areas and (4) two time-separate turbidity current events with no recognisable bedding contact. Where there was a difference in flow orientation recorded, only directions obtained from sole structures were used in the palaeocurrent compilation of Figure 5.5. At one locality groove casts which formed in two different directions were seen (Plate 5.5). These must represent the local deviation of currents in a single flow event.

Groove casts are considered to represent tool marks, formed by the impression of objects (e.g. twigs and branches) moving through newly deposited sediment. Flute casts, on the other hand, represent scouring formed by current eddies passing over the sediment surface. Flutes can be sub-divided into different morphological types, e.g. asymmetrical, spindle and parabolic. Spindle types are almost always observed.

An interesting small "tear-shaped" sole mark was observed near the type section (Plate 5.5). It is considered to represent an early stage in flute development as it is asymmetrical, small and with a high length to width ratio. Alternatively the structure may be the result of small grains carried by the current and impacting with the sediment surface. No gravel grade sediment necessary to form such impressions were found in the medium grained sandstone and the relatively deep scour does not suggest an origin as prod, skip or bounce structures either. Because of the ambiguity of the structure a unidirectional palaeocurrent could not be obtained.

Soft sedimentary deformation is indicated in some beds by the presence of convolute bedding. The convolutions appear to have formed by the movement of discrete horizons of sediment, that plastically deformed in response to slip along bedding parallel horizons, rather than by dewatering. Differential internal shearing led to the development of soft sediment sheath folds which, when cut by an erosion surface at a high angle to the principle axial surface, exposes the structure as an eye fold (Plate 5.6). Mostly, convolutions are randomly orientated, but in some horizons the

preferential vergence of folding gives an indication of the sediment movement direction (Plate 5.6).

### **Petrography**

Petrographical examination of Pindos Flysch Formation sandstone reveals a variety of angular to sub-rounded components, generally moderately to poorly sorted, and including clasts of volcanic, metamorphic and sedimentary origin (Plate 5.3). Quartz is the dominant constituent with both strained polycrystalline and monocrystalline varieties present. There are lithoclasts of quartz-rich schistose metasediment, also abundant muscovite mica and chlorite. Individual clasts of plagioclase are infrequently seen and microcline was observed in one thin section. Some thin sections contain large proportions of relatively undegraded volcanic debris, chiefly of basalt (some with trachyte textures) and dolerite. Also seen are clasts with quartz/feldspar vermicular intergrowths (symplectic texture). Carbonate allochems are volumetrically important constituents and comprise micrite, coarse spar and skeletal debris (shell and echinoderm fragments). The sandstone cement is a calcite spar. Carbonaceous material observed in hand specimen has been identified in thin section where it occurs as dark, network structures (e.g. Plate 5.3).

#### **5.3.1.2 Siltstone**

Siltstone bedding is generally thinner than in sandstones, up to 20cm thick, and of light brown or olive green colour. The siltstones are laterally continuous, but often have erosive bedding contacts with overlying sandstone beds. Internal structures are infrequently seen and are restricted to bedding parallel laminations. Siltstones are often found as component parts of graded sandstone beds, overlying coarser sediment. They are also found as individual beds bounded by definite bedding surfaces. The constituent grains of the siltstones are the same as those of the sandstones, except that they are of smaller grain size. Mica flakes are common on upper bedding planes.

#### **5.3.1.3 Pelite**

The pelites associated with sandstone and siltstone are argillaceous and contain a variable carbonate content, generally low. They are mostly dark brown to black. The shales are thin, less than 2cm, but may be up to 5cm and they often form thin bedding partings. No geochemical or mineralogical analysis was made of the pelites, but the colour and association with sand- and siltstones suggests that they are derived from similar source areas.

#### 5.3.1.4 Pink Marlstone

Pink to red marlstone beds are sometimes observed in flysch sections, but the stratigraphic position has never been ascertained. Bedding is usually thin (less than 10cm) except on the Kato Klitoria to Drimos road, where a 35cm thick bed was seen. As well as being pink, the rock reacts with dilute hydrochloric acid and thus appears to be distinct from other Pindos Flysch Formation mudstones. The pink marls may correspond to copious red marlstones that were deposited during the Lower Palaeocene in the Sub-Pelagonian Zone (Celet 1962) and that were also frequently observed in the Vardoussia and Parnassus Zones (AHF Robertson & PJ Degnan, unpublished data).

### 5.3.2 Distribution and Depositional Environment

#### Distribution

The formation is present throughout the study area where erosion has not denuded the lithology. The best exposures are found within synformal structures, or immediately below major thrust planes that have placed protective older stratigraphies above the less resistant flysch. Because the formation contains much pelite, and interlayering containing pelite, it generally forms low-lying relief with poor exposure. For this reason continuous vertical sections are not found. The best exposure of the Pindos Flysch Formation is observed in a broad synform south of Kato Klitoria (Figure 1.1, Enclosure 1) where the type section is found (Section 2.3.6).

#### Depositional Environment

The Pindos Flysch Formation forms a terrigenous sedimentary deposit that was laid down conformably upon the Kataraktis Passage Member. The ichnofacies indicate deposition at abyssal depths and sedimentary structures are classically attributed to sediments deposited by turbidity currents. For example, normal graded bedding representing the Bouma Ta interval, abundant ripple laminations of the Tc interval and sole marks of both tool and current scour origin.

The presence of schistose lithoclasts, metamorphic quartz and mica indicates the erosion of continental basement. Unlike the Late Triassic Priolithos Formation where metamorphic fragments are also found, a western source is less tenable for the Pindos Flysch Formation as the Ionian Zone formed a deep intraplatfomal basin, inboard of the Pindos Ocean. Thus, the Pindos domain was effectively isolated by at



least one major depocentre from any potentially significant Gondwanaland or Apulian basement detrital source. Palaeocurrents are mainly from the north and the possible significance of this is discussed below in a depositional model.

### 5.3.3 Discussion

The beginning of Tertiary terrigenous sedimentation in the Pindos Basin (Katarktis Passage Member) is dated as Late Maastrichtian to Lower Palaeocene (Fleury 1970). However, the deposition of the Pindos Flysch Formation (defined as the last occurrence of carbonate by Fleury 1980) is dated as Upper Maastrichtian in northern Greece, Cretaceous/Palaeocene in southern continental Greece, and Palaeocene in the northern Peloponnese (Fleury 1980). On the Hellenide scale, the earliest incursion of siliciclastic deposition has also been established as being diachronous. For example, it is of Maastrichtian age in the Pelagonian Zone (Mercier 1966, Bignot *et al.* 1971) and of Palaeocene age in the Sub-Pelagonian (Richter & Mariolakos 1977) and Parnassos Zones (Celet 1962). Flysch sediments were not deposited in the Gavrovo-Tripolitza Zone until Middle to Late Eocene times (Section 7.3.2.2).

The following discussion is intended to briefly examine possible controls which might have affected the observed change in sedimentation at the Mesozoic/Cenozoic boundary, from calcareous to terrigenous deposition. Consideration of these factors leads to a depositional model.

#### 5.3.3.1 Eustatic Control

The transitional facies examined near the Pindos front and at Livardzi (Section 5.2.4.1) indicate that carbonate debris flows, derived from the Gavrovo-Tripolitza slope and platform, were deposited immediately prior to the first siliciclastic sediment. It is possible that there was tectonic activity along the margin. Alternatively, the deposits could represent the sedimentary response to a sea level fall as the time period corresponds to a fall on the eustatic curves of Vail *et al.* (1977) and Haq *et al.* (1987, 1988). During regressive periods large volumes of unconsolidated slope sediment become unstable and more terrigenous detritus can be supplied by erosion in the hinterland. It is suggested that the earliest terrigenous sediments passively infilled parts of the Pindos Basin (see below). Interbedded turbiditic sandstones and mudstones are commonly interpreted as channel-levee complexes within a fan. However, stratigraphic correlation difficulties and a lack of

continuous outcrop means that no model of fan development (e.g. Normark 1970, Mutti & Ricci Lucchi 1972, Walker 1978, Stow *et al.* 1984) can usefully be applied to the Pindos Flysch Formation in the study area (such research might be more applicable to the thick sequence of flysch preserved in the Pindos Zone north of the Gulf of Corinth). Therefore, equally valid is the suggestion that vertical successions of interbedded sand and pelite could reflect eustatic fluctuations, with arenite beds indicative of extensive sand sheet deposition during low stands and the mudstone units expressing high stands (c.f. Mutti 1985).

#### 5.3.3.2 Palaeogeographic control

The consistently north to south axial trends reflected in the palaeocurrents of Figure 5.5 (also noted by Green, north of the Gulf of Corinth, and inferred by Fleury 1970, 1980) indicates basement erosion and sediment transport from the north. The Cretaceous-Early Tertiary Pindos Ocean is envisaged as a "V"-shaped embayment of Neotethys (Figure 9.5), narrowing to the north (Robertson & Dixon 1984, Dercourt *et al.* 1986, Robertson *et al.* 1991). Thus, compressive deformation would have resulted in continent-continent overthrusting between equivalents of the Pelagonian and Apulian continental units in the north, prior to Pindos Ocean subduction and continental collision in the south (Figure 5.6). This might have occurred as early as the Maastrichtian and provides an explanation for: (1) the north to south diachroneity of the Pindos Flysch Formation (Fleury 1980); (2) the observed palaeocurrent orientations and (3) the long period of time (c.a. 30-35my) between terrigenous sedimentation in the study area and tectonic activity (expressed by deformation in the Pindos Group in the Upper Eocene/Lower Oligocene).

#### 5.3.3.3 Depositional Model

The tectono-sedimentary environment proposed for the Pindos Flysch Formation evolves with time and can be considered in three stages:

1) Initially, the earliest siliciclastic sediments were not deposited uniformly. They appear first in the Aroania to Dendra areas during Maastrichtian times, followed by deposition at certain localities near to the Pindos front and Livardzi. Later, after the deposition of black cherts, terrigenous sedimentation affects areas in the extreme east and west of the study area. There is no distinctive east to west progressive onlap of terrigenous sediment, as would be expected for a foreland basin deposit derived from a mountain front to the east. Nor are models of fan development easily applicable, thus the earliest flysch-type sediment is interpreted as a passive, basin-

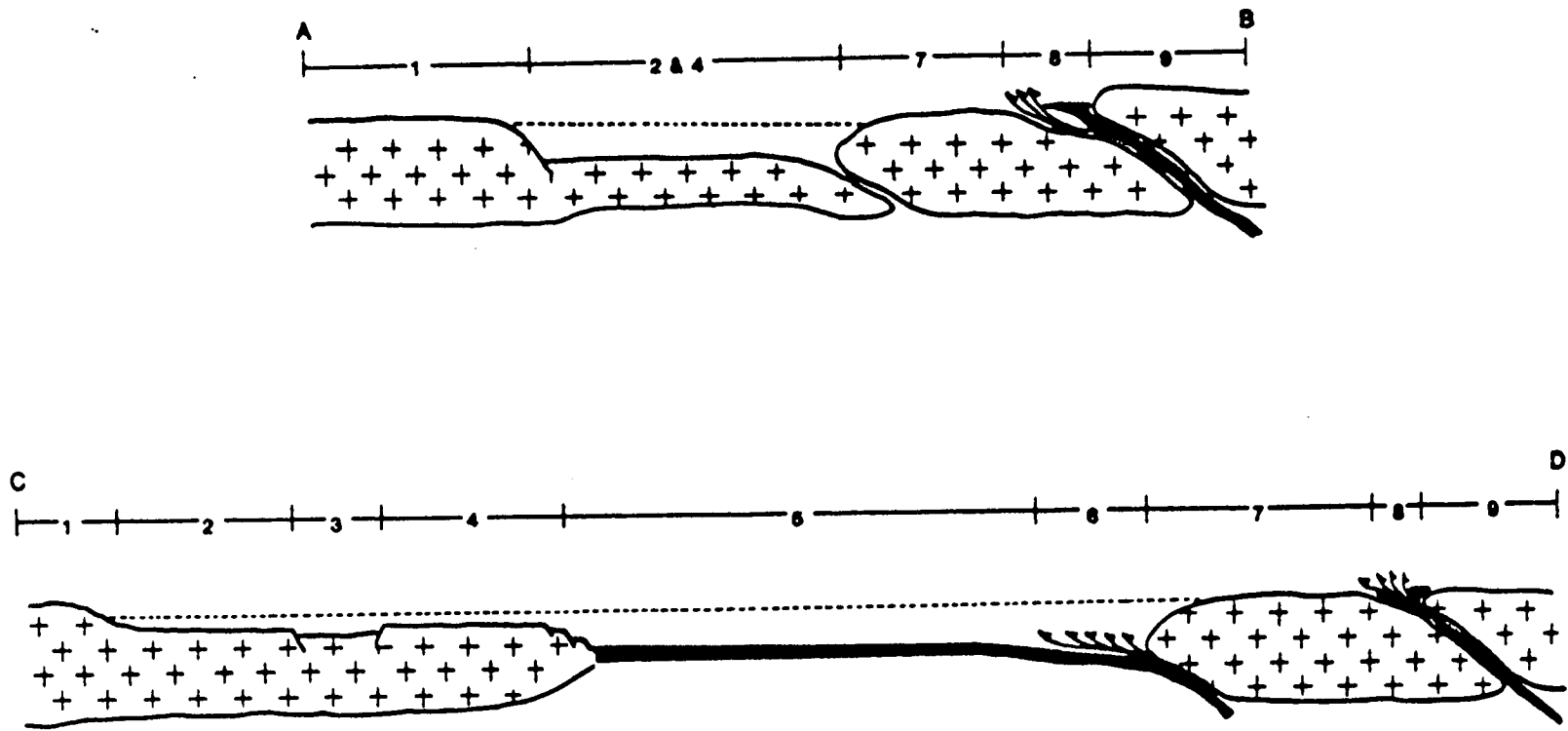
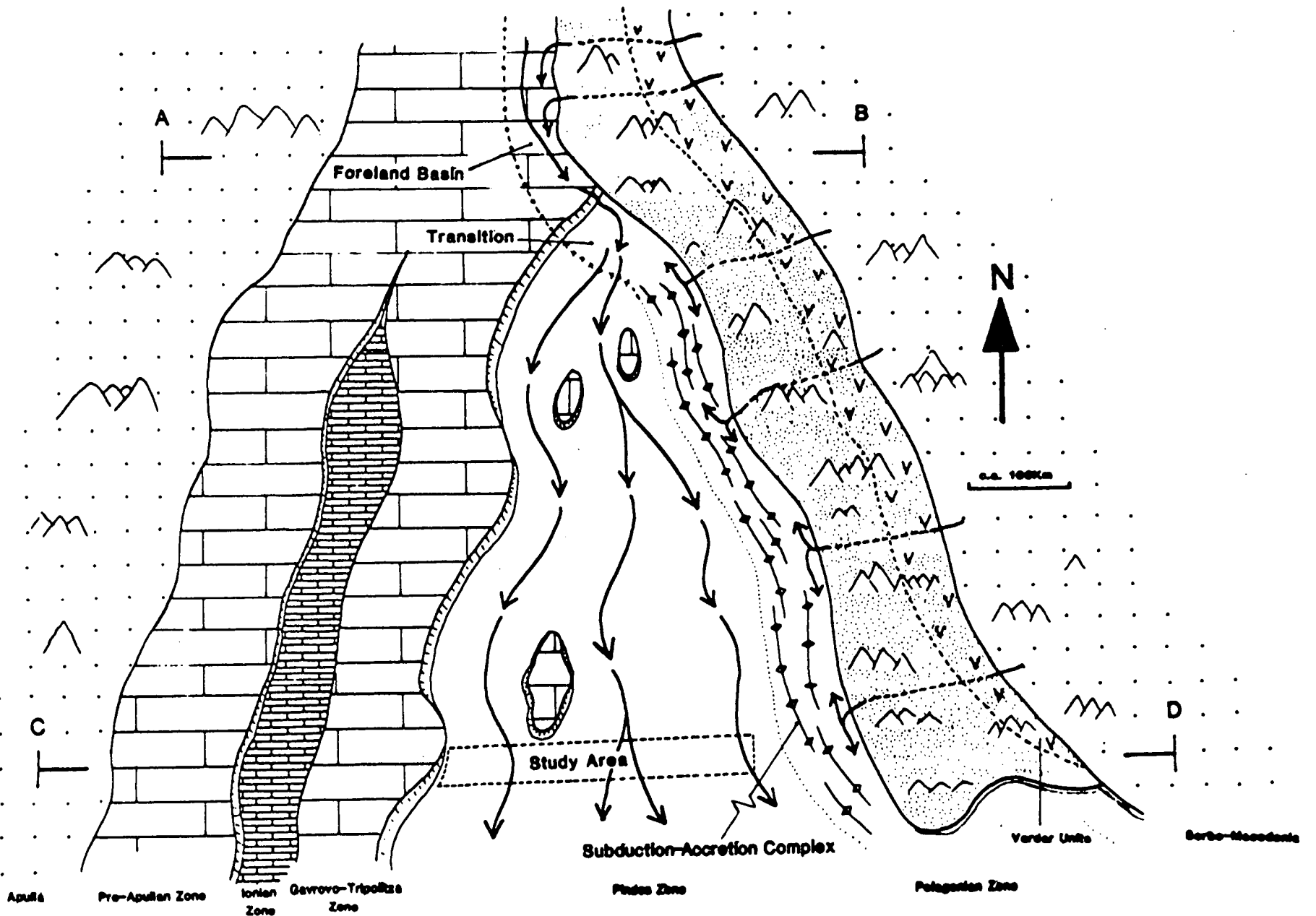


**Fig. 5.6** Schematic reconstruction illustrating the palaeogeography of the Pindos Ocean and opposing margins during the Palaeocene. Arrows indicate dominant palaeocurrent directions (note that E-W flow in the Pindos basin is restricted by the developing subduction-accretion complex). The proposed palinspastic reconstruction of the study area is also shown. The cross sections are across the continent-continent collision zone in the north (Section A-B), with the development of a foreland basin on the under-thrusting platform. Further south (Section C-D) the Pindos Ocean subducts eastwards and an accretionary complex forms by the folding and imbrication of off-scraped oceanic sediment. 1=Apulian Continent; 2=Pre-Apulian Platform; 3=Ionian Basin; 4=Gavrovo-Tripolitza Platform; 5=Pindos Ocean; 6=Pindos subduction-accretion complex; 7=Pelagonian Micro-continent; 8=Vardar derived units; 9=Serbo-Macedonian Continent.

plain-fill (Mutti & Ricci Lucchi 1975) representing the erosional products of the eroding Pelagonian Zone in the north.

It is envisaged that proximal localities of the Pindos Basin received debris flows off the platform as the result of a sea level fall. This period corresponds to the Late Mesozoic/Cenozoic sea level fall of Vail *et al.* (1977) and Haq *et al.* (1987, 1988). Compressive tectonics cannot have affected the Apulian margin (locally) at this time as the minimum width of the Pindos Basin is inferred to have been approximately 300Km (Section 6.3.7).

2) To the east of the study area (present day Euboea and Argolis), Hellenide compression emplaced remnants of the Vardar Ocean onto the Pelagonian microcontinent during the Palaeocene (Robertson & Dixon 1984, Robertson 1990, Clift 1990, I. Sharp, unpublished data), due to ocean closure between the Serbo-Macedonian and Pelagonian Zones. This formed a lithospheric load that down-flexed the thinner Pindos oceanic crust adjacent to Pelagonia. Simplistically, it is suggested that the propagation of deformation through alternative continental and oceanic units in the Neotethyan realm was like the shunting of a train. Thus, a certain build-up of stress would first be necessary before the next tectonic unit could be deformed. It is envisaged that there was a degree of imbrication and lithospheric loading within the Pelagonian domain, prior to strain accommodation by subduction in the Pindos Zone. The precise classification of the Pindos Basin at this time (i.e. foreland basin or trench) depends on whether subduction had been initiated in the Pindos basin prior to, or at the same time as, crustal downwarping due to lithospheric loading (c.f. Allen *et al.* 1986). It is possible that the flexure of oceanic lithosphere, due to loading in the hinterland, initiated subduction. Thus, it is envisaged that the transition from a passively filling basin to an accretionary prism was via a foredeep stage. This was earlier in the north and may correspond to the earliest influx of siliciclastics into the study area (Maastrichtian).

3) The Hellenide deformation front continued to migrate westward with time, due to major plate reorganisations (Section 6.5.1); the Pelagonian Zone began to overthrust the Pindos Basin and subduction of the ocean crust was initiated. Because of the high competency contrast between the Pindos oceanic substratum and the overlying sedimentary cover, a detachment plane developed at this interface (Section 6.5.1). Subduction of the Pindos basement led to the off-scraping of the Pindos Group sediment, supported by a backstop of Pelagonian continental crust. Sediment

continued to be deposited (axially) in the deforming Pindos Basin and the off-scraped Pindos Group formed a subduction-accretion complex. Upper sections of the Pindos Flysch Formation are not preserved in the Peloponnese, but can be found in continental Greece where olistostromal horizons (including basalt and ultramafic rocks) are observed (Kerasia-Milia Complex, Beck 1980, Robertson & Degan 1992, Section 9.3.1).

The rarity of east to west palaeocurrents and the apparent paucity of Pindos-derived clastics in the Pindos Flysch Formation suggests that the developing wedge of off-scraped Pindos sediment may not have been subaerial during pre-Upper Eocene times. Rather, the subduction-accretion complex may have formed a submarine barrier to fans shedding off the uplifted orogen (formed by the Pelagonian and Serbo-Macedonian landmass, Figure 5.6).

#### 5.3.4 Ancient Comparisons

Essentially, the Pindos Flysch Formation represents a sedimentary response to compressional tectonics in the hinterland. The initiation of Pindos basement subduction was probably due to overthrusting by the Pelagonian Zone. Ocean crust subduction and pelagic sediment off-scraping implies that Pindos Zone analogues should include subduction-accretion complexes, however, due to the particular tectonic circumstances of the Pindos Basin and mechanical similarities between subduction-accretion complexes and foreland basin sedimentary settings, the latter would represent closer analogues to the early stages of Tertiary terrigenous sedimentation in the Pindos Basin. Furthermore, differences in the sedimentary fill of foreland basins and subduction-accretion complexes only become apparent at high stratigraphic levels, when strong unconformity surfaces are formed (e.g. due to perched basin sedimentation on rotated thrust slices). At lower stratigraphic levels (e.g. in an accretion related stratigraphy), high sedimentation rates can completely fill the morphological trench and conformably blanket the subducting crust (e.g. as off the Washington-Oregon coast). Thus, both types of sediment pattern are initially similar and difficult to differentiate. In the stratigraphy of the study area, the highest stratigraphic levels have been eroded off and the preserved terrigenous fill is conformable.

Many foredeep deposits have been described since the concept of thrust-loaded flexural basins was first proposed by Dickinson (1974). Particularly well studied

foreland basins include the Ebro basin of the Southern Pyrenees (Puigdefabregas *et al.* 1986, Hirst & Nichols 1986), the Alpine foreland basin (Sinclair *et al.* 1990), the Himalayan foreland basin (Burbank *et al.* 1986, Najman *et al.* 1992) and the Upper Cretaceous Muti Formation of Oman (Robertson 1987, Warburton *et al.* 1990). Fossil subduction-accretion complexes preserved on land include the Southern Uplands Prism (Leggett *et al.* 1982), the Makran Complex of Pakistan (Platt *et al.* 1985) and the Shimanto Accretion Complex in southern Japan (Taira 1985).

### 5.3.5 Modern Comparisons

Present day foreland basins, undergoing subsidence and active deposition, are all adjacent to currently active orogens. Well studied examples include the Taiwan Basin (Covey 1986) and the Timor foreland basin of the Banda Arc, Indonesia (Audley-Charles 1986). Examples of present day subduction-accretion complexes include Nias Island (Karig *et al.* 1978) and the Sunda Arc Complex (Breen *et al.* 1986) both in Indonesia, the Nankai Accretionary Complex (Le Pichon *et al.* 1987) and the Barbados Complex (Westbrook 1982).

## 5.4 CONCLUSIONS

The Paos Limestone member records the transition from siliceous to calcareous sedimentation during the Lower and Middle Cretaceous. Pink micrite, siltite, marl, and conglomerate, rich in argillite, dominate the Member and a proximal-distal facies distribution is established. Sedimentation may have been near the contemporary CCD. A short period of Lower Cretaceous terrigenous sedimentation is recorded by the deposition of the Klitoria Sandstone Member in more distal localities. The Erymanthos Limestone Member is the dominant relief-forming lithology of the Pindos Group and a clear facies pattern is observed, with calcirudite characterising the westerly outcrops, and calcisiltite and micrite the more easterly. Depositional mechanisms were debris flows and rock falls, which developed outboard into turbidity currents, while the background sedimentation consisted of the pelagic settling-out of hemipelagic ooze. At the end of the Mesozoic, terrigenous sediment derived from the north became increasingly more significant in central areas. In the west, a sea level fall led to slope instabilities and large scale debris flows were initiated. This was followed by the intercalation of locally derived (?)

calcareous sediment and siliciclastics with a northern provenance. The resultant lithostratigraphic unit is termed the Kataraktis Passage Member.

The oblique convergence of Pelagonia and Apulia led to the initiation of foredeep deposition in the north, prior to <sup>deposition</sup> in the south of the Pindos Basin. Thus, more southerly areas (e.g. the study area) were not necessarily regions of down-flexed lithosphere during Maastrichtian and Palaeocene times. In the model proposed, the oldest terrigenous deposits of the Kataraktis Passage Member and Pindos Flysch Formation can best be considered as passively infilling the Pindos Basin. As deformation and crustal thickening occurred in more southerly areas of the Pelagonian microcontinent during the Palaeocene, the adjacent Pindos basement was down-flexed (to form a foreland basin that developed on oceanic crust). Westward migration of the Hellenide deformation front thrust the Pelagonian Zone over the eastern Pindos margin and oceanic crust began to subduct. Deep sea sediments were detached from the oceanic basement and, along with the continued terrigenous input, formed a subduction-accretion complex.

## PLATES

### PLATE 5.1: Lambia & Pindos Flysch Formations

(A) Regularly bedded pink limestone of the Paos Limestone Member. Above the figure for scale on the road, is a package of the Klitoria Sandstone Member. (B) Elongate streaks of green reduced argillaceous limestone in a dominantly pink, hematite-rich and oxidised argillaceous limestone. The reduced areas are believed to represent horizons of intense bioturbation, flattened by compaction. Hammer for scale. (C) Alternating sandstone and siltstone beds of the Pindos Flysch Formation. Section youngs to the left and is c.a. 7m wide. (D) White porcellanous, *Calpionellid*-bearing limestone deposited above the Aroania Chert Member at Alepohorio. (E) Thin to medium bedded calciturbidite and pelagic limestone of the Erymanthos Limestone Member. Hammer for scale at bottom right.

### PLATE 5.2: Erymanthos Limestone Member

(A) Thin section of a clast from a Cretaceous rock fall deposit containing *Calpionellid* sp, (centre of field of view). PPL, Scale bar = 0.3mm (B) Bioclastic micrite containing scattered, poorly sorted siltstone grade carbonate clasts and *Globotruncana asymetrica* of Santonian/Campanian age. PPL, scale bar = 0.8mm (C) Sub-angular monomict debris flow from the proximal thrust sheets. Hammer for scale. (D) Micrite and siltstone grade limestone with bedding parallel laminations of calciturbidite origin. Note burial compaction induced stylolites. Lens cap for scale.

### PLATE 5.3: Lambia & Pindos Flysch Formations - Petrology

(A) Coarse-grained calcarenite of the Paos Limestone Member. Many clasts display an interlocking jigsaw-stylolite fabric due to compaction induced pressure solution. PPL, Scale bar = 1.2mm (B) Mixed source arenite of the Klitoria Sst Mbr. Contains a mixture of reworked carbonate, quartz and metamorphic lithic fragments. XP, Scale bar = 0.6mm (C) A more carbonate rich mixed source arenite of the Klitoria Sst Mbr. Clasts include reworked Upper Jurassic chert (centre of photograph) PPL, Scale bar = 0.8mm (D) Bioclastic micrite from the Kataraktis Passage Mbr. Contains the pelagic foraminifera *Globorotalid* sp and *Globigerina* sp. PPL, Scale bar = 0.8mm (E) Poorly sorted arenite of the Pindos Flysch Fm, dominated by mono- and polycrystalline quartz, metamorphic lithic fragments and subsidiary carbonate. Note the black skeletal network of a carbonaceous fragment seen in the centre of the field of view. XP, Scale bar = 0.8mm (F) Fine-grained calciturbidite of the Erymanthos Lst Mbr. The main grainstone fabric passes upwards into a micrite which shows the hydraulic sorting of suspended carbonate clasts. PPL, Scale bar = 1mm (G) Pindos Flysch Formation arenite particularly rich in volcanic and schistose lithic fragments in addition to abundant mono- and polycrystalline quartz. XP, Scale bar = 1.8mm

### PLATE 5.4: Pindos Flysch Formation - Ichnofacies

(A) *Palaeodictyon* cast in a fine-grained calcarenite. Pencil for scale. (B) Wandering trace fossil cast of *Helminthopsis*, with two parallel ridges and a central furrow on the underside of an arenite bed. Hammer for scale. (C) A *Chondrites*-type trace fossil comprising irregular dendritic burrows. Compass for scale. (D) An overturned arenite bed with a *Diplocraterion* burrow and spreite. Pen for scale.



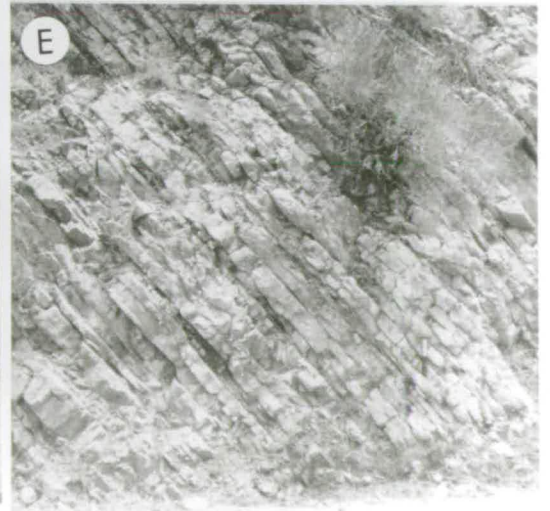
**PLATE 5.5: Pindos Flysch Formation - Palaeocurrent Indicators**

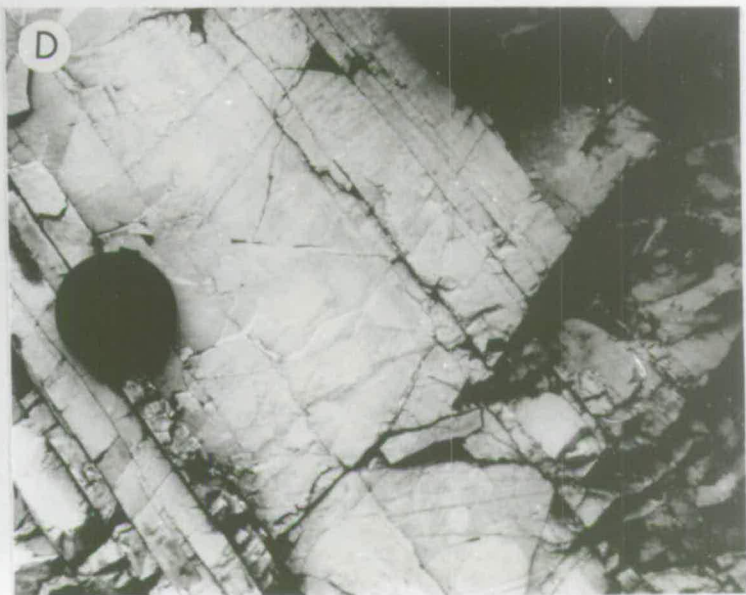
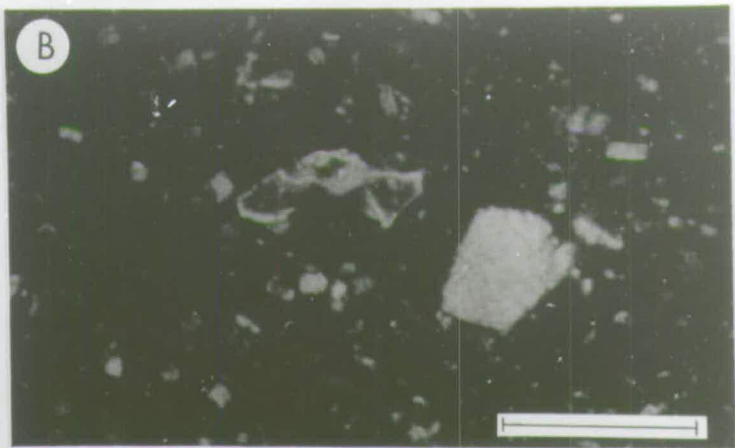
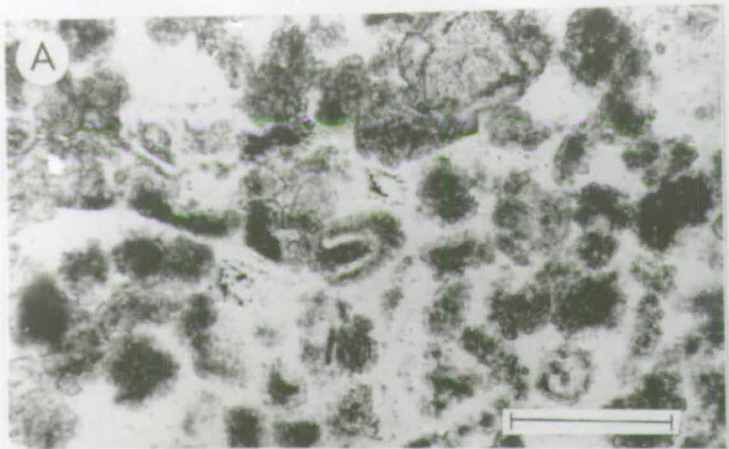
(A) Bi-directional groove casts on the underside of a turbiditic sandstone. The field of view is approximately 1.5m . (B) Spindle-type flute casts on the underside of a turbiditic arenite bed. Field of view approximately 2.5m . (C) Flute casts on the underside of an arenite bed, these particular casts may represent an early stage in the flute development, due to size, depth and a high length versus width ratio. Discussion in text. Lens cap for scale. (D) Primary current lineation on the upper surface of a turbiditic sandstone bed. Pen for scale. (E) Trough-cross lamination observable in three dimensions. Pen for scale (F) The preferred orientation of elongate carbonaceous fragments ("Tea-leaf lineation"). Lens cap for scale.

**PLATE 5.6: Pindos Flysch Formation - Sedimentary Structures**

(A) Over-turned bedding as indicated by asymptotic trough-cross lamination. Lens cap for scale. (B) Climbing ripple lamination. Hammer for scale. (C) Contorted slump horizon in turbiditic sandstone. Note the development of an "eye-fold". Lens cap for scale. (D) Slump horizon showing the preferred orientation of soft-sedimentary folds providing a palaeoslope indicator. Compass for scale.

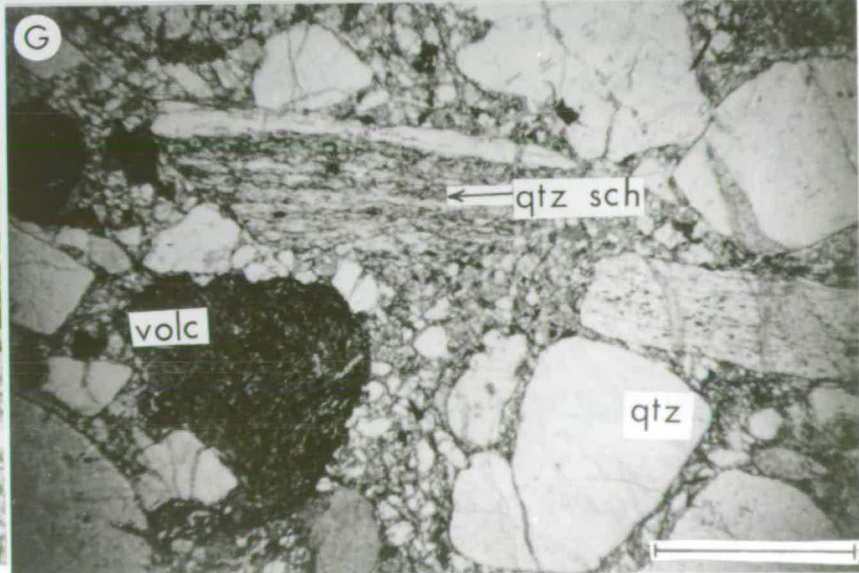
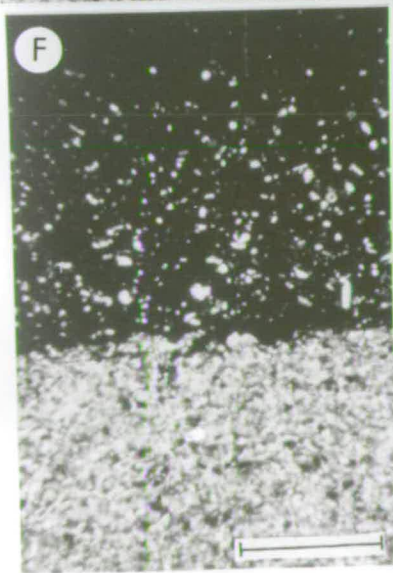
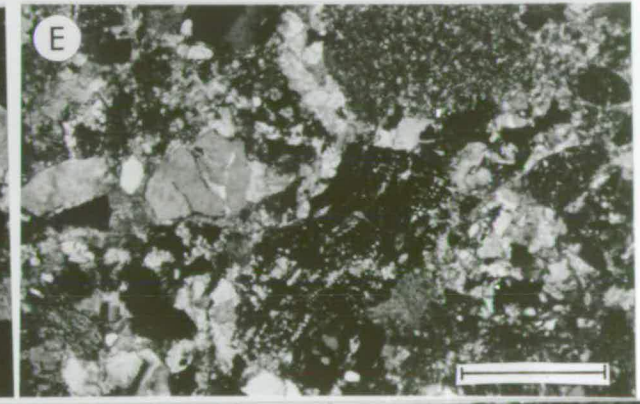
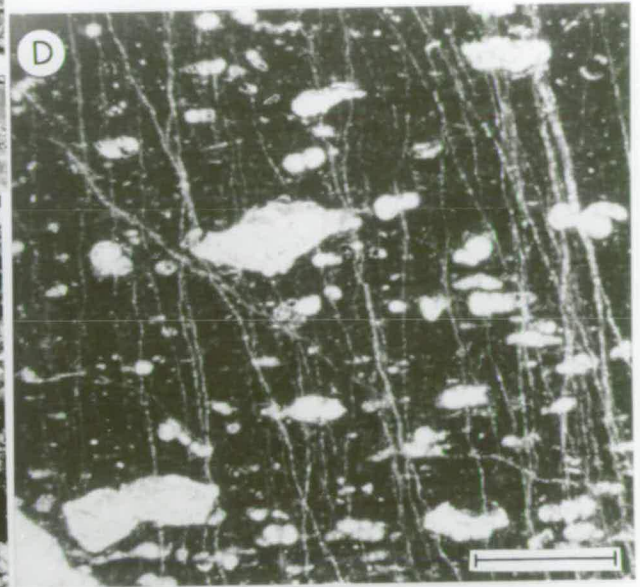
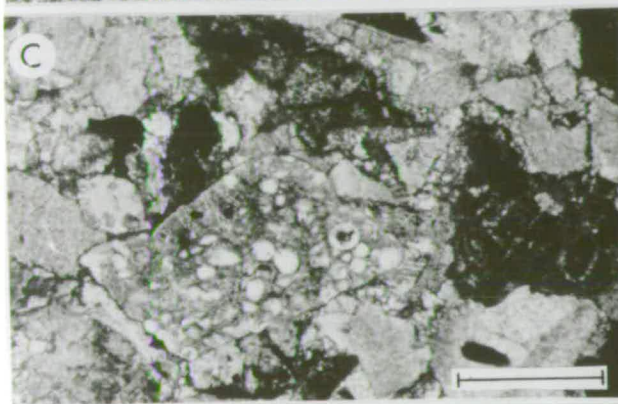
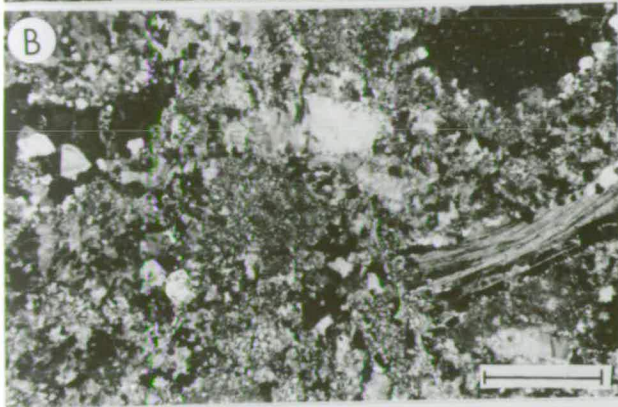
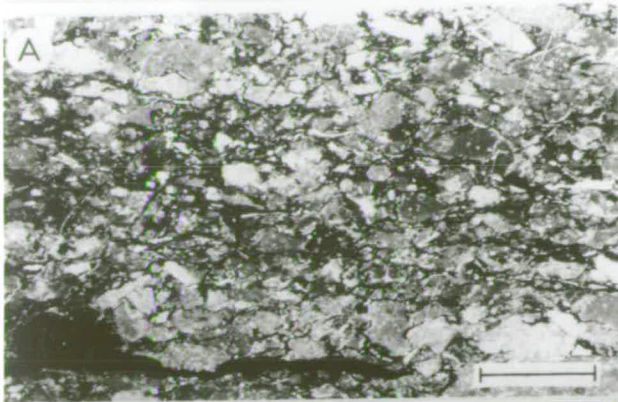
# PLATE 5.1







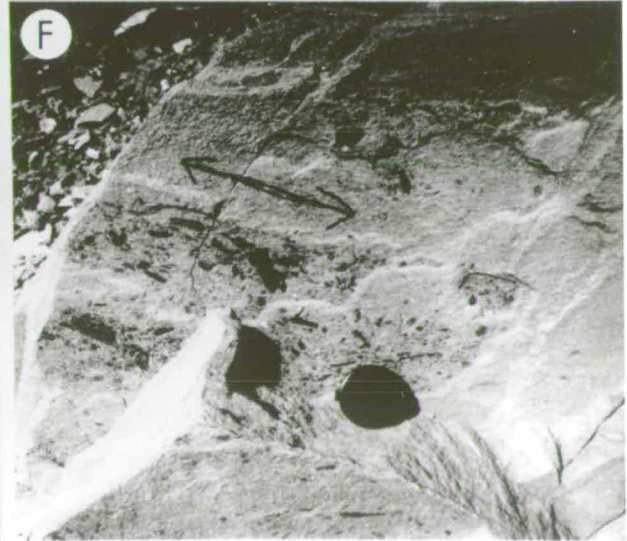
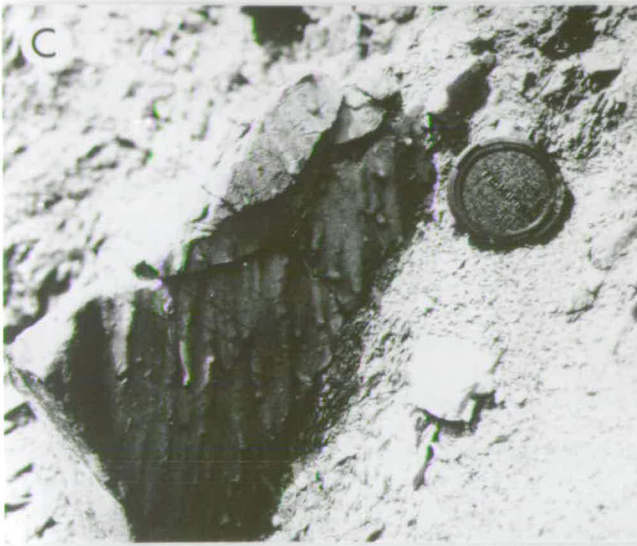
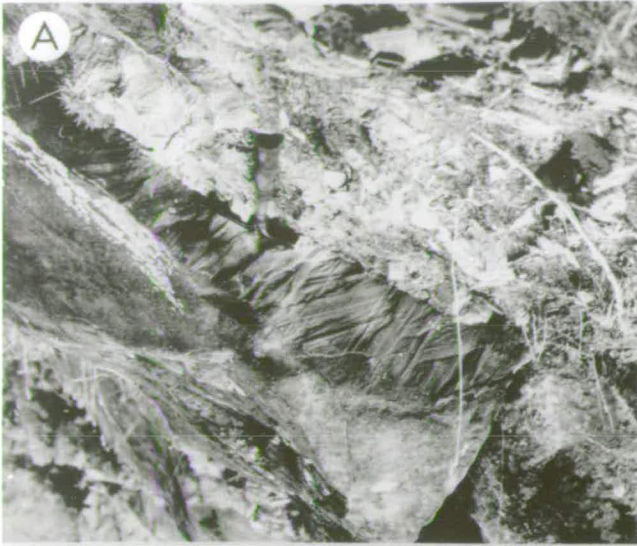
# PLATE 5.3



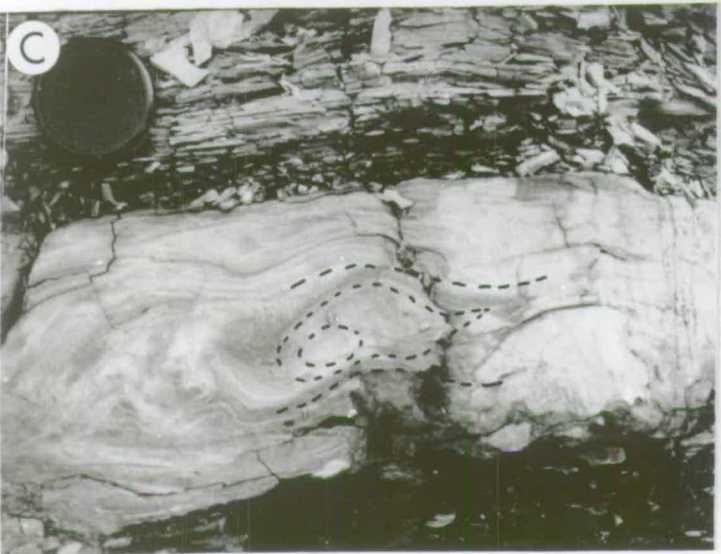
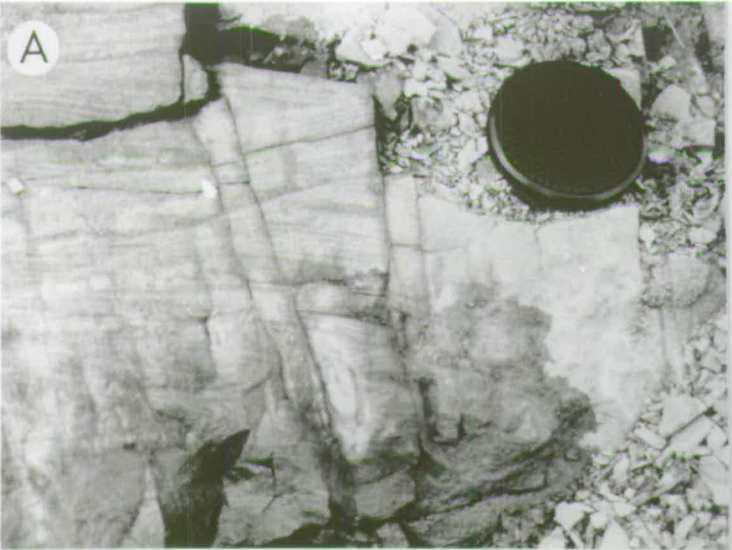












## CHAPTER 6: STRUCTURAL ANALYSIS OF THE PINDOS ZONE

### 6.1 INTRODUCTION

The sedimentary sequences of the Pindos Group, described in preceding chapters, were deformed in a compressive stress regime during the Eocene/Oligocene. The basinal sediments were telescoped and emplaced westwards onto the adjacent Apulian carbonate platform, represented by the Gavrovo-Tripolitza Zone (Chapter 7). This chapter describes the structural style and deformational mechanisms of the Pindos Zone along a structural transect made across the study area. In order to simplify the dissemination of data, the study area is divided into three regions. These areas are the frontal imbricate region, the central imbricate region and the eastern imbricate region. The boundaries are shown on Enclosure 1. Facies analysis indicates that proximal Pindos Group sedimentary sequences are preserved at low structural levels in the west, while more distal deposits characterise the higher structural level thrust sheets in the east. This arrangement, and field mapping, indicates that there has been no significant out-of-sequence thrusting and that the thrust stack was deformed in a relatively simple and systematic manner.

Shortening in the Pindos Zone was accommodated by extensive folding and thrust faulting, while ancilliary structures such as contemporaneous transverse faulting and pervasive cleavage development, are also present. Analysis of the structures within the three regions has led to the development of a thin-skinned, foreland propagating fold and thrust model, with stratal buckling followed by fault propagation folding and thrusting as a result of the eastward subduction of oceanic crust beneath the Pelagonian microcontinent.

Late stage deformation is briefly considered as there is evidence for a south to north directed compressional event that affected the Gavrovo-Tripolitza and Pindos Zones equally, subsequent to the emplacement of the basinal sequences onto the platform. The dating of this event is poorly constrained, but occurred prior to the Plio-Quaternary extensional regime that currently affects the NW Peloponnese and which is also discussed.



### 6.1.1 Structural Terminology

It is not the intention here to exhaustively describe the various structural features that can develop as the result of compressional stresses. Rather, the terminology of folds and faults is generally well known and the nomenclature used here follows well accepted definitions as found in modern structural text books (e.g. Ramsay & Huber 1987, Price & Cosgrove 1990). Moreover, several papers specifically address the terminology of the various structures in thrust terranes (e.g. Boyer & Elliott 1982, Butler 1982, 1987, Morley 1986, 1988, McClay 1992), while the geometry of numerous thin-skinned thrust systems has been explained in detail (e.g. Price & Mountjoy 1970, Elliott & Johnson 1980, Suppe 1980, Butler 1985, Searle & Cooper 1986) and many of the features described in such studies are to be found in the Pindos Zone of the NW Peloponnese.

Field evidence suggests a hierarchy of thrust and fold structures. First order thrusts are defined here as those that are mappable features, where appreciable stratigraphic separation and displacement can be demonstrated. Secondary thrusts are discrete thrust planes where the juxtaposition of different lithostratigraphic units is common (but not a prerequisite) and where displacement can be established as insignificant compared to first order thrusting. These faults can be map scale features (1:10,000) and some are confirmed to be splays off first order thrust faults. Third order thrusts are usually intra-formational and very localised. They place individual beds, or short sequences of beds, above stratigraphically similar lithologies. The fault planes are discrete features that do not generally create a significant fault gouge, unlike first and second order thrusts. Many third order thrusts are present in the study area and have been either rotated along with bedding during later movements, or they are late-stage structures that cut previously rotated bedding (Plate 6.7).

Kinematic indicators are often present on fault planes. In general, the type of indicator present depends on several factors, for example the depth of burial, the orientation of deviatoric stresses, the amount of instantaneous slip along the fault plane and the lithological competence of the footwall and hangingwall. In this study, several structures found on fault planes could be used as kinematic indicators. They are of either syn-orogenic or neotectonic significance, depending on orientation, the geometry of the fault plane and the type of fault plane structure. Relative movement directions of fault blocks were determined where possible, based on at least one of the criteria illustrated in Figure 6.1. Striations found on fault planes were often used in the field to approximate stress orientations. However, their use in this study is

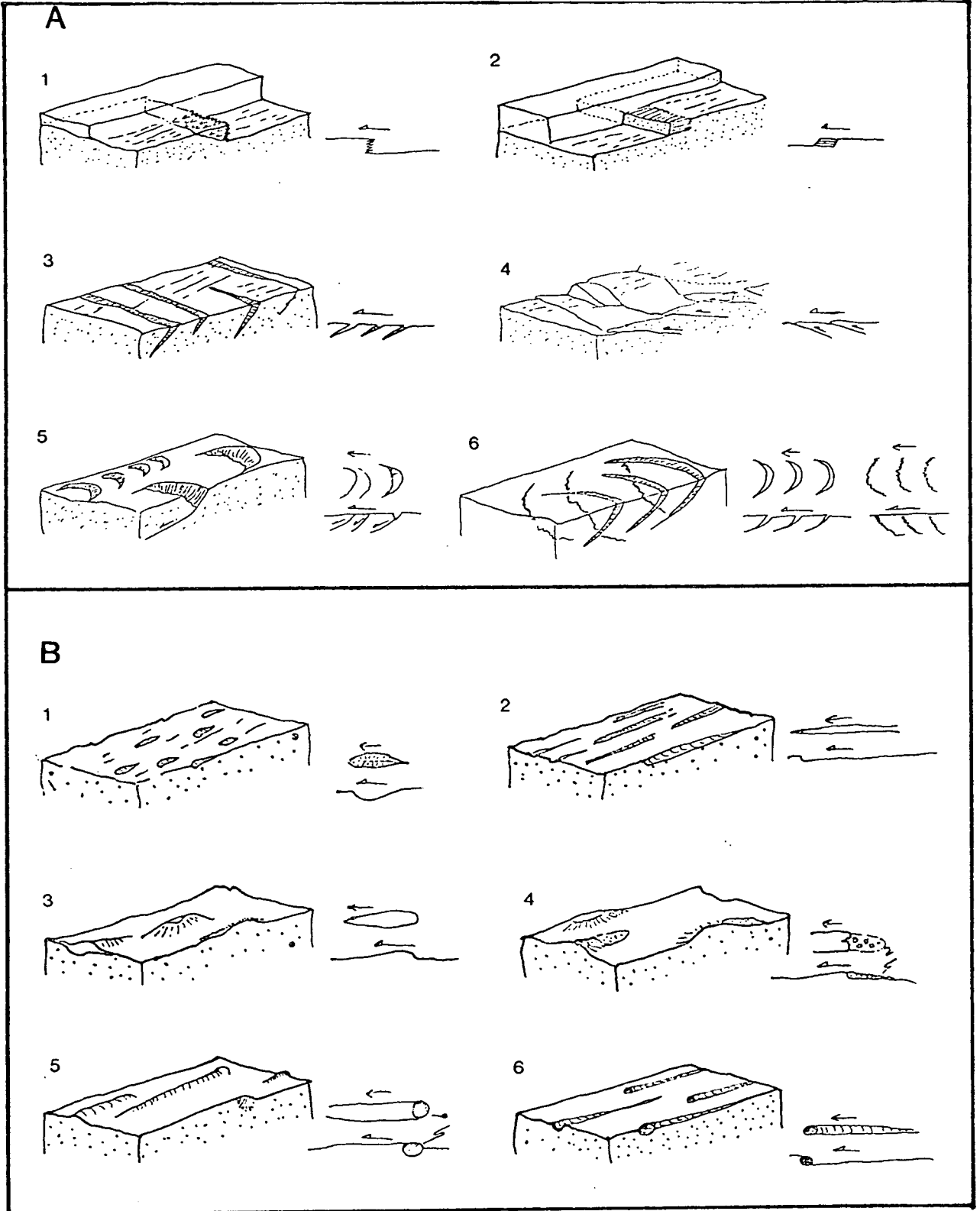


**Fig. 6.1** Kinematic indicators present on fault planes. Note upper block movement right to left in each case. Cross section (and plan view) shown.

(A) Indicators perpendicular to movement. 1) Stylolitic steps; 2) Crystal fibres; 3) Riedel fractures; 4) Micro-thrusts; 5) Micro-extensional faults; 6) Lunate fractures, compressional and extensional.

(B) Indicators parallel to movement. 1) "Pluck" marks; 2) Elongate scour marks; 3) Tectonic equivalents of "roche moutonnee"; 4) Position of surficial gouge; 5) Resistant fault plane irregularity; 6) Tectonic breccia or sediment scour (*in-situ*).

limited as it is recognised that they record only the latest slip movements on faults, many of which were reactivated during the present neotectonic regime.

The fold analysis section in this chapter, focuses attention on meso-scale folds (i.e. those folds which are directly measurable at outcrop scale) and macro-scale folds which are loosely defined as map scale (1:10,000) structures, often discernable only by the systematic measurement of bedding and outcrop patterns.

The stereonetts shown in Figures 6.3 to 6.8 are lower hemisphere equal area stereographic projections constructed using the program "Stereonet" (N. Mancktelow). On the contoured nets which indicate the plunge and trend of fold hinge lineations, the local shortening (emplacement) direction has been established through the use of the orientation and sense of asymmetry of folding. This is inferred to have formed in the same stress field as the thrusting, as both syn-orogenic fault kinematic indicators and vergence derived from folded layers give similar directions. The methodology used to convert fold hinge data into emplacement direction is a variation of the separation-arc method of Hansen (1971), whereby a best-fit great circle can be constructed along the girdle formed by contoured fold hinge lineations plunging in two directions (N.B. hinge axes are considered to be perpendicular to the principle stress axis). The direction orthogonal to this great circle indicates the mean (bi-directional) azimuth of shortening, while the facing directions of asymmetric folds confirm the emplacement direction.

## 6.2 REGIONAL STRUCTURAL DESCRIPTIONS

### 6.2.1 The Frontal Imbricates

The frontal imbricates are bounded to the west by the frontal Pindos thrust which overlies chaotic, massive, debris flow deposits of the Gavrovo Tripolitza Zone (Section 7.3.2.2). A discrete thrust plane is not exposed, rather, the underlying GTZ conglomerates become progressively more deformed upwards and, similarly, the basal strata of the Pindos Group degenerates into broken formation at lower levels, with more coherent bedding upwards. The position of the base of the Pindos thrust sheets can often be inferred from a general break of slope. Along the strike of the basal thrust, a section of Priolithos Formation is observed at Alepohorio, while in other areas, to the north and south, the Drimos Formation or (more usually) the Lesteena Formation is seen as the oldest sequence above the basal decollement

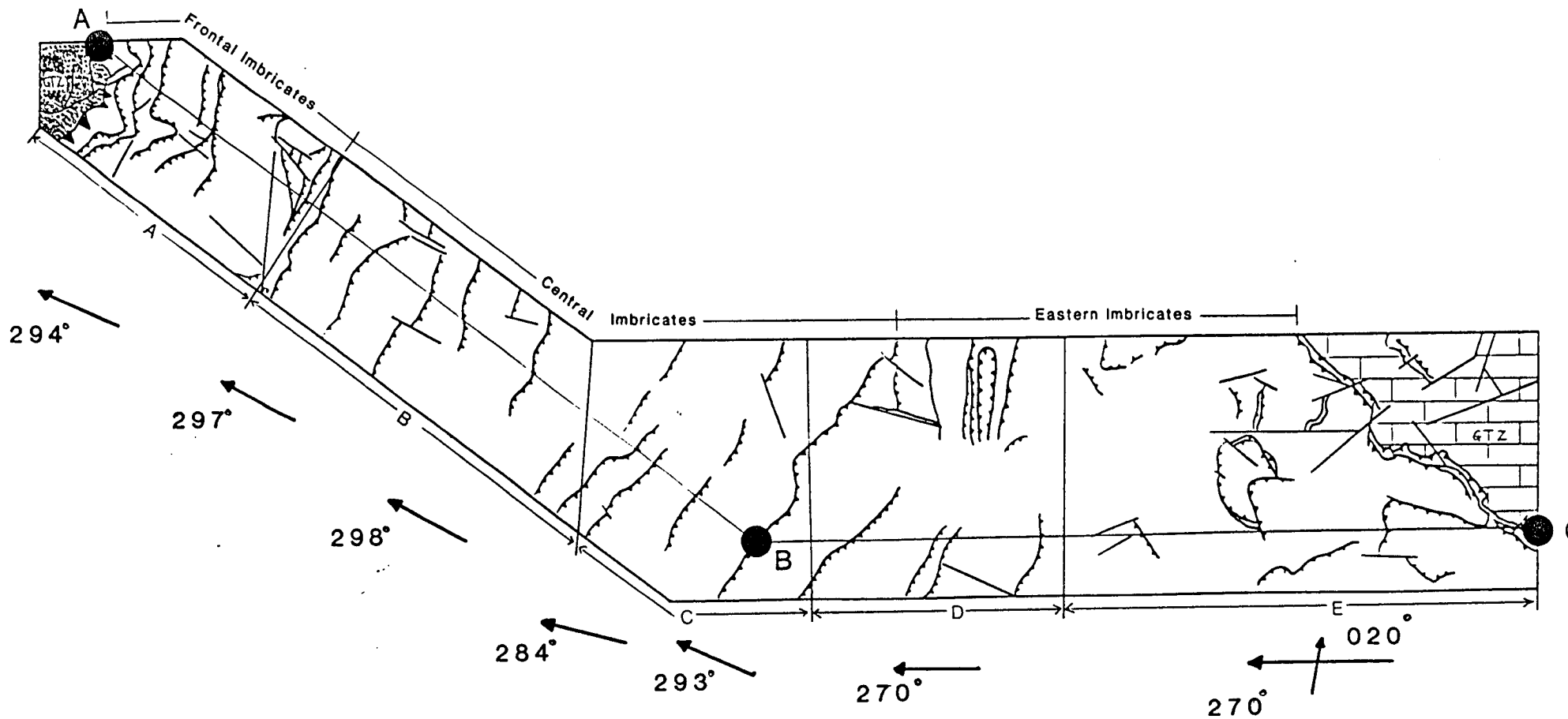


**Fig. 6.2** Outline of the geological map (Enclosure 1) showing the division into frontal, central and eastern imbricate regions. Also shown are the sub-areas A to E, corresponding to Figures 6.3-6.7. The arrows represent the mean shortening direction for each sub-area derived from mesoscopic fold hinge data.

(Enclosure 1). This indicates that the basal detachment cuts up and down section variably along strike. The Pindos basal thrust is a moderately (20-30°) east dipping feature at the thrust front.

The frontal region is dominated by limestones of the Lambia Formation. Many third order thrust planes are present within this unit and the rocks have been disharmonically folded with respect to underlying units. This is especially obvious where the Alephorio valley dissects the most westerly thrust sheets. Inaccessible cliffs show the presence of numerous highly contorted folds and third order thrusts. Above Kalendzi (Figure 1.1), several low amplitude concentric fold trains are seen. The fold interlimb angles are generally open with wavelengths of up to ca. 15m and the axial surfaces are steeply inclined (eastward) to vertical. Section thicknesses of largely intact (but inaccessible) sequences in the Erymanthos Limestone Member, of the frontal imbricate region, are estimated at 250-300m thick. As the rugged topography of the area exposes apparent Cretaceous limestone thicknesses up to 500-600m, it is likely that the rocks have been substantially thickened in the frontal imbricates, by folding and possibly by the development of intraformational duplexes in more intensely deformed horizons.

At the head of the Alephorio valley (Figure 1.1 and Enclosure 1) a macroscopic synform (amplitude at least 300m) is present in the footwall to a first order thrust. The axial surface is horizontal to weakly eastward-dipping and strikes towards 020°. On the south side of the valley, both limbs of the major synform are preserved. The oldest sediments beneath the lower limb are exposed, but the equivalent lithologies in the eastern limb have been dissected by a later thrust. Mesoscale folds are preserved in the lower limb and intense ductile deformation is demonstrated by the observation of an east vergent isoclinal fold with chevron folds developed on the upper limb (Plate 6.4). On the north side of the valley the upper limb of the macroscopic fold has been largely thrust-out but, the enveloping surfaces of a fold train comprising a series of chevron folds defines part of the synform (Plate 6.4). The folded strata consist of the Paos Limestone Member. The gross structure on the north side of the Alephorio valley is shown on Plate 6.1. Figure 6.3 illustrates bedding orientations near the Pindos front (A) and in the area of the head of the Alephorio valley (B).

Mapping of the thrust sheets in the eastern part of the frontal imbricate region demonstrates that a splay of second order thrusts is connected in the footwall to a

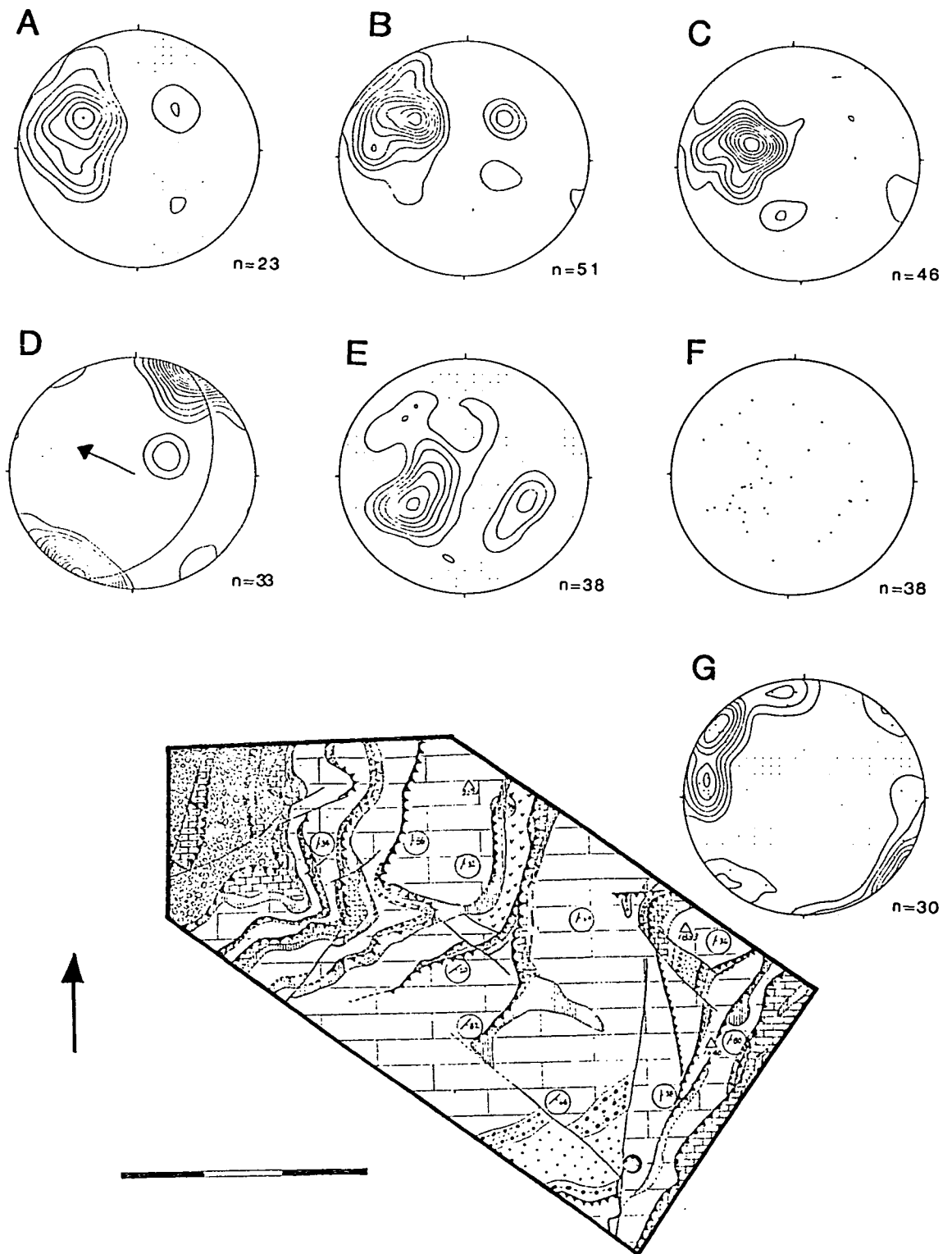


**Fig. 6.3** Stereographic projections of the structural data from sub-area A. Contoured plots (A), (B) and (C) indicate poles to bedding for the Pindos front, the head of the Alephorio valley and the SE of the sub-area respectively. (D) Mean emplacement direction derived from contoured plots of mesoscopic fold hinge orientations. (E) Contoured plot of poles to third order reverse fault planes and (F) is a scatter-plot of the same data. (G) Contoured plot of poles to normal fault planes. Scale bar = 3Km

first order thrust fault, by branch lines that converge to the south and north. The third thrust sheet corresponds at the present level of erosion to a hanging wall cut-off. Figure 6.3 (C) indicates bedding orientations in this sub-area.

Generally, throughout the frontal imbricate region bedding is found to be moderately to steeply eastward-dipping. This is because the folding of the frontal imbricates is often asymmetric and antiformal frontal limbs are overturned in many cases. The dominant mesoscale fold style is as chevron folds with fold hinges gently plunging, both NE and SW, while axial planes are moderately to steeply east-dipping. The stereographic projection of fold hinge lineations (Figure 6.3 D) indicates that the mean emplacement direction in the frontal imbricates is towards  $294^{\circ}$ . Figure 6.3 (E and F), illustrate third order thrust orientations within the frontal imbricates and shows a wide spread of data points. This indicates that the thrust faults have variably dipping planes, but are concentrated as moderately dipping structures with a mean NE-SW strike. Normal faults are also well developed and show a wide spread of fault plane orientations (Figure 6.3 G). Kinematic indicators are more frequently observed on these neotectonic surfaces and they are dominated by north-down normal faulting, although strike-slip (dextral and sinistral) movement is also indicated.

### 6.2.2 The Central Imbricates

The central imbricate region, from the thrust sheet immediately east of Platanitza to the Aroania thrust sheet (Enclosures 1 and 2), has generally thinner bedding than in the frontal imbricate area, due to the facies change from debris flow deposits and proximal calciturbidites, to more distal type sediments (Chapters 3-5). In the central area, folds are observed on a number of scales, ranging from "tectonic ripples" with amplitudes and wavelengths of less than a centimetre, to large scale folds with wavelengths of several hundred metres.

Mesoscopic fold structures are commonly present, especially in the Erymanthos Limestone Member, disharmonically overlying folded cherts of the Lesteena Formation. Chevron folds are commonly developed with approximately  $60^{\circ}$  interlimb angles, although a later flattening strain has in places over-tightened such folds (Figure 6.9). Where alternations of competent limestones with less competent shale horizons exist, folding becomes strongly disharmonic between layers. In other places, straight limbed folds with rounded hinge areas are observed in thicker

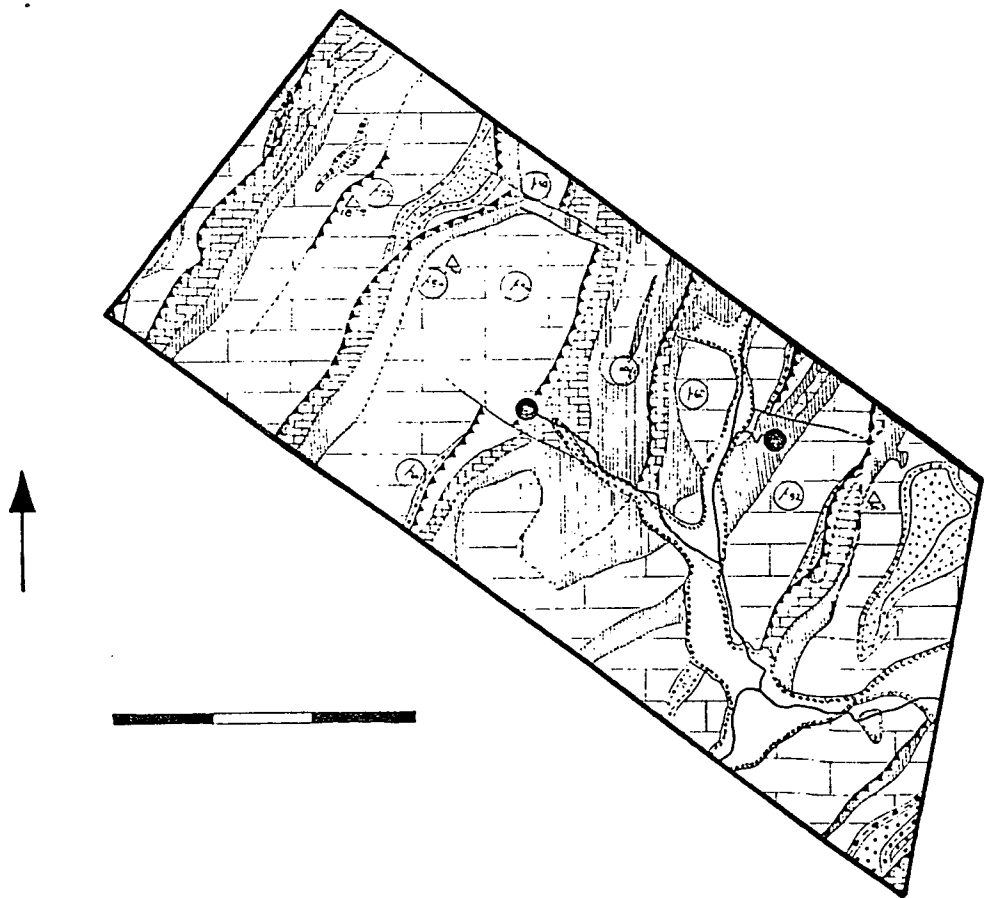
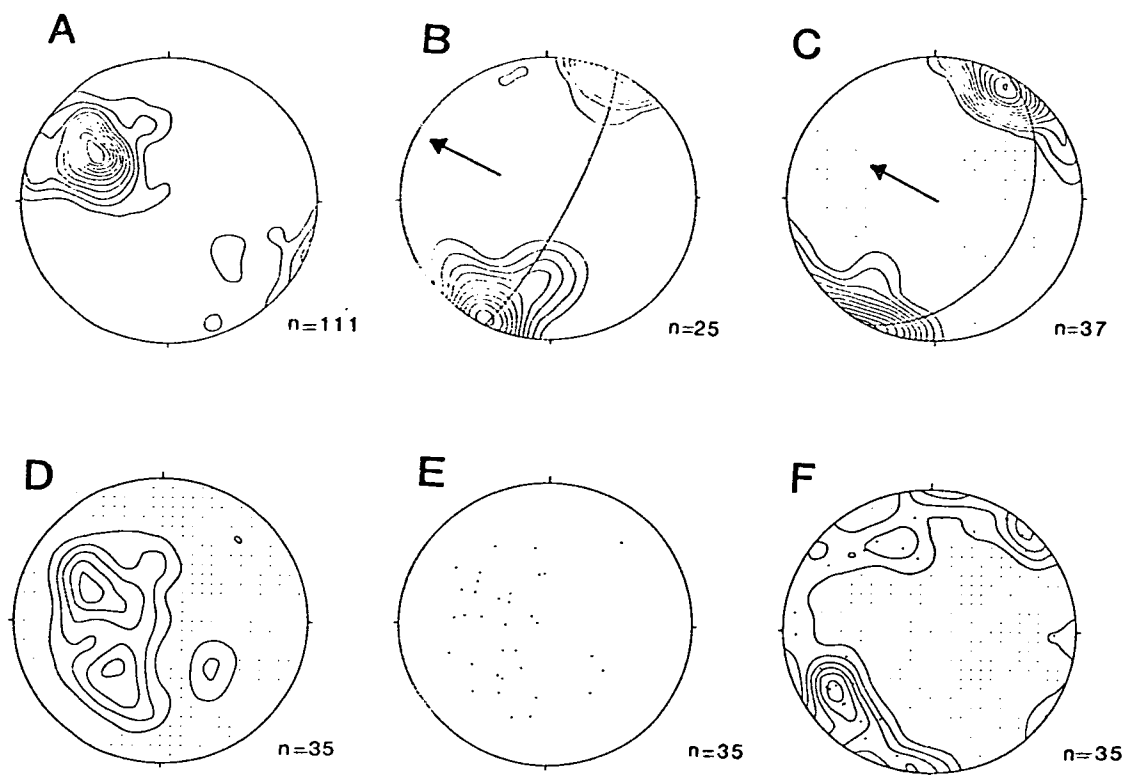


**Fig. 6.4** Stereographic projections of the structural data from sub-area B. (A) Contoured plot of poles to bedding planes. (B) and (C) indicate the mean emplacement directions derived from contoured plots of mesoscopic fold hinge orientations for the NW and SE parts of the sub-area respectively. (D) Contoured plot of poles to reverse faults and (E) is a scatter-plot of the same data. (F) Contoured plot of poles to normal fault planes. Scale bar = 3Km



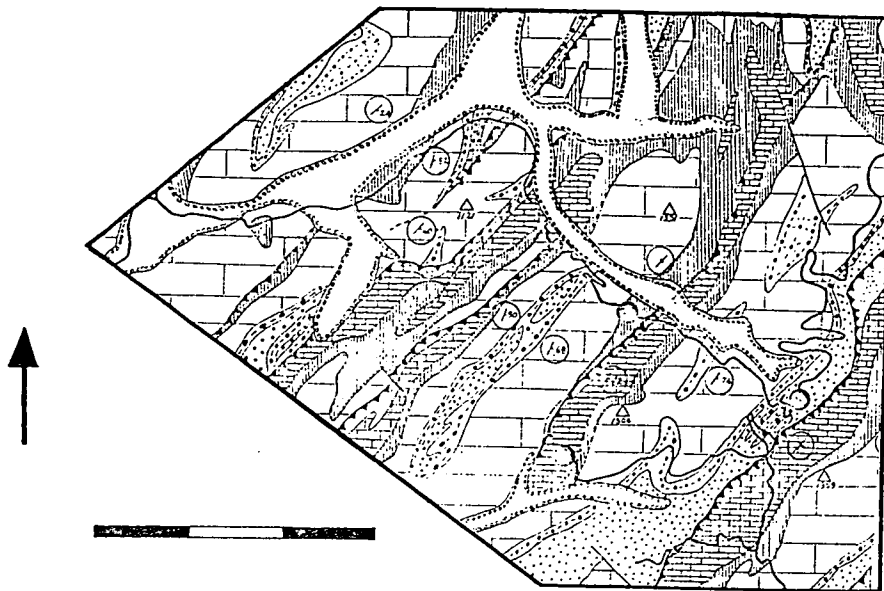
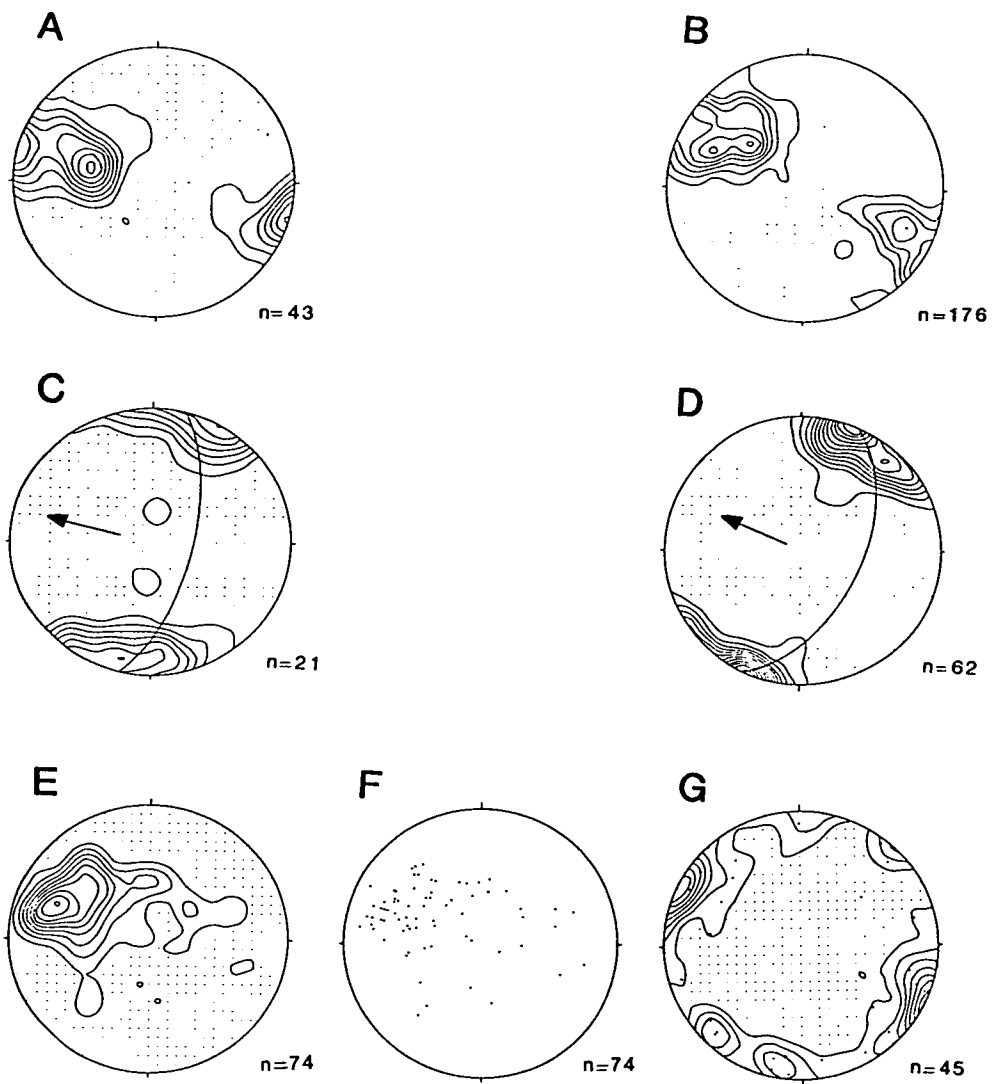


**Fig. 6.5** Stereographic projections of the structural data from sub-area C. (A) and (B) are contoured plots of poles to bedding planes from the west and east of the sub-area respectively. (C) and (D) indicate the mean emplacement directions derived from contoured plots of mesoscopic fold hinge orientations for the west and east of the sub-area respectively. (E) Contoured plot of poles to reverse faults and (F) is a scatter plot of the same data. (G) Contoured plot of poles to normal fault planes. Scale bar = 3Km

bedded units, suggesting a generic relationship with chevron folds (Plate 6.6 and discussion below). The folds are sometimes asymmetric; thus, vergence directions, and often facing directions, are measurable.

Larger scale folds are well seen at many localities, including Livardzi (Figure 6.11) where the folding is most prevalent in thickly-bedded, competent, intraformational limestone beds within the Aroania Chert Member, and also at Drimos (Plate 6.2). The folding is highly irregular with wavelengths of approximately 100-300m. Fold surfaces comprise smaller scale folded strata, generally as chevron and sometimes box folds; these formed prior to the larger scale folding as fold train enveloping surfaces are themselves folded. The larger wavelength folds appear to correspond to the tightening of a "single layer" (see below) resulting in irregular buckle folds.

First and second order thrust planes are generally not well exposed as the adjacent, weakened or incompetent, lithologies often weather recessively to form gully features which are covered with superficial alluvial sediment (Plate 6.3). Mapping indicates that most of the first and second order thrust faults cropping out at the surface are hangingwall and footwall flats, as the underlying and overlying bedding approximately parallels both the fault plane and each other. Occasionally however, hangingwall or footwall cut-offs can be inferred, although it is important to realise that these often represent the thrusting of pre-existing folds rather than thrusts cutting-up through an undeformed layer cake sequence (mesoscale example see Plate 6.5 C). The thrusting of previously folded strata can account for younger on older stratigraphic juxtaposition, although thrusts placing older rocks on younger lithologies is generally observed. First order thrust planes are usually at high angles and are steeper than the modelling of thrust systems would suggest for an in-situ reverse fault (30°, e.g. Boyer & Elliott 1982).

Many of the thrust faults die out along strike as doubly plunging structures, with maximum stratigraphic separation in the centre and displacement dying out to zero at either end of the fault trace, whereafter asymmetric antiformal folds are developed at the surface (e.g. thrust immediately west of Livardzi).

Stereographic projections of structural orientation data are provided in Figures 6.4 and 6.5 which correspond to two sub-areas within the central imbricate region (Figure 6.2). Figures 6.4 (A) and 6.5 (A and B) indicate that bedding is moderately to steeply inclined towards the SE. Thrust sheet shortening directions have been

derived from mean fold hinge lineations (Figures 6.4 [B and C], and 6.5 [C and D]) and these indicate 297 and 298° in the westerly sub-area, and 284 and 293° in the easterly sub-area. Third order thrusts exhibit a wide spread of orientations (Figures 6.4 E and 6.5 F), but the contoured stereonet confirms the dominance of E to SE dipping fault planes. Late-stage normal faulting (Section 6.6.2) is typically high angled and shows a wide spread of data points (Figures 6.4 F and 6.5 G).

### 6.2.3 The Eastern Imbricates

The eastern imbricate region comprises the thrust sheets east of Aroania and those westwards of the Chelmos antiform, where the underlying GTZ sediments are exposed beneath the Pindos basal thrust (Enclosures 1 and 2).

Overall, the area is structurally different to the central and frontal imbricate regions because the spacing between first order thrust faults is wider, bedding flattens (on a map scale) into more gently folded antiform/synform couplets and higher stratigraphic horizons outcrop more widely. Thrust planes are at high angles in the west, but are mapped as becoming less steep eastwards (e.g. commonly 20-30° at Krinofta, Enclosure 1).

Mesoscopic deformation, i.e. folding and minor faulting, is as extensive in the eastern imbricate region as in the more western regions. Mesoscopic folds often form fold trains, with enveloping surfaces connecting fold inflection points and these surfaces are themselves seen to be folded at several localities (e.g. Krinofta, Drimos, Aroania). The folded enveloping surfaces define the limbs of the larger mesoscopic folds, as in the central imbricate region, although some folds resulted from later south to north directed compression (Section 6.5.1) and this accounts for the wide spread of bedding and hinge lineation orientations in many of the eastern localities (Figure 6.7).

Generally, the Aroania Chert Member is the oldest lithologic unit exposed in the east of this sub-area. In several places east of Kato Klitoria, volcanic rocks of the TSM (Chapter 8) are found directly under the Jurassic cherts with sheared contacts. The Priolithos Formation (Section 3.2) is no longer exposed and outcrops of the Drimos Formation (Section 3.3) are more rare and always as an incomplete sequence. It is believed that the change in stratigraphy (from a full Triassic-Eocene sequence west of Kato Klitoria, to mainly the Cretaceous Erymanthos Limestone Member to the

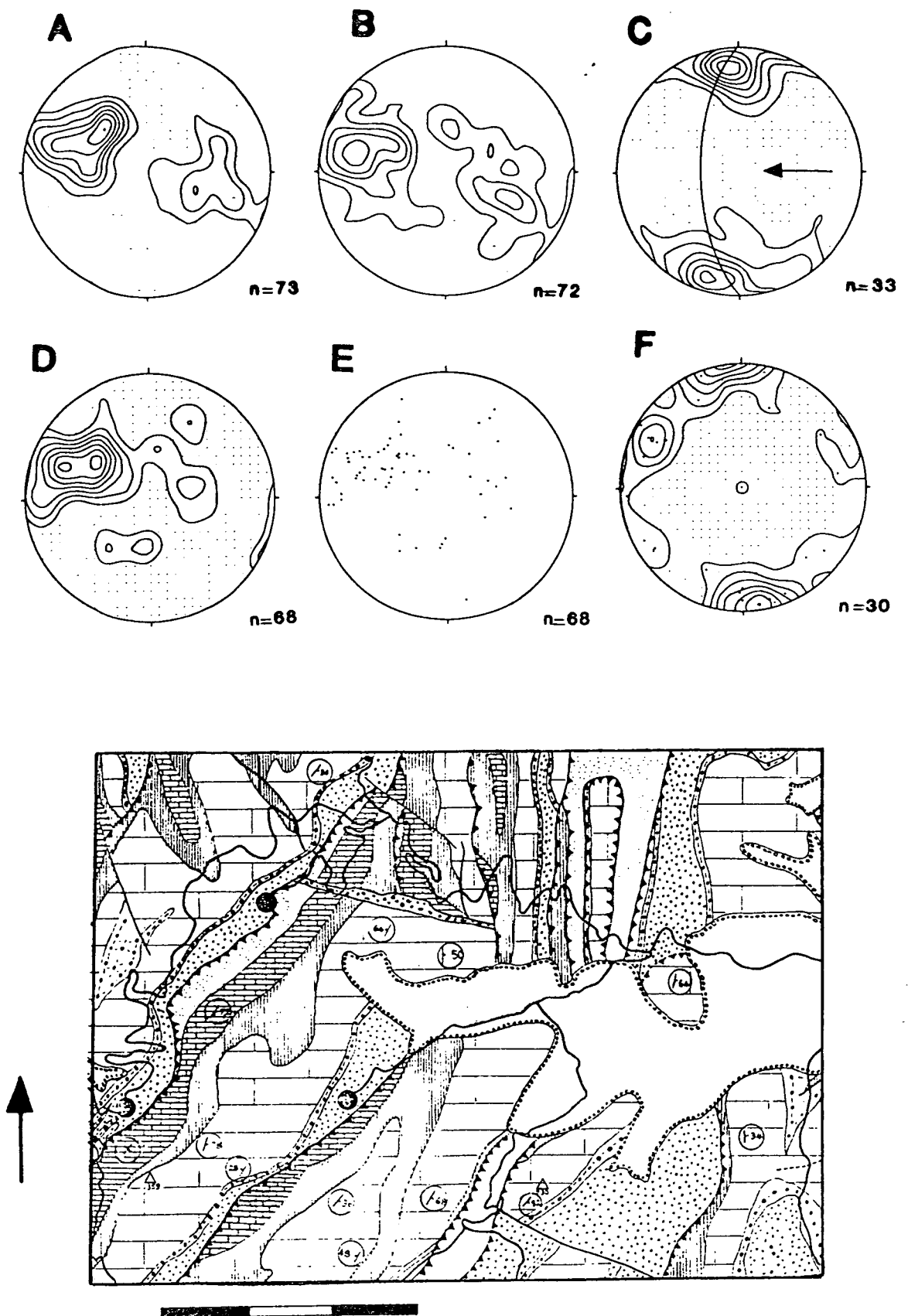


**Fig. 6.6** Stereographic projections of the structural data from sub-area D. (A) and (B) are contoured plots of poles to bedding planes from the west and east of the sub-area respectively. (C) Mean emplacement direction derived from contoured plot of mesoscopic fold hinge orientations. (D) Contoured plot of poles to reverse faults and (E) is a scatter-plot of the same data. (F) Contoured plot of poles to normal fault planes. Scale bar = 3Km

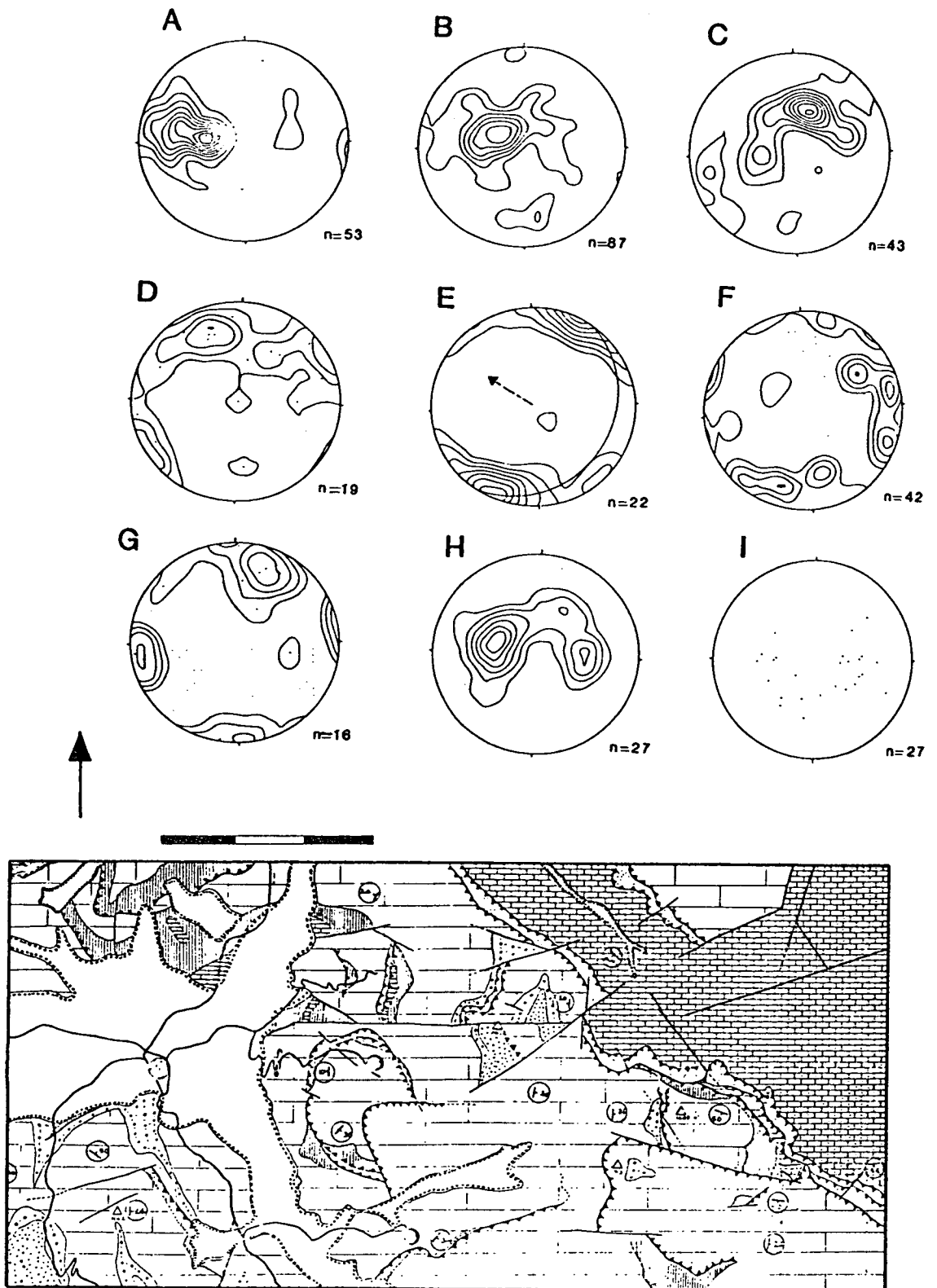


**Fig. 6.7** Stereographic projections of the structural data from sub-area E. (A), (B) and (C) are contoured plots of poles to bedding planes from the west, centre and east of the sub-area respectively. (D) Contoured plot, with over-printed scatter-plot, of poles to normal fault planes. (G) Contoured plot, with over-printed scatter-plot, of poles to normal fault planes within the Gavrovo-Tripolitza Zone. (E) and (F) are contoured plots of mesoscopic fold hinge orientations, from the west and east of the sub-area respectively. Note that there is a later N-S fold event present and the method used for deriving mean emplacement directions from contoured fold hinge data is not valid. (G) Contoured plot of poles to reverse faults and (I) is a scatter-plot of the same data. Scale bar = 3Km

east) contributes to the difference in structural style between the Arcadia region to the east of Chelmos Mountain and the imbricates of the frontal and central areas (Sections 6.5.3 & 1.1).

In the far east of the mapped area, an important reverse fault striking NW-SE and dipping  $60^\circ$  south, separates the Pindos and Gavrovo-Tripolitza Zone lithologies. Striae indicate that it was reactivated as both a high angle strike-slip and normal fault. The basal thrust is continued further NW where the major detachment flattens to sub-horizontal to very gently west dipping. The footwall Eocene limestone of the Tripolitza Zone dips quite steeply to the south ( $50-70^\circ$ ) and abundant post emplacement faults indicate that there have been substantial later movements at this point of juxtaposition between the two tectono-stratigraphic zones, (marked by a thin 0-20m thickness of TSM, Chapter 8). As described in Chapter 7 (Section 7.5.1) it is envisaged that the Pindos thrust sheets were emplaced onto the Chelmos region as it was actively flexing (due to the forelandward propagation of stress into the neritic sequences). The non-congruancy of bedding between the Pindos and Gavrovo-Tripolitza Zones, an east dipping Pindos basal thrust in the east of the Chelmos area, but west dipping in the west (i.e. folded detachment) and the presence of N to NE-directed reverse faults suggests post-emplacement tightening of the Chelmos periclinal structure, possibly resulting in strike-slip and normal relative movement (culmination collapse) between the two tectono-stratigraphic units as the Chelmos pericline developed.

A westerly sub-area of the eastern imbricate region (Figure 6.2) displays bedding dips which are mostly inclined to the ESE, but also westwards (Figure 6.6 A and B). Shortening directions derived from fold hinge orientations show mean emplacement to  $270^\circ$ . Thus, between this sub-area and the easterly part of the central imbricate region, there has been an angular change in the emplacement direction of  $23^\circ$ . Third order thrusts (Figure 6.6 D and E) show a wide spread of fault plane orientations, but with a concentration of data points dipping ESE. Similarly, normal faults are widely dispersed, although WSW-ENE striking high-angle fault planes are statistically more significant.

Figure 6.7 (A, B and C) show contoured poles to bedding (from the west, eastwards) in the most easterly sub-area. A and B show a dominance of moderately eastward dipping inclinations (although with less concentration of data points in B). Fold hinge lineations in the west of the sub-area (Figure 6.7 E) show a wide spread of

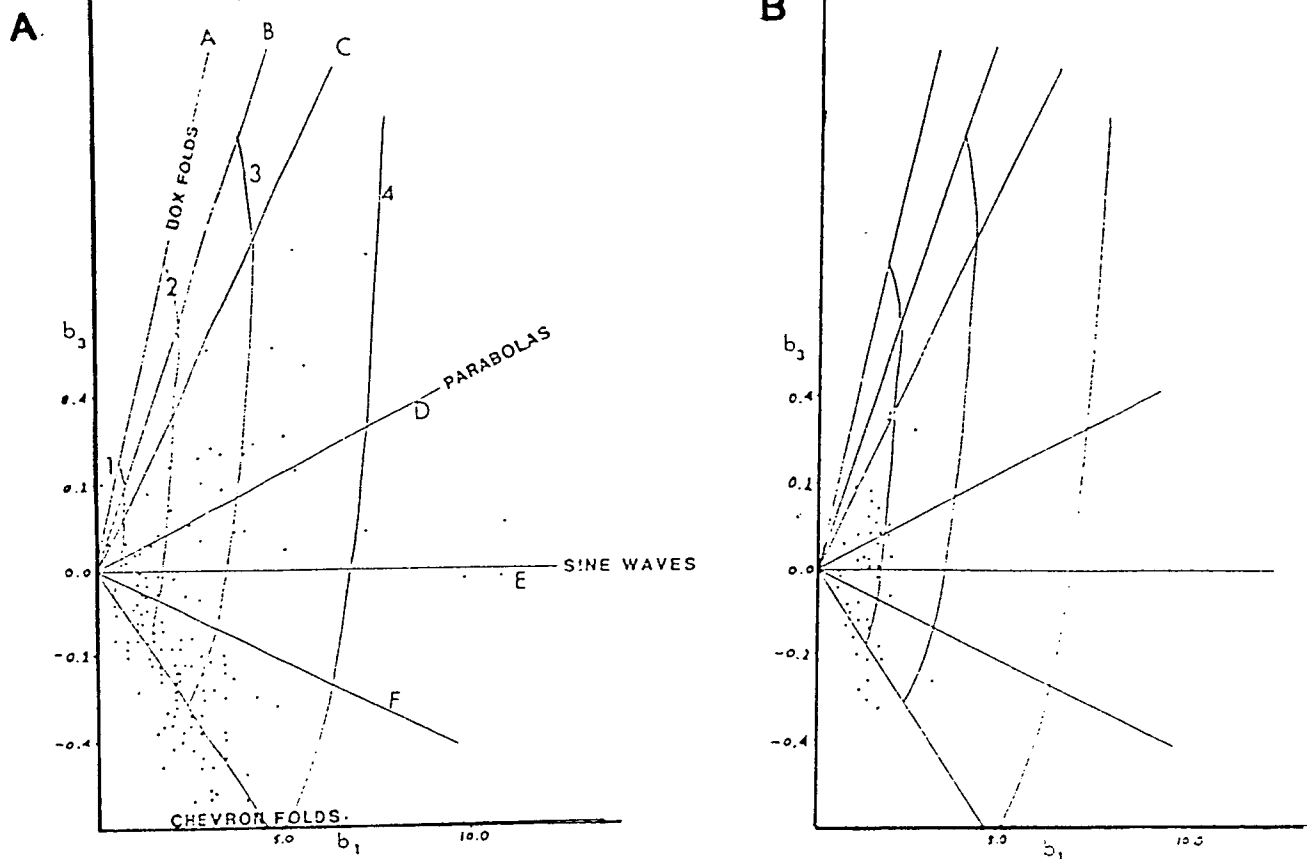
gently plunging orientations and the mean shortening direction is shown to the NW. However, this is largely an artefact of the wide spread of data and the dominant direction is more probably due west. Figure 6.7 (C) shows bedding measurements adjacent to where the Gavrovo-Tripolitza platformal lithologies are exposed through a major tectonic window. Here it is clear that the majority of bedding measurements are dipping towards the SW. Close to the tectonic window, fold hinge lineations are dominantly N-S and E-W (Figure 6.7 F). This area is considered to have been subject to later south to north directed compression (Section 6.6.1); thus, a single mean shortening direction cannot be obtained. Third order thrust planes are mostly orientated east-west (Figure 6.7 H and I) for the complete sub-area. Normal faulting in the Pindos Zone of the eastern imbricate region is shown in Figure 6.7 (D) as high angled and striking both NE-SW and NW-SE. This is compared with normal faults within the platform (Figure 6.7 G) which are largely orientated N-S and E-W.

### 6.3 ANALYSIS OF PINDOS ZONE DEFORMATION

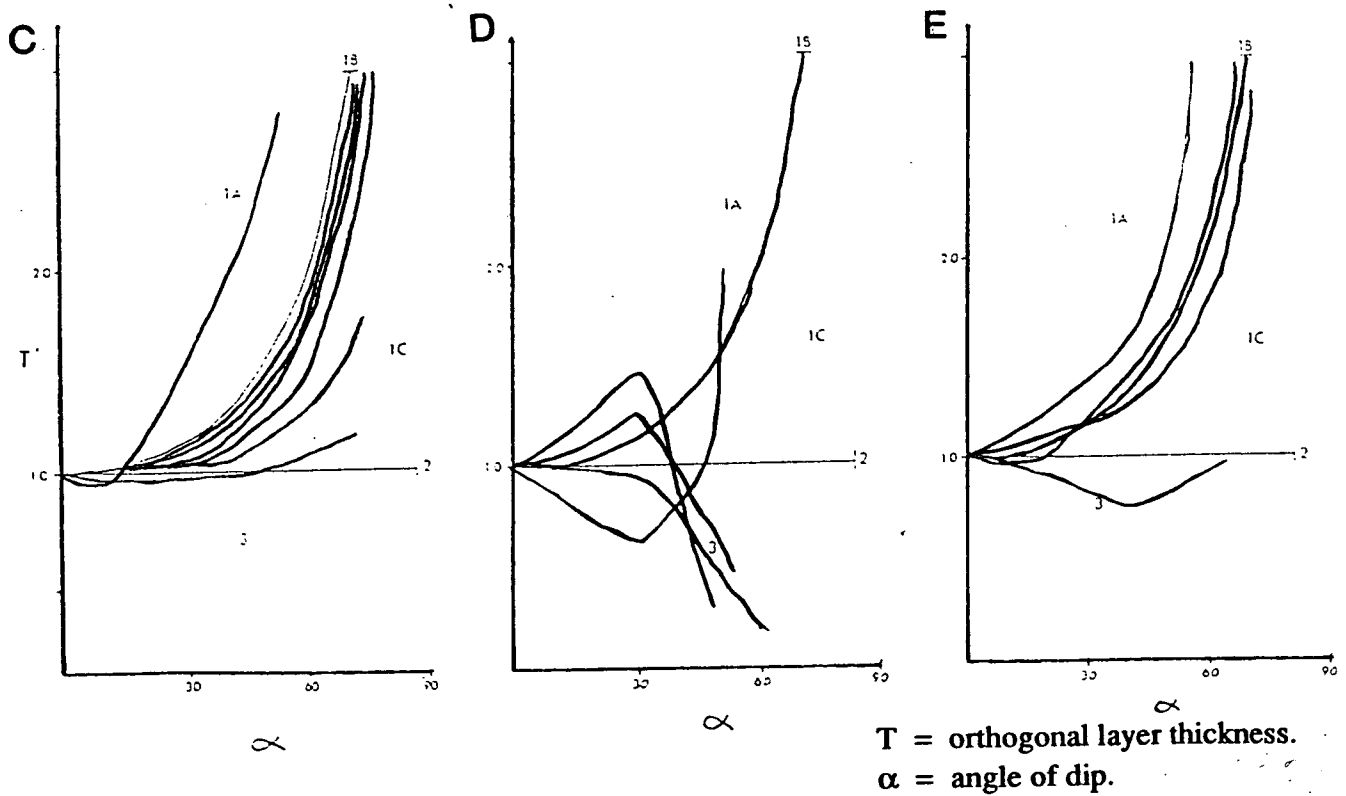
#### 6.3.1 Introduction to Fold Analysis

In this study, folds are separated into mesoscopic and macroscopic scales, although this classification is not dependent on any absolute criteria. Furthermore, different types of mesoscopic and macroscopic folding are distinguished. Differences in fold morphology are largely the result of mechanisms that depend on whether the rocks have behaved as single or multilayers (in the case of mesoscopic folds), or on the relationship between thrust faulting and folding (in the case of some mesoscopic folds and the macroscopic folding).

North of the Gulf of Corinth, Green (1982) carried out an in-depth study of the styles of mesoscopic folding within the Pindos thrust stack and the results of his layer shape and surface shape analysis are illustrated in Figure 6.8. Layer shapes were found to approximate Class 1B (parallel) geometries while 20-25% conformed to Class 1A or Class 3, with many folds displaying composite geometries. The surface shape analysis indicates that chevron folding predominates. The results of Green's analysis are considered equally applicable to many of the mesoscopic folds of the present study area, based on the analysis of layer shape from a small number of folds in multilayer piles. Field observations confirm the dominance of chevron geometries in the NW Peloponnese.



$b_1$  &  $b_3$  are Fourier coefficients.



$T$  = orthogonal layer thickness.  
 $\alpha$  = angle of dip.

**Fig. 6.8** Plots indicating the surface shape of folds in limestone (A) and chert and shale lithologies (B), derived from harmonic coefficients. Fold layer shape analysis using the dip isogon and layer thickness method (Ramsay 1967) for folds in limestone (C) and (D) and interbedded chert and shale (E). All data from the Pindos Zone north of the Gulf of Corinth. From Green (1982).



### 6.3.2 Meso-scale Folding

Two main types of mesoscopic folding are distinguished. The first consists of structures with wavelengths commonly up to 10m; these comprise sinusoidal to chevron fold morphologies in multi-layer sequences of low ductility contrast (Type 1 mesoscopic folds). The second type of mesoscopic folding is restricted to mechanical single layers (i.e. individual beds, or sequences of beds, intercalated with lithologies of high rheological contrast); these have irregular morphologies with wavelengths between 1-50m, depending on the layer thickness (Type 2). There are also mesoscopic examples of fault-related folding, particularly in thinly-bedded limestone sequences (Plate 6.5). This type of folding is considered more fully in relation to larger scale thrust faults (Section 6.3.3) but the mechanisms leading to the development of such folds are equally applicable on smaller scales.

#### 6.3.2.1 Type 1 Mesoscopic Folds

##### Field Observations

The type 1 outcrop scale folds are dominated by close to tight chevron morphologies (angular hinge area and straight limbs) in the competent limestones of the Drimos and Lambia Formations (Figure 6.9, Plates 6.5 and 6.6). Also observed, but less commonly, are sinusoidal to concentric folds with more open interlimb angles. Such folds sometimes occur isolated within multilayers or, as at Kalendzi, in fold trains of several hundred metres length. There is evidence in the field to support Green's (1982) claim that there is a genetic link between the sinusoidal folds and chevron morphologies, as a spectrum of interlimb angles is observed. Where the interlimb angles of folds approach 70-60° the limbs are always straight, although sometimes with rounded hinge areas (Plate 6.6). The degree of roundness, or angularity in the hinge zone appears to depend on the ratio of bed thickness to wavelength and amplitude. No attempt to quantify this relationship was undertaken in this study. Thickness variations in the multilayer succession often lead to strain accommodation by hinge collapse and this is especially prevalent where intercalated incompetent material is expelled from the dilated fold cores, leading to the development of saddle reef structures (Figure 6.9, Ramsay 1974).

Folding was accomplished by a concurrent combination of flexural slip and tangential longitudinal strain. The flexural slip mechanism is not only confined to limestones intercalated with thin shale interbeds, but is also evident where limestone

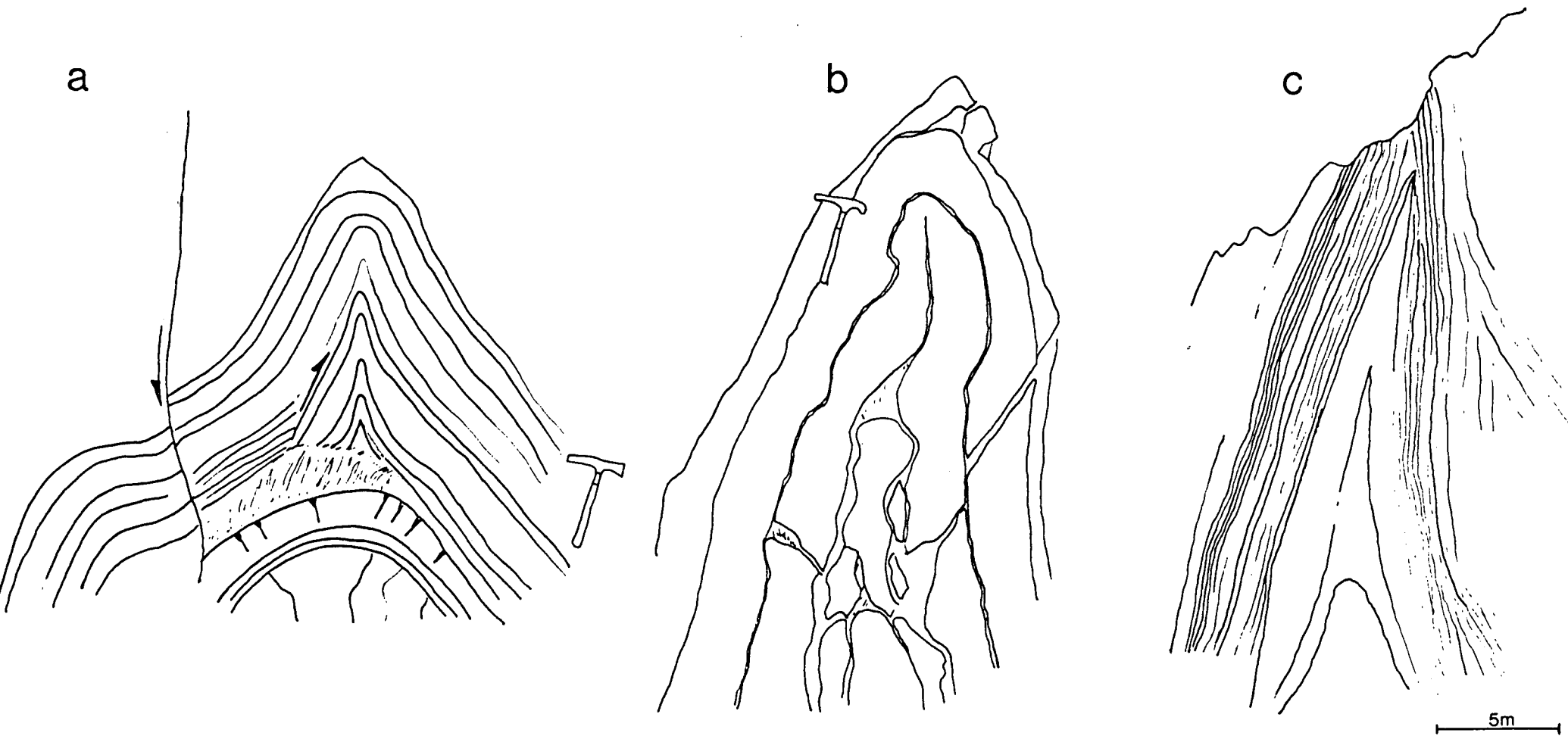


**Fig. 6.9** Sketches of field examples of mesoscopic folding. Note in (A) the rounded hinge formed by a thick layer in the fold core, with extensional fractures in the outer arc. Also, thrusting along the limb of the fold formed by thinner bedded layers. (B) Fold hinge collapse and boudinage in fold core. (C) Superposed flattening strain present in overtightened chevron folds.

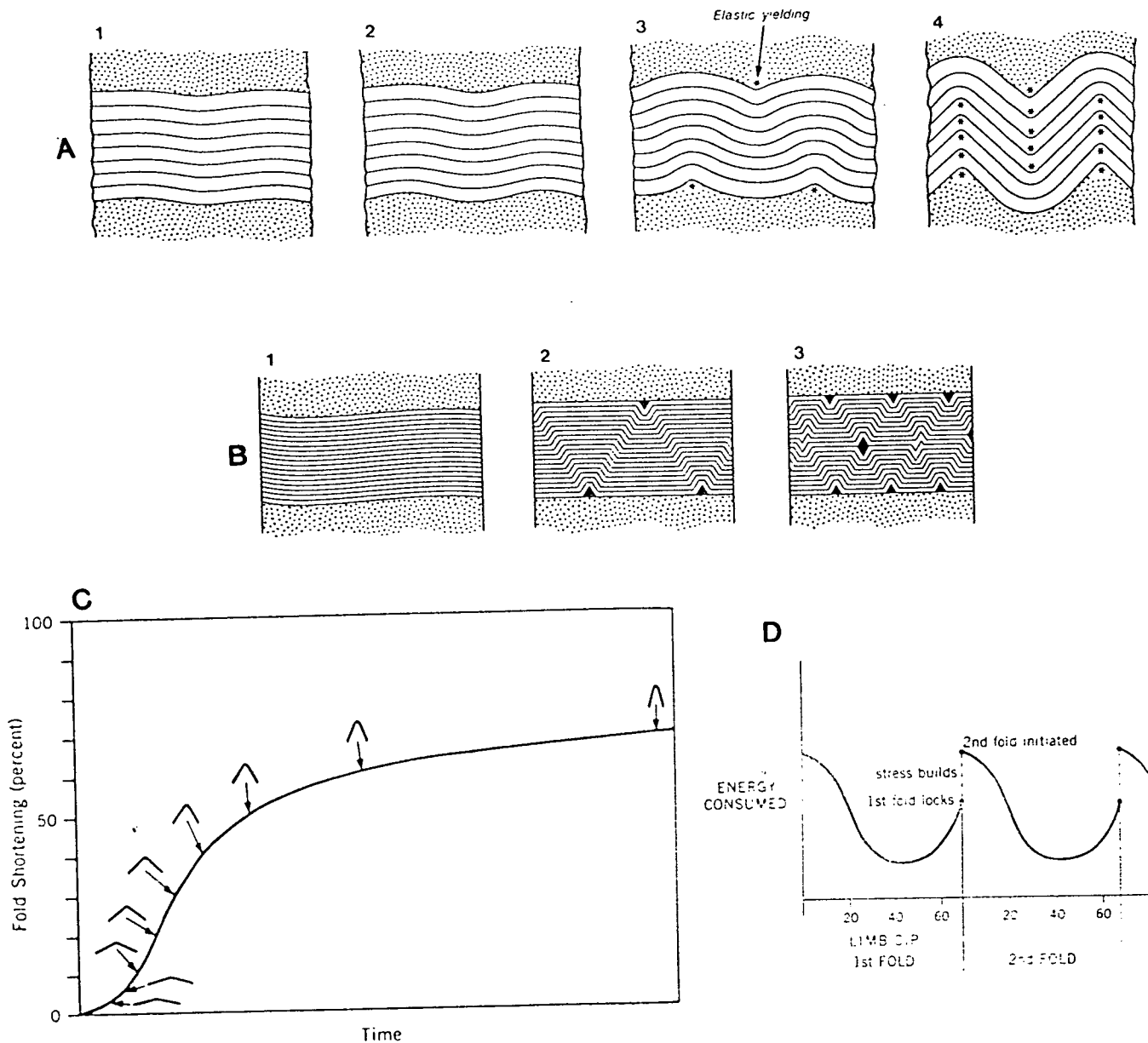


**Fig. 6.10** (A) and (B) Sequence of fold forms developed when an elastic multilayer is compressed. Sequence (A) begins with a sinusoidal form and evolves through a concentric form into chevron folds. Sequence (B) begins with a broad sinusoidal form, evolves to kink forms which eventually intersect to form local chevron folds (from Johnson 1977). (C) Diagrammatic representation of Ramsay's analysis (1974) showing that a constant applied stress will cause increasingly rapid fold formation to limb dips of c.a. 50-60°, thereafter there is a marked decrease in limb tightening until the fold "locks-up". (D) Diagrammatic representation of the expected energy consumption (in arbitrary units) versus limb dip. The energy required to initiate a fold is large but drops significantly as the fold develops, until limbs begin to lock-up at about 60°. Thereafter stress levels begin to build up until they are large enough to initiate a new fold.

beds are juxtaposed, as shown by the presence of slickensides on exposed limbs perpendicular to hinge axes. Tangential longitudinal strain was also important, often leading to minor thrusting along the fold limbs within fold inner arcs and extensional fracturing in fold outer arcs above the neutral surface (Figure 6.9).

### Theories of Multi-Layer Fold Development

Modelling by Cobbold (1976) and Johnson (1977) shows that both concentric and chevron folds can form in the same experiment and that the sinusoidal folds can develop into chevrons with increasing strain. Figure 6.10 illustrates the results of an experiment by Johnson (1977) showing this progressive change whereby hinge geometry changes but not hinge location, which is established at the time of sinusoidal fold creation and is directly controlled by the thickness of the competent layer. Also shown in Figure 6.10 is an alternative development of chevron folds from the interference of conjugate kink bands. Faill (1969) explained the geometry of fold complexes in the Central Appalachians in terms of conjugate kink bands whereby several intersecting kink bands could produce a chevron fold complex. Such a mechanism is not considered valid in the Pindos Zone as it requires the migration of fold hinges with the sequential thickening and thinning of beds as migration proceeds. Such a process would lead to extensive penetrative deformation along the entire length of a fold limb and this is not observed. Rather, accommodation features related to fold development in multilayers with different bed thicknesses indicate that the hinge zone tightens *in-situ* (saddle-reef and pinch and swell structures, Figure 6.9).

Ramsay (1974) considered the timing of chevron fold development and illustrated how the initial stages of folding are relatively slow, but folding proceeds rapidly as interlimb angles approach  $110^\circ$ , beyond which the rate decelerates until folds are locked up at  $60^\circ$  (Figure 6.10). Additionally, the degree of stress necessary to initiate a fold is greater than that needed to continue fold tightening to "lock-up". The stress/strain relationship for the serial development of folding is diagrammatically shown on Figure 6.10. Cobbold (1975) illustrated how folds are created serially in nature, whereby the folds are grouped into complexes where fold amplitude decreases away from a central fold which develops at the site of a perturbation formed by an inhomogeneity (e.g. a sedimentary structure or facies change?).

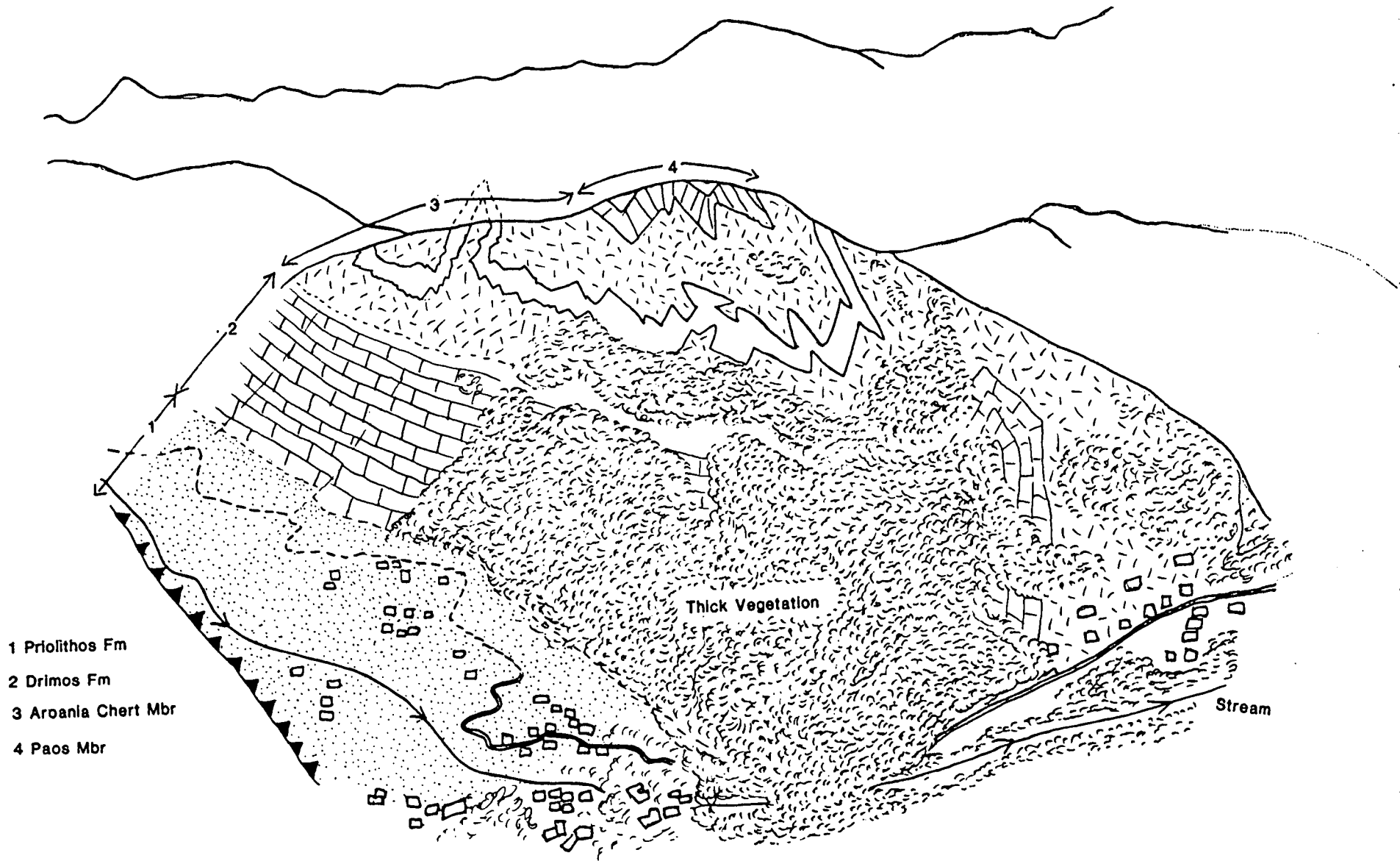


Fig. 6.11 Field sketch, towards the NE, over the village of Livardzi showing the buckling of an already folded intraformational limestone within the Aroania Chert Member. Note the folded limb of the Drimos Formation on the right of the sketch.

### 6.3.2.2 Type 2 Mesoscopic Folds

#### Field Observations

This style of folding is principally observed in the intraformational limestones within the Aroania Chert Member of the central imbricate region. The limestones form discrete lithological units of 5-15m thickness, intercalated between cherts and mudstones. The competency contrasts and differing rheologies effectively mechanically isolate the limestone as a single layer and shortening within this stratigraphic sequence is reflected in the development of upright, but irregular, buckle folds.

Figure 6.11 illustrates a fold train of buckles in an intraformational limestone (Lesteena Formation) near Livardzi (Figure 1.1). The irregular style of folding is seen clearly and there is a similarity of wavelength and amplitude. The locality also exemplifies the mesoscale folds forming longer wavelength macroscopic folding. This demonstrates that the already deformed mesoscale buckled layer acted later as a thicker layer, in response to continued stress.

In places, shear zones are seen between the limestones and surrounding cherts and mudstones. Although never measured directly, it is probable that the more incompetent lithologies have flowed into zones of thickening within the cores of limestone folds in such areas.

#### Theories of Single Layer Fold Development

Many authors have analysed the development of folding in single layers. Biot (1961) and Ramberg (1961) influenced later work. Both these authors considered the initiation of folding and, in particular, the significance and interdependence of layer thickness, competence contrast and fold wavelength. They independently derived a similar equation to relate these parameters:-

$$L = 2\pi a \sqrt[3]{\eta_1/6\eta_2}$$

where L is the wavelength of the buckles, a is the layer thickness and  $\eta_1$ ,  $\eta_2$  are the viscosities of the layer and matrix respectively. The equation can be modified to:-

$$L/a = 2\pi \sqrt[3]{\eta_1/6\eta_2}$$

and this defines the "slenderness ratio", whereby from field observations of layer thickness and fold wavelength, the significance of the ratio of rheological properties (i.e. competency contrast) in the single layer and matrix can be appreciated. Sherwin & Chapple (1968) measured the slenderness ratio of over 800 natural folds where the values were found to be between 5/1 and 10/1. This is an order of magnitude smaller than proposed theoretically by Biot (1961); thus, the many simplifications of the earlier theories needed modification. In particular, an incremental increase in fold amplification was found to modify the layer thickness under consideration. An extensive discussion of the various models proposed to develop theoretical ideas of single layer buckling, including finite element analysis, is provided by Price & Cosgrove (1990).

### 6.3.3 Macro-scale Folding

#### 6.3.3.1 Field Observations

Macroscopic folds are generally inferred through bedding dips, sediment younging directions and outcrop patterns rather than by direct observation. There are some geological observations which lead to deductions about the mode of formation of these large scale fold structures:-

The youngest Pindos Group sediments, comprising the Pindos Flysch Formation, are generally poorly preserved due to erosion. Where present, the formation is generally found in cores of synformal structures with steeply eastward-inclined axial surfaces and hinge lines that roughly parallel thrusting. Many (but not all) synforms are adjacent to thrust planes which lie immediately to the east (i.e. they are in the immediate footwall), while other synforms are dissected by thrusts and only forelimbs are preserved.

The axial traces of macroscopic antiformal folds are often sinuous and sometimes bifurcate (e.g. west of Agridi). In places antiformal folds increase in amplitude and then develop into thrusts along strike (e.g. immediately east of Agridi). Thus, such antiforms are clearly in the hangingwall to blind thrusts, which become emergent along strike. Sinuous antiforms that develop into thrusts along strike with congruent axial traces and fault planes, can most readily be considered as having folding and thrusting that developed contemporaneously and they are therefore different expressions of the same deformation mechanism. However, where a relatively linear

thrust trace does not parallel a fold axial trace, but dissects the sinuous synform (e.g. NW of Livardzi) or antiform, it is clear that the faulting post dates the folding and they therefore cannot be part of the same structure.

The above observations suggest that there are two types of macroscopic folding present. It is clear that while folding may influence the trajectory of later thrusting, as in the case of many faulted antiformal folds, it does not necessarily always control faulting (as with the dissected folds). In the eastern imbricate region, most macroscopic folds are not associated with observable thrusts at all (SE of Kato Klitoria) and thus the fault-related origin of folding cannot be established. This does however, offer additional evidence for the assertion that much macroscopic folding locally preceded faulting, although formed in the same regional deformation event.

Lastly, large scale folds that are occasionally observed in well exposed cliff sections, are of sinusoidal, chevron and box fold morphologies, generally upright or west-vergent. The fold geometries are suggestive of buckle folding, rather than being related to thrust fault-related folding (fault bend and fault propagation folds), which are quite characteristic.

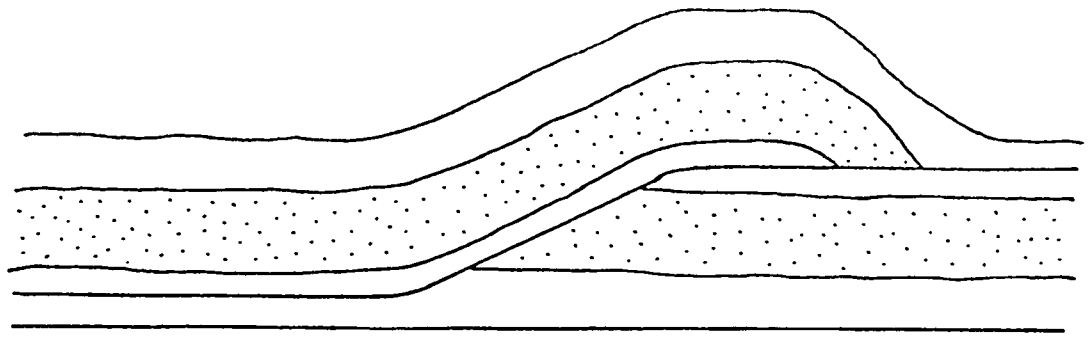
#### 6.3.3.2 Theories of Fold/Fault Interaction

There are several models to explain the development of folding (a ductile response to deformation), associated with faulting (a brittle mechanism). The geometries of three specific types of folding have been identified in thrust terranes (Figure 6.12). (1) Fault bend folding. Such folds develop after ramp formation and the fold is the geometrical consequence of a thrust sheet moving over a footwall ramp onto a flat (Suppe 1983). (2) Fault propagation folding. This fold type develops as a deformation front migrates into rocks ahead of a ramping thrust tip (Williams & Chapman 1983, Suppe 1985), the folding is therefore synchronous with fault development. (3) Detachment folding is the "rucking" of strata caused by the synchronous shortening of rocks above a flat lying, propagating, decollement plane. Jamison (1987) has described the characteristics of each of these fold types and proposed geometrical constraints to distinguish the various types. Theories of fold/fault interaction considered relevant to the Pindos Zone are discussed here.

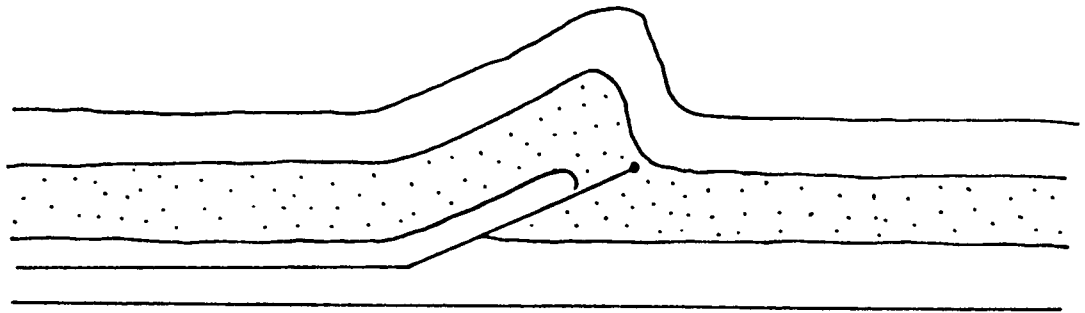
#### **Detachment Folding**

If decoupling is initiated along a relatively ductile interface between over and underlying competent units due to compressive stress applied disproportionately to

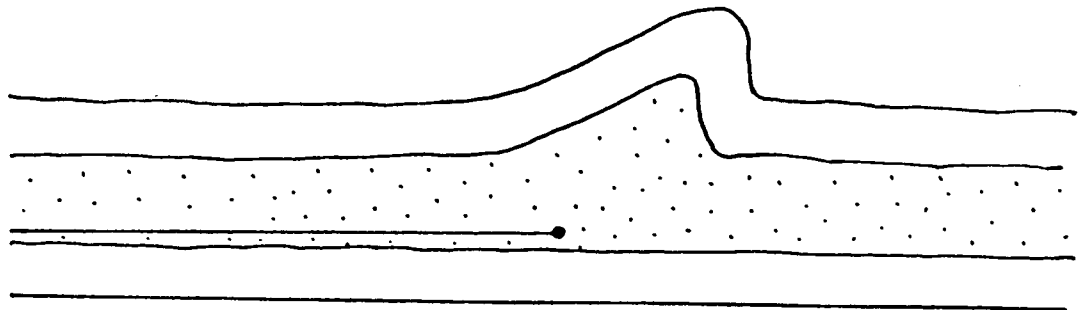




Fault Bend Fold



Fault Propagation Fold



Detachment Fold

**Fig. 6.12** Folding associated with faulting; fault bend, fault propagation and detachment folding. Explanations in text. From Jamison (1987).

one block rather than the other, the hangingwall can be expected to move in relation to the footwall. Depending on the efficiency of fault propagation, either strain will be accommodated by the creation of a fast-moving, flat-lying detachment or, if sticking points are encountered and stress builds up locally in the upper block, the hangingwall must necessarily shorten by either folding, faulting or pressure solution. Detachment folding is effectively the ductile lithological response to deviatoric compressive stress in a hangingwall block. Depending on local factors, e.g. competence, anisotropy, layer thickness and inherent weaknesses, a variety of fold structures could become established that are strongly disharmonic with respect to the footwall.

An elaborate view of detachment folding was conceived by Thompson (1981) for folding in the northern Rocky Mountains. In his model, blind thrusts were considered to merge and flatten at an "upper detachment zone" which was unobservable at the surface. As the propagation of blind thrusting proceeded, a sub-surface back thrust developed which allowed overlying strata to behave independently of underlying, relatively rigid rocks. Shortening in the hangingwall block was expressed as disharmonic folding. If the folding kept pace with forelandward thrust tip propagation, then folding would be the only structure to develop in the hanging wall. However, if the folding could not accommodate strain sufficiently quickly then splays would develop from the basal thrust and cut up to the surface as a "release valve" to adjust for the hanging wall shortening imbalance. The model presented by Thompson implies that thrusts breaking surface will develop in the foreland to the folding, although there is no reason for thrusts not to splay off a basal detachment within the fold complex.

Jamison (1987) has related the angle of fold backlimb dip (i.e. the acute angle between the decollement surface and fold backlimb) to the fold interlimb angle for detachment folds. However, this relationship is itself dependent on the ratio of fold amplitude to layer thickness and also to any forelimb thickening or thinning. Thus, there is a vast spectrum of fold geometries possible for detachment folding. This author is of the opinion that there is a limitless combination of factors that could co-exist to alter or localise the initiation and development of detachment folds. The geometrical treatment of Jamison is therefore considered applicable only to isolated folds created within very tight constraints and the analyses cannot easily be applicable to geologically realistic situations.

In the study area, where macroscopic folding is demonstrably unrelated directly to thrust faults at the surface, and the style of folding is best appreciated as irregular buckle folds, the initiation of folding is here considered as being due to shortening above a flat-lying subsurface thrust tip. The continued development of the large-scale detachment style of folding can be perceived in the same manner as mesoscale single layer buckle folds (Section 6.3.2.2), as the Pindos Group is effectively a mechanically isolated single layer on the scale being considered. That is, a detachment at the sedimentary/igneous interface effectively defines the bottom surface and the upper surface would have been either free (if folding continued up to the surface) or the relatively unconsolidated, rheologically different, overlying flysch. Thus, the macroscale structures often represent first order buckle folds which develop due to the whole Pindos Group sedimentary sequence acting as a mechanical single layer.

#### Fault Propagation Folding

As a thrust fault propagates up a footwall ramp, a region of ductile deformation precedes the thrust tip. This region was termed the "ductile bead of deformation" by Elliott (1976) and the strain is commonly expressed as folding. Antiformal structures will develop above the fault surface and some footwall deformation (synforms) should also exist (Cooper & Traynor 1986).

Suppe & Medwedeff (1984) and Jamison (1987) have derived theoretical relationships between the footwall ramp angle and the antiformal fold interlimb angle. For example, where layer thickness remains constant through folding and the ramp angle is  $25^\circ$ , the interlimb angle is calculated to be  $67^\circ$ . It is possible to accurately measure macroscopic interlimb angles; however, the analysis of Jamison (1987) presupposes layer-cake stratigraphy, staircase fault trajectory and kink-band type folding. Where such constraints are not valid, or where there are additional complicating factors, the measuring of interlimb angles and relating them to hypothetical ramp angles is not considered justified.

One of the major differences between a detachment and fault propagation fold is that in the latter the antiform is truncated against the thrust that formed it, while detachment folds form above thrust flats. Clearly, in the Pindos Zone both truncated and non-truncated folds are present. A difficulty arises when a thrust cuts up from a basal detachment, through a detachment fold. Given the wide range of detachment fold morphologies possible, which can mimic fault propagation fold morphologies,

it is proposed that the only sure way to differentiate the two fold types is to determine whether the folds and thrusts are of the same structure, as determined from field mapping and as described above (Section 6.3.3.1, e.g. the dissection of sinuous axial traces by linear thrust traces indicates that faulting clearly post-dates folding and they are not directly related).

#### 6.3.4 The Relative Timing of Folding

The field observations and theoretical modelling, outlined above, suggest a possible chronology, whereby mesoscopic folds are followed by the folding of meso-scale fold enveloping surfaces into first order macroscopic folds, as the Pindos Zone sedimentary cover was detached from the igneous substratum. This, in turn, was followed by macroscopic folding related to thrust faulting cutting up-section from a basal decollement. The relative timing and the ramifications of the fold progression can be postulated:

The development of mesoscopic multilayer folding in the Pindos Group is considered to have developed as follows: An initial increase in deviatoric stress was accommodated by strain concentration and nucleation at inhomogeneities in the sedimentary sequence. From a local flexure, the rocks deformed into sinusoidal folds, the initial wavelength of which depended on the thickness and competence of the multilayer. Continued stress reduced the interlimb angles of folds and asymmetry was sometimes induced, possibly by simple shear. As the stresses required to initiate a fold are greater than those needed to continue its development, the local strain field relaxed once folding was initiated, only to gradually increase as the fold limbs tightened and "lock-up" was imminent. At this stage the stress front propagated efficiently to the foreland and a new cycle of folding was initiated. Continued stress in the hinterland induced some superposed flattening strain and third order thrust rock failure.

The mesoscopic multilayer folding was probably contemporaneous with a different fold style that developed in mechanical single layers, whereby irregular buckling was initiated in competent horizons within a more ductile matrix. Strain accommodation continued serially until folds locally locked-up and a thicker mechanical single layer was formed by the folded strata that was itself able to deform as a first order buckle fold. The single layer folding, in relation to

surrounding multilayers, was disharmonic with substantial shearing at boundaries where there were strong competence contrasts.

At several locations, mesoscopic folds are often found along the limbs of first order folds (of a greater wavelength and amplitude) and they have a parasitic relationship with the macroscopic folds, whereby vergence directions are similar and enveloping surfaces, connecting inflection points, are themselves clearly re-folded.

The first order folding may have been detachment folding above a flat-lying decollement propagating along the igneous/sediment interface. Axial planar lines of weakness may have been exploited by later thrusts that cut up through the sedimentary column and dissected pre-existing folds. Additionally, the regular relationship between some antiforms and thrust surfaces indicates that fault propagation folding also occurred ahead of migrating thrust tips.

The fold/thrust model suggested for deformation in the Pindos Zone is based on the geometries of observed macroscopic folds and an inferred sequence of deformation. The validity of detachment folding and fault propagation folding existing contemporaneously in nature is strengthened by analogue modelling using scaled stratigraphic sequences under centrifuge conditions by Dixon & Tirrul (1991). In the experiments, deformation proceeds towards the foreland by the nucleation of periclinal folds ahead of higher amplitude folds above a decollement horizon. Increasing fold amplitude and hinge length occur as strain increases and individual antiforms can join up along strike. Internally, folds develop with listric axial surfaces which through time resemble incipient imbricate thrust faults. When discrete thrusts do develop, they propagate through previously folded strata as "smooth trajectory" thrusts (Cooper & Traynor 1986), rather than with staircase geometries. As a result of the modelling, a conclusion is that the folding of particularly competent units determines the position of thrust ramps by localising strain beneath antiforms. Dixon & Liu (1992) demonstrate how the fault-related folds which nucleate as detachment folds, develop into fault propagation folds as faulting is localised in the antiformal core. Finally, thrust ramps propagate upwards through the forelimb of the fold and there is the potential for fault bend folding.

### 6.3.5 Thrust Surface Geometries

Rich (1934) was the first to demonstrate how faults propagating towards the foreland, detach along flats within incompetent layers and cut up-section in the transport direction, along footwall ramps through more competent lithologies. The ramp-flat staircase trajectory of the "Rich" model can be contrasted with the fault plane geometry created by the smooth trajectory thrusting model of Cooper & Trayner (1986). Both of these models are "conventional" in that they involve a foreland propagating, linked thrust system. Alternatively, Eisenstadt and De Paor (1987) propose a system whereby reverse faulting is initially isolated and the failure of a "solid beam" is achieved by fault nucleation on a ramp. Thrust propagation then occurs both up and down section along the ramp and an interconnected thrust system is formed by the later capture of ramping faults along flats.

The sedimentary lithologies of the Pindos Group are extensively folded and thrustured in the NW Peloponnese and, with due regard to the study of other fold and thrust belts (Dahlstrom 1969, Elliott & Johnson 1980, Boyer & Elliott 1982) a thin-skinned foreland propagating linked thrust system geometry is considered applicable. The general characteristics of such fault systems are low angle, hinterland-dipping reverse faults that rise to higher stratigraphic levels in the transport direction, duplicating stratigraphy.

There are many thrust geometries that potentially can develop in such a system; however, mapping indicates that the Pindos thrust stack was deformed in a simple and systematic manner, where faulting cut through an already folded sedimentary pile with no major out-of-sequence thrusting or back thrusting. The field evidence (principally the lack of footwall flat/ramp intersections and fault bend folding) suggests that smoothly curving thrust trajectories are applicable. It has already been noted that most of the thrust outcrops are characterised by flats. Where cut-offs are present, they may often represent the thrusting of pre-existing folds (Section 6.3.3). At the surface, most of the structures (bedding and thrust planes) are steeply eastward dipping. Such an arrangement suggests tightening of the imbricate stack, possibly associated with <sup>t</sup>butressing against the Apulian margin (Section 6.5.3) and the back rotation of pre-existing thrusts.

### 6.3.6 Timing of Deformation

The timing of thrust faulting in the Pindos Zone cannot be determined absolutely as there are no syn-tectonic sedimentary strata preserved. However, minimum and maximum ages can be established, based on the presence of the youngest strata in both the Pindos Group and the Tripolitza Zone.

The clastic beds of the Pindos Flysch Formation were deposited ahead of the deformation front (Section 5.3) as the sedimentary response to tectonism in the hinterland. Conformable sedimentary sequences are present through to the Upper Eocene (41my B.P. Dercourt *et al.* 1977), thus the actual deformation front cannot have affected the area of the NW Peloponnese prior to this time, but may well have existed in more easterly parts of the Pindos Basin.

The youngest sediments preserved in the foreland basin that formed ahead of the Pindos thrust stack on the Gavrovo-Tripolitza platform are dated as Upper Oligocene (Section 7.3.2.2) (or Aquitanian north of the Gulf of Corinth, Dercourt *et al.* 1977) and these are directly overlain by the Pindos thrust stack. The youngest age possible for the emplacement of the Pindos thrust sheets is therefore Upper Oligocene (c.a. 20my B.P.). Evidence (Section 7.5.1) indicates that there was movement on thrust faults in the platform while the Pindos unit was being emplaced. By the Miocene, footwall collapse had propagated the deformation front through to the Ionian Zone further west (Underhill 1985, Clews 1989). Thus, the best estimate for the period of deformation within the Pindos Zone is approximately 21my, between the Upper Eocene and the Upper Oligocene.

### 6.3.7 Estimates of Orogenic Shortening

The concept of balanced cross sections was introduced by Dahlstrom (1969) and discussed by Hossack (1979) and Elliott & Johnson (1980) in an attempt to constrain the degree of shortening in an orogenic system and more accurately model high level crustal structures at depth. In recent years some geologists (J.G. Ramsay in particular, TSG conference 1989, Himalayan conference at Oxford 1992) have stated their strong disapproval for "balanced sections" that are constructed in "unbalance<sup>a</sup>ble situations", where essential assumptions about geometries and thrust fault mechanisms can not be justified.

The palinspastic restoration of a thrust system relies on the conservation of volume between the deformed and undeformed states. There are two principle types of balancing in compressional regimes; area balancing and line balancing. Area balancing critically requires that the depth to detachment in the thrust stack can be ascertained and from this the area of an undeformed portion of the thrust sheet can be derived. Unfortunately, neither bore hole nor seismic data are available for the study area and area balancing cannot be accomplished.

Line balancing involves determining the length of a horizon between two marker points (pins) common to both the deformed and undeformed sections, where movement of the hangingwall relative to the footwall is zero at the frontal pin. If the line lengths in both states are equal the section balances. Naturally, in grossly allochthonous terranes there are seldom obvious pin points available, thus the absolute displacement of the Pindos Zone relative to the Gavrovo-Tripolitza autochthon cannot be accomplished. In the case of thrusting within the Pindos Zone, strong lithological contrasts present in the Pindos sedimentary sequences (e.g. Lesteena Formation, between the overlying Lambia and underlying Drimos Formations), preclude the recognition of accurate pin points as there has invariably been a great deal of bedding parallel slip through thrust movement and flexural slip folding.

In attempting to constrain the shortening within the NW Peloponnese section of the Pindos Zone, a number of other difficulties lessen the accuracy of any restoration, such that only a minimum shortening estimate can be provided. In order for a line section to be restored to a permissible pre-deformation state, several requirements must be fulfilled:-

(1) Restorable sections which depict surface geological data extrapolated to depth must involve fold and thrust geometries that are not unrealistic. The sub-surface detail in Enclosure 2 is only one of several possible interpretations of geometrically permissible configurations. Note that the basal detachment of Enclosure 2 is folded. This is partly a schematic "space-filling solution", but it is also considered more realistic than a flat-lying detachment (due to post emplacement strain, Section 6.6.1 and 7.5.1.5).

(2) The section must be along a line of plain strain, where volume loss is minimised. To accomplish this (without the use of out of plane approximations) the structural section (Enclosure 2) parallels, as much as possible, the local shortening direction



**TABLE 6.1: OROGENIC CONTRACTION**

**A: NW PELOPONNESE STUDY AREA**

Frontal Imbricate Region ( $L_{1a}$ ) = 7Km  
Central Imbricate Region ( $L_{1b}$ ) = 15Km  
Eastern Imbricate Region ( $L_{1c}$ ) = 21Km  
Present Width = ( $L_{1a} + L_{1b} + L_{1c}$ ) = 43Km

Initial Restored Width ( $L_{01}$ ) = 77Km

Mesoscopic Folding Restoration

Frontal Imbricate Region 100m = 140m  $\therefore L_{1a} + 2.8\text{Km}$   
Central Imbricate Region 100m = 180m  $\therefore L_{1b} + 12\text{Km}$   
Eastern Imbricate Region 100m = 170m  $\therefore L_{1c} + 14.7\text{Km}$

New Restored Width ( $L_{02}$ ) = 107Km

Volume Loss Through Pressure Solution  
3mm in 3cm over width of 10Km = 1Km

Final Restored Width ( $L_{03}$ ) = 108Km

**B: ARCADIA**

Present Width ( $L_{1d}$ ) = 56Km

Restored Width ( $L_{04}$ ) = 112Km

**C: PINDOS ZONE**

Present Width ( $L_{1a} + L_{1b} + L_{1c} + L_{1d}$ ) = ( $L_1$ ) = 99Km

Total Restored Width ( $L_{03} + L_{04}$ ) = ( $L_0$ ) = 220Km

Shortening =  $L_1 - L_0 / L_0 = 55\%$

Deformation Time Period = 21my

Shortening Rate = 5.8 mm/y

Thrust Propagation Rate = 10.5 mm/y

derived from folding. It is significant that kinematic indicators at Aroania and Agridi indicate that first order thrust planes were utilised as strike-slip faults during later movements and this phase possibly corresponds to the post emplacement south-to-north phase of compressive stress (Section 6.5.1) which has also accentuated out-of-plane strain.

(3) The stratigraphic template must be accurate. Note that no Priolithos Formation rocks are exposed east of Kato Klitoria and the Drimos Formation is only sporadically exposed as incomplete sections.

The result of a restorable cross section which incorporates the accurate portrayal of surface structural information and fulfils the criteria established above, is a geometrically permissible line of section. These criteria are not established for the cross section (Enclosure 2) due mainly to unquantifiable out of plane strain and bedding parallel slip. The Pindos thrust system is therefore clearly "leaky", both mechanically and chemically. Nevertheless, the extrapolation of the base of the Lambia Formation to link hangingwall and footwall cut-offs (with minimum values) allows the estimation of orogenic contraction in the Pindos Zone, as preserved in the northern Peloponnese. Table 6.1 incorporates the restored line length with an appraisal of shortening due to mesoscale folding and volume loss through dissolution. From three localities in each of the imbricate regions (at Aleporio, Livardzi and Aroania), meso-scale folding over a 100m section was measured and shortening estimated. Similarly, pressure solution effects were evaluated within the Erymanthos Limestone Member by measuring the distance of adjacent stylolite peak to peaks and cleavage domains. In the frontal region, cleavage spacing is approximately 1-6cm (average 3cm) and peak-to-peak stylolite widths, which are appreciable, have been estimated as 2-5mm per stylolite (average 3mm). The stylolitic pressure solution is not commonly observed east of Livardzi. The width of the area with bedding perpendicular pressure solution development is therefore 27Km perpendicular to the principle shortening direction, although concentrated areas of pressure solution cover perhaps 10Km. Volume loss through dissolution is estimated at 1Km with an upper and lower limit of perhaps 5Km and 0.33Km

The above methodology, to deduce mesoscopic shortening and volume loss through dissolution, is crude and it is appreciated that such measurements may have no regional validity; however, a more legitimate quantification of the degree of shortening due to meso-scale folding and volume loss through pressure solution would require a much wider systematic study.

There has been at least 60% shortening in an area that is currently 43Km wide, the area studied here (Table 6.1). The Pindos Zone exposed throughout the northern Peloponnesse is a total of 99Km wide (the additional 56Km comprising the Arcadian region ("Table d'Arcadie", Dercourt 1964), almost exclusively consisting of flat lying deformed Cretaceous Erymanthos Limestone Member rocks to the east of Chelmos, Section 1.1, Figure 1). It is difficult to evaluate orogenic contraction in the Arcadian area but 50% was arbitrarily considered by Fleury (1980) as a reasonable value. The total orogenic contraction for the Pindos Zone of the Peloponnesse is therefore estimated at 55% and this indicates that the pre-deformed Pindos ocean, represented by the preserved sediments, was at least 220Km wide. It is proposed that a more realistic estimate would restore the preserved Pindos Group to a width of approximately 300Km which represents 67% shortening. (North of the Gulf of Corinth, Green (1982) has estimated orogenic contraction within the Pindos Basin at 63%).

The period of deformation when the Pindos sedimentary sequences were telescoped from a width of 220Km to 99Km has been estimated at 21 m.y. between the Upper Eocene and the Upper Oligocene. Thus, the average shortening rate of the orogen can be estimated at 5.8 mm/y. This rate is similar to rates established in other mountain systems, e.g. 5mm/y in the Canadian Rockies (Elliott 1976) and 6mm/y in the Pyrenees (Williams & Fischer 1984).

The thrust propagation rate is calculated by determining the initial distance between two points affected by deformation (i.e.  $L_0$ ) over a given period of time. The result, 220Km/21my gives a thrust propagation rate of 10.5 mm/y although it must be remembered that this is a time averaged rate and long periods of zero displacement would have been punctuated by instantaneous slip rates of several millimetres.

## 6.4 ANCILLARY STRUCTURES

### 6.4.1 Coeval Transverse Faulting

There is a great deal of faulting present in the Pindos Zone which is perpendicular to the strike direction of thrust faulting. The transverse fault planes contain a variety of kinematic indicators which indicate that normal faulting is dominant but, strike-slip movement is also prevalent. It must be remembered that most faults, as planes of weakness, can be utilised in different stress fields; therefore, these indicators only

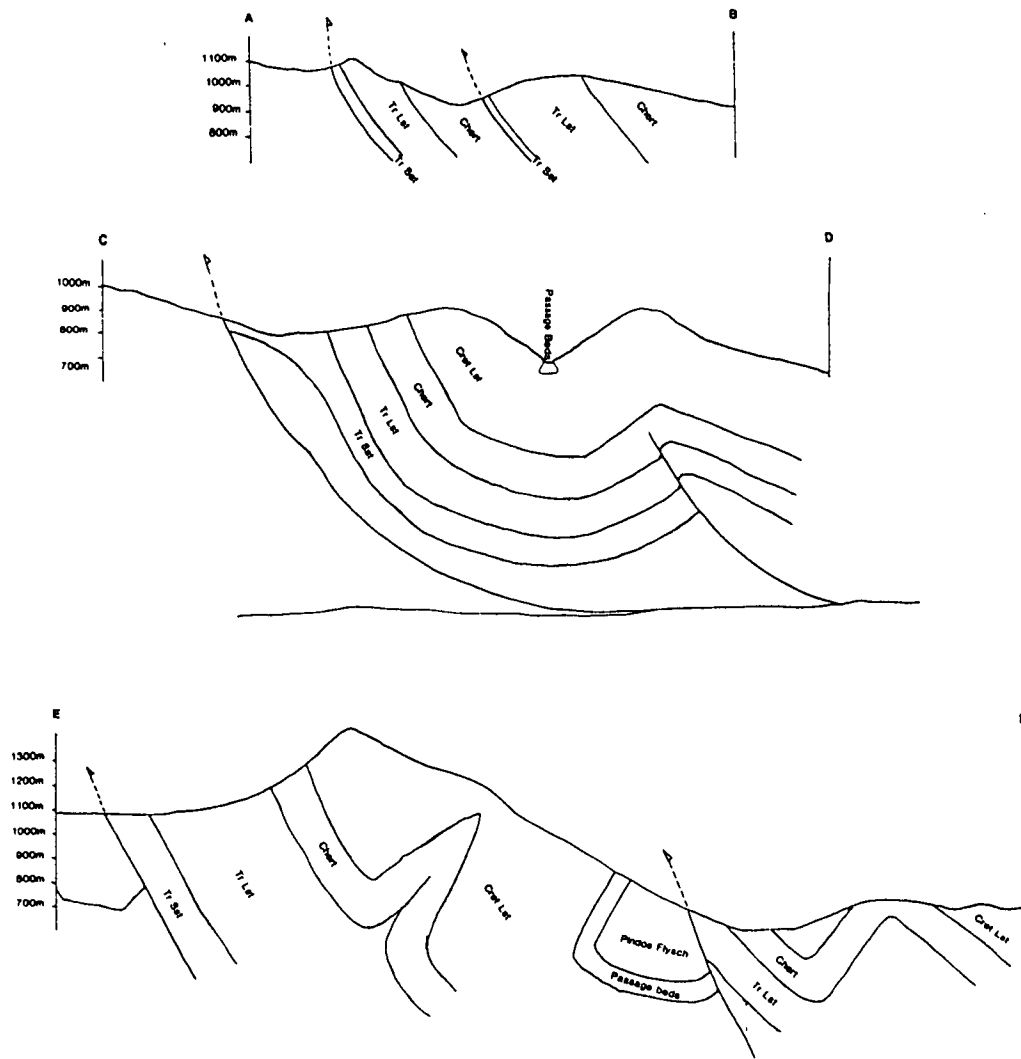
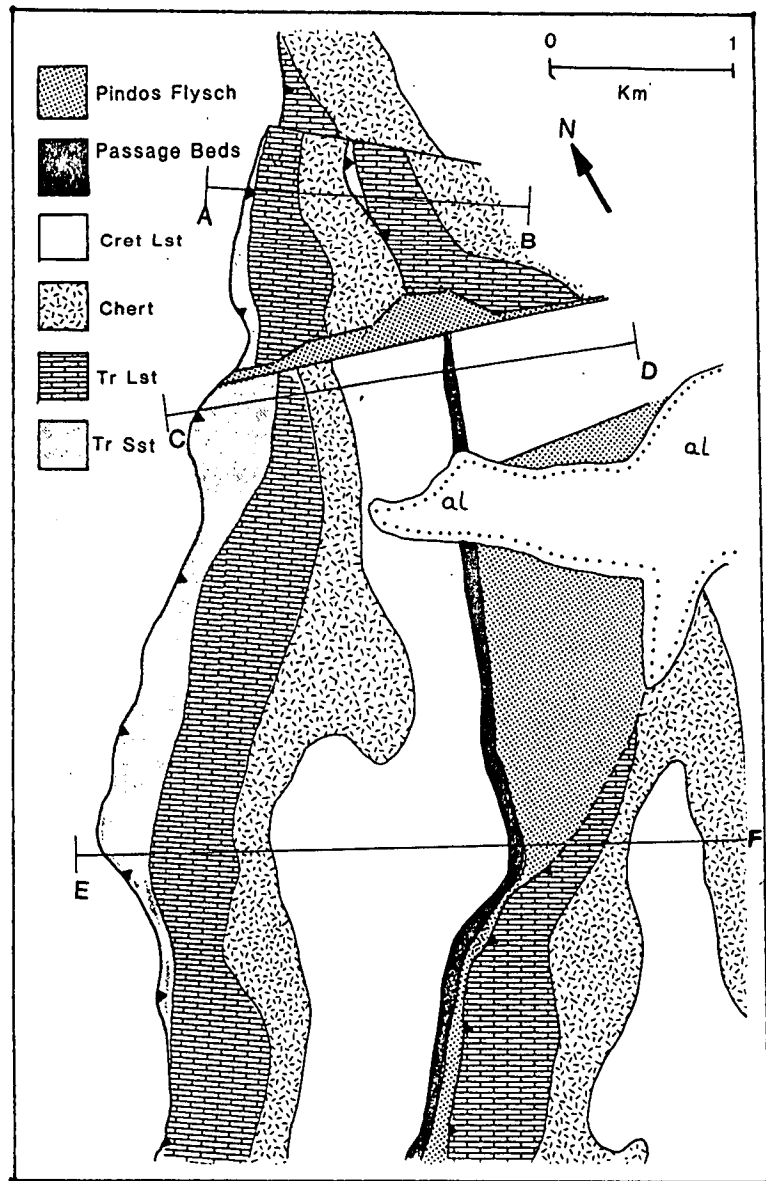


**Fig. 6.13** Geological map and cross sections in the area around Drimos (see Figure 1.1 and Enclosure 1 for location). Cross section A-B indicates two closely spaced thrust faults breaking surface. Immediately north of cross section C-D a graben infilled with Pindos Flysch Formation sandstone is truncated against the frontal thrust. The transverse fault is a tear fault, associated with thrusting, that was reactivated in the present day neotectonic regime. The line of section C-D shows a broad synform with a core of the Kataraktis Passage Member. Cross section E-F illustrates the southward plunge and more open aspect of the synform, also the back limb cut by a later thrust.

represent the latest fault movements, which may or may not, be of neotectonic origin. Two particular transverse faults were studied in some detail in an attempt to determine whether they formed coevally with thrusting.

At Drimos, mapping indicates that two sub-parallel transverse structures are present and these create a narrow graben (Figure 6.13 and Plate 6.2). The normal faults die out gradually eastwards as stratigraphic separation diminishes, while they are abruptly truncated by a major thrust fault in the west. Immediately north of the transverse structure (cross section A-B) the stratigraphic sequence is duplicated by a second thrust. This thrust is not present south of the area of transverse faulting, where a tight synform is instead developed in the higher stratigraphy of the Lamba Formation (cross section C-D). Yet further south, the folding is less tight still (cross section E-F). It is also shown here that the folding is cut by a thrust fault that formed after the folding (Plate 6.2). It can thus be inferred that differential along strike tightening took place, expressed by thrust faulting north of the transverse structure (which acted as a tear fault) and folding to the south. The area south of the transverse fault cannot simply be the downthrown side of a normal fault as the fault plane is truncated at the forelandward thrust and slickensides show that the latest movement at least, downthrew the northern side.

At Kerasia (Figure 1.1 and Enclosure 1) a transverse fault separates a second order thrust sheet to the north from folded strata to the south. The degree of folding present in the Aroania Chert Member is more intense north of the fault and the underlying Drimos Formation is exposed as a small hangingwall antiform (not inferred to be a fault propagation fold). On the southside of the transverse fault the Aroania Chert Member is very much less affected by folding and the Drimos Formation is not exposed. The deduction is that more intense strain was developed in the thrust sheet north of the transverse fault.

As noted above, the transverse fault at Drimos is truncated in the foreland by a thrust fault, and the thrust fault trace is itself unbroken at the juncture with the transverse fault. This indicates that the transverse faulting must have developed prior to being cut by the thrust. Transcurrent faulting (i.e. faults with strike-slip displacement) are integral components of thrust systems and have been considered to form by either hangingwall movement over an irregular footwall topography (e.g. with tear faults developing in a thrust sheet hangingwall moving over lateral ramps in the footwall), or by differential movement within the thrust sheet. In either case, an offset in the

position of a frontal thrust either side of the transverse structure would be expected. To cut a transcurrent fault formed by thrusting, and to create a continuous thrust trace in the foreland, would require breaching by an out-of-sequence thrust, or alternatively, a simpler explanation proposed for the study area would involve the development of tear faulting by strain partitioning (expressed as differential along strike folding) above a flat-lying basal detachment. Thrusts splaying off the basal detachment, after folding, and using axial planar weaknesses, would cut up-section and transport the hangingwall (with the transverse fault termination) over the footwall away from the transcurrent structure in the footwall. In this model, tear faulting is therefore unrelated to any underlying footwall topography, but rather, purely to differential strain above the basal detachment.

The transverse faults form a radial arrangement throughout the NW Peloponnese. These structures are perpendicular to the arcuate arrangement of thrusting (Figure 1.2). The neotectonic normal faults along the Gulf of Corinth and the Olympia graben (Section 6.6.2) are mostly orientated parallel to one another in a WNW-ESE direction, suggesting that neotectonic faults in between should also be parallel. Thus, it is likely that originally thrust related transverse faults were reactivated in the neotectonic regime, between the above mentioned bounding structures, as normal faults.

#### 6.4.2 Rock Cleavage

Two types of cleavage are developed in the limestones of the Pindos Group. The first is a relatively rarely observed, regularly spaced, fracture cleavage seen generally in bedding thicker than c.a. 30cm. The cleavage forms a bedding-intersection lineation, parallel to meso-scale fold hinges (Plate 6.7) and the cleavage planes are always sub-axial planar, forming both divergent and convergent fans with slight cleavage diffraction across layers of differing competence. Most cleaved bedding surfaces exhibit extensional offsets, while microthrusts also form a fracture cleavage with discrete, compressional fractures sometimes leading to the development of "cleavage duplexes" (Plate 6.7). The axial planar fracture fabric was never seen to develop over a significantly large area although the cleavage is considered to be directly related to the folding of particularly competent rock units.

The second cleavage type is a stylolitic pressure solution cleavage that is more common than the extensional fractures described above and was frequently observed

in the calciturbidites of the Erymanthos Limestone Member in the frontal imbricate region. The pressure solution cleavage is not to be confused with bedding parallel pressure solution that is commonly present throughout the study region and which is considered to develop from compaction due to overburden pressures. The stylolitic cleavage forms an anastomosing array of "sharp-peak" stylolites (Guzzeta 1984) that are approximately axial planar to macroscopic folds (Plate 6.7). The stylolites form orthogonally to the direction of maximum compressive stress and were one of the criteria used to define the local shortening direction in the field.

Multi-layer folding by tangential longitudinal strain, as opposed to flexural slip mechanisms, commonly involves the development of extension in the outer arc of a fold and compression in the inner arc (Figure 6.9), however, this mechanism is not believed to be responsible for the stylolitic pressure solution cleavage seen in the frontal imbricate region. This is because the pressure solution is observed both on the limbs as well as hinges of macroscopic folds, and also in the outer arc (inferred) of folds. The cleavage development is considered to have followed folding as a strain accommodation mechanism where the compression of competent units results in volumetric changes through dissolution. The fact that the cleavage is restricted to the frontal imbricate region suggests that it may be related to additional strain induced by the <sup>t</sup>butressing of the Pindos thrust stack against the Apulian margin (Section 6.5.3). The extent of the pressure solution has important repercussions for the construction of balanced sections (Section 6.3.7) and an attempt was made to estimate shortening by such volume loss.

#### 6.4.3 Joints and Veining

At the <sup>n</sup>beginning of the study, an attempt was made to systematically measure joint and vein populations. However, the cross-cutting relationships and orientations were too complicated at the level of study to yield any meaningful interpretation. It is probable that the compressional stress field, while regionally consistent, was locally variable with several phases of structural overprinting. Rotation of thrust sheets implied by the promontory impingement model (Section 6.5.3) would have locally complicated stress and strain orientations. Furthermore, vein and joint structures were also created during the later Plio-Quaternary extensional phase.

#### 6.4.4 Palaeomagnetic Study

A brief palaeomagnetic study was made along the strike of a single thrust sheet to determine whether there were significant local rotations about a vertical pole. Such movements could invalidate, or confirm, palaeocurrent and structural vergence data. Additionally, as the thrust sheet transport directions are seen to systematically swing from a NW orientation in the south of the study area, to the WSW in the north, it was hoped that this work would test the promontory impingement model proposed in Section 6.5.3, whereby original sediment patterns were rotated by thrust sheet impingement onto an Apulian margin promontory, creating the concave (westward) aspect to the thrust traces of the NW Peloponnese (Figure 6.15).

##### 6.4.4.1 Methodology

Two hand specimens were carefully orientated and taken from each of four localities. The localities are from similar stratigraphic intervals within the Paos Limestone Member, close to the transition from the underlying Aroania Chert Member and along the strike of the same extensive thrust sheet. The pink pelagic limestone is hematite-rich and, based on earlier palaeomagnetic investigations from other localities in Greece (Morris 1990), this lithology was considered likely to retain a measurable remnant magnetism. Each hand specimen was cored and several plugs were obtained with the aid of Dr A. Morris at Newcastle University.

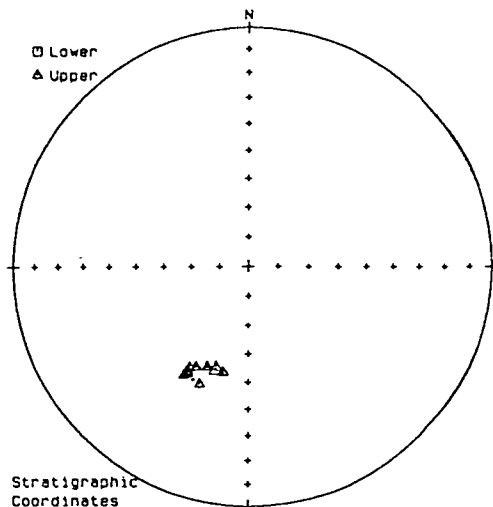
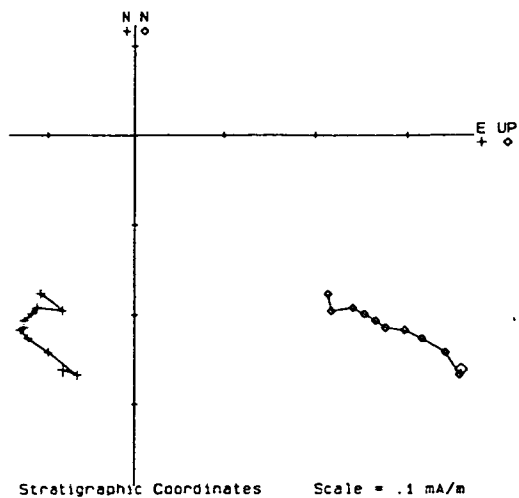
At Edinburgh University, Dr R. Enkin supervised measuring successive demagnetizations by means of the alternating field method. Each of the plug axes were automatically reorientated in a set sequence within the alternating field and any secondary remnant magnetization (sNRM) was removed until the pNRM was established (the magnetic grains holding the least stable remanence are removed, leaving the more stable primary remanence). The magnitude of the induced magnetic fields was 0 to 600 oersted (Oe), with 100 Oe steps.

##### 6.4.4.2 Results

Only three of the core plugs were actually measured. The results were not coherent and it was decided that until a proper palaeomagnetic study could be carried out there was little point in continuing the analysis. The vector component (Zijderveld) diagrams and equal-area projections for each core plug, are illustrated in Figure 6.14. The results indicate that each of the samples yielded a completely different series of natural remnant magnetization vectors which, viewed individually, seem reasonable but, taken together were deemed uninterpretable. The reason for such a

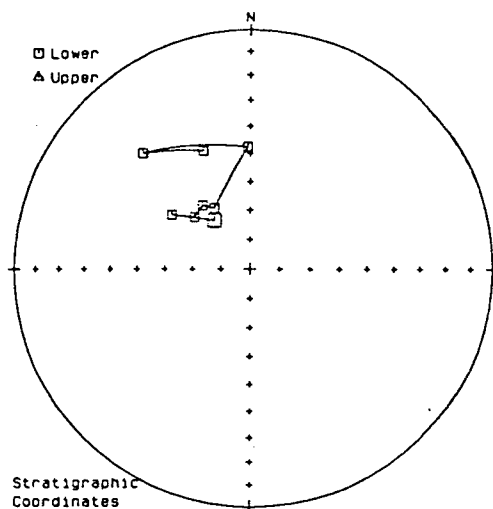
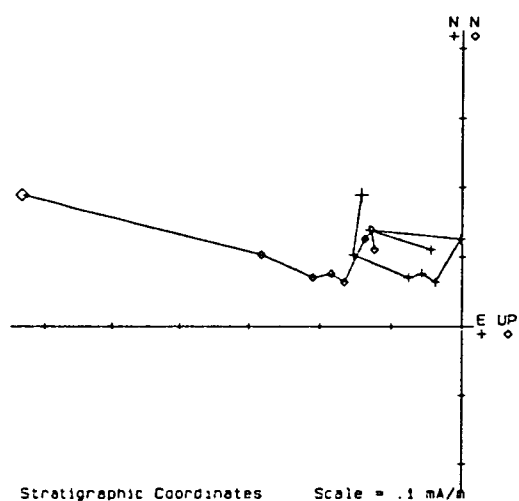


A/2



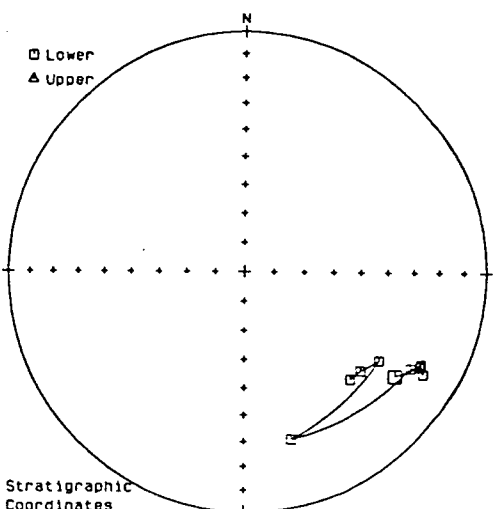
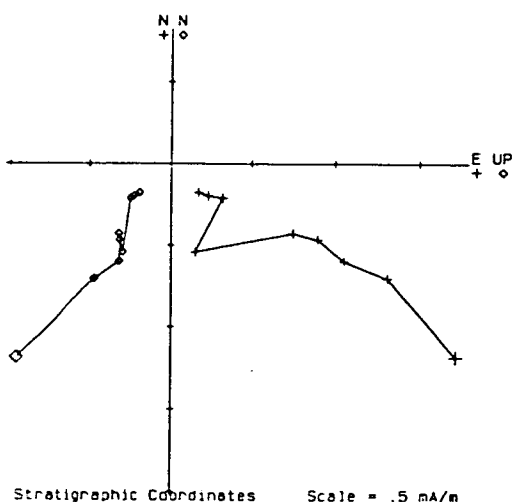
05-26-1992

B/1



05-26-1992

B/2



05-26-1992

**Fig. 6.14** Results of palaeomagnetic examination of three samples (A/2, B/1 and B/2) from the Paos Limestone Member. Both the Zijderveld diagrams and the stereographic plots indicate that there is no data correspondence between any of the samples. Explanation in text.

result is unknown; however, it could be one, or a combination, of several possibilities:-

(1) The samples may have been subjected to a strong magnetic field during transport or while in storage (unlikely). (2) The samples were orientated in the field but may have become disorientated while cores were being drilled (unlikely). (3) The alternating field demagnetizer was known to be malfunctioning during the period preceding measurements (probable). (4) Hematite contained in the red shales of the Kastelli Mudstone Member is considered to be, at least in part, detrital. Alternatively, it could have formed from a goethite precursor during burial diagenesis (Section 4.3.1.4). By comparison with the shales, if the Paos Limestone Member hematite is mainly detrital and the samples are from the same stratigraphic interval, a consistent detrital remanent magnetism (DRM) should be observed. However, if hematite formation is mainly diagenetic, the remnant magnetization recorded would be chemical (CRM) and this does not necessarily correspond to the primary remanence. The authigenic precipitation of hematite (and thus the CRM) could vary in time for different locations as it is the growth of individual grains in the prevailing magnetic field that determines the magnetic moment, and this will depend on local conditions (possible). (5) Bioturbation can destroy the validity of DRM (arguable) as can the alteration or removal of ferromagnetic particles by later pore fluid movements (unlikely).

It is suggested that the palaeomagnetic aspects of the Pindos Zone merit an in-depth study in their own right, but time constraints meant that the topic could not be brought to fruition during this study.

## **6.5 COMPRESSIONAL DEFORMATION MODEL**

Based on all the structural evidence outlined above, a sequence of deformation can be inferred which accounts for the structural development of the Pindos Zone and incorporates the proposed tectonic setting of the Pindos Basin.

### **6.5.1 Regional Setting**

Deformation in the Hellenides propagated from the east towards the west during the Early Tertiary and is considered to be related to the anti-clockwise movement of Africa, with respect to Eurasia, around a north European pole (Smith 1971, Dewey

*et al.* 1973, Robertson & Dixon 1984, Dercourt *et al.* 1986). The subsequent rearrangement of plate configurations led to the initiation of subduction in the Tethyan realm during the Cretaceous. The Tethyan Vardar Ocean is considered to have been consumed by the closure and suturing of the Serbo-Macedonian and Pelagonian micro-continentals in the Late Cretaceous (Dercourt *et al.* 1986) and/or during the Palaeocene-Eocene (Robertson & Dixon 1984, Robertson 1990b, Clift 1990). The deformation front advanced westward of the Pelagonian Zone, into the Pindos Basin, during the Early Tertiary. The Pindos Basin at this time is considered to have been floored by remnant oceanic crust (Jones 1990, Robertson *et al.* 1991), present since Upper Jurassic subduction emplaced ophiolite lithologies onto the Pelagonian margin.

During the Eocene, the Pelagonian continental crust overthrust the denser and thinner Pindos oceanic crust which began to subduct with an eastward polarity. The initial site of subduction must have been at, or close to, the Pelagonian continental/oceanic margin, as ophiolites were not emplaced onto Apulia, although fragmentary outcrops of serpentinite and harzburgite are present west of Pamassos (Beck 1980) and these are cited as evidence for oceanic crust in the Pindos Basin during the Cretaceous (Robertson & Degnan 1992a Section 9.3.1). Due to the rheological contrast between the *oceanic basement* and the "thin veneer" of overlying pelagic sediments (the Pindos Group), underthrusting led to the initiation of a detachment at the sediment/igneous interface and the sedimentary sequences were progressively off-scraped into a thickening wedge.

### 6.5.2 Earliest Deformation

Initial compression was expressed in the Pindos Group multilayer by the generation of sinusoidal meso-scale folds which developed at lithological inhomogeneities. Continued shortening was accommodated by the serial development of sinusoidal folds tightening into chevron morphologies, while incompetent units experienced bedding parallel shear. Contemporaneously, lithological sections, isolated between rocks with strong competence contrasts, acted as mechanical single layers that buckled into irregular folds. Fold amplification and tightening continued until locally, sticking necessitated strain accommodation by rock failure and flattening in the multilayers. Synchronously, larger scale detachment folding developed in the sedimentary pile as the igneous-sediment interface decoupled. As the deformation front migrated westwards, thrust faults propagated upwards from the basal

detachment along axial planar lines of weakness formed by the folding. Some additional folding may be directly attributable to fault propagation folding. Folding and faulting migrated westwards with the progressive development of hinterland to foreland deformation. In this manner, initial folding in the Pindos foreland (adjacent to the Apulian margin) would have been synchronous with active thrust faulting in the hinterland.

### 6.5.3 Later Pre-Emplacement Deformation

The observation that an imbricate fan developed in the area studied, but not in the Arcadian region to the east (Figure 1.2), is ascribed to the "solid beam" of thick Cretaceous limestones in the east concentrating detachment surfaces along the ductile igneous/sediment interface. This compares with the relatively heterogeneous older stratigraphic succession present further west (i.e. the present study area) containing incompetent inter-layering which provided the rheological contrasts necessary for the development of a linked thrust stack system (see also Section 8.3.3 & Figure 8.5). A corollary of this model is that the Pindos sheets formed an accretionary prism with the successive off-scraping of the sedimentary cover from an igneous basement as the remnant Pindos Basin ocean crust was subducted.

Massive limestones are highly folded and contorted in the frontal imbricate region and stylolitic pressure solution and duplexing is well developed. Furthermore, thrust planes are at a high angle, becoming less steep eastward of Klitoria. The general pattern of thrust fault traces in the NW Peloponnese forms an arcuate outcrop pattern that is concave towards the west (Figure 1.2). During the course of this study it was discovered that there are many more map-scale thrusts present than previously appreciated and that the emplacement directions, derived from fold geometry, vary systematically in the region (consistently orthogonal to the thrust traces, Figure 6.15). It is proposed that the curvature of thrust traces, the radial arrangement of transverse faulting and emplacement vectors and the apparent concentration of strain in the frontal region can be incorporated into a model whereby the orogenic front was buttressed by a promontory of the Apulian margin (inferred to represent a steep by-pass margin, Section 3.3.3.2) which, although collapsed may still have had significant topographic relief.

The possible presence of continental margin promontories or embayments has been deduced for several areas in mountain belts, e.g. the Appalachians (Lash 1988),

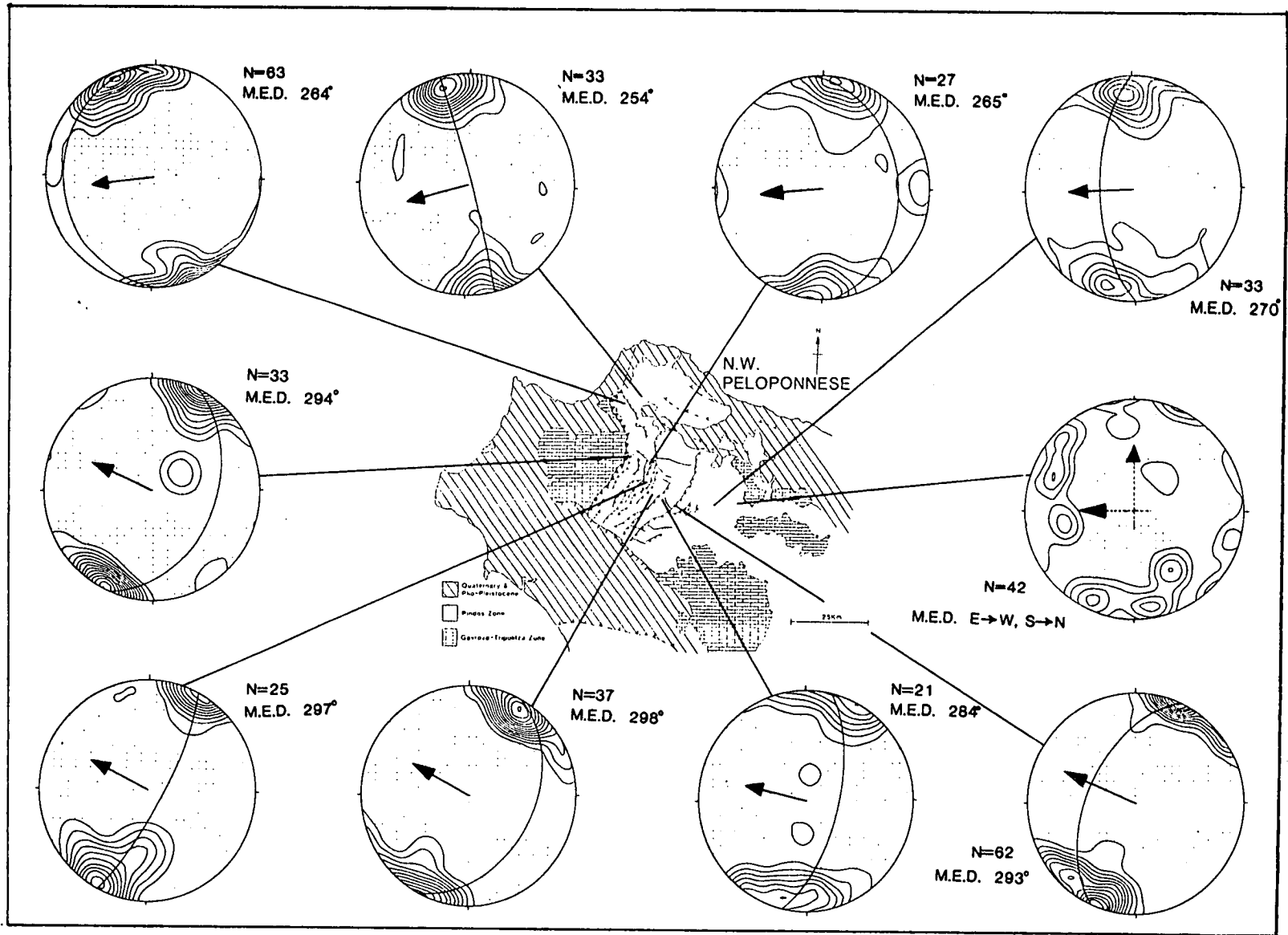


Fig. 6.15 Stereographic projections indicating the mean emplacement directions (M.E.D.) derived from contoured plots of mesoscopic fold hinge data. The approximate locations of the data sites are indicated on the map of the NW Peloponnese. Note the convex (to the east) aspect of the thrust traces and how the mean emplacement directions swing from WSW in the north, to NW in the south.

Oman (Cooper 1986, Searle and Cooper 1986) and the north Indian (Zanskar) margin (Robertson & Degan, 1992b in press). Buttressing has also long been recognised as a potential mechanism for altering the otherwise simple structural style of foreland propagating thrust belts (Lash 1988, Searle & Cooper 1986, Kulik & Schmidt 1988, Couples & Lewis 1988). The hypothetical involvement of a foreland buttress has several consequences for rocks being shortened by an effective hinterland-push. Because a progressive build-up of strain will develop at an immobile "sticking point" adjacent to a buttress, the accumulation of stress can potentially be dissipated by several methods:-

(1) The development of an out-of-sequence (break back) thrust system (Butler 1987, Hunter 1988, Morley 1988). (2) The back rotation and tighter imbrication of pre-existing thrusts. (3) The formation of layer parallel shortening fabrics, especially pressure solution (Craddock *et al.* 1988). (4) The partial dissipation of strain into the footwall. (5) The deflection of hangingwall fold hinges to sub-parallelism with the strike of the foreland buttress (Corbett 1983, Searle & Cooper 1986) and the possible rotation *en-masse* of thrust sheets where the topographic slope of a foreland buttress does not parallel, or lie perpendicular, to the transport direction of the thrust sheets.

Apart from the break-back of the locus of thrust faulting, all of the above features appear to be relevant to the Pindos Zone of the NW Peloponnese and the conclusion reached in this study is that the Pindos thrust sheets locally impinged onto an Apulian promontory (Figure 6.16). Evidence to support this contention chiefly includes the radial arrangement of tear faults, which parallel the local emplacement directions, and the arcuate outcrop pattern of thrust faulting. (N.B. Palaeocurrent studies in the north of the Peloponnese are not conclusive enough to provide additional evidence for a promontory).

It is further tentatively suggested that the northern limit of the proposed Apulian promontory corresponds roughly to the present day Gulf of Corinth lineament and that this may, therefore, correspond to a fundamental basement weakness that may represent a transform offset. There are a number of other lines of evidence to support this contention;- (1) The emplacement vectors deduced for the Pindos Zone north of the Gulf of Corinth suggest transport to the SW (Green 1982, Leigh 1991). (2) Implicit in work by Fleury (1980) is the presence of a transform fault along the present day Gulf of Corinth. (3) Underhill (1985) suggests that there may be a major

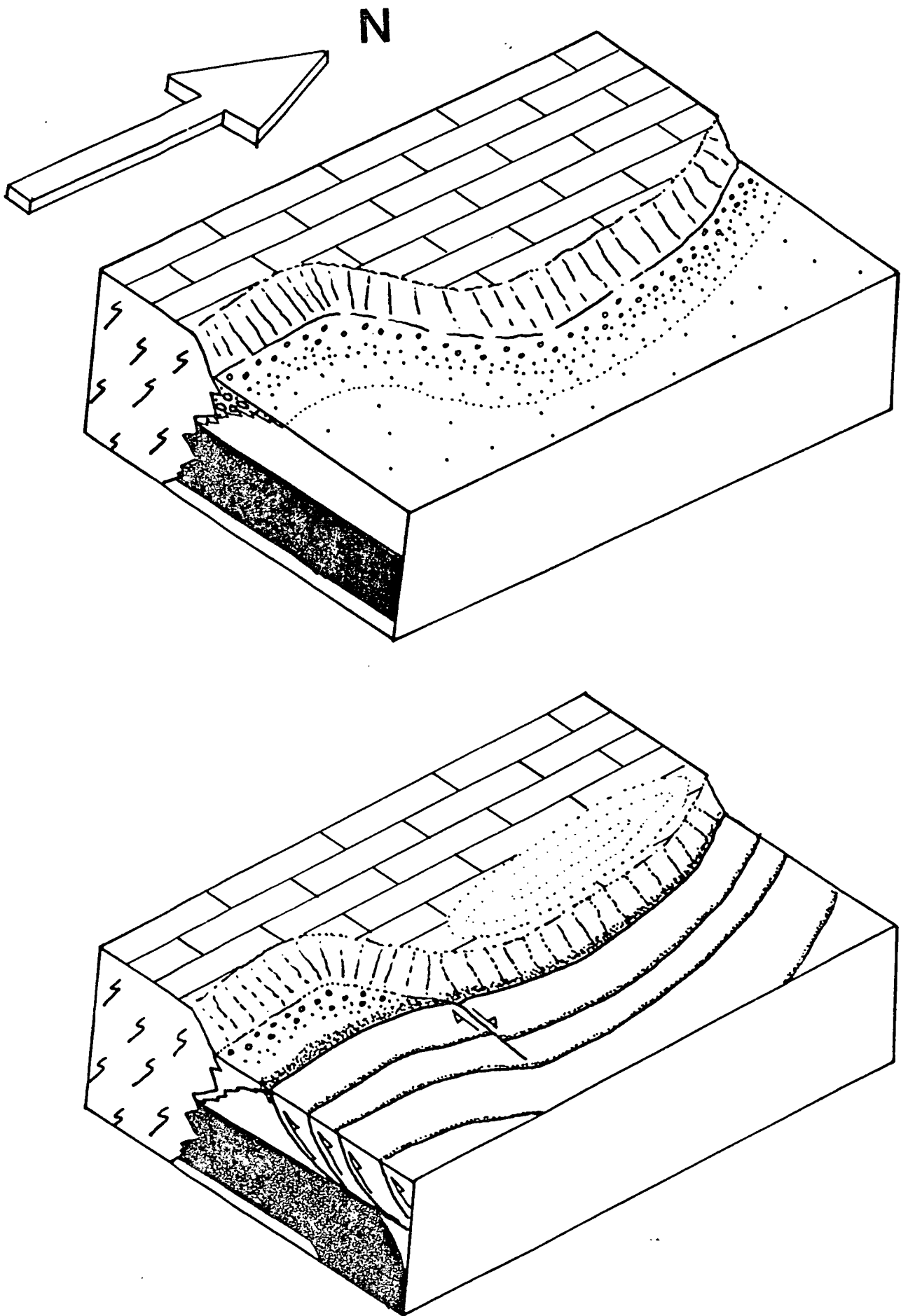


**Fig. 6.16** Schematic representation of a continental margin promontory. In the lower diagram, as the margin approaches the site of subduction, the collapsed platform still represents a pronounced footwall topography to the thrust stack comprising off-scraped pelagic sediments. When the westward moving thrust sheets impinge on the promontory, differential strain results in transverse fracturing and the bulk rotation of the thrust sheets

transverse fault accommodating differential Hellenide thrust movement between the islands of Zakynthos and Cephalonia in the Ionian Sea. Such an east-west fault could be extrapolated into the present day Gulfs of Patras and Corinth. (4) Degnan (unpublished data 1989) and Leigh (1991) propose that the provenance of flysch debouching into the foreland basin covering the Gavrovo-Tripolitza and Ionian Zones suggests a major structural feature in the area of the Gulf of Corinth. Palaeocurrents were seen to be north to south, south of the Gulf of Corinth (Section 7.4.2 and Izart 1976), while north of the Gulf of Corinth the palaeoflow is south to north (Leigh 1991). All the above evidence suggests that a significant basement lineament, active during the Hellenide orogeny, is centred on the Gulf of Corinth area and that the present extensional regime may be utilising this crustal weakness.

#### 6.5.4 Emplacement

As described more thoroughly in Section 7.5, the continuation of compressive stress, due to subduction of the remaining oceanic crust, eventually led to the underthrusting of the Gavrovo-Tripolitza sequences beneath the Pindos Group and a frontal and lateral ramp system was initiated at the continental rise and slope. Emplacement of the Pindos thrust stack was soon followed in the Late Oligocene (?) and Miocene by the final collision of Apulia with Pelagonia...

### 6.6 POST EMBLACEMENT TECTONICS

#### 6.6.1 Compressional Tectonics

At several locations throughout the study region, structures were noted which indicate south to north directed compression. This takes the form of both folding and reverse faults which are orientated transverse to the main thrust direction. Minor folding is largely confined to thin calciturbidites in the Erymanthos Limestone Member around Chelmos and Krinofta in the east and, less commonly, near to Platanitza in the west (Figure 1.1). Outcrop patterns south of Filia show NW-SE striking macroscopic fold axes. Large east-west and NW-SE reverse faults, with slickensides showing south to north movement, are present south of Chelmos and immediately south of Kato Klitoria. Furthermore, major thrust planes, striking NE-SW, to the east and west of Agridi in the central imbricate region have a strong strike-slip overprint. De Wever (1975) mapped an area south and east of the present study region where macroscopic fold axis strike NW-SE and NE-SW. All of these



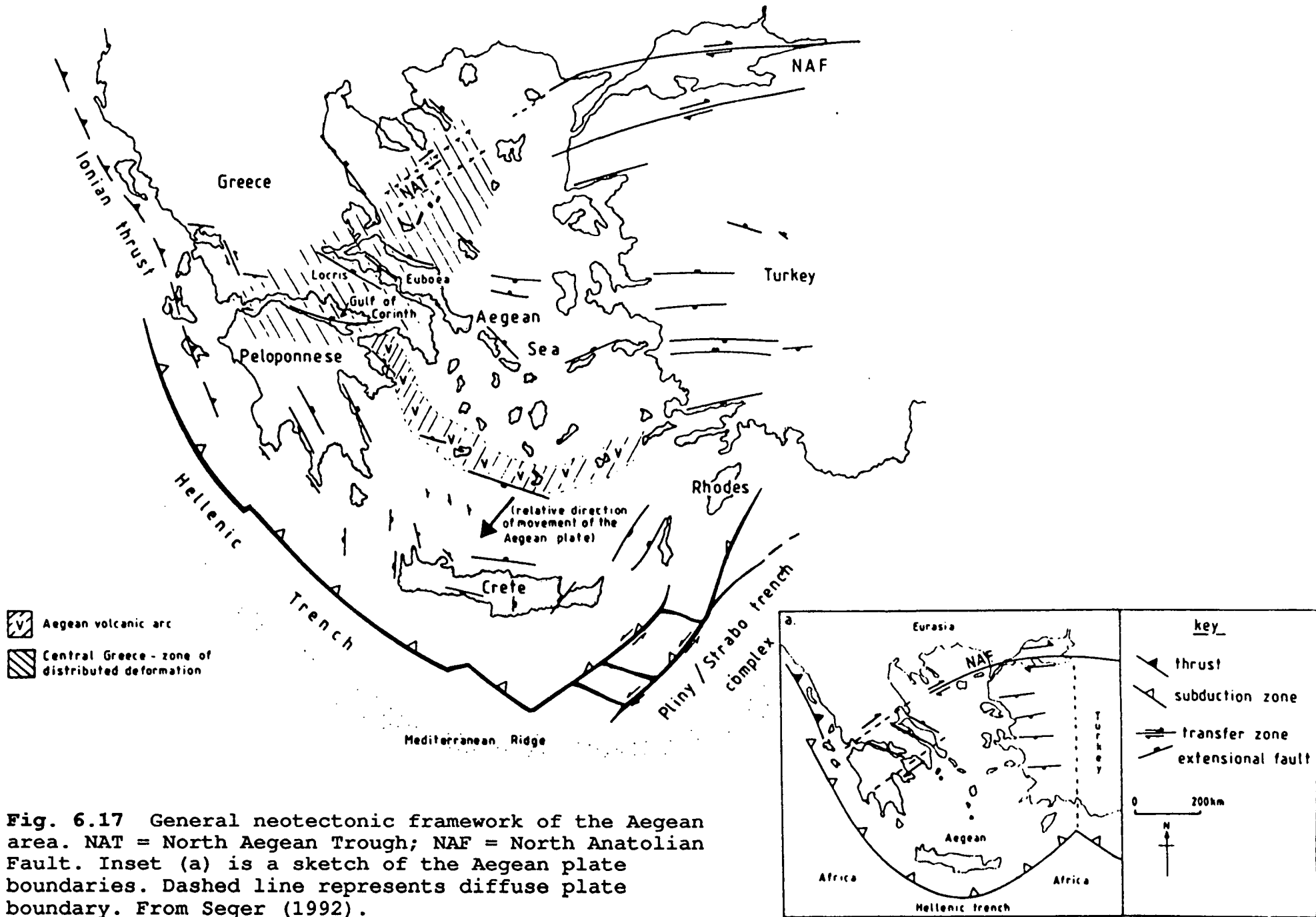


**Fig. 6.17** General neotectonic framework of the Aegean area. NAT = North Aegean Trough; NAF = North Anatolian Fault. Inset (a) is a sketch of the Aegean plate boundaries. Dashed line represents diffuse plate boundary. From Seger (1992).

features are difficult to reconcile with the stress field established for the contraction and emplacement of the Pindos Zone during the Oligocene. It is possible that some structures may be local accommodation features due to thrust sheet sticking or lateral culmination collapse. However, the concentration of north to south directed deformation around Chelmos, equally in both the Gavrovo-Tripolitza and Pindos Zones, leads to the conclusion that the post emplacement compression was concentrated around the Chelmos periclinal structure.

Later neotectonic faulting cuts across the folded Pindos and Gavrovo-Tripolitza rocks equally; thus, the timing of south to north directed deformation can only be constrained between the start of neotectonic activity (Pliocene?) and the Late Oligocene emplacement of the Pindos thrust sheets. Mercier (1983) has identified two compressional phases in the Aegean based on micro-structural studies. These events he dated as Miocene-Pliocene and Pleistocene. Jackson *et al.* (1982) dispute the occurrence of such compression in the neotectonic history, but the structures observed in this study may correspond to the earlier (or both?) of Mercier's phases.

The compression could be related to the far field effects of the initiation of subduction along the Hellenic trench. There is disagreement over the timing of this event. Mercier *et al.* (1976) suggested an age of 5-10 m.y. based on the oldest age of volcanics in the the Aegean arc. Le Pichon (1982) using the maximum depths of slab related seismicity suggested an age of 12-13 m.y., while Meulenkamp *et al.* (1988) and Wortel *et al.* (1988) propose that 800Km of subducted slab exists in the Aegean area and this implies a minimum of 26my of subduction at maximum rates of convergence between the African and Eurasian plates.

### 6.6.2 Extensional Neotectonics

All of the structures described in the preceeding sections are cut by later high angle extensional faulting. Stereographic plots of the field data are incorporated in Figures 6.3-6.7. The late-stage extensional faulting is attributed to the neotectonic regime presently active throughout the Aegean region. The Aegean Sea and the Gulfs of Corinth and Patras are currently one of the most seismically active regions in the world. Figures 6.17 and 6.18 indicate the main neotectonic features of the region. The present day stress field in the northern Peloponnese is north-south and tensional, as derived from numerous earthquake fault plane solutions (Jackson & McKenzie 1988). The extensional faulting observed throughout the north Peloponnese is

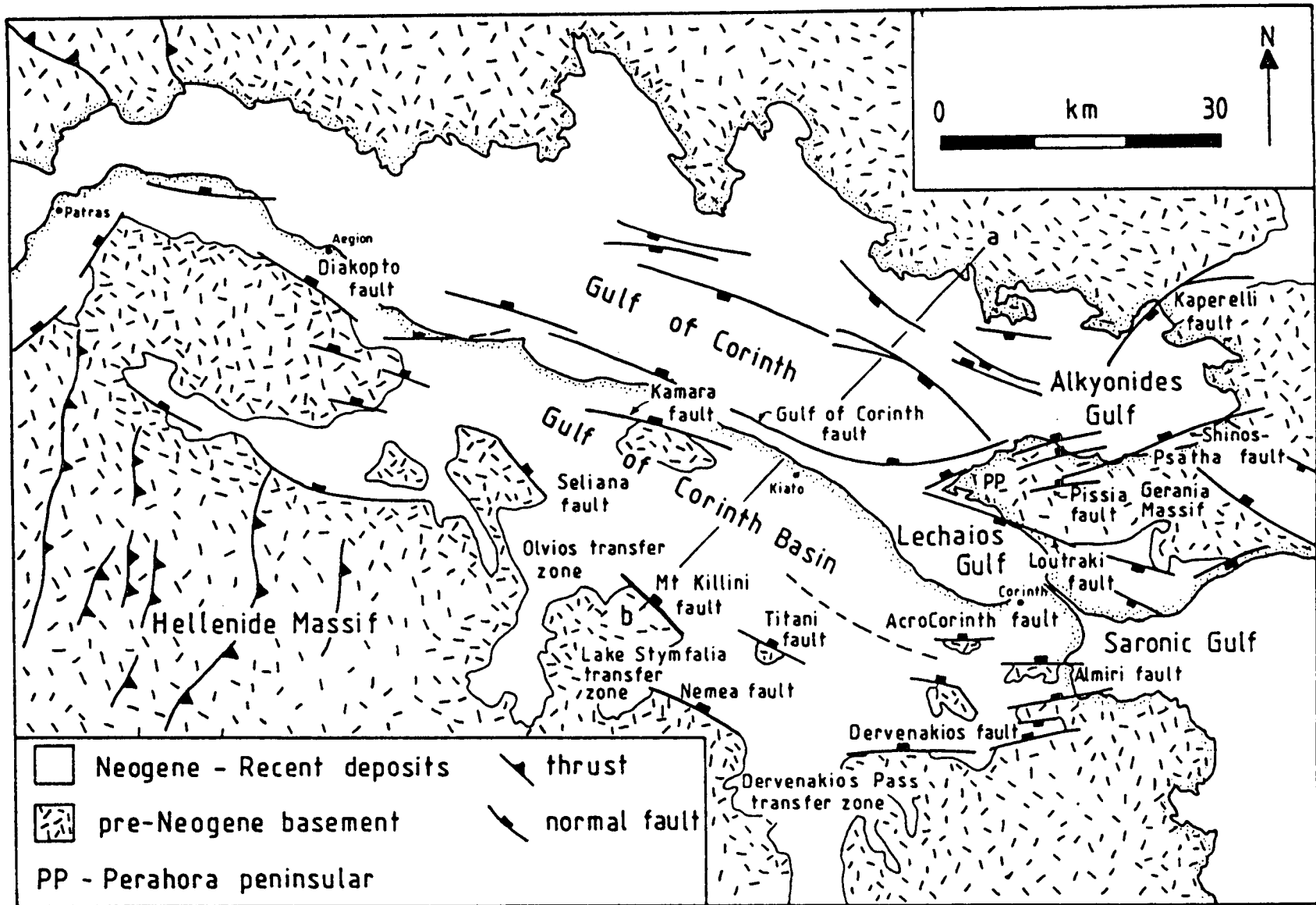


**Fig 6.18** Generalised map of the Gulf of Corinth showing the distribution of major normal faults. After Seger (1992).

generally ascribed to back-arc extension, induced by the lithospheric roll-back of the underthrust African plate (Le Pichon & Angelier 1979, Angelier *et al.* 1982, Meulenkamp *et al.* 1988).

Although the Gulf of Corinth block is downthrowing with respect to the north Peloponnese, the Peloponnesian land-mass is actually rising in absolute terms. The reasons for this are largely speculative. Mercier *et al.* (1976) suggest that uplift is a response to outer arc compression, although Jackson & McKenzie (1988) demonstrate that most of the compression related to subduction is accommodated along the Mediterranean ridge to the south of the trench. Compressional uplift (transpressional) was also invoked by Stiros (1988) based on "morphotectonic" data. The general absence of any major neotectonic compressional structures in the NW Peloponnese would appear to invalidate both proposals and the minor compressional structures described above (Section 6.6.1) have an extensional overprint. Le Pichon & Angelier (1979, 1981), Angelier *et al.* (1982), Le Pichon (1982) and Jackson & McKenzie (1988) propose that uplift is the result of sediment underplating and accretion under the Hellenic arc. Although much oceanic sediment has accreted at the Mediterranean ridge, a 4Km thickness is available for subduction. The subducted slab beneath the Aegean microplate has a dip of 30-40° near the trench. Beneath the Peloponnese however, the plate has been identified as a flat lying structure (Hatzfeld *et al.* 1989) and this, it is suggested, represents a zone of subducted sediment. Under the Gulf of Corinth the dip of subduction is imaged to return to 45°. As the subducted sediment is less dense than most of the overlying crust, the area is potentially buoyed-up as the accumulation of sediment adds to the crustal root of the Aegean plate and thus the Peloponnese rises with respect to the Gulf of Corinth.

## 6.7 CONCLUSIONS

Deformation in the Pindos Zone was probably initiated during the Eocene due to the eastward subduction of the Pindos basement beneath the Pelagonian micro-continent. It continued until the final emplacement of the basinal sediments onto the Apulian margin during the Upper Oligocene. A chronology of deformation has been established whereby mesoscopic folds preceeded large scale folding, in turn dissected by thrust faulting. Mesoscopic folds vary throughout the region and two main types are recognised; (1) sinusoidal to chevron folds in multilayers and (2) irregular buckle folds in single layers. The variation is believed to be a function of

the sedimentary sequence anisotropy, including layering, litho-type rheology (competence), individual layer thickness and the degree of deviatoric stress. Large scale folding is attributed to the rucking of strata above a detachment zone as the sedimentary/igneous interface decoupled. Additional strain release was accommodated by thrust faults cutting up section from the basal decollement. A palinspastic reconstruction based on line length restoration and volume loss through dissolution indicates that the basin (as represented by preserved sediments) was at least 220Km wide. A more realistic width of approximately 300Km is proposed. The thrust propagation rate is calculated to have been 10.5 mm/y and the shortening rate was at least 5.8 mm/y.

There is evidence for a post-emplacment south to north directed compressional event in the study area. Lastly, all preceding structures are cut by high angle normal faulting related to the extensional neotectonic regime currently affecting the Aegean region.

## PLATES

### PLATE 6.1: Alepohorio Area, Structural Features

Panorama of the north side of the Alepohorio valley section. Field of view approximately 4Km across. The low lying sediments of the foreland basin, to the left of the collage, were deposited on neritic carbonates of the Gavrovo-Tripolitza Zone and later overthrust by the Pindos thrust sheets. Note the well defined hanging wall cut-off and antiform in the centre of the photograph.

### PLATE 6.2: Drimos Area, Structural Features

(A) View towards the NE in the Drimos area, showing the outcrop of mapped structures. Note the transverse faults which are interpreted as reactivated tear faults. These form a graben structure which is truncated at a thrust to the west. A second thrust is developed on the north side of the transverse fault. (B) View of the same area but looking back towards the SSW. The mountain in the background is strongly folded, the extrapolated limbs being cut by a later thrust fault. The trace of the transverse normal faults are visible in the foreground as the margins of low-lying Pindos Flysch.

### PLATE 6.3: Thrusts

(A) Directly under the base of a major thrust sheet in the Pindos thrust stack (Agridi) a strongly sheared pelite with phacoidal blocks of limestone is observed. Hammer for scale. (B) The typical relief formed by the major thrusts is gulleys infilled by gravels and muds, obscuring the actual thrust contact (Lesteena). (C) A secondary Pindos thrust fault without the development of sheared pelite or phacoids. The thrust places Drimos Formation limestones over cherts of the Lesteena Formation. Field of view approximately 8m.

### PLATE 6.4: Fold Structures

(A) Complex folding in the footwall to a major thrust at the head of the Alepohorio valley. Note that the tight chevron folds on the upper limb of an elongate isoclinal fold. Field of view 300m. (B) Massive chevron folds which form a footwall synform to the same thrust, on the north side of the Alepohorio valley, indicating that minor folding preceded faulting. Note the overturned Aroania Chert Member beds in the far distance, over-thrusting the folded limestones with displacement diminishing towards the north. Field of view c.a. 800m .

### PLATE 6.5: Fold Structures

(A) Hanging wall antiform developed above a minor bedding parallel thrust detachment. Hammer for scale. (B) Similar detachment style fold developed above a small scale thrust where movement was subsequently transferred to a lower bedding parallel detachment. Hammer for scale. (C) Chevron folds in an evenly bedded limestone. Note the planar thrust cutting a chevron limb after folding. Outcrop c.a. 4m high. (D) Very highly folded exposure of monotonous limestone, making the degree of shortening in the beds difficult to ascertain.

**PLATE 6.6: Fold Structures**

(A) Tight to isoclinal recumbent folding in a thick-bedded limestone, as picked-out by bedding parallel replacement chert. Field of view c.a. 2m . (B) A sheaf fold in limestone in which the dominant transport direction is to the left (west), with the second closure developed perpendicular to the main shortening axis (south). Field of view c.a. 4m across. (C) West facing asymmetric fold, note the rounded hinge typical of thicker bedded limestone. Field of view c.a. 3m across. (D) Asymmetric chevron fold where the vergence direction can be established. Field of view c.a. 3m across.

**PLATE 6.7: Other Structures**

(A) Anastomosing stylolitic pressure solution cleavage. This is especially well developed in the Erymanthos Limestone Member of the frontal thrust sheets where the dominant cleavage direction is axial planar to major folds. Compass for scale. (B) A late stage minor reverse fault cutting bedding already rotated to vertical. Note the development of a conjugate back thrust in the upper left of the photograph and a conjugate fracture in the lower right. Field of view approximately 3m . (C) An axial planar fracture cleavage. Hammer for scale. (D) Two generations of axial planar fracture cleavage developed orthogonally to one another. Compass for scale.



- 1 Priolithos Fm
- 2 Drimos Fm
- 3 Drimos Fm volc sst
- 4 Lesteena Fm
- 5 Erymanthos Lst Mbr

- 6 Kataraktis Mbr
- 7 Pindos Flysch Fm
- 8 GT platform
- 9 GT flysch

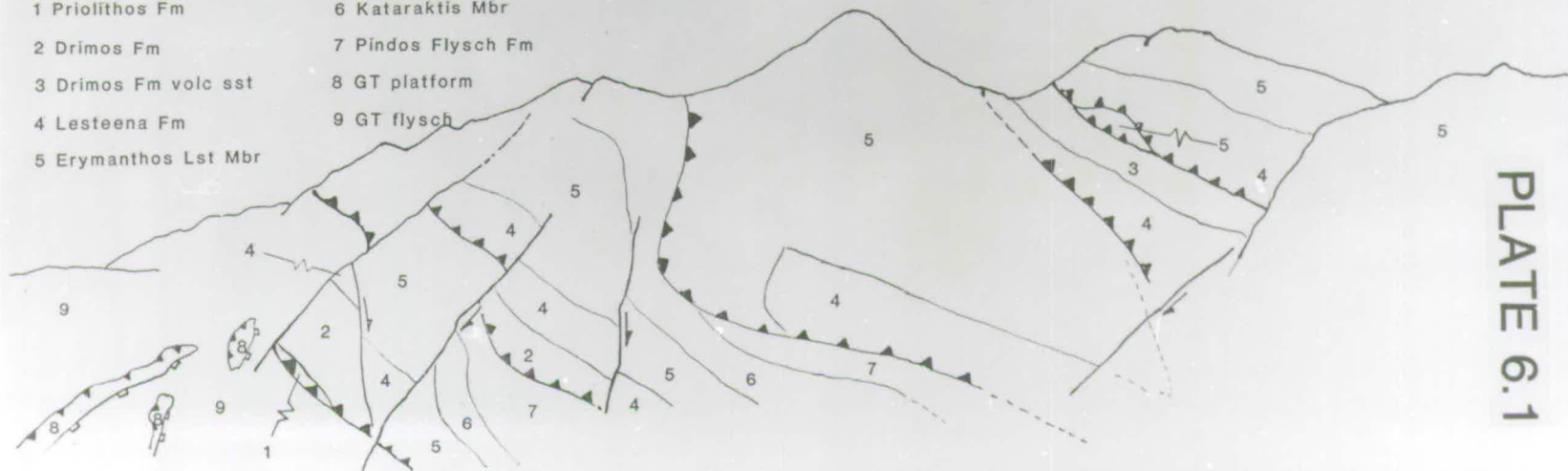
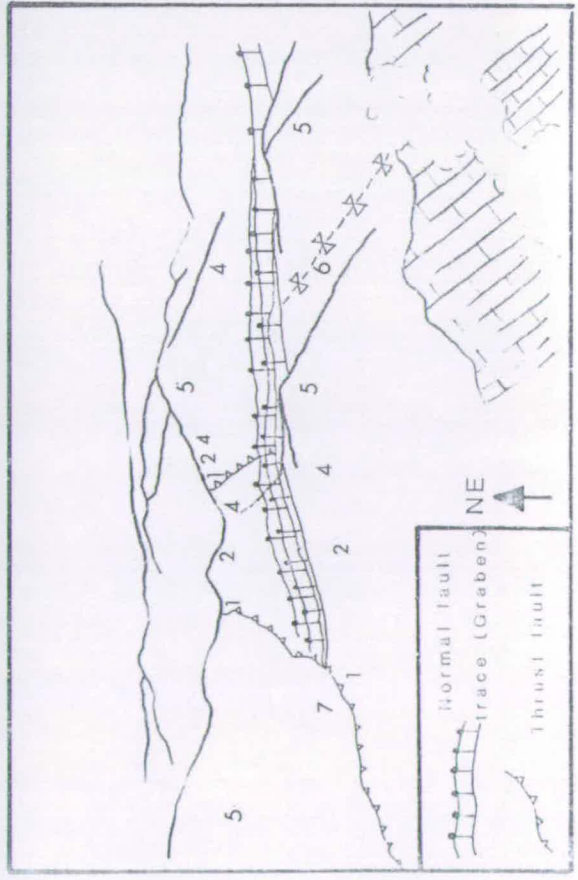
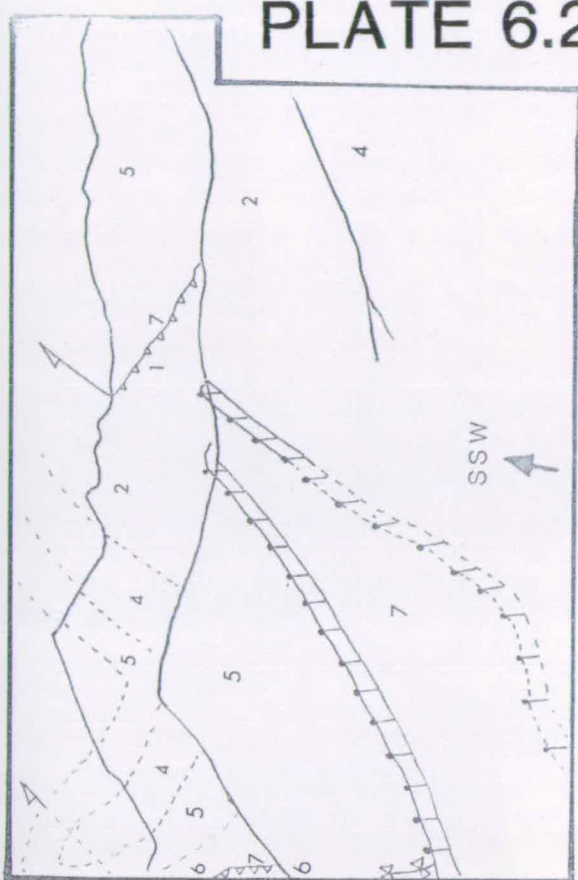


PLATE 6.1



# PLATE 6.2



# PLATE 6.3

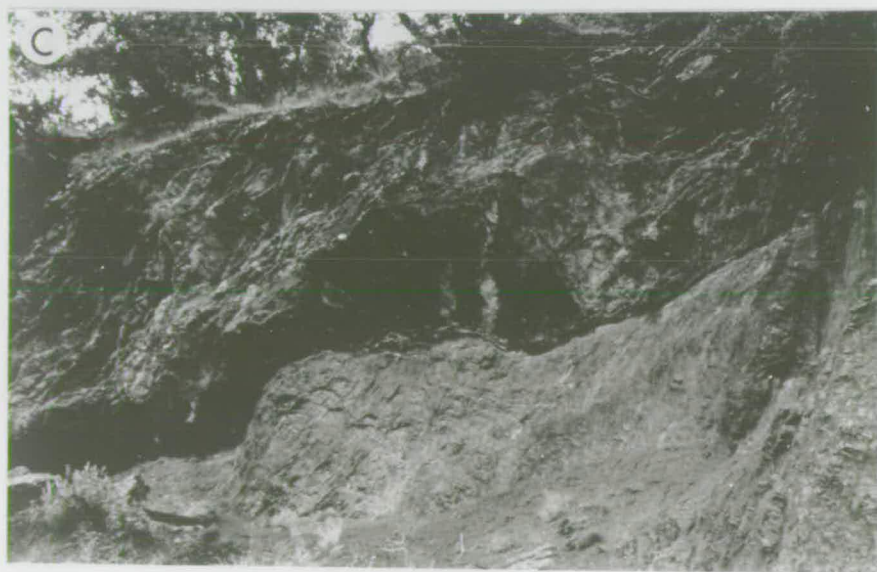


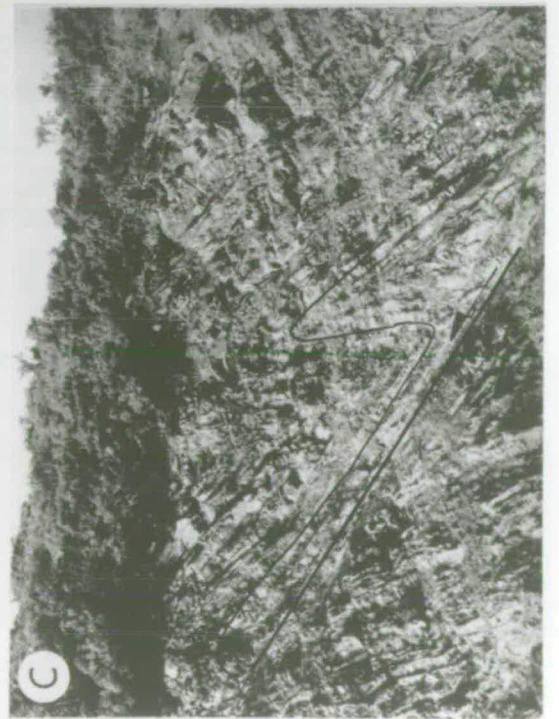


# PLATE 6.4





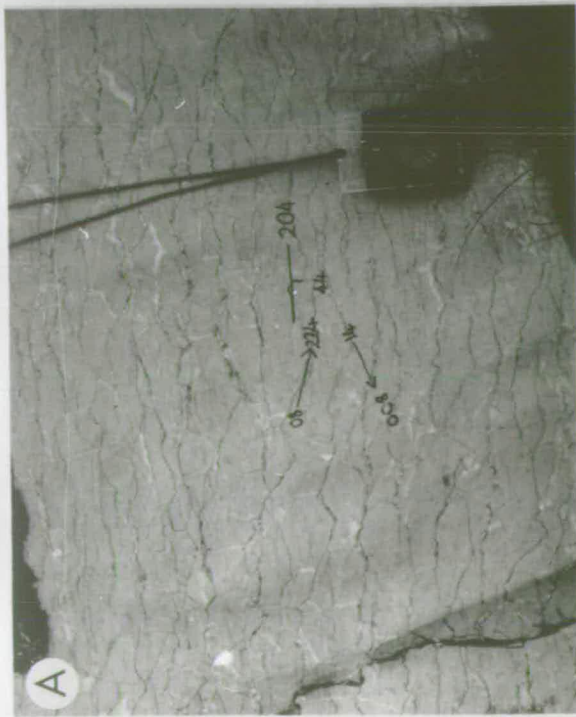
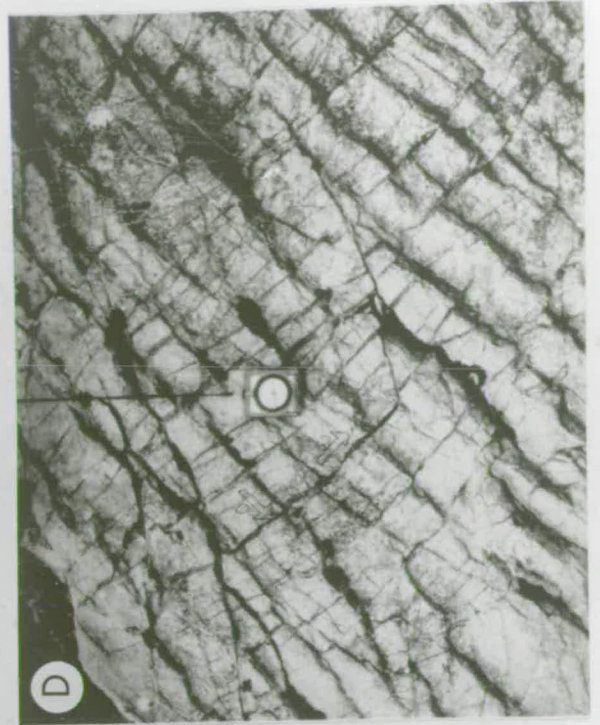
# PLATE 6.5



20m







**SECTION C: ADDITIONAL TECTONO-  
SEDIMENTARY COMPONENTS**

**CHAPTER 7: THE GAVROVO-TRIPOLITZA ZONE**

**CHAPTER 8: TECTONO-SEDIMENTARY MELANGE**



## CHAPTER 7 THE GAVROVO-TRIPOLITZA ZONE

### 7.1 INTRODUCTION

8 + The Gavrovo-Tripolitza Zone (GTZ) is a tectono-stratigraphic terrane dominated by shallow water carbonates. Two sub-zones are recognised, based on stratigraphic differences and palaeoenvironment. In the Tripolitza sub-zone, outcropping in the Peloponnese, Rhodes, Crete and Kithyra (Renz 1955), sub-tidal sediments accumulated during Cenomanian-Lower Turonian times, while the Gavrovo sub-zone of continental Greece and the Peloponnese records a period of emergence during this time. The first tentative connection between the Gavrovo sub-zone and the Apulian margin (the "Adriatico-Ionian Zone") was proposed by Phillipson (1890, 1898). Dercourt (1964) recommended combining the two sub-zones into the "Gavrovo-Tripolitza Zone", as he inferred that they probably formed a continuous palaeogeographic high separating the deeper water Ionian basin to the west from the Pindos basin to the east. In general, the nature of the facies suggest that the Gavrovo sub-zone formed the more inboard (westerly), and the Tripolitza sub-zone the more outboard (easterly), part of an extensive carbonate platform that formed the Apulian continental shelf. The relative position of the two sub-zones is retained today. The Gavrovo sub-zone crops out to the west of the Tripolitza sub-zone in the central and southern Peloponnese and forms the immediate foreland of the Pindos nappes. Blumenthal (1933) was the first to establish that the Tripolitza carbonates are exposed within tectonic windows, structurally beneath the Pindos Group in the Peloponnese.

In recent years the stratigraphy of the GTZ has been extensively studied, primarily through the work of Dercourt (1964), De Wever (1975), Fleury (1980) and Thiebault (1982). Age determinations based on microfossil zonation have allowed the history of the platform to be determined and the following stratigraphic descriptions are based on their work. The Gavrovo sub-zone outcrops to the west of the Pindos front as tectonic inliers within flysch sediment and it is not described in any detail. The basement lithologies and the stratigraphy of the Tripolitza sub-zone are discussed here. The main objective of this chapter is to present new evidence for the Early Tertiary development of a foreland basin related to lithospheric flexure caused by the crustal loading of the Pindos orogen. This is reflected in the break-up



of the platform, intra-plaformal deformation and the transition to a deeper water environment with flysch deposition.

## 7.2 GTZ BASEMENT

### 7.2.1 Introduction

The basement of the GTZ is seen in the southern Peloponnese and on Crete as the Phyllite Series (Lekkas & Papanikolaou 1978). It is a complex metamorphosed unit believed by most workers to be allochthonous (c.f. Jacobshagen *et al.* 1978a), overthrusting the Ionian Zone with westward transport, and comprising two components. The lower is a metaflysch with Ionian Zone affinities, first described by Ktenas (1926) and dated palaeontologically as Oligocene (Lekkas 1980, Thiebault 1982). The upper unit, of Upper Palaeozoic to Middle Triassic age (Thiebault 1982), is considered as the base of the GTZ proper and is informally termed the "Tyros Beds" (Ktenas 1926).

In the NW Peloponnese a basement consisting of Permo-Triassic low grade meta-sediment and volcanics is preserved beneath the GTZ Mesozoic carbonate sequence. It was named the Zaroukla Group by De Wever (1975) and is believed to be lithologically equivalent to the Tyros Beds of the Phyllite Series (Thiebault 1982). From the base upwards, five formations are described (De Wever 1975):-

- 1) The Fenou Quartzophyllite Formation; comprising 250m of schist with abundant sericite, also quartzose phyllite with chloritoid and rare quartzite.
- 2) The Goura Calcareous Formation; 60m consisting of black and grey carbonates interbedded with pelitic schist, sometimes rich in mica.
- 3) The Aghios Ilias Eruptive Formation; this comprises a variable thickness (20-500m) of alternating phyllite and volcanics. Several igneous specimens from this formation were taken for examination and are described below.
- 4) The Aghios Nikolas Detrital Formation; comprising 50m of phyllite, meta-sandstones and rare conglomerates.
- 5) The Kinigou Greenschist Formation; comprising 100m of phyllites with calcareous nodules.

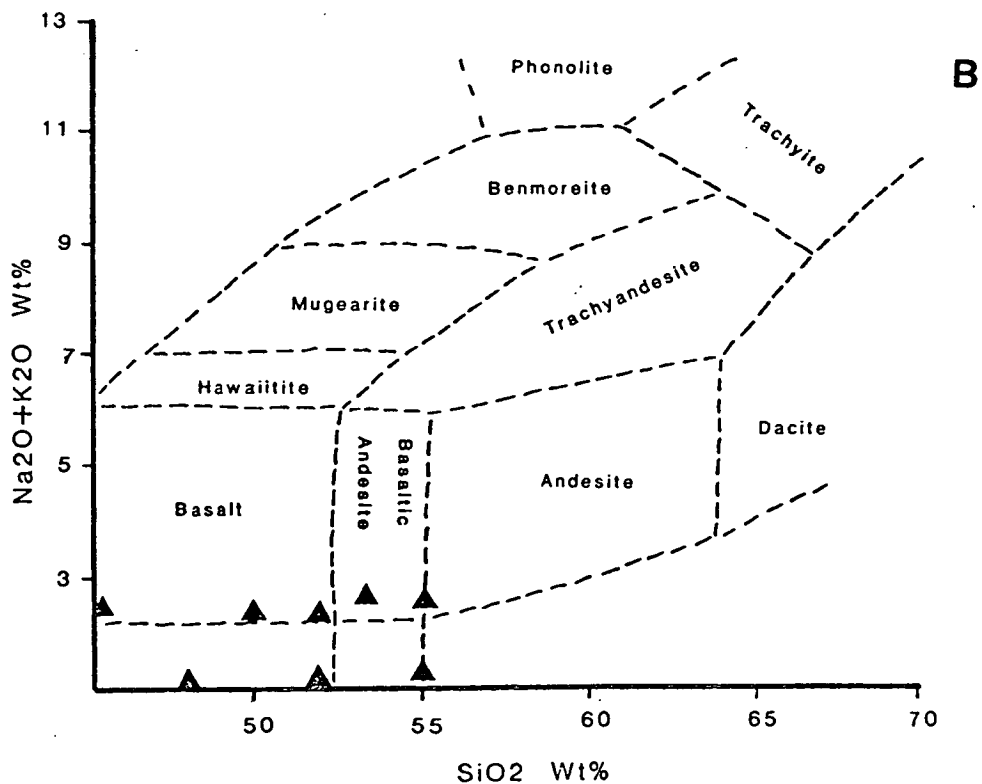
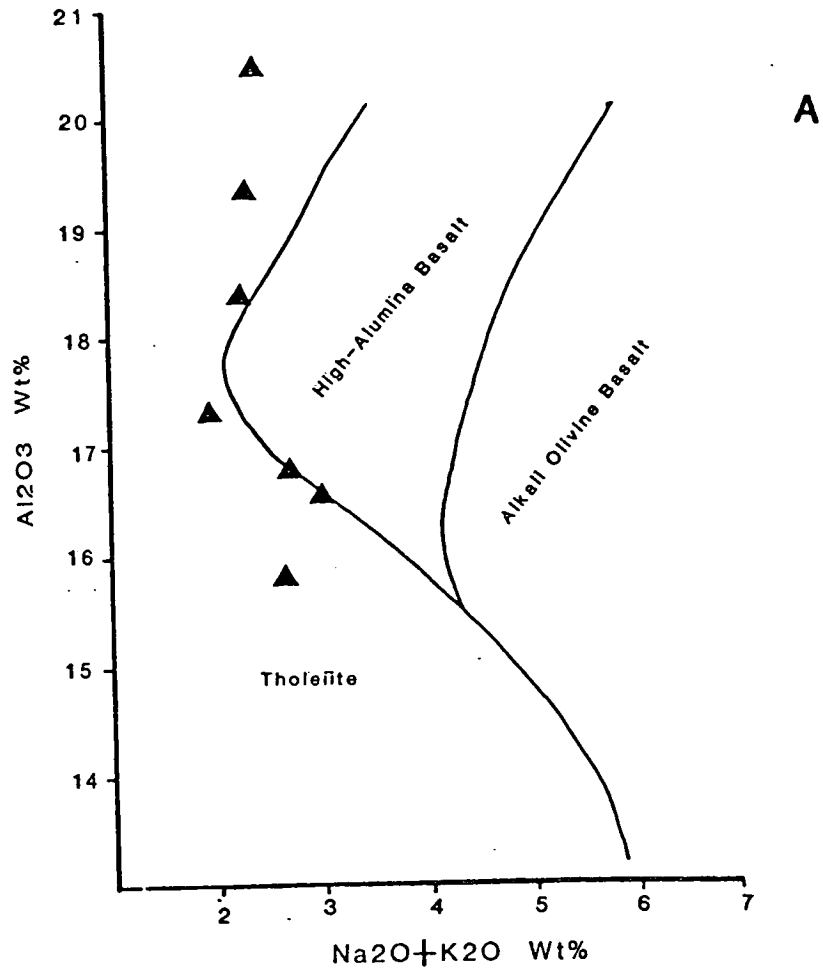


**Fig. 7.1** (A) Plot of alkali content/ $Al_2O_3$  for several GTZ samples indicating the tholeiitic character of the analysed rocks (after Kuno 1960). (B) Diagram showing the plots of several GTZ samples with the lithological boundaries of Cox et al. (1987)

### 7.2.2 GTZ Volcanics: Petrography

Several igneous samples (PD/89/323-325 and 717-722) belonging to the Aghios Ilias Eruptive Formation were taken from near to the village of Zarouchla. The rocks were collected for petrographic and geochemical comparison with igneous specimens collected from the tectono-sedimentary melange (TSM). The Zarouchla specimens all appear aphyric in hand specimen and are olive green in colour with a strong schistose overprint. In thin-section three distinct rock types were identified and all have mineral assemblages characteristic of low grade metamorphism with a variable hydrothermal contribution.

#### Metabasite

Samples 323-325 are highly altered with quartz and epidote porphyroblasts surrounded by a dark unresolvable groundmass. Alteration has largely obscured any primary groundmass textures but there are traces of an original porphyritic texture with an intergranular-intersertal matrix. Quartz occurs in a variety of forms; many porphyroblasts are single crystals with straight extinction. These commonly have secondary overgrowths of acicular amphibole that grow in from the margin towards the centre of the quartz crystals. There are also strained polycrystalline quartz aggregates present with serrated internal contacts. Epidote is ubiquitous as isolated small anhedral grains, often with zoning. Rosettes of pumpellyite are visible. There are outlines of remanent feldspar phenocrysts, almost totally replaced by chlorite, sericite and pumpellyite; the last is also a major constituent of the groundmass. Other replaced phenocrysts are polygonal in outline and often symmetrical, unlike the more rectangular feldspar pseudomorphs. These are inferred to have been pyroxene phenocrysts.

#### Meta(trachy)andesite

The second rock-type is a more matrix-rich extrusive rock that displays a preferred orientation of quartz and pseudomorphed phenocrysts of feldspar and pyroxene. The matrix appears to have undergone a small degree of shear, but there are no pressure shadows around phenocrysts, nor is there evidence for later brittle alignment. The preferred orientation is thus considered a flow texture and the groundmass may have been trachytic feldspar. There is more chlorite present than in the preceding sample, otherwise the mineralogy is similar.

### Meta-acidic Tuff

Sample 719 was identified as a fine grained tuff. It exhibits several diagnostic features such as a clastic fabric, with good sorting of grains, and adjacent tuff particles having distinctly different volcanic textures showing a range of degrees of quenching. Some grains have cracks that do not continue into the matrix, and others are clearly broken fragments in which the clast boundary cuts phenocryst pseudomorphs. Many of the clasts have dark rims which are indicative of rapid chilling. There are stringers of polycrystalline quartz through the sample but it is not possible to ascertain whether these are pre-metamorphic or syn-metamorphic veins. The mineralogy is again quartz, epidote, actinolite, chlorite, sericite and pumpellyite.

### 7.2.3 GTZ Volcanics: Electron Probe Analysis

In order to further identify the mineralogy and history of metamorphism, sample PD/89/324 was studied with the electron probe. Plate 7.1 illustrates a back-scattered electron image and map showing where some of the data points were. The analyses are provided in Table 7.1 along with the mineral formulae.

#### Amphibole

The analyses show that the amphibole is actinolite. There are 6 amphibole analyses. AM1/1 is an analysis point from the grain boundary of a stubby subhedral actinolite crystal that has grown in from the edge of a quartz porphyroblast margin. AM1/3 is from an actinolite crystal core within the same porphyroblast and AM1/2 is an analysis from an intermediate position. AM2/1-3 are from a single, much more phyrical, actinolite crystal and the analyses are also from the rim to the core. The overall chemistry of AM2 is similar to AM1 except that the core is slightly more enriched in SiO<sub>2</sub> and depleted in Al<sub>2</sub>O<sub>3</sub> and FeO.

#### Epidote

There are two sets of three analyses from the rim towards the core of two epidote crystals (EP1/1-3 & EP2/1-3). The crystals are often quite well zoned and this is reflected in the increased Fe<sub>2</sub>O<sub>3</sub> and lower Al<sub>2</sub>O<sub>3</sub> in the cores. No specific REE analyses were performed but several REE's were evident on an energy dispersive scan and REE concentrations rise towards the core. The darker REE-rich cores suggest that these epidotes may have overgrown primary allanite crystals that are often rich in REE's.

Sample PD/89/324

Electron Microprobe Results

Concentration	am1/1	am1/2	am1/3	ep1/1	ep1/2	ep1/3	ep2/1	ep2/2	ep2/3	gm1	gm2
NA2O	0.146	0.403	0.477	0.016	0.02	0.003	0.012	0.018	0.013	0.055	0.026
MGO	15.065	14.866	15.161	0.043	0.013	0.025	0.025	0.015	0.04	4.737	3.092
AL2O3	0.76	0.601	0.667	24.789	22.692	20.574	23.678	22.191	20.2	22.803	23.658
SiO2	54.667	54.612	54.736	37.827	37.309	36.122	37.194	37.035	35.136	38.817	38.253
K2O	0.012	0.033	0.02	0	0.007	0	0	0.002	0.01	0.012	0.002
CAO	12.661	12.237	12.244	23.639	23.467	19.057	23.313	22.847	18.473	17.841	22.474
TiO2	0.005	0.012	0.032	0.05	0.092	0.053	0.077	0.053	0.057	0.06	0.068
MNO	0.266	0.239	0.285	0.097	0.128	0.301	0.141	0.226	0.217	0.24	0.136
FEO	13.647	13.916	13.763	9.628	11.904	13.059	10.953	12.571	12.991	8.96	5.489
NiO	0.008	0.008	0.032	0.032	0	0	0.025	0.001	0.047	0.043	0.023
TOTAL	97.236	96.926	97.418	96.121	95.632	89.193	95.418	94.961	87.183	93.57	93.22

Formula

Na	0.041	0.113	0.134	0.005	0.007	0.001	0.004	0.006	0.005	0.018	0.008
Mg	3.25	3.22	3.267	0.01	0.003	0.006	0.006	0.004	0.011	1.158	0.757
Al	0.13	0.103	0.114	4.764	4.447	4.312	4.623	4.393	4.336	4.415	4.586
Si	7.938	7.964	7.94	6.181	6.219	6.443	6.177	6.237	6.418	6.39	6.301
K	0.002	0.006	0.004	0	0.002	0	0	0	0.002	0.002	0
Ca	1.968	1.91	1.901	4.135	4.186	3.636	4.143	4.117	3.609	3.143	3.964
Ti	0.001	0.001	0.003	0.006	0.011	0.007	0.01	0.007	0.008	0.007	0.009
Mn	0.033	0.03	0.035	0.013	0.018	0.045	0.02	0.032	0.033	0.034	0.019
Fe	1.655	1.694	1.667	1.314	1.657	1.944	1.519	1.767	1.98	1.232	0.755
Ni	0.001	0.001	0.004	0.004	0	0	0.003	0	0.007	0.006	0.003
O	23	23	23	25	25	25	25	25	25	25	25

Concentration	gm3	am2/1	am2/2	am2/3	plag1/1	plag1/2	plag1/3	plag1/4	chl1/1	chl2/1	chl3/1
NA2O	0.059	0.417	0.355	0.166	11.479	11.989	12.013	11.87	0.02	0	0.009
MGO	2.58	14.609	14.538	15.118	0.091	0.022	0.032	0.061	16.186	15.163	16.267
AL2O3	24.513	1.181	1.037	0.595	19.727	19.622	19.675	19.667	18.275	18.807	19.11
SiO2	39.063	54.077	54.533	54.909	68.583	68.168	67.886	67.82	26.968	26.125	27.225
K2O	0.01	0.029	0.043	0.022	0.052	0.049	0.039	0.053	0.018	0.014	0.008
CAO	21.267	12.351	12.351	12.614	1.139	0.304	0.555	0.869	0.319	0.322	0.175
TiO2	0.05	0.025	0.005	0.012	0.017	0.005	0.03	0.072	0.013	0.062	0.03
MNO	0.189	0.253	0.302	0.289	0.012	0.019	0.009	0.021	0.378	0.382	0.373
FEO	5.814	14.391	14.783	13.453	0.436	0.247	0.174	0.307	24.794	25.239	25.025
NiO	0.006	0.02	0.032	0.023	0.025	0.02	0.02	0.013	0.039	0.034	0.031
TOTAL	93.552	97.352	97.978	97.2	101.562	100.445	100.432	100.753	87.011	86.149	88.253

Formula

Na	0.019	0.117	0.099	0.046	3.849	4.058	4.071	4.016	0.008	0	0.004
Mg	0.626	3.162	3.13	3.259	0.024	0.006	0.008	0.016	5.101	4.846	5.044
Al	4.708	0.202	0.177	0.102	4.022	4.037	4.053	4.045	4.574	4.774	4.706
Si	6.376	7.879	7.903	7.967	11.865	11.902	11.866	11.836	5.747	5.646	5.708
K	0.002	0.005	0.008	0.004	0.011	0.011	0.008	0.012	0.005	0.004	0.002
Ca	3.717	1.926	1.915	1.959	0.211	0.057	0.104	0.162	0.072	0.074	0.039
Ti	0.006	0.003	0	0.001	0.002	0.001	0.004	0.01	0.002	0.01	0.005
Mn	0.026	0.031	0.037	0.036	0.002	0.003	0.001	0.003	0.068	0.069	0.066
Fe	0.793	1.75	1.789	1.63	0.063	0.036	0.025	0.045	4.387	4.529	4.357
Ni	0.001	0.002	0.004	0.003	0.004	0.003	0.003	0.002	0.007	0.006	0.005
O	25	23	23	23	32	32	32	32	28	28	28

am=amphibole, ep=epidote, gm=groundmass, plag=plagioclase, chl=chlorite.

Table 7.1 Electron microprobe results for sample PD/89/324.

### Feldspar

The groundmass contains a variety of minerals which have replaced relict crystals. Some of these are pseudomorphed feldspar. The feldspar present is albite. The texture and occurrence suggest it is an alteration product of more calcic plagioclase. The analyses were obtained by rastering the beam to overcome volatilization problems.

### Pumpellyite, Chlorite & Groundmass phases

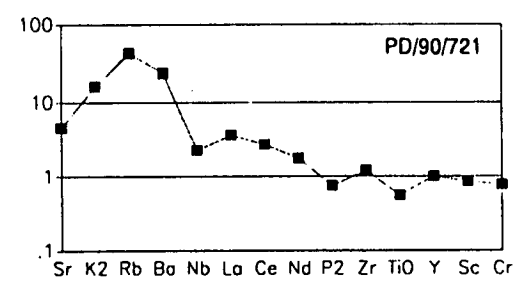
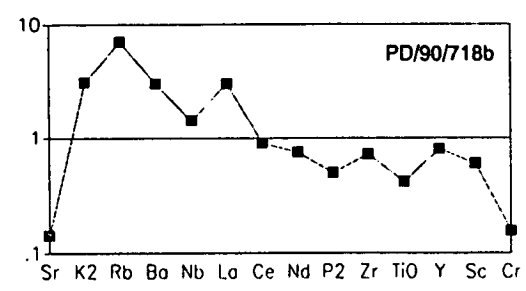
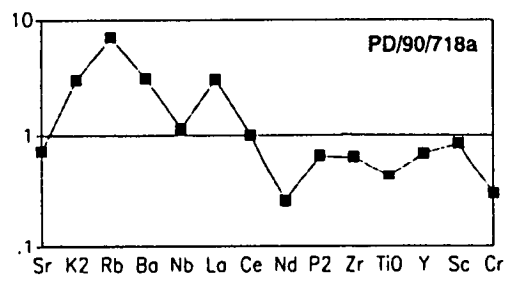
The presence of abundant fine-grained pumpellyite in the groundmass is indicated by the analyses GM1-3 as the mineral formula, recalculated on a 25 oxygen basis, can be compared with the pumpellyite formula from Deer, Howie and Zussman (1983):  $\text{Ca}_4(\text{Mg}, \text{Fe}^{2+})(\text{Al}, \text{Fe}^{3+})_5\text{O}(\text{OH})_3[\text{Si}_2\text{O}_7]_2 \cdot 2\text{H}_2\text{O}$ . The other main groundmass phase is chlorite as shown by CHL 1/1-3. It is closely associated with the pumpellyite and also as a replacement phase in the altered pseudomorphs after pyroxene as well as plagioclase. Lastly there is an unidentified groundmass mineral with abundant K, and with Si, Al, Fe & Mg. No discrete crystals were visible. The elements present suggests that there may be a celadonic or another potassic mica phase possibly intergrown with chlorite on a scale not resolvable with the probe.

### 7.2.4 Geochemistry

Nine igneous samples were analysed by XRF for major oxide and trace element composition (Appendix 5). The operating conditions and method are described in Appendix 2. Sample 718c has high silica content and negligible MgO and has clearly suffered extensive hydrothermal alteration. It is not considered further. The remaining samples plot in the basalt or basaltic andesite fields of Cox *et al.* (1987) with  $\text{SiO}_2$  contents of 42-55% (Figure 7.1). Total alkali content is low (0.56-3.1%), and the total MgO values are low to moderate (3.2-5.7%).  $\text{Al}_2\text{O}_3$  is quite high, between 15.8 and 20.4% and  $\text{Fe}_2\text{O}_3$  content is moderate, (8.5-10.9%). The basalts all have low  $\text{TiO}_2$  values of 0.55-0.8%. The rocks fall in the sub-alkaline tholeiite field of Kuno (1960, Figure 7.1) but it is clear from the textures that the silica values are inherently unreliable and that the alkalis may also have been substantially modified.

Trace elements were plotted on MORB normalised spidergrams (Pearce 1980, Figure 7.2). This gives a direct visual indication of the relative abundance of several elements. Large ion lithophile (LIL) elements (Sr-Ba) are relatively mobile and are

ROCK/MORB



ROCK/MORB

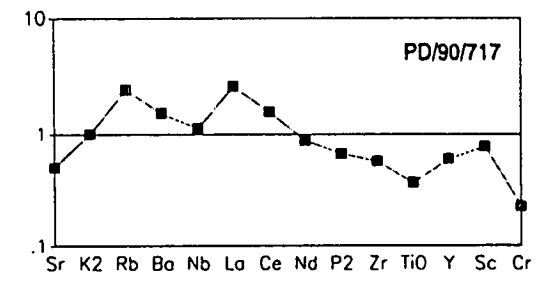
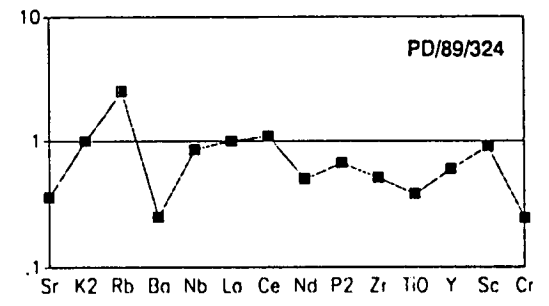
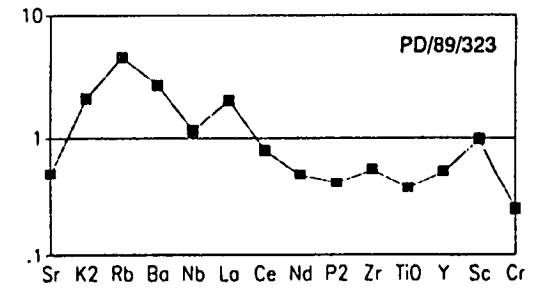


Fig. 7.2 MORB-normalised multi-element plots (Pearce 1975) for selected igneous samples of the GTZ.

enriched relative to MORB. This may be a primary feature or the product of secondary alteration. In comparison, the less mobile high field strength (HFS) elements (Nb-Y) show relative depletion, except for sample PD/90/721 which has a flat, MORB-like trace. Cr levels are low, consistent with the generally low MgO values. The suite is dominated by moderately evolved rocks yet the incompatible trace elements are not as enriched as would be expected if a MORB or WPB had been the parent. All six plots show a slight relative depletion in Nb compared to La, a characteristic signature of above subduction-zone influence, either contemporaneous or inherited. Immobile elements were also plotted on selected variation diagrams which indicate possible tectonic settings (Pearce 1980, Pearce 1982). The data plot in the fields of overlap between island arc tholeiite (IAT) and MORB (Figures 7.3 & 7.4).

### 7.2.5 Interpretation

The samples have undergone pumpellyite-actinolite grade metamorphism. Even under such low-grade metamorphism, many elements are mobile (Gillis & Robinson 1986). Boyle (1984) studied altered lavas from the Troodos ophiolite and he compared these rocks, which had undergone greenschist and zeolite facies metamorphism, with similar but relatively unaltered samples. Chemical compositions differed, notably there was a loss in Si and Fe oxides while Mg and K oxides were increased. Conversely, Pearce (1975) indicates that there is enrichment in Si, Fe and Na oxides with loss in Al during greenschist metamorphism. The chemical data presented here are evaluated with due regard to possible element mobility.

The mineral assemblage of Qtz+Act+Epi+Chl+Alb+Sph+Pump is characteristic of 300–400°C and 2–4 Kbar conditions. The assemblage, geochemistry and texture further indicate that the protoliths were igneous rocks, probably a basaltic andesite. The development of the mineral assemblage, including the unstrained quartz, probably results from prograde metamorphic reactions. The most probable geochemical pathway involves the breakdown of calcic plagioclase and any pyroxene that was present. For example:-



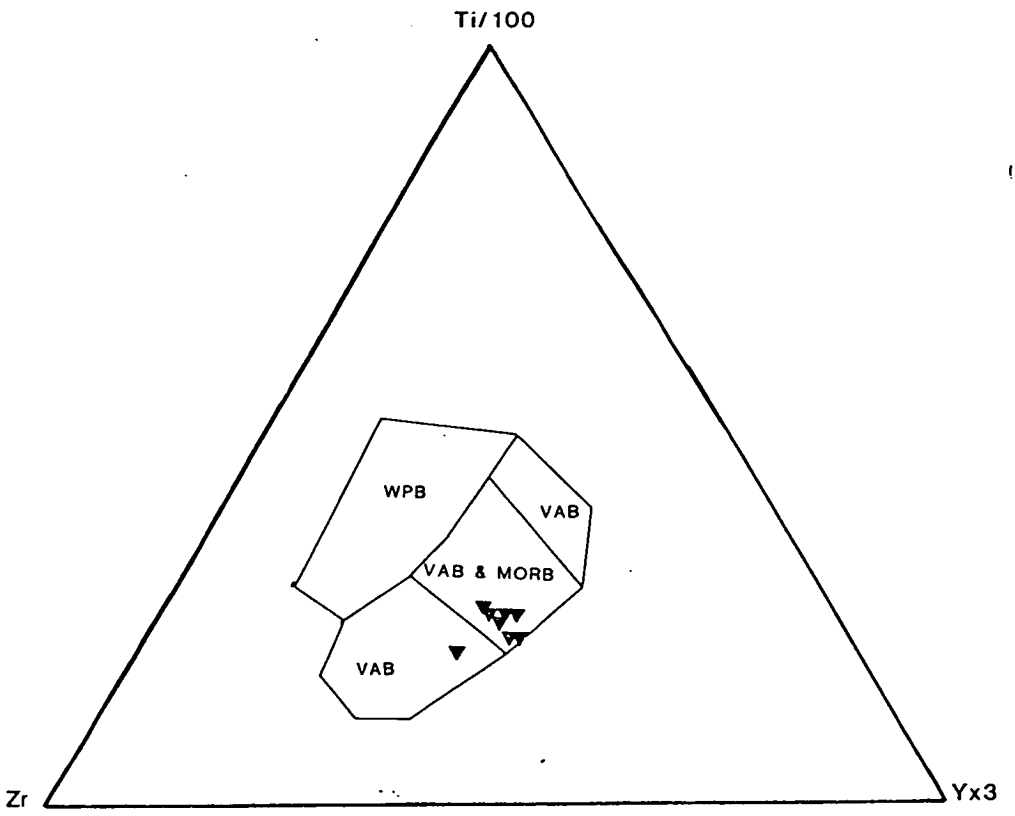
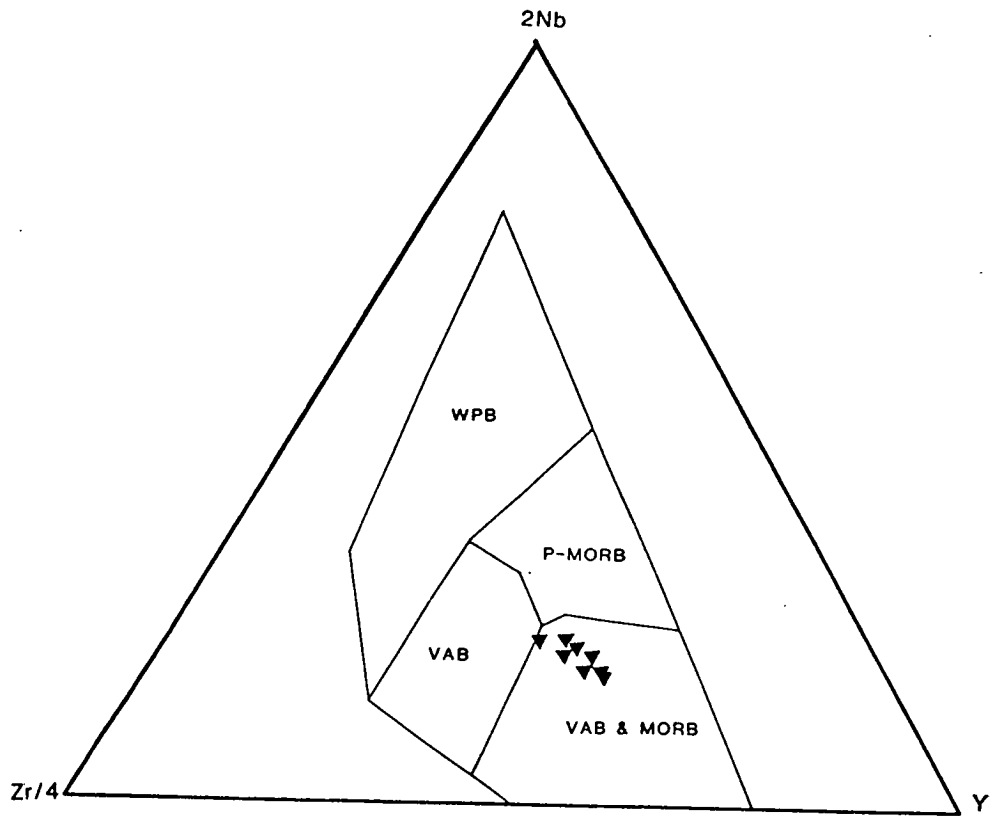


**Fig. 7.3** Ternary tectono-magmatic discrimination diagrams (Meschede 1986, Pearce & Cann 1973) for selected samples of the GTZ.

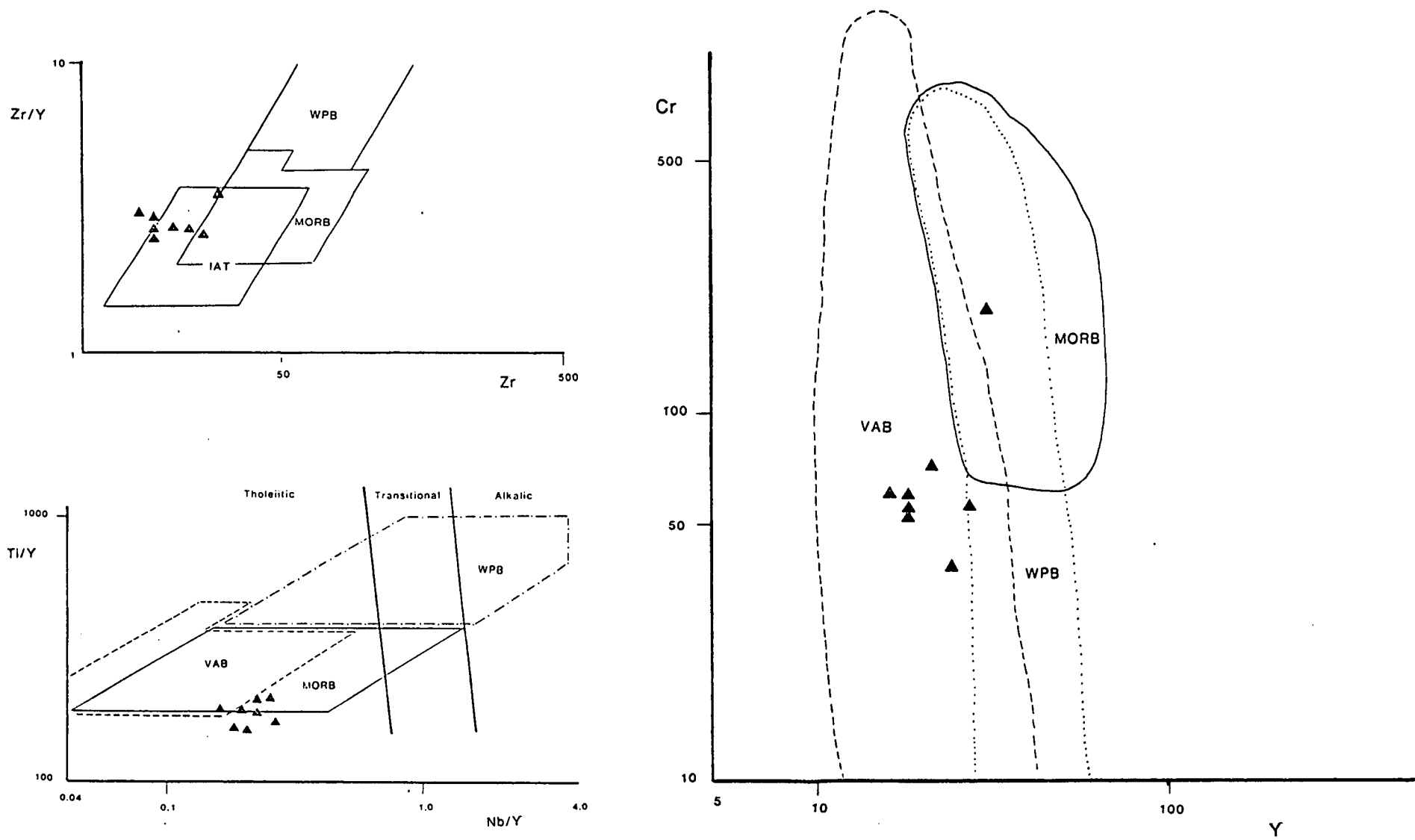
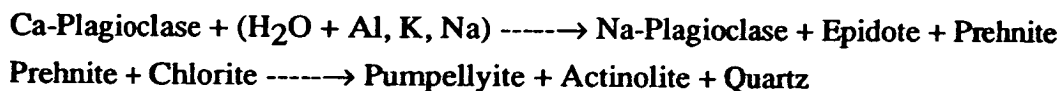


**Fig. 7.4** Tectono-magmatic variation diagrams (Pearce 1980, Pearce 1982, Pearce et al. 1981) for selected samples of the GTZ.



The polycrystalline quartz with stylolitic grain boundaries, internal deformation and a foliated texture in thin-section is indicative of moderate strain. This could have been accomplished purely by burial loading although intensive mesoscale folding within the metasediments of the GTZ basement (De Wever 1975) indicates that dynamic structuration accompanied the metamorphism and schistosity development. This most probably relates to Tertiary thrusting and collision. The metamorphism is not apparent in the lower-most neritic carbonates of the GTZ and confirms the view of Dercourt (1964) that there must be a major thrust decollement between the two units.

Geochemical diagrams based on immobile element concentrations indicate that the likely tectonic provenance was above a subduction zone. The rocks have close geochemical affinities with the basaltic andesites found in the tectono-sedimentary (TSM) melange as described in Chapter 8. In this study, the GTZ and TSM volcanic rocks are considered to reflect the same Middle Triassic rifting event that formed the Pindos Basin and their "arc" character is thought to reflect their derivation from a lithospheric source previously modified by volatiles from subducted pelagic sediment, much as inferred for the extensional Basin and Range volcanics of the western USA (Fitton *et al.* 1991). They are discussed more fully in Section 8.4 .

### 7.3 TRIPOLITZA ZONE STRATIGRAPHY & SEDIMENTOLOGY

#### 7.3.1 Tripolitza Platform

The greater part of the Tripolitza sub-zone comprises a shallow-water carbonate sequence. This was not studied in detail and the following section is largely compiled from the literature. The transition from neritic to deeper water sedimentation, described in later sections of this chapter, is based on new work that integrates the Tertiary sedimentology of the Gavrovo-Tripolitza Zone with the tectonic evolution of the Apulian margin.

Dercourt (1964) described a horizon between the metamorphic basement and the unmetamorphosed neritic limestone consisting of gypsum and "Cargneule" (a French Alpine term for Triassic brecciated dolomite often associated with evaporites). It

appears that this horizon acted as a decollement with unknown movement and is assigned a Triassic age. Triassic evaporites are known from the Ionian zone (BP 1971, Underhill 1985) but are not proven to be beneath the Gavrovo zone. De Wever (1975) studied several incomplete sections from the Tripolitza sub-zone to the east of Chelmos. From this data he was able to synthesise a coherent stratigraphic column which is reproduced in Figure 7.5 .

**T:** The basal section comprises laminated limestone for approximately 80m, containing the thick bivalve *Neomegalodon complanatum*. This indicates an Upper Triassic age.

**TJ:** A minimum of 220m of dolomitic limestones and dolomites, not dated.

**J1:** Consists of partially dolomitised limestone containing algae, gastropods and thin shelled megalodont bivalves. Dercourt (1964) cites a bed containing *Polygonella* sp and dates the unit as Liassic. It is approximately 350m thick.

**J2:** The unit was not dated. It consists of 250m of limestone and dolomite.

**J3:** This unit is rich in fauna including *Cladocoropsis mirabilis*, *Clypeina jurassica* and *Kurnubia* sp. It is dated as Kimmeridgian-Tithonian and is 120m thick.

**JC:** Contains alternations of limestone and dolomite. *Salingoporella grudi* and *Actinoporella podolica* indicate an Upper Jurassic to Lower Cretaceous age. The unit is approximately 220m thick.

**CS1:** 280m thick but generally poor in microfossils, this lithology is dominated by limestone of Cenomanian age.

**CS2:** Approximately 80m thick the unit is dolomitic at the base, towards the top rudists become abundant. It corresponds to the Turonian stage.

**CS3a:** This richly fossiliferous unit is 300m thick and contains laminated and massive limestones. Among the fauna are *Dicyclines gr. schlumbergi* and *Aeolisaccus kotori*.

**CS3b:** This unit is only distinguishable from the preceding CS3a by recognition of the appearance of *Murciella orbitoides* sp. and *Raadshoovenia* sp. along with the disappearance of *D. schlumbergi*. It is 150m thick and dated as Campanian-Maastrichtian.

**CS3c:** The identification of *Rhapydionina liburnica* dates this 100m thick unit as Maastrichtian. It consists of alternating limestone and dolomite.

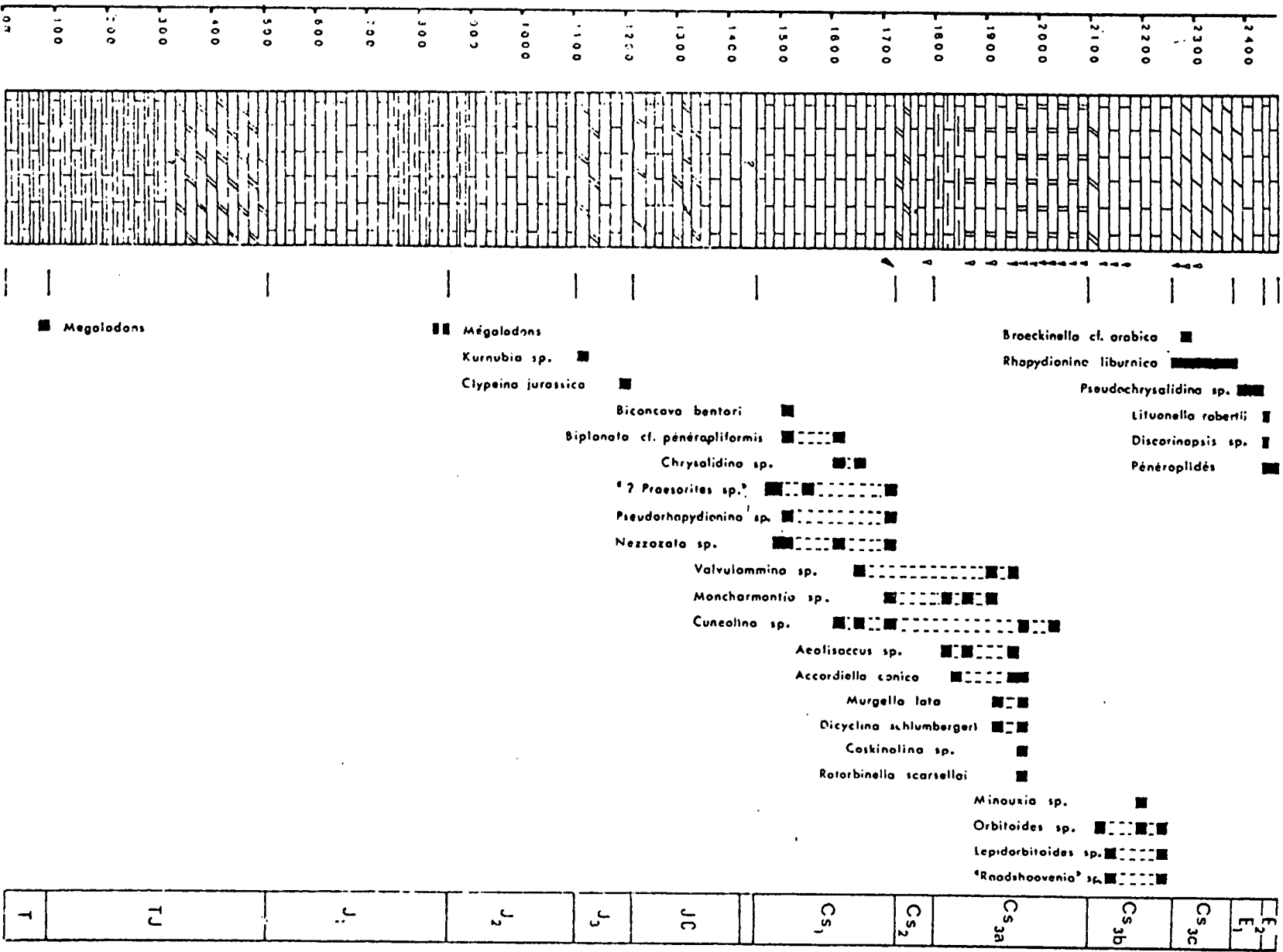


Fig. 7.5 Composite log and biozonation of the Tripolitza zone (from De Wever 1975).

E1: Also composed of alternations of limestone and dolomite, this 50m thick unit is dated as Palaeocene by the disappearance of *R. liburnica* and rudists, and with the appearance of *Pseudochrysalidina* sp.

E2: At least 25m of limestone containing *Lituonella roberti* dates this unit as Upper Eocene.

The sedimentary history of the platform is complicated by several well documented periods of emergence with bauxite development and the formation of erosional surfaces. De Wever (1975) indicates that an Upper Jurassic hardground is locally developed in neritic limestones. He is not specific regarding the exact date. It is possible that this corresponds to the period of sea level fall inferred from the interbedded micrite, breccia and conglomerate of the Aroania Chert Member (Section 4.4.3.2). Tsalia-Monopolis (1977) states that there are breaks in sedimentation recorded in measured and dated sections from Feneos, the area from which De Wever's composite log was constructed. These correspond to the "Early-Late Cretaceous" boundary. In other areas, up to 80m of breccias are intercalated within the neritic sequences. This time period corresponds to the interval during which copious quantities of brecciated micrite were deposited within the laterally equivalent Cenomanian Erymanthos Limestone Member. The implications of the shedding of such vast amounts of platform breccia through erosion, while sedimentation continued in adjacent areas, is that there was active block faulting during the Middle Cretaceous along the Apulian margin. Clasts of neritic limestone with Triassic fauna (Fleury 1980) in these Cretaceous breccias indicate that there was strong uplift and erosion in parts of the platform while other areas were unaffected.

### 7.3.2 Early Tertiary Syn-Orogenic Sediments

#### 7.3.2.1 Break-up Breccia

Lekkas (1978) reports Cretaceous to Eocene Tripolitza-derived coarse sediments redeposited during the Upper Eocene, prior to flysch sedimentation. He acknowledges that parts of the platform must have emerged, and been eroded, prior to overthrusting by the Pindos sheets as there are areas where Oligocene flysch directly overlies Jurassic strata. Bassias & Lekkas (1988) report an Upper Cretaceous to Palaeocene (?) carbonate breccia series above neritic sediments. This lithology is intercalated between the Tripolitza and Pindos Group sediments. The

authors suggest a phase of normal faulting within the platform during the Upper Cretaceous and prior to the deposition of flysch sedimentation. However, the stratigraphic and structural position of the sections described by Lekkas (1978) and Bassias & Lekkas (1988) suggest that they are all related to the same uplift event, considered here as Eocene. Similar outcrops are widespread in the Northern Peloponnese between Tripolis and Argos (IGME mapping) but no particular significance has previously been attributed to them. Similar breccias are absent to the west of Tripolis.

#### 7.3.2.2 GTZ Flysch

The GTZ flysch is found both beneath the Pindos thrust sheets and also in the foreland to the thrust front. At several localities around Chelmos and Drakovouni (Figure 1.1) the transition from neritic carbonate to flysch sedimentation was observed. Conglomerates and mixed beds of carbonate and sandstone ("couches de passage") are reported by Dercourt *et al.* (1976) and are dated as Eocene (upper Lutetian to lower Priabonian). In other areas, e.g. Drakovouni, the transition is sharp with medium- to coarse-grained turbiditic sandstone and shale deposited upon neritic carbonate (Plate 7.4). Siltstones from the transition contain both benthic platform derived fauna and planktonic forams more typical of deeper-water pelagic deposits. A sample from the platform immediately beneath the flysch yielded Middle Eocene *Discocyclina* sp (Plate 7.2). A thin-section of the overlying sandstone indicates it to be a fine-grained sandstone with sub-rounded, moderately sorted grains, dominantly of calcite and quartz. The cement is sparry calcite.

In the foreland to the Pindos thrust sheets, the platform is covered by a variable thickness of turbiditic sandstone. Within the basin several inliers of Gavrovo zone neritic limestone are exposed. The lowermost flysch sediments above the Gavrovo zone platform are palaeontologically dated as Late Eocene or Early Oligocene (Dercourt *et al.* 1976) and there is, therefore, clear evidence for diachronism across the Tripolitza to Gavrovo zones in the onset of syn-orogenic flysch deposition. The sedimentology of the flysch has been studied in the Peloponnese by Izart (1976) and north of the Gulf of Corinth by Leigh (1991). At Alepohorio a 500m thick section was measured which records the upward transition from flysch to a massive unit of conglomerates and breccias (Figure 7.6). Three major facies groups are seen in this section.

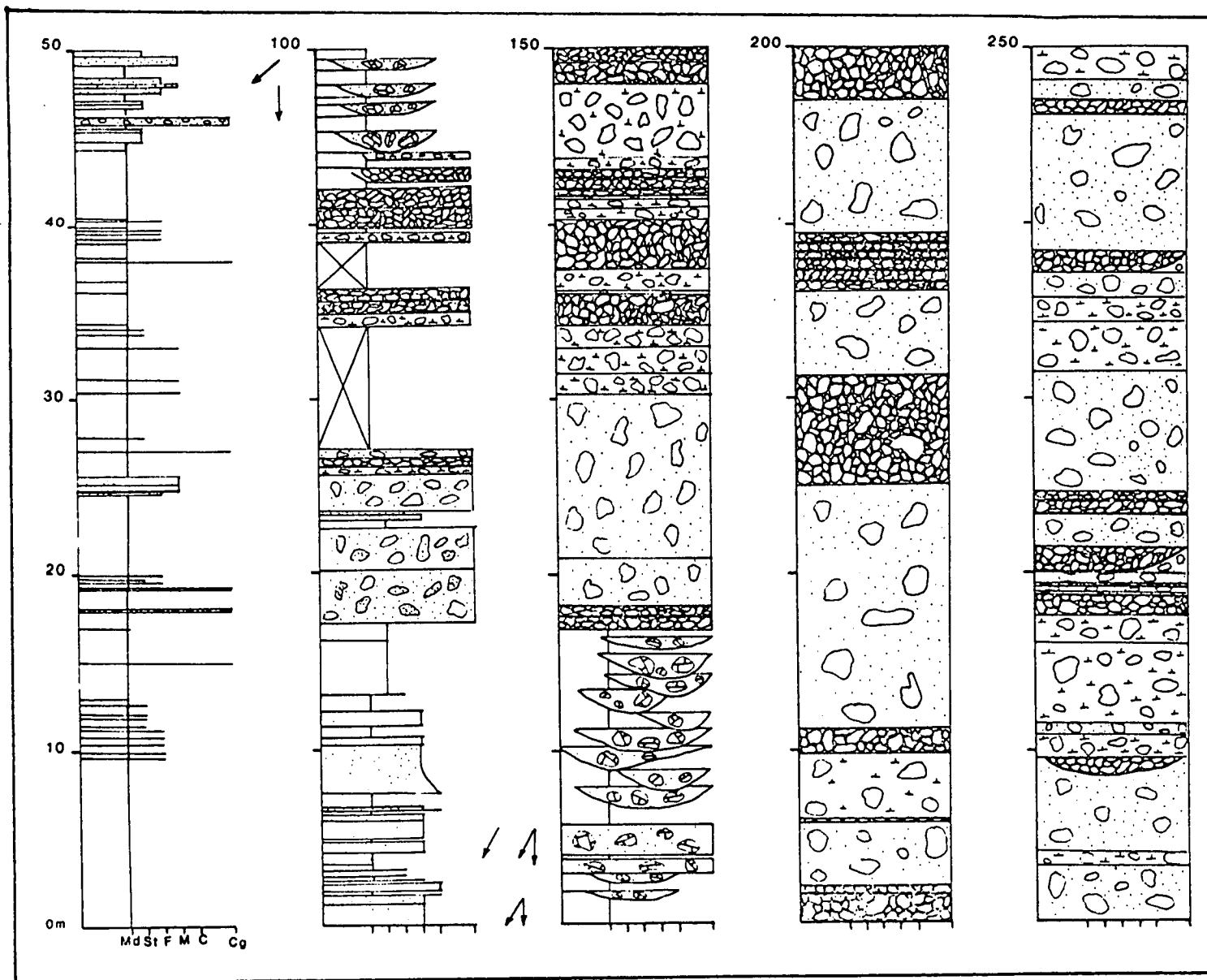


**Fig. 7.6** Graphic log from the Pindos foreland showing the transition from mainly pelitic distal turbidites, through a short arenite interval, into massive debris flow deposits. The chaotic gravity flows continue upwards for a further 200m.



### Conglomerate Facies

There are three distinct end-member types of conglomerate facies:-

- (1) Clast-supported, sub-rounded, conglomerate with clasts to 21x12cm and bed thickness to 6.2m. All clasts are micrite or carbonate grainstone.
- (2) Matrix-supported conglomerate with limestone clasts as above. The matrix is fine-grained carbonate and the lithology is well cemented. Bed thickness is up to 4m with a maximum sized clast of 89x50cm observed.
- (3) Matrix-supported conglomerate with mixed source clasts of sandstone and carbonate, also shale and chert. The matrix is a green flysch-like pelite and the lithology is relatively unconsolidated. Generally, the beds are massive, to 13.8m in thickness and with individual clasts to 45x30cm.

All three types of deposit are demonstrably channelised on various scales. A neritic limestone clast yielded *Actinocyclus* sp and *Nummulites* sp together. The sample was dated as Upper Eocene (pers.comm. C. Betzler) and the conglomerates must be younger than this. Unfortunately, a contemporary *Nummulite* sp found in shale could not be dated. The conglomerates are 535m thick, the correct way-up and above at least several hundred metres of flysch that has been dated as dominantly Oligocene (Izart 1976). Mansy (1971) reports 300m of conglomerate from the central Peloponnese that is dated as Upper Oligocene.

### Sandstone Facies

Stratigraphically below the conglomeratic facies, a 15m interval of thick bedded (to 272cm), dominantly medium grained sandstone was deposited. Bedding is tabular on the scale observed and grading is often present. Sole structures, e.g. flute and groove casts, "tealeaf lineation" and rare trough cross lamination show north to south and east to west palaeocurrent directions. Thin section examination indicates that the sandstones are litharenites. They contain mostly quartz and carbonate grains with subsidiary feldspar, chert and volcanic fragments.

### Mudstone Facies

Intercalated within the sandstones, and becoming volumetrically more important down-section, pelite is present in beds up to 120cm thick. Subordinate siltstone is present. In similar beds north of the Gulf of Corinth, a diverse trace fossil assemblage was noted, including *Spirophycus*, *Palaeodictyon*, *Zoophycus* and *Diplocraterion* (Alexander & Degnan, unpublished data). The mudstones were not studied further, however, an interesting sub-facies is a pebbly mudstone seen at

Alepohorio below a thrust fault within the flysch. It contains well rounded pebbles of carbonate of unknown derivation.

For a fuller account of the sedimentology of the GTZ flysch, the reader is referred to Izart (1976) and Leigh (1991).

## 7.4 DEPOSITIONAL ENVIRONMENT

### 7.4.1 GTZ Carbonates

The composite section from the Tripolitza sub-zone in the NW Peloponnese records at least 2400m of continuous neritic sedimentation from the Upper Triassic to the Upper Eocene. The Tripolitza zone is considered contiguous with the Gavrovo zone, in turn connected to the Ionian Zone which was a shallow marine environment until the Early Jurassic when it underwent a sudden deepening (Fleury 1980). The Ionian Zone was palaeogeographically connected to the Pre-Apulian Zone in the west, an area of continuous shallow marine sedimentation from the Triassic to Tertiary times. It is clear that the Apulian margin essentially formed a wide, shallow shelf that experienced various degrees of extension during the Mesozoic and Cenozoic, leading to the formation of a deep intra-platformal trough, the Ionian basin. The Apulian platform can be considered analogous in many ways to the present-day Bahama Banks which measure 700 km north-south and 300 km east-west (Tucker 1990). Fleury (1980) provides an extensive comparison between the two areas which are characterised by the following:-

- (1) Both have variable types of neritic carbonate microfacies, underlain by evaporites from an initial rifting phase.
- (2) The platforms are/were long lived areas with episodic tectonic activity that created local sediment hiatuses on uplifted blocks within thick neritic sequences. The probable controls are/were basement faults.
- (3) Deep depressions exist, e.g. the Florida Straights, Tongue of the Ocean and the Exuma Sound, that dissect the 300km wide Bahama platform. This bathymetry can be compared with the large scale arrangement inferred for the external Hellenides. Upon unstacking, the Pre-Apulian, Ionian and Gavrovo-Tripolitza tectono-stratigraphic zones may have been of a similar width.

(4) The steep by-pass margin of the Bahama Banks is probably the fault controlled transition from continental crust to Atlantic oceanic crust (Mullins & Lynts 1977). This is thought analogous to the boundary between the GTZ and Pindos Zones.

The Upper Eocene transitional sediments and the thick locally derived platform breccia of the GTZ record the break-up of the margin as the advancing Pindos thrust front began to load the adjacent crust. Extensional faulting ahead of an orogenic wedge has been recorded elsewhere (e.g. Jaca Basin in the Spanish Pyrenees, Jolley 1988) where it is related to the passage of a peripheral forebulge. It is envisaged that the platform margin was a line of major crustal weakness that formed a topographic buttress to the Pindos orogen, even after collapse (Section 6.5.3). Thrust sheet loading in the Pindos Basin led to the development of a flexural forebulge on the platform with significant extension (Section 7.5.1), probably utilising basement faults related to Triassic rifting. A horst and graben topography on the forebulge initiated deep erosion and the development of bauxite and karst on topographic highs (Section 7.3.1), while contemporaneous carbonate breccia was deposited in topographic lows (Section 7.3.2). The sudden deepening of the platform records the passage of the forebulge inboard. Continued subsidence led to a general blanketing by flysch sediments.

A likely modern-day analogue for the above processes is the subduction of the Australian continental margin beneath the Banda forearc in Indonesia. Audley-Charles (1986) suggests that further crustal shortening in the region would lead to footwall collapse and southward thrusting of the Australian shelf over foredeep deposits.

#### 7.4.2 GTZ Flysch

The depositional environment of the Ionian and Gavrovo Zones during the Oligocene has been described in terms of a foreland basin that formed as a lithospheric flexural response to the advancing Pindos orogen (Underhill 1985, Clews 1989, Leigh 1991). It is broadly similar to many other ancient examples of flexural foredeeps described elsewhere (Allen, Homewood & Williams 1986, and references therein). The syn-orogenic sediments of the GTZ are important in that they record the transition from a passive margin to a foredeep migrating over continental crust.

As will be shown below (7.5.1 & 7.5.2), deformation ahead of the Pindos front imbricated the platform soon after extensional collapse. In the Gavrovo Zone, slices of the uppermost platform were detached and thrust onto flysch sediments during the Oligocene. These formed folded inliers within the photic zone that became colonised by shallow water benthic forams during the Oligocene as shown by the contemporary specimens in shale (PD/90/750). At the same time the backshedding of sediment into a thrust-sheet top (or piggy-back) basin by debris-flow and rockfall mechanisms occurred (Section 7.3.2.2). Mixed-source conglomerate was derived additionally from the Pindos thrust front. Similar allochthonous Gavrovo limestone was studied north of the Gulf of Corinth (Alexander & Degnan; and S. Leigh, unpublished data) and is considered to have been a topographic feature on the basin floor as there is palaeocurrent divergence seen in flysch lithologies. Izart (1976) suggested a deep sedimentary environment for the flysch deposits, based on the clear turbidite origin of the sediment and the trace fossil assemblage. However, Leigh (pers. comm. 1989) found symmetrical ripples indicative of wave action in some flysch beds implying a sea floor above storm-wave base. Stockmal *et al.* (1986) show how the depth of a foreland basin is strongly dependent on the thrust load. Covey (1986) details the evolution of the Taiwan foreland basin and shows how depositional environments become progressively shallower with time due to sediment thickness out-pacing sediment-load induced subsidence for a steady-state orogen (i.e. the magnitude of the tectonic load remains constant). The Pindos foreland basin may not have been as deep as commonly presumed for other flysch basins (possibly a few hundred metres rather than several hundreds or thousands of metres) due to inconsiderable thrust loading or the attainment of a steady-state wedge once emplacement onto the margin occurred.

## 7.5 GTZ STRUCTURE

### 7.5.1 Intra-platform Deformation

The study of deformation within the GTZ was restricted to the measurement of large-scale structures which allow the Tertiary tectonic history to be better determined. The area of the Tripolitza zone studied had difficult access and limited exposure. Most of the intra-platform deformation was recorded from the Planeterio valley and a geological map is shown in Figure 7.7. Mapping of this area provided a number of important observations.

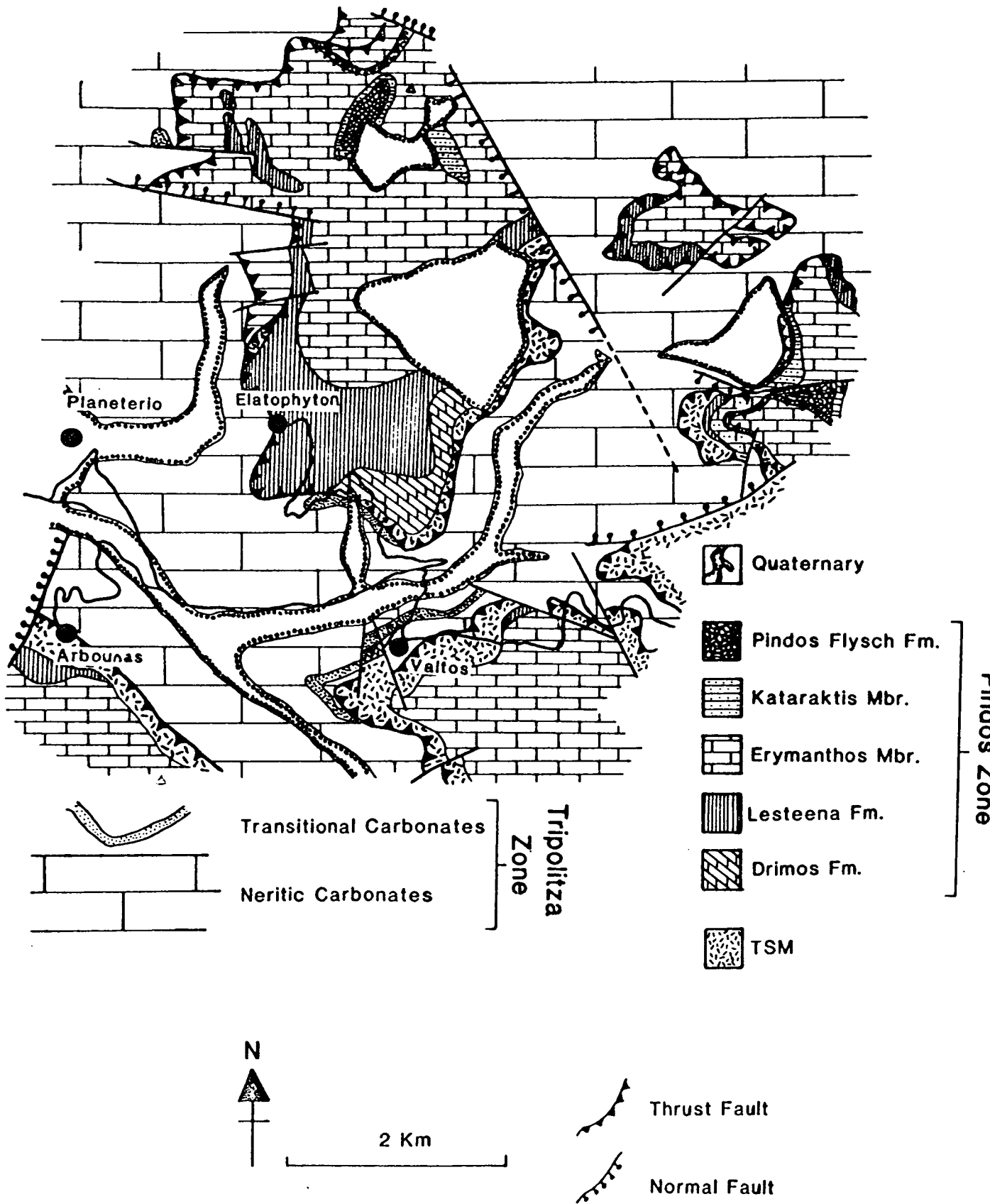


Fig. 7.7 Geological Map of the Planeterio valley in the Chelmos Mountain area.

### 7.5.1.1 Extensional Faulting

At Valtos there are two extensional faults which cut platform lithologies and approximately 20m of normal movement is indicated from bedding offsets. However, no slickensides were observed and strike-slip movement is not ruled-out. The sediments are Eocene (IGME sheet Kaledsi), and the basal Pindos thrust was mapped to cut the extensional faults across both the hangingwall and footwall regions in a continuous plane. This indicates that there was post-depositional (Eocene) extensional faulting prior to emplacement of the Pindos thrust sheets on this part of the platform. N.B. The extensional faults were reactivated after Pindos emplacement as the faulting presently extends into the overlying Pindos Group.

### 7.5.1.2 Folding

At the head of the valley, beneath Chelmos Mountain, a large fold is seen (Plate 7.4). It is bounded to the west by a neotectonic fault that downthrows at least 100m of Cretaceous Pindos Zone sediment against Tripolitza zone Eocene carbonate. Access is difficult but the fold has an axial plane of 350/55. The fault has a dip & strike of 330/80. They are both roughly perpendicular to the gross Tertiary transport direction which is also parallel to the inferred Triassic rift orientation. The geometry and juxtaposition of both the fold and fault strongly suggests that they are kinematically linked as a fault propagation fold (Jamison 1987) due to west-directed compressive stress above an original rift-related fault, reactivated as an inversion structure (Figure 7.8, A1 & A2). The deformed platform was then overthrust by the Pindos basal thrust. During the Plio-Pleistocene, neotectonic activity reactivated the fault again to give the present day extensional expression.

### 7.5.1.3 Thrusting

A steep cliff of folded Tripolitza zone Eocene sediment has been heavily imbricated by thrust faults (Plate 7.4). The folding is along strike from the fold described above. Only five fault plane measurements were possible due to inaccessibility and no kinematic indicators are preserved. The GTZ outcrop is overlain by relatively undeformed sub-horizontal Pindos Zone Upper Jurassic and Cretaceous sediments that have not experienced the same folding and thrusting event. The observations indicate that the platform was folded and then cut by numerous intraplatformal thrusts with unknown displacement. Later, the Pindos thrust sheets were emplaced onto the already deformed Tripolitza platform.

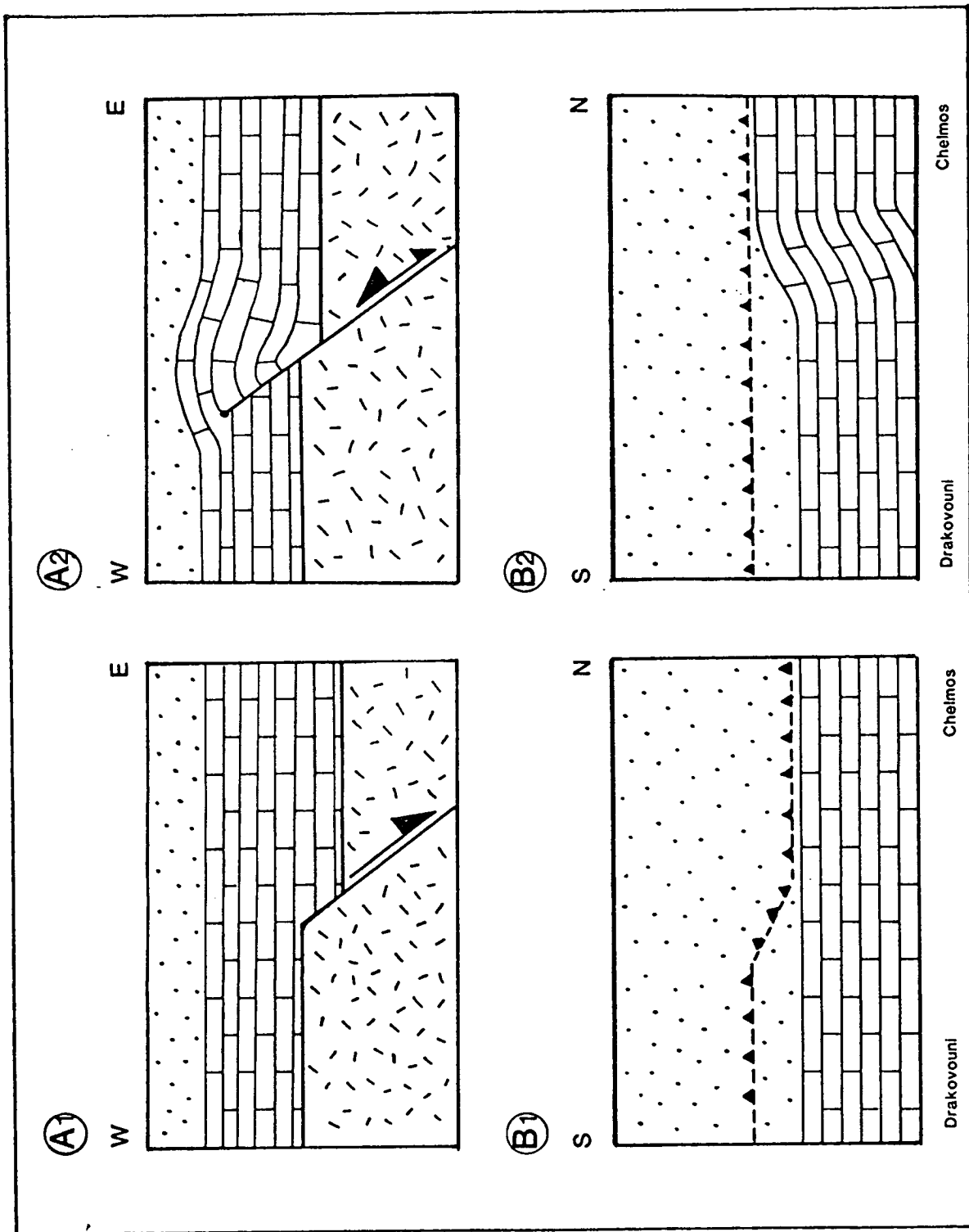


**Fig. 7.8** Schematic diagrams to indicate the inversion of a rift related extensional fault (A1) to form the Chelmos fold (A2) shown in Plate 7.4 and alternative explanations for the observation that the Pindos basal detachment is approximately 50m above the GTZ carbonate/flysch interface at Drakovouni but directly along the platform carbonates at Chelmos (B1 & B2, hangingwall sections). Explanation in text.

At Drakovouni (Figure 1.1), Eocene neritic carbonate is thrust onto Upper Eocene flysch sediments. This locality was described by De Wever (1975) and was mapped during this study (Figure 8.2).

#### 7.5.1.4 The Basal Pindos Thrust Horizon

At Chelmos, the basal Pindos thrust sheet is locally detached along the top of the Tripolitza platform with only a few centimetres of Tripolitza flysch present (Plate 7.4). At Elatophyton, 4 km further west, there is approximately 30m of flysch-like debris flow sediment intercalated between nummulitic Eocene neritic carbonate. At Drakovouni, approximately 20km to the south, 50m of Tripolitza flysch was observed overlying the platform (Plate 7.4). This compares with several hundreds of metres of foreland flysch structurally beneath the Pindos frontal thrust. The presence of structurally intercalated flysch at Elatophyton means that non-deposition of flysch at Chelmos was unlikely. Thus, there must have been a structural control causing the different stratigraphic level of the basal Pindos decollement. Either there was a north dipping lateral ramp through flysch sediment and the Chelmos area was later folded (Figure 7.8, B1.), or as is more likely, the platform at Chelmos was originally topographically higher than the Drakovouni area, forming a frontal ramp (Figure 7.8, B2). It is proposed that the Pindos thrust-sheet was transported over an already folded Chelmos area which caused frontal ramping. At Drakovouni to the south, the basal decollement was a thrust-flat within the flysch. The initial fold may have been of relatively weak amplitude. Between Chelmos and the Pindos front the basal decollement cut up-section to its present position.

#### 7.5.1.5 Post Emplacement Folding

The Chelmos region presently exposes the Tripolitza zone through a large tectonic window. It is best described in terms of a large pericline with the metamorphic core exposed beneath folded Tripolitza zone and Pindos Zone sediments. The large scale warping of crust to form this structure obviously post-dates the emplacement of the Pindos thrust sheets onto the platform as both Pindos and Tripolitza lithologies are grossly concordant with a common, folded, intervening thrust plane. The pericline is centred on the same locality as the pre-emplacment folding described above. It is reasonable to suppose that the Chelmos structure formed initially by basement fault reactivation with some folding prior to Pindos emplacement. The folding was then enhanced by longer wavelength warping, after emplacement of the Pindos thrust sheets, and was caused by continued thrusting as the Apulian margin was imbricated at deeper crustal levels on collision with the Pelagonian microcontinent.



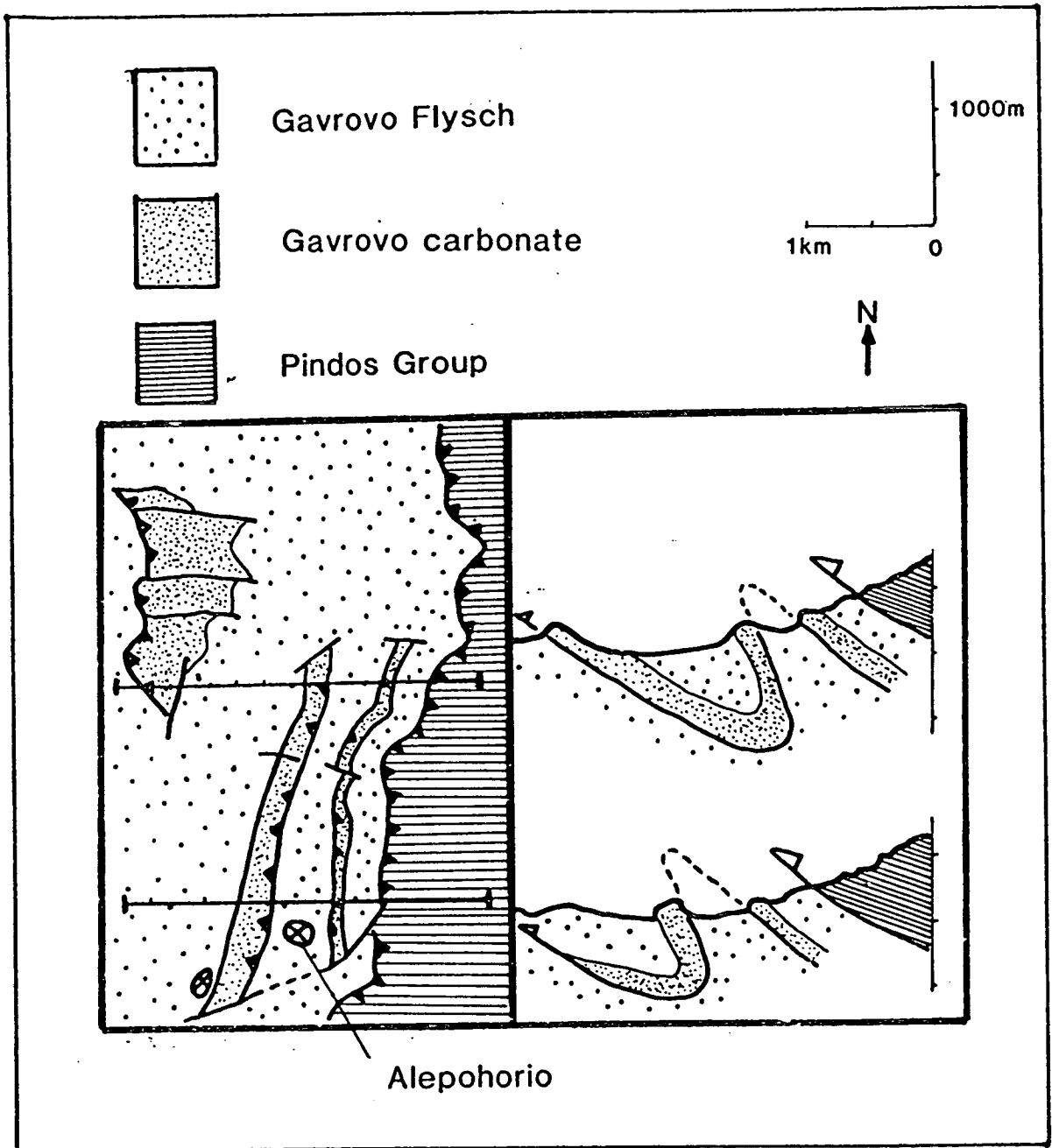


**Fig. 7.9** Simplified geological map and cross sections across the immediate Pindos foreland at Alepohorio showing the folding of an Eocene platform thrust sliver as proposed by Fleury (1980).

A similar structure is observed in the Jebbel Akhdar of Oman (Cooper 1986, Searle & Cooper 1986, Hanna 1990) the essential feature of which is the development of a culmination above a blind thrust in the basement, coeval with, or after, emplacement of the Hawasina nappes. This is considered a likely mechanism for the development of the Chelmos post-emplacement folding.

### 7.5.2 Foreland Deformation

In the foreland to the west of the Pindos front, several inliers of Gavrovo zone limestone are known (Dercourt 1964, Izart 1976, Fleury 1980). These are clearly thrust slices of the uppermost platform, detached and emplaced onto the Oligocene flysch deposits. Fleury (1980) has studied the facing directions of limestone immediately to the west of the Pindos front and has concluded that they represent an antiformally folded thrust slice (Figure 7.9).

Within the flysch itself there are several folds and minor thrusts that were taken into account during the construction of the measured section (Figure 7.6). The base of the log is at a major thrust detachment. Several large scale thrusts are known in the basin (Izart 1976).

## 7.6 DISCUSSION

### 7.6.1 Foreland Basin Model

The sedimentary and structural record of the Gavrovo-Tripolitza platform is integral to an understanding of the regional Early Tertiary tectonic history. It allows an accurate picture to be constructed illustrating the collapse of a carbonate platform and the transition to a foreland basin. The development of foreland basins has been modelled by many authors (e.g. Beaumont 1981, Karner & Watts 1983). Actualistic examples have been described from most orogenic systems (Allen & Homewood 1986). There are also examples of the transition of a platform to foreland basin from Tethyan regions. For example, several papers have been published detailing the flexural history of the Oman margin (Robertson 1987a,b, Patton & O'Connor 1988, Warburton *et. al.* 1990). Robertson (1987a,b) demonstrates how the Oman margin was uplifted and eroded in Turonian times due to forebulge uplift. Cratonward migration of the bulge was followed by submergence as the platform collapsed and this was accompanied by gravitational mass flows of limestone debris. The

subsequent foredeep was then filled with turbiditic siliciclastics. Maximum uplift (600m) is inferred for the platform edge. Alternatively, Paron & O'Connor (1988) suggest a maximum upwarp of 244m, corresponding to a more inboard palaeo-position, while Warburton *et. al.* (1990) use seismic and field data to show an essentially fixed, non-migrating forebulge located well into the foreland.

In northern Euboea, Robertson (1990b) demonstrates the development of an Early Tertiary foreland basin in response to loading from an advancing orogenic wedge formed above subducting Vardar Zone oceanic crust. On the Pelagonian platform, neptunian dykes, breccia and metalliferous sediments formed during the Maastrichtian. Collapse (possibly rift related) was accompanied by deeper water hemipelagic sedimentation. Later trench/margin collision is considered to have occurred in the Palaeocene/Eocene with the development of a foreland basin on an already submerged platform. The transition is not considered similar in this respect to the Pindos foreland basin development.

#### **7.6.2 Interpretation of Field Data: Platform Collapse**

Platform collapse is here inferred to have been due to the passage of a flexural bulge in advance of the Pindos orogenic front and foredeep depocentre. Such flexural forebulges have been established in the rock record (above references) and are predicted to be of variable amplitude depending on the elastic/viscoelastic properties of the lithosphere. In the shallow water shelf area of a carbonate platform, small amounts of uplift can lead to the development of hardgrounds and bauxite horizons, as seen in the Tripolitza and Gavrovo zone during the early Middle Eocene (Fleury 1980). More extreme and intense uplift could have resulted in the erosion of vast tracts of platform to expose Jurassic and Cretaceous horizons (Section 7.3.2.1) that were subsequently unconformably overlain by flysch sediments. The break-up breccia of monomict limestone is poorly constrained temporally, being composed of reworked clasts. The breccia is found at the inferred shelf-break, as given by the present-day structural and geographic position, and it is inferred to be the product of intense forebulge-generated denudation. Sudden deepening of the Tripolitza zone in the Middle to Upper Eocene records the migration towards the foreland of the forebulge, as does the Upper Eocene to Oligocene deepening seen in the Gavrovo zone.

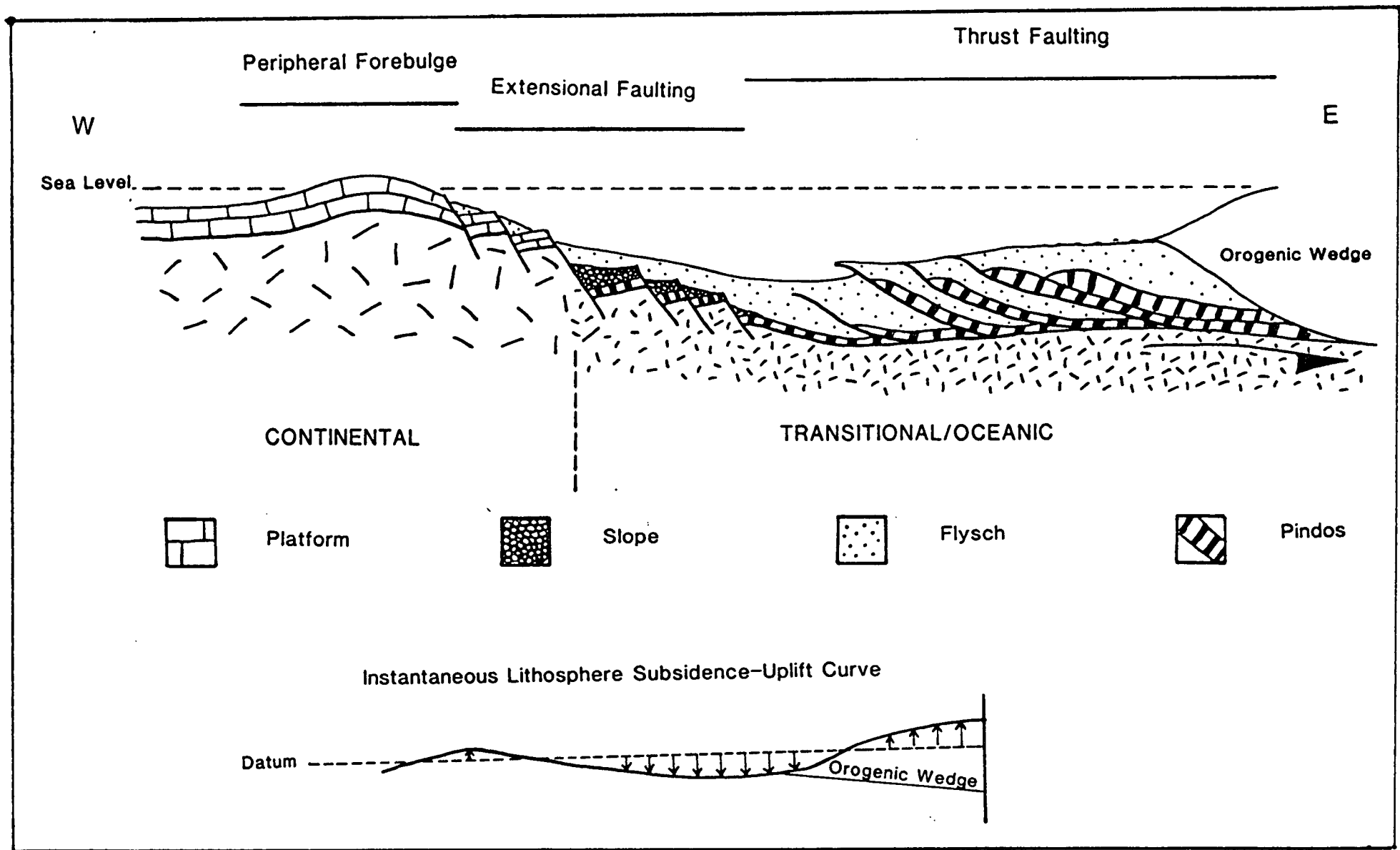


**Fig. 7.10** Proposed model for the collapse of the Apulian margin and the development of a peripheral forebulge (followed ultimately by the transition to a foreland basin) in response to lithospheric flexure ahead of the advancing Pindos/Pelagonnian orogenic wedge.

### 7.6.3 Migration of the Foreland Basin

On homogenous lithosphere a depocentre will migrate steadily and in tandem with the orogenic front. A simplistic Pindos/Gavrovo-Tripolitza foreland basin model is shown in Figure 7.10, however, the migration of the foreland basin was potentially complicated by two main factors.

#### 7.6.3.1 Continental Margin Palaeogeographic Control

The Pindos Flysch Formation was deposited conformably on sediments overlying transitional/oceanic crust (initially as a passive basin-fill, then as a trench deposit; Section 5.3.3) while the GTZ flysch was deposited on top of a collapsed shallow water platform, with many unconformities. The Pindos subduction-accretion complex was probably restrained for a time at the continental slope after the margin had collided with a poorly developed trench (Section 6.5.3). Prior to margin collapse the slope appears to have been a steep by-pass margin rather than a ramp, based on sedimentary evidence (Section 3.3.3.2). On collapse it is inferred that there was a distinct footwall topography to be surmounted by the Pindos thrust sheets. With sufficient compressive stress either the slope would imbricate by footwall collapse, or the Pindos thrust sheets would overthrust by frontal ramping. Both are seen to have occurred and, from the evidence in Section 7.5.1, footwall collapse preceded Pindos overthrusting, which was therefore a large scale out-of-sequence event. Prior to the overthrust, the Pindos orogenic load built up through back-rotation of thrusts and telescoping of sediments. Thus "over-loading" at the margin would initially lead to a deeper and narrower basin on the platform than would otherwise have occurred on homogenous lithosphere.

The effects of an irregular Apulian margin on the subsequent deformation of the Pindos thrust sheets are considered in Section 6.5.3. Lash (1988) demonstrates how an irregular margin can complicate the platform response to an approaching orogen in precisely the way inferred in this study, i.e. promontories would undergo uplift while lateral re-entrants would have relatively little lithospheric response initially. It is clear that along an irregular Apulian margin, there would theoretically be areas of coeval uplift and subsidence along strike, parallel to the orogenic front. This would undoubtedly mean the erosion of elevated areas with sediment deposition in adjacent, topographically lower regions along the continental margin during platform collapse.

### 7.6.3.2 Continental Basement Structural Control

Most foreland basin sediments are assumed to have been deposited diachronously according to the foreland onlap model (Allen & Allen 1990), with migration of the locus of sedimentation equal to the propagation rate of the thrust tip. This is probably an oversimplification for the Pindos foreland basin on the platform as although a "flysch blanket" covered the Ionian Zone and the Gavrovo zone, thick proximal deposits do not appear to have been deposited on the Pre-Apulian Zone (Clews 1989). A possible explanation involves reactivation of pre-existing weaknesses in the Ionian Zone that may have compartmentalised the ensuing flexural basin. Once the main depocentre coincided with the Ionian trough, the basin may not have migrated any further. This would have led to the gradual narrowing of the basin with time as the Pindos orogen migrated to its present position. Turcotte & Schubert (1982) show how, for a fractured plate with a small effective elastic thickness, the width of a foreland basin is narrower than for an unfractured plate of otherwise similar characteristics.

### **7.6.4 Palaeocurrent Orientation**

Palaeocurrent measurements from the flysch of the GTZ in the Peloponnese are recorded by Izart (1976) as dominantly from north to south and from east to west. Several palaeocurrent measurements from Alepohorio also demonstrate north to south palaeoflows. Leigh (1991 and pers. comm. 1989) has measured several hundred palaeocurrents north of the Gulf of Corinth dominantly showing south to north palaeoflows. There was obviously a point source approximately located in the Gulf of Corinth area supplying detritus. Major fluvial systems are often developed in structural lows and hanging wall re-entrants due to transverse faulting (Allen & Allen 1990) and it is suggested that the Gulf of Corinth point-source drainage feature may have been related to a pre-existing basement lineament.

## **7.7 CONCLUSIONS**

The basement to the GTZ is a structurally distinct unit of Late Palaeozoic and Early Mesozoic sediments and volcanics that have undergone pumpellyite-actinolite metamorphism. The protolith was most probably air-fall tuff, tholeiitic basalt and basaltic andesite, petrogenetically related to the igneous lithologies of the TSM. Above the basement is an evaporite horizon that acted as an effective structural

detachment with the overlying thick platformal sequence of Triassic to Upper Eocene age. It is likely that there was limited tectonic activity on the platform in the Jurassic and Cretaceous. From the Middle Eocene onwards, normal faulting was initiated both parallel and perpendicular to the margin, as a peripheral forebulge developed on the platform. This led to differential uplift and subsidence and was caused by thrust sheet loading as the Gavrovo-Tripolitza platform approached the Pindos subduction-accretion complex due to the eastward subduction of intervening oceanic crust. The faulting was especially concentrated along the shelf-break and copious amounts of locally derived breccia were deposited.

The peripheral forebulge migrated towards the foreland and rapid subsidence of the outer platform followed, resulting in the deposition of turbiditic sandstones and shales in a basin formed by lithospheric flexure. This was diachronous across the collapsed platform, Middle to Upper Eocene in the Tripolitza zone, and Upper Eocene to Oligocene more inboard in the Gavrovo zone. The flysch sediment was mostly supplied axially but was also derived from the Pindos orogen to the east.

As the Pindos thrust sheets impinged on the continental margin they were restricted by a collapsed slope buttress. This allowed the transmission of west-directed compressive stresses into the platform causing first folding and then thrust faulting. After this deformation, the Pindos thrust sheets ramped up the variable footwall slope and a basal detachment formed along the platform-flysch interface in the Chelmos area, which at the time was a relative high. Along strike at Drakovouni there was a basal thrust flat approximately 50m above the platform-flysch contact.

The emplacing thrust sheets cut up-section through the flysch. In the foreland, thrust slices from the top of the platform were detached and thrust onto Oligocene flysch. These inliers rose to near the sea surface allowing colonisation by neritic organisms. Debris-flows and rock falls were shed backwards into a thrust-sheet top basin. In addition mixed sediment was periodically supplied from the approaching orogenic front.

After the emplacement of the Pindos nappes during the Oligocene, full continental collision between the Pelagonian microcontinent and Apulia, possibly in the Early Miocene, led to broad scale crustal warping and potentially to blind thrusting involving the underlying basement.

## PLATES

### PLATE 7.1: GTZ Metabasite Electron Image and Map

A backscattered electron image and map of the analysis points from sample PD/89/324, a pumpellyite/actinolite metabasite of the Aghios Ilias Eruptive Formation.

### PLATE 7.2: GTZ Foraminifera

(A) *Alveolina* sp. within a clast in the GTZ conglomerates. The fauna indicate an age no younger than Middle Eocene (probably Lower Eocene). Field of view 10mm. (B) Abundant Eocene *Discocyclina* sp. and red algae from the GTZ platform. Field of view 10mm. (C) *Nummulites* sp. of Lower to Middle Eocene (?) age. Field of view 15mm. (D) A clast within conglomerates of the GTZ foreland basin includes a diverse faunal assemblage including *Discocyclina* sp., *Actinocyclina* sp., *Nummulites* sp. and planctonic foraminifera of Upper Eocene age. Field of view 10mm.

### PLATE 7.3: GTZ Conglomerate Facies

(A) Clast supported, sub-rounded conglomerate with clasts of micrite or carbonate grainstone. (B) More matrix-rich conglomerate, very poorly sorted and containing sub-angular to sub-rounded clasts of limestone. (C) Poorly consolidated, matrix supported oligomict conglomerate with an over-printed shear fabric. (D) Poorly consolidated pelitic conglomerate with abundant angular sandstone and limestone clasts. (E) Well cemented channel of clast supported conglomerate within pelitic flysch beds, developed near the transition to the conglomerate facies. (F) Base of an extremely large channel infilled by well cemented clast supported limestone conglomerate. Underlying bed is matrix supported oligomict containing limestone and sandstone clast components.

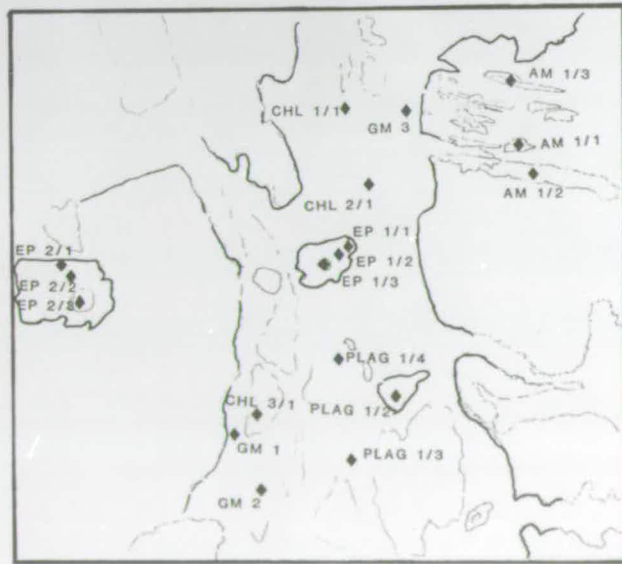
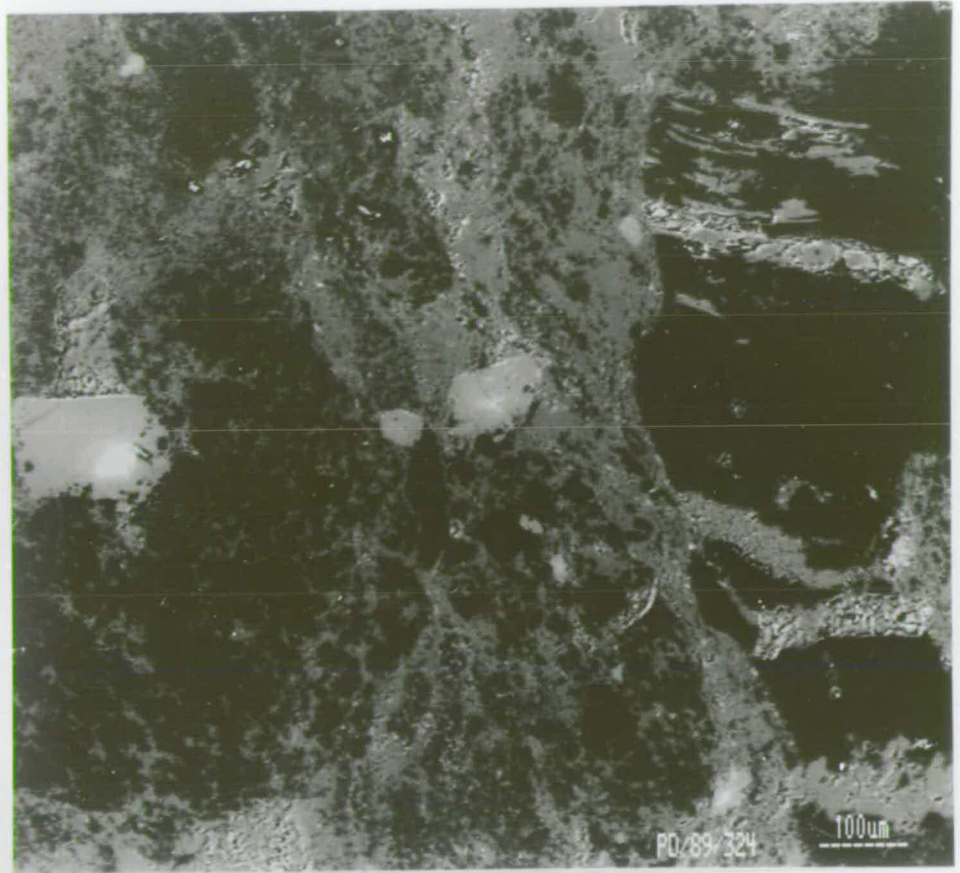
### PLATE 7.4: GTZ Structures

(A) Large fold developed in the platformal limestones at Chelmos. The geometry and close proximity of the fold to a neotectonic normal fault (Trace seen in the left of photograph) suggest the possible reactivation of Triassic extensional faults; explanation in text. Cliff section c.a. 300m high. (B) Intense folding and thrusting is recognisable in the GTZ platform at Chelmos. The top of the neritic sequence is a planar thrust contact with over-lying Pindos lithologies emplaced onto the already deformed platform. Cliff section c.a. 350m high. (C) In the area of Chelmos, the principle thrust surface between the Pindos and GTZ lithologies detaches along the top of the carbonate platform, seen here dipping east at c.a. 30°. (D) In the area of Drakovouni, 20Km to the south, 50m of Tripolitza zone flysch overlies the platform carbonate. Explanation for structural consequences in the text.

⊕ Arrowed



# PLATE 7.1



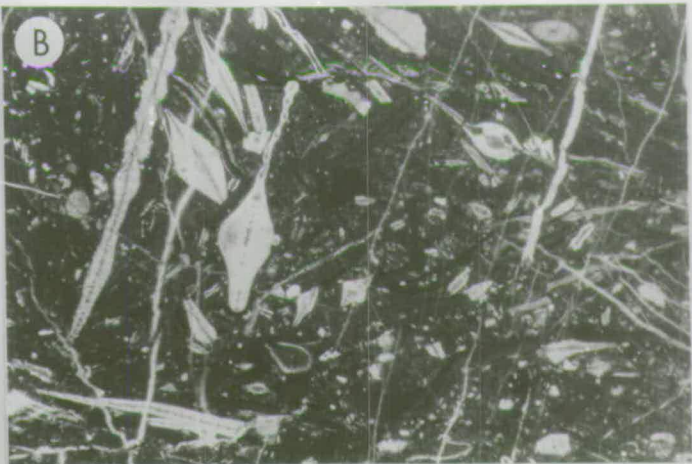
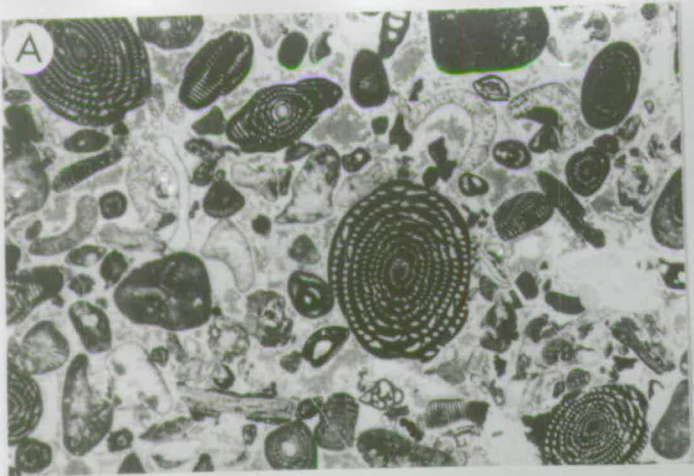
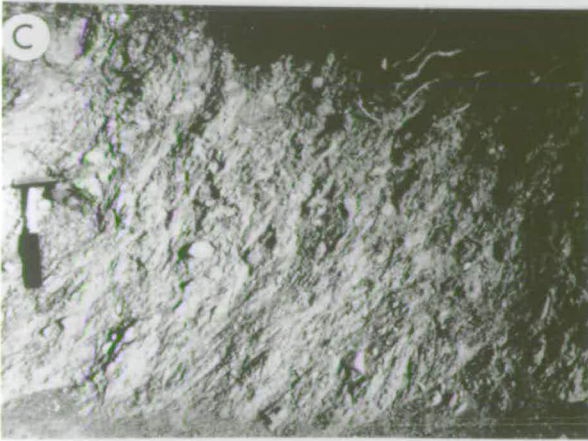
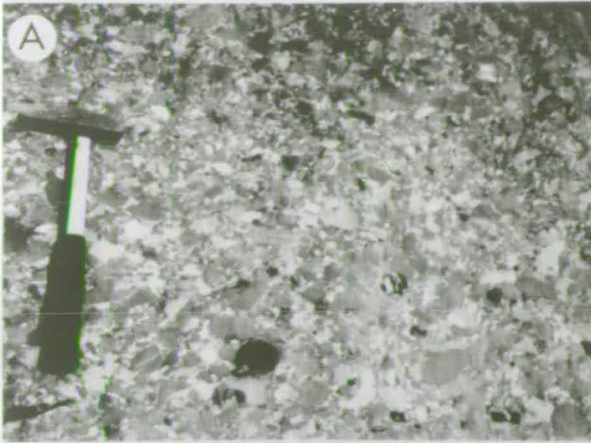




# PLATE 7.3





## CHAPTER 8: TECTONO-SEDIMENTARY MELANGE

### 8.1 INTRODUCTION

In this chapter the geological setting of several melange outcrops in the Peloponnese will be discussed. Melange fabrics are described and interpreted in the context of the thrust regime established in Chapter 6. A detailed study of the igneous rocks present in the melange uses petrographic and geochemical data to help elucidate the early development of the Pindos Basin, and a model of rift magmatism is inferred.

Melange has been defined as "a mappable, internally fragmented and mixed rock body containing a variety of blocks, commonly in a pervasively deformed matrix" (Silver & Beutner 1980). Greenly (1919) was the first to use the term melange for deformed, olistostromal deposits of the Gwna Group, Angelsey. Thus, there is historical precedence for using "melange" to describe a chaotic sedimentary unit. Hsu (1974) preferred a purely tectonic definition for melange and contrasted this with olistostromes, while Raymond (1984) states that the term is applicable to mixed rock units of a sedimentary, diapiric and/or tectonic origin. It is commonly accepted that melange conforms to the loose definition of Raymond (1984), however, more restrictive terminology is useful, thus Rast & Horton (1989) distinguish olistostrome, for solely sedimentary melange formation, from olistostromal melange, in which both sedimentary and tectonic deformation is involved.

Within the study area, several outcrops are found where a variety of deformed lithologies are recognised, conforming to the loose definition of melange. The assemblages include extrusive and hypabyssal igneous rocks, debris flows, turbiditic sandstones and various sediments of the Pindos Group, Gavrovo-Tripolitza Zone and of unknown derivation. The melange is found at the base of Pindos thrust sheets, where the Pindos Group tectonically overlies the Gavrovo-Tripolitza Zone, and also locally intercalated within the Pindos thrust stack. There is a strong tectonic fabric, characterised by the layer-parallel extension of rock bodies. Certain features indicate that mass flow sedimentary processes produced a degree of rock mixing. Thus, the melange is considered to be primarily the result of tectonic deformation, but also of subordinate sedimentary processes and is here termed a tectono-sedimentary melange (TSM).

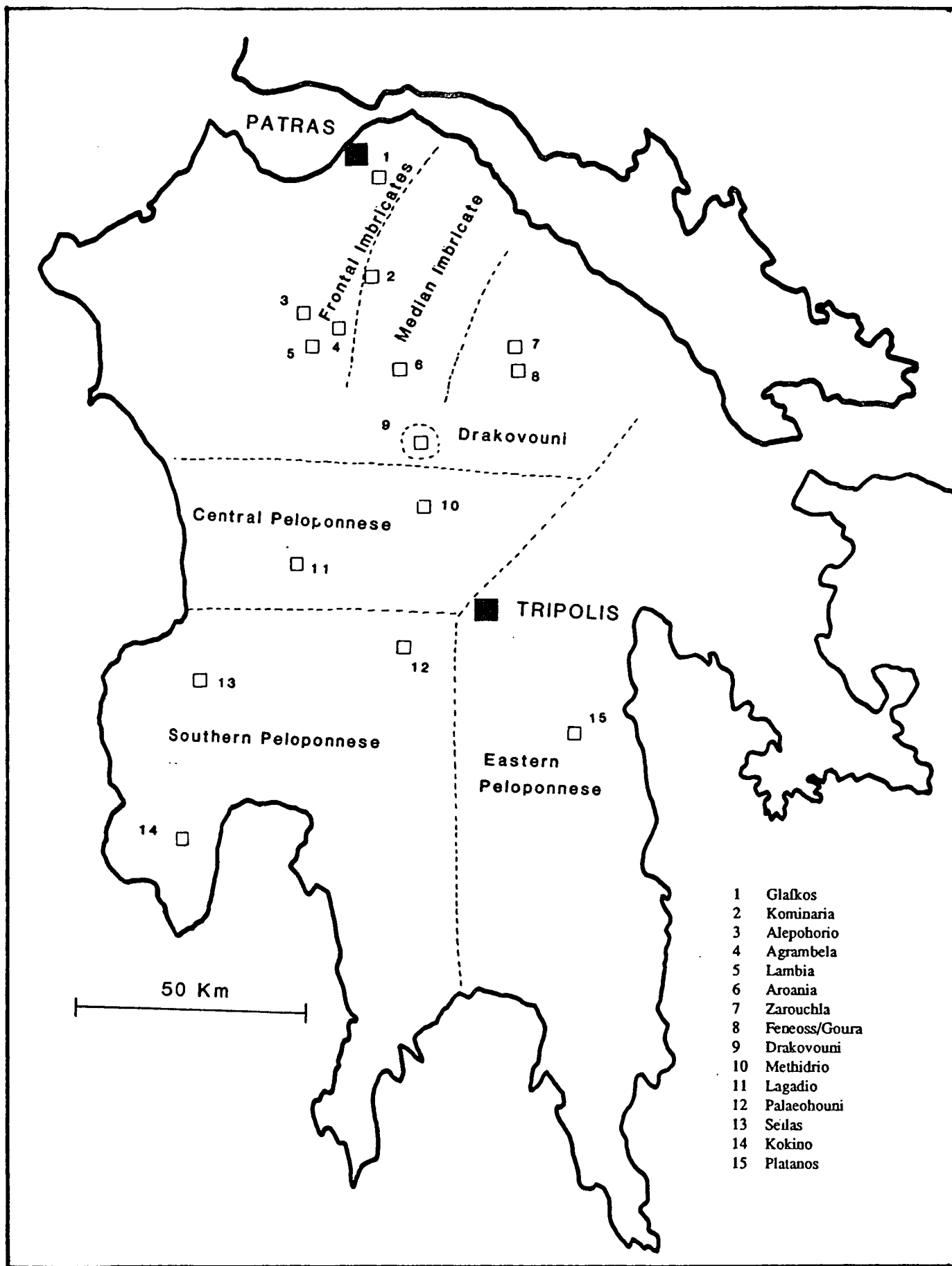


**Fig. 8.1** Locality map of sites where igneous rocks were collected for analysis.



## 8.2 TSM GEOLOGICAL SETTING

The presence of melange has been reported from a number of localities in the Peloponnese (De Wever 1975, 1976a,b, Richter & Lensch 1977, 1989, Pe-Piper & Piper 1984, 1990). De Wever (1975) was the first to recognise the tectonic setting of the TSM, while Richter & Lensch (1977, 1989) describe (in German) the petrography of extrusive rocks from several outcrops. They initially considered the rocks to be ophiolitic and of Lower Cretaceous age. Pe-Piper & Piper (1990) used XRF data to postulate the formation of arc-related volcanism in a back arc basin, related to the southward subduction of Palaeotethys.

Because of the apparent uncertainty in the tectonic setting of the igneous rocks, and the potential for better understanding the development of the Pindos Basin, it was decided to document the field settings of the TSM sites and to establish an independent database of igneous geochemical analyses. Figure 8.1 indicates the localities where samples of igneous rocks were taken.

### 8.2.1 Drakovouni

Drakovouni is the most extensive area in the Peloponnese where the TSM is observed (Figure 8.1). The locality was first described and mapped by De Wever (1975). An independent map was constructed during this study (Figure 8.2). Near the village of Kerpini, Upper Eocene Tripolitza flysch is seen in depositional contact with the underlying Tripolitza carbonate platform (Plate 7.4). The flysch is coherent for approximately 50m before bedding becomes severely disrupted, resulting in a "broken formation" (definition after Hsu 1974), and continues upwards into a chaotic pelitic unit containing floating blocks of sandstone. There are many faults present, notably neritic carbonate is observed overthrusting the Tripolitza flysch in the Paos stream bottom. Other faults, e.g. the south-eastern TSM boundary, are high angle normal faults downthrowing the TSM against the Tripolitza zone carbonate. Locally, radiolarian cherts of the Pindos Zone overlie the TSM. Thus the melange is clearly located between the top of the Tripolitza zone flysch and beneath the Pindos Group.

The Tripolitza flysch grades into the TSM, which is here between 50 and 100m thick. Near the top of the TSM, a 20m thick horizon consists mostly of sheared pelite, sandstone and matrix supported conglomerate of Tripolitza platform origin.

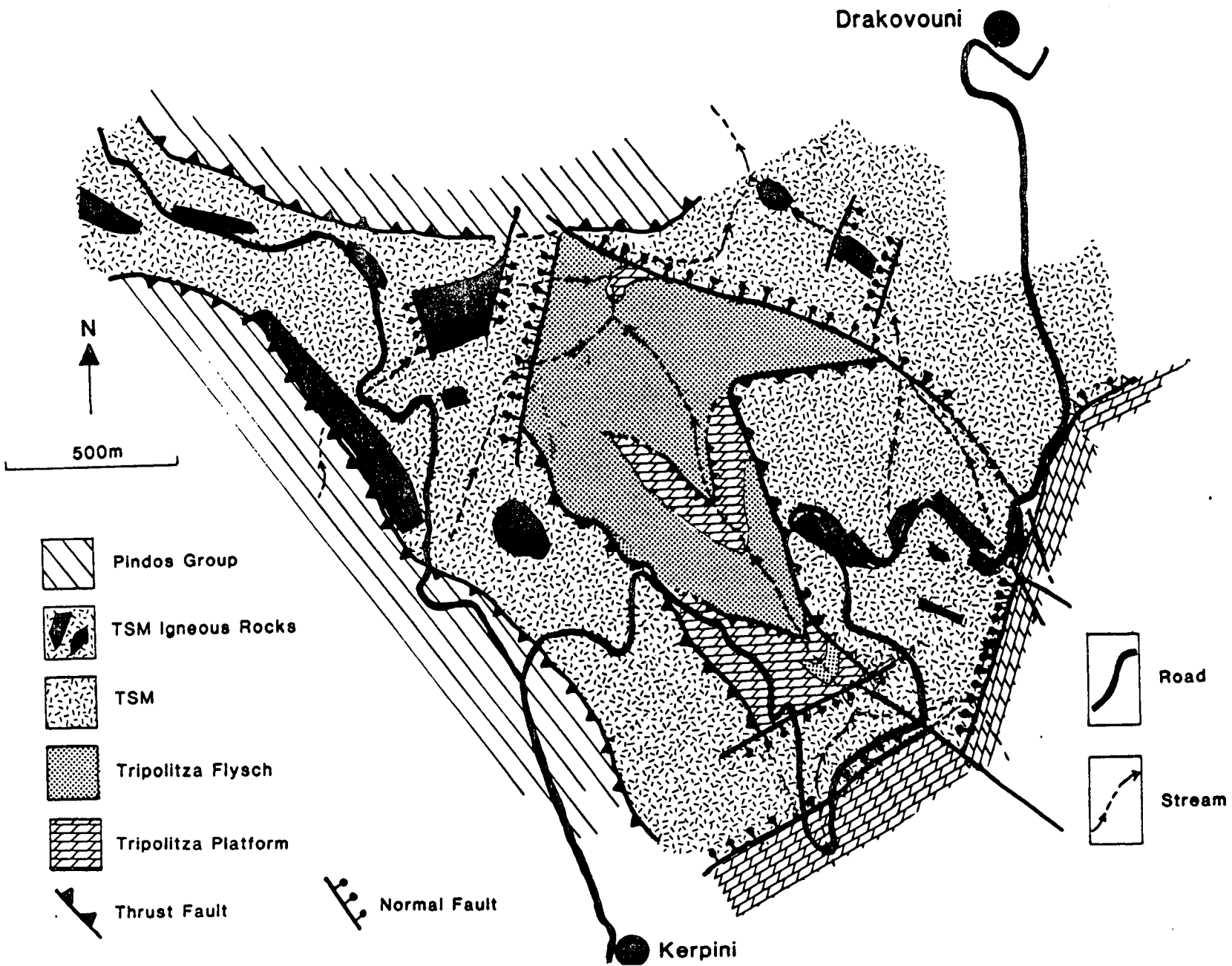


Fig. 8.2 Geological map of the TSM outcrop in the area of Drakovouni.



Above is a horizon, approximately 30-40m thick, in which clasts are found floating in a phacoidal pelitic matrix. The clasts range from gravel grade to 30x30x10m. Mostly the blocks are of decimetric size and are phacoid shaped sandstone (Section 8.3.1), but many large, metre-scale igneous blocks are also observed (Plate 8.1). The igneous blocks are purple/violet to black, aphyric, sometimes with calcite filled amygdalae. Most of the blocks are rounded and some may be pillows. Cracks are seen, possibly representing inter-pillow interstices, infilled with pelagic sediment (attempts at faunal extraction were unsuccessful). Hydrothermal calcite and celadonite is also present within some cracks. Outcrops of pyroclastic tuff, agglomerate and lava conglomerate are also present and are found directly below Pindos radiolarian chert in some cases, where it appears as if there might be a depositional contact, although this is not proven.

An important fault bounded outcrop was found where a dolerite (PD/90/464 & 465) could be traced up into basalt, overlain by tuff and volcanoclastic conglomerate. The eastern boundary of the dolerite is a high-angle, NNE-SSW trending normal fault, down-throwing an unidentified (presumed GTZ) limestone-bearing pelitic sediment of the TSM against the igneous rock. This sediment is itself downfaulted further east against GTZ flysch. Towards the west the dolerite passes up into basalt, tuff and volcanoclastics. The coarse igneous lithology consists of a green weathering rock with randomly orientated phenocrysts of feldspar, up to to 3x1cm in size. Near the transition to a finer grain size, a patchy pattern suggestive of partial remelting of the feldspar phenocryst-bearing rock, was seen (Plate 8.2 & Section 8.4.1.2). Passing upwards, grain size becomes progressively smaller until, at the transition to the tuff and volcanoclastic sediment, it is not possible to differentiate igneous from very fine grained pyroclastic lithologies in the field. Green (1982) describes a sill of dolerite near the village of Moschophyton, north of the Gulf of Corinth, intruding *Halobia*-bearing carbonate rocks and with chilled margins. No unambiguous chilled margins were noted at Drakovouni, but it is suggested that the Drakovouni dolerite outcrop represents a similar high crustal level sill.

Large phacoids (greater than 5m<sup>3</sup>) of sedimentary lithologies are found in the melange and these comprise: (1) Pindos Group Kataraktis Passage Member limestone with black cherts. (2) undated, similarly sized blocks of pelagic limestone (Plate 8.1). (3) Large irregular blocks of platform derived sub-angular to sub-rounded matrix-supported conglomerate, containing *Alveolina* and *Nummulites*

(Plate 8.1). (4) A block of shallow marine limestone, heavily recrystallised but containing neritic fauna.

Amongst other sedimentary blocks, usually of fist size, the following were found:-

(1) *Halobia*-bearing black micritic limestone. (2) 1-2cm scale alternating bands of green and purple siliceous, fine-grained limestone. (3) Black chert. (4) Grey micrite (5) Blue-grey calcareous grainstone with micrite top (or base?). (6) Red and yellow hydrothermally stained jasper with distinctive "wavy" mm-scale laminations. (7) Green vitreous chert. (8) Sub-angular quartzose breccia. (9) Recrystallised calcareous, gravel grade limestone breccia. (10) Dark, bituminous limestone. (11) Hard, dark grey siliceous calc-grainstone.

## 8.2.2 Central Peloponnese

### 8.2.2.1 Methedrio

Near the village of Methedrio, a flat-lying thrust sheet, with radiolarian-bearing cherts of the Aroania Chert Member, overlies flysch sediment of the Gavrovo-Tripolitza Zone. The zone of detachment is represented by a typical melange outcrop of igneous and sedimentary lithologies. Many of the rock bodies have slickensided surfaces, attesting to the intense shearing and deformation necessary to create chaotic outcrop. Sedimentary lithologies include matrix-supported conglomerate (with clasts of neritic limestone, micritic limestone and black chert), phacoids of sandstone (rich in mica and carbonaceous fragments) and isolated blocks of recrystallised grainstone carbonate, all found in a sheared pelite matrix. Disrupted beds of volcanic breccia are present with clast sizes up to 3x2cm. Some of the clasts have a strong pumice texture. Igneous blocks are mostly dark and aphyric, some possibly pillow lava, while violet and purple amygdaloidal lava blocks are also present.

### 8.2.2.2 Lagadio

Pink micritic limestones, probably of the Paos Limestone Member, overlie flysch sediments of the Gavrovo-Tripolitza Zone. The contact is poorly exposed because of much loose surficial sediment, but isolated blocks of igneous rocks and conglomerate are found at the presumed thrust contact. The largest igneous block (2x2x1m) is a purple, amygdaloidal lava. Several blocks are found in recent scree deposits further down slope.

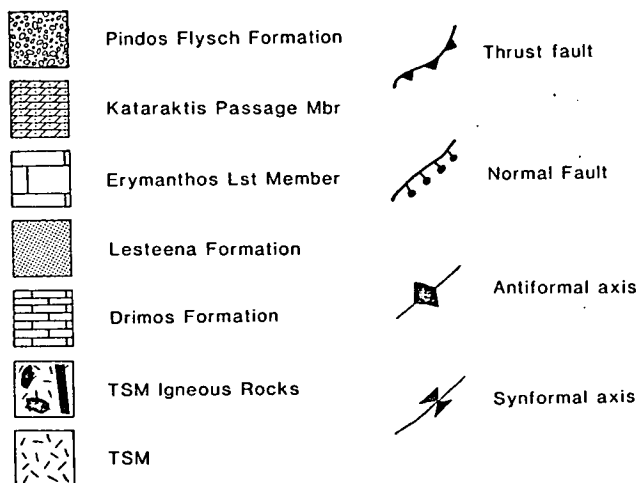
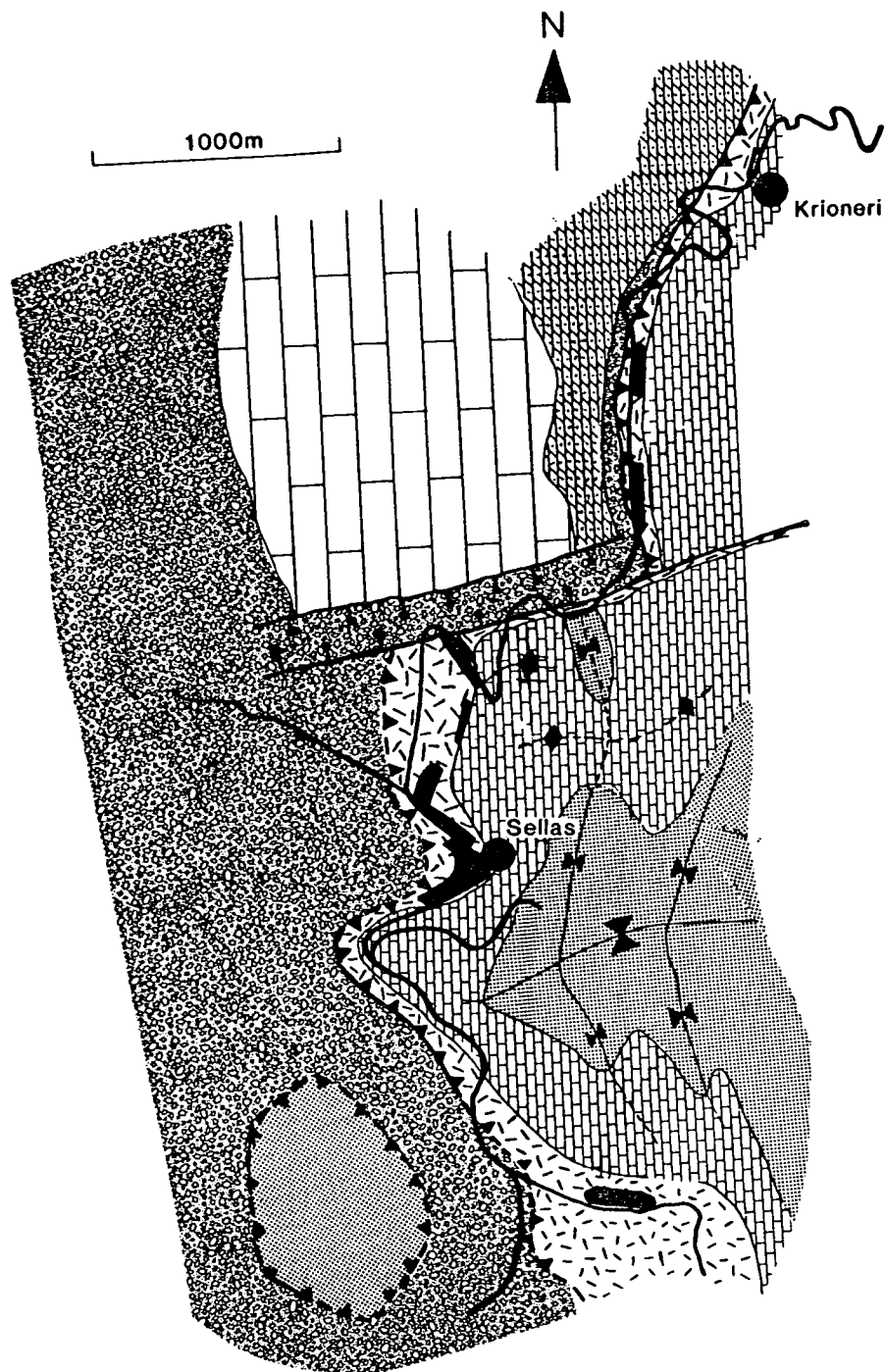


Fig. 8.3 Geological map of the TSM outcrop in the area of Sellas.

### 8.2.3 Southern Peloponnese

#### 8.2.3.1 Sellas

In the southern Peloponnese, to the east of Kyparissia, volcanic lithologies are found at the base of the Pindos thrust sheets between the villages of Sellas and Krioneri. The area was mapped (Figure 8.3), with the best exposure of igneous lithologies being found on the road between the two villages and around Sellas. The rocks are generally highly altered blocks of lava in a sheared red mudstone matrix, or within pyroclastic tuff deposits. Near Sellas the lava resembles pillow lava, with rims of hydrothermal calcite and celadonite. Fresh specimens were taken from the cores of the pillow structures and the surrounding tuff, which was found to contain zeolites. The total lava thickness observed is never more than 3m. Clear contacts are not seen with the underlying lithologies, which are fine- to medium-grained turbiditic sandstone with abundant mica and carbonaceous plant fragments. This lithology is correlated with the Tertiary Pindos Flysch Formation, rather than the Triassic Priolithos Formation. The lava is therefore interpreted as being at the base of thrust sheets rather than intercalated within contemporary turbiditic sandstones. Upper contacts, above the lava, always consist of sheared green to red pelite. Above this, without exception, micrites and grainstones, some *Halobia*-bearing, were found. A thin series of red cherts is present in the limestone and the sequence is assigned to the Drimos Formation, as described in Chapter 3. Thus, the lavas are stratigraphically below the Drimos Formation, and of Middle to Late Triassic age. This is not in accord with the field setting described by Pe-Piper & Piper (1990) who state that the igneous lithologies are stratigraphically below Jurassic radiolarite of the Aroania Chert Member.

#### 8.2.3.2 Kokino

In the southern Peloponnese, west of the village of Kokino (Figure 8.1), a thrust sheet of Drimos Formation limestone overlies turbiditic pelites and siltstones with subordinate sandstones of the Pindos Flysch Formation. At the base of the thrust sheet, over 20m of volcanic rocks and volcanoclastics are exposed. The lowermost 12-15m of the extrusive rocks are competent, relatively undegraded lavas. There is evidence for the presence of sills, with well-defined cooling joints, intruded into pillow lavas and with hyaloclastite basalt breccia filling interpillow interstices. Above this intact lava sequence, a sheared horizon of lava breccia passes upwards into volcanoclastic muds. Pink *Halobia*-bearing thin limestones are found towards the top of the breccia and intercalated within the pelite. These limestones were

deposited coevally with the volcanoclastics and are not sheared-in. Above the purple volcanoclastic muds, regularly bedded *Halobia*-bearing hemipelagic, and calciturbidite, beds of the Drimos Formation were deposited (Plate 8.2). The calciturbidite is coarse arenite to gravel grade and contains reworked basalt in minor quantities. At 8m above the volcanoclastic-Drimos Formation interface, there are several decimetric interbeds almost totally composed of locally derived volcanic breccia.

#### 8.2.3.3 Palaeohouni

The TSM at Palaeohouni (Figure 8.1) is found on the main Kalamata to Tripolis road, with the best exposure in, and around, a stream cut to the south of the road. The TSM consists mainly of lava and volcanoclastic conglomerate. It is found at the base of an Erymanthos Limestone Member thrust sheet, below a 2-5m thick radiolarian chert horizon at the base of the thrust sheet. There is a detachment surface composed of sheared tuff and mudstone between the overlying Pindos Group rocks and the volcanic sequence. Because of the tectonic contact, an age cannot be assigned to the volcanics of this locality. The complete thrust sheet, including volcanics, overlies pelites and sandstones of the Tripolitza zone.

In the stream cut, volcanoclastic conglomerates of sub-rounded to rounded, cobble grade are found within a green volcanoclastic pelite matrix. Intercalated is a thick (30-40cm) horizon of black, aphyric lava (Plate 8.2). The volcanoclastic sediment infills depressions on the underside of the lava and does not have chilled margins. Thus, this is considered to be an inverted sequence, although the evidence is not conclusive. Overlying the conglomerates are volcanoclastic mudstones and siltstones, with parallel laminations and scoured channel bases, which indicate that they are the correct way-up and the result of high-energy current deposition.

On the north side of the road and further downstream, loose blocks of purple-blue, slightly vesicular and aphyric lava is found, sometimes with celadonite and hydrothermal calcite margins. In the excavated foundations of a house, spheroidally weathered blocks of lava, severely degraded, are observed (Plate 8.2).

#### **8.2.4 Eastern Peloponnese**

Approximately 15km SE of Astros, near to the village of Platanos, blocks of lava and radiolarian bearing cherts and mudstones are found entrained at the base of an

Erymanthos Limestone Member thrust sheet that has overthrust turbiditic Tertiary shales and sandstones of the Tripolitza zone.

Near the road, aphyric non-vesicular and amygdaloidal lava is observed forming an approximately 10m long, 3-4m wide zone. It is interpreted as a tectonic slice at the base of the Pindos thrust sheet. The lava is mostly spheroidally weathering.

The main TSM outcrop is found further south, following the base of the thrust sheet, and comprises degraded lava, similar to that described above, at the base of a radiolarian chert section. There is evidence for metasomatic mineralisation along joint planes, shown by patchy silicification and secondary mineralisation, possibly of fine chalcedony.

### 8.2.5 Other localities

The TSM is widely exposed in the area around Chelmos Mountain. From the village of Arboynas, SE towards Likoria (Figure 1.1) and east towards the head of the Elatophyton valley, a roughly planar melange zone is observed as shown on the field map of Figure 7.7. The TSM lies directly above Eocene platform carbonates of the Tripolitza zone. Near Arboynas the uppermost Tripolitza zone dolomitic limestones have been heavily tectonised and a leaching process is apparent. Consequently the rocks have a "dusty" tectonite texture; they are pale, soft and are easily weathered. This horizon is generally 20 to 30m thick and indicates that locally, the Pindos thrust sheets were emplaced directly onto the platform, with hydraulic fracturing and the alteration of platform rocks due to tectonically induced high pore pressure. The TSM is between 6 and 20m thick, and consists of green pelite with a phacoidal fabric, subordinate flysch-type sandstone, red chert and red pelite. Blocks of calciturbidite (of unknown age), up to 15x10x10m are also found floating in the matrix. In the SE of the TSM "corridor" an approximately 100m long area was discovered with abundant rounded blocks of amygdaloidal, purple lava. Similarly, at the head of the Elatophyton valley, a small outcrop was discovered of purple, amygdaloidal pillow lavas. Above the TSM, Erymanthos Limestone Member and Aroania Chert Member lithologies are found.

Below the village of Elatophyton, the Pindos thrust overlies Eocene platform carbonates and debris flow deposits; a TSM zone is largely missing. Instead, a chaotic broken formation of radiolarian chert of the Lesteena Formation is present.

On the eastern side of Chelmos mountain, 1km NE of the village of Goura (Figure 8.1) a poorly exposed, 20m<sup>2</sup> outcrop was found where two types of igneous lithology were exposed. Purple, amygdaloidal lava blocks of fist size, and similarly sized light green aphyric igneous rocks are found in a sheared green pelite. The geological setting is uncertain as no boundaries could be observed. The outcrop is flat-lying and at the inferred base of the Pindos basal thrust, which has been eroded-away locally. Alternatively, the volcanics could belong to the Gavrovo-Tripolitza Zone basement (Aghios Ilias Eruptive Formation, De Wever 1975) described in Section 7.2.2 .

Above the village of Likouria, an outcrop consisting of 2m-thick blocks of lava-breccia and tuff is present. The outcrop is situated at the base of the Pindos thrust and is overlain by cherts of the Aroania Chert Member. The northern boundary is a south-dipping lateral ramp of Tripolitza zone carbonate.

At all the above TSM localities, volcanic rocks are found at the juncture of the Pindos Group and the Tripolitza zone. Extrusive rocks, from detachment horizons between thrust sheets involving only Pindos lithologies, are also found in the NW Peloponnese (Figure 8.1) at Glafkos, Alepohorio, Agrambela, Kakotari, Lambia, Aroania and Krinofta. At all these locations the TSM is much reduced in thickness and phacoidal fabrics are generally less well developed.

#### **8.2.6 Jurassic Chert Association**

In the NW Peloponnese, igneous rocks are found beneath Upper Jurassic radiolarian cherts of the Aroania Chert Member. This setting contrasts with the igneous/chert relation of areas described above, where a depositional contact is unproven due to intense deformation. The field setting of the two major localities, Aroania and Kombigadi is described in Section 4.5.2. Volcanic blocks are also found below Aroania Chert Member rocks between Platanitsa and Ano Vlasia. A depositional contact is not totally clear in this case, and the igneous lithologies may instead represent undated lavas from the TSM entrained along the basal Pindos thrust.

## 8.3 TSM FABRIC STUDIES

### 8.3.1 Fabric Descriptions

The TSM is dominated by a pelitic matrix, within which various sedimentary and igneous blocks are found. The most obvious aspect of the TSM is a phacoidal fabric (Plate 8.1). This is an intense deformation fabric present in the pelitic matrix as two dominant sets of sub-parallel shear bands. The two sets are formed at approximately 60° to one another (acute angle) and create decimetric, to several metre-wide, criss-crossing arrays of shear zones containing rhombohedral domains (Plate 8.1). On a smaller scale (millimetre to a few centimetres), anastomosing fabrics are seen within the pelite, forming a cleavage parallel to one or the other main set of shear bands.

Within the sheared matrix are usually found competent blocks of various sizes comprising sandstone, pelagic/calciturbiditic limestone, debris flow deposits and igneous lithologies. The sandstones and pelagic/calciturbidite limestones form blocks that are either diamond shaped or slightly sigmoidal. Such lenticular bodies are generally symmetrical. Upper and lower bounding surfaces are almost exclusively bedding planes, to either a single bed, or series of beds. The bedding plane surfaces are usually parallel to the dominant shear zones in the pelite. Frontal and rear surfaces of the competent blocks are at about 60° to the bedding.

Within the Drakovouni melange, a block consisting of several limestone beds, with bedding parallel chert horizons, was observed in the pelitic matrix. Normal faults were seen to be dissecting the beds into the typical phacoidal shape. Bedding parallel slip is developed along several bedding planes with displacement transferred to lower bedding planes via normal faults that cut across bedding. The normal faults are at approximately 60° to the dominant shear zone, while the bedding planes are parallel to it (Figure 8.4). Thus, there is clear evidence from the field that the phacoidal structures are formed by the layer parallel extension of competent rock bodies. Such boudinaged beds became successively strung out until they were totally separated from parent blocks, and with time and extensive movement, a chaotic assemblage of varied rock types can be juxtaposed.

The igneous and debris flow blocks of the TSM are often rounded, rather than being phacoidal. This may indicate (a) the sedimentary reworking of the lithology as a clast, (b) the weathering of the block prior to inclusion in the matrix, or (c) tectonic erosion. It is considered that (c) is most likely.

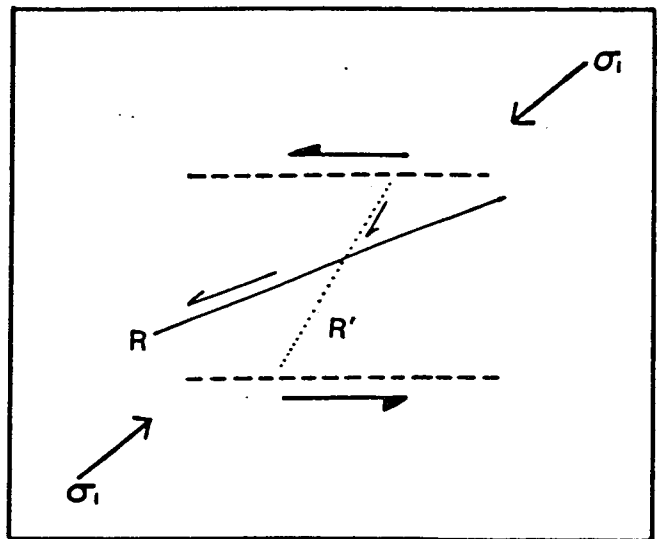
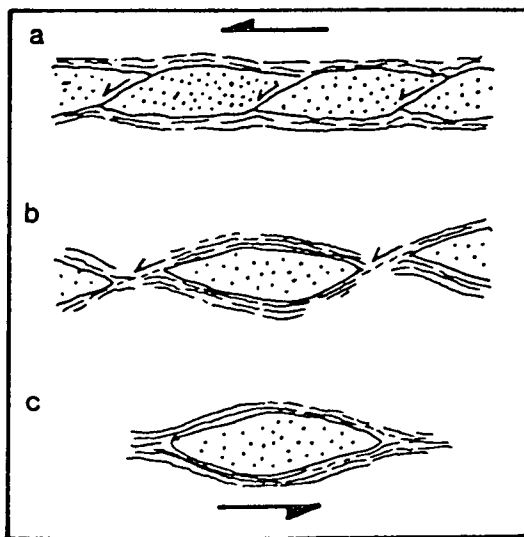
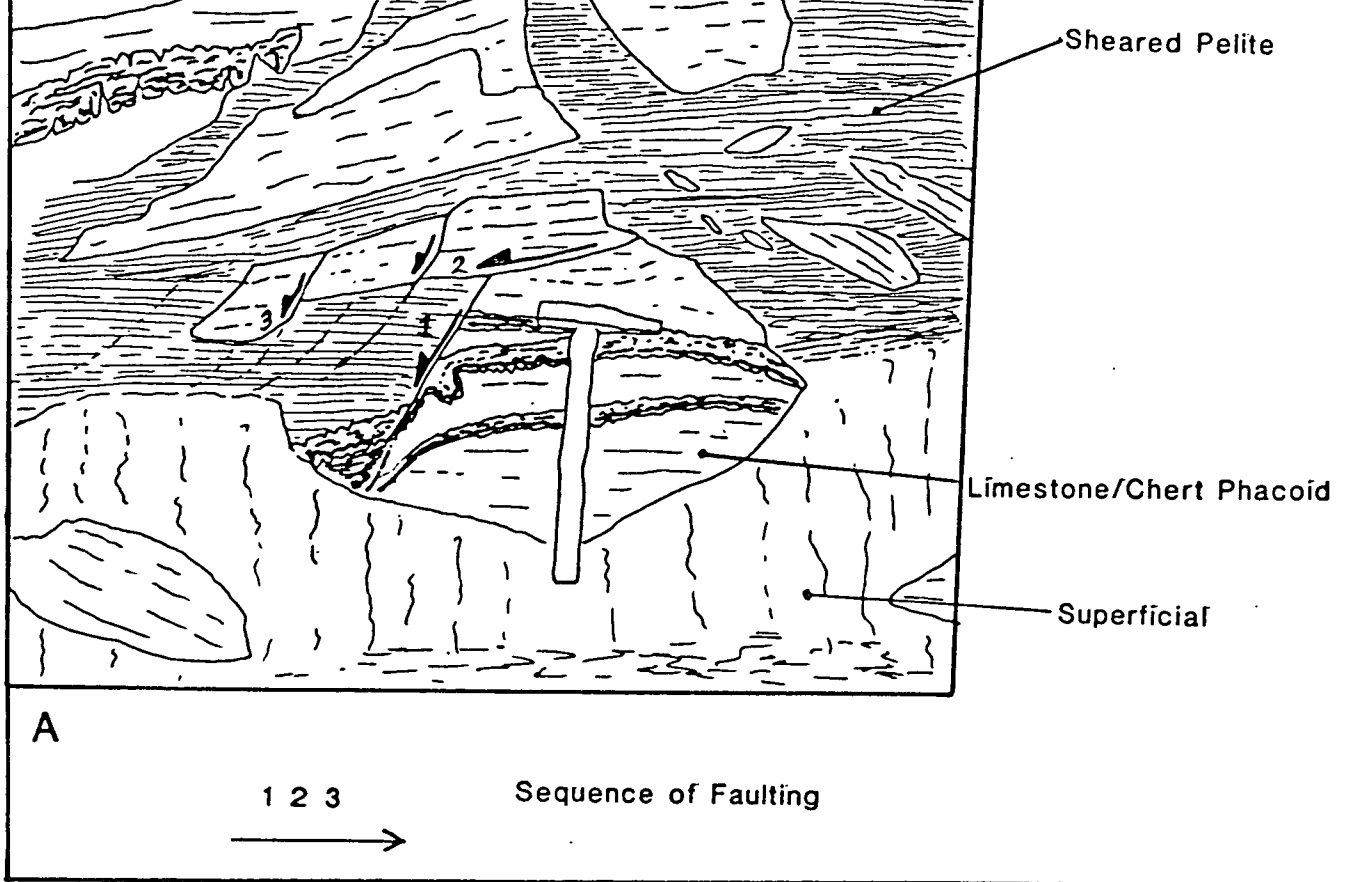


The fact that blocks of debris flow origin do not exhibit the distinctive phacoidal shape is presumably controlled by the lack of suitable planar weaknesses. Tectonically induced shear around the periphery of a debris flow block would tend to irregularly break-up the unit along the non-planar lines of greatest weakness, i.e. individual clast boundaries. Therefore, it is the overall competency of the debris flow unit (determined by cementation), and the shape and size of the component clasts, that will control the eventual shape of the block on shearing. Igneous blocks which have no inherently consistent lines of weakness may similarly not develop phacoidal shapes. It is reasonable to suppose that such blocks, once detached from their substrate, act as "ball-bearings" between shear planes and are rotated and systematically eroded with each successive movement, thus creating a smooth surface to a rounded block.

At several sites, cleaved pebbly mudstones form an integral part of the TSM (Section 7.3.2.2). These beds are considered to reflect cohesive mud-dominated debris flows that formed in the foreland basin ahead of the orogenic wedge, and later were incorporated into the melange. Pebbly mudstones were observed in flysch sequences at Alepohorio (Figure 1.1), Megdovas (north of the Gulf of Corinth) and at other localities on mainland Greece. Within these pebbly mudstone beds there is no preferred alignment of the long axis of clasts (with length:width ratios of at least 3:1). However, south of Chelmos (Figure 1.1), and at other locations on mainland Greece (AHF Robertson & PJ Degnan, unpublished data) where pebbly mudstones constitute part of a melange, such clasts show a preferred alignment of long axis. Debris flows rarely show a well developed imbrication of clasts. This is even more unlikely when large amounts of pelitic matrix is present, as mud-dominated debris flows "freeze" when internal shear stresses become less than the cohesive strength of the matrix. "Freezing" can occur at any time and included clasts are being continuously rotated up until that moment. It is suggested that pebble alignment can be used as a tectonic kinematic indicator, as the long axes are in parallelism with the transport direction of the over-riding Pindos thrust sheets, as seen at Drakovouni.

### 8.3.2 A Model for Fabric Development

Examination of shear bands in the field indicates that the dominant planes are orientated approximately parallel to the transport direction of the overlying Pindos thrust sheets. Blocks of bedded rock are often locally the same size. It is possible that the size of the block is a function of the thickness between an over- and under-



B

C

**Fig. 8.4** (A) Field sketch of a limestone/chert phacoid in the TSM at Drakovouni displaying clear evidence for the formation of blocks in sheared matrix by extension according to the Reidal shear model. 1, 2, 3 indicates the relative timing of three minor faults. A thin chert bed is downthrown in the hangingwall of fault 1 while there are drag folds present in the footwall. Fault 2 is parallel to the main shear movement with top to the west. Faults represented by 3 propagate into the pelite where they are refracted due to competency contrast. (B) Illustrates the development of competent bed boudinage (after Needham 1987) leading eventually to isolated blocks in matrix. (C) Indicates the orientation of R and R' shear fractures in relation to the principle compressive stress ( $\sigma_1$ ) and the dominant shear bands. Note that the youngest faults in (A) are at a relatively higher angle to the shear bands than the ideal R fracture, in the competent limestone, but flatten listrically in the matrix.

lying dominant shear zone. Thus large blocks are developed between widely spaced shear zones, while smaller blocks are developed between less widely spaced shear zones. However, the main shear zones appear to be developed at reasonably evenly spaced intervals in the pelite and it is clear that the shear zones exploit bedding planes either side of an individual bed. Thus, the size of smaller blocks, at least, is controlled to a large degree by bed thickness rather than by shear zone spacing.

The geometry of the shear zones (i.e. the dihedral angles of the two sub-sets) is considered to be governed according to the Riedel shear model whereby a series of secondary fractures develop at an angle to a major through-going shear (Needham 1987, Figure 8.4). The angles of the secondary fractures are controlled by the internal angle of friction of the particular lithology being fractured (a measure of the resistance to movement, itself particular to an individual lithology). The normal faulting observed in the field, which creates boudinaged bedding, is developed in the R1 direction of the Riedel model, i.e. as a synthetic fracture to the main shear zone. The R1 direction is also the orientation of the second sub-set of shears present in the pelitic matrix. Minor shears are found in the pelite which could correspond to the R2 and P directions.

Extensional features are found in the TSM, rather than structures indicative of shortening, despite the regionally compressional stress regime. Tensional stresses are set-up in the melange because of the tractional effects caused by the movement of the over riding, highly competent, Pindos thrust sheets above the melange, and the GTZ platform below. These units act as two rigid bodies relative to the rheologically weak TSM, which acts as a lubricant between the two, with highly distributed strain accommodating the friction induced stresses.

### 8.3.3 Melange Formation in the Pindos Overthrust Terrane

The TSM comprises a variety of lithologies; volcanic rocks, Pindos Group sediments and those derived from the Tripolitza platform. All the components of the TSM are chaotically mixed in a deformed pelitic matrix located between the Pindos Group and the underlying Tripolitza platform, with minor TSM development in between thrust sheets of the Pindos thrust stack (Section 8.2). In the southern Peloponnese the TSM is found below Triassic rocks of the Drimos Formation. In the west of the Pindos Zone, the stratigraphically lowermost sediments are of the Priolithos Formation, while many of the more easterly outcrops have basal thrust detachments

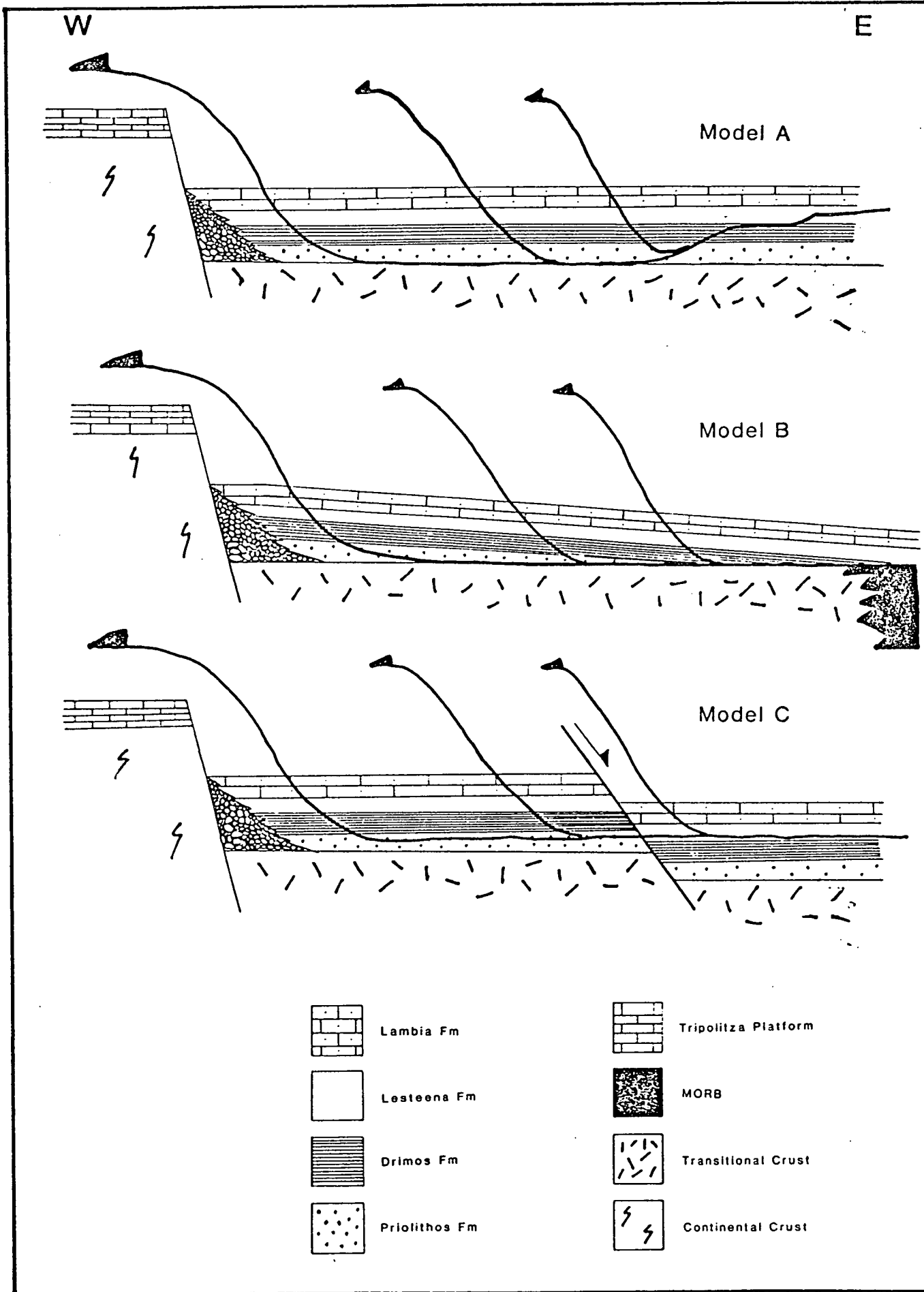


**Fig. 8.5** Postulated models to account for the observation that the basal Pindos detachment apparently cuts down section in the transport direction, from the base of the Cretaceous Lambia Formation to within the Upper Triassic Priolithos Formation. Of the three models (B) is preferred. Explanation in text.

located beneath the Lambia Formation, or more rarely, below the radiolarites of the Aroania Chert Member. There are three alternatives proposed to account for the apparent downstepping of the basal Pindos thrust in the transport direction, from below Cretaceous limestone in the east to below Upper Triassic sandstones in the west (Figure 8.5):-

(a) The Pindos basal thrust cuts down the stratigraphic section in the transport direction. This is the model proposed by Fleury (1980), where it was presumed that the Pindos Basin formed on thinned continental crust. Therefore, all the stratigraphic horizons would have been deposited throughout the basin in a layer-cake stratigraphic manner.

(b) The Priolithos and Drimos Formations were deposited largely on Middle Triassic transitional crust. The overlying Aroania Chert Member was deposited both upon these formations and on younger oceanic crust further to the east. During Tertiary compression the MORB crust was entirely consumed with an east-dipping polarity. Thin remnants of chert and the bulk of the Lambia and Pindos Flysch Formations were off-scraped and incorporated into an orogenic wedge. The basal detachment was located at the sediment/igneous interface and, as it propagated westward into the older part of the Pindos Basin, it developed under progressively older stratigraphic horizons.

(c) With the advancement from the east of an orogenic wedge, a foreland basin formed on the oceanic crust. The western edge of this downwarp could have developed east-dipping extensional faults in the crust. Thus, the propagating basal thrust would be transferred from higher to lower stratigraphic horizons across a non-ramping plane.

Of the above models, (b) is preferred, both because it is the simplest and also because it is in accord with present day subduction models (Westbrook 1982).

The sparse inclusion of volcanic lithologies in the TSM may be due to the frontal accretion of raised volcanic edifices on the Pindos Basin sea floor off-scraped into the orogenic wedge, while most of the igneous basement was consumed as part of a subducting slab. This would account for the TSM sometimes being without igneous rocks and adequately explains the presence of lavas beneath the Upper Jurassic Aroania Chert Member at Aroania (Mn locality), where surrounding lithologies are of Upper Triassic and Lower Jurassic age. The presence of TSM, with and without igneous rocks, intercalated within the Pindos thrust stack indicates that thrusting

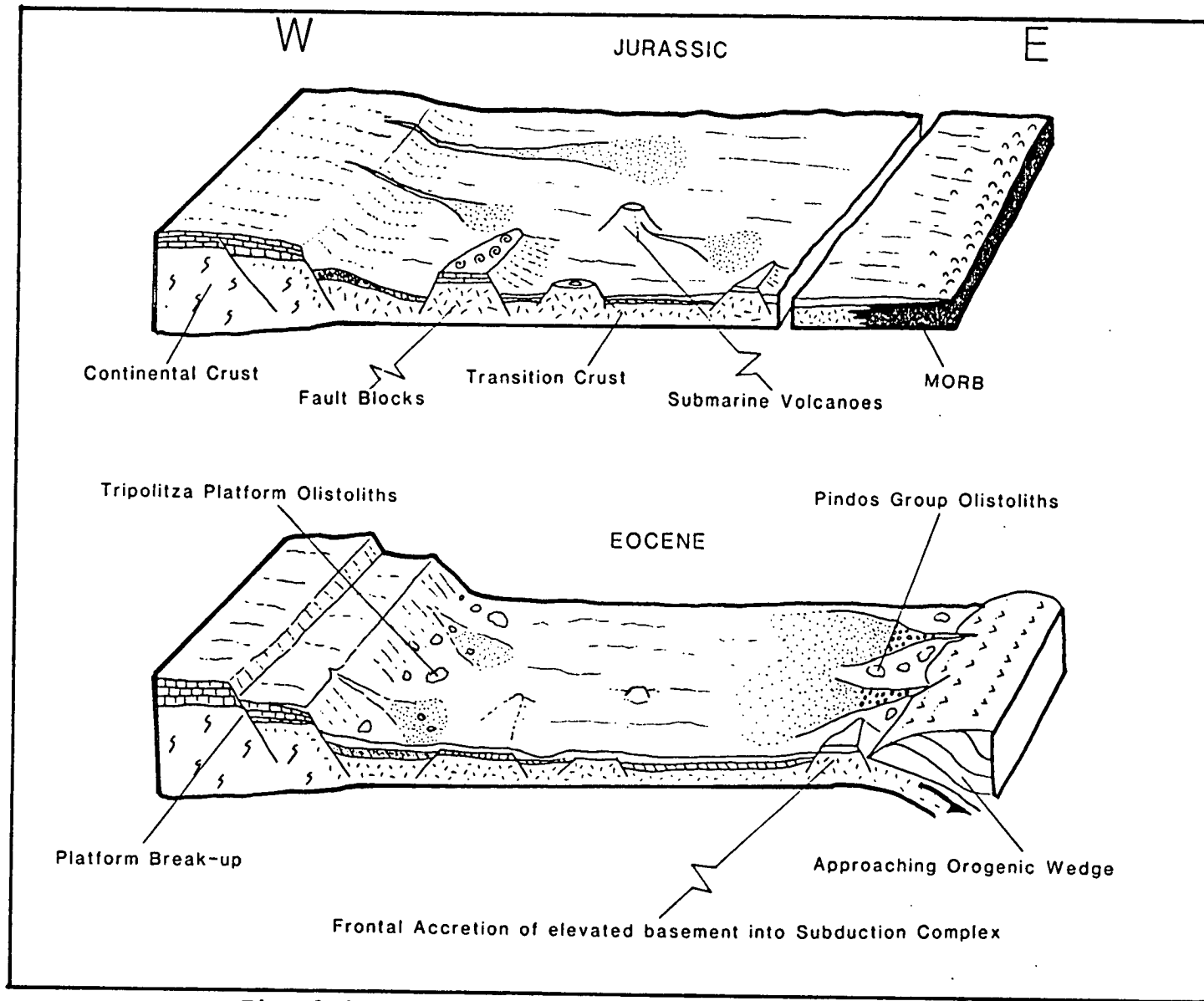


**Fig. 8.6** Proposed model showing the irregular Pindos basin Jurassic palaeobathymetry which during the Eocene was blanketed in turbidites and chaotic gravity flows shed off both an advancing orogenic wedge and the collapsing GTZ platform. These sediments were later over-riden and incorporated into the TSM, as were frontally accreted elevated basement areas.

must have occurred in the Pindos Basin, prior to emplacement onto the Tripolitza platform. Most of the TSM is made-up of pelite with an admixture of sedimentary lithologies, including debris flows. It is suggested that these represent turbidite deposits, olistoliths and debris flows shed off both the advancing Pindos thrust sheets and the collapsed platformal area. Similar debris flow lithologies, relatively undeformed in comparison to the TSM, are found at Alepohorio where the lack of deformation indicates that the Pindos thrust sheets did not over-ride sufficiently far westwards to induce melange formation. A schematic diagram of the proposed model is shown on Figure 8.6.

## 8.4 IGNEOUS LITHOLOGIES

### 8.4.1 Petrography

With the exception of the feldspar-phyric rocks found at Drakovouni, all the igneous lithologies of the TSM are fine-grained and aphyric in hand specimen. Some are vesicular or with calcite-filled amygdales. The various rock types have been classified according to the nomenclature for volcanic rocks of Cox, Bell & Pankhurst (1987, Figure 8.7). Petrological and geochemical analysis clearly indicates that many of the rocks have been severely affected by hydrothermal and weathering processes. Major element geochemistry in these cases is extremely unreliable as many elements, particularly MgO, CaO and alkalis, are mobile. The igneous classification of Figure 8.7 is therefore considered unreliable. The rocks have also been plotted on a Ti/Y:Nb/Y diagram which indicates that they belong to the tholeiitic suite. In this section, representative petrological descriptions are given for igneous rocks in the TSM. The variety of igneous textures and mineral constituents does not relate to any particular location, nor to the gross chemical composition. The rocks are therefore simply divided into (a) basalt/andesite and (b) dolerite. The characteristics of volcanoclastic rocks in the TSM, including pyroclastic deposits, is also presented.

#### 8.4.1.1 Basalt and Andesite

The rocks described here are termed basalt and andesite because of differences in silica content, as indicated by XRF analysis (Appendix 5). There is a continuum of lithologies from low silica varieties (less than 40%) to highly siliceous rocks (greater than 65%). Evaluation of the volatiles (CO<sub>2</sub> & H<sub>2</sub>O) lost on ignition (LOI,

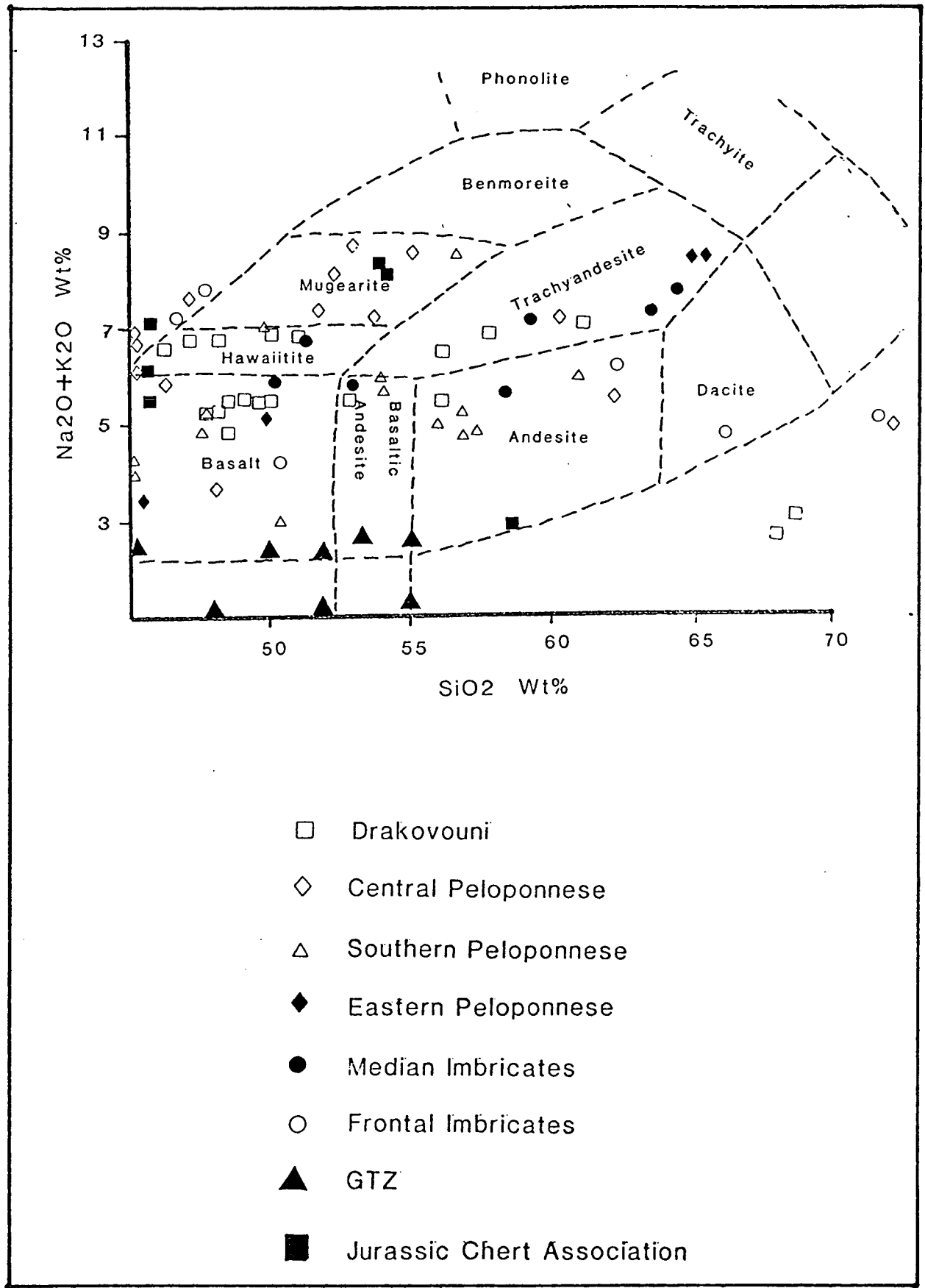


**Fig. 8.7** Igneous lithological boundaries after Cox et al. (1987) with selected TSM samples plotted.



Appendix 5) suggests that the silica values could have been higher in some cases, as every 1% of LOI will add 1-2% SiO<sub>2</sub> to the rock major-element content totals.

The basalts and andesites are aphyric in hand specimen, although many rocks are seen to contain micro-phenocrysts of feldspar and sometimes zoned augitic clinopyroxene and occasionally orthopyroxene (Plate 8.3). Generally, the rocks are equigranular and dominated by feldspar. The feldspar varies from albite, with much replacement by chlorite, to andesine. Fibrous pumpellyite and chlorite are seen to replace feldspar and clinopyroxene in some thin sections. Additionally, chlorite may pseudomorph biotite and/or amphibole. Other specimens consist of an unaligned glassy feldspathic and opaque mineral groundmass without a phenocryst assemblage.

Many of the samples display trachytic textures formed by the sub-parallel alignment of elongate feldspar laths (albite and/or oligoclase, Plate 8.4). Where ellipsoidal amygdales are present they also show a preferred alignment, parallel to the trachytic texture; however, larger plagioclase phenocrysts are often at high angles to it. A second groundmass texture, observed in a pillow basalt thin section, consists of discrete spherulites formed by a fan-like arrangement of variolitic feldspars (Plate 8.4). Such a texture is common in pillow lavas and is often associated with rapid quenching.

Many of the basalts and andesites are amygdaloidal, the vesicles being up to a centimetre in width and filled with calcite and/or silica. Other minerals observed in the groundmass include apatite, iron oxides, sphene, ilmenite and rutile.

#### 8.4.1.2 Dolerite

Coarse-grained igneous rocks of the TSM are found at Drakovouni. The dolerite ranges from microplagioclase-phyric to distinctly plagioclase-phyric. Two textures can be seen closely associated in an otherwise petrographically identical rock, possibly suggesting the assimilation of a partially (and slowly) cooled magma back into a melt, which then cooled at a faster rate (Plate 8.2). The mineralogy of the dolerite is dominated by feldspar phenocrysts without a preferred orientation (andesine). The rock also contains isolated anhedral phenocrysts of augitic clinopyroxene and minor orthopyroxene. Some pyroxene encloses plagioclase laths sub-ophitically. A thin section which displays a gradational transition from coarser to finer dolerite, indicates that the pyroxenes are preferentially concentrated in the more phyric areas. The groundmass texture is intergranular and consists of laths of

unorientated plagioclase and opaque minerals, comprising anhedral iron oxides and ilmenite. There has been extensive alteration and replacement by sericite, secondary chloritisation and an unidentified acicular amphibole (actinolite?). The chlorite is patchy and often fibrous, replacing plagioclase and clinopyroxene equally.

#### 8.4.1.3 Volcaniclastic Rocks

Two volcaniclastic lithologies are recognised in the field. (1) Pyroclastic and (2) epiclastic (redeposited) conglomerates.

The particle size of the volcaniclastic lithologies ranges from ash to cobble grade. The lithified pyroclastic rocks are classified as tuff, lapillistone, agglomerate and conglomerate, after Suthren (1985). The tuff is often a poorly consolidated purple-violet mudstone-like lithology that crumbles easily. XRD analysis indicates that albite is the major constituent, with ancillary quartz and saponite (a smectite clay formed by the weathering of volcanic ash). At Kokino and Sellas, fibrous zeolites (natrolite) are found in the tuff, while at Drakovouni the zeolite analcime is present. The homogeneity of the tuff and consistent grain-size suggests an air-fall origin, rather than reworking in the marine environment.

A more lithified tuff, with no apparent secondary clay alteration, is also present at Drakovouni and grades imperceptibly into coarser lapillistone and agglomerate. These pyroclastics are green or purple/violet. In hand specimen, the tuff and lapillistone often resemble igneous lithologies, except that planar beds are present, up to 14cm thick. In thin section the beds are seen to contain a variety of diverse, well sorted, to poorly sorted, volcanic clasts (Plate 8.5). Most of the clasts are angular to sub-rounded, comprising trachytic textured basalt, amygdaloidal basalt and individual grains of quartz, feldspar fragments and opaque oxides. In some thin sections, larger clasts of more glassy material are present and could represent primary volcanic ejecta. The agglomerate is largely devoid of matrix material, being well cemented by (hydrothermal?) carbonate or silica. It is often difficult to differentiate pyroclastic volcanic lithic fragments from epiclastic deposits. However, the facies association with tuff, and some plastic indentation of clasts, suggests that this rock can be considered as pyroclastic at Drakovouni. Other agglomerate beds may well be epiclastic, representing the reworking of volcanic ejecta, and therefore not strictly agglomerate. At Drakovouni a block of distinctive blue-green arkose contains a bimodal assemblage of plagioclase feldspar and quartz (Plate 8.5). Also at Drakovouni, blocks containing inter-bedded agglomerate with jasperised chert (Fe-

rich) are found. The clasts are poorly sorted angular feldspar-phyric lava and quartz. It is likely that most of the "agglomerate" has been reworked, although the field setting and thin-sections clearly indicate a relatively local source.

The agglomerate of Drakovouni coarsens upward into several metres of clast-supported volcanic conglomerate. Bedding is between 10cm and 60cm thick, it is not graded and component clast sizes are up to 5x2cm. Clasts are well rounded and consist of purple, aphyric, non-amygdaloidal lava. Other isolated blocks of basaltic breccio-conglomerates are found elsewhere in the TSM.

#### 8.4.2 Geochemistry

One hundred samples of hypabyssal and extrusive igneous rocks were analysed by X-ray fluorescence (operating conditions and data are provided in Appendix 2 and Appendix 5). From each of the geological settings described above (Section 8.2), several fresh-looking samples were taken from different outcrops and/or different igneous blocks within the TSM. Due to the possible effects of low-grade metamorphism, burial diagenesis and weathering, not all the rocks analysed were used in the compilation of geochemical discriminant diagrams, nor were they considered for further petrogenetic evaluation. They are nevertheless included in Appendix 5 as they may prove of value to later researchers. The criteria used to screen unsuitable specimens include extensive alteration seen in thin section and samples with an excess, or deficiency, in certain oxides and elements. As a rough guide, samples with SiO<sub>2</sub> outside 35 to 80%, MgO outside 3 to 9% and CaO outside 5 to 15% were mostly omitted. Details of the screened samples are provided here.

##### 8.4.2.1 Major Oxides

###### SiO<sub>2</sub>

SiO<sub>2</sub> is mobile during weathering and metamorphism (Pearce 1975). There are no discernable patterns in the SiO<sub>2</sub> values from the various locations, possibly indicating both a degree of silica mobilisation and the development of secondary quartz bearing phases. Concentrations range from 33.89 to 77.55%.

###### Al<sub>2</sub>O<sub>3</sub>

Al<sub>2</sub>O<sub>3</sub> is rarely mobile during greenschist metamorphism, and immobile during weathering processes (Pearce 1975). Except for two low-alumina samples from the

Central Peloponnese (6.31 & 8.92%), all the TSM samples fall in the range 13.06 to 20.27%.

### Fe<sub>2</sub>O<sub>3</sub>

Fe<sub>2</sub>O<sub>3</sub> is moderately mobile during alteration inducing processes. It ranges from 4.33 to 12.77% in the TSM.

### MgO

MgO is very mobile during weathering and moderately mobile in low-grade metamorphic reactions (Pearce 1975). Generally, the analysed samples contain more than 3%, but less than 9% MgO. The majority of screened samples contain 4-6%.

### CaO

CaO is very mobile during alteration processes (Pearce 1975). There is a correspondingly wide range of values present.

### Na<sub>2</sub>O

Na<sub>2</sub>O is mobile during weathering and low grade metamorphic reactions (Pearce 1975). In the analysed rocks, the range is 2.97 to 8.26%. This makes up most of the total alkali content shown on Figure 8.7

### K<sub>2</sub>O

K<sub>2</sub>O is very mobile during weathering and moderately to very mobile under metamorphic conditions (Pearce 1975). The K<sub>2</sub>O values are always lower than those for Na<sub>2</sub>O, except for five samples of the Jurassic Chert Association which are very potassic, with up to 6.95%. Due to the potentially high mobility, no significance is given to this value. The TSM K<sub>2</sub>O ranges from 0.02 to 3.75% and generally measures less than 1%.

### TiO<sub>2</sub>

TiO<sub>2</sub> is effectively immobile during weathering and low-grade metamorphism (Pearce 1975). Most of the samples have moderate TiO<sub>2</sub> values, between 0.7 to 1.7%. At Drakovouni, two high-titanium basalts are present (2.01% & 2.07%). All but two of the GTZ volcanics are below 0.7%.

#### 8.4.2.2 Trace Elements

The 17 trace elements measured by X-ray fluorescence in this study can be divided into groups reflecting different chemical characteristics.

Incompatible elements are those which are preferentially concentrated in the liquid phase during melting and crystallization. The compatibility of an element varies with the crystallising mineral under consideration, thus for any mineral there is a partition coefficient,  $D$  ( $D = \text{concentration in mineral}/\text{concentration in liquid}$ ) which reflects compatibility ( $D < 1 = \text{incompatible}$ ).

Large ion lithophile elements (LIL) are incompatible with respect to normal mantle minerals (e.g. olivine and pyroxene) and include Rb, Sr, K, Ba, Zr, Th and the light rare earth elements, e.g. La, Ce and Nd. Another group of trace-elements comprises the high field strength elements (HFS) which are defined as having an ionic radius/charge of less than 0.2 (Saunders *et al.* 1980). The incompatible HFS elements include Ti, P, Zr and Nb.

The rare earth elements (REE) are strictly LILs but react as HFS elements. Along with HFS elements they are most useful for tectono-magmatic discrimination purposes as they tend to remain in the solid products of weathering, being less likely to be removed in solution as hydrated cations (Pearce, undated Users Guide to Discrimination Diagrams). These elements are thus "immobile".

Absolute trace-element abundances found in even a single rock suite can vary a great deal. Of much more relevance is the ratio of a certain group of elements to another group, e.g. LIL to HFS. Such ratios are the basis for the creation of many of the tectono-magmatic discrimination diagrams discussed below.

#### 8.4.3 Tectono-magmatic Discrimination Diagrams

The geochemical data were plotted on immobile element and multi-element diagrams (Figure 8.8 and 8.9) which attempt to discriminate between possible tectono-magmatic environments (Pearce 1980, Pearce 1982, Pearce & Cann 1973, Meschede 1986). The various fields shown on the diagrams are within plate basalt (WPB), which typically represents continental rift and ocean island environments; mid-ocean ridge basalts (MORB), which are erupted at constructive oceanic plate boundaries; and volcanic arc basalt (VAB) or island arc tholeiites (IAT), which

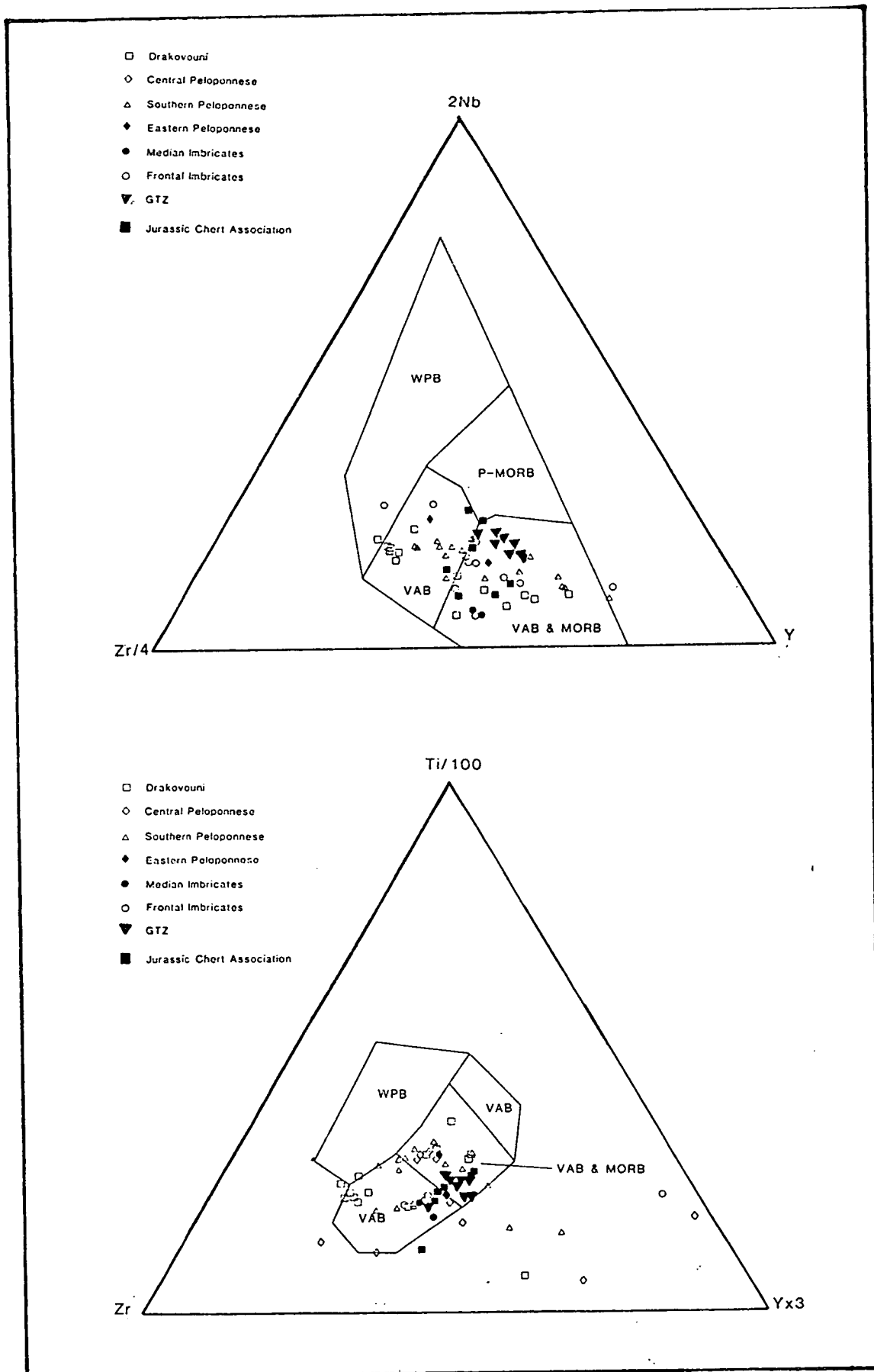


**Fig. 8.8** Ternary tectono-magmatic discrimination diagrams (Meschede 1986, Pearce & Cann 1973) with selected TSM samples plotted. Explanation in text.

characterise the igneous rocks forming above subduction zones at destructive plate boundaries.

#### **2Nb:Zr/4:Y (Meschede 1986)**

Almost all of the data points plot in the fields of VAB or VAB/MORB (Figure 8.8a). Samples from Drakovouni show a wide spread, with a distinct cluster close to the VAB and WPB boundary.

#### **Ti/100:Zr:Yx3 (Pearce & Cann 1973)**

On this discriminant diagram (Figure 8.8b) the majority of samples from all locations plot in the VAB or VAB/MORB fields. There is again a cluster of Drakovouni samples close to the VAB and WPB boundary.

#### **Ti:Zr (Pearce 1980)**

This diagram suggests that the data selected represent essentially basic rocks (Figure 8.9a). These are of greater value in assessing tectonic environments (from trace-element composition) than more evolved rocks, as the effects of fractional crystallisation are greatly reduced. Data points are concentrated in the MORB field, which overlaps with both VAB and WPB. A Drakovouni cluster is present in the WPB field alone.

#### **Cr:Y (Pearce *et al.* 1981)**

Several samples are deficient in Cr, probably representing extensive fractional crystallisation as Cr partitions into olivine and clinopyroxene (Section 8.4.5). The rest of the samples plot in overlapping VAB/MORB & WPB/MORB fields or VAB alone, except for a single sample each from the frontal imbricates and Drakovouni, which are found in the WPB field (Figure 8.9b).

#### **Zr/Y:Zr (Pearce 1980)**

In this diagram (Figure 8.9c), it is noticeable that the GTZ volcanics have lower Zr values than the TSM samples. Zr depletion is a feature commonly observed in subduction related rocks. The majority of TSM analyses plot throughout the VAB, MORB and WPB fields, however there is a distinct sub-group comprising several samples from Drakovouni which plot well within the WPB field.

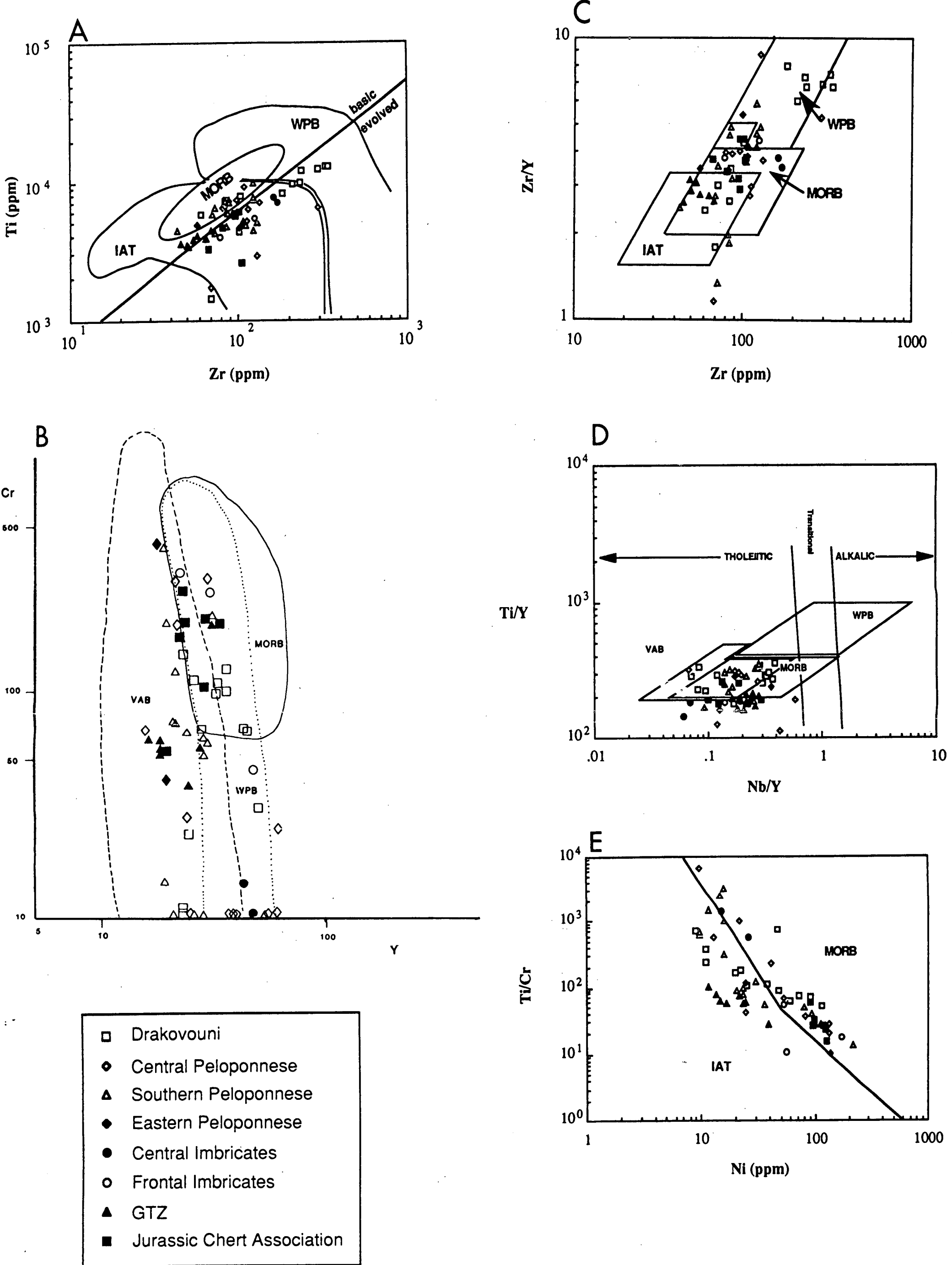


**Fig. 8.9** Tectono-magmatic discrimination diagrams (Pearce 1980, 1982, Pearce et al. 1982, Beccaluva et al. 1979) with selected TSM samples plotted. Explanation in text.



**Ti/Y:Nb/Y (Pearce 1982)**

Most of the analyses fall into the overlapping MORB/VAB field, apart from the majority of the GTZ volcanics which are in, or near, the MORB field (Figure 8.9d). There is a cluster of Drakovouni and southern Peloponnese samples near to the WPB boundary with VAB. This diagram is also used to distinguish tholeiitic from alkaline rocks. This is because it has been demonstrated that there is marked enrichment of Nb, relative to Ti, in alkaline relative to tholeiitic basalts (Pearce 1982).

**Ti/Cr:Ni (Beccaluva *et al.* 1979)**

This diagram (Figure 8.9e) attempts to separate the MORB and VAB tectono-magmatic provinces. There are two clear clusters, one (A) comprises GTZ volcanics in the IAT field, and the other (B) shows the volcanics associated with the Jurassic cherts plotting solely in the MORB field. The TSM samples appear to have the usual scatter in both IAT and MORB fields. However, there is a clear negative correlation between Ti/Cr and Ni, as seen in most samples from Drakovouni and the southern Peloponnese (C & D). The best fit negative correlation line through the two sets of data are parallel. In general Ni is positively correlated with Mg (Section 8.4.5.2). Both elements partition into olivine although this mineral is not present in the samples. It is therefore suggested that the best-fit lines C & D represent a pyroxene fractionation trend in the TSM lavas, from a more basic magma source to more differentiated types.

**8.4.4 Discussion**

The "French school" of geology that worked in the Pindos Zone during the 1950-70s (Aubouin 1959, Dercourt 1964, Fleury 1980) considered that the Pindos Basin represented attenuated continental crust. Such a setting was suggested for other Neotethyan basins, e.g. the Hawasina Basin in Oman (Bechennec 1987, Bechennec *et al.* 1990) and the Triassic to Middle Jurassic basin represented by extrusives and deep water sediments of the Antalya Complex in Turkey (Waldron 1984, Dercourt *et al.* 1986). In the Pindos Zone there is a wealth of data which cannot be easily reconciled with a model supporting a simple rift interpretation. For example, there are deep-water continental margin/oceanic-type sediments present (Chapters 3, 4 & 5); there is evidence for MORB-type igneous rocks and supra-subduction zone ophiolites (Pindos, Othris, Erymioni) being derived from the same Pindos oceanic basin and emplaced onto the Pelagonian microcontinent during the Upper Jurassic (Section 1.2.1 and references therein); backstripped subsidence curves (Green 1982,

Thiebault 1982) indicate geological settings comparable to present day passive margins, and lastly, the geochemistry of igneous rocks considered here are not simply of continental rift origin.

After much detailed work in Oman (Cooper 1986, Robertson 1986, Robertson & Searle 1990), Turkey (Robertson & Woodcock 1984) and Greece (Smith *et al.* 1979, Green 1982, Jones 1990, Robertson *et al.* 1991) it is now more certain that basins such as the Hawasina, Antalya and Pindos Basins probably represented transitional domains to oceanic crust proper. Such an interpretation is conceded by several authors who had previously held opposing views (e.g. Stampfli *et al.* 1991). Thus, for many, the question is no longer "was the Pindos Basin formed on thinned continental crust or oceanic crust"?; but, "did the Pindos Basin develop as an oceanic back-arc basin or in a Red Sea-type rift to drift setting"?

Many of the GTZ and TSM igneous rocks are basalts or andesites which appear to have subduction-related components, as shown by marked HFS depletion (e.g. Nb & Ti) relative to enrichment in LIL elements. Crucial to an understanding of the development of the Pindos Basin is an appraisal of the significance of this signature. Pe-Piper and Piper (1990) suggest that copious pyroclastic deposits, the presence of plagiogranites at Drakovouni, shoshonites on the basin margin (Kremasta and Lakmon, north of the Gulf of Corinth) and the VAB geochemical signature in discriminant diagrams, all indicate that the Pindos Basin developed as a back-arc basin related to the southwestward subduction of Palaeotethys beneath Apulia. While not discounting a back arc basin hypothesis out of hand, it is pertinent to provide a possible alternative explanation to account for the presence of basalts and andesites, apparently with a VAB tectono-magmatic signature. This approach is valid as there are a number of inconsistencies with a subduction-related hypothesis with regard to the Pindos Zone, viz.:-

1) The basalts and andesites analysed here have some geochemical features which are not consistent with typical analyses of subduction-zone (VAB) rocks (Pearce 1976, 1982), e.g. they are generally low in  $K_2O$  and some have significantly higher amounts of  $MgO$ ,  $CaO$ ,  $Cr$  and  $Zr$ . Many of the spidergrams show a marked Nb depletion relative to La, but others have flat MORB-like trends. Additionally, there is little evidence of depletion in other HFS elements, nor is there enrichment in LIL elements for all samples. It is debatable whether the geochemistry really does contain a significant primary subduction-related component, and if so whether this is

directly the result of coeval subduction with the development of an arc, or the incorporation of magma sources which have been modified by an earlier subduction event.

2) Most basalts from present day back-arc basins are MORB and are apparently unaffected by subduction-modified magma sources (Saunders *et al.* 1980). (NB. recent work by P. Clift [pers. comm.] suggests that this may not be true for the Lau Basin).

3) Pyroclastic deposits are particularly voluminous in volcanic arc provinces, but are not restricted to this setting. They can, for example, be significant in areas of active and extensive continental rifting where magmatism can be highly explosive (e.g. Ethiopia). It is also argued that although pyroclastic deposits are present in the Peloponnese, the scattered and fragmentary outcrops do not allow a valid estimation of volume. Furthermore many of the fine-grained volcanoclastics are epiclastic rather than primary volcanic ejecta. Extensive pyroclastic deposits in other parts of the Pindos Zone cannot be proven.

4) Despite several weeks work on the TSM locations, plagiogranites (which are distinctive in the field, and were seen in the Aspropotamos Complex (Jones 1990) of the Pindos Zone in northern Greece) were not observed at Drakovouni. Rhyolites were observed in the Drimos Formation volcanoclastic sandstone facies (Section 3.3.1.3) but not elsewhere. Other highly siliceous igneous rocks, including those from Drakovouni, contain much chalcedony and quartz of secondary origin.

5) There is no suitable candidate for a Palaeotethyan arc terrane to the east of the Pindos Basin. In addition, it appears that microcontinental fragments have successively rifted-off Gondwana and drifted across Palaeotethys and Neotethys to accrete with the southern Eurasian margin due to the northward subduction of oceanic crust (Robertson & Dixon 1984, c.f Sengor 1984).

6) Middle Triassic igneous rocks reported from other Pindos Zone localities do not always exhibit an island arc character, e.g. Green (1982) indicates that TSM equivalents north of the Gulf of Corinth are WPB, while Kostopoulos (1989) and Jones (1990) describe Triassic WPB and MORB lavas from the Pindos Zone (Avdela Melange) in northern Greece. Thus, it appears that along strike magma evolution was varied through the Pindos Basin during the Middle to Late Triassic.

7) Both basalts and andesites are found in the Pindos Zone of the NW Peloponnese. Andesites are classically considered to result from subduction-related magmatism, above the Benioff zone of down-going oceanic plates. Although the presence of andesitic lithologies in the NW Peloponnese would appear to support Pe-Piper & Piper's (op. cit.) explanation for the subduction-related signature indicated by the geochemistry, it must be remembered that the composition of an igneous rock is affected by a diverse series of processes, including fractional crystallisation, partial melting, mantle heterogeneity and contamination by crustal rocks.

The significance of the last point is pursued further here. Anorogenic andesites, although uncommon, are recognised from several present day areas, including a mid-ocean ridge/plume association (Iceland; Carmichael 1964), propagating rift segments (Galapagos, Byers *et al.* 1983) and continental flood basalt provinces (e.g. Parana, Brazil [Fodor 1987] and the Karoo, South Africa [Duncan 1987, Cox 1983]). Hall (1987) states that the bulk composition of the whole continental crust is not dissimilar to that of andesite, thus, very extensive melting of continental crust would theoretically give a magma of an intermediate composition. Myers & Marsh (1981) cite andesites produced by the mixing of basaltic magma, with melt produced from crustal anatexis (Alaska) while other authors have also shown how the partial melting of amphibolite facies rocks at shallow depth, or eclogite at deeper depths, can form andesitic magma. Pichler & Ziel (1972) suggest this mechanism (Andes) while Burnham (1979) proposes that the injection of basaltic magma provides a suitable heat source.

Both basaltic and andesitic magmas have been produced in the Basin and Range extensional setting of the western USA (Fitton *et al.* 1988, Gans *et al.* 1989, Fitton *et al.* 1991). Many of the basaltic lavas have subduction-related geochemical signatures (enrichment in Ba, depletion in Nb), despite the cessation of subduction locally at least 20my earlier. A mechanism to provide a subduction-related overprint has been suggested by Fitton *et al.* (1991), whereby an active asthenospheric mantle plume may sufficiently soften the lithosphere and allow lithospheric mantle, enriched in LIL elements inherited from a subducted slab, to contribute to a magma reservoir by mass assimilation. Without such plume softening, extending cold lithosphere can be thought of as essentially "cracking", allowing the rapid passage of uncontaminated asthenospheric melt. Furthermore, Fitton *et al.* (1988) indicate that the involvement of silica-saturated magma was greatest around the periphery of the Basin and Range region, i.e. where extension was greatest. With continued rifting

and asthenosphere involvement, such an environment is likely to become the site of a future passive margin.

There are other areas where immobile trace-element data do not accurately reflect the known tectono-magmatic setting of extrusive rocks. In the southern province of the Karoo basalt terrane of South Africa, many lavas plot in the subduction-related basalt field, despite clear geological evidence for a within plate origin (Duncan 1987). Cox (1983) appeals to mantle heterogeneity to explain these anomalous trace-element levels in the Karoo basic lavas. Dostal & Dupuy (1984) suggest that continental tholeiites of Nova Scotia are similar to oceanic tholeiites, but were affected by crustal contamination, thereby providing negative Nb anomalies.

Despite the above examples, there is generally a low level of recognition given to the occurrence of subduction-like signatures in extending terranes away from recognised sites of subduction.

#### 8.4.5 Interpretation of the Geochemical Results

The igneous rocks of the TSM are tholeiitic and basic to acidic in composition. Alkalies versus silica diagrams show a wide scatter of data points that may, or may not, represent original lava compositions. The results of plotting the more immobile element data on to tectono-magmatic discrimination diagrams indicates that, within the wide spread of data, there are several distinct suites of igneous lithologies possibly present.

The first is the well clustered GTZ group which plots consistently in the VAB field. As seen in the spidergrams of Chapter 7 (Figure 7.2), all the GTZ samples are depleted in Nb relative to La. A second group of igneous samples, associated with the Jurassic cherts, plot in the MORB field of the Ti/Cr:Ni diagram. The third suite is a sub-set of samples from Drakovouni which plot in the VAB field, close to the WPB boundary. The majority of TSM lithologies exhibit a wide spread of data points, occupying the overlapping VAB/MORB fields.

Many of the analysed rocks display varied geochemical compositions, usually with an apparent subduction zone affinity. It is necessary to determine whether the geochemical variation observed in the Pindos Zone igneous rocks is due to source heterogeneity or whether the evolution from a parental magma can be deduced.

Because many of the rocks have been altered by post-eruptive reactions involving the migration of elements into and out of the rocks during low grade metamorphism, burial diagenesis and weathering, the above tectono-magmatic discrimination diagrams are not necessarily considered an accurate reflection of the contemporary volcanic environment. More beneficial is a critical appraisal of the trace element data.

In assessing the relevance of the trace element data, it is worthwhile to consider some of the factors which may influence the concentration of trace elements. Partial melting and fractional crystallisation are briefly considered here, although the following remarks can in no way adequately cover all aspects involved in the generation of magmas.

#### 8.4.5.1 Partial Melting

Partial melting, for a source rock of any given composition, occurs when the geothermal gradient intersects the solidus; with increasing degrees of partial melting a particular rock type will be progressively consumed. Under normal conditions the geotherm in old lithosphere would never intersect the dry solidus, thus melting must be induced by anomalous thermal perturbations of the geotherm, adiabatic decompression or by the addition of volatiles.

MORB is depleted in incompatible elements, being derived from the upper mantle which has undergone incompatible element extraction throughout geological time with the progressive concentration of those elements in continental crust. Tholeiitic basalt magmas are generated by quite large degrees of partial melting (20-30%) of sub-lithospheric, upper mantle lherzolite, at depths of 80Km upwards (McKenzie & Onions 1991). Basalts may evolve from the differentiation of more picritic melts, or by the mixing of picritic melts with more evolved magmas in crustal reservoirs. Latin *et al.* (1991) have attempted to constrain the degree of partial melting of either a MORB-source mantle, or an enriched asthenosphere source, by considering the trace element contents of Jurassic North Sea volcanics.

A real complication in lithospheric extensional situations is that melts from enriched lithospheric mantle may be combined with melts from depleted asthenosphere in varying proportions, dependant upon the enrichment history and the subsequent melting episode. Thus, in order to understand the contribution that partial melting makes to the final composition of igneous rocks, the source characteristics and the

enrichment and melting circumstances must be known. This cannot be ascertained for the rocks studied here. However, the partial melting of continental lithosphere and its incorporation into a MORB melt, is clearly a potential mechanism to derive igneous rocks displaying varying degrees of enrichment. This is because various minerals will be preferentially consumed into a melt depending on local conditions. For example, incompatible enriched phases, such as amphibole, biotite and apatite require only small degrees of partial melting for incorporation into a magma.

#### 8.4.5.2 Fractional Crystallization

A magma at a temperature between its solidus and liquidus will include a variety of crystals within the melt and the crystals will form at varying temperatures depending on the magma composition. In a basalt, the crystallizing sequence in a high pressure system will usually include olivine as one of the earliest crystallizing phases, followed by clinopyroxene and then plagioclase (Carmichael *et al.* 1974). This sequence may not hold for low pressure systems. With each successive crystallization, if the bulk composition of the melt changes due to the separation of the solid phase from the liquid, the process is termed fractional crystallization. A consequence of fractional crystallization is a progressive change in the elemental ratios found in the differentiating magma if the elements concerned partition differently into the crystallising phases. It is therefore probable that extensive fractional crystallization would involve the concentration of incompatible elements in later crystallizing phases as a magma approaches its solidus.

There are several geochemical characteristics that indicate fractional crystallization in a suite of lavas. The use of Harker variation diagrams displays correlations between  $\text{SiO}_2$  and another element. If there is a strong correlation between an element and an increasing  $\text{SiO}_2$  content, this may indicate the evolution of a liquid line of descent due to fractional crystallization. A major problem with using  $\text{SiO}_2$  as an index of fractional crystallization is that  $\text{SiO}_2$  can be very mobile and it is difficult to determine the degree of that mobility in the altered rocks studied here.

MgO content is commonly used as an inverse measure of the degree of fractionation from a primary magma as it is largely unaffected by partial melting, but it is sensitive to fractional crystallization. Cr and Ni are closely allied with MgO values as they are both strongly compatible ( $D > 1$ ) in olivine and pyroxene. Where Cr, Ni and MgO all correlate, as their content falls, it strongly suggests extensive crystal fractionation. A variation diagram of MgO versus Ni (Figure 8.10a) indicates that Ni

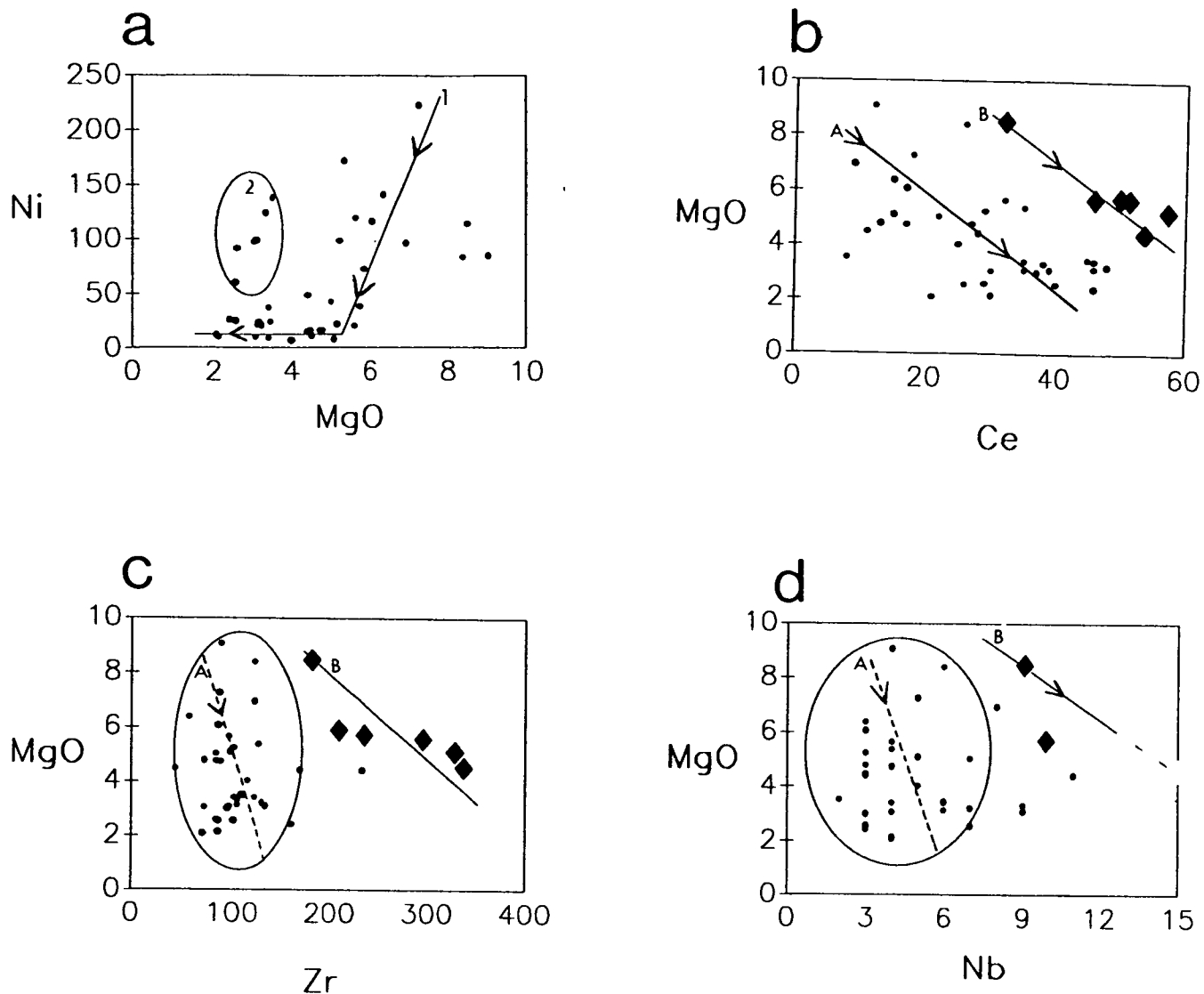


**Fig. 8.10** Variation diagrams. (a) MgO v Ni showing a fractionation trend (1) with Ni falling gradually until flattening-out at an MgO value of c.a. 5.5%. Sub-field (2) has initially low MgO values with little reduction in MgO as Ni falls.

(b) MgO v Ce; (c) MgO v Zr; (d) MgO v Nb; all showing trace element enrichment with fractionation. Note that line B (points plotted as diamonds represent samples 276, 453, 454, 459, 464 & 475; all from Drakovouni) represents a more enriched source and evolution trend. Explanations in text.



falls with MgO to approximately 5.5% MgO. Thereafter Ni values are at a base level while MgO continues to fall. This 5.5% MgO value most probably corresponds to the point where olivine and pyroxene largely ceased to crystallise. There are a few isolated points with high Ni but low MgO and these suggest the loss of MgO for a reason other than fractional crystallisation (possibly weathering). MgO is used here as a reliable index of fractional crystallisation and the Ni/MgO relation is used as a filter to remove suspect analyses.

Figure 8.10 (b-d) plots MgO versus the incompatible elements Ce, Nb and Zr. Appraisal of each of the diagrams indicates that there are two suites of lava present where incompatible enrichment is observed as MgO falls. The first suite recognised (1) has a basic end member with 8.5% MgO. The set shows Nb increasing from 9 to 15 ppm, Ce from 32 to 54 ppm and Zr from 183 to 336 ppm (i.e. an increase of c.a. 160%) and this set corresponds to the WPB of Drakovouni identified in Section 8.3.3. The second set is widely scattered and shows a lower level of absolute enrichment because of the initially low level of incompatible element concentration (e.g.  $10 \times 160\% = 16$ ) and the degree of precision at very low values, especially for Nb. PD/89/276 (MgO 8.5%) is considered a suitable candidate for the more enriched parental magma, and sample PD/89/605 (MgO 9.05%) possibly represents the parental lava of a second suite that is relatively depleted in incompatibles.

#### 8.4.5.3 Multi-Element Plots

Many of the samples considered as basic to moderately evolved, based on SiO<sub>2</sub> content, show enrichment in LILEs and HFS elements relative to MORB. They also display a marked depletion in Nb relative to La, a feature considered indicative of a subduction character. However, the evidence provided above shows that most samples have been subjected to extensive fractional crystallisation and are more evolved than simple analysis of the Ti versus Zr graph (Figure 8.9a) and SiO<sub>2</sub> content might suggest. For these evolved basaltic andesites, direct comparisons with modern-day basalts are not justifiable. This conclusion diminishes, but does not obviate, the validity of the tectono-magmatic discrimination diagrams described earlier (Section 8.4.3) and by other authors (Pe-Piper & Piper 1990).

The principle concern of this geochemical investigation is to relate the Pindos Zone magma generation to a likely tectono-magmatic environment. To establish this aim, it is necessary to consider only the most basic of the lavas present in the TSM, i.e. those few analyses of samples with at least 5.5% MgO. MORB normalised multi-

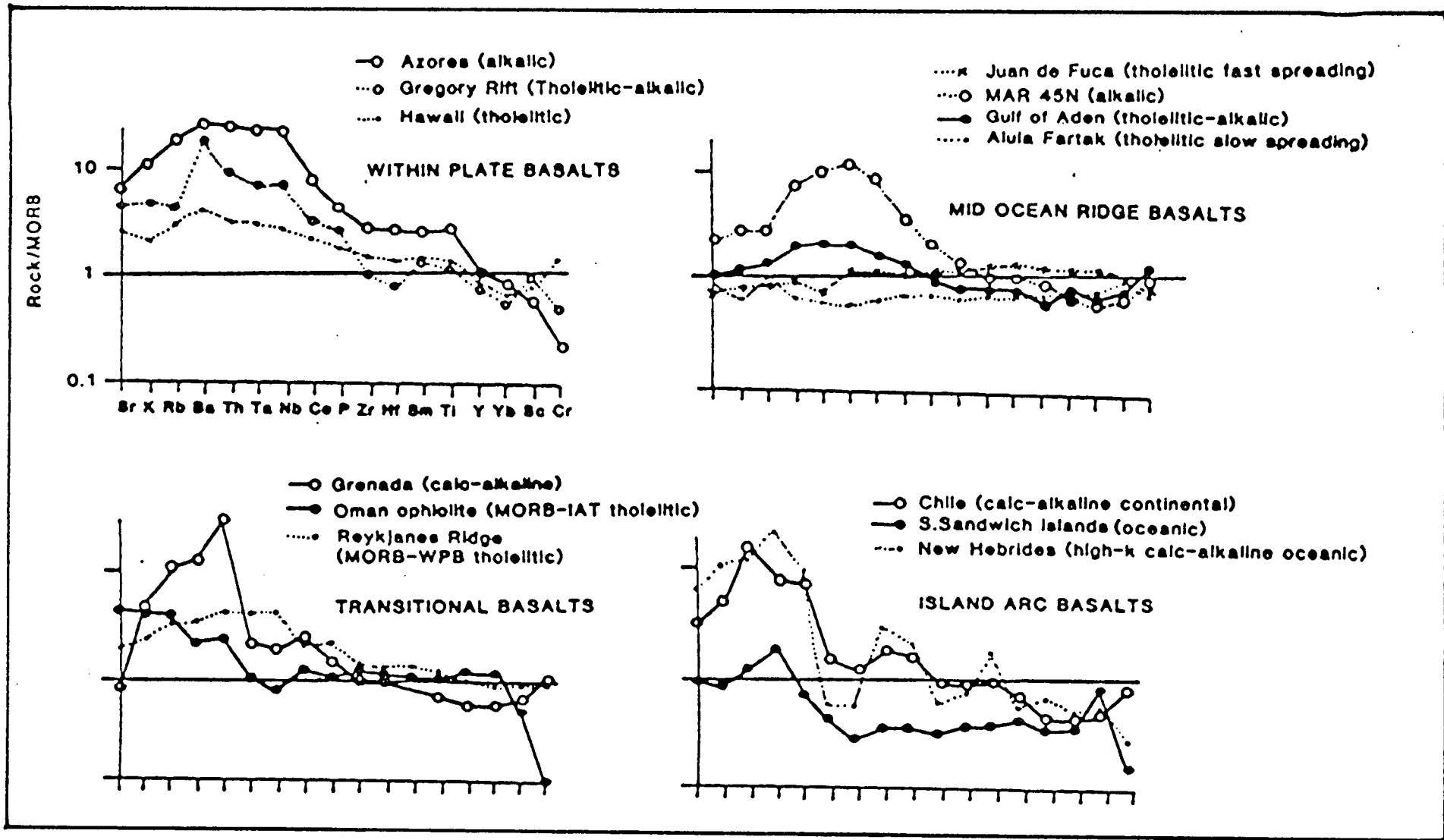
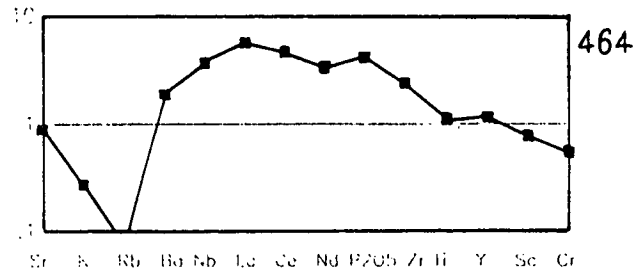
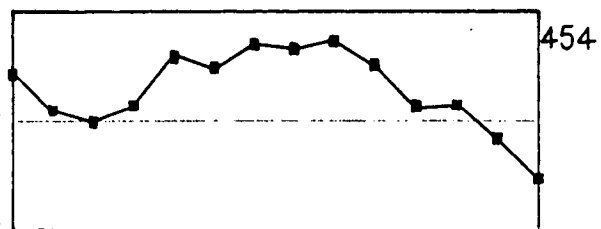
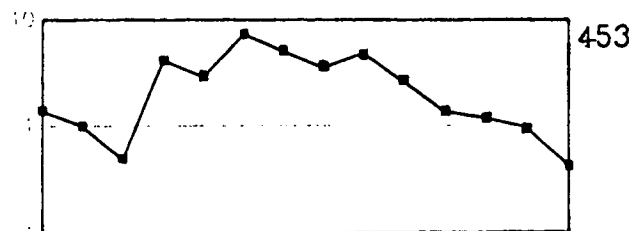
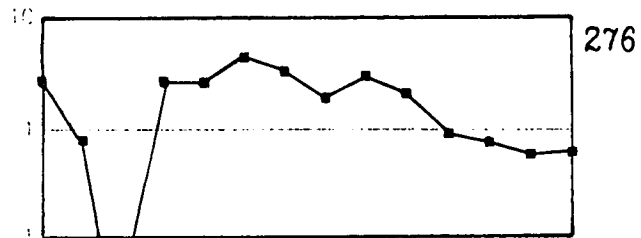
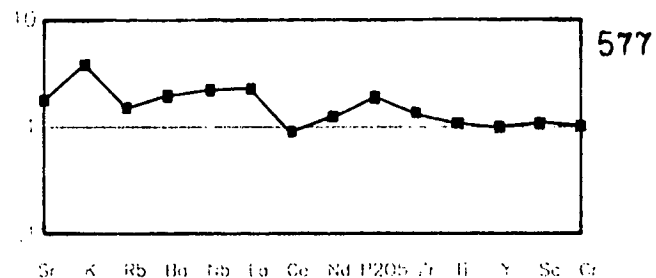
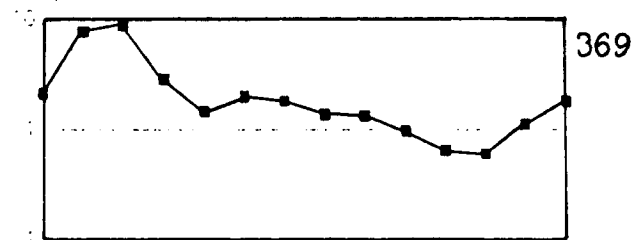
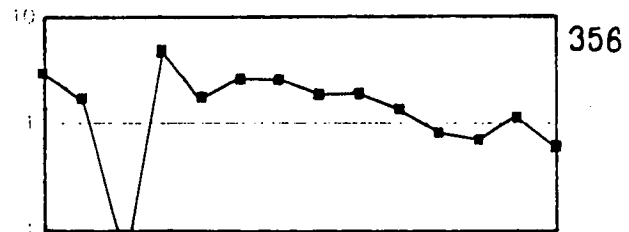
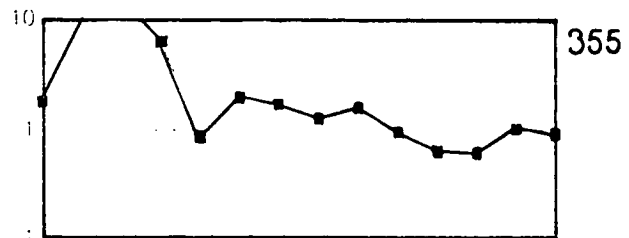


Fig. 8.11 Typical multi-element "spidergram" plots for within plate basalts, mid-ocean ridge basalts, transitional basalts and island arc basalts; normalised against MORB (from Pearce, unpublished users guide to basalt discrimination diagrams).

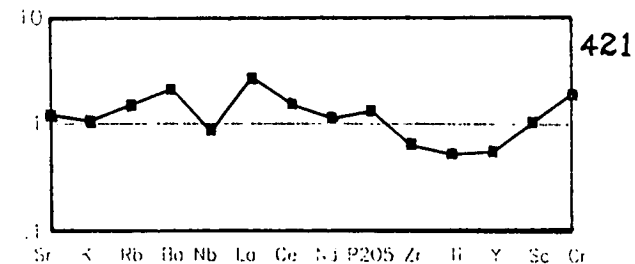
### DRAKOVOUNI



### SOUTHERN PELOPONNESE



### EASTERN PELOPONNESE



### CENTRAL PELOPONNESE

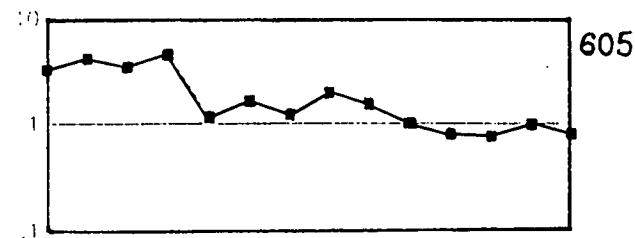


**Fig. 8.12** Multi-element "spidergram" plots for selected TSM samples from (A) Drakovouni, (B) Central Peloponnese, (C) Southern Peloponnese and (D) other areas. Explanation in text.

element spidergram plots (after Pearce 1980) were constructed for such samples (Figure 8.12). The elements are arranged so that the incompatibility of the mobile and immobile elements increases from the outside to the inside of the diagrams. On the left are the more mobile LIL elements Sr, K, Rb and Ba. For comparison with the TSM spidergrams, typical MORB normalised spidergrams from P-MORB, VAB and WPB environments are provided in Figure 8.11 (from Pearce, unpublished "User Guide to Discrimination Diagrams").

At Drakovouni, samples 276, 453, 454 and 464 show LIL levels similar to, or lower than, those of MORB lavas. The LIL elements can be extremely mobile and should be viewed with suspicion due to the possible effects of alteration. However, comparison with the LILEs values present in many other TSM rocks suggests smaller degrees of LILE mobility in these more basic samples. Overall, the more immobile HFS incompatible elements are more enriched than in MORB, the elements Ti and Y are approximately equivalent to MORB levels and Sc and Cr are relatively depleted. Nb/La ratios are low, normalised Nb even exceeds La in sample 454. In this suite Rb is depleted with respect to Ba, a feature which Gans *et al.* (1989) suspects indicative of the partial melting of continental crust. The suite has a "humped" pattern indicative of WPB but the most parental lava (276) is less enriched and more akin to MORB.

Samples 605 (Central Peloponnese) and 421 (Eastern Peloponnese) are both potential parent lavas to the more widespread occurrence of evolved basaltic andesites. The trace element patterns are relatively flat, MORB-like and there is no significant Nb depletion relative to La.

In the Southern Peloponnese, there are four samples with greater than 5.5% MgO. The more mobile LILEs show some enrichment relative to MORB (except for Rb in 356) while the more immobile elements have very flat MORB-like patterns with only a weak Nb-depletion relative to La, a feature markedly more obvious in the more evolved lavas.

#### 8.4.5.4 Conclusion

It is concluded that there are two distinct suites of lava present in the TSM. One suite is present at Drakovouni and was either derived from a relatively enriched source, possibly due to the partial melting of continental lithosphere, or the suite is the product of a small degree of melting. The second suite is considered to be

derived directly from a more depleted upper mantle source and is comparable to MORB, but with a weak (relative) Nb depletion. Both suites have undergone fractional crystallisation and alteration and this has obscured the true geochemical character by mobilising LILEs and generally enriching the magmas in HFS elements. If the weak Nb-depletion relative to light REEs (and the equally moderate LILE enrichment) in the southern Peloponnese suite is a real feature indicating the influence of a subducted slab, the question arises as to whether it reflects contemporaneous subduction, as argued by Pe-Piper & Piper 1990, or whether it could be an inherited feature derived from underlying enriched continental lithospheric mantle.

#### 8.4.6 A Proposed Model for Pindos Zone Magmatism

It is suggested that lithospheric stretching, and the rifting of the Pelagonian microcontinent from Apulia, began in the Permo-Triassic as a result of the thermal weakening of the continental crust (Section 9.2.1.4). Accelerated rifting occurred in the Middle Triassic when extensive volcanism was a feature of both the opposing margins of the Pindos Basin. Widespread partial melting of the asthenosphere and the overlying lithospheric mantle, due to adiabatic decompression, led to the generation of picritic melts from a depleted mantle lherzolite source. Extensive olivine fractionation created tholeiitic basaltic magma and buoyancy facilitated the transport of the differentiated magma towards high level reservoirs. It is probable that fractionation continued *en-route*, thus inherent heat and latent heat supplied from continued crystallization caused anatexis of the surrounding lithospheric mantle and lower crust. The Apulian lithospheric mantle is inferred to have been volatile-enriched with fluids expelled from pelagic sediments and the hydrated crust of a subducting slab during an earlier (Hercynian?) phase of subduction (Robertson *et al.* 1991). This facilitated the depression of the solidus due to the inclusion of volatiles and led to the subsequent mixing of asthenosphere-derived, depleted, tholeiitic magma with an enriched (arc character) lithospheric melt. Thus, lavas of basic to intermediate composition, variably enriched in incompatible elements and relatively deficient in Nb, were produced.

The igneous rocks of the Gavrovo-Tripolitza Zone and Pindos Zone in the NW Peloponnese are here considered as transitional, representing a spectrum of lithologies. The rocks range from enriched within-plate tholeiitic basalt (minor quantities) to basaltic andesites which appear to be derived from the fractional

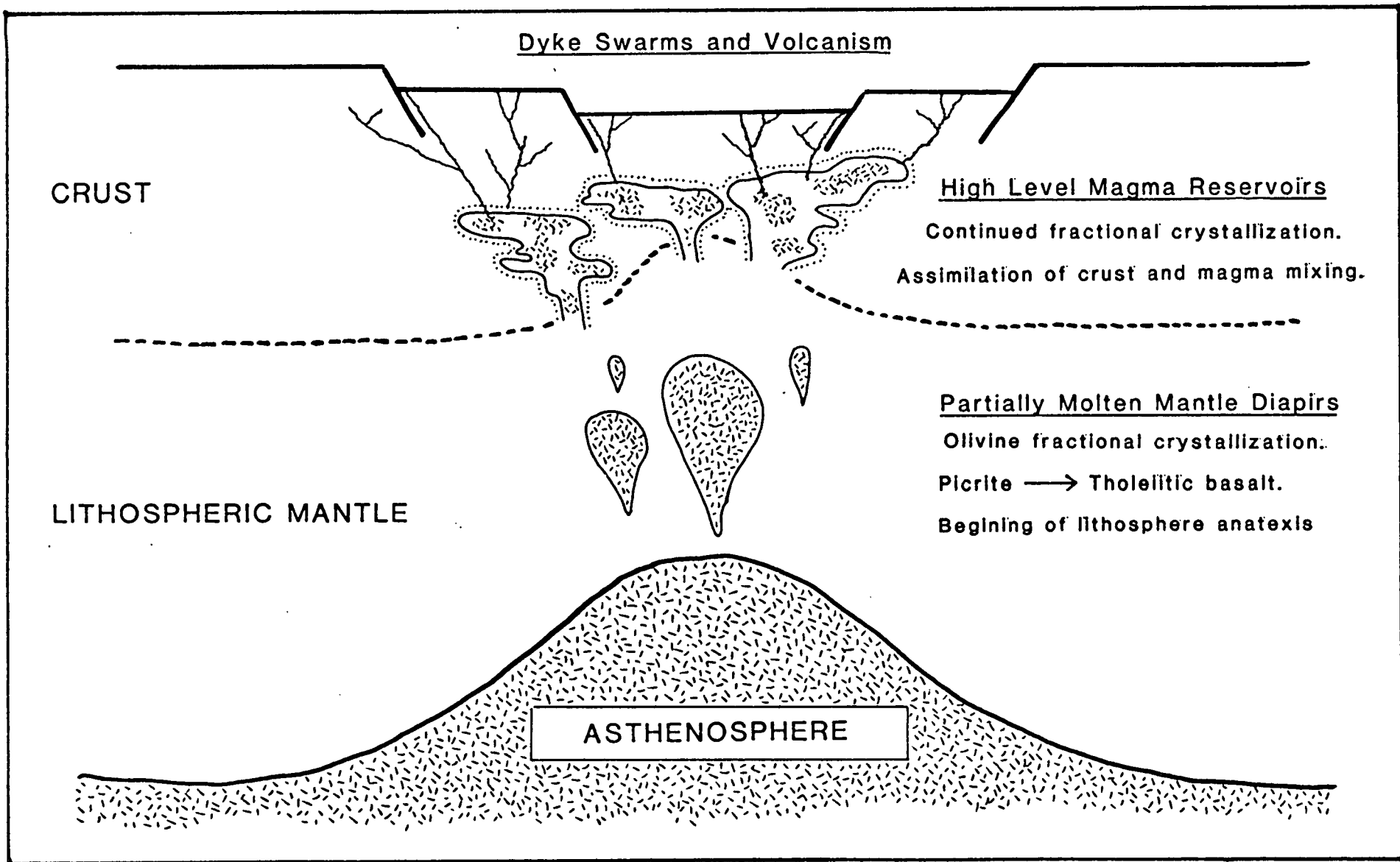


**Fig. 8.13** Proposed magmatic model for the generation of Pindos Zone igneous rocks with subduction zone modification of WBR to MORB signatures

crystallisation of a MORB source rock. Additionally, it is inferred that there is a variable component derived from magma mixing with modified lithospheric mantle. Once mid-ocean ridge magma generation was properly established, typical depleted MORB would have dominated at the Pindos Ocean spreading ridge, away from the contaminating effects of the continental crust. Such basalts are not widespread in the Peloponnese due to Eocene/Oligocene subduction (Chapter 6 and 7), but they are preserved in the northern Pindos Mountains (Jones 1990).

The favoured model is schematically illustrated in Figure 8.13. This model, if true, would indicate that the rifted Gondwana margin probably consisted of former arc and microcontinental exotic terranes accreted onto the main cratonic landmass. Such a scenario is analogous to the western and eastern periphery of present day North America, which consists of a mosaic of accreted terranes.

## 8.5 CONCLUSIONS

The lavas of the TSM were extruded in submarine environments and have, in most cases, undergone weathering and low-grade metamorphic alteration. Hypabyssal dolerite is the equivalent of such extrusive rocks. These lithologies, with volcanoclastic rocks, formed the basement to the overlying sediments of the Pindos Group. It is envisaged that the sea floor bathymetry was irregular.

Petrological and geochemical examination of lithologies in the TSM suggest a model whereby Middle Triassic extension was accompanied by the copious outpouring of tholeiitic lavas which were mostly basic and intermediate in composition. The magmas were formed by the combination of a depleted asthenosphere derived tholeiitic melt, mixed with the products of subduction modified lithospheric mantle and crust. The result of such assimilation and mixing, as well as fractional crystallization, produced the observed wide range of lavas and generally caused enrichment in incompatible trace-elements, in many cases to give a superficial VAB tectono-magmatic signature. It is proposed here that the trace-element data in fact indicate WPB (minor amounts) and MORB, contaminated by the incorporation of fluids and phases derived from an earlier (Hercynian?) subduction event.

During Eocene collisional deformation, elevated areas of volcanic basement were off-scraped and incorporated into a westward advancing orogenic wedge. Also

incorporated into the wedge were olistoliths of Pindos Group and Tripolitza zone affinity. The thrust sheets ramped over the Tripolitza platform. The basal detachment horizon was subjected to intense layer parallel extension which facilitated the further mixing of lithologies to produce the sheared tectono-sedimentary melange found today between the two units.



## PLATES

### PLATE 8.1: TSM Blocks & Fabric

(A) A large rounded block of basalt within pelite of the TSM at Drakovouni. Hammer to top right of block for scale. (B) A block of debris flow conglomerate, with clasts containing Eocene neritic fauna, from within the TSM at Drakovouni. Hammer for scale. (C) Large phacoid, c.a. 3m high, of thinly bedded pelagic limestones within sheared pelites of the TSM at Drakovouni. (D) Typical TSM fabric developed in the pelite at Drakovouni with numerous shear bands defining rhombohedral domains and enclosing phacoids of more competent lithologies. Hammer in the centre of picture for scale.

### PLATE 8.2: TSM Igneous Rocks

(A) *Halobia*-bearing limestones of the Drimos Formation over-lying volcanoclastic mudstones, themselves over-lying lavas, at Kokino. Hammer for scale. (B) Severely degraded and spherically weathering basalts from Palaeohouni. Hammer for scale. (C) Possibly overturned thin lava flow and lava breccias from the TSM at Palaeohouni. (D) Well defined irregular margins between a feldspar phenocryst bearing and more aphyric dolerite at Drakovouni, interpreted as a re-melting texture. Explanation in text. Lens cap for scale.

### PLATE 8.3: TSM Igneous Petrography

(A) Clinopyroxene subophitically enclosing laths of plagioclase in the dolerite of Drakovouni. XP. Scale bar = 0.2mm. (B) Randomly orientated plagioclase laths in a partially chloritised groundmass of interstitial glass. A clinopyroxene crystal is subophitically enclosing a plagioclase lath in the centre of the field of view. XP. Scale bar = 1mm.

### PLATE 8.4: TSM Igneous Petrography

(A) Radiating laths of plagioclase forming a spherulitic textured rock, typically found along the margins of pillow basalts. Note the carbonate filled vesicle to the top left of the photograph being replaced by chalcedonic silica. XP. Scale bar = 1mm. (B) Sub-parallel laths of plagioclase in a glassy groundmass forming a trachytic textured rock. XP. Scale bar = 2mm.

### PLATE 8.5: TSM Volcanoclastic Petrography

(A) Volcanoclastic sandstone containing a diverse assemblage of igneous components with doleritic and basaltic clasts including trachytic and vesicular varieties. PPL. Scale bar = 1mm. (B) XP, and (C) PPL, of an arkosic volcanoclastic sandstone dominated by clasts of sub-angular twinned plagioclase set in an altered, partially chloritised matrix. At the top of the photograph a large clast of basalt, with unaligned microphenocrysts of plagioclase, is set in an altered groundmass. Scale bar = 0.4mm.





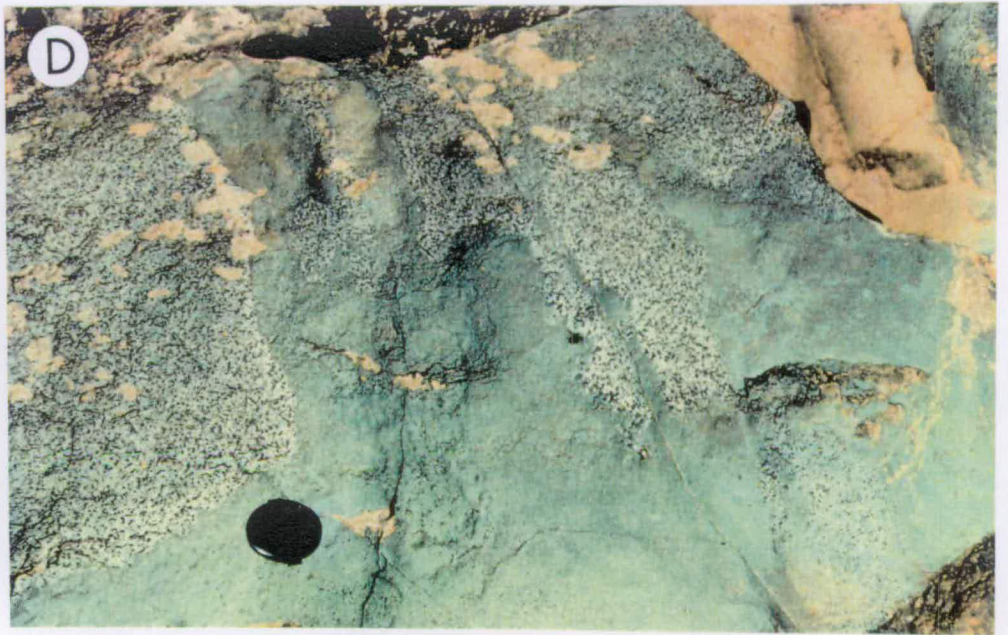
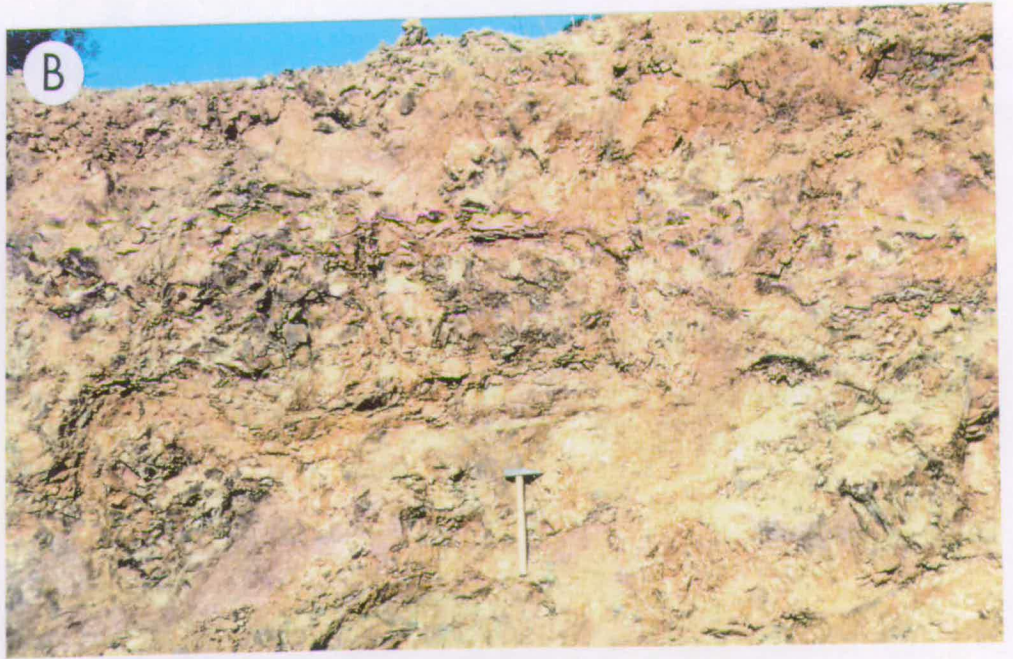




# PLATE 8.3

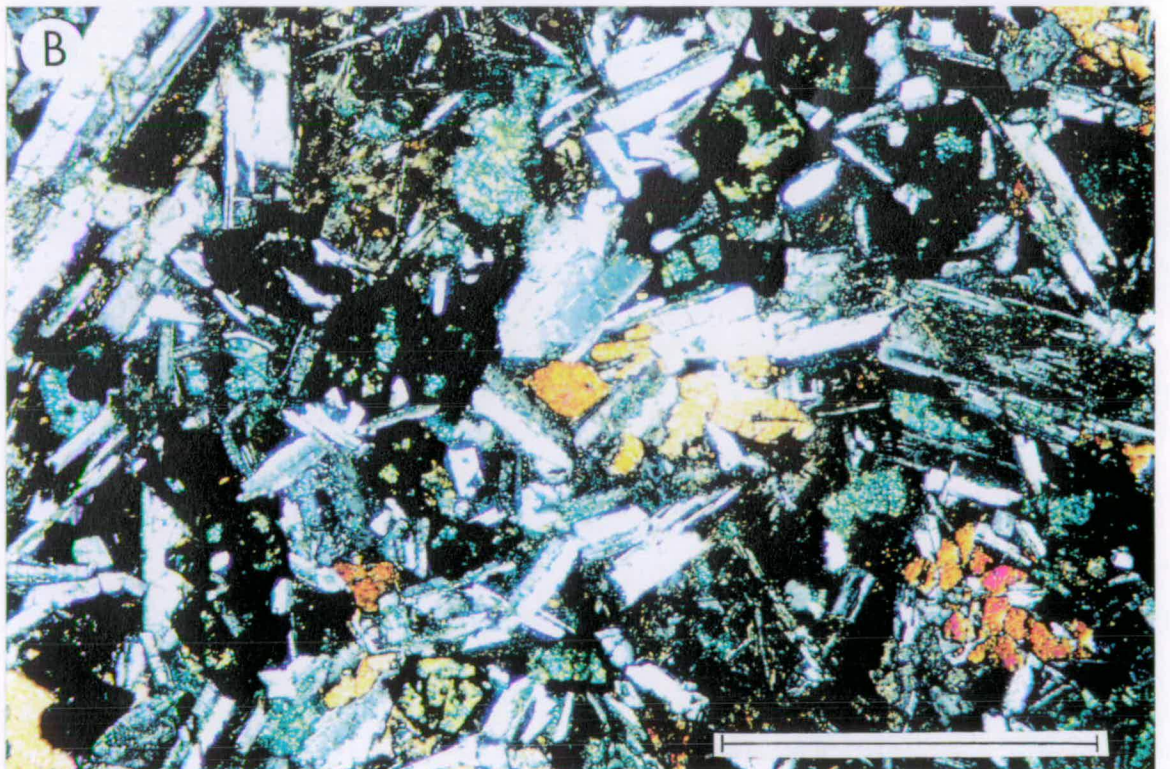
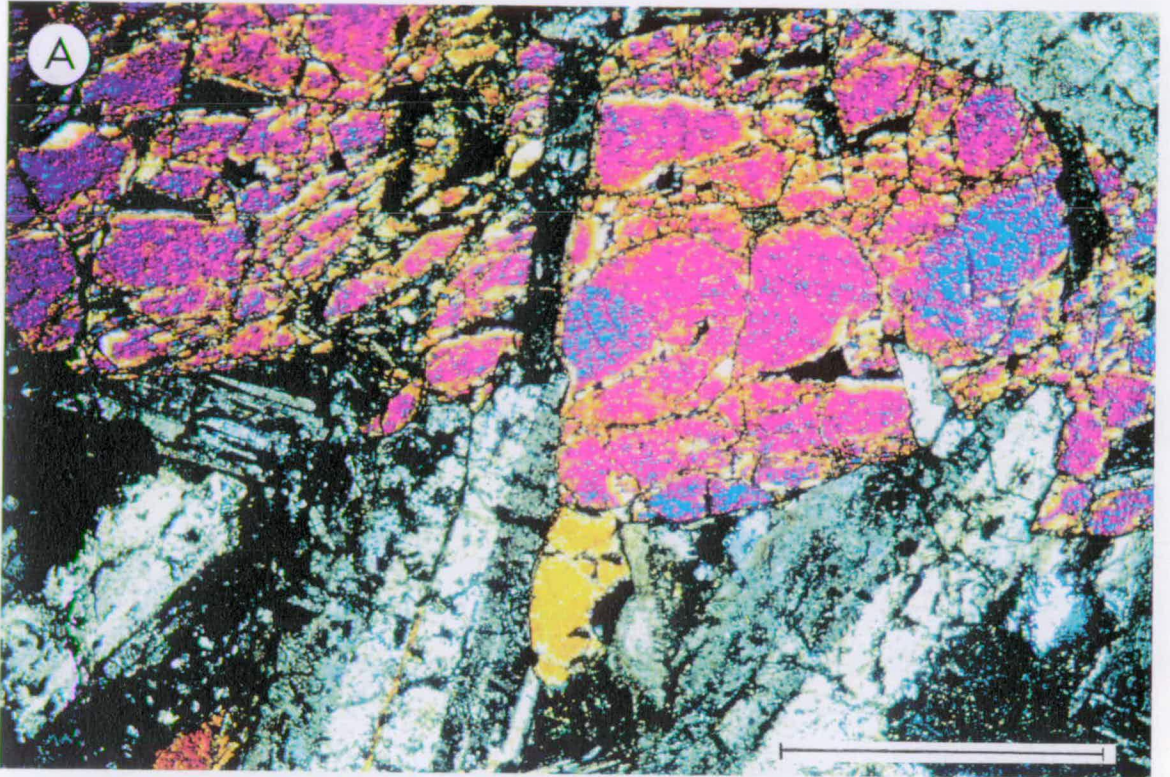




# PLATE 8.4

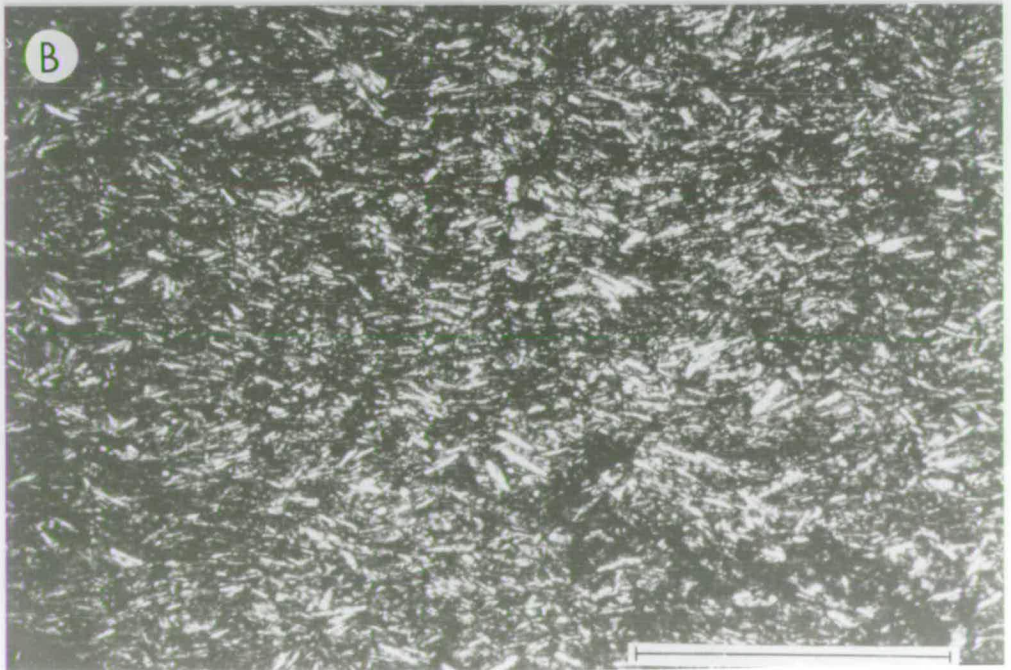
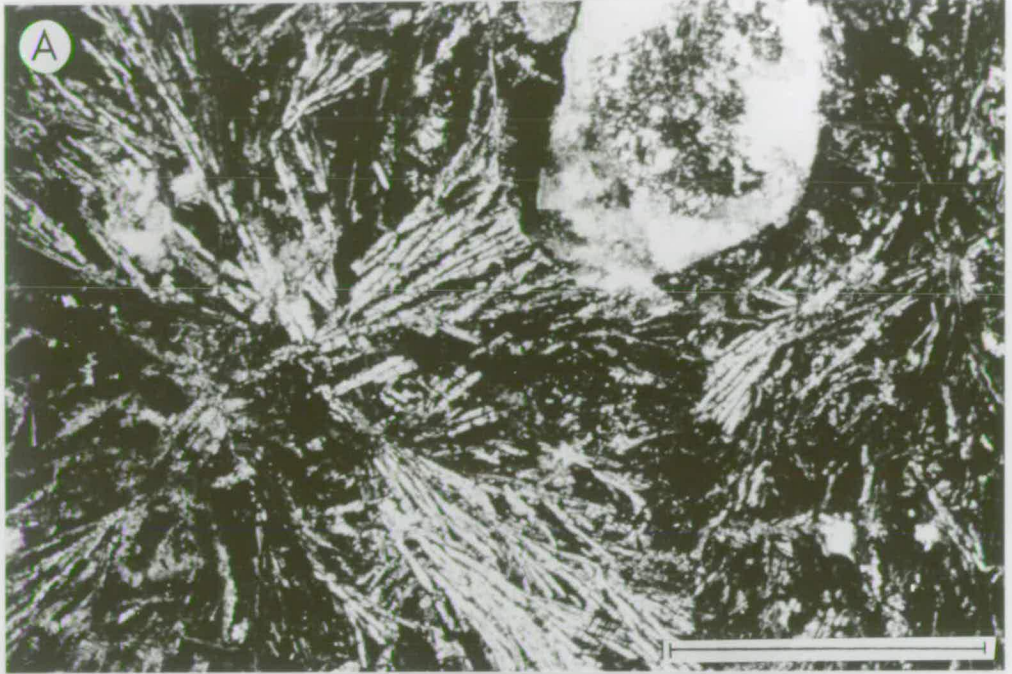
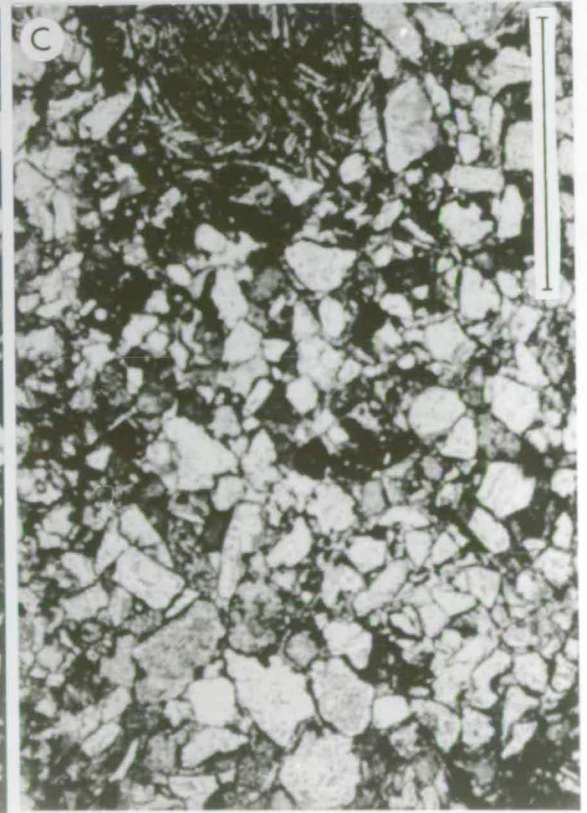
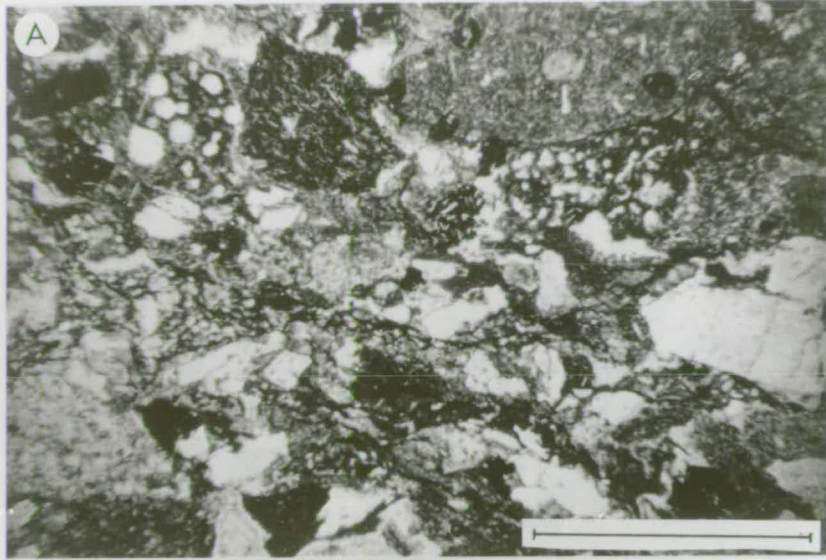


PLATE 8.5





**SECTION D: SYNTHESIS**

**CHAPTER 9: TECTONO-SEDIMENTARY EVOLUTION OF  
THE PINDOS ZONE**

## CHAPTER 9: TECTONO-SEDIMENTARY EVOLUTION OF THE PINDOS ZONE

### 9.1 INTRODUCTION

Preceding chapters have described the sedimentology and deformation of the Pindos Zone (Chapters 3-6) and of the Gavrovo-Tripolitza Zone (Chapter 7), as exposed in the NW Peloponnese. Additionally, the field relationships and composition of a tectono-sedimentary melange, found at the base of the Pindos thrust sheets (Chapter 8), have also been discussed. The purpose of this concluding chapter is to integrate all of the above data into a simplified evolutionary framework. To supplement what has already been described, additional material pertinent to the proposed palaeogeographic model is also presented. This includes supplementary information derived from the literature and the results of field work undertaken in collaboration with Dr A.H.F. Robertson north of the Gulf of Corinth.

The approach used here is to firstly consider the development of the Pindos Basin, from inception to the beginning of final closure (Section 9.2), and secondly to describe the factors responsible for deformation in the Pindos Zone during the Early Tertiary (Section 9.3).

### 9.2 BASIN EVOLUTION

#### 9.2.1 Basin Formation

The origins of the Pindos Basin can be best understood by assessing the significance of the regional geology and interpreting the geochemistry of volcanic lithologies. The dating of the rifting event can be ascertained from the ages of contemporaneous sediments overlying rift volcanics in adjacent zones and also dating the underlying lithologies on rifted continental units. Igneous and sedimentary rocks from the Pindos, Tripolitza, Vardoussia and Sub-Pelagonnian Zones are considered here.

##### 9.2.1.1 Pindos and Tripolitza Zones

The oldest coherently preserved sedimentary deposits of the Pindos Zone are intercalated sandstones, siltstones and subsidiary limestones of the Priolithos Formation, dated as Carnian (Section 3.2). These rocks were deposited upon a



volcanic substratum that is sparsely preserved as blocks in melange. Extrusive and epiclastic lithologies are also occasionally present as short sequences beneath *Halobia*-bearing limestones (Section 8.2.3.2). The volcanic rocks are tholeiitic basalts and andesites that are interpreted as transitional, from WPB to MORB. Geochemical analysis suggests that depleted magmatic intrusions rose through continental crust which had previously been hydrated with fluids derived from a subduction slab, and the resultant volcanics therefore possess an apparent arc-like geochemical signature. Similar geochemical attributes are found in greenschist metamorphosed volcanic and pyroclastic rocks present at the base of the Tripolitza zone (Section 7.2.2). These rocks were extruded onto a previously metamorphosed and folded basement. In the southern Peloponnese, Carboniferous to Permian neritic carbonates are found unconformably overlying the equivalent metamorphic basement ("Phyllite Series", Lekkas & Papanikolaou 1978, Jacobshagen *et al.* 1978a).

#### 9.2.1.2 Vardoussia Zone

North of the Gulf of Corinth, the Vardoussia Zone is inferred to represent the western margin to the Parnassos Zone, a Pindos Ocean intra-basinal high (Robertson *et al.* 1991). The Parnassos unit is floored by continental crust and capped by a shallow-water Mesozoic carbonate sequence. Sedimentary and igneous rocks were studied in the Vardoussia Mountains between Kerassia and Melia and around the town of Lidohorio. Sheets of massive and pillow lava, up to 80m thick, are depositionally overlain by silicified *Halobia*-bearing limestone and ribbon-bedded chert. Also present are individual blocks of shallow water limestone (e.g. stromatolitic and megalodont-bearing limestones). The sediments are confirmed to be of Upper Triassic age (Beck 1980, Robertson & Degnan 1992a) and the igneous lithologies are geochemically similar to the volcanic rocks found in the main study area (Figure 9.1). Also found are serpentinite sheets and WPB of Cretaceous age, discussed in Section 9.3.1.

#### 9.2.1.3 Sub-Pelagonnian Zone

The Othris Mountains of the Sub-Pelagonnian Zone contain rocks considered to represent the opposing (eastern) margin to the Pindos Basin (Smith *et al.* 1975). The succession was deposited upon a pre-Upper Permian continental basement. The lowest non-metamorphosed sedimentary formation in the sequence (Gavriani Formation) contains Upper Permian to Lower Triassic fauna, including gastropods, ammonites and lamellibranchs (Smith *et al.* op. cit.). The formation is considered to



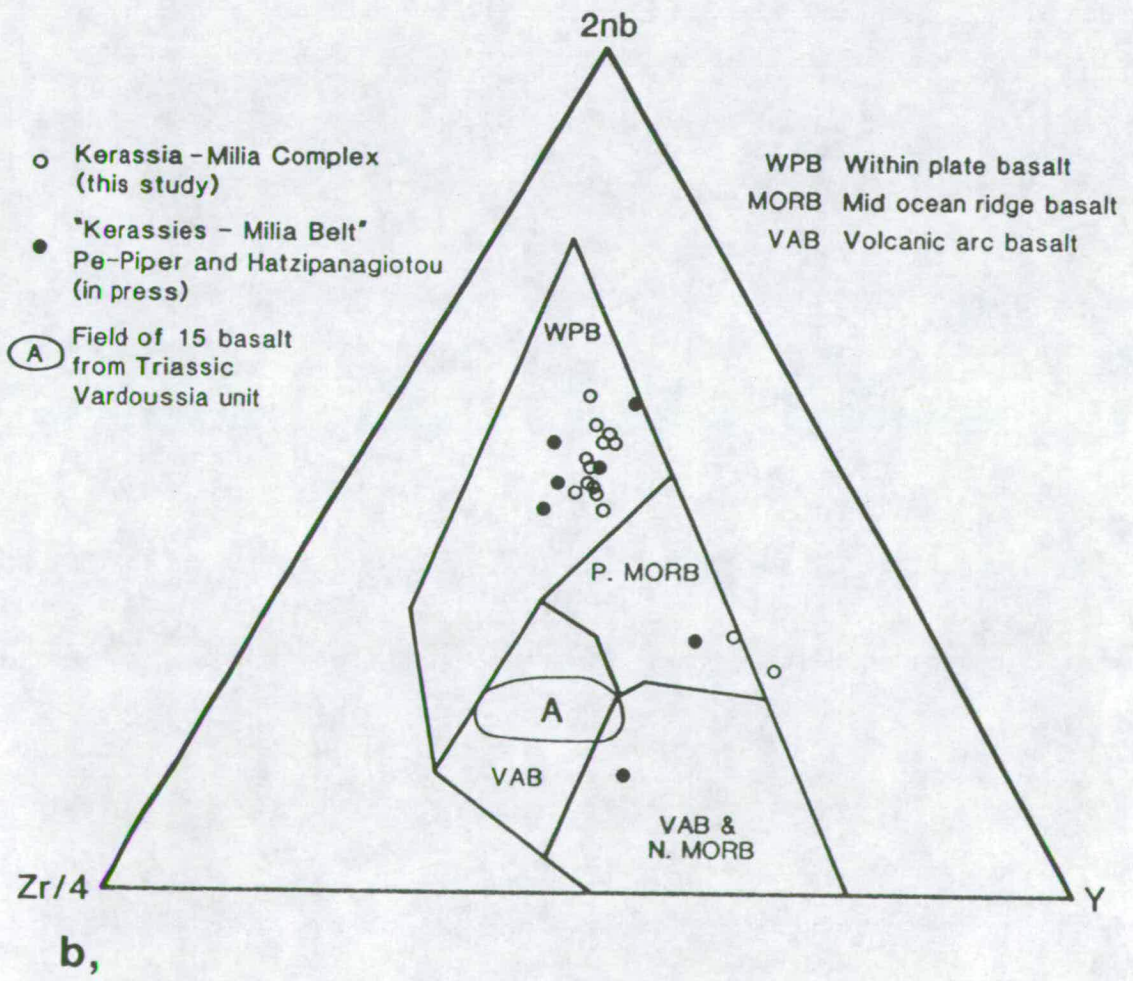
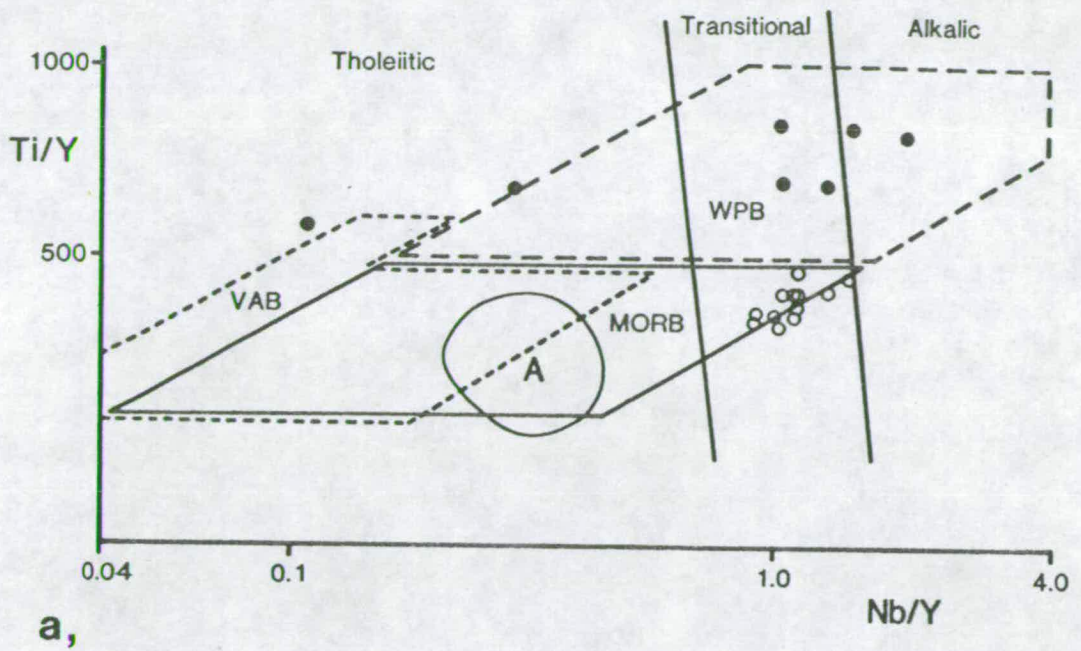


**Fig. 9.1** Tectono-magmatic discrimination diagrams for basalts from the Vardoussia Zone (Robertson & Degnan 1992). Note that the Triassic rock analyses (field A) are similar to the igneous rocks of the Pindos Zone tectono-sedimentary melange and the volcanics of the Tripolitza Zone. The basalts of the Kerassia-Melia Complex are associated with serpentinite sheets. They plot in the WPB field but may represent seamount settings.



have been deposited in a shallow water environment. From Middle to Upper Triassic times the Othris region was subjected to volcanism. After this period, eastern Othris continued as a site of shallow carbonate deposition, while in the west deepening is indicated by the deposition of reworked neritic facies and pelagic carbonates.

#### 9.2.1.4 Pre-rift Palaeogeography

There is a distinctive stratigraphic symmetry to the opposing margins of the Pindos Basin, with Middle Triassic volcanics overlying Permian to Triassic neritic carbonates, themselves unconformably overlying the metamorphosed basement of the Phyllite Series (Apulian domain) and the Sub-Pelagonian Zone. The close similarity in the early sedimentary history of the Apulian and Pelagonian basement lithologies, and the similar age of volcanics, suggest that the pre-Middle Triassic Apulian and Pelagonian regions may once have formed a continuous area of shallow water sedimentation. The presence of Permian to Lower-Middle Triassic shallow water carbonates further suggests that regional lithospheric extension began at the close of the Palaeozoic (c.a. 255my). The Middle to Upper Triassic volcanic rocks from the NW Peloponnese, Vardoussia and the Sub-Pelagonian Zone, all appear to be geochemically transitional and they are considered to represent a phase of accelerated rifting during the Middle Triassic. Final continental break-up was completed by Carnian times (c.a. 225my).

#### 9.2.1.5 Rifting Mechanisms

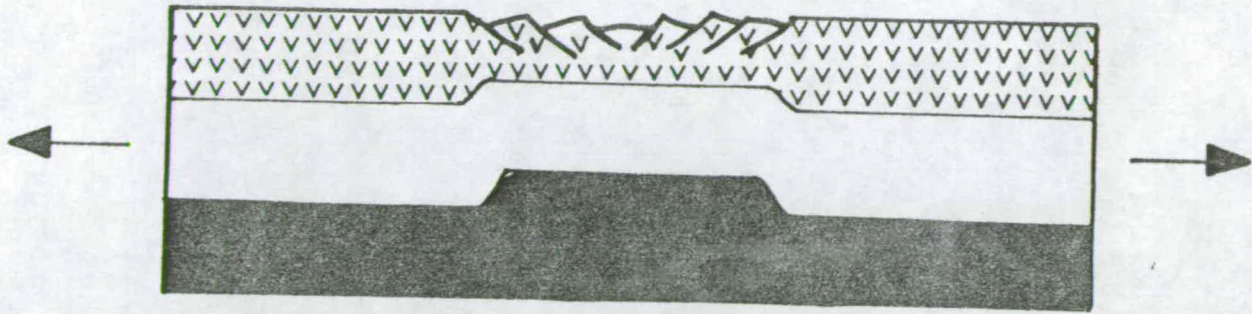
Due to the complexities of Tertiary deformation, there is little hard evidence that can be used to postulate a rifting mechanism within the developing Pindos Basin (e.g. the uniform stretching model of McKenzie 1978; the simple shear model of Wernicke 1981; or an intermediate model, Barbier *et al.* 1986, Fig. 9.2). However, two elementary observations suggest alternative rifting models and no particular mechanism is favoured here:-

1) The transitional rift related volcanics are found on both of the opposing basin margins, and also surrounding the Parnassos intra-basinal high. A basic tenet of the Wernicke model is asymmetric basin development which results in volcanic activity concentrated on one margin only (upper plate, Figure 9.2).

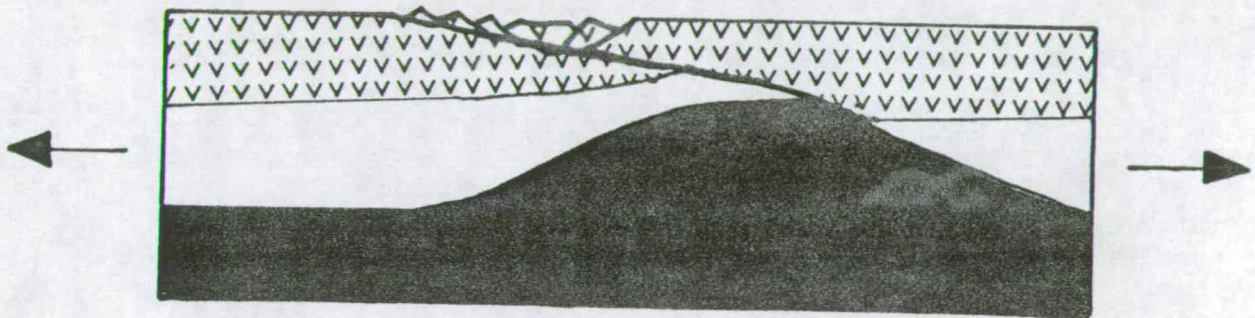
2) It is probable that the shelf of the Apulian margin (comprising the Pre-Apulian, Ionian and Gavrovo-Tripolitza Zones) can be restored to a width comparable with that of the present day Bahamas, i.e. 200-300Km. In contrast, the carbonate platform



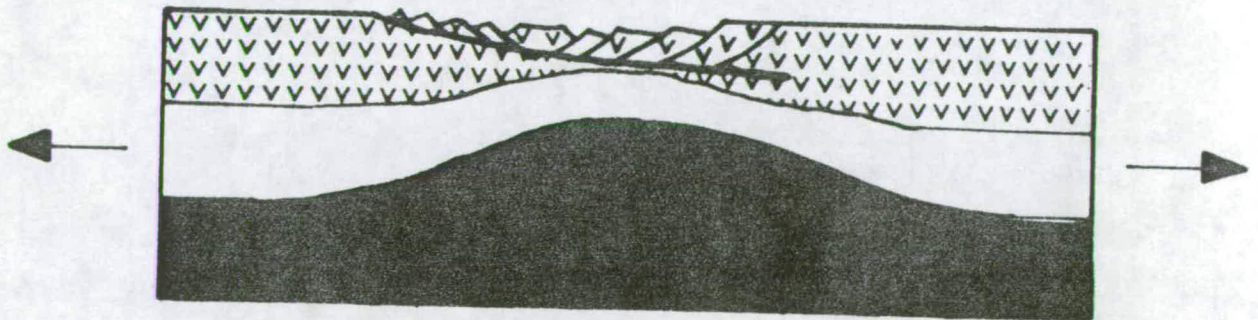
### PURE SHEAR



### SIMPLE SHEAR



### COMBINED SHEAR



CRUST



SUBCRUSTAL LITHOSPHERE



ASTHENOSPHERE

Fig. 9.2 Models of lithospheric stretching after McKenzie (1978), Wernicke (1981) and Barbier et al. (1986).



that developed along the western margin of the Pelagonian Zone was probably a few tens of kilometres wide at most. This is based on the present day width of the complete Pelagonian terrane (which preserves both east and west facing shelf lithologies) and presumes that Pelagonian Zone continental basement has not overthrust a large proportion of the western platform (this does not appear to be the case as the Sub-Pelagonian Zone represents the principal thrust leading-edge, overriding the Pindos Basin). Asymmetric rifted margins are predicted by the Wernicke model, with wide shelves developing on the lower plate.

### 9.2.2 Sedimentary Evolution of the Pindos Zone

The sedimentary evolution of the Pindos and Gavrovo-Tripolitza Zones can be summarized by the time versus stratigraphy/activity diagram illustrated in Figure 9.3. In addition to the principal litho-types present, this diagram also indicates the eustatic sea level curve of Haq *et al.* (1988), inferred periods of platform erosion (emergence), and the approximate level of the CCD relative to the Pindos basin sediment/water interface.

#### 9.2.2.1 Upper Triassic

From Middle-Upper Triassic times a passive margin became established between the Apulian continental terrane and the Pindos Ocean. Adjacent to the rifted margin of Apulia, volcanic seamounts, or horsts of rifted continental basement were capped by Ladinian-Lower Carnian-aged ammonite-bearing nodular limestones (Section 3.3.1.2). Rifted continental slivers close to the margin, as represented by Meghdovas (Section 3.3.2.2), were covered by prograding shallow water carbonates, while more outboard seamounts (e.g. as represented by Glafkos), subsided. In the southern Peloponnese volcanoclastics and volcanic mudstones underlie *Halobia*-bearing limestones of Upper Triassic age. These limestones are lithologically correlated with the Drimos Formation, however, they may be older than, or temporal equivalents to the Priolithos Formation. The siliciclastics of the Priolithos Formation were unevenly deposited around basement highs from coalescing fans shed off the Apulian shelf (Section 3.2.2.2). The formation comprises clasts indicating both a metamorphic and volcanic provenance, mixed with components derived from a shallow water carbonate platform. These sediments are considered to be rift-related, i.e. the erosional products of uplifted rift-shoulders, and derived mainly from the Apulian hinterland.

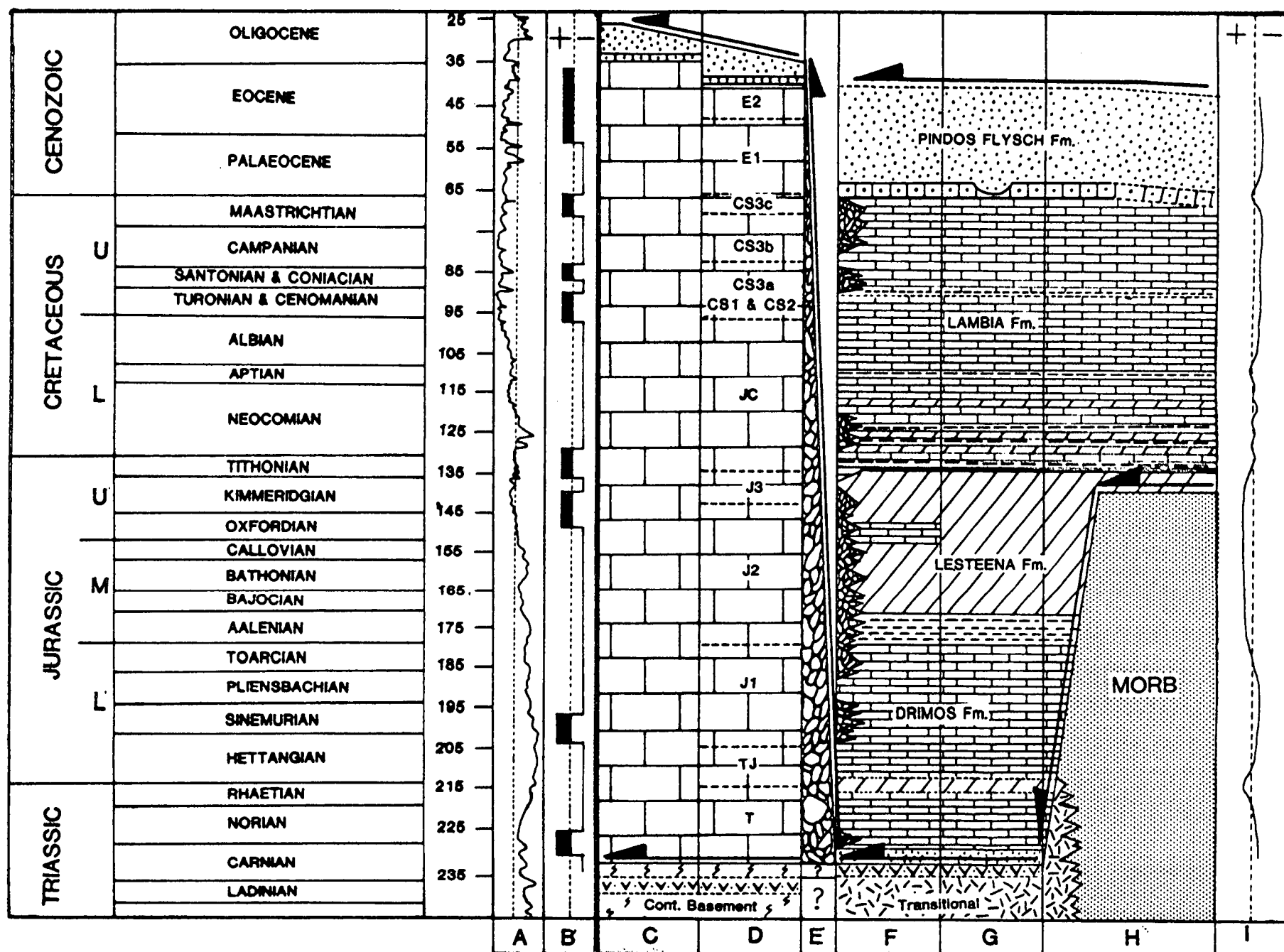


Fig. 9.3 Time v lithology/activity diagram. A = 2nd order sea level curve, dashed line represents present day +100m (after Haq et al. 1988). B = Periods of platform erosion (+ = probable emergence), based on Tsalia-Monopolis (1977), De Wever (1975) and this study. C = Gavrovo Zone. D = Tripolitza Zone; stratigraphy after De Wever (1975). See also Section 7.3.1. E = Slope facies (not exposed). F = Proximal Pindos Zone, this study. G = Distal Pindos Zone, this study. H = Pindos Zone of the "Table d'Arcadie" (Dercourt 1964). I = Inferred relationship of the CCD to the sediment/water interface (dashed line). + = CCD above the sediment surface. Also shown are the principal thrust surfaces. Note: 1) Apparent down cutting of the basal thrust through the stratigraphy in the transport direction. In fact the thrust plane represents the base of the sedimentary succession. 2) The Pindos thrust stack ramped up the slope facies onto the Gavrovo-Tripolitza platform.

### 9.2.2.2 Upper Triassic-Lower Jurassic

The Drimos Formation (Section 3.3) preserves cherts, hemipelagic micrites and turbiditic calcisiltites that were deposited in more distal areas of the Pindos Basin, while coarse calcirudites, derived from rock falls and debris flows, were deposited further inboard to the west. There was probably some subsidence and erosion of volcanic slopes and edifices close to the margin, as volcanoclastic detritus was supplied to certain proximal areas (Section 3.3.2.2). The Drimos Formation represents the establishment of a quiescent phase of passive margin sedimentation. The deposition of calcareous rocks continued until Aalenian times when a profound change in the nature of sedimentation occurred.

### 9.2.2.3 Middle-Upper Jurassic

The Kastelli Mudstone Member (Section 4.3) records a reduction in the supply of calcareous sediment into the basin, with a concomitant increase in the importance of siliceous deposition. Mudstones dominate the interval and illite is the principal clay mineral present. The change is inferred to have been due to a relative sea level rise and an increase in the productivity of siliceous micro-organisms (radiolarians). These factors combined to have the effect of raising the CCD and reducing the supply of off-platform carbonate.

From Bajocian to Tithonian times most of the sediments of the Lesteena Formation were deposited below the CCD, a local exception being the thick calcirudite of the Kakotari Member (Section 4.2), found in the extreme south-west of the study area. The base of the Aroania Chert Member (Section 4.4) is represented by an interval of green chert which is mainly silicified calciturbidite. Ribbon-bedded red argillaceous chert, intercalated with siliceous mudstones and vitreous chert overlies the green chert and dominates most of the member. The regular inter-layering of these facies could be related to Milankovitch cyclicity. A notable period of manganese enrichment occurred during the Upper Jurassic and the Mn is shown to be of hydrothermal origin (Section 4.5). Local volcanic activity led to the development of hydrothermal systems and water circulating through conduits in these systems became enriched in certain elements, principally iron and manganese. Manganese was fractionated from iron-bearing phases in sub-surface mounds due to variations in temperature, Eh and pH. Manganese charged fluids were then debouched from low temperature vents into the Pindos water column, where much of the Mn rapidly precipitated-out. However, some Mn micro-particles remained buoyant and were carried for considerable distances from the exhalative sites and, in doing so, sorbed

additional trace elements from the water column. Dateable volcanic activity, soft sedimentary deformation and minor faulting is evident at Aroania and Kombigadi and the volcanism is considered to relate to a period of renewed extension (transtension?) along the Apulian margin, a feature recognised in other Tethyan regions (Robertson & Boyle 1983).

During the Upper Jurassic, outwith the immediate study area, significant tectonic events were underway along both margins of the Pelagonian Zone (Section 9.2.3). At this time ophiolites derived from the Pindos Ocean were emplaced onto the Pelagonian micro-continent to the east. Thereafter the Pindos Basin became a "remnant ocean", estimated as at least 220Km wide. The effects of the ophiolite emplacement were not reflected in the contemporary sediments studied here, but work by Thiebault & Fleury (1991) suggests that Lower Cretaceous mudstones do contain a partial ophiolite mineralogy.

#### 9.2.2.4 Lower Cretaceous

During the Tithonian the CCD fell below the sediment/water interface in the most proximal areas of the Pindos Basin, allowing the deposition of porcellanous *Calpionellid*-bearing limestones (Section 5.2.1). After this short interval, the CCD apparently fluctuated near the sediment/water interface for a considerable period of time (Tithonian to Coniacian/Santonian). This interval is represented by the condensed sequence of the Paos Limestone Member (Lambia Formation), consisting mostly of pink micrites and calcisiltites. There is a short interval when terrigenous sandstones were deposited in central parts of the study area although it has not been established whether this sediment influx was due to sea level fluctuation or tectonics.

#### 9.2.2.5 Upper Cretaceous

The Erymanthos Limestone Member (Section 5.2.3) indicates a return to depositional conditions similar to those prevailing during the Upper Triassic/Liassic (Drimos Formation), i.e. deposition of coarse carbonate sediments, derived from the platform and slope, in the west and hemipelagic and turbiditic carbonate deposited in more outboard areas.

A distinctive interval of black chert within, or at the base of the overlying Kataraktis Passage Member (Section 5.2.4) is dated as straddling the Mesozoic/Cenozoic boundary. Close to the boundary, carbonate debris flow deposits are more



commonly encountered in the west, while terrigenous sediment began to attain significance in central parts of the study area. The initiation of debris flows may reflect a sea level fall. The siliciclastic sediment was principally derived from the north and the terrigenous component is interpreted to represent detritus eroded from an uplifted site of continental collision, caused by the diachronous closure of the Pindos Basin. However, low stands also favour the development of turbidite systems and eustatic sea level variations may also have been contributory factors.

#### 9.2.2.6 Palaeocene-Oligocene

During the Palaeocene the proportion of terrigenous sediment entering the Pindos Basin increased significantly, eventually swamping carbonate deposition throughout the basin (Section 5.3). Palaeocurrents indicate dominantly axial flows derived from the north and clasts show a mixed provenance. It is considered likely that the oldest preserved siliciclastic sediment represents the passive infilling of the Pindos Basin, while younger terrigenous material covered an over-supplied trench and became unconformably incorporated into a subduction-accretion complex. The lithostratigraphic unit (the Pindos Flysch Formation) continues up to the Upper Eocene. There is no syn-sedimentary deformation evident in the succession, although it is very sparsely preserved. Thus, the structural effects of the approaching orogen are not discernable at this time. When the deformation front did finally reach the region represented by the study area, structuration and break-up of the Tripolitza platform was relatively rapid, as platform collapse is dated as Upper Eocene-Lower Oligocene.

#### 9.2.2.7 Palaeogeography

The sediments of the Pindos Group record a period of passive margin sedimentation between the Upper Triassic and the Eocene. Pindos Group facies distributions suggest deposition in a deep water environment, adjacent to a steep carbonate slope that lay to the west. The reconstruction of proximal facies indicates that coarse-grained carbonate sediment entry into the basin was mostly along linear sources, rather than from point sources, and that a base-of-slope apron was supplied with slope and platform derived detritus. There was, however, some channelisation of the coarse sediment to more outboard localities and the channels may have originated on the slope. There is also evidence for a Jurassic canyon or upper fan environment at Kakotari (Section 4.2). Further outboard, calciturbidites and hemipelagic sediments were deposited on an abyssal plain. Through time, the basin was subjected to a

fluctuating CCD due to various combinations of sea level change (eustatic and local) and biogenic productivity.

#### 9.2.2.8 Subsidence Curves

The sedimentary evolution of the Pindos and Gavrovo-Tripolitza Zones provide some insight into the bathymetric history of the region. Green (1982) and Thiebault (1982) have both attempted to decompact sedimentary columns of the zones in order to characterise the nature of the subsidence. Green (op. cit.) used the data of Fleury (1980) to construct a subsidence curve for the Gavrovo-Tripolitza Zone, while Thiebault used his own data and that of De Wever (1975) and Tsalia-Monopolis (1977) for the Tripolitza zone only. It was inferred by both authors that Tripolitza zone sedimentation occurred at depths less than 200m. Green (op. cit.) concluded that the Gavrovo-Tripolitza Zone represents an area in which the overall degree of subsidence was low, and could be accounted for principally by sediment loading. Thiebault (1982) calculated that the Tripolitza zone subsidence curve indicated a crustal thinning equal to a  $\beta$ -factor of 1.3.

Green (op. cit.) utilised the proposed Tethyan depositional depths of Bosselini and Winterer (1975) to estimate depositional depths for Pindos Group sediments. In subsidence modelling, he argued that the Pindos Zone underwent a relatively rapid exponential subsidence which quickly led to deep water sedimentation during the Upper Triassic. Green considers that this pattern is similar to that of oceanic lithosphere. Thiebault's subsidence curve is similar to Green's, although he suggests that a  $\beta$ -factor of only up to 3 is valid.

#### **9.2.3 The Pindos Basin as a Neotethyan Ocean**

There is much evidence presented in this thesis suggesting that a true oceanic substratum underlay distal sediments of the Pindos Zone and that this basement was almost totally subducted during Tertiary times. The tectonic development of the Pindos Basin according to this model can be simply synthesised in a series of cartoons relating the Pindos Zone to the adjacent Gavrovo-Tripolitza and Pelagonian Zones through time (Figure 9.4). The evidence provided here for the validity of such a model includes: (1) the presence and spatial distribution of deep sea sedimentary facies; (2) similarities between the inferred Pindos margin palaeogeography with the present day Red Sea and Bahama regions; (3) the characteristics of the subsidence curves contrasting the Pindos and Gavrovo-Tripolitza Zones; (4) the transitional

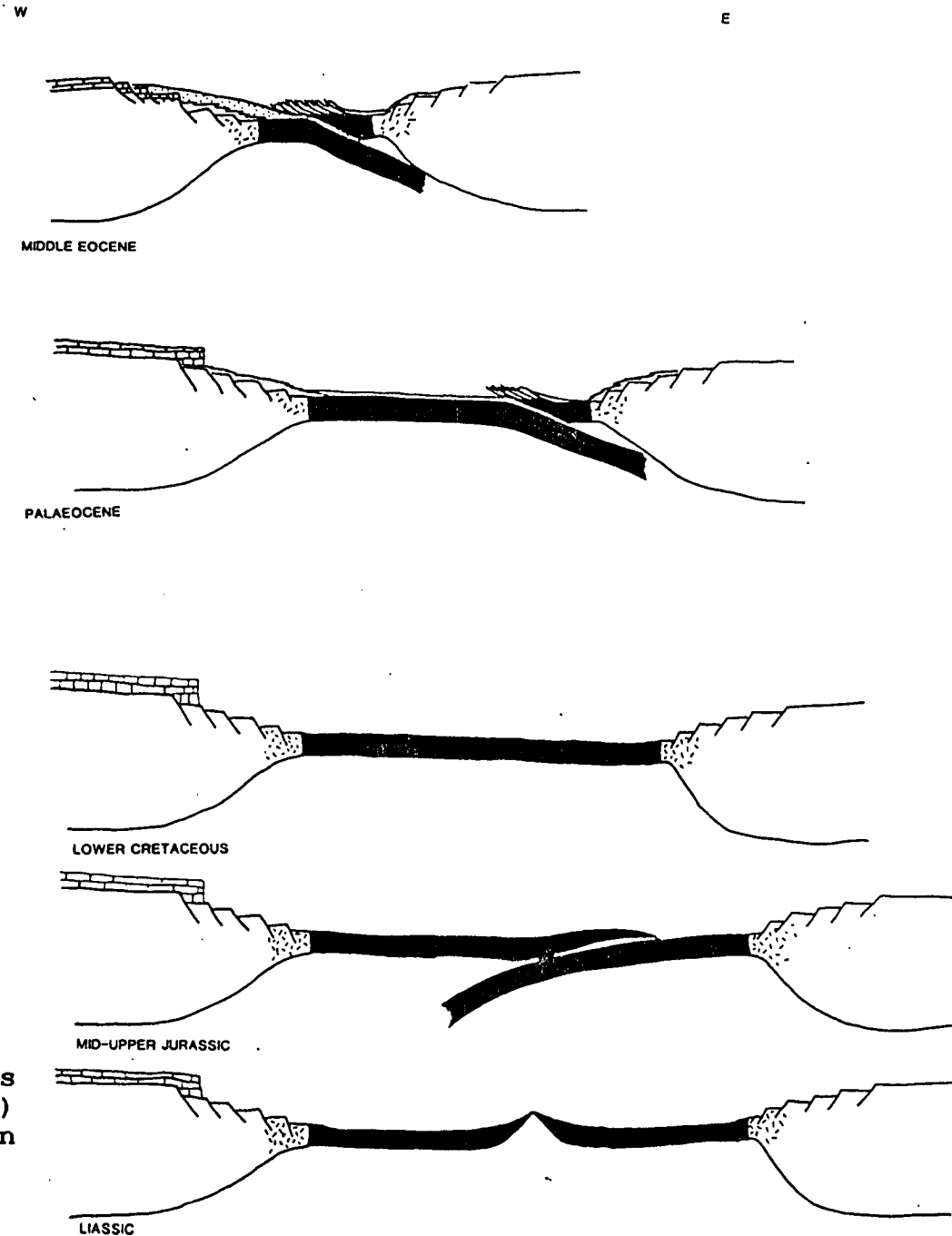
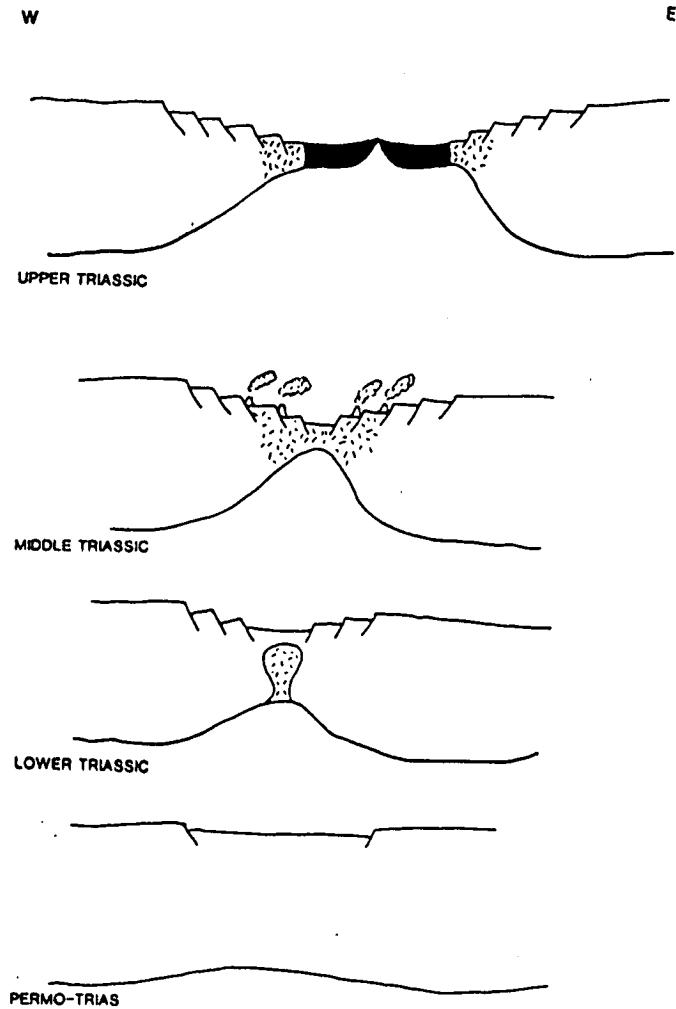


**Fig. 9.4** Simplified tectonic evolution of the Pindos Zone, from initial lithospheric extension (Upper Permian) through to the development of a Tertiary subduction complex. Explanations in text.

nature of the preserved volcanics; (5) Late Cretaceous Vardoussia Zone ultramafic lithologies (Section 9.3.1); and lastly (6) the large difference in the timing of trench/foreland basin migration across the Pindos and Tripolitza Zones (Section 9.3.3). Additional evidence can be gained from other studies:-

Jones (1990) has studied the tectono-stratigraphy of the Pindos ophiolite and associated sedimentary units, preserved in northern Greece. Intact sheets of Triassic-Jurassic extrusives are of WPB to MORB-type and preserved sequences of Upper Jurassic chert, also Cretaceous deep water limestones, are equivalent to the Lesteena and Lambia Formations. Dismembered intrusive and extrusive ophiolitic igneous rocks include boninite and island arc tholeiite. These indicate the development of supra-subduction zone spreading within an oceanic basin. Ophiolite emplacement onto the western Pelagonian margin occurred during the Upper Jurassic. The dating of the amphibolite sole at the base of the ophiolite indicates initial displacement at 165my. Evidence is provided from structural and petrological analyses, suggesting that the Pindos and Vourinos ophiolites are continuous beneath the Meso-Hellenic Trough and that they were both derived from the same basin that lay to the west of the Pelagonian micro-continent, viz. the Pindos Ocean.

In the Argolis area of the Peloponnese, Clift (1990) studied sparsely preserved ophiolitic rocks. Structural measurements from the ophiolite and underlying sediments indicate derivation from the NE, however, subsequent micro-plate rotations of the Argolis, verified by palaeomagnetic study (Morris 1990), reveals derivation from the NW, i.e. the Pindos Basin.

Further supporting evidence for a Pindos Ocean is to be found in the Sub-Pelagonian Zone. This includes high temperature fabrics and folding in the Othris ophiolite (interpreted as the along strike continuation of the Pindos and Vourinos ophiolite bodies) and facies trends, sedimentary structures and deformation in the underlying basinal and continental margin lithologies (Smith *et al.* 1975, 1979).

Taken in isolation, any one argument for an oceanic substratum can be criticised. However, in combination the above evidence would appear to conclusively support the assertion that the Pindos basin was a small Neotethyan ocean, separating the rifted micro-continental fragment of Pelagonia from Apulia. A fuller account of the evolution of the Pindos basin as an oceanic domain is provided in Robertson *et al.* (1991).

## 9.3 BASIN CLOSURE AND DEFORMATION

### 9.3.1 Initiation of Basin Closure

The partial closure of the Pindos Ocean and the emplacement of ophiolites onto the Pelagonian micro-continent during the Upper Jurassic, corresponds to the beginning of sea floor spreading in the Central Atlantic. This major tectonic event induced sinistral movement between Africa and Laurasia, in turn reorganising the alignment of neighbouring micro-plates. Significantly for the Tethyan realm, the Western Mediterranean underwent transtensional stresses and oceanic crust formed in the Ligurian-Piedmont Basin while eastward movement of the African plate caused compression along the margins of Neotethyan basins (e.g. Pindos and Vardar) and the intervening oceanic areas began to close. In the Pindos Basin, complete closure in the north (Yugoslavia) is evidenced by ophiolite obduction, suturing of platforms and transgressive shallow water sedimentation (Karamata 1988). Further south (Albania and Greece), closure was only partial, and a remnant ocean remained until Early Tertiary times (Robertson *et al.* 1991).

Until Late Cretaceous times, there is little evidence for major tectonic activity in the Pindos Basin, although Europe and Africa continued to move in a sinistral fashion with respect to one another. An exception is provided by the presence of ultramafic lithologies found within the Kerassia-Milia Complex, in the Vardoussia Zone (Beck 1980, Robertson & Degnan 1992a). Sheets of serpentinitised harzburgite, dunite, pyroxenite and minor gabbro are found tectonically intercalated within Tertiary flysch deposits. Extrusive rocks are also present as pillow lavas and these have been geochemically analysed by Robertson & Degnan (Fig. 9.1, 1992a). They plot in the WPB fields of tectono-magmatic discrimination diagrams. However, the close association with ultramafic lithologies and the fact that they are clearly geochemically different to the Triassic extrusives, suggests that they may represent remnants of oceanic seamounts. The presence of ophiolitic clasts within overlying Cretaceous pelagic carbonates of the Vardoussia Zone (correlated with the Lambia Formation) indicates that faulted oceanic crust was exposed on the Pindos Ocean floor during the Upper Cretaceous, well before the appearance of flysch locally. It is not known if extensional or compressional faulting was responsible, but the event probably relates to continuing plate reorganisations. Harbury & Hall (1988) suggest that Late Cretaceous extension in the SE Aegean was related to the formation of oceanic crust to the east (Cyprus and Turkey).

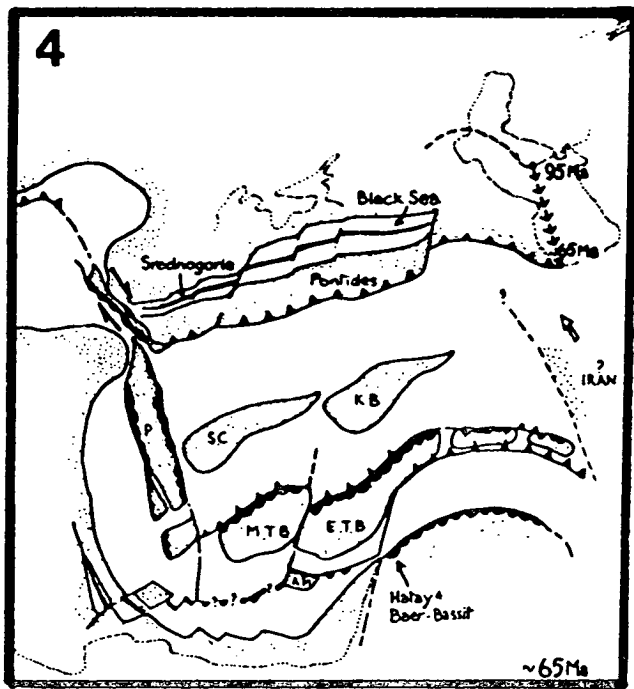
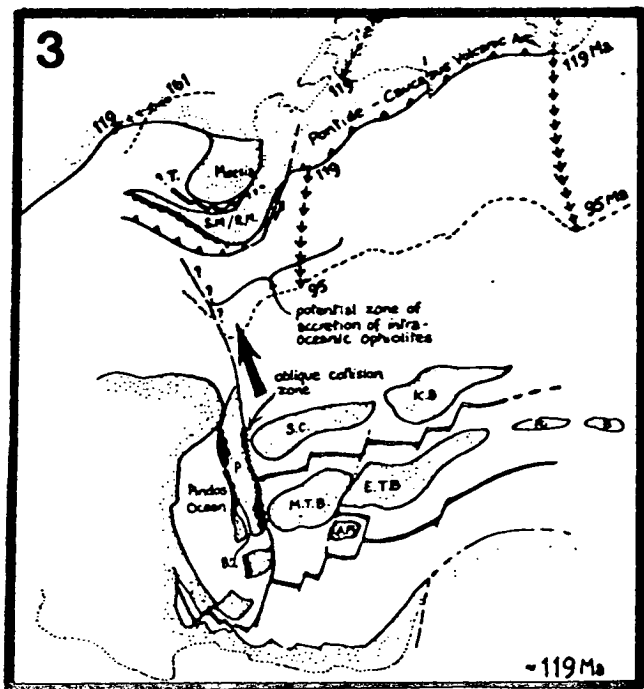
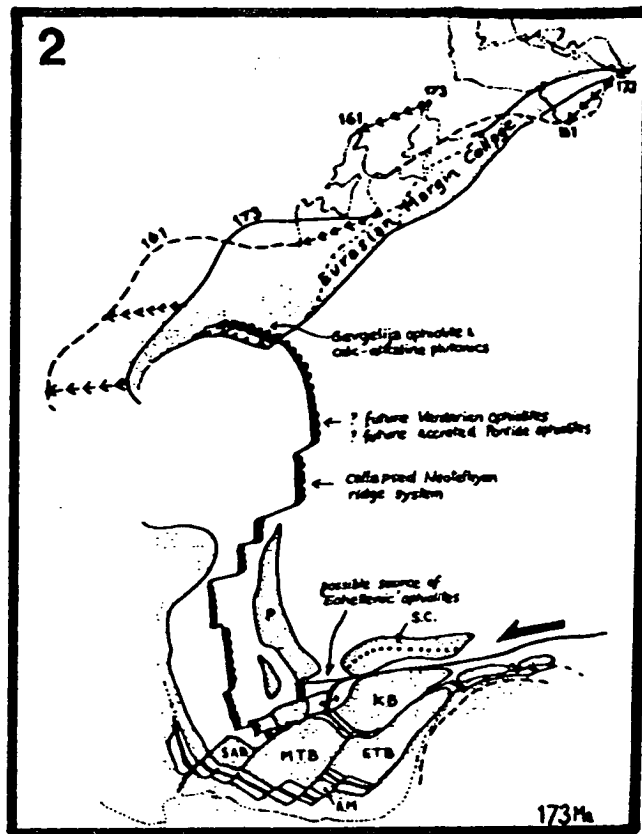
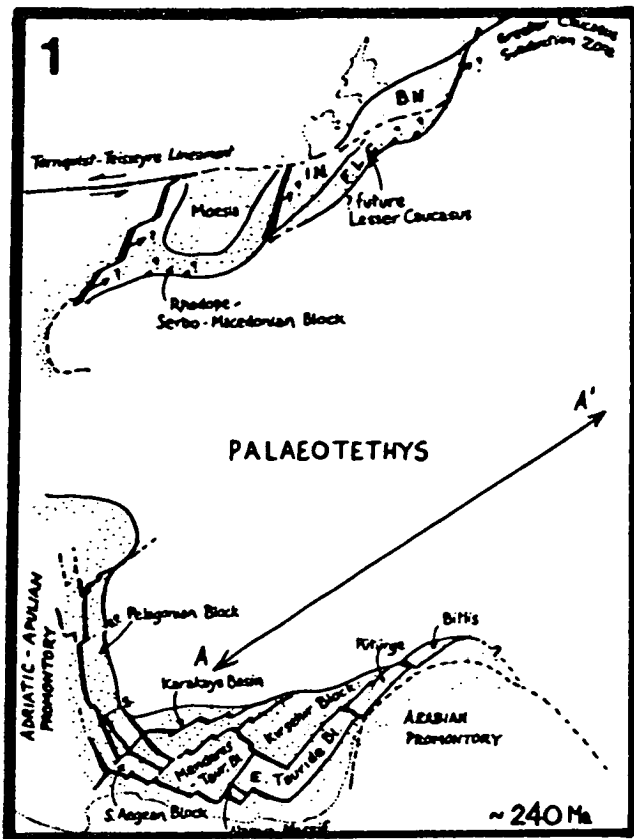


Fig. 9.5 Palaeogeography of the Eastern Mediterranean/Middle East for the: 1) Mid-Triassic, 2) Mid-Jurassic, 3) Lower Cretaceous, 4) Late Cretaceous. (From Robertson & Dixon 1984).

The final closure of the Pindos and other Neotethyan basins began in the Upper Cretaceous, coeval with the opening of the South Atlantic-Indian Ocean (causing northward movement of Africa and the anti-clockwise movement of Apulia). The initial sedimentary response to this second phase of Hellenide compression was apparently coeval in adjacent basins (Pindos and Vardar) although by Eocene times Vardar derived thrust sheets had been emplaced onto the Pelagonian Zone (Robertson 1990a). Due to the configuration of the remnant Pindos Basin (i.e. narrowing to the north, Figs. 5.6 & 9.5), east-west compression resulted in strongly diachronous continental collision between the Apulian and Pelagonian areas. This partially explains the long period of time between the earliest sedimentary response to collisional tectonics, at the end Maastrichtian, and actual deformation during the Late Eocene.

### 9.3.2 Pindos Subduction-Accretion

The Pindos Group, as studied here, represents the most westerly region of the Pindos Basin. The Pindos thrust stack is inferred to represent an accretionary complex formed by the progressive eastward subduction of oceanic and transitional crust, with the decoupling of pelagic sediments from a volcanic substratum and their incorporation into a developing thrust wedge. In this manner, the deformation of the sedimentary succession proceeds towards the foreland, emplacing older rocks onto younger strata (Fig 9.6). Some sediments were supplied to the trench from the hinterland (Pelagonia) via the inner trench slope, however most palaeocurrents are axial, a feature commonly observed in subduction complexes (Underwood & Bachman 1982). The palaeocurrent evidence, along with the paucity of reworked Pindos material, suggests that the accretionary wedge formed a submarine barrier. Ponded sediments on the wedge, trench olistoliths and unconformities are not recognised in the Pindos Flysch Formation due to the erosion of the youngest sediments. Blocks within the tectono-sedimentary melange may, however, represent trench deposits and the decapitated portions of down-going edifices (Fig. 8.6).

There is no evidence for the development of a volcanic arc within the Pelagonian Zone. The lack of a recognisable arc terrane could be due to a number of factors. Most significantly, the width of the remnant Pindos Ocean is inferred to be only 220-300km. Magma generation occurs at approximately 120km beneath the over-riding plate. With a subduction dip of just 20°, at least 350km of lithosphere would need to be subducted before magma generation started and with shallower dips even

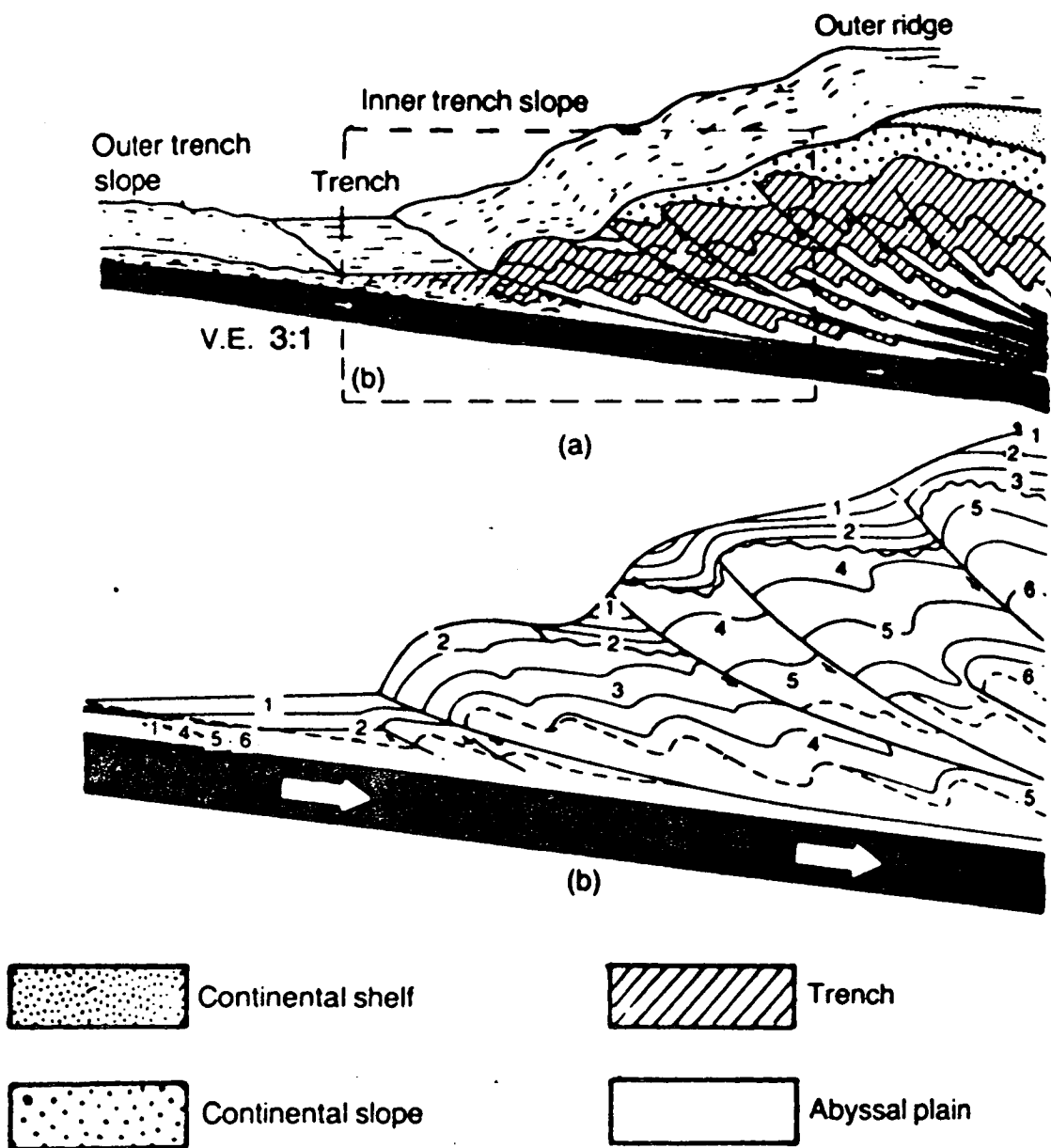


**Fig. 9.6** Model of subduction-accretion (after Seely et al. 1974). a) Distribution of facies. b) Distribution of isochrons (stratigraphy), 1 = youngest, 6 = oldest. The dashed line represents the boundary between trench turbidites (above) and sediments from the abyssal plain. The wavy line represents the boundary between ponded sediments deposited on the wedge (above) and accreted trench turbidites. Explanations of relevance to the Pindos Group in text.



more crust would need to be consumed. Furthermore, the continental collision between the Pelagonian and the Serbo-Macedonian continental units would have thickened the crust, making magmatic intrusions more unlikely to reach the surface. Lastly, orogenic granites and calc-alkaline volcanics of Oligo-Miocene age are found further east within the Serbo-Macedonian and Rhodope Zones of northern Greece. These may have formed due to the subduction of Neotethyan oceanic crust from other basins. However, recent work (N. Kolokotroni, pers. comm.) suggests that they represent magmatic intrusions which have an inherited "subduction-like" character. They were intruded during an extensional event that occurred immediately after Hellenide compression locally.

### 9.3.3 Platform Collapse and the Transition to a Foreland Basin

During the Upper Eocene, at the approximate time that Pindos successions were being actively deformed, the Tripolitza platform began to break-up. This was expressed by extensional faulting both parallel, and at high angles, to the margin. Portions of the platform were uplifted and eroded, resulting in "break-up" breccias being shed down the slope. According to classical models of foreland basin development, lithospheric flexure due to orogenic loading forms significant depocentres adjacent to the thrust wedge, while crustal flexures in the foreland create a peripheral forebulge (Fig. 7.10). Complications arise where a continental margin approaches a site of subduction and the thrust load of a subduction-accretion complex formed on oceanic crust begins to cause instabilities at the transition to continental crust. Such is the case for the Gavrovo-Tripolitza and Pindos Zones. Consequently, rather than the straight-forward migration of a foreland basin across homogenous crust, thrust sheet loading may well have initiated a significant rupture at the pre-existing zone of weakness marking the edge of the Apulian passive margin. It could be inferred that if the Pindos Group succession had been deposited on continental crust then foreland basin migration would have been smooth. As it is, there is a considerable time gap between terrigenous sedimentation in the Gavrovo-Tripolitza and Pindos Zones and this corresponds to depocentre migration from an oceanic to a continental domain and the transition from trench sedimentation to foreland basin sedimentation.

In the model proposed here (Section 6.5), when the Apulian continental basement reached the subduction trench, although the platform had collapsed, the margin would have still formed a significant topographic barrier, jamming the subduction

system. Compression would have continued however, and the subduction-accretion complex would have become locked. Further tightening within the thrust stack would lead to additional structuration (Section 6.5). At this stage, stress was transferred through to the neritic sequences which deformed by folding and thrusting. Finally, prior to complete continental collision between the Pelagonian and Apulian units, the Pindos thrust stack ramped up a relatively narrow zone of slope facies sediment and was emplaced onto the Gavrovo-Tripolitza platform.

#### **9.3.4 Emplacement of the Pindos Thrust Stack**

Emplacement of the Pindos thrust stack occurred during the Oligocene and continued until the Upper Oligocene. The Pindos basal thrust generally cut up-section through the flysch, but utilised a broad crustal flexure in the region of Chelmos, creating a detachment at the platform/flysch interface. By the emplacement stage it is probable that the Pindos thrust stack was sub-aerial, as massive debris flows comprising well rounded cobble-grade material were being shed into the flysch basin depocentre from the Pindos thrust stack. The main basin consisted of a series of minor thrust-sheet-top basins, developed on the back of the platform, that were systematically over-ridden by the Pindos thrust stack. Intra-platformal thrusting ahead of the main Pindos thrust placed tectonic inliers of neritic carbonate onto the flysch, sometimes at photic depths. These inliers were colonised by shallow water benthic organisms. They also formed topographic highs that deflected palaeoflows within the foreland basin.

#### **9.3.5 Post-Emplacement Tectonics**

The Hellenide deformation front migrated westward and was still active up to Pliocene times (Underhill 1985). Today it could be argued that the final subduction of the Ionian Sea is also related to the Hellenide orogeny. In the study area, structures indicating post emplacement, south to north directed compression are probably related to far-field stresses caused by the initiation of subduction along the Hellenic trench (Section 6.6.1). After subduction became established, tensional stresses were centred around the Aegean area due to back arc extension (Section 6.6.2). This resulted in an east-west extensional fault system, of which the Gulf of Corinth is a major expression. The Peloponnese has actively undergone uplift during the neotectonic period and this has been modelled to be the result of sediment

underplating, with a major change in the dip of the subducting slab beneath the Gulf of Corinth.

#### **9.4 EPILOGUE**

In conclusion, this study has attempted to provide a fuller understanding of the evolution of the Pindos Basin, from inception through to final emplacement on to the adjacent Apulian margin. It is hoped that this contribution to Tethyan studies, integrating sedimentological, geochemical and structural data, provides relevant information that will allow a fuller understanding of the sedimentary and tectonic processes affecting ancient and modern passive margins at various stages of development.

## REFERENCES

- Allen, P.A., & Allen, J.R. (1990) Basin Analysis: Principles and Applications. Blackwell Scientific Publications, Oxford.
- Allen, P.A. & Homewood, P. (1986) Foreland Basins. Special Pub. Int. Ass. Sediment. 8.
- Allen, P.A., Homewood, P. & Williams, G.D. (1986) Foreland basins: an introduction. In: Foreland Basins, P.A. Allen & P Homewood (eds.). Special Pub. Int. Ass. Sediment. 8. pp. 3-12.
- Angelier, J., Lyberis, N., Le Pichon, X., Barrier, E. & Huchon, P. (1982) The tectonic development of the Hellenic arc and the sea of Crete: a synthesis. Tectonophysics 86, pp. 159-196.
- Ardaens, R. (1978) Geologie de la chaine du Vardoussia, comparaison avec le Massif du Koziakas (Grece continentale). These 3eme cycle, University of Lille.
- Arrenheius, G., Kjellberg, G. & Libby, W.F. (1951) Age determination of Pacific chalk ooze by radiocarbon and titanium content. Tellus 3, pp. 222-229.
- Aubouin, J. (1959) Contribution a l'etude geologique de la Grece septentrional: Les confins de l'Epire et de la Thessalie. Ann. Geol. Pays Hell. 10. pp. 403.
- Aubouin, J. (1974) Des tectoniques superposees et de leur signification par rapport aux modeles geophysiques: l'exemple des Dinarides; paleotectonique, tectonique, tarditectonique, neotectonique. Bull. Soc Geol. France, (7) 15pp.426-420
- Aubouin, J., Bonneau, M., Celet, P., Charvet, J., Clement, B., Degardin, J.M., Dercourt, J., Ferriere, J., Fleury, J.J., Guernet, C., Maillot, H., Mania, J., Mansy, J.L., Terry, J., Thiebault, F., Tsoflias, P. and Verrieux, J.J. (1970) Contribution a la geologie des Hellenides: Le Gavrovo, le Pinde et la zone ophiolitique subpelagonian. Ann. Soc. Geol. du Nord, 90. pp. 277-306.
- Aubouin, J., Bonneau, M., Davidson, J., Leboulenger, P., Matesco, S. & Zambetakis, A. (1976) Esquisse structurale de l'arc egeen externe: des Dinarides aux Taurides. Soc. Geol. France Bull. 18, pp. 327-336.
- Audley-Charles, M.G. (1986) Timor-Tanimbar Trough: the foreland basin of the evolving Banda orogen. In: Foreland Basins, P.A. Allen & P. Homewood (eds.). Spec. Pub. Int. Ass. Sediment. 8, pp. 91-102.
- B.P. (See British Petroleum Company).
- Baker, P.A. & Burns, S.J. (1985) Occurrence and formation of dolomite in organic-rich continental margin sediments. Am. Ass. Petrol. Geol. Bull. 69, pp. 1917-1930.
- Baker, P.A. & Kastner, M. (1981) Constraints on the formation of sedimentary dolomite. Science 213, pp 214-216.
- Ball, M.M. (1967) Carbonate sand bodies of Florida and the Bahamas. J. Sed Petrol. 37, pp 556-591.
- Ball, M.M. (1979) Petroleum potential of passive margin slopes. In: Geology of continental slopes (eds Doyle & Pilkey). S.E.P.M. Spec. Pub. 27.
- Baltuck, M. (1982) Provenance and distribution of Tethyan pelagic and hemipelagic siliceous sediments, Pindos mountains, Greece. Sedimentary Geol. 31, pp. 63-88.
- Baltuck, M. (1983) Some sedimentary and diagenetic signatures in the formation of bedded radiolarite. In: Siliceous deposits in the Pacific region. (Ed. Iijima, Hein & Siever). Developments in sedimentology 36, pp.299-316.

- Barbier, F., Duverge, J. & Le Pichon, X. (1986)** Structure profonde de la marge Nord-Gascogne. Implications sur la mechanisme de rifting et formation de la marge continentale. *Bull. Cent. Res. Expl.-prod. Elf-Aquitane* 10, pp. 105-121.
- Barrett, T.J. (1979)** Origin of bedded cherts overlying ophiolitic rocks in the Italian North Appenines, and implications of the ophiolite-pelagic sediment sequences for seafloor processes. Unpublished D. Phil. thesis, University of Oxford.
- Barrett, T.J. (1981)** Chemistry and mineralogy of Jurassic bedded chert overlying ophiolites in the northern Appenines, Italy. *Chemical Geology* 34, pp.289-317.
- Bassias, Y. & Lekkas, S. (1988)** La serie de transition entre les zones de Tripolitza et du Pinde dans la region d'Eleokhorion-Mont Parthenion (Peloponnese, Grece). *Ann. Soc. Geol. Nord* 107, pp. 297-304.
- Bathurst, R.G.C. (1976)** Carbonate sediments and their diagenesis. *Developments in sedimentology* 12, Elsevier, Amsterdam.
- Beaumont, C. (1981)** Foreland Basins. *Geophys. J.R. Astro. Soc.* 65, pp. 291-329.
- Beccaluva, L., Ohnenstetter, D. & Ohnenstetter, M. (1979)** Geochemical discrimination between ocean-floor and island arc tholeiites-application to some tholeiites. *Can. J. Earth Sci.* 16, pp. 1874-1882.
- Bechennec, F. (1987)** Geologie des nappes Hawasina dans les parties orientale et centrale des montagnes d'Oman. These Doctorat d'Etat, Universite Pierre et Marie Curie, Paris 6. Documents du Bureau de Recherches Geologiques et Minieres 127.
- Bechennec, F., Le Metour, J., Rabu, D., Bourdillon-De-Grissac, CH., De Wever, P., Beurrier, M. & Villey, M. (1990)** The Hawasina nappes: Stratigraphy, palaeogeography and structural evolution of a fragment of the south-Tethyan passive continental margin. In: *The Geology and Tectonics of the Oman Region*. (Eds: Robertson, Searle & Ries). *Geol. Soc. Special Pub.* 49, pp. 213-223.
- Beck, C.M., (1980)** Essai d'interpretation structurale et paleogeographique des roches vertes du Pinde d'Etoile (Grece continentale meridionale). *Ann. Soc. Geol. Nord* 99, pp. 355-365.
- Berger, W.H. (1974)** Deep sea sedimentation. In: *The geology of continental margins* (Ed C.A Burk & C.L. Drake) Springer-Verlag, New York, pp. 213-241.
- Berger, W.H. & Winterer E.L. (1974)** Plate stratigraphy and the fluctuating carbonate line. In: *Pelagic sediments: on land and under the sea*. (Ed. K.J. Hsu & H.C. Jenkyns), pp.11-48 *Spec. Publ. Int. Ass Sediment.* 1
- Bernoulli, D. & Laubscher, H.P. (1972)** The palinspastic problem of the Hellenides. *Eclog. Geol. Helv.* 65, pp. 107-118
- Bignot, G., Fleury, J.J. & GGuernet, C. (1971)** Sur la stratigraphie du cretace superieur et du flysch en Eubee moyenne (zone pelagonienne, Grece). *Bull. Geol. Soc. France*, 7, pp. 484-489.
- Biot, M.A. (1961)** Theory of folding of stratified visco-elastic media and its implications in tectonics and orogenesis. *Geol. Soc. Am. Bull.* 72, pp. 1595-1620.
- Bischoff, J.L. (1969)** Red Sea geothermal brine deposits: their mineralogy, chemistry and genesis. In: *Hot brines and recent heavy metal deposits in the Red Sea*. (Eds. Degens & Ross). Springer-Verlag, Berlin, pp. 368-401.
- Bischoff, J.L. & Rosenbauer, R.J. (1977)** Recent metalliferous sediments in the north Pacific manganese nodule area. *E.P.S.L.* 33, pp. 379-388.
- Blumenthal, M. (1933)** Zur Kenntnis der querprofilen des zentralen und nordlichen Peloponnes. *N. Jb. Mineral. Geol. Palaont.* 70, pp. 449-514.

- Bonatti, E.** (1975) Metallogenesis at oceanic spreading centres.  
E.P.S. Ann. Rev. 3, pp. 401-431.
- Bonatti, E., Fisher, D.E., Joensuu, O., Rydell, H.S. & Beyth, M.** (1972) Iron-manganese-barium deposit from the northern Afar Rift (Ethiopia).  
Econ. Geol. 67, pp. 717-730.
- Bonatti, E. & Nayudu, Y.R.** (1965) The origin of manganese nodules on the ocean floor.  
Am. J. Sci. 263, pp. 17-39.
- Bonatti, E., Zerbi, M., Kay, R. & Rydell, H.** (1976) Metalliferous deposits from the Apennine ophiolites: Mesozoic equivalents of modern deposits from oceanic spreading centres.  
Geol. Soc. Am. Bull. 87, pp. 83-94.
- Bosellini, A. & Winterer, E.L.** (1975) Pelagic limestone and radiolarite of the Tethyan Mesozoic: a genetic model.  
Geology 3, pp. 279-282.
- Bostrom, K.** (1973) The origin and fate of ferromanganoan active ridge sediments.  
Stockholm Cont. Geol. 27, pp. 149-243.
- Bostrom, K., Joensuu, O., Moore, C., Bostrom, B., Dalziel, M. & Horowitz, A.** (1973) Geochemistry of barium in pelagic sediments.  
Lithos 6, pp. 159-174.
- Bouma, A.H.** (1962) Sedimentology of some flysch deposits. A graphic approach to facies interpretation.  
Elsevier, Amsterdam.
- Boyer, S.E. & Elliott, D.** (1982) Thrust systems.  
Bull. Am. Ass. Petrol. Geol. 66, pp. 1196-1230.
- Boyle, J.F.** (1984) The origin and geochemistry of metalliferous sediments of the Troodos Massif, Cyprus.  
Unpublished PhD thesis, University of Edinburgh.
- Boyle, J.F.** (1990) The composition and origin of oxide metalliferous sediments from the Troodos ophiolite, Cyprus. In: Ophiolites: Oceanic crustal analogues (eds. Malpas, Moores, Panayiotou & Xenophontos).  
Cyprus Geol. Survey Department. pp. 705-717.
- Bramlette M.N.** (1961) Pelagic sediments.  
Publ. Am. Ass. Adv. Sci. 77, pp. 345-366.
- Breen, N.A., Silver, E.A. & Hussong, D.M.** (1986) Structural styles of an accretionary wedge south of the island of Sumba, Indonesia, revealed by seaMarc II side scanner.  
Bull. Geol. Soc. Am. 97, pp. 1250-1261
- British Petroleum Company Limited.** (1971) The geological results of Petroleum exploration in western Greece.  
Institute for Geology and Subsurface Research (now I.G.M.E.), Spec. Report 10, Athens.
- Brunn, J.H.** (1956) Contribution a l'etude geologique du Pinde septentrional et d'une partie de la Macedoine centrale.  
Ann. Geol. Pays Hell. 12.
- Burbank, D.W., Reynolds, R.G.H. & Johnson, G.D.** (1986) Late Cenozoic tectonics and sedimentation in the NW Himalayan foredeep: II Eastern limb of the Northwest syntaxis and regional synthesis. In: Foreland Basins (eds. Allen & Homewood).  
Spec. Pub. Int. Ass. Sediment. 8, pp. 293-307.
- Burnham, C.W.** (1979) Hydrothermal fluids at the magmatic stage. In: Geochemistry of hydrothermal ore deposits (ed. Barnes).  
J. Wiley & Sons, New York.
- Burns, R.G. & Burns, V.M.** (1977) Mineralogy. In: Marine manganese deposits. (Ed. Glasby).  
Elsevier, New York, pp. 185-249.
- Butler, R.W.H.** (1982) The terminology of structures in thrust belts.  
J. Struct. Geol. 4, pp. 239-245.
- Butler, R.W.H.** (1985) The restoration of thrust systems and displacement continuity around the Mont Blanc Massif. NW External Alpine thrust belt.  
J. Struct. Geol. 7, pp. 569-582.

- Butler, R.W.H.** (1987) Thrust sequences.  
J. Geol. Soc. London 144, pp. 619-634.
- Byers, C.D., Muenow, D.W. & Garcia, M.O.** (1983) Volatiles in basalts and andesites from the Galapagos spreading centre, 85° to 86° W.  
Geochim. Cosmochim. Acta 47, pp. 1551-1558.
- Calvert, S.E.** (1966) Accumulation of diatomaceous silica in the sediments of the Gulf of California.  
Bull. Geol. Soc. Am. 77, pp. 569-596.
- Cann, J.R., Winter, D.K. & Pritchard, R.G.** (1977) A hydrothermal deposit from the floor of the Gulf of Aden.  
Mineral. Mag. 41, pp. 193-199.
- Carmichael, I.S.E.** (1964) The petrology of Thingmuli, a Tertiary volcano in eastern Iceland.  
J. Petrol. 5, pp. 435-460.
- Carmichael, I.S.E., Tuner, F.J. & Verhoogen, J.** (1974) Igneous Petrology.  
McGraw-Hill Publ. New York.
- Carter, R.M.** (1988) The nature and evolution of deep-sea channel systems.  
Basin Res. 1, 41-54.
- Celet, P.** (1962) Contribution a l'etude geologique du Parnasse-Kiona et d'une partie des regions meridionales de la Grece continentale.  
Ann. Geol. des Pays Hell. 13, pp. 425.
- Celet, P., Clement, B. & Ferriere, J.** (1976) La zone Beotienne en Grece: implications paleogeographiques et structurales.  
Eclogae Geologicae Helveticae 69, pp. 577-599.
- Clews, J.E.** (1989) The Mesozoic and Cenozoic evolution of the Ionian zone, Western Greece.  
Unpublished PhD thesis, University of Wales, Cardiff. pp. 176.
- Clift, P.D.** (1990) Mesozoic/Cenozoic sedimentation and tectonics of the southern Greek Neotethys (Argolis Peninsula).  
Unpub. PhD thesis, University of Edinburgh
- Clift, P.D. & Robertson, A.H.F.** (1990) A Cretaceous Neotethyan carbonate margin in Argolis, Southern Greece.  
Geol. Mag. 127, pp. 299-308.
- Cobbold, P.R.** (1975) Fold propagation in single embedded layers.  
Tectonophysics 27, pp. 333-351.
- Cobbold, P.R.** (1976) Fold shapes as functions of progressive strain.  
Phil. Trans. Roy. Soc. Lon. A283, pp. 129-138.
- Compton, J.S. & Siever, R.** (1985) Diffusion and mass balance of Mg during early dolomite formation, Monterey Formation.  
Geochimica et Cosmochimica Acta, 50, pp. 125-135.
- Cooper, D.J.W.** (1986) The Hamrat Duru Group: Evolution of a Mesozoic passive carbonate margin in the Oman mountains.  
Unpublished PhD thesis, University of Edinburgh, pp. 504.
- Cooper, D.J.W.** (1989) A longitudinal carbonate fan from the Jurassic of the Oman Mountains: The Guweyza Limestone Formation of the Hamrat Duru.  
Sedimentary Geology 61, pp. 253-275.
- Cooper, D.J.W.** (1990) Sedimentary evolution and palaeogeographical reconstruction of the Mesozoic continental rise in Oman: evidence from the Hamrat Duru Group. In: Robertson, Searle & Ries (Eds.). The geology and tectonics of the Oman region.  
Geol. Soc. London Spec. Pub. 49, pp. 161-187.
- Cooper, M.A. & Trayner, P.M.** (1986) Thrust surface geometry: Implications for thrust belt evolution and section balancing techniques.  
J. Struct. Geol. 8, pp. 305-312.
- Corbett, M.K.** (1983) Superposed tectonism in the northern Idaho-Wyoming thrust belt. In: Geologic studies of the Cordilleran thrust belt (ed. Powers).  
Rocky Mountain Ass. Geol. 1, pp. 341-356.

- Corliss, J.B., Lyle, M., Dymond, J. & Crane, K. (1978)** The chemistry of hydrothermal mounds near the Galapagos rift.  
E.P.S.L. 40, pp. 12-24.
- Corliss, J.B., Dymond, M., Gordon, L.I., Edmond, J.M., von Herzen, R.P., Ballard, R. D., Green, K., Williams, D., Bainbridge, A.E., Crane, K. & Van Andel, T.H. (1979)** Submarine thermal springs on the Galapagos rift.  
Science 203, pp. 1073-1083.
- Couples, G.D. & Lewis, H. (1988)** "Thrust belt" structures with "foreland" influence: The interaction of tectonic styles. In: Interaction of the Rocky Mountain foreland and the Cordilleran Thrust Belt. (eds. Schmidt & Perry).  
Geol. Soc. Am. Mem. 171, pp. 99-110.
- Covey, M. (1986)** The evolution of a foreland basin to steady state: evidence from the western Taiwan foreland basin. In: Foreland Basins, Allen & Homewood (eds.).  
Spec. Pub. Int. Ass. Sed. 8, pp. 77-90
- Cox, K.G. (1983)** The Karoo igneous province of southern Africa: origin of trace element enrichment patterns.  
In: Continental basalts and mantle xenoliths. (Eds. Hawkesworth & Norry. Nantwich, Shiva (Publishers), pp. 139-157.
- Cox, K.G., Bell, J.D., & Pankhurst, R.J. (1987)** The interpretation of igneous rocks. 5<sup>th</sup> Edition.  
George, Allen & Unwin (Publishers).
- Craddock, J.P., Kopania, A.A. & Wiltsoch, D.V. (1988)** Interaction between the northern Idaho-Wyoming thrust belt and bounding basement blocks, central west Wyoming. In: Interaction of the Rocky Mountain foreland and Cordilleran thrust belt (eds. Schmidt & Perry).  
Mem. Geol. Soc. Am. 171.
- Crerar, D.A., Cormick, R.K. & Barnes, H.L. (1980)** Geochemistry of manganese: an overview. In: Geology and geochemistry of manganese. (Ed. Varentsov).  
Hungarian Acad. Sci. 1, pp. 293-334.
- Crerar, D.A., Namson, J., So Chyi, M., Williams, L. & Feigenson, M.D. (1982)** Manganiferous cherts of the Franciscan assemblage: 1 General geology, ancient and modern analogues, and implications for hydrothermal convection at oceanic spreading centres.  
Bull. Soc. Econ. Geol. 77, pp. 519-540.
- Cronan, D.S. (1969)** Inter-element associations in some pelagic deposits.  
Chem. Geol. 5, pp. 99-106.
- Cronan, D.S. (1976)** Basal metalliferous sediments from the eastern Pacific.  
Geol. Soc. Am. Bull. 87, pp. 928-934.
- Cronan, D.S. (1980)** Underwater minerals.  
Academic Press, London.
- Dahlstrom, C.D.A. (1969)** Balanced cross sections.  
Canadian J. Earth Sci. 6, pp. 743-757.
- Davis, E.F. (1918)** The radiolarian chert of the Franciscan Group.  
Univ. Calif. Publ. Dept. Geol. 11, pp. 236-432.
- De Boer, P.L. & Wonders, A.A. (1984)** Astronomically induced rhythmic bedding in Cretaceous pelagic sediments near Moria (Italy). In: Milankovitch and climate. (Eds. Berger et al.)  
NATO Series C-126, pp. 177-190.
- Deer, W.A., Howie, R.A. & Zussman, J. (1983)** An introduction to the rock forming minerals.  
Longman Publ. London.
- Delaune-Mayere, M. Marcoux, J., Parrott, J-F. & Poisson, A. (1977)** Modele d'evolution Mesozoique de la paleomarge Tethysienne au niveau des nappes radiolaritiques et ophiolitiques du Taurus Lycien, d'Antalya et du Baer-Bassit. In: Structural history of the Mediterranean basins, Biju-Duval & Montadert (eds.).  
Technip, Paris, pp. 79-94
- Dercourt, J. (1964)** Contribution a l'etude geologique d'un secteur du Peloponnese septentrional.  
Ann. Geol. Pays Hell. 15.



- Dercourt, J., Aubouin, J., Savoyat, E., Desprairies, A., Terry, J., Vergely, P., Mercier, J., Godfriaux, I., Ferriere, J., Fleury, J.J., Celet, P. & Clement B. (1977) Reunion extraordinaire de la societe geologique de France en Grece.  
Bull. Soc. Geol. France 19, pp. 5-70.
- Dercourt, J., De Wever, P. & Fleury, J.J. (1976) Donnees sur le style tectonique de la nappe de Tripolitza en Peloponnese septentrional (Grece).  
Bull. Soc. Geol. France 18, pp.317-326.
- Dercourt, J., Flament, J.M., Fleury, J.J. & Meilliez, F. (1973) Stratigraphie des couches situees sous les radiolarites de la zone du Pinde-Olonos (Grece): Le Trias Superieur et le Jurassique Inferieur.  
Ann. Geol. Pays Hell. 25, pp. 397-406.
- Dercourt, J. & Magne, J. (1973) Sur l'age de l'apparition du flysch dans la partie interne de la nappe du Pinde en Peloponnese.  
Ann. Geol. Pays Hell. pp. 501-504.
- Dercourt, J., Zonenshain, L.P., Ricou, L.E., Kazmin, V.G., Le Pichon, X., Knipper, A.L., Grandjacquet, C., Sshortshikov, I.M., Geyssant, J., Lepvrier, V., Pechersky, D.H., Boulin, J., Sibuet, J.C., Savostin, L.A., Sorokhtin, O., Westphal, M., Bazhenov, M.L., Laver, J.P., and Biju-Duval, B., (1986) Geological evolution of the Tethys belt from the Atlantic to the Pamirs since the Lias.  
Tectonophysics, 123, pp. 241-315.
- De Wever, P., (1975) Etude geologique des series apparaissant en fenetre sous l'allochtone pindique (serie de Tripolitza et serie epimetamorphique de Zarouchla). Peloponnese septentrional, Grece.  
Thesis 3eme cycle, Universite de Lille.
- De Wever, P. (1976a) La "formation a blocs": olistostrome chevauche par la nappe du Pinde-Olonos (Peloponnese Grece).  
C.R. Acad. Sci. (Paris) 282, pp. 21-24.
- De Wever, P. (1976b) Mise en evidence d'importants affleurements de roches eruptive a la base de la nappe du Pinde-Olonos au sein de la "formation a blocs" (peloponnese Grece).  
Ann. Soc. Geol. Nord 97, pp. 123-126.
- De Wever, P. (1987) Radiolarites rubanees et variations de l'orbite terrestre.  
Bull. Soc. Geol. France 8, pp. 957-960.
- De Wever, P. (1989) Radiolarians, radiolarites and Mesozoic palaeogeography of the circum-Mediterranean Alpine belts. In: Siliceous deposits of the Tethys and Pacific regions. (Eds. Hein & Obradovic). Springer-Verlag, New York, pp. 31-50.
- De Wever, P. & Cordey, F. (1986) Datation par les radiolaires de la formation Radiolarites s.s. de la serie du Pinde-Olonos (Grece): Bajocian(?)-Tithonique.  
Eurad IV-Marine Micropalaeontology 11, pp. 113-127
- De Wever, P & Origlia-Devos, I (1982a) Datations nouvelles par les radiolaires de la serie des radiolairites s.l. du Pindos-Olonos, Grece.  
C.R. Acad. Soc. (Paris) 294, pp. 1191-1198.
- De Wever, P & Origlia-Devos, I (1982b) Datation par les radiolaires des niveaux siliceux du Lias de la serie du Pinde-Olonos, (Presqu'ile de Koroni, Peloponnese meridional, Grece).  
Geobios (Lyon) 14, pp. 577-609.
- De Wever, P., Ricou, L.E. & Fourcade, E. (1986) La fin brutale de l'optimum radiolaritique au Jurassique terminal: l'effet de la circulation oceanique.  
C.R. Acad. Sci. (Paris) 302, pp. 665-670.
- De Wever, P. & Thiebault, F. (1981) Les radiolaires d'age Jurassique superieur a Cretace superieur dans les radiolarites du Pinde-Olonos (presqu'ile de Koroni, Peloponnese meridional, Grece)  
Geobios (Lyon) 14 (5), pp. 577-609.
- Dewey, J.F., Pitman, W.C., Ryan, W.B. & Bonin, J. (1973) Plate tectonics and the evolution of the Alpine system.  
Bull. Geol. Soc. Am. 84, pp. 3137-3180.

- Dickinson, W.R.** (1974) Plate tectonics and sedimentation. In: Tectonics and sedimentation (ed. Dickinson)  
Spec. Pub. S.E.P.M. 22, pp. 1-27.
- Dickinson, W.R. & Suczek, C.A.** (1979) Plate tectonics and sandstone compositions.  
Bull. Am. Ass. Petrol. Geol. 63, pp. 2164-2182.
- Dickinson, W.R., Beard, L.S., Brakenridge, G.R., Erjavec, J.L., Ferguson, R.C., Inman, K.F., Knepp, R.A., Lindberg, F.A. & Ryberg, P.T.** (1983) Provenance of North American Phanerozoic sandstones in relation to tectonic setting.  
Geol. Soc. Am. Bull. 94, pp. 222-235.
- Dixon, J.M. & Liu, S.** (1992) Centrifuge modelling of the propagation of thrust faults. In: Thrust Tectonics (ed. McClay)  
Chapman & Hall, London, pp. 53-69.
- Dixon, J.M. & Tirrul, R.** (1991) Centrifuge modelling of fold-thrust structures in a tripartite stratigraphic succession.  
J. Struct. Geol. 13, pp. 3-20.
- Dostal, J. & Dupuy, C.** (1984) Geochemistry of the North Mountain basalts (Nova Scotia, Canada).  
Chemical Geology 45, pp. 245-261.
- Dumont, J.F. Gutnic, M., Marcoux, J., Monod, O. & Poisson, A.** (1972) Le Triass des Taurides occidentales (Turquie). Definition du bassin pamphylien: Un nouveau domaine a ophiolithes a la marge externe de la chaine taurique.  
Zeitschrift der Deutschen Geol. Gesellschaft 123, pp. 385-409.
- Duncan, A.R.** (1987) The Karoo igneous province-a problem area for inferring tectonic setting from basalt geochemistry.  
J. Volcanol. Geotherm. Res. 32, pp. 13-34.
- Edmond, J.M., Measures, C., Mangum, B., Grant, B., Sclater, F.R., Collier, R., Hudson, A., Gordon, L.I. & Corliss, J.B.** (1979) On the formation of metal-rich deposits at ridge crests.  
E.P.S.L. 46, pp. 19-30.
- Eisenstadt, G. & De Paor, D.G.** (1987) Alternative model of thrust propagation.  
Geology 15, pp. 630-633.
- Elliott, D.** (1976) The energy balance and deformation mechanisms of thrust sheets.  
Phil. Trans. Roy. Soc. Lon. 283, pp. 289-312.
- Elliott, D. & Johnson, M.R.W.** (1980) Structural evolution in the northern part of the Moine thrust belt, NW Scotland.  
Trans. Roy. Soc. Edinburgh, Earth Sci. 71, pp. 69-96.
- Fail, R.T.** (1969) Kink band structures in the Valley and Ridge province, Central Pennsylvania.  
Geol. Soc. Am. Bull. 80, pp. 2539-2550.
- Fitton, J.G. & Dunlop, H.M.** (1985) The Cameroon Line, West Africa and its bearing on the origin of oceanic and continental alkali basalt.  
E.P.S.L. 72, pp. 23-38.
- Fitton, J.G., James, D., Kempton, P.D., Ormerod, D.S. & Leeman, W.P.** (1988) The role of lithospheric mantle in the generation of Late Cenozoic basic magmas in the western United States.  
J. Petrol., Special lithosphere issue, pp. 331-349.
- Fitton, J.G., James, D. & Leeman, W.P.** (1991) Basic magmatism associated with Late Cenozoic extension in the western United States: Compositional variations in space and time.  
J. Geophys. Res. 96, pp. 13,693-13,711.
- Flament, J.M.** (1973) De l'Olonos au Chelmos, etude geologique d'un secteur de la nappe du Pinde-Olonos.  
These 3eme cycle, Universite Lille.
- Fleury, J.J.** (1970) Sur les modalites d'installation du flysch du Pinde au passage Cretace-Eocene (Grece continentale et Peloponnese septentrional).  
Bull. Geol. Soc. France 7, pp. 1110-1117

- Fleury, J.J.** (1980). Evolution d'une plateforme et d'un bassin dans leur cadre alpin: Les zones de Gavrovo-Tripolitza et du Pinde-Olonos. Soc. Geol. du Nord, Spec. Pub. 4. pp. 651.
- Fodor, R.V.** (1987) Low and high TiO<sub>2</sub> flood basalts of southern Brazil: origin from picritic parentage and a common mantle source. E.P.S.L. 84, pp. 423-430.
- Folk, R.L.** (1966) Petrology of sedimentary rocks. Hemphills Publ. Austin, Texas.
- Folk, R.L. & McBride, E.F.** (1978) Radiolarites and their relation to subjacent "oceanic crust" in Liguria, Italy. J. Sedim. Petrol. 48, pp. 1069-1102.
- Frey, R.W.** (1975) The study of trace fossils. A synthesis of principles, problems and procedures in ichnology. Springer-Verlag, Berlin.
- Friedman, G.M.** (1964) Early diagenesis and lithification in carbonate sediments. J. Sediment. 34, pp. 777-813.
- Friedman, G. & Saunders, J.** (1978) Principles of sedimentology. J. Wiley & Sons, New York.
- Galanopolous, V.P.** (1982) Managing manganese: A world commodity service with special reference to the sedimentary manganese resources of Greece. Unpublished M.Sc. thesis, University of London, Imperial College.
- Gans, P.B., Mahood, G.A. & Schermer, E.** (1989) Synextensional magmatism in the Basin and Range Province. Geol. Soc. America Special Paper 233.
- Garrison, R.E.**, (1974) Radiolarian cherts, pelagic limestones and igneous rocks in eugeosynclinal assemblages. In: Pelagic sediments: on land and under the sea. (Eds. Hsu & Jenkyns). Spec. Publ. Int. Ass. Sediment. 1, pp. 367-399.
- Geeslin, J.H. & Chaetz, H.S.** (1972) Ordovician aleman ribbon cherts: an example of silicification prior to carbonate lithification. J. Sed. Petrol. 52, pp. 1283-1293.
- Gillis, K.M. & Robinson, P.T.** (1986) Low temperature alteration of the extrusive sequence, Troodos ophiolite, Cyprus. Can. Min. 23, pp. 431-441.
- Ginsburg, R.N. & James, N.P.** (1974) Holocene carbonate sediments of continental shelves. In: The geology of continental margins (eds Burke & Drake). S.E.P.M. Springer-Verlag, Berlin. pp. 137-155
- Glasby, G.P.** (Ed.) (1977) Marine manganese deposits. Elsevier oceanography series, Amsterdam.
- Graf, D.L. & Goldsmith, J.R.** (1956) Some hydrothermal syntheses of dolomite and protodolomite. J. Geol. 64, pp. 173-187
- Green, T.J.** (1982) Structural and sedimentological studies of the Pindos zone, central Greece. Unpublished PhD thesis, University of Cambridge.
- Greenly E.** (1919) The Geology of Anglesey. Great Britain Geological Survey Memoir 1.
- Guzzeta, G.** (1984) Kinematics of stylolite formation and physics of pressure solution process. Tectonophysics 101, pp. 383-394.
- Hall, A.** (1987) Igneous Petrology Longman Scientific and Technical (Publishers) UK.
- Hanna, S.S.** (1990) The Alpine deformation of the Central Oman Mountains. In: The geology and tectonics of the Oman region (eds. Robertson, Searle & Ries). Spec. Pub. Geol. Soc. Lon. 49, pp. 341-359
- Hansen, E.** (1971) Strain facies. Springer-Verlag, New York & Berlin.

- Haq, B.U., Hardenbol, J. & Vail, P. (1987)** Chronology of fluctuating sea levels since the Triassic.  
*Science* 235, pp. 1156-1167
- Haq, B.U., Hardenbol, J. & Vail, P.R. (1988)** Mesozoic and Cenozoic chronostratigraphy and Eustatic cycles. In: *Sea level changes: an integrated approach* (eds. Wilgus, Hastings, Kendall, Posamentier, Ross & Van Waaner).  
 SEPM Spec. Publ. 42, pp. 71-108.
- Harbury, N.A. & Hall, R. (1988)** Mesozoic extensional history of the southern Tethyan continental margin in the SE Aegean.  
*J. Geol. Soc. London* 145, pp. 238-301.
- Hardie, L.A. (1987)** Perspectives. Dolomitization: A critical view of some current views.  
*J. Sed. Petrol.* 57, pp. 166-183.
- Harland, W.B., Armstrong, R.L., Cox, A.V., Craig, L.E., Smith, A.G. & Smith, D.G. (1989)** A geologic time scale.  
 Earth Science Series, Cambridge University Press.
- Hatzfeld, P.E., Pedotti, G., Hatzidimitiou, P., Panagiotopoulos, D., Scordilis, M., Drakopoulos, I., Makropoulos, K., Delibasis, N., Latousakis, I., Baskoutas, J. & Frogneux, M. (1989)** The Hellenic subduction beneath the Peloponnesos: First results of a micro-earthquake study.  
*E.P.S.L.* 93, pp. 283-291.
- Hedberg, H.D. (1976)** International stratigraphic guide.  
 Wiley, New York.
- Hein, J.R., Scholl, D.W., Barron, J.A., Jones, M.G. & Miller, J. (1978)** Diagenesis of Late Cenozoic diatomaceous deposits and formation of the bottom simulating reflector in the southern Bering Sea.  
*Sedimentology* 25, pp. 155-181.
- Hein, J.R. & Karl, S.M. (1983)** Comparisons between open ocean and continental margin chert sequences. In: *Siliceous deposits in the Pacific region* (eds. Iijima, Hein & Siever)  
*Developments in sedimentology* 36, pp. 25-43.
- Hein, J.R., Scholl, D.W., Barron, J.A., Jones, M.G., & Karl, S.M. (1983)** Comparisons between open ocean and continental margin chert sequences. In: *Siliceous deposits in the Pacific region*. (Eds. Iijima, Hein & Siever). *Developments in sedimentology* 36, Elsevier, Amsterdam, pp. 25-44.
- Hirst, J.P.P. & Nichols, G.J. (1986)** Thrust tectonic controls on Miocene alluvial distribution patterns, southern Pyrenees. In: *Foreland Basins* (eds. Allen & Homewood)  
*Spec. Pub. Int. Ass. Sed.* 8, pp. 247-258.
- Holland, C.H., Audley-Charles, M.G., Bassett, M.G., Cowie, J.W., Curry, D., Fitch, F.J., Hancock, J.M., House, M.R., Ingham, P.E., Kent, P.E., Morton, N., Ramsbotom, W.H.C., Rawson, P.F., Smith, D.B., Stubblefield, C.J., Torrens, H.S. & Woodland, A.W. (1978)** A guide to stratigraphic procedure.  
*Geol. Soc. Lon. Spec. report* 11, pp. 1-18.
- Hossack, J. R. (1979)** The use of balanced cross sections in the calculation of orogenic contraction: A review.  
*J. Geol. Soc. Lon.* 136, pp. 705-711.
- Howell, D.G., (1989)** Tectonics of suspect terranes. *Topics in Earth Sciences* 3.  
 Chapman & Hall, England
- Hsu, K. (1974)** Melanges and their distinction from olistostromes. In: *Modern and Ancient Geosynclinal Sedimentation* (Eds. Dott & Shaver).  
 SEPM Special Publication 19, pp. 321-333.
- Hsu, K. (1976)** Palaeoceanography of the Mesozoic Alpine Tethys.  
*Geol. Soc. Am. Spec. Paper.*
- Hunter, R.B. (1988)** Timing and structural interaction between the thrust belt and foreland, Hoback Basin, Wyoming. In: *Interaction of the Rocky Mountain foreland and Cordilleran thrust belt* (eds. Schmidt & Perry).  
*Mem. Geol. Soc. Am.* 171.

- Iijima, A., Hein, J.R. & Siever, R. (1983)** An introduction to siliceous deposits in the Pacific region.  
Developments in sedimentology 36, Elsevier, Amsterdam, pp. 1-6.
- Iijima, A., Kakuwa, Y., Yamazaki, K., & Yanagimoto, Y., (1978)** Shallow-sea, organic origin of the Triassic bedded chert in central Japan.  
J. Fac. Sci. Uni. Tokyo (II) 19, pp. 369-400.
- Iijima, A. & Utada, M. (1983)** Recent developments in sedimentology of siliceous deposits in Japan. In: Siliceous deposits in the Pacific region (Eds. Iijima, Hein & Siever).  
Developments in sedimentology 36, Elsevier, Amsterdam, pp. 45-64.
- Institute Francaise du Petrole (IFP), (1966)** Etude geologique de l'Epire (Grece nord-occidental).  
Paris (Edition Technipress).
- Izart, A. (1976)** Etude geologique d'un secteur du Peloponnese nord-occidental (Grece): la carte de Goumeron.  
These 3eme cycle, Universite Lille.
- Jackson, J.A., Gagnepain, J., Houseman, G., King, G.C.P., Papadimitiou, P., Soufleris, C. & Virieux, J (1982)** Seismicity, normal faulting and the geomorphological development of the Gulf of Corinth (Greece): the Corinth earthquakes of February and March 1981.  
E.P.S.L. 57, pp. 377-379.
- Jackson, J.A. & McKenzie, D. (1988)** The relationship between plate motions and seismic moment tensors and the rates of active deformation in the Mediterranean and the Middle East.  
J. Geophys. 93, pp. 45-73.
- Jacobshagen, V., Durr, S., Kockel, F., Kopp, K.O., and Kowalczyk, G. (1978a)** Structure and Geodynamic evolution of the Aegean region.  
In: Closs, Roeder & Schmidt (Ed.); Alps, Apennines, Hellenides. pp. 537-564.  
Schweitzerbart she Verlag, Stuttgart.
- Jacobshagen, V., Kopp, K.O. and Makris, J. (1978b).** Investigations in the Aegean region: an introduction.  
In: Closs, Roeder & Schmidt (Ed.); Alps, Apennines, Hellenides. pp. 389-391.  
Schweitzerbart she Verlag, Stuttgart.
- Jamison, W.R. (1987)** Geometric analysis of fold development in overthrust terranes.  
J. Struct. Geol. 9, pp. 207-219.
- Jaques, A.L. & Green, D.L. (1980)** Anhydrous melting of peridotite at 0-15 kb pressure and the genesis of tholeiitic basalts.  
Contrib. Mineral. Petrol. 73, pp. 287-310.
- Jenkyns, H.C. (1974)** Origin of red nodular limestones (Ammonitico rosso, Knollenkalke) in the Mediterranean Jurassic: a diagenetic model.  
Spec. Pub. Int. Ass. of Sediment. 1, pp. 249-271.
- Jenkyns, H.C. & Winterer, E.L. (1982)** Palaeoceanography of Mesozoic ribbon radiolarites.  
Earth Planet Sci. Letts. 60, pp. 351- 375.
- Johns, D.R. (1978)** Mesozoic carbonate rudites, mega-breccias and associated deposits from central Greece.  
Sedimentology 25, pp. 561-573.
- Johnson, A.M. (1977)** Styles of folding: Mechanics and mechanisms of natural elastic materials.  
Elsevier Scientific Publ. Amsterdam.
- Jolley, E.J. (1988)** Thrust tectonics and alluvial architecture of the Jaca Basin, Southern Pyrenees.  
Unpub. PhD thesis, Univ. of Wales College Cardiff.
- Jones, G., (1990)** Tectonostratigraphy and evolution of the Pindos ophiolite and associated units, northwest Greece.  
Unpublished University of Edinburgh PhD thesis, 397pp.
- Jones, G. & Robertson, A.H.F. (1991)** Tectono-stratigraphy and evolution of the Mesozoic Pindos ophiolite and related units in northwest Greece: an integrated supra-subduction zone spreading and subduction-accretion model.  
J. Geol. Soc. London 148, pp. 267-288

- Karamata, S.** (1988) The "Diabase-Chert Formation". Some genetic aspects.  
Bull. Acad. Serbe. Sci. Nat. 95, 28: pp. 1-11.
- Karig, D.E., Suparka, S. & Moore, G.F.** (1978) Structure and Cenozoic evolution of the Sunda Arc in the central Sumatra region. In: Contributions to knowledge of tectonics & mineral resources in east Asia (ed. Sano).  
Asia Offshore Areas Tech. Bull. 12, pp. 87-106.
- Karner, G.D. & Watts, A.B.** (1983) Gravity anomalies and flexure of the lithosphere at mountain ranges.  
J. Geophys. Res. 88, pp. 10449-10477.
- Kastner, M. & Gieskes, J.M.** (1983) Opal-A to Opal-CT transformation: A Kinetic study. In: Siliceous deposits in the Pacific region (Eds. Iijima, Hein & Siever).  
Developments in sedimentology 36, Elsevier, Amsterdam, pp. 211-228
- Kickmaier, W. & Peters, T.J.** (1991) Chert-hosted manganese deposits in the Wahrah Formation: A depositional model. In: Ophiolite genesis and evolution of the oceanic lithosphere (Ed Peters *et al.*).  
Kluwer Publ., Dordrecht.
- Kober, L.** (1929) Die Grossgliederung der Dinariden.  
Zentralbl. Mineral., B, pp.425-437.
- Kossmatt, F.** (1924) Geologie der zentralen Balkanhalbinsel.  
Bornträger, Berlin.
- Kostopoulos, D.** (1989) Geochemistry and tectonic setting of the Pindos ophiolite, northwestern Greece.  
Unpublished PhD thesis, University of Newcastle-upon-Tyne.
- Krauskopf, K.B.** (1957) Separation of manganese from iron in sedimentary processes.  
Geochimica & Cosmochimica Acta 12, pp. 61-84.
- Ktenas, C.** (1926) Sur le developement du primaire au Peloponnese central.  
Prakt. Acad. Athenes 1, pp. 53-59
- Kulik, D.M. & Schmidt, C.J.** (1988) Region of overlap and styles of interaction of Cordilleran thrust belt and Rocky Mountain foreland. In: Interaction of the Rocky Mountain Foreland and Cordilleran thrust belt (eds. Schmidt & Perry).  
Mem. Geol. Soc. Am. 171, pp. 75-98.
- Kuno, H.** (1960) High-alumina basalt.  
J. Petrol. 1, pp. 212-145.
- Kushnir, J. & Kastner, M.** (1982) Adsorption of sulphate ions on calcite, aragonite and dolomite: Their role in inhibiting dolomitization. (Abstract).  
E.O.S. 63, p. 999.
- Lalou, C., Brichet, E., Jehanno, C. & Perez-Leclaire, H.** (1983) Hydrothermal Mn-deposits from Galapagos mounds. D.S.D.P. Leg 70, hole 509b and Alvin dives 729 and 721.  
E.P.S.L. 63, pp. 63-75.
- Lancelot, Y.** (1978) Relations entre evolution sedimentaire et tectonique de la plaque Pacifique depuis le Cretace inferieur.  
Mem. Soc. geol France 134, 40pp.
- Land, L.S.** (1967) Diagenesis of skeletal carbonates.  
J. Sed. Petrol. 37, pp. 914-930.
- Lash, G.G.** (1988) Along-strike variations in foreland basin evolution: Possible evidence for continental collision along an irregular margin.  
Basin Research 1, pp. 71-83.
- Latin, D.M., Dixon, J.E. & Fitton, J.G.** (1991) Rift related magmatism in the North Sea basin. In: Tectonic evolution of North Sea rifts (eds. Blundell & Gibbs).  
Oxford Univ. Press
- Laubscher, H.** (1971) The large scale kinematics of the western Alps and the northern Appenines and its palinspastic implications.  
Am. J. Sci. 271, pp. 193-226.

- Leggett, J.K., McKerrow, W.S. & Casey, D.M. (1982)** The anatomy of a Lower Palaeozoic accretionary forearc: the Southern Uplands of Scotland. In: *Trench-forearc geology: Sedimentation and tectonics on modern and ancient plate margins* (Ed. Leggett). Spec. Pub. Geol. Soc. London 14, pp. 495-520.
- Leigh, S.P. (1991)** The sedimentary evolution of the Pindos foreland basin, Western Greece. Unpub. PhD Thesis, University of Wales, Cardiff.
- Lekkas, S. (1978)** Phenomenes d'ecailages dans la zone de Tripolitza en Peloponnese central (Grece). C.R. Somm. Soc. Geol. France. pp. 108-111
- Lekkas, S. (1980)** Les phyllades du Peloponnese: un metaflysch Ionien chevauche par le serie de Gavrovo-Tripolitza. C.R. Acad. Sci. Paris. 291, pp. 21-24.
- Lekkas, S. & Papanikolaou, D. (1980)** On the phyllite problem in the Peloponnese. An. Geol. Pays Hell. 29, pp. 395-410.
- Le Pichon, X. (1982)** Land-locked oceanic basins and continental collision: The Eastern Mediterranean as a case example. In: *Mountain building processes* (ed. Hsu). Academic Press, New York. pp. 201-211.
- Le Pichon, X. & Angelier, J. (1979)** The Hellenic Arc and trench system: a key to the neotectonic evolution of the eastern Mediterranean area. *Tectonophysics* 60, pp. 1-42.
- Le Pichon, X. & Angelier, J. (1981)** The Aegean Sea. *Phil. Trans. Roy. Soc. Lon.* A300, pp.357-372.
- Le Pichon, X., Bergerat, F. & Roulet, M.J. (1988)** Plate kinematics and tectonics leading to the Alpine belt formation: a new analysis. *Geol. Soc. A. Spec. Pub.* 218, 111-131.
- Le Pichon, X., Iiyama, T., Chamley, H., Charvet, J., Faure, M., Fujimoto, HY., Furata, T., Ida, Y., Kagami, H., Lallemon, S., Leggett, J., Murata, a., Okada, h., Rangin, C., Renard, v., Taira, A., & Tokuyama, H. (1987)** Nankai trough and the fossil Shikoku Ridge: Results of box 6 Kaiko survey. *E.P.S.L.* 83, pp. 186-198.
- Lisitzyn, A. P., (1972)** (Ed.) *Sedimentation in the worlds oceans.* Soc. Econ. Paleont. Mineral. Spec. Publ. 17.
- Lonsdale, P. (1977)** Deep tow observations at the mounds abyssal hydrothermal field, Galapagos rift. *E.P.S.L.* 36, pp. 92-110.
- Lowe, D.R. (1979)** Sediment gravity flows: Their classification and some problems of application to natural flows and deposits. In: *Geology of continental slopes* (eds Doyle & Pilkey) *S.E.P.M.* 27, pp. 75-82.
- Lowe, D.R. (1982)** Sediment gravity flows: II. Depositional models with special reference to the deposits of high-density turbidity curenets. *J. Sed. Petrol.* 52, pp. 279-297.
- Lyberis, N (1978)** Etude geologique de la partie meridionale des montagnes d'Agrapha (euritanie, Grece) *These Doct. Ing. Univ. Paris.*
- Lyberis, N., Chotif, P. & Doubinger, J. (1980)** Precisions stratigraphiques sur la serie du Pinde (Grece): La duree de sedimentation des "radiolarites". *C.R. Acad. Sci. (Paris)* 290, pp. 1513-1516.
- Lyle, M. (1983)** The brown-green colour transition in marine sediments: a marker of the Fe(III)-Fe(II) redox boundary. *Limnol. Oceanogr.* 28, pp. 1026.
- Lynn, D.C. & Bonatti, E. (1965)** Mobility of manganese in diagenesis of deep-sea sediments. *Marine Geol.* 3, pp. 457-474.
- Mackel, H.G. & Mountjoy, E. (1986)** Chemistry and environments of dolomitization-a reappraisal. *Earth Science Reviews* 23, pp. 175-232

- Mansy, J.L. (1971) Etude geologique des monts de Kyparissia (Messenie, Grece).  
Ann. Soc. Geol. Nord, 91, pp. 57-63.
- McBride, E.F. (1963) A classification of common sandstones.  
J. sedim. Petrol. 33, pp. 664-669.
- McBride, E.F. & Folk, R.L. (1979) Features and origin of Italian Jurassic radiolarites deposited on continental crust.  
J. Sedim. Petrol 49, pp. 837-868.
- McClay, K.R. (1992) Glossary of thrust tectonics terms. In: Thrust Tectonics (ed. McClay).  
Chapman & Hall Publ. London, pp. 419-433.
- McIlreath, I.A. (1977) Accumulation of a Middle Cambrian, deep water, basinal limestone adjacent to a vertical, submarine carbonate escarpment, Southern Rocky Mountains, Canada. In: Deep-water carbonate environments (eds Cook & Enos).  
S.E.P.M. 25, pp. 113-124
- McIlreath, I.A. & James, N.P. (1979) Carbonate Slopes. In: Facies Models (ed Walker).  
Geoscience Canada Reprint Series 1, pp. 133-144.
- McIlreath, I.A. & James, N.P. (1984) Carbonate Slopes. In: Facies Models (2nd Edition, ed Walker).  
Geoscience Canada Reprint Series 1, pp. 245-257
- McKenzie, D. (1978) Some remarks on the development of sedimentary basins.  
E.P.S.L. 40, pp. 25-32
- McKenzie, D.P. & Bickle, M.J. (1988) The volume and composition of melt generated by extension of the lithosphere.  
J. Petrol. 29, pp. 625-679.
- McKenzie, D. & O'Nions, R.K. (1991) Partial melt distributions from inversion of rare element concentrations.  
J. Petrol. 32, pp. 1021-1091.
- McKenzie, J.A., Isern, A., Karpoff, A.M. & Swart, P.K. (1990) Basal dolomitic sediments, Tyrrhenian Sea, ODP Leg 107. In: Proceedings of the ODP. Scientific results (eds. Kastern, Mascle *et al.*). Vol. 107, pp. 141-152.
- Meilliez, F. (1971) Etude geologique de la region d'Aroania, Achaie, Peloponnese central, Grece.  
D.E.A. Universite Lille.
- Menzies, M., Seyfried, W. & Blanchard, D. (1979) Experimental evidence of rare earth immobility in greenstones.  
Nature 282, pp. 398-399.
- Mercier, J. (1966) Palaeogeographie, orogenese, metamorphisme et magmatisme des zones internes des Hellenides en Macedoine (Grece).  
Bull. Soc. Geol. France 8, pp. 1020-1049.
- Mercier, J. (1983) Some remarks concerning the paper "The neotectonics of the Aegean; an alternative view", By J.A. Jackson, G. King & C. Vita-Finzi.  
E.P.S.L. 66, pp. 321-325.
- Mercier, J., Carey, E., Philip, H. & Sorel, D. (1976) La neotectonique plio-quatenaire de l'arc egeen externe et de la mer egee et ses relations avec la seismicite.  
Bull. Soc. Geol. France 29, pp. 663-672.
- Meschede, M. (1986) A method of discriminating between different types of mid-ocean ridge basalts and continental tholeiites with the Nb-Zr-Y diagram.  
Chem. Geol. 56, pp. 207-218.
- Meulenkamp, J.E., Wortel, M.J.R., Van Wornel, W.A., Spakman, W. & Hoogerduyn Strating, E. (1988) On the Hellenic subduction Zone and the gyodynamic evolution of Crete since the late Middle Miocene.  
Tectonophysics 146, pp. 203-215.
- Miall, A.D. (1986) Eustatic sea level changes interpreted from seismic stratigraphy: a critic of the methodology with particular reference to the North Sea Jurassic record.  
Bull. Am. Ass. Petrol. Geol. 70, pp 131-137.



- Milankovitch, M. (1941)** Kanon der Erdbestrahlung und seine Anwendung auf das Eiszeitenproblem.  
Acad. Roy. Serbe, edit. spec. 133, Belgrade.
- Miller, J. (1978)** Diagenesis of Late Cenozoic diatomaceous deposits and formation of the bottom simulating reflector in the southern Bering Sea.  
*Sedimentology* 25, pp. 155-181.
- Miller, J. (1988)** Catholuminescence microscopy. In: *Techniques in sedimentology* (ed. Tucker). Blackwell Scientific Pub. Oxford, pp. 174-190.
- Mitchell, A.H.G. & Reading, H.G. (1989)** Sedimentation and tectonics. In: *Sedimentary environments and facies*. (2nd Edition. Ed. Reading). Blackwell Scientific Pub. Oxford. pp. 471-519
- Moorby, S.A., Cronan, D.S. & Glasby, G.P. (1984)** Geochemistry of hydrothermal Mn-oxide deposits from the SW Pacific island arc.  
*Geochim. Cosmochim. Acta* 48, pp. 433-441.
- Moore, W.S. & Vogt, P.R. (1976)** Hydrothermal manganese crusts from two sites near the Galapagos spreading axis.  
*E.P.S.L.* 29, pp. 349-356.
- Morley, C.K. (1986)** A classification of thrust fronts.  
*Am. Ass. Petrol. Geol. Bull.* 70, pp. 12-25.
- Morley, C.K. (1988)** Out-of-sequence thrusts.  
*Tectonics* 7, pp. 539-561.
- Morris, A. (1990)** Palaeomagnetic studies in Cyprus, Turkey and Greece.  
Unpubl. PhD thesis, Univ. of Edinburgh.
- Morrow, D. (1982)** Diagenesis 2, Dolomite-part 2, dolomitization models and ancient dolostones.  
*Geosci. Can.* 9, pp. 95-107.
- Muller, P.J. & Mangini A. (1980)** Organic carbon decomposition rates in sediments of the Pacific manganese nodule belt dated by  $^{230}\text{Th}$  and  $^{231}\text{Pa}$ .  
*E.P.S.L.* 51, pp. 94-114.
- Mullins, H.T., Heath, K.C., Van Buren, M. & Newton C.R. (1984)** Anatomy of a modern open-ocean carbonate slope: northern Little Bahama Bank.  
*Sedimentology* 31, pp. 141-168
- Mullins, H.T. & Lynts, G.W. (1977)** Origin of the northwestern Bahama platform: Review and reinterpretation.  
*Geol. Soc. Am. Bull.* 88, pp. 1447-1461.
- Mullins, H.T. & Neumann, A.C. (1979)** Deep carbonate bank margin structure and sedimentation in the northern Bahamas.  
*S.E.P.M.* 27, pp. 165-192.
- Murata, K.J. & Larson, R.R. (1975)** Diagenesis of Miocene siliceous shales, Temblor Range, California.  
*J. Res. US Geol. Surv.* 3, pp.553-566.
- Murata, K.J., Friedman, I. & Gleason, J.D. (1977)** Oxygen isotope relations between diagenetic silica minerals in Monterey shale, Temblor Range, California.  
*Am. J. of Sci.* 277, pp. 259-272.
- Murray, J.W. (1974)** The surface chemistry of hydrous manganese dioxide.  
*J. Colloid Interface Sci.* 46, pp. 357-371.
- Mutti, E. (1985)** Turbidite systems and their relations to depositional sequences. In: *Provenance of arenites* (Ed Zuffa). NATO Series Dordrecht, Holland.
- Mutti, E. & Ricci-Lucchi, F (1972)** Le turbiditi dell'Appennino settentrionale: Introduzione all'analisi di facies.  
*Mem. Soc. Geol. Ital.* 11, pp. 161-199.
- Mutti, E. & Ricci-Lucchi, F. (1975)** Turbidite facies and facies associations. Field trip guidebook, 9th Int Sed. Congres. Nice, France, pp. 21-36
- Myers J.D. & Marsh, B.D. (1981)** Geology and petrogenesis of the Edgumbe volcanic field, SE Alaska: The interaction of basalt and sialic crust.  
*Contrib. Mineral. Petrol.* 77, pp. 272-287

- Nardin, T.R., Hein, F.J., Gorsline, D.S. & Edwards, B.D. (1979)** A review of mass movement processes, sediment and acoustic characteristics, and contrasts in slope and base of slope systems versus canyon-fan-basin floor systems. In: *Geology of continental slopes* (eds. Doyle & Pilkey). S.E.P.M. 27, pp. 61-73.
- Najman, Y., Clift, P., Johnson, M. & Robertson, A. (1992)** Early stages of foreland basin evolution in the Lesser Himalaya, N. India. *Special Publ. Geol. Soc. London* (In press).
- Needham, D.T. (1987)** Asymmetric extensional structures and their implications for the generation of melanges. *Geol. Mag.* 124, pp. 311-318.
- Negrís, P. (1908)** Sur la répartition des Halobies dans le Peloponnese occidental. *C.R. Acad. Sci. (Paris)*, 147, pp. 1008-1010.
- Nisbet, E.G. & Price, I. (1974)** Siliceous turbidites: bedded cherts as redeposited ocean ridge derived sediments. *Spec. Pub. Int. Ass. Sediment.* 1, pp. 351-366.
- Normark, W.R. (1970)** Growth patterns of deep sea fans. *Bull. Am. Ass. Petrol. Geol.* 54, pp. 2170-2195.
- Normark, W.R. (1978)** Fan valleys, channels and depositional lobes on modern submarine fans: characters for recognition of sandy turbidite environments. *Bull. Am. Ass. Petrol. Geol.* 62, pp. 912-931.
- Panagos, A.G. & Varnavas, S.P. (1984)** On the genesis of some manganese deposits from eastern Greece. In: *Syngeneses and epigenesis in the formation of mineral deposits*. (Eds Wauschkuhn et al.). Springer-Verlag, Berlin, pp. 553-561.
- Papaniikolaou, D. & Sideris, C. (1979)** Sur la signification des zones "ultra pindique" et "beotienne" d'après la géologie de la région de Karitsa: l'unité de Thessalie occidentale. *Ecl. Geol. Helv.* 72, pp. 251-261.
- Patton, T.L. & O'Connor, S.J. (1988)** Cretaceous flexural history of northern Oman Mountain foredeep, United Arab Emirates. *Am. Ass. Petrol. Geol. Bull.* 72, pp. 797-809.
- Pearce, J.A. (1975)** Basalt geochemistry used to investigate past tectonic environments on Cyprus. *Tectonophysics* 25, pp. 41-67.
- Pearce, J.A. (1980)** Geochemical evidence for the genesis and eruptive setting of lavas from Tethyan ophiolites. In: *Proceedings of the International Ophiolite Symposium, Cyprus 1979*. (Ed. Panayiotou). pp. 261-272.
- Pearce, J.A. (1982)** Trace element characteristics of lavas from destructive plate boundaries. In: *Andesites* (Ed. Thorpe). J. Wiley (Publisher). pp. 525-548.
- Pearce, J.A., Alabaster, T., Shelton, A.W. & Searle, M.P. (1981)** The Oman ophiolite as a Cretaceous arc-basin complex: Evidence and implications. *Phil. Trans. R. Soc. A* 300, pp. 299-317.
- Pearce, J.A. & Cann, J.R. (1973)** Tectonic setting of basic volcanic rocks determined using trace element analysis. *Earth & Plan. Sci. Letters* 19, pp. 290-300.
- Pe-Piper, G. & Koukouvelas, I. (1990)** Petrology and geochemistry of granitic pebbles in the Pliocene fluvial deposits of the northwest Peloponnese (Greece) and their regional significance. *Neues Jahrbuch Miner. Abh.* 161, pp. 327-343.
- Pe-Piper, G. & Piper, D.W.J. (1984)** Tectonic setting of the Mesozoic Pindos basin of the Peloponnese, Greece. In: *Dixon & Robertson (Eds.) The geological evolution of the eastern Mediterranean*. *Geol. Soc London Spec. Pub.* 17, pp. 563-568.
- Pe-Piper, G. & Piper, D.W.J. (1989)** The geological significance of manganese distribution in Jurassic-Cretaceous rocks of the Pindos Basin, Peloponnese, Greece. *Sed. Geol.* 65, pp. 127-137.

- Pe-Piper, G. & Piper, D.W.J.** (1990) Early Mesozoic oceanic subduction-related volcanic rocks, Pindos Basin, Greece.  
Tectonophysics 192, pp. 273-292
- Perry, E.A. & Hower, J.H.** (1972) Late stage dehydration in deeply buried pelitic sediments.  
Am. Ass. Petrol. Geol. Bull. 56, pp. 2013-2021.
- Phillipson, A.** (1890) Über die Altersfolge der sedimentformationen in Griechenland.  
Zeit. der Deutsch. Geol. Gesell. 42, pp. 150-159.
- Phillipson, A.** (1892) Der Peloponnes.  
Friedlander Sohn, Berlin.
- Phillipson, A.** (1898) La tectonique de l'Egeide.  
Ann. Geogr. 7, pp. 112-141.
- Pichler, H. & Ziel, W.** (1972) The Cenozoic rhyolite-andesite association of the Chilean Andes.  
Bull. Volcanol. 35, pp. 424-452.
- Pickering, K.T., Hiscott, R.N. Hein, F.J.** (1989) Deep Marine Environments.  
Unwin Hyman, London
- Pindell, J.L.** (1985) Alleghenian reconstruction and subsequent evolution of the Gulf of Mexico, Bahamas and proto-Caribbean.  
Tectonics 4, pp. 1-39.
- Piper, D.J.W.** (1978) Turbidite muds and silts on deep sea fans and abyssal plains. In: Sedimentation in submarine canyons, fans and trenches (Ed. D.J. Stanley & G. Kelling). pp 163-175. Dowden, Hutchinson & Ross, Stroudsburg, Pa.
- Piper, D.J.W. & Pe-Piper, G.** (1980) Was there a western (external) source of terrigenous sediment to the Pindos Zone of the Peloponnese (Greece).  
Neues Jahrb. Geol. Palaontol., Monatsh 2, pp.107-115.
- Pitman, III W.C.** (1979) The effect of eustatic sea level changes on stratigraphic sequences of Atlantic margins.  
Am. Ass. Petrol. Geol. Mem. 29, pp. 453-460.
- Platt, J.K., Leggett, J.K., Young, J., Raza, H. & Alam, S.** (1985) Large-scale sediment underplating in the Makran accretionary prism, southwest Pakistan.  
Geology 13, pp. 507-511.
- Poisson, A.** (1977) Recherches géologiques dans les Taurides occidentales (Turquie).  
Thesis, Univ. Orsay, Paris, France.
- Price, L.** (1977) Facies distinction and interpretation of primary cherts in a Mesozoic continental margin succession, Othris, Greece.  
Sed. Geol. 18, pp. 321-335.
- Price, N.B. & Calvert, S.E.** (1970) Compositional variation in Pacific Ocean ferromanganese nodules and its relationship to sediment accumulation rates.  
Marine Geol. 9, pp. 145-171.
- Price, N.J. & Cosgrove, J.W.** (1990) Analysis of geological structures.  
Cambridge University Press, Cambridge.
- Price, R.A. & Mountjoy, E.W.** (1970) Geologic structure of the Canadian Rocky Mountains between Bow and Athabasca Rivers-progress report.  
Geol. Ass. Canada Spec. Paper 6, pp. 7-25.
- Puidifabrigas, C., Munoz, J.A. & Marzo, M.** (1986) Thrust belt development in the eastern Pyrennes and related depositional sequences in the southern foreland basin. In: Foreland basins (eds. Allen & Homewood)  
Spec. Pub. Int. Ass. Sed. 8, pp. 229-246
- Ragan, D.M.** (1985) Structural geology-An introduction to geometrical techniques.  
Wiley, New York.
- Ramberg, H.** (1961) Contact strain and folding instability of a multilayered body under compression.  
Geol. Rundsch. 51, pp. 405-439.
- Ramsay, J.G.** (1967) Folding and fracturing of rocks.  
McGraw-Hill, New York and London.

- Ramsay, J.G. (1974)** Development of chevron folds.  
Bull. Geol. Soc. Am. 85, pp. 1741-1745.
- Ramsay, J.G. & Huber, M.I. (1987)** The techniques of modern structural geology, Vol. II.  
Academic Press Publ.
- Rast, N. & Horton, J.W. (1989)** Melanges and olistostromes in the Appalachians of the United States and mainland Canada; an assessment.  
Geol. Soc. of America Special Paper 228, pp. 1-15.
- Raymond, L.A. (1984)** Classification of melanges. In: Melanges, their nature, origin and significance.  
Geol. Soc. of America Special Paper 198, pp. 7-20.
- Read, J.F. (1984)** Carbonate platforms of passive (extensional) continental margins: types, characteristics and evolution.  
Tectonophysics 81, pp. 195-212.
- Reading, H.G. (1989)** Sedimentary environments and facies. (2<sup>nd</sup> Edition)  
Blackwell scientific publishing, Oxford.
- Renz, C., (1955)** Die vorneogene stratigraphie der normalsedimentaren Formationen Griechenlands.  
Inst. Geol. Subs. Res. Athens.
- Rich, J.L. (1934)** Mechanics of low angle overthrust faulting as illustrated by Cumberland thrust block, Virginia, Kentucky and Tennessee.  
Am. Ass. Petrol. Geol. Bull. 18, pp. 1584-1587.
- Richter, D. & Lensch, G. (1977)** Die ophiolitigchen vulkanit-vorkommen der Olonos-Pindos decke im zentralpeloponnes (Griechenland).  
N. Jb. Miner. Abh. 129, pp. 312-332.
- Richter, D. & Lensch, G. (1989)** Neue vulkanit-vorkommen der Pindos-decke auf dem Peloponnes (Griechenland).  
Z. Geol. Wiss. Berlin 17, pp.947-961.
- Richter, D. & Mariolagos, I. (1977)** Paleorelif & beginn der flysch-sedimentation in der subpelagonischen zone, nordlich Lamia (ostgriechenland).  
ZSG Wiss. 5, pp. 361-372.
- Ricou, L.E. (1976)** Evolution structurale des Zagrides. La region clef de Neyriz (Zagros Iranien).  
Mem. Soc. Geol. France 125, pp. 1-140.
- Rio, M. (1982)** Les accidents siliceux dans la Cretace du bassin Vocontien (sud-est de la France).  
Contributions a l'etude de la silicifications des formations calcaires.  
Doc. Lab. Geol. Fac. Lyon, 84.
- Robertson, A.H.F. (1977)** The origin and diagenesis of cherts from Cyprus.  
Sedimentology 24, pp. 11-30.
- Robertson, A.H.F. (1978)** Metallogenesis along a fossil oceanic fracture zone: Arakapas fault belt, Troodos Massif, Cyprus.  
E.P.S.L. 41, pp. 317-329.
- Robertson, A.H.F. (1981)** Metallogenesis on a Mesozoic passive continental margin, Antalya Complex, southwest Turkey.  
E.P.S.L. 54, pp. 323-345.
- Robertson, A.H.F. (1986)** Geochemical evidence for the origins of Late Triassic melange units in the Oman Mountains as a small ocean basin formed by continental rifting.  
E.P.S.L. 77, pp. 318-332.
- Robertson, A.H.F. (1987a)** Upper Cretaceous Muti Formation: Transition of a Mesozoic passive margin to a foreland basin in the Oman Mountains.  
Sedimentology 34, pp. 1123-1142.
- Robertson, A.H.F. (1987b)** The transition from a passive margin to an Upper Cretaceous foreland basin related to ophiolite emplacement in the Oman Mountains.  
Geol. Soc. Am. Bull. 99, pp. 633-653.
- Robertson, A.H.F. (1990a)** Pliocene basal dolomitic and Fe-Mn sediments from the Tyrrhenian Sea, Western Mediterranean, ODP Leg 107.  
Proceedings of the Ocean Drilling Program, Scientific results, 107, pp. 129-139

- Robertson, A.H.F. (1990b) Late Cretaceous oceanic crust and Early Tertiary foreland basin development, Euboea, Eastern Greece.  
Terra Nova 2, pp. 333-339.
- Robertson, A.H.F. & Boyle, J.F. (1983) Tectonic setting and origin of metalliferous sediments in the Mesozoic Tethys. In: Hydrothermal processes at seafloor spreading centres. (Ed. P.A. Rona). NATO Conference series, Plenum, New York & London, pp 595-663.
- Robertson, A.H.F., Clift, P.D., Degnan, P.J. & Jones, G. (1991) Palaeogeographic and palaeotectonic evolution of the eastern Mediterranean Neotethys.  
Palaeogeography, Palaeoclimatology, Palaeoecology 87, pp 289-343.
- Robertson, A.H.F. & Degnan, P.J. (1992a) The palaeogeographic setting of the Parnassos carbonate platform in the Mesozoic Pindos Ocean: Evidence from the Kerassia-Milia Complex.  
6th Cong. Geol. Soc. Greece, Athens May 1992. (In press).
- Robertson, A.H.F. & Degnan, P.J. (1992b) Sedimentology of the Lamayuru Complex: Mesozoic deep water facies of the Indian passive margin. Indus Suture Zone, Ladakh Himalaya.  
Special Publ. Geol. Soc. Lon. (In press).
- Robertson, A.H.F. & Dixon, J.E. (1984) Introduction: aspects of the geological evolution of the eastern Mediterranean. In: Dixon & Robertson (Eds), The geological evolution of the eastern Mediterranean.  
Geol. Soc. London Spec. Pub. 17, pp. 1-74.
- Robertson, A.H.F. & Fleet, A.J. (1976) The origins of rare earths in metalliferous sediments of the Troodos massif, Cyprus.  
E.P.S.L. 28, pp. 385-394.
- Robertson, A.H.F. & Searle, M.P. (1990) The northern Oman Tethyan continental margin: stratigraphy, structure, concepts and controversies. In: Robertson, Searle & Ries (Eds.). The geology and tectonics of the Oman region.  
Geol. Soc. London Spec. Pub. 49, pp. 3-26.
- Robertson, A.H.F., Varnavas, S.P. & Panagos, A.G. (1987) Ocean ridge origin and tectonic setting of Mesozoic sulphide and oxide deposits of the Argolis peninsula of the Peloponnesus, Greece.  
Sed. Geol. 53, pp. 1-32.
- Robertson, A.H.F. & Woodcock, N.H. (1981) Alakir Cay Group, Antalya Complex, SW Turkey: A deformed Mesozoic carbonate margin.  
Sed. Geol. 30, pp. 95-131.
- Robertson, A.H.F. & Woodcock, N.H. (1981b) Bileyeri Group, Antalya Complex: deposition on a Mesozoic passive continental margin, south-west Turkey.  
Sedimentology 28, pp. 381-399.
- Robertson, A.H.F. & Woodcock, N.H. (1982) Sedimentary history of the southwestern segment of the Mesozoic-Tertiary Tethyan continental margin, southwestern Turkey.  
Eclogae Geologicae Helveticae 75. pp. 517-562.
- Rona, P.A. (1978) Criteria for recognition of hydrothermal mineral deposits in oceanic crust.  
Bull. Soc. Econ. Geol. 73, pp.135-160.
- Rossi, P.L., Bocchi, G. & Lucchini, F. (1980) A manganese deposit from the south Tyrrhenian region.  
Oceanol. Acta 3, pp. 107-113.
- Ruiz-Ortiz, P.A., Bustillo, M.A. & Molina, J.M. (1989) Radiolarite sequences of the subbetic, Betic Cordillera, Southern Spain. In: Siliceous deposits of the Tethys and Pacific regions. (Eds. Hein & Obradovic). Springer-Verlag, New York, pp.107-128.
- Rupke, N.A. (1975) Deposition of fine-grained sediments in the abyssal environment of the Algero-Balearic basin, Western Mediterranean sea.  
Sedimentology 22, pp. 95-109.
- Saunders, A.D., Tarney, J., Marsh, N.G. & Wood, D.A. (1980) Ophiolites as ocean crust or marginal basin crust: A geochemical approach. In: Proceedings of the International Ophiolite Symposium, Cyprus 1979. (Ed. Panayiotou) pp. 193-204.

- Scandone, P.** (1967) Studi di geologia lucana: la serie calcareo-silico-marnosa e i suoi rapporti con l'Appennino calcareo.  
Boll. Soc. Naturalisti in Naples 76, pp. 3-175.
- Scandone, P.** (1975) Triassic seaways and the Jurassic Tethys Ocean in the central Mediterranean area.  
Nature 256/5513, pp. 117-119.
- Scholle, P.A.** (1971) Sedimentology of fine-grained deep-water carbonate turbidites, Monte Antola Flysch (Upper Cretaceous) Northern Apennines, Italy.  
Bull. Geol. Soc. Am. 82, pp. 629-658.
- Schroeder, J.H. & Siegel, F.R.** (1969) Experimental dissolution of calcium, magnesium and strontium from Holocene biogenic carbonates: a model of diagenesis.  
Bull. Am. Ass. Petrol. Geol. 53, pp. 741
- Schwarzacher, W. & Fischer, A.G.** (1982) Limestone-shale bedding and perturbations of the Earth's orbit. In: Cyclic and event stratification. (Eds. Einsele & Seilacher). Springer-Verlag, Berlin, pp. 72-95.
- Searle, M.P. & Cooper, D.J.W.** (1986) Structure of the Hawasina window culmination, central Oman Mountains.  
Trans. Roy. Soc. Edinburgh 77, pp. 143-156.
- Sebrier, M.** (1977) Tectonique recent d'une traversale a l'arc Aegeen. Le Golfe de Corinthe et ses regions peripheriques.  
Universite de Paris-sud (Orsay), PhD thesis.
- Seely, D.R., Vail, P.R. & Walton, G.G.** (1974) Trench-slope model. In: Geology of continental margins (eds. Burke & Drake).  
Springer-Verlag, New York, pp. 249-260.
- Seilacher, A.** (1964) Biogenic sedimentary structures. In: Approaches to palaeoecology (eds. Imbrie & Newell).  
Wiley, New York, pp. 296-313.
- Sengor, A.M.C.** (1984) The Cimmeride orogenic system and the tectonics of Eurasia.  
Geol. Soc. Am. Spec. Pub. 195, pp. 82.
- Seyfried, W. & Bischoff, J.L.** (1977) Hydrothermal transport of heavy metals by seawater: The role of seawater/basalt ratio.  
E.P.S.L. 34, pp. 71-77.
- Sherwin, J.A. & Chapple, W.M.** (1968) Wavelengths of single layer folds: a comparison between theory and observation.  
Am. J. Sci. 266, pp. 167-179.
- Shimmield, G.B. & Price, N.B.** (1984) Recent dolomite formation in hemipelagic sediments off Baja California, Mexico. In: Dolomites of the Monterey Formation and other organic-rich units. (eds Garrison, Kastner & Zenger).  
S.E.P.M. Pacific Section 41, pp. 5-18.
- Siever, R.** (1983) Evolution of chert at active and passive continental margins. In: Siliceous deposits in the Pacific region. (Eds. Iijima, Hein & Siever).  
Developments in sedimentology 36, Elsevier, Amsterdam, pp. 7-24.
- Silver, E.A. & Beutner, E.C.** (1980) Melanges.  
Geology 8, pp. 32-34.
- Sinclair, H.D., Coakley, B., Allen, P.A. & Watts, A.B.** (1990) Simulation of foreland basin stratigraphy using a diffusion model of mountain belt erosion: an example from the Alps of eastern Switzerland.  
Tectonics 10, pp. 599-620.
- Smith, A.G.** (1971) Alpine deformation and the oceanic areas of the Tethys, Mediterranean and Atlantic.  
Bull. Geol. Soc. Am. 82, pp. 2039-2070.
- Smith, A.G., Hynes, A.J., Menzies, M., Nisbet, E.G., Price, I., Welland, M.J.P. and Ferriere, J.** (1975) The stratigraphy of the Othris Mountains, eastern central Greece: a deformed Mesozoic continental margin sequence.  
Eclogae Geologicae Helveticae 68, 463-481.



- Seeger, M.J.** (1992) Tectonic influences on lacustrine sedimentation in the Gulf of Corinth half graben, Greece.  
PhD Thesis, University of Wales College, Cardiff.

- Smith, A.G. & Moores, E.M. (1974)** The Hellenides. In: *Mesozoic and Cenozoic Orogenic Belts*. Spec. Pub. Geol. Soc. London 4, pp. 159-185.
- Smith, A.G. & Woodcock, N.H. (1982)** Tectonic synthesis of the Alpine-Mediterranean region: a review. In: *Alpine-Mediterranean Geodynamics*. Am. Geophys. Un. Geodynamics Series 7, pp. 15-39.
- Smith, A.G., Woodcock, N.H. & Naylor, M.A. (1979)** The structural evolution of a Mesozoic continental margin, Othris Mountains, Greece. *J. Geol. Soc. London* 136, pp. 589-603.
- Sorem, R.K. & Fewkes, R.H. (1977)** Internal characteristics. In: *Marine manganese deposits*. (Ed. Glasby). Elsevier oceanography series, Amsterdam, pp.147-184.
- Stampfli, G., Marcoux, J. & Baud, A. (1991)** Tethyan margins in space and time. *Palaeogeography, Palaeoclimatology, Palaeoecology* 87, pp. 373-409.
- Steinberg, M., Bonnot-Courtois, C. & Tlig, S. (1983)** Geochemical contribution to the understanding of bedded chert. In: *Siliceous deposits in the Pacific region*. (Eds. Iijima, Hein & Siever). *Developments in Sedimentology* 36, Elsevier, Amsterdam, pp. 193-210.
- Steinberg, M., Desprairies, A., Fogelgesang, J.F., Martin, A., Caron, D. & Blanchet, R. (1977)** Radiolarites et sediments hypersiliceux oceaniques: une comparaison. *Sedimentology* 24, pp. 547-563.
- Stiros, S.C. (1988)** Model for the N. Peloponnesian (C. Greece) uplift. *J. Geodynamics* 9, pp. 199-214.
- Stockmal, G.S., Beaumont, C. & Boutilier, R. (1986)** Geodynamic models of convergent margin tectonics: Transition from rifted margin to overthrust belt and consequences for foreland-basin development. *Am. Ass. Petrol. Geol. Bull.* 70, pp. 181-190.
- Stow, D.A.V., Howell, D.G. & Nelson, C.H. (1984)** Sedimentary, tectonic and sea level controls on submarine fan and slope-apron turbidite systems. *Geo-Marine Letts.* 3, pp. 57-64.
- Stow, D.A.V., Wezel, F.C., Savelli, D., Rainey, S.C.R. & Angell, G. (1984)** Depositional model for calcilutites: Scaglia-Rossa Limestones, Umbro-Marchean Apennines. In: *Fine-grained sediments: Deep-water processes and facies* (eds. Stow & Piper). *Spec. Pub. Geol. Soc. London* 15, pp. 611-645
- Suppe, J. (1980)** A retrodeformable cross section of Northern Taiwan. *Geol. Soc. China* 23, pp. 45-55.
- Suppe, J. (1983)** Geometry and kinematics of fault bend folding. *Am. J. Sci.* 283, pp. 684-721.
- Suppe, J. (1985)** Principles of structural geology. Prentice-Halls Publ. New Jersey, USA.
- Suppe, J. & Medwedeff, D.A. (1984)** Fault-propagation folding. *Geol. Soc. Am. Ann. General Meeting* 16, pp. 670.
- Suthren, R.J. (1985)** Facies analysis of volcanoclastic sediments: a review. In: *Sedimentology, recent developments and applied aspects*. (eds. Brenchley & Williams). Blackwell Scientific Publications, Oxford.
- Swarbrick, R.E. (1979)** The sedimentology and structure of southwest Cyprus and its relationship to the Troodos Complex. Unpub. PhD thesis, Cambridge University.
- Swarbrick, R.E. & Robertson, A.H.F. (1980)** Revised stratigraphy of the Mesozoic rocks of southern Cyprus. *Geol. Mag.* 177, pp. 547-563
- Taira, A. (1985)** Sedimentary evolution of the Shikoku subduction zone: The Shimanto belt and Nankai Trough. In: *Formation of active margins* (ed. Nasu). Terrapub. Tokyo. pp. 835-851.
- Temple, P.G. (1968)** Mechanics of large scale gravity sliding in the Greek Peloponnese. *Bull. Geol. Soc. Am.* 79, pp. 687-700.

- Terry, J.** (1969) Etude geologique d'un secteur de la Messenie occidentale.  
D.E.A. Universite Lille.
- Thiebault, F.** (1982) Evolution geodynamique des Hellenides externes en Peloponnese meridionale (Grece).  
Soc. Geol. du Nord Spec. Pub. 6, pp. 574.
- Thiebault, F., De Wever, P. & Raoult, J.F.** (1986) Marqueurs mineralogique et geochemique au passage Jurassique-Cretace dans les Pinde du Peloponnese meridional (Grece). Signification geodynamic.  
Rev. Geol. Dyn. Geogr. Phys. 27, pp. 351-362.
- Thiebault, F. & Fleury, J.J.** (1991) Essai d'identification des sources et des vecteurs de l'alimentation en argiles du bassin du Pind-Olonos pendant le Mesozoique. In: Proceedings of the 5<sup>th</sup> Geol. Cong., Thessaloniki 1990.  
Bull. Geol. Soc. Greece 25, pp. 369-386.
- Thompson, R.L.** (1981) The nature and significance of large "blind" thrusts within the northern Rocky Mountains of Canada. In: Thrust and nappe tectonics (eds. McClay & Price).  
Spec. Publ. Geol. Soc. London. 9, pp 449-462.
- Torrent, J & Schwertmann, U.** (1986) Influence of hematite on the colour of red beds.  
J. Sed. Petrol. 57, pp 682-686
- Toth, J.T.** (1980) Deposition of submarine crusts rich in manganese and iron.  
Geol. Soc. Am. Bull. 91, pp. 44-54.
- Tsalia-Monopolis, S.** (1977) Study of the Tripolitza Zone micropalaeontology and stratigraphy. (In Greek with English summary).  
I.G.M.E. Publ. 20, pp. 96-99.
- Tsoflias, P.** (1969a) Sur la decouverte d'ammonites triasiques au front de la nappe du Pinde en Peloponnese septentrional (Grece).  
C.R. Soc. Geol. France pp. 118-119
- Tsoflias, P.** (1969b) Sur la presence de Trias detritique dans la serie du Pinde-Olonos, en Peloponnese septentrional (province d'Achaie, Grece).  
C.R. Soc. Geol. France, pp. 77-78.
- Tsoflias, P.** (1984) 1:50000 Geological Map of Greece, Halandritsa sheet.  
Pub. I.G.M.E. Athens.
- Tucker, M.E.** (1974) Sedimentology of Palaeozoic pelagic limestones: the Devonian Griotte (Southern France) and Cephalopodenkalk (Germany). In: Pelagic sediments: on land and under the sea (eds. Hsu & Jenkyns).  
Spec. Pub. Int. Ass. Sed. 1, pp. 71-92.
- Tucker, M.E.** (1990) Modern carbonate environments. In: Carbonate sedimentology (eds. Tucker & Wright).  
Blackwell Scientific Publ. Oxford.
- Turcotte, D.L. & Schubert, G.** (1982) Geodynamics: Applications of continuum mechanics to geological problems.  
Wiley, New York.
- Underhill, J.** (1985) Neogene and Quaternary tectonics and sedimentation in western Greece.  
Unpublished University of Wales, Cardiff PhD thesis.
- Underhill, J.** (1988) Triassic evaporites and Plio-Quaternary diapirism in western Greece.  
J. Geol. Soc. London 145, pp. 269-282.
- Underhill, J.** (1989) Late Cenozoic deformation of the Hellenide foreland, western Greece.  
Bull. Geol. Soc. Am. 101, pp. 613-634.
- Underhill, J.** (1991) Controls on Late Jurassic seismic sequences, Inner Moray Firth, UK North Sea: A critical test of a key segment of Exxon's global cycle chart.  
Basin Research 3, pp. 79-98.
- Underwood, M.B. & Bachman, S.B.** (1982) Sedimentary facies associations within subduction complexes. In: Trench-Forearc Geology (ed. Leggett).  
Spec. Pub. Geol. Soc. London 10, pp. 537-550.



- Vail, P.R. & Mitchum, R.M. (1979) Global cycles of relative changes of sea level from seismic stratigraphy. In: Seismic stratigraphy-applications to hydrocarbon exploration (Ed. by C.E. Payton).  
Mem. Am. Ass. Petrol. Geol. 29, pp 469-472.
- Vail, P.R., Mitchum, R.M. & Thompson S. (1977) Seismic stratigraphy and global changes of sea level. In: Seismic stratigraphy-applications to hydrocarbon exploration (Ed. by C.E. Payton).  
Mem. Am. Ass. Petrol. Geol. 26, pp 83-97.
- Vail, P.R. & Todd, R.G. (1981) Northern North Sea Jurassic unconformities, chronostratigraphy and sea level changes from seismic stratigraphy. In: Petroleum Geology of the continental shelf of North-West Europe: Proceedings of the 2nd conference. (eds. Illing & Hobson) Heydon, London, pp. 216-235.
- Van Andel, T.H., Thiede, J., Sclater, J.G. & Hay, W.W. (1977) Depositional history of the south Atlantic Ocean during the last 125 million years.  
J. Geol. 85, pp. 651-698.
- Varnavas, S.P. (1987) Marine barite in sediments from deep sea drilling project sites 424 and 424a (Galapagos Hydrothermal Mounds Field).  
Marine Chemistry 20, pp. 245-253.
- Varnavas, S.P. & Cronan, D.S. (1981) Partition geochemistry of sediments from DSDP 424 in the Galapagos hydrothermal mounds field.  
Mineral. Mag. 44, pp.325-331
- Varnavas, S.P. & Cronan, D.S. (1988) Arsenic, antimony and bismuth in sediments and waters from the Santorini hydrothermal field, Greece.  
Chemical Geology 67, pp. 295-305.
- Varnavas, S.P. & Cronan, D.S. (1991) Hydrothermal metallogenic processes off the islands of Nisiros and Kos in the Hellenic Volcanic arc.  
Marine Geology 99, pp. 109-133.
- Varnavas, S.P., Cronan, D.S. & Anderson, R.K. (1990) Spatial and time series analysis of Santorini hydrothermal waters. In: Thera and the Aegean world III. (Eds Doumas et al.) The Thera Foundation, London.
- Varnavas, S.P., Moorby, S.A. & Cronan, D.S. (1983) Partition geochemistry of sediments from holes 506 and 509B, DSDP Leg 70.  
Initial Report. DSDP 70, pp. 297-302.
- Varnavas, S.P. & Panagos A.G. (1982) Geochemistry, mineralogy and genesis of manganese deposits from the Pindos geotectonic zone, Greece,  
Proc. of Int. Mineral. Ass., Varna, Bulgaria.
- Varnavas, S.P. & Panagos, A.G. (1986) The Mesozoic ocean-ridge deposits of Hermioni area, Greece.  
Geol. Zb. Geol. Carpathica 37.
- Varnavas, S.P., Papaioannou, J. & Catani, J. (1988) A hydrothermal manganese deposit from the Eratosthenes seamount, Eastern Mediterranean Sea.  
Marine Geology 81, pp. 205-214.
- Vecsei, A., Frisch, W., Pirzer, M. & Wetzell, A. (1989) Origin and tectonic significance of radiolarian chert in the Austroalpine rifted continental margin. In: Siliceous deposits of the Tethys and Pacific regions. (Eds. Hein & Obradovic). Springer-Verlag, New York, pp. 65-80.
- Vergely, P. (1976) Chevauchement vers l'ouest et retrocharriage vers l'est des ophiolites: Deux phases tectoniques au cours du Jurassique superieur-Eocretace dans les Hellenides internes.  
Bull. Soc. Geol. France (7) 18. pp. 231-244.
- Vergely, P. (1984) Tectonique des ophiolite dans les Hellenides internes. Consequence sur l'evolution des regions Tethysiennes occidentales.  
Thesis, Universite de Paris-sud (Orsay).
- Waldron, J.F. (1984) Evolution of carbonate platforms on a margin of the Neotethys ocean: Isparta angl, southwestern Turkey.  
Eclogae Geol. Helv. 77, pp. 553-581.

- Walker, R.G.** (1978) Deep water sandstone facies and ancient submarine fans: models for exploration for stratigraphic traps.  
Bull. Am. Ass. Petrol. Geol. 62, pp. 932-966.
- Walker, R.G.** (1979) Facies Models.  
Geoscience Canada Reprint Series 1.
- Warburton, J., Burnhill, T.J., Graham, R.H. & Isaac, K.P.** (1990) The evolution of the Oman Mountains foreland basin. In: The geology and tectonics of the Oman Region (eds. Robertson, Searle & Ries).  
Geol. Soc. London, Spec. Pub. 49, pp.419-427.
- Watts, K. & Garrison, R.E.** (1986) Sumeini Group, Oman-Evolution of a Mesozoic carbonate slope on a south Tethyan continental margin.  
Sediment. Geol. 48, pp. 107-168.
- Wernicke, B.** (1981) Low angle normal faults in the Basin and Range province: Nappe tectonics in an extending orogen.  
Nature 291, pp. 645-647.
- Westbrook, G.K.** (1982) The Barbados Ridge Complex: Tectonics of a mature forearc system. In: Trench-Forearc geology (ed. Leggett).  
Spec. Pub. Geol. Soc. London 10, pp. 275-290.
- Whittaker, A., Cope, J.C.W., Cowie, J.W., Gibbons, W., Hailwood, E.A., House, M.R., Jenkins, D.G., Rawson, P.F., Rushton, A.W.A., Smith, D.G., Thomas, A.T. & Wimbledon, W.A.** (1991) A guide to stratigraphical procedure.  
J. Geol. Soc. Lon. 148, pp. 813-824.
- Williams, A., Parks, G.A. & Crerar, D.A.** (1985) Silica diagenesis 1. Solubility controls.  
J. Sed. Petrol. 55, pp. 301-311.
- Williams, G.D. & Chapman, T.** (1983) Strain developed in the hangingwalls of thrust sheets due to their slip/propagation rate: a dislocation model.  
J. Struct. Geol. 5, pp. 563-571.
- Williams, G.D. & Fischer, M.W.** (1984) A balanced section across the Pyrenean orogenic belt.  
Tectonics 3, pp. 773-780.
- Williams, L. & Crerar D.A.** (1985) Silica diagenesis 2. General mechanisms.  
J. Sed. Petrol. 55, pp. 312-321.
- Wilson, M.** (1989) Igneous Petrogenesis.  
Unwin Hyman Ltd (publishers), London.
- Winterer, E.L. & Bosellini, A.** (1981) Subsidence and sedimentation on Jurassic passive continental margin, southern Alps, Italy.  
Bull. Am. Ass. Petrol. Geol. 65, pp. 394-421.
- Wise, S.W. & Weaver, F.M.** (1974) Chertification of oceanic sediments.  
Spec. Pub. Int. Ass. Sediment. 1, pp. 301-326.
- Woo, C.C.** (1973) SEM of marine manganese micronodules, marine pebble-sized nodules and fresh water manganese nodules. In: Papers on the origin and distribution of manganese nodules in the Pacific and prospects for exploration. (Ed. Morgenstein). Hawaii Inst. Geophysics, pp. 165-171.
- Wortel, M.J.R., Spakman, W., Van Wamel, W.A., Meulenkamp, J.E., Hoogerduyn, S.E.** (1988) On the relation between the subduction process and the Neogene Geological evolution of the Aegean area: a new perspective. In: The structural and sedimentary evolution of the neotectonic Aegean basins. London (Abstracts).
- Zimmerman, J.** (1971) Emplacement of the Vourinos Ophiolite Complex, Northern Greece.  
Mem. Geol. Soc. Am. 132, pp. 225-239

**APPENDIX 1**

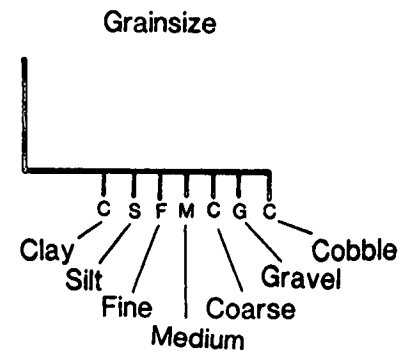
**GRAPHIC SEDIMENTARY LOGS**

## LITHOLOGY

	Limestone		Green Vitreous chert
	Limestone with nodules		Argillaceous chert
	Dolomitic Limestone		Sandstone
	Limestone with chert interbeds		Carbonate matrix support conglomerate
	Mudstone/chert interbeds		Mudstone matrix support conglomerate
	Siltstone		Clast support conglomerate
	Mudstone		Volcaniclastic Sediment

## SEDIMENTARY STRUCTURES

	Graded bedform
	Channeled bedform
	Erosive base
	Planar base
	Trough cross lamination
	Planar cross lamination
	Planar lamination
	Pelagic bivalve
	Ooids
	Globotruncana
	Burrows
	Manganese enrichment
	Igneous intraclasts
	Palaeocurrent orientation



Chert  
"Pinch & Swell"

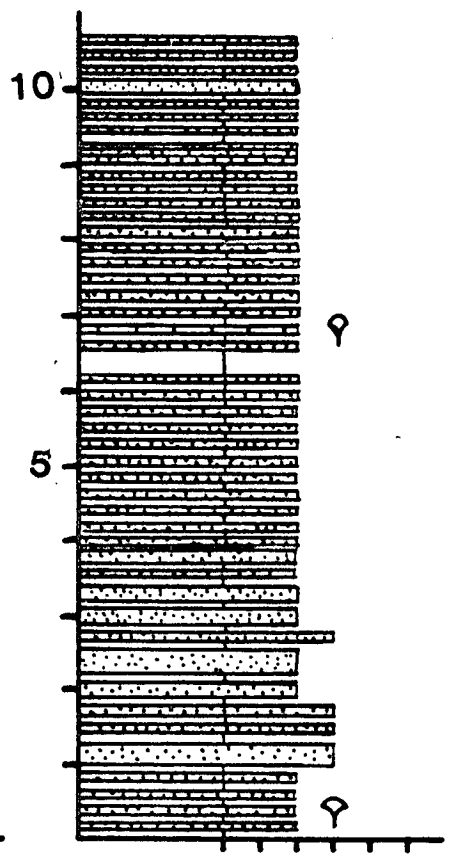
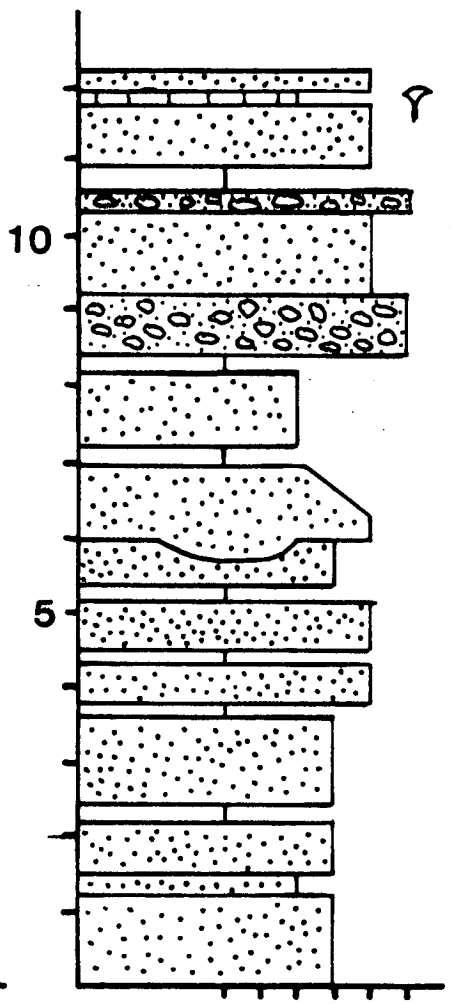
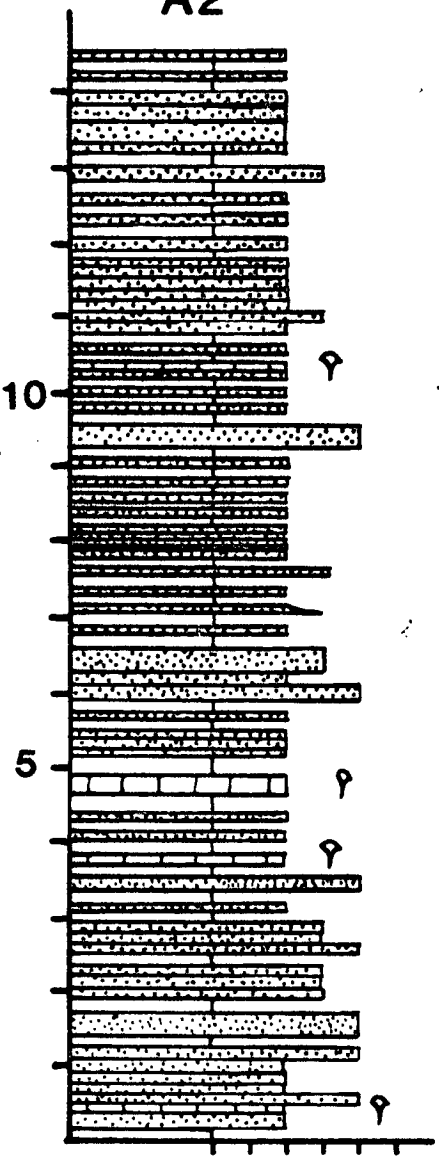
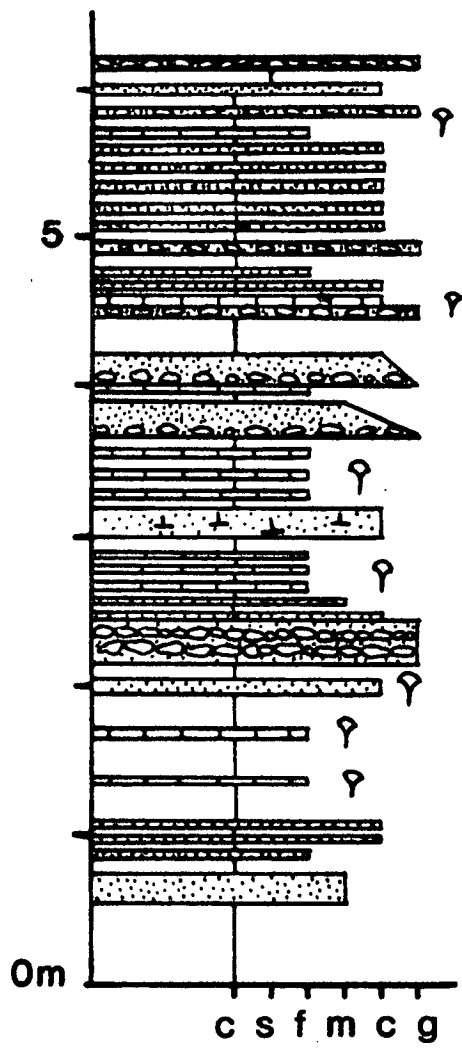
## KEY TO GRAPHIC SEDIMENTARY LOGS

A2

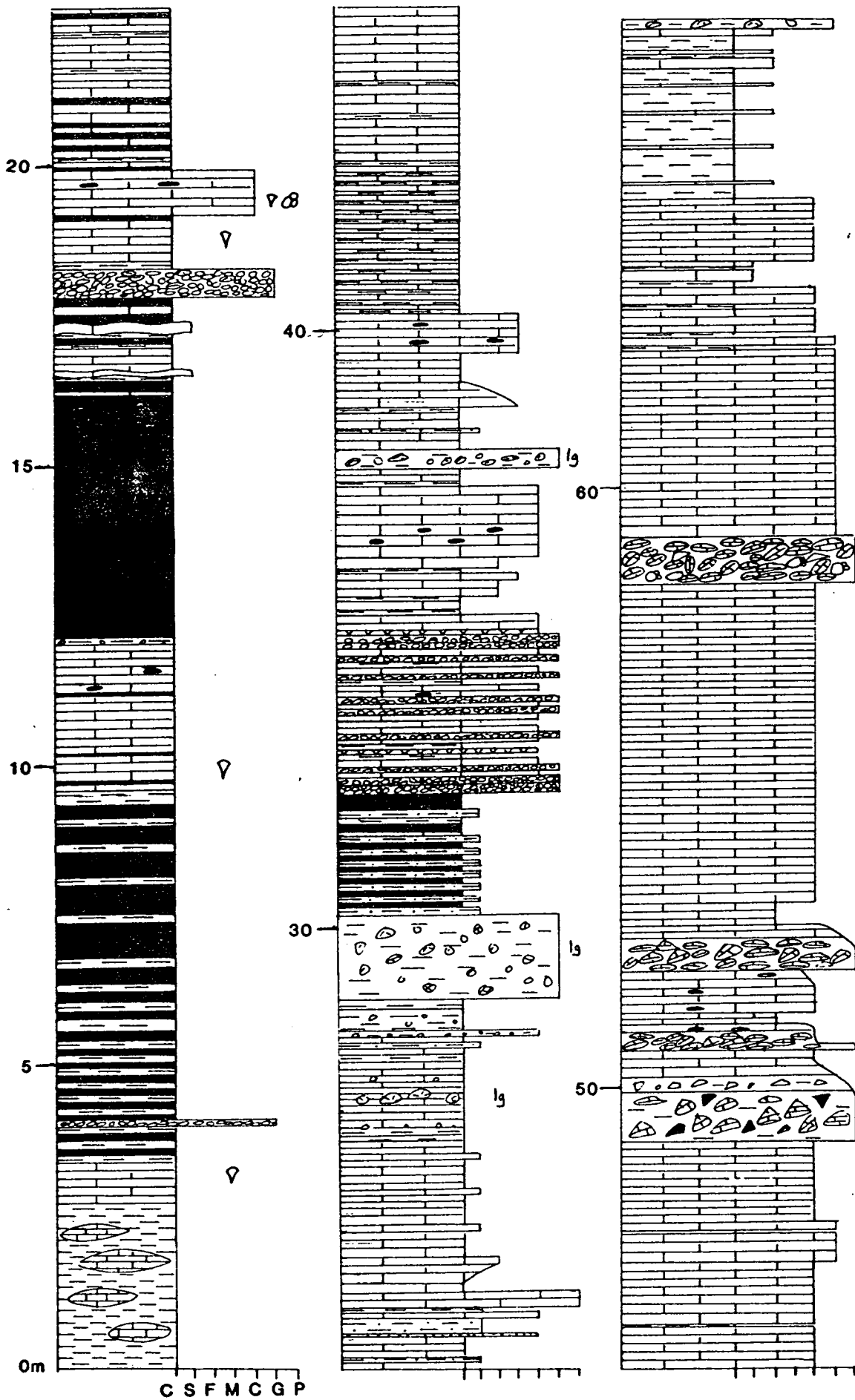
A1

A3

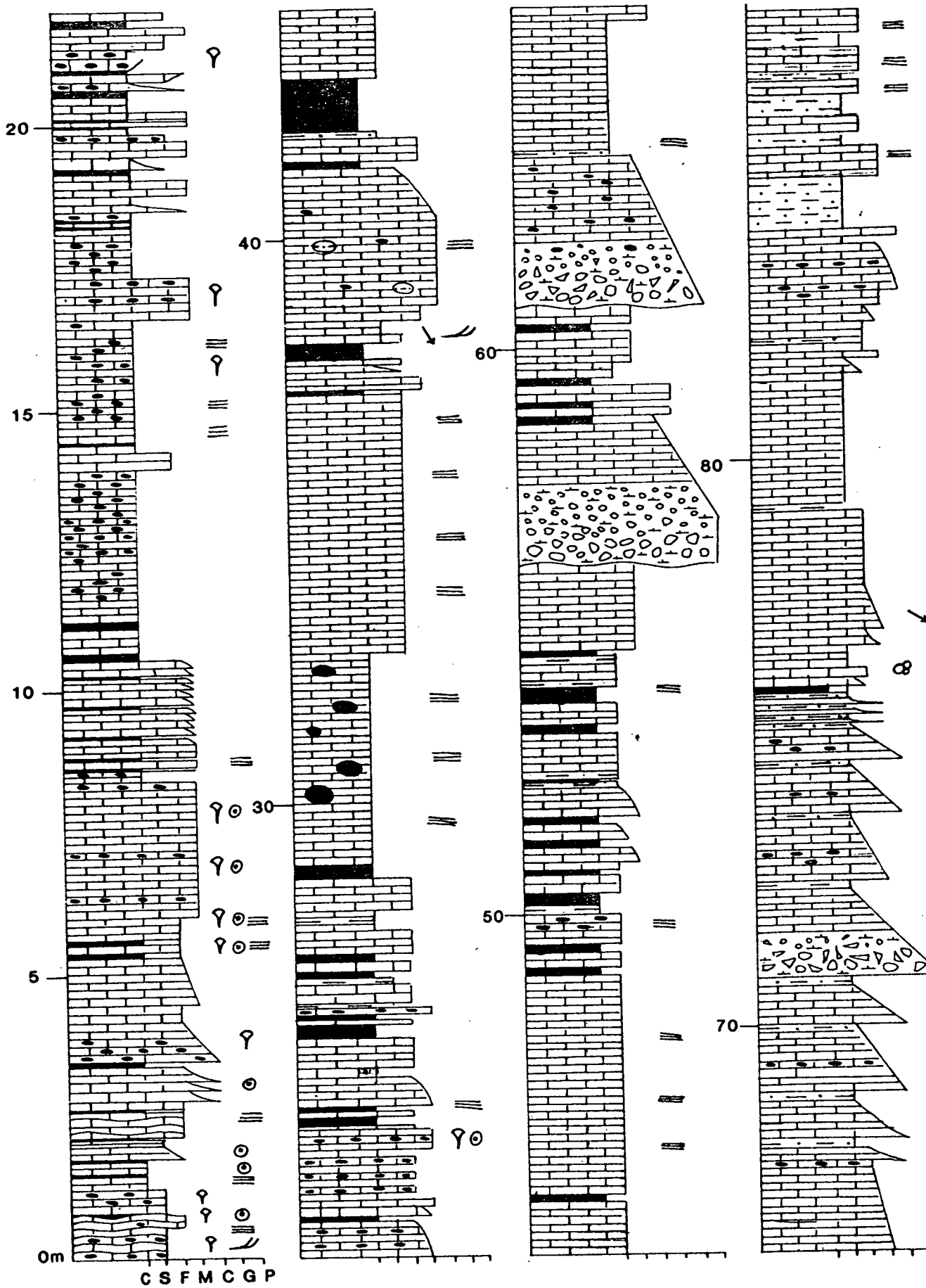
A4



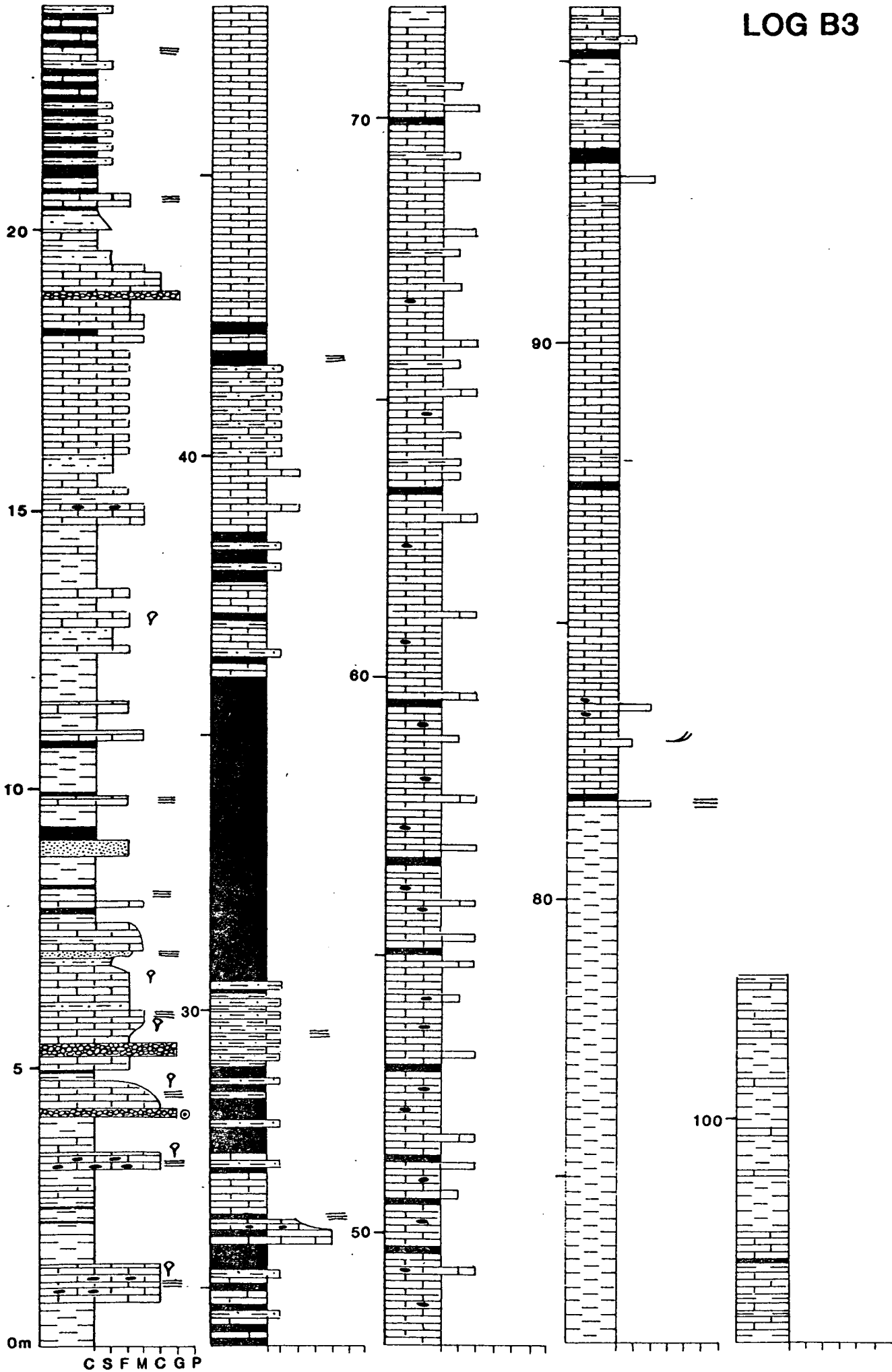
# LOG B1



# LOG B2

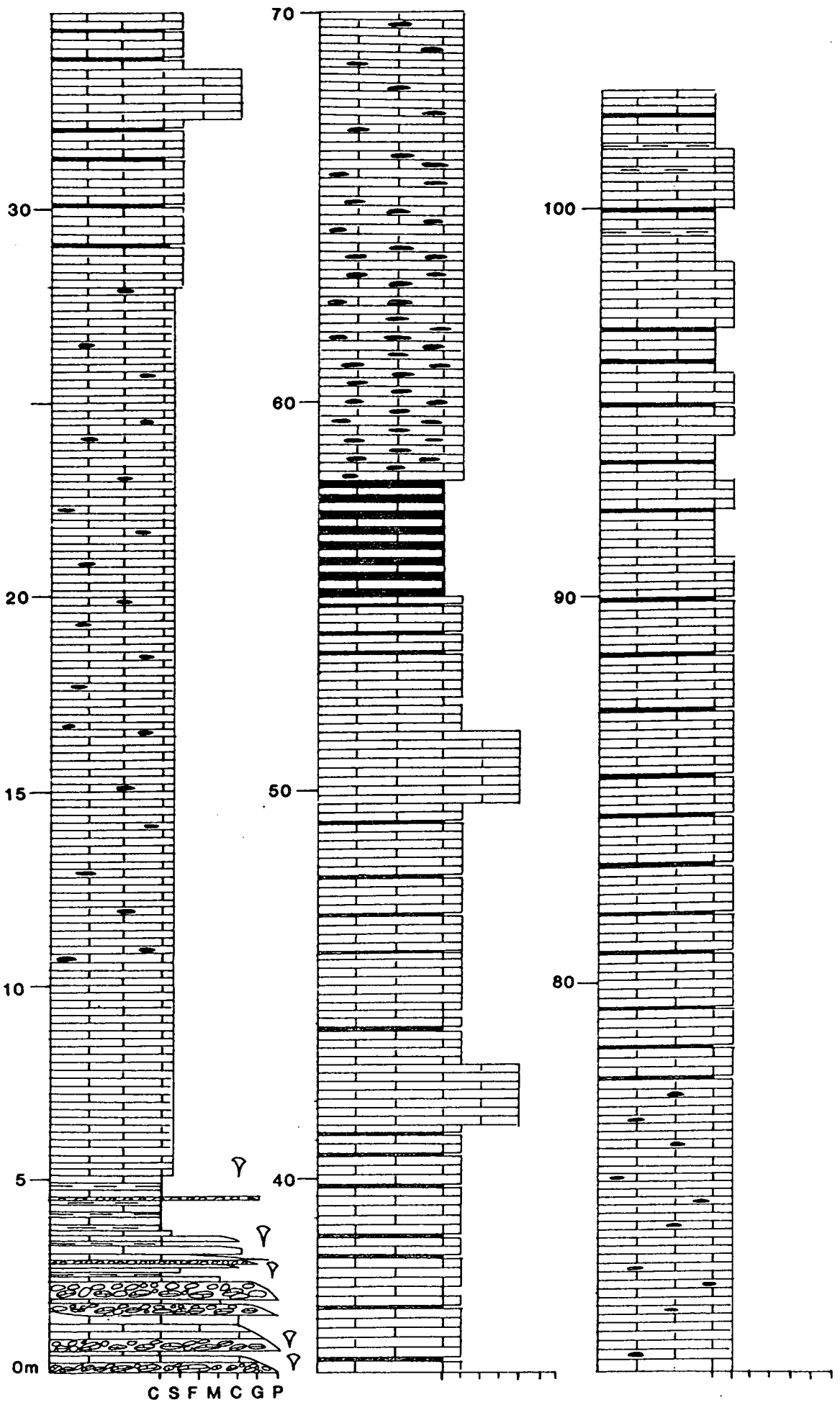


# LOG B3

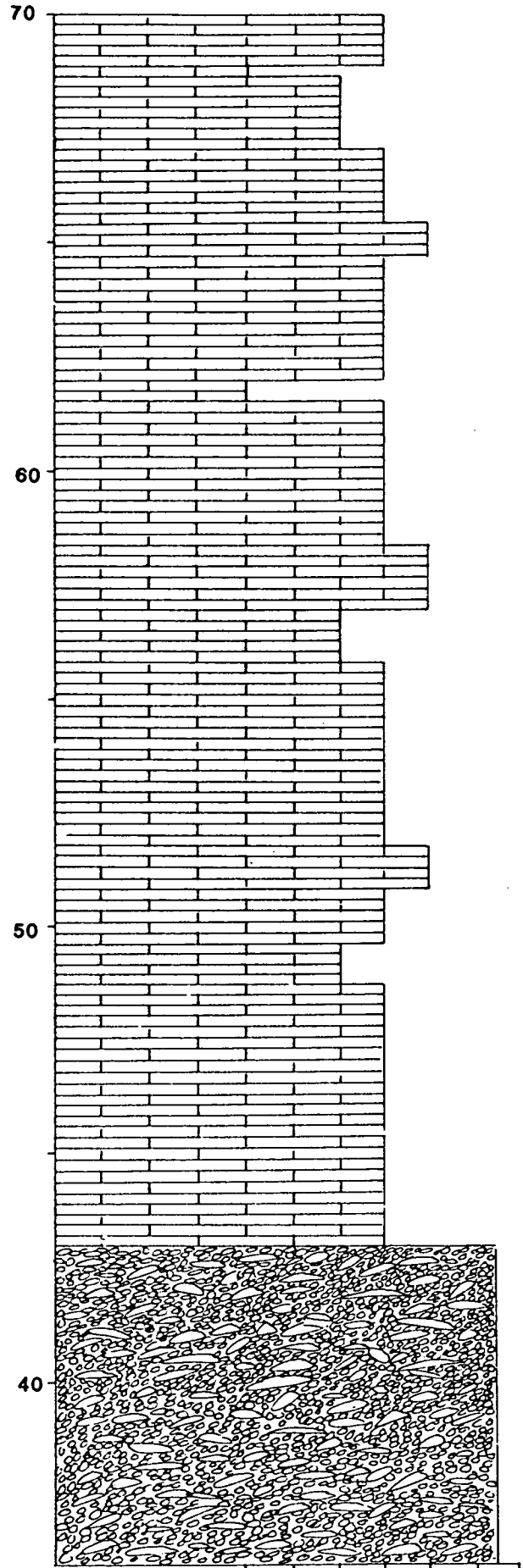
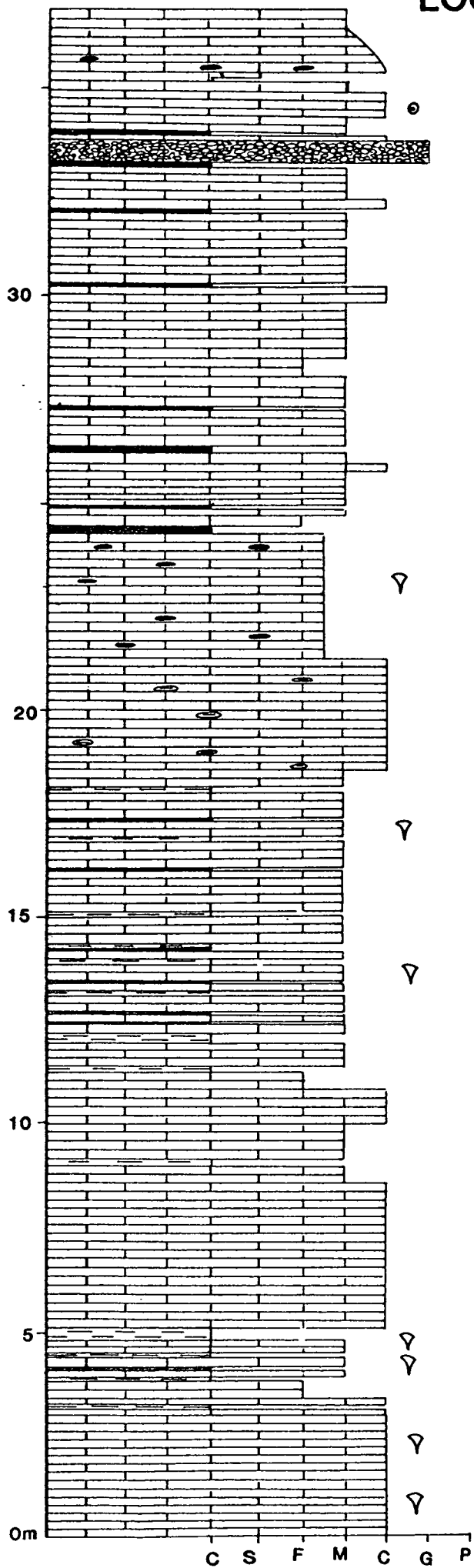




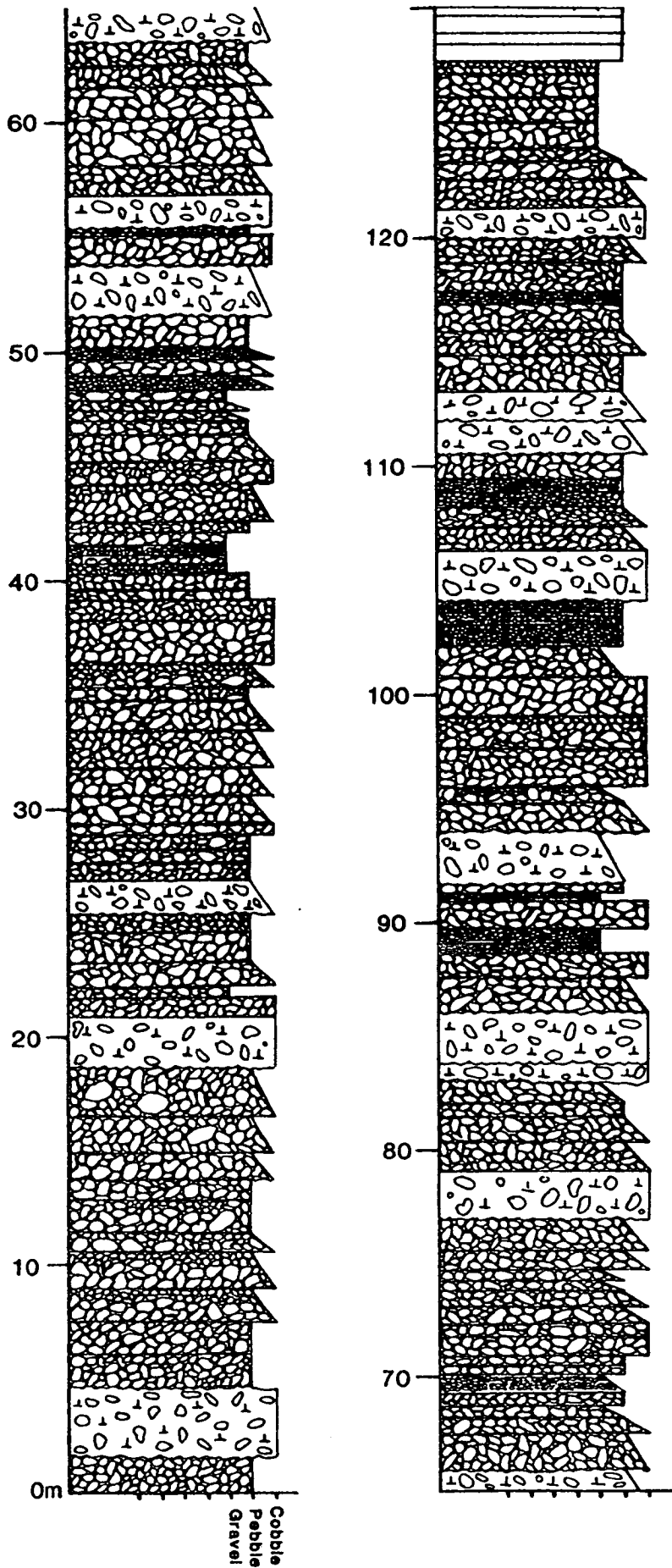
# LOG B4

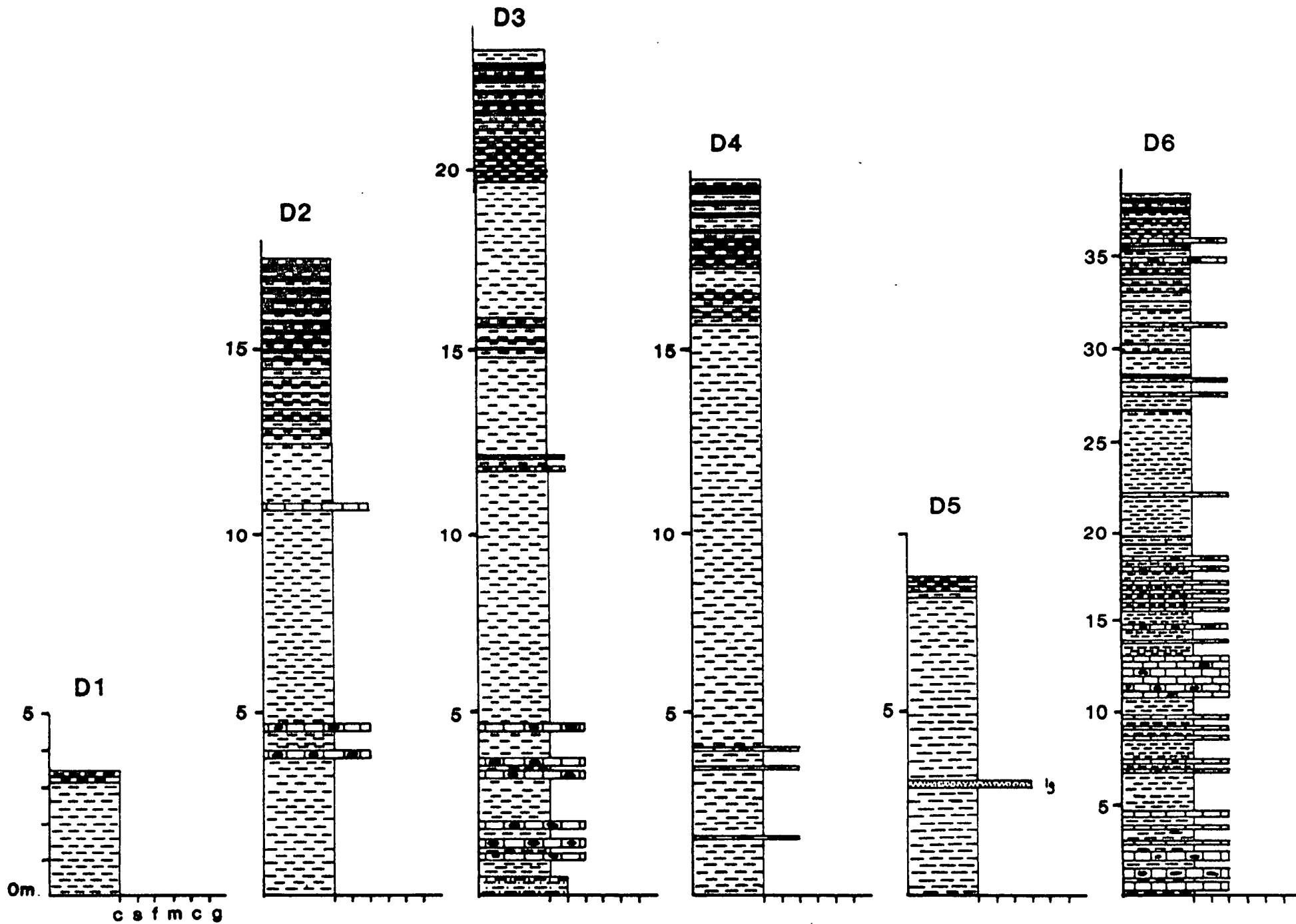


# LOG B5

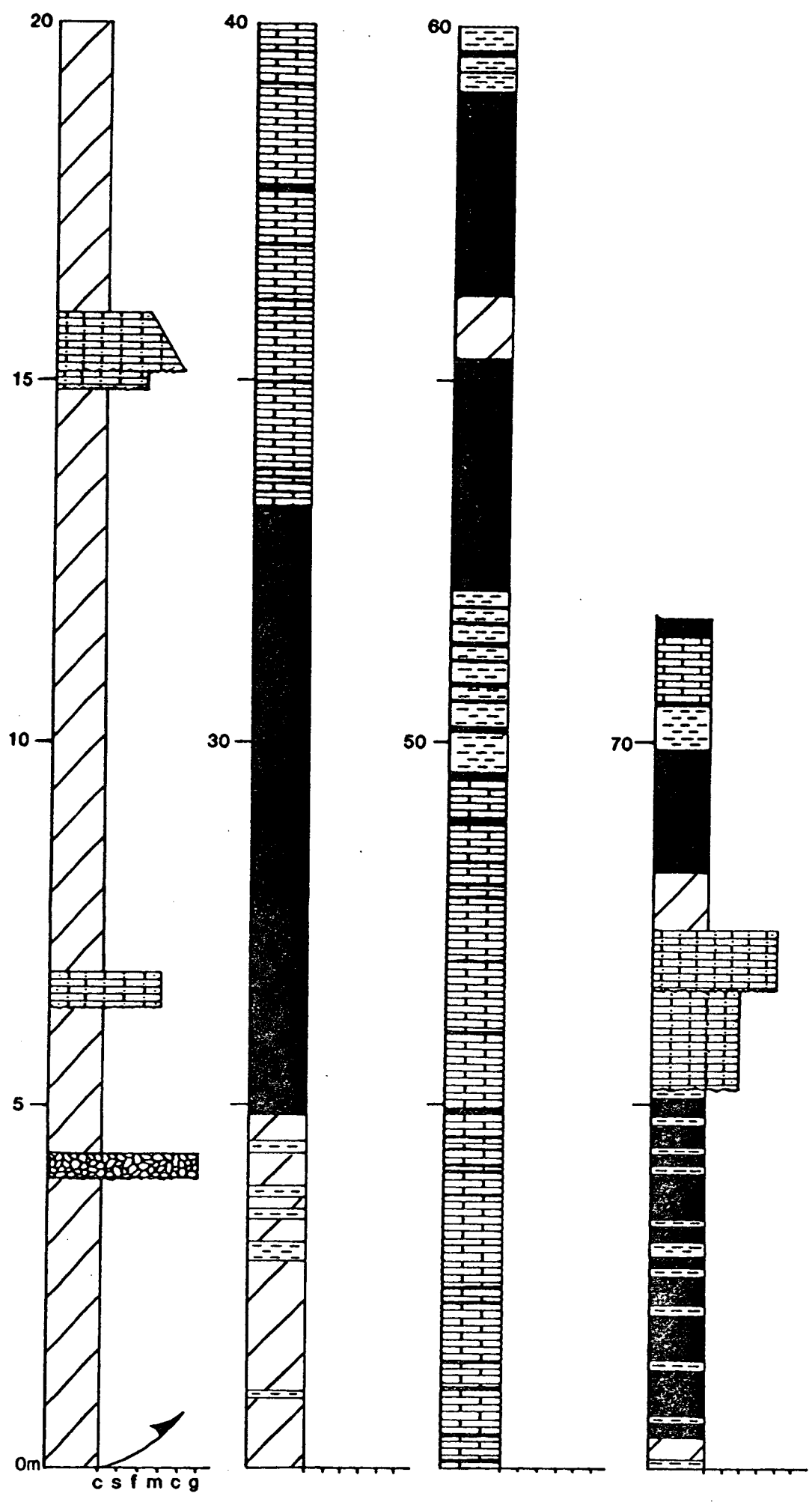


# LOG C1

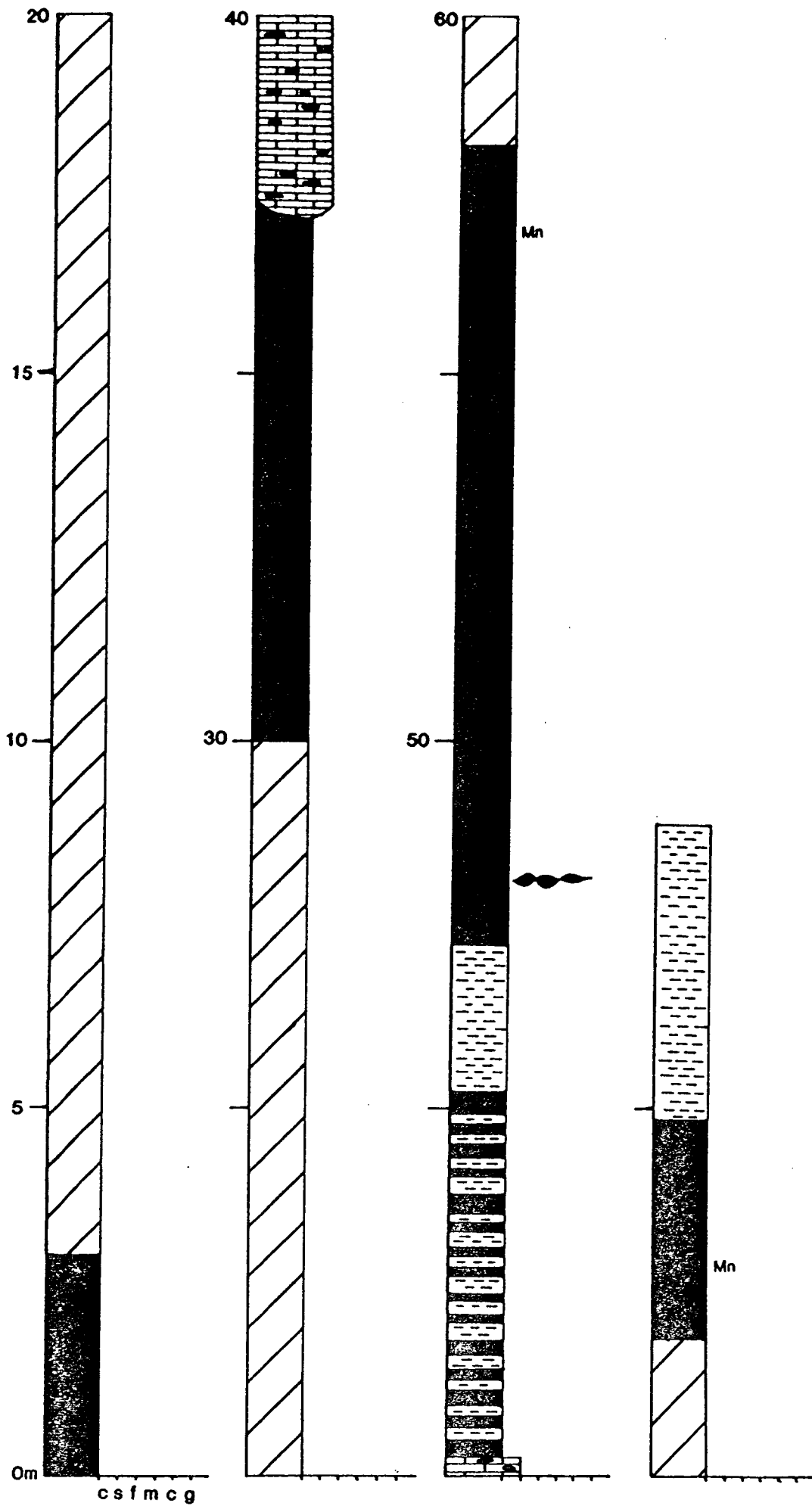




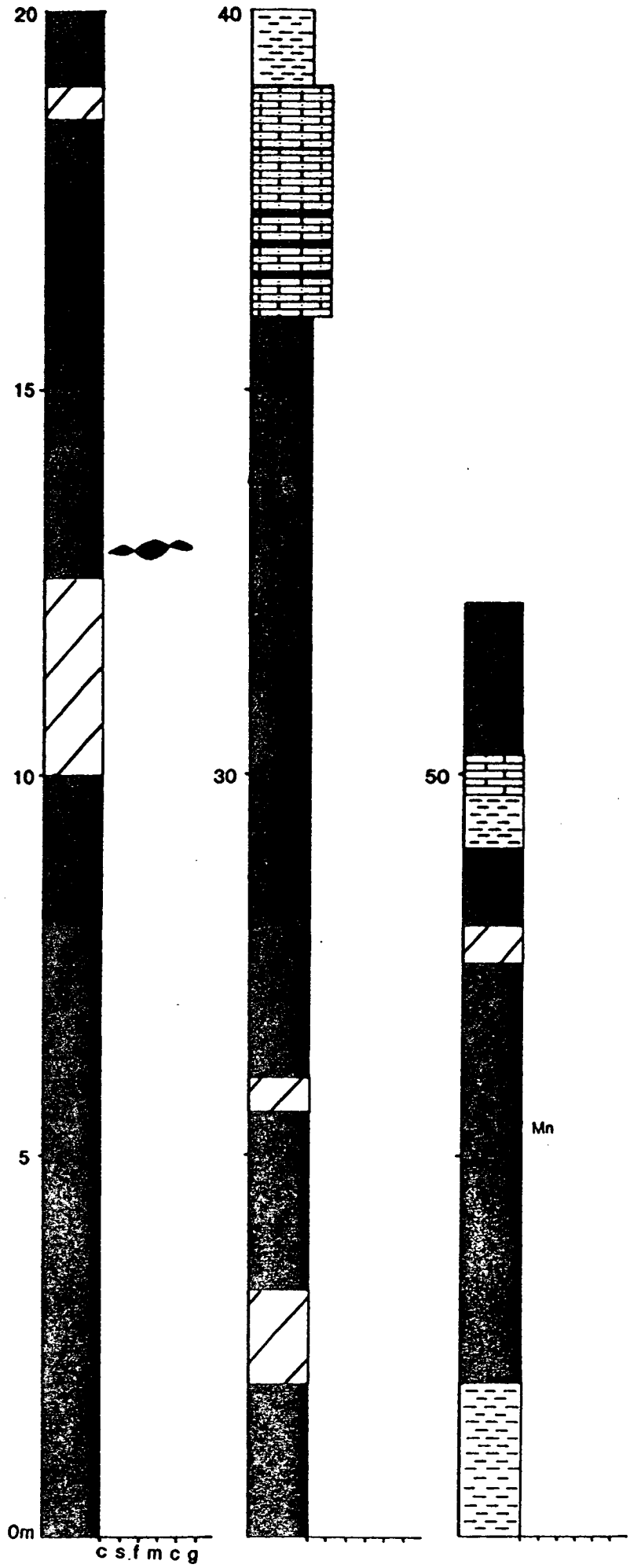
# LOG E1



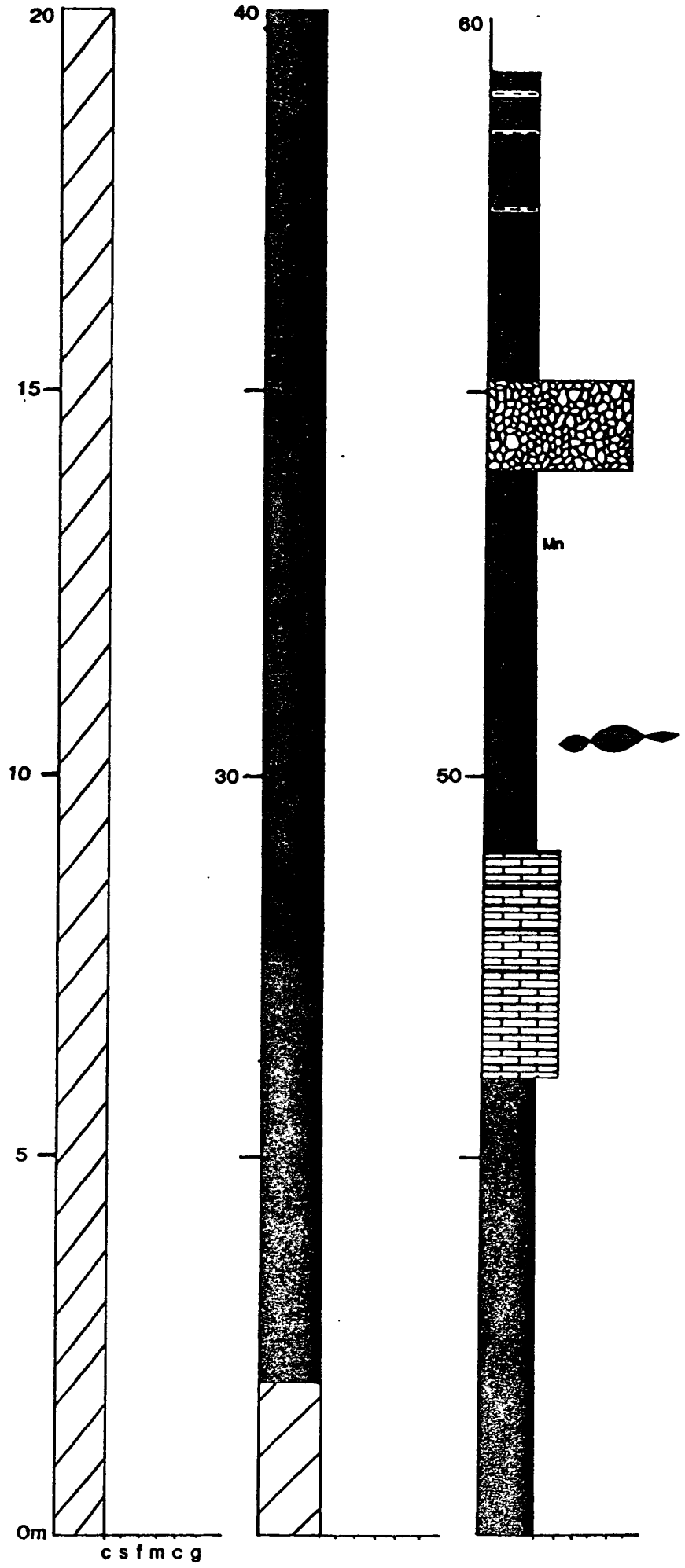
# LOG E2



# LOG E3

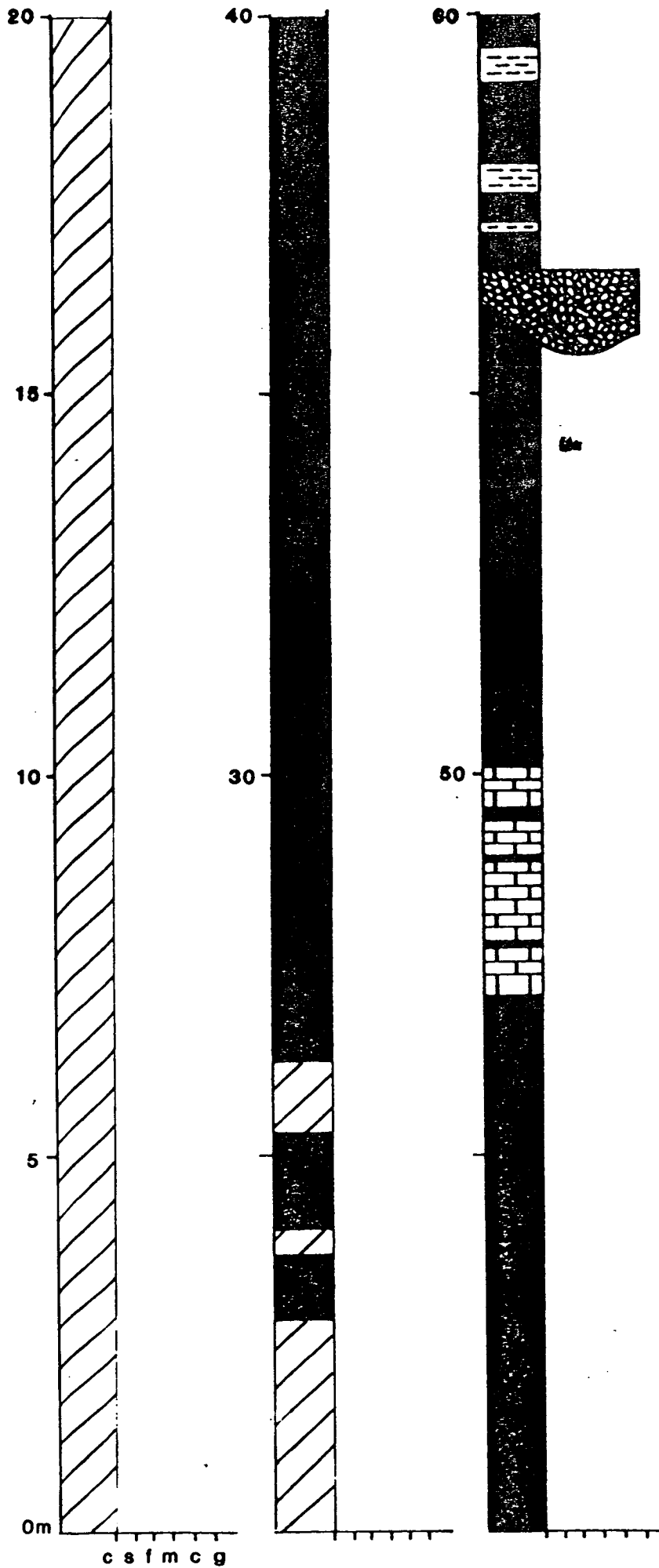


# LOG E4

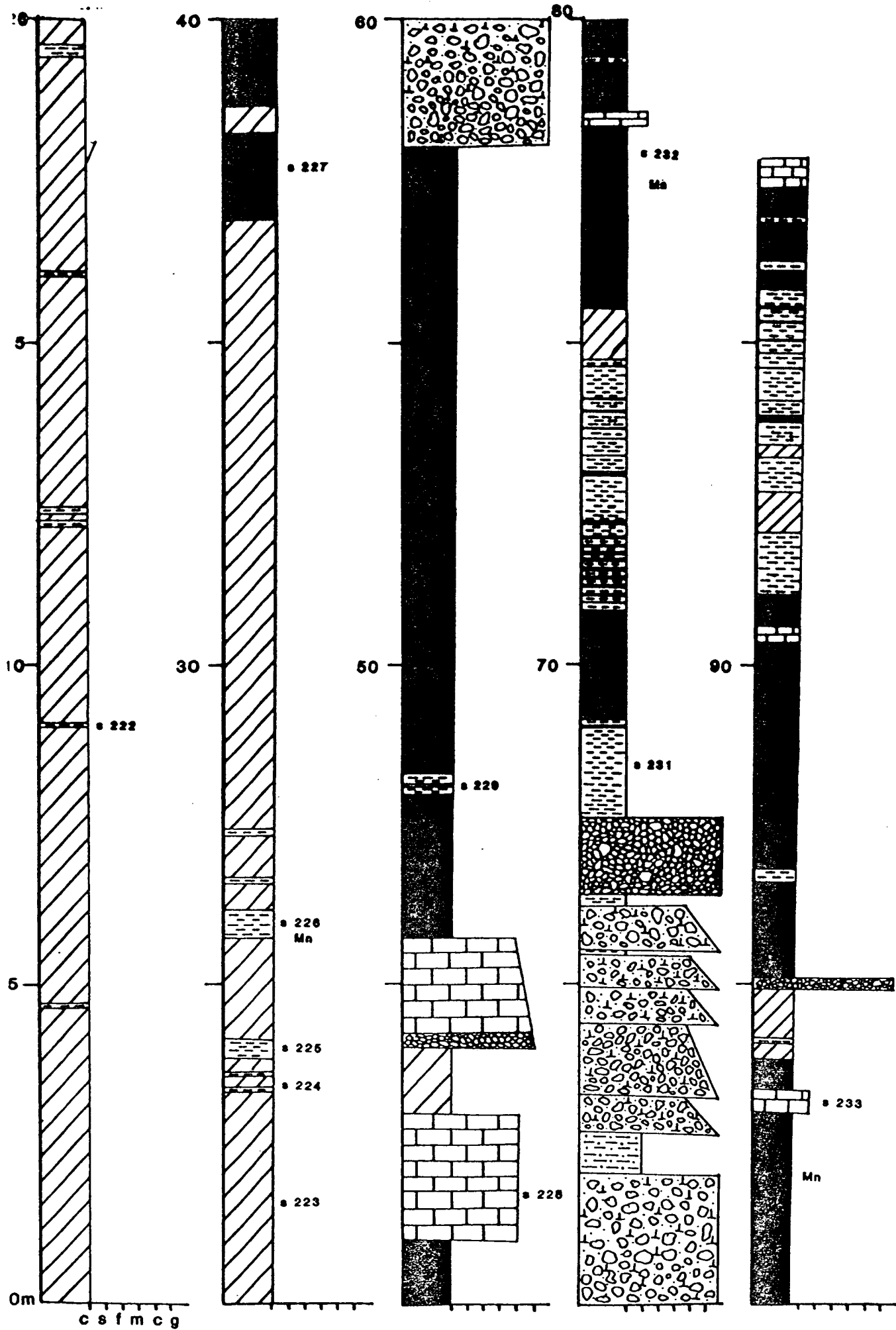




# LOG E5

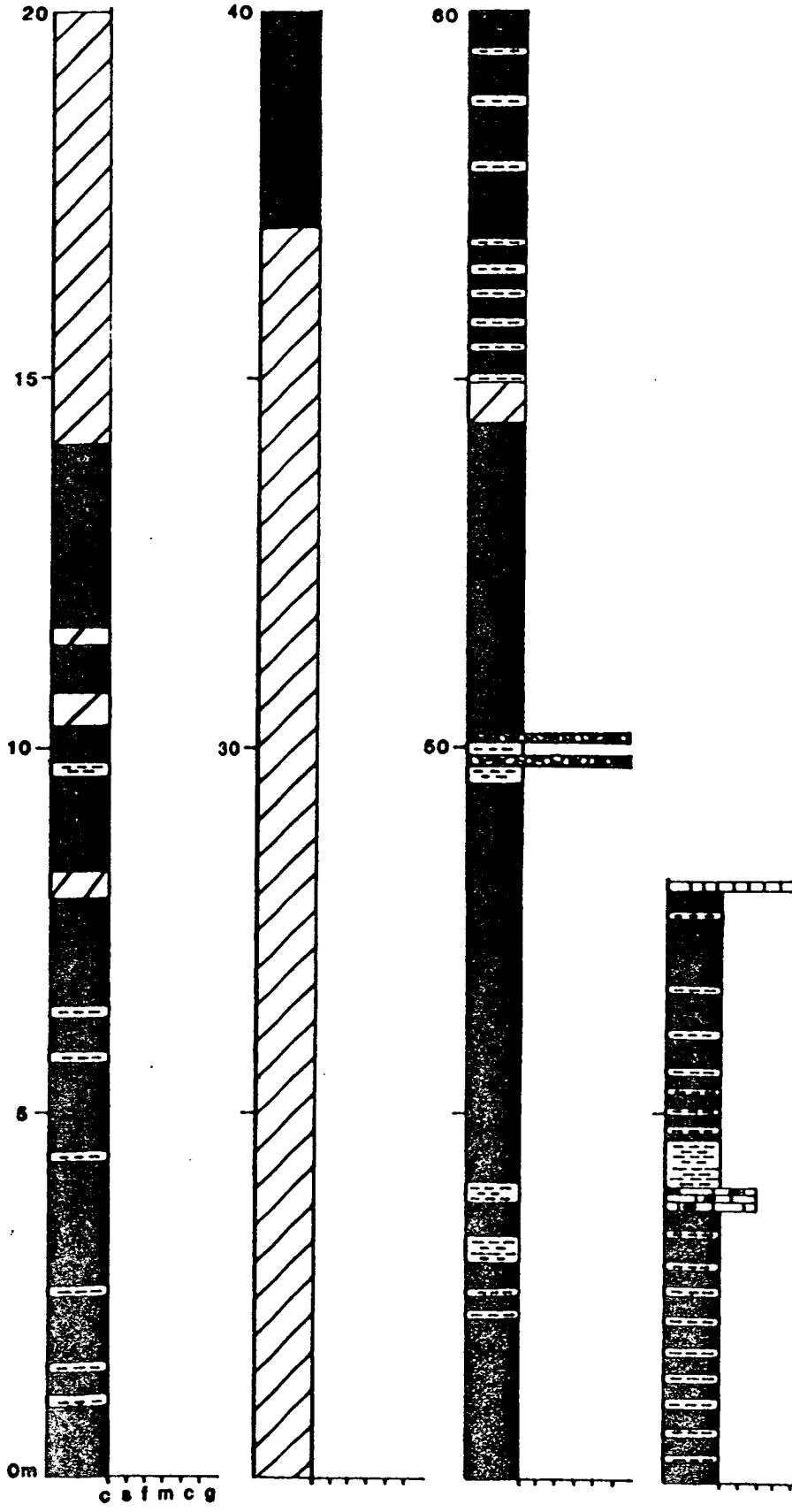


# LOG E6

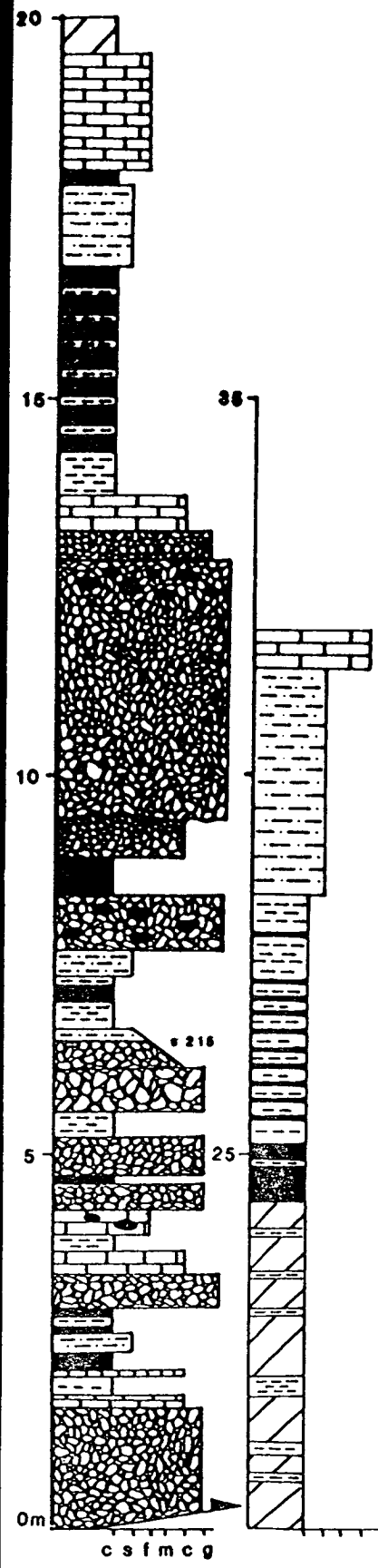




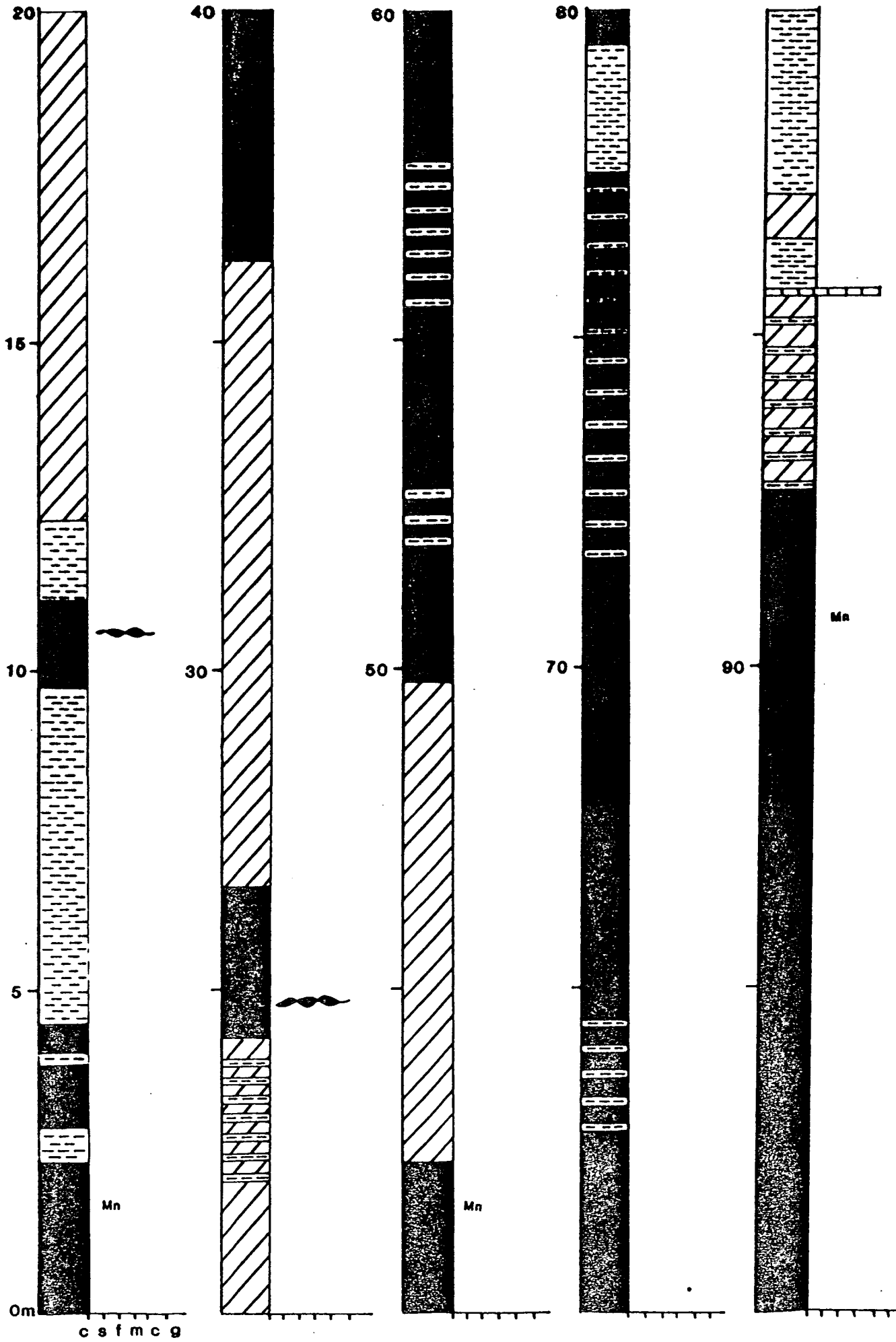
# LOG E8a



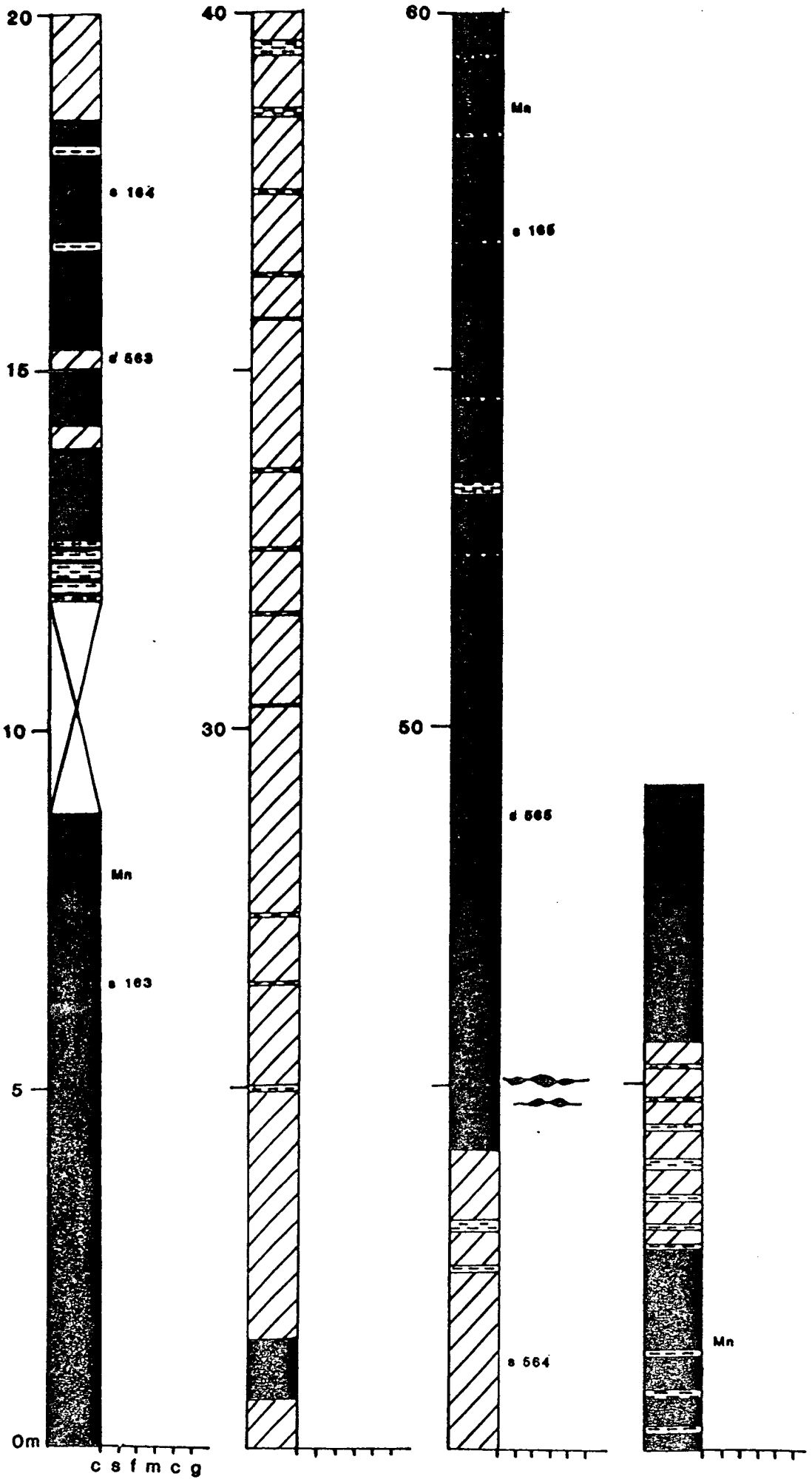
# LOG E8b



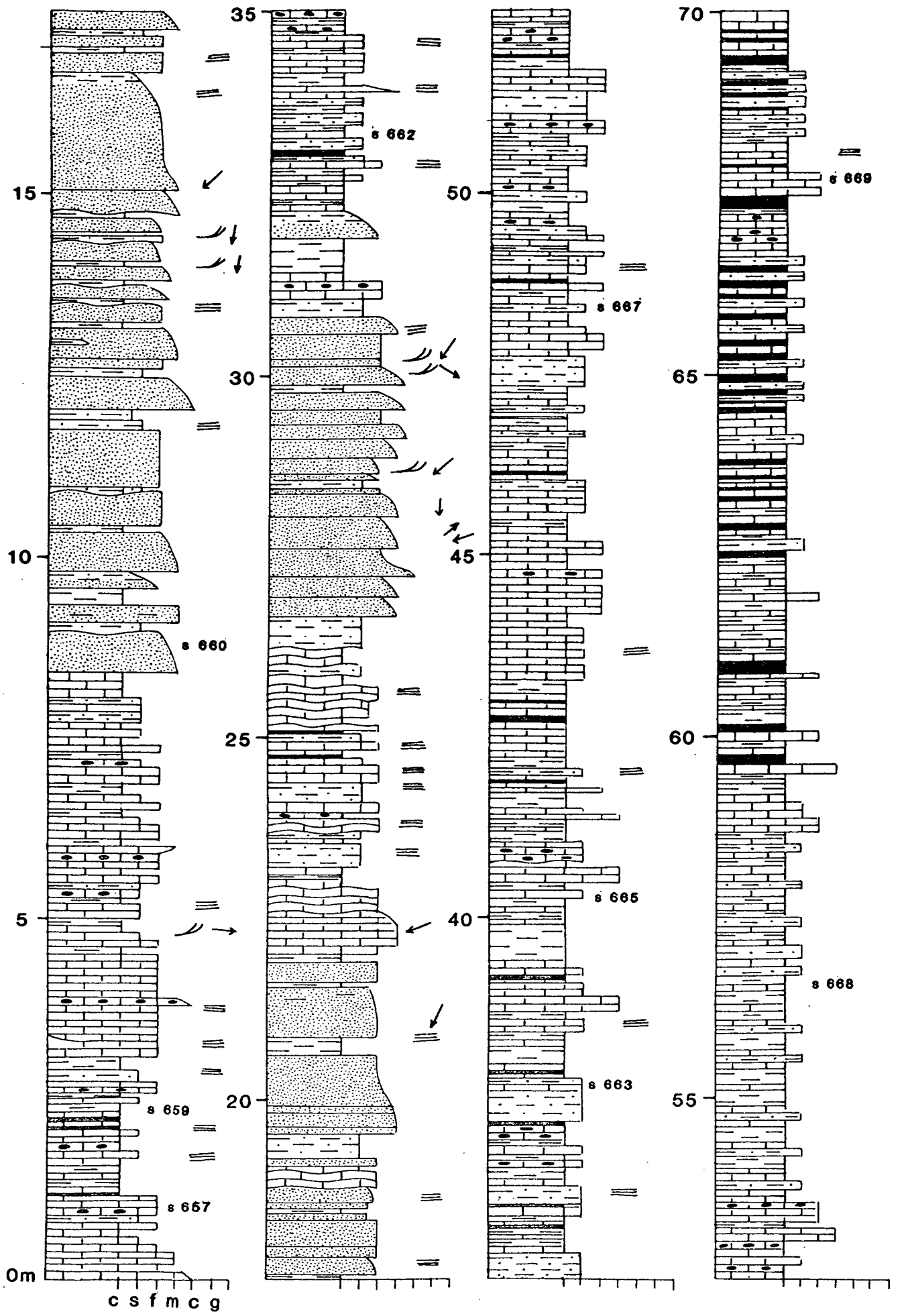
# LOG E9



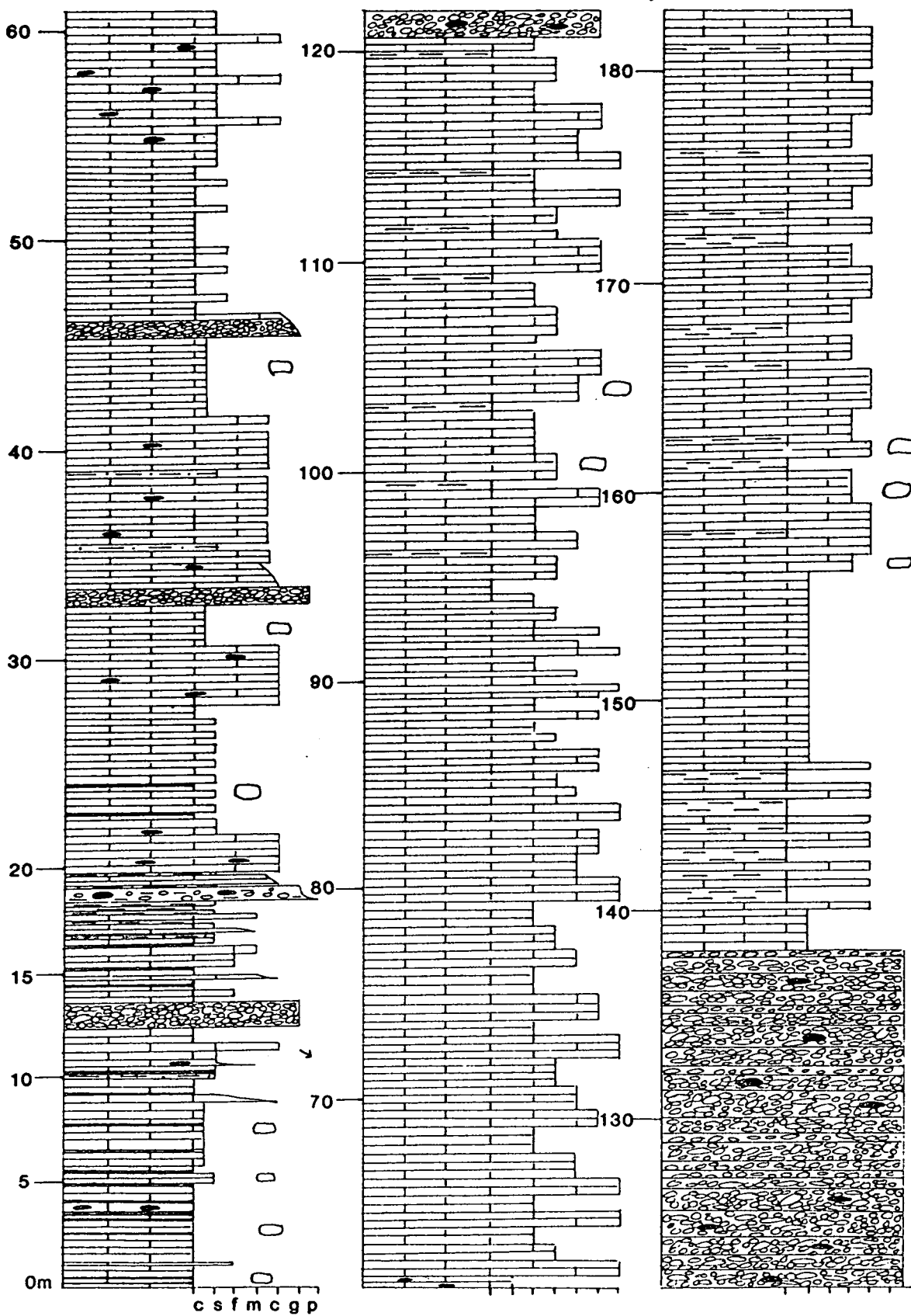
# LOG E10



# Log F1

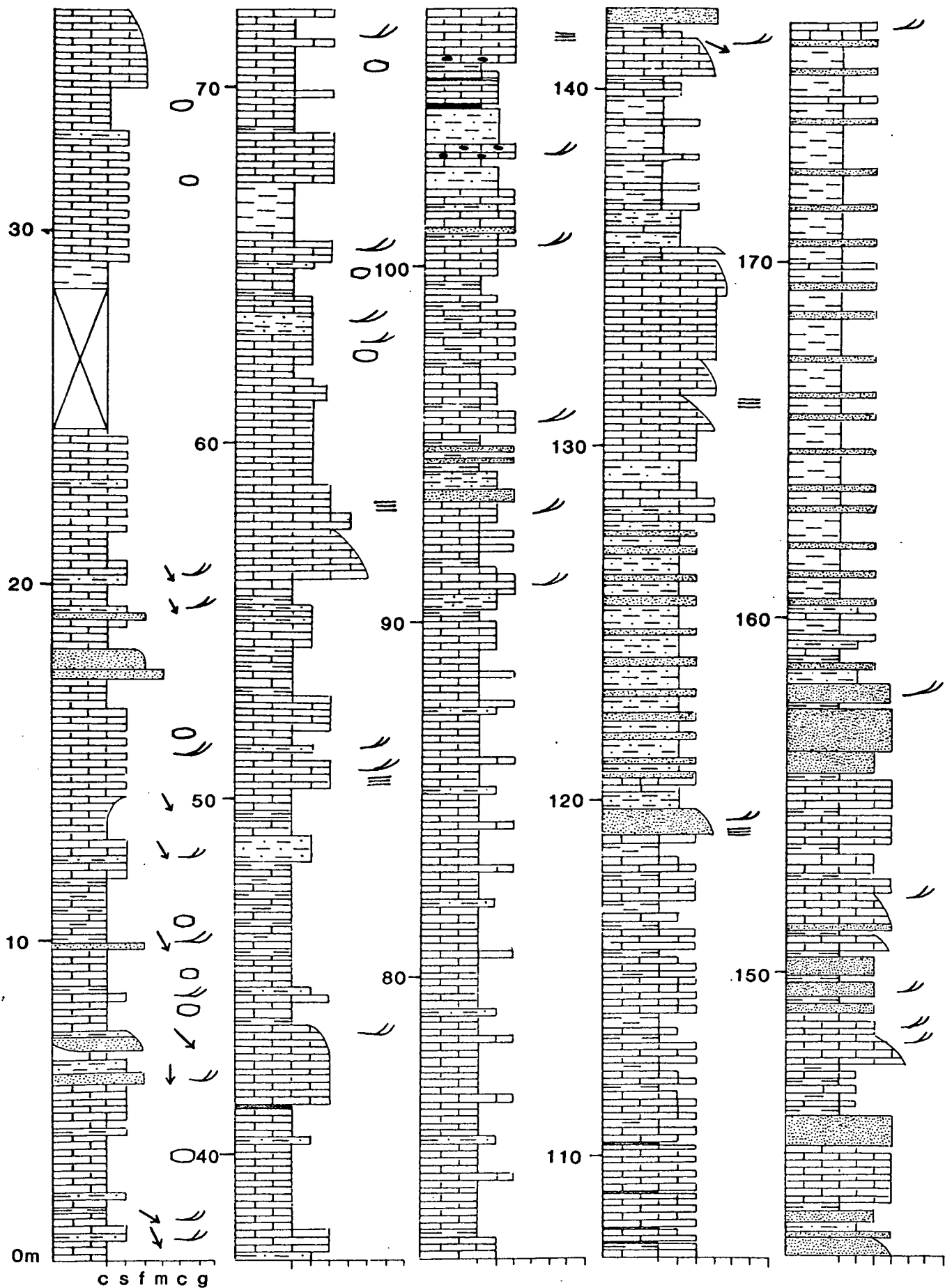


# LOG G1

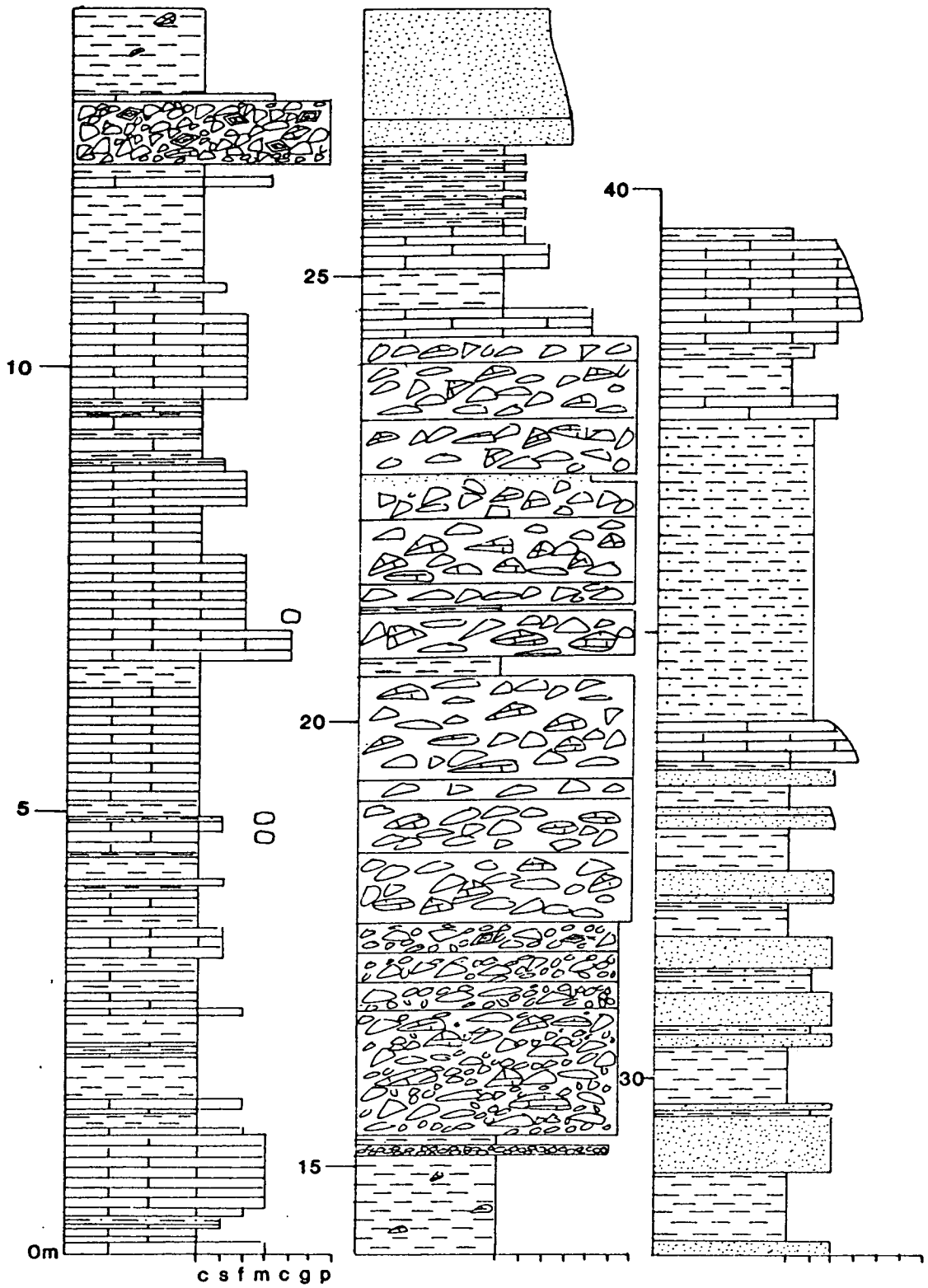




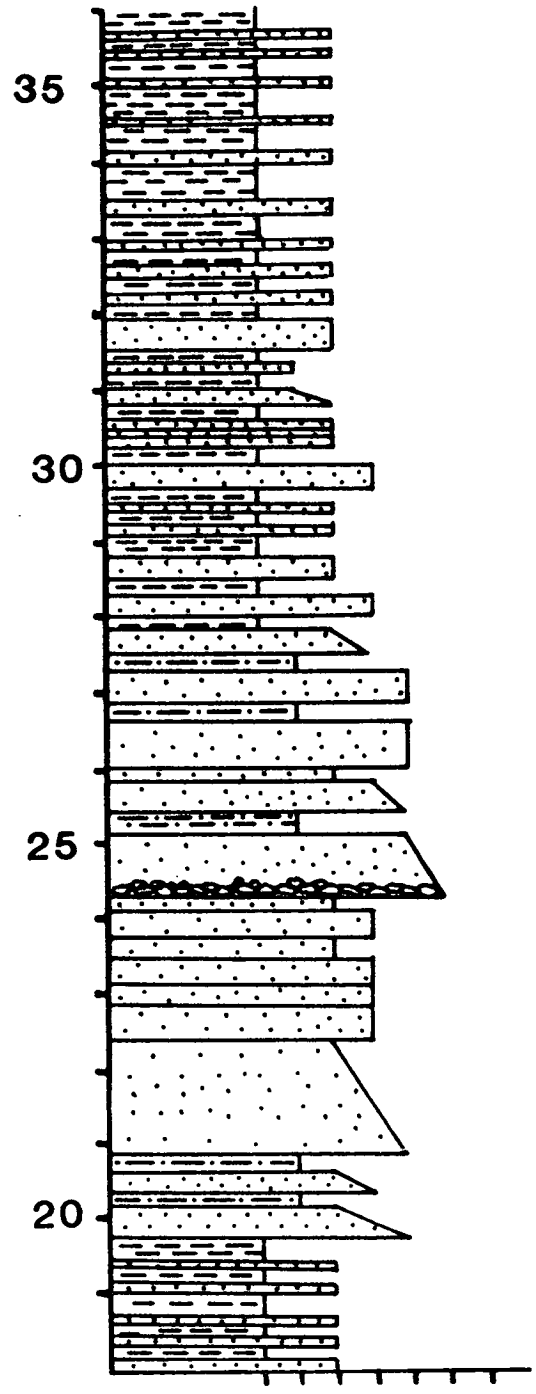
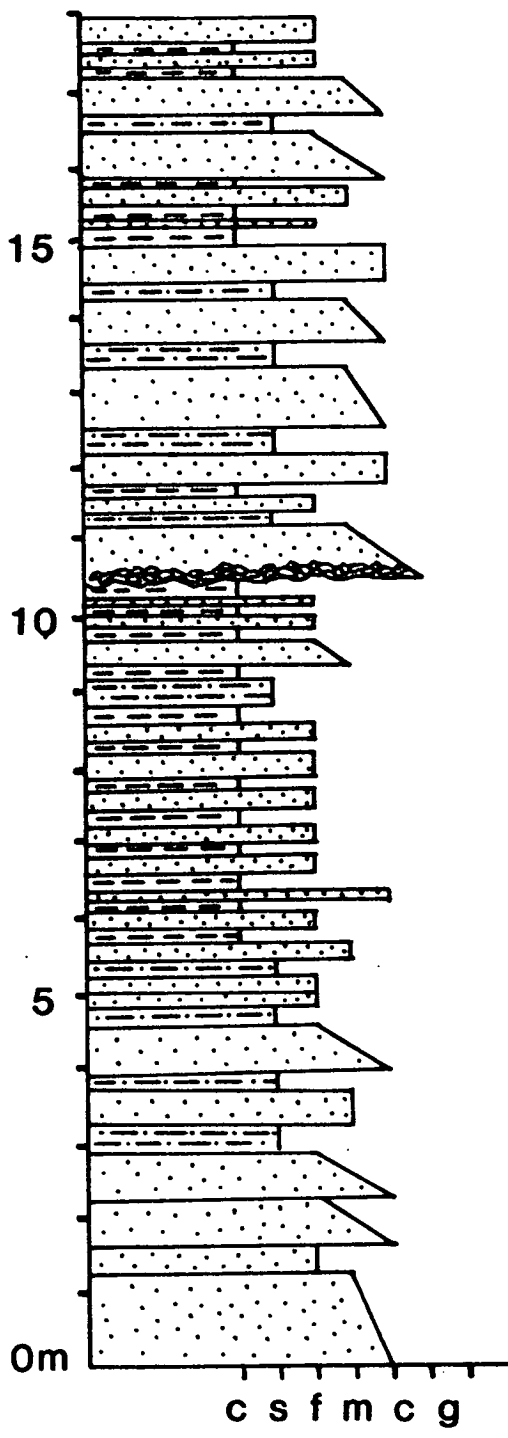
# Log H1



# LOG H2



# Log I1



## APPENDIX 2

### ANALYTICAL TECHNIQUES

#### X-RAY FLUORESCENCE

Selected igneous and sedimentary samples were subjected to whole rock geochemical analysis at Edinburgh University Geology department by X-ray fluorescence. Samples were prepared according to the techniques described by Fitton & Dunlop (1985). This involves the crushing of fresh rock chips to obtain a uniform powder which is suitable for determining major element oxides and trace element content. For major element analysis a measured quantity of lithium flux (Johnson-Mathey Spectroflux) was added to the rock powder and the preparation was fused at 1100°C to obtain glass discs. Samples from the 1988 field season were analysed on a Phillips PW 1450/20 spectrometer, while those from 1989 and 1990 were analysed on a Phillips PW 1480. For trace element analysis, pressed powder pellets were manufactured and all samples were analysed on a Phillips PW 1450/20 machine.

Samples were calibrated using USGS and CRPG international standards, and interference and matrix corrections were applied. A representative sample was prepared and analysed six times to demonstrate the level of analytical consistency obtained by the above methods. The resultant range, mean and standard deviations are shown overleaf. In the tables of Appendix 3 & 5, LOI represents loss on ignition of volatiles, e.g. H<sub>2</sub>O and CO<sub>2</sub>. N/C means that there was no convergence of the spectral lines necessary for determining trace element concentration. Sample numbers in Appendix 5 with bars and underlined were not used in the multi-element discrimination diagrams of Chapter 8 because of alteration.

#### X-RAY DIFFRACTION

The clay-sized fraction of mudstones was separated, after ultrasonic disaggregation, with distilled water in a settling column as outlined in Tucker (1988). The sediment was then allowed to settle in a beaker onto a glass slide. The beaker was placed in an oven at 60°C until the specimen was dry. A departmental, fully automated, Phillips PW 1808 diffractometer with a Cu K-alpha source was used to measure intensity and 2 theta. The resultant traces were compared with mineral analyses contained in an extensive databank of standardised minerals and compounds. Where necessary, manual peak matching was possible and a hard-copy obtained.

#### ELECTRON MICROPROBE ANALYSIS

Two samples (PD/89/323 & 504) were subjected to electron microprobe analyses using the Edinburgh University Geology department Cameca Camebox Microbeam, fitted with four wavelength dispersive crystal spectrometers. The samples were prepared as double polished, uncovered thin-sections and then carbon coated under vacuum. Silicate, oxide and pure metal standards were used for calibration. Adsorption fluorescence effects were corrected using Cameca PAP software. The operating conditions were:-

Accelerating potential-20Kv,  
Beam current-20 n.a.,  
Count times of 30 secs. for peaks and 15 secs for background,  
Focused beam diameter-1µm

	Maximum	Minimum	Mean	Standard Deviation
<b>SiO<sub>2</sub></b>	49.93	49.4	49.74	0.21
<b>Al<sub>2</sub>O<sub>3</sub></b>	16.47	16.16	16.29	0.12
<b>Fe<sub>2</sub>O<sub>3</sub></b>	10.69	10.48	10.6	0.08
<b>MgO</b>	5.2	5.11	5.16	0.04
<b>CaO</b>	6.73	6.5	6.64	0.1
<b>Na<sub>2</sub>O</b>	5.6	5.48	5.55	0.05
<b>K<sub>2</sub>O</b>	0.19	0.19	0.19	0
<b>TiO<sub>2</sub></b>	2.17	2.09	2.13	0.03
<b>MnO</b>	0.19	0.18	0.18	0
<b>P<sub>2</sub>O<sub>5</sub></b>	0.59	0.57	0.58	0.01
<b>LOI</b>	3.07	2.87	2.95	0.07
<b>Total</b>	100.3	99.83	100.02	0.19
<b>Ni</b>	23	21	21.83	0.75
<b>Cr</b>	71	67	69.5	1.38
<b>V</b>	213	204	209.19	3.19
<b>Sc</b>	26	24	24.67	1.03
<b>Cu</b>	53	50	51.17	1.47
<b>Zn</b>	89	87	87.83	0.75
<b>Sr</b>	313	310	312.17	1.17
<b>Rb</b>	4	3	3.3	0.52
<b>Zr</b>	323	312	319.5	4.04
<b>Nb</b>	14	13	13.83	0.41
<b>Ba</b>	37	28	30.5	3.27
<b>Pb</b>	4	1	2.33	1.03
<b>Th</b>	1	0	0.67	0.52
<b>La</b>	23	16	19.33	2.94
<b>Ce</b>	66	44	56.33	7.47
<b>Nd</b>	34	23	28.33	4.23
<b>Y</b>	44	43	43.5	0.55

The above table represents the typical accuracy (i.e. a measure of the absolute quality of the analyses) of the geochemical results achieved by XRF.

### SCANNING ELECTRON MICROSCOPY

Selected rock samples and extracted radiolarian microfossils were analysed on an Edinburgh University, Botany department, Cambridge S90B scanning electron microscope. Samples were fixed to aluminium stubs with adhesive and then gold coated in a sputter machine. The samples were bombarded with electrons under a vacuum in the SEM and viewed with a video monitor.

### CATHODOLUMINESCENCE MICROSCOPY

Double-polished thin-sections of coarse grained rock specimens were analysed with a Nuclide Corporation ELM-2B luminoscope. The specimens were placed under partial vacuum (0.55-0.95 millitorr) in a chamber. A collimated electron beam (0.7-0.9 mA current accelerated to 13-14 Kv) from a cold cathode (tungsten/steel) source bombarded the sample. Certain luminescent centres related to crystal lattice irregularities are excited by the electron beam and electrons in an excited atom are raised to a higher energy level. On returning to the original energy level, energy can be released in the form of visible electromagnetic radiation. The principles and technique is described by Miller (1988).

### RADIOLARIAN EXTRACTION

Chert samples were analysed in the field for the probable presence of radiolarian microfossils. In the laboratory, the samples were broken into rock chips to maximise surface area. Manganiferous cherts were pre-treated by boiling in concentrated HCl for two hours. All samples were then transferred to plastic beakers and left for two hours in 10% HF. The chips and residue were passed through sieves of 300 and 70 mesh while being copiously sprayed with water. The microfossils are just visible with the naked eye and were collected with a few drops of water along the edge of the sieve. The water and specimens were transferred into small containers by pipette. The rock chips were returned to the plastic beakers with a 5% HF solution for six hours, then again sieved. The samples were once again returned to the beakers, this time with a 2% HF solution, however, it was found that the greatest yield of radiolarians was extracted on the first and second sieving.

**APPENDIX 3**

**RESULTS OF GEOCHEMICAL ANALYSIS, BY XRF, ON  
SEDIMENTARY SAMPLES OF THE PINDOS GROUP**

# Shale

Sample No.	311	312	313	314	536	537	538	539	540	541	542	543	544
SiO <sub>2</sub>	63.64	72.2	67.25	76.19	58.2	63.26	67.33	78.84	76.97	71.36	75.89	81.83	67.81
Al <sub>2</sub> O <sub>3</sub>	15.02	12.52	13.06	9.74	15.2	16.39	11.47	8.22	8.71	11.51	9.16	6.73	6.53
Fe <sub>2</sub> O <sub>3</sub>	7.54	3.27	7.54	4.38	7.53	3.57	5.93	3.74	3.25	5.55	4.85	3.65	4.09
MgO	2.97	2.72	3.07	1.61	2.69	2.95	2.49	1.72	1.75	2.7	2.13	1.64	1.7
CaO	0.54	0.52	0.56	0.37	2.65	1.48	2.29	0.47	0.53	0.71	0.48	0.55	8.35
Na <sub>2</sub> O	0.47	0.18	0.22	0.13	0.24	0.31	0.13	0.13	0.04	0	0.16	0.04	0
K <sub>2</sub> O	4.787	3.496	3.859	2.958	6.188	6.708	4.056	2.597	2.636	3.514	2.548	1.997	2.035
TiO <sub>2</sub>	0.795	0.606	0.653	0.609	0.789	0.848	0.524	0.358	0.35	0.546	0.418	0.307	0.287
MnO	0.093	0.031	0.051	0.005	0.13	0.112	0.094	0.04	0.117	0.028	0.038	0.021	0.094
P <sub>2</sub> O <sub>5</sub>	0.108	0.11	0.136	0.057	0.09	0.115	0.095	0.086	0.09	0.176	0.063	0.111	0.228
LOI	4.16	3.91	4.19	3.96	5.53	4.79	5.1	3.03	3.29	4.14	3.34	2.68	8.63
Total	100.1	99.57	100.6	100	99.25	100.5	99.52	99.24	97.73	100.2	99.07	99.56	99.7
V	78	252	181	94	112	166	71	53	81	83	70	72	59
Ba	270	190	211	155	282	274	178	123	123	108	149	117	142
Sc	20	14	17	11	18	23	16	11	14	27	13	11	14
La	38	34	42	22	43	41	30	23	21	40	19	18	32
Nd	31	35	36	16	33	36	26	24	19	40	16	22	35
Ce	103	94	95	46	108	118	101	79	76	52	39	36	49
Cr	76	64	85	57	80	85	56	42	41	127	103	88	109
Ni	53	92	107	101	74	86	63	56	62	104	108	102	130
Cu	21	70	33	55	29	86	31	67	90	110	67	47	62
Zn	84	94	83	151	106	178	86	64	65	99	75	58	76
Pb	11	11	10	44	31	121	9	9	9	21	9	13	10
Th	5	5	3	3	6	9	3	1	2	0	1	0	0
Rb	136	119	127	67	145	154	118	85	85	108	94	71	64
Sr	79	65	66	49	67	72	51	44	37	28	34	32	60
Y	28	25	34	15	28	30	24	27	21	33	17	22	40
Zr	152	113	115	132	151	162	101	65	66	77	73	55	53
Nb	16	14	13	15	16	18	11	7	8	6	7	6	5
Fe <sub>2</sub> O <sub>3</sub> /Al <sub>2</sub> O <sub>3</sub>	0.502	0.261	0.577	0.45	0.495	0.218	0.517	0.455	0.373	0.482	0.529	0.542	0.626
SiO <sub>2</sub> /CaO	117.9	138.9	120.1	205.9	21.96	42.74	29.4	167.7	145.2	100.5	158.1	148.8	8.121



# Shale

Sample No.	563	564	565	566	567	568
SiO <sub>2</sub>	69.81	76.01	65.38	66.2	65.01	71.92
Al <sub>2</sub> O <sub>3</sub>	12.22	10.23	13.82	10.95	12.75	11.66
Fe <sub>2</sub> O <sub>3</sub>	5.02	4.89	7.29	9.13	8.89	4.4
MgO	2.84	1.93	3.44	4.19	3.76	2.86
CaO	0.95	0.43	0.54	1.74	0.87	0.64
Na <sub>2</sub> O	0	0.43	0.44	0.61	0.58	0.6
K <sub>2</sub> O	3.864	2.49	3.616	2.633	3.062	2.91
TiO <sub>2</sub>	0.457	0.463	0.652	0.514	0.602	0.635
MnO	0.043	0.065	0.132	0.364	0.126	0.153
P <sub>2</sub> O <sub>5</sub>	0.198	0.094	0.17	0.133	0.226	0.094
LOI	2.268	3.42	4.2	4.73	4.23	3.81
Total	98.05	100.5	99.68	101.2	100.1	99.68
V	104	78	71	71	79	97
Ba	118	172	265	173	205	190
Sc	25	14	24	25	22	15
La	35	22	39	28	36	35
Nd	36	22	29	29	30	30
Ce	67	55	62	69	73	70
Cr	44	112	222	563	594	190
Ni	71	105	250	944	670	349
Cu	110	69	118	128	147	328
Zn	99	75	113	124	122	127
Pb	8	12	15	21	26	12
Th	3	1	3	2	1	3
Rb	130	91	128	93	113	97
Sr	41	40	50	56	59	53
Y	50	21	35	31	43	28
Zr	90	80	113	85	103	129
Nb	9	8	12	8	10	13
Fe <sub>2</sub> O <sub>3</sub> /Al <sub>2</sub> O <sub>3</sub>	0.411	0.478	0.528	0.834	0.697	0.377
SiO <sub>2</sub> /CaO	73.48	176.8	121.1	38.05	74.72	112.4

# Mn Chert

Sample No	63	64	65	66	67	68	69	80	81	90	94	95	96	124	158
SiO2	75.034	83.144	52.337	75.948	77.064	75.553	92.242	63.3	87.69	46.43	81.98	52.996	90.53	83.65	86.79
Al2O3	0.584	0.467	1.045	1.29	1.058	1.081	0.391	1.05	2.18	0.6	0.32	0.7	1.16	0.55	3.53
Fe2O3	0.087	0.0001	0.384	0.406	0.285	0.263	0	0.07	0.82	0.33	0	0.25	0.51	1.59	1.4
MgO	0.165	0.13	0.39	0.5	0.116	0.4	0.02	1.267	0.423	0.56	0.552	1.073	0.8	0.29	0.66
CaO	0.5	0.297	0.846	0.463	0.509	0.486	0.186	0.323	0.309	1.2	0.55	1.07	0.8	4.64	0.21
Na2O	0	0.02	0	0.095	0.12	0.027	0.182	0	0.188	0.01	0	0.01	0.11	0.14	0.41
K2O	0.047	0.07	0.11	0.11	0.21	0.107	0.022	0.054	0.5	0.41	0.1	0.29	0.26	0.13	0.98
TiO2	0.03	0.02	0.05	0.05	0.05	0.04	0.02	0.03	0.097	0.05	0.02	0.04	0.05	0.02	0.167
MnO	19.328	12.405	38.095	17.429	16.181	18.304	4.429	25.66	3.93	29.955	11.639	25.712	2.913	2.71	2.41
P2O5	0.025	0.024	0.032	0.042	0.023	0.035	0.023	0.02	0.03	0.04	0.02	0.03	0.03	0.26	0.049
LOI	4.227	3.413	6.813	3.668	4.378	3.703	2.519	8.15	3.83	20.41	5.3	18.23	3.21	6.02	1.91
Total	100	100	99.99	100	100	99.99	100	100	100	100	100	100	100	100	98.51
V	53	39	117	50	50	52	11	359	52	467	268	425	99	23	47.9
Ba	705	521	1583	636	1058	379	273	7143	1273	20707	6138	21055	813	844	784
Sc	0	0	0	0	0	0	0	0	0	0	0	0	0	1	5.3
La	0	0	0	0	0	0	0	0	0	0	0	0	0	18	8.3
Nd	0	2	0	1	0	0	0	5	3	37	7	26	9	19	4.7
Ce	3	9	9	18	12	15	0	16	9	58	14	13	35	81	38
Cr	4	10	29	7	12	3	0	20	6	14	6	10	9	2	18
Ni	76	35	130	81	71	55	15	270	65	113	73	150	110	45	57
Cu	95	47	151	115	33	99	16	323	43	444	26	59	20	35	54
Zn	23	10	47	42	29	24	5	87	17	53	21	45	30	13	30
Pb	6	6	20	15	5	13	3	0	2	197	0	0	86	31	15
Th	0	0	0	0	0	0	0	0	0	0	0	0	0	0	2
Rb	0	0	5	4	3	4	0	3	16	0	0	0	10	2	33
Sr	6	50	66	52	59	47	21	1009	172	30705	11745	24211	2897	73	103
Y	57	4	9	9	7	9	3	13	5	25	11	26	11	23	7
Zr	5	3	12	12	7	10	2	17	18	0	58	158	24	8	33
Nb	1	2	3	2	2	2	1	2	3	1	0	1	3	2	5
Fe2O3/Al2O3	0.14897	0.00021	0.36746	0.31473	0.26938	0.24329	0	0.06667	0.37615	0.55	0	0.35714	0.43966	2.8909	0.3966
Fe2O3/MnO	0.0045	8.06E-06	0.01008	0.0233	0.01761	0.01437	0	0.00273	0.20865	0.01102	0	0.00972	0.17508	0.58672	0.58091

# Mn Chert

Sample No	174	345	347	354	439	440	452	486	504	510	600	601	614	702
SiO2	94.13	70.53	76.98	89.67	92.39	88.87	74.61	22.56	88.53	72.67	84.71	29.28	46.67	94.27
Al2O3	0.61	1.21	1.48	1.06	0.81	0.77	2.05	0.61	2.43	0.3	2.71	0.58	0.82	0.74
Fe2O3	1.29	0.54	0.71	0.64	0.32	0.33	4.91	0.34	0.8	0.24	1.12	0.38	0.36	1.35
MgO	0.38	0.15	0.12	0.1	0.06	0.12	0.78	0.26	0.6	0	0.56	0.36	0.44	0.18
CaO	0.13	0.09	0.12	0.07	0.08	0.08	0.21	1.03	0.33	0.21	0.28	0.7	0.54	0.18
Na2O	0.22	0	0	0.07	0	0.01	0.04	0.06	0.33	0	0.35	0.18	0	0.05
K2O	0.079	0.25	0.28	0.25	0.12	0.118	0.51	0.98	0.648	0.03	0.7	1.4	0.148	0.19
TiO2	0.036	0.05	0.06	0.05	0.03	0.043	0.1	0.04	0.107	0.02	0.13	0.058	0.07	0.048
MnO	1.058	20.77	15.36	5.31	6.98	6.36	10	69.54	3.32	21.18	5.907	59.24	48.42	1.56
P2O5	0.021	0.05	0.04	0.02	0.03	0.035	0.04	0.13	0.03	0.01	0.06	0.084	0.05	0.07
LOI	1.1	4.5	3.11	1.87	1.68	2.16	3.32	7.32	1.96	3.99	2.43	6.96	1.64	1.29
Total	99.06	98.13	98.45	99.12	102.45	98.89	96.75	102.88	99.08	98.59	98.96	99.22	99.14	99.93
V	40	102	27	62	53	43	50	373	56	177	79	N/C	63	33
Ba	417	148	1238	460	2905	2318	7499	11996	348	1501	227	N/C	285	150
Sc	0	0	1	1	0	1	0	0	4	0	6	N/C	0	1
La	0	2	4	2	1	5	21	0	0	0	11	N/C	0	6
Nd	0	0	13	9	7	0	32	11	1	0	1	N/C	0	7
Ce	3	2	24	35	7	0	54	57	19	0	14	N/C	4	12
Cr	117	15	14	21	8	6	14	17	15	15	22	N/C	9	16
Ni	177	139	57	42	54	53	88	138	82	223	43	N/C	38	72
Cu	11	330	287	110	135	137	136	2079	8	26	153	N/C	92	86
Zn	19	76	55	26	30	28	35	80	19	54	34	N/C	25	25
Pb	3	16	2	39	0	5	35	0	4	0	5	21	6	23
Th	0	0	0	0	0	0	0	0	2	0	3	0	1	2
Rb	3	8	12	7	3	4	11	13	23	1	21	7	5	6
Sr	47	130	84	65	77	71	309	346	1956	364	293	1249	145	47
Y	4	17	19	10	8	8	15	27	3	4	12	33	6	10
Zr	7	10	14	11	6	9	23	23	52	3	28	24	10	12
Nb	3	3	2	2	2	2	4	4	4	1	4	0	2	2
Fe2O3/Al2O3	2.1148	0.44628	0.47973	0.60377	0.39506	0.42857	2.3951	0.55738	0.32922	0.8	0.41328	0.65517	0.43902	1.8243
Fe2O3/MnO	1.2193	0.026	0.04622	0.12053	0.04585	0.05189	0.491	0.00489	0.24096	0.01133	0.18961	0.00641	0.00743	0.86538

N/C = No Convergence

## APPENDIX 4

### LOCATIONS OF SEDIMENTARY SAMPLES ANALYSED BY XRF

#### SHALE

311 Kominara	542 Dendra
312 Kominara	543 Dendra
313 Kominara	544 Dendra
314 Kominara	563 Drimos
536 Dendra	564 Drimos
537 Dendra	565 Drimos
538 Dendra	566 Drimos
539 Dendra	567 Drimos
540 Dendra	568 Drimos
541 Dendra	

#### MN CHERT

63 Drimos	94 Aroania	440 Kontovazani
64 Drimos	95 Aroania	452 Platanitza
65 Drimos	96 Aroania	486 Drakovouni
66 Drimos	124 Lambia	504 Aroania
67 Drimos	158 Aroania	510 Aroania
68 Drimos	174 Agridi	600 Likouria
69 Drimos	345 Lesteena	601 Likouria
80 Aroania	347 Lesteena	614 Elatophyton
81 Aroania	354 Figalia	702 Alepohorio
90 Aroania	439 Kontovazani	

**APPENDIX 5**

**RESULTS OF GEOCHEMICAL ANALYSIS, BY XRF, ON  
IGNEOUS SAMPLES OF THE TECTONO-SEDIMENTARY  
MELANGE, GAVROVO-TRIPOLITZA ZONE AND  
ASSOCIATED WITH UPPER JURASSIC RADIOLARIAN  
CHERT.**

Drakovouni

IGNEOUS

	<u>1</u>	<u>2</u>	<u>3</u>	6	<u>8</u>	9	<u>11</u>	274	276	453	464	469	470
SiO2	56.71	68.81	58.42	53.67	41.35	46.13	37.75	61.82	51.36	49.07	49.07	47.71	68.98
Al2O3	15.18	8.53	13.19	17.51	13.36	16.88	13.5	15.66	18.3	17.12	17.95	15.44	8.87
Fe2O3	6.5	3.63	4.73	7.9	12.11	13.82	11.56	7.02	8.09	10.09	8.13	8.87	6.06
MgO	0.78	1.87	0.33	2.33	1.27	2.67	1.95	3.39	8.5	5.74	5.85	2.58	2.22
CaO	6.24	6.64	8.7	7.03	12.44	5.43	8.46	1.21	2.17	8.45	7.8	8.46	4.7
Na2O	5.78	2.15	6.42	4.93	5.89	6.13	5.52	5.72	6.39	4.77	5.27	5.32	2.54
K2O	0.91	0.64	0.35	0.57	0.3	0.36	0.02	1.1	0.12	0.15	0.04	1.3	0.48
TiO2	0.82	0.49	1.04	1.33	1.1	1.34	1.04	0.72	1.37	2.01	1.6	1.21	0.24
Mno	0.09	0.07	0.03	0.17	0.1	0.07	0.08	0.11	0.15	0.2	0.13	0.11	0.06
P2O5	0.2	0.07	1.13	0.34	0.21	0.2	0.12	0.11	0.35	0.56	0.5	0.23	0.12
LOI	N/A	N/A	N/A	N/A	N/A	N/A	N/A	3.17	4.81	3.83	3.8	8.65	5.52
Total	93.22	92.89	94.33	95.77	88.14	93.03	80.5	100.04	101.6	99.99	100.13	99.88	99.78
Ni	6	95	6	25	47	46	25	9	114	38	72	91	7
Cr	2	290	21	75	20	11	8	6	157	107	131	101	0
V	110	63	94	392	354	420	459	94	152	248	179	195	11
Sc	27	9	14	47	38	51	47	27	24	38	30	45	18
Cu	0	5	0	2	5	4	0	13	34	38	4	10	0
Zn	65	46	9	159	188	277	187	88	64	79	23	157	107
Sr	76	142	106	125	119	66	102	87	324	166	108	117	57
Rb	26	22	9	16	7	9	0	30	0	1	0	29	13
Zr	108	133	139	103	66	72	60	102	183	237	210	84	70
Nb	4	7	4	2	2	2	2	4	9	10	13	3	3
Ba	73	125	82	72	20	29	41	372	53	83	38	56	63
Pb	5	20	5	7	11	10	5	2	1	0	0	4	1
Th	3	5	4	2	0	3	0	3	0	0	3	3	3
La	12	15	16	6	6	10	9	14	13	22	17	12	11
Ce	21	31	39	23	14	10	7	35	32	50	46	29	29
Nd	21	13	46	12	12	4	7	20	15	28	26	17	18
Y	49	15	66	28	31	24	24	24	23	35	35	32	39
	1	?	?	1	1	1	1	1	2	2	2	1	1

## Drakovouni

## IGNEOUS

	473	454	456	459	475	707
SiO2	48.54	50.13	49.56	48.75	49.82	56.68
Al2O3	15.16	16.02	17.79	16	16.24	13.25
Fe2O3	8.45	9.42	8.43	10.76	10.48	10.75
MgO	2.54	5.62	4.41	4.51	5.17	3.47
CaO	8.48	7.07	8.14	8.14	6.67	3.68
Na2O	5.54	5.5	5.47	5.12	5.55	5.37
K2O	1.17	0.192	0.076	0.099	0.193	0.05
TiO2	1.22	2.073 <sup>1.2</sup>	1.64 <sup>1.0</sup>	2.15 <sup>1.3</sup>	2.14 <sup>1.3</sup>	0.96
Mno	0.13	0.18	0.16	0.18	0.18	0.12
P2O5	0.2	0.64	0.45	0.7	0.58	0.11
LOI	8.55	3.24	3.51	3.23	2.98	4.94
Total	99.98	100.08	99.45	99.65	100.01	99.37
Ni	60	20	48	11	22	11
Cr	115	73	108	34	71	24
V	307	210	167	243	204	360
Sc	43	28	20	25	27	40
Cu	20	59	43	62	53	17
Zn	106	69	71	83	88	95
Sr	171	338	223	137	313	145
Rb	24	2	1	1	2	1
Zr	86	297	233	336	329	61
Nb	3	14	11	15	14	2
Ba	37	28	39	52	30	2
Pb	3	3	5	5	2	5
Th	2	3	2	4	2	2
La	10	9	13	16	17	8
Ce	26	51	28	54	57	15
Nd	15	36	21	31	34	10
Y	25	43	32	50	44	25

1

2

2

2

2

1

## Central Peloponnese

## IGNEOUS

	320	<u>322</u>	<u>331</u>	333	338	339	<u>340</u>	343	588	604	605	<u>606</u>	<u>607</u>
SiO2	53.54	34.93	52.04	52.84	54.24	60.51	72.46	62.75	46.64	44.16	48.7	45.45	45.34
Al2O3	20.27	13.47	16.85	16.45	18.27	14.93	11.48	13.27	14.81	15	18.1	15.57	14.94
Fe2O3	5.79	3.94	8.14	8.59	9.18	9.64	5.23	7.3	8.74	9.38	6.19	6.28	5.3
MgO	3.09	1.89	1.69	4.01	5.09	2.75	1.54	3.31	4.21	5.02	9.05	1.43	1.57
CaO	3.15	21.1	6.38	3.87	1.33	1.37	0.96	2.68	11.46	9.92	7.32	12.48	12.57
Na2O	4.5	2.26	7.27	7.34	7.24	7.01	4.9	4.45	4.81	4.44	3.06	5.49	5.63
K2O	3.87	3.24	0.02	0.55	0.04	0.05	0.12	1.03	0.945	1.65	0.63	1.43	1.32
TiO2	1.15	0.83	0.81	1.02	1.19	0.84	0.72	0.73	1.06	1.07	1.18	1.55	1.51
MnO	0.11	0.19	0.09	0.2	0.1	0.13	0.04	0.09	0.11	0.13	0.15	0.12	0.09
P2O5	0.59	0.26	0.32	0.24	0.18	0.32	0.18	0.09	0.178	0.42	0.18	0.51	0.52
LOI	4.54	18.21	6.34	4.92	4.02	2.59	2.12	3.86	7.45	9.39	4.9	10.32	10.51
Total	100.59	100.32	99.95	100.02	100.88	100.13	99.75	99.57	100.42	100.57	99.46	100.65	99.29
Ni	22	22	8	7	8	7	5	13	136	42	85	15	14
Cr	7	4	0	0	0	0	0	8	328	29	201	16	14
V	187	148	132	117	218	115	28	193	310	321	244	220	199
Sc	27	15	22	31	24	32	21	25	37	25	40	22	20
Cu	38	11	59	21	47	19	0	233	20	44	60	67	116
Zn	86	53	67	153	146	119	71	134	53	59	73	55	55
Sr	192	225	65	102	95	31	47	104	403	309	397	372	317
Rb	63	43	0	10	0	1	2	31	13	28	7	26	36
Zr	134	106	99	115	98	112	73	3	82	84	89	177	176
Nb	9	8	5	5	5	5	4	46	4	7	4	12	11
Ba	70	117	350	30	123	4	0	252	75	47	93	123	93
Pb	2	0	3	5	2	5	2	4	3	2	4	4	5
Th	3	0	3	2	4	4	3	6	1	2	3	2	4
La	20	15	5	11	5	12	8	40	3	4	5	6	15
Ce	39	38	12	25	15	23	16	92	28	22	12	39	41
Nd	27	25	13	16	9	13	13	47	19	13	16	24	25
Y	37	31	44	39	25	41	37	63	21	25	23	30	31



## Central Peloponnese

	611	<u>623</u>	700	711	713	<u>715</u>
SiO2	50.31	47.39	55.41	41.49	77.55	83.58
Al2O3	16.95	14.9	16.4	6.31	8.92	6.69
Fe2O3	10.04	5.36	5.97	13.77	6.79	4.91
MgO	3.51	1.48	2.06	4.82	2.46	1.8
CaO	6.16	11.57	5.59	13.55	0.15	0.1
Na2O	7.04	5.56	8.26	0.09	0.43	0.33
K2O	0.06	1.9	0.4	0.155	0.57	0.4
TiO2	1.52	0.78	1.04	0.28	0.47	0.51
Mno	0.1	0.12	0.18	2.19	0.03	0.03
P2O5	0.16	0.44	0.48	0.04	0.097	0.06
LOI	4.1	10.39	4.98	16.79	2.51	1.94
<b>Total</b>	<b>99.93</b>	<b>99.9</b>	<b>100.77</b>	<b>99.48</b>	<b>99.98</b>	<b>100.34</b>

## Eastern Peloponnese

	421	<u>422</u>	423	<u>425</u>	<u>427</u>
SiO2	45.56	50.11	52.28	65.94	65.15
Al2O3	14.8	16.9	15.4	16.19	16.66
Fe2O3	7.85	7.02	4.46	4.25	4.23
MgO	6.36	11.08	2.54	1.66	1.36
CaO	11.16	3.07	9.79	1.23	1.72
Na2O	4.34	5.05	4.08	8.15	8.33
K2O	0.16	0.01	2.69	0.18	0.21
TiO2	0.79	0.94	0.75	0.58	0.62
Mno	0.15	0.14	0.1	0.06	0.07
P2O5	0.16	0.17	0.3	0.19	0.21
LOI	9.3	5.96	7.46	1.27	1.38
<b>Total</b>	<b>100.62</b>	<b>100.46</b>	<b>99.85</b>	<b>99.71</b>	<b>99.94</b>

Ni	138	17	10	55	25	22	141	172	25	6	6
Cr	339	14	1	26	71	82	475	587	41	0	0
V	228	81	38	50	96	80	257	238	194	32	35
Sc	40	12	19	14	14	11	42	46	16	6	8
Cu	53	6	5	25	9	27	4	93	44	2	3
Zn	82	42	132	178	121	74	61	81	54	60	67
Sr	424	96	209	72	31	22	145	152	307	142	177
Rb	1	19	6	6	19	14	3	0	22	2	2
Zr	109	154	297	70	129	104	58	67	101	223	231
Nb	2	9	25	5	9	8	3	3	7	16	15
Ba	43	29	41	559	114	73	42	23	53	19	19
Pb	3	3	4	9	4	3	2	2	1	6	3
Th	1	4	4	6	6	5	1	3	2	9	8
La	4	20	28	23	25	14	8	6	16	36	34
Ce	8	32	67	48	44	24	15	20	40	85	87
Nd	5	24	36	24	20	13	9	8	24	38	36
Y	29	53	57	61	15	10	17	16	19	31	33

Southern Peloponnese

IGNEOUS

	355	356	360	369	386	387	389	390	399	400	401	405	408
SiO2	39.66	50.65	40.72	40.66	56.3	57.37	59.57	54.27	50.19	57.07	57.53	54.33	47.93
Al2O3	15.25	17.48	13.81	14.86	16.4	15.88	16.28	18.01	16.55	18.64	13.32	15.52	18.17
Fe2O3	8.48	5.42	8.04	8.17	6.92	5.6	4.53	4.33	7.33	7.28	9.56	11.37	12.77
MgO	6.06	8.38	3.13	7.25	3.45	3.12	3.39	3.2	3.04	2.13	4.46	4.77	4.72
CaO	12.24	7.96	15.68	14.25	8.51	8.25	8	9.44	8.41	3.16	4.85	4.22	6.16
Na2O	1.71	2.97	3.17	1.53	3.2	3.28	4.3	4.25	6.92	7.83	4.25	5.44	4.8
K2O	2.36	0.26	1.62	1.15	1.71	2.02	0.5	1.93	0.06	0.58	0.13	0.04	0.02
TiO2	0.99	1.21	1.26	0.96	0.79	0.76	0.71	0.82	0.69	0.76	0.71	1.06	1.14
Mno	0.11	0.12	0.11	0.06	0.14	0.12	0.09	0.11	0.23	0.19	0.17	0.2	0.18
P2O5	0.19	0.23	0.32	0.16	0.23	0.2	0.17	0.22	0.23	0.14	0.07	0.12	0.14
LOI	13.01	5.57	12.14	11.22	3.19	3.51	2.32	3.56	6.25	2.25	4.88	3.63	4.13
Total	100.06	100.24	100.01	100.27	100.83	100.12	99.85	100.14	99.9	100.03	99.94	100.71	100.16
Ni	116	83	31	223	24	24	37	21	10	10	16	16	16
Cr	226	149	66	454	51	60	82	58	7	7	14	2	7
V	274	288	251	180	188	168	167	169	172	175	267	457	367
Sc	41	46	41	45	29	29	28	31	37	37	37	42	43
Cu	14	85	43	12	14	15	34	14	18	28	90	43	93
Zn	59	67	51	109	56	49	52	66	107	119	79	91	104
Sr	217	357	283	255	300	300	343	328	156	269	45	51	46
Rb	22	0	29	18	43	54	3	11	1	9	4	0	0
Zr	86	122	123	87	110	105	122	130	73	86	44	73	88
Nb	3	6	6	5	6	6	6	7	4	4	3	3	4
Ba	123	99	147	56	312	258	210	196	15	73	17	24	17
Pb	0	0	1	0	3	3	4	4	5	4	3	5	4
Th	0	2	0	1	7	5	8	7	1	2	1	3	2
La	6	8	12	6	21	17	17	23	11	14	3	7	6
Ce	17	26	35	18	45	46	46	48	30	30	11	13	17
Nd	10	15	21	11	21	22	22	25	15	18	5	7	8
Y	19	21	27	18	27	24	21	27	55	47	18	21	28

## Southern Peloponnese

## IGNEOUS

	409	<u>410</u>	413	577	<u>770</u>	<u>771</u>
SiO <sub>2</sub>	57.36	61.31	48.24	45.14	36.06	39.69
Al <sub>2</sub> O <sub>3</sub>	16.25	15.58	17.37	14.98	11.65	11.24
Fe <sub>2</sub> O <sub>3</sub>	8.17	7.2	12.2	8.35	7.52	8.05
MgO	2.08	0.8	4.74	6.93	1.42	1.53
CaO	7.34	5.83	6.43	12.04	20.07	18.73
Na <sub>2</sub> O	4.71	5.29	5.07	3.34	3.64	2.58
K <sub>2</sub> O	0.02	0.06	0.21	0.59	1.34	1.71
TiO <sub>2</sub>	0.94	0.87	1.17	1.6	0.87	0.904
MnO	0.1	0.11	0.13	0.17	0.12	0.117
P <sub>2</sub> O <sub>5</sub>	0.11	0.09	0.55	0.23	0.252	0.181
LOI	3.61	2.56	3.98	7	16.54	14.97
Total	100.7	99.7	100.09	100.38	99.48	99.7
Ni	12	8	15	96	184	195
Cr	4	4	3	256	581	529
V	358	343	524	330	109	103
Sc	40	34	52	43	27	29
Cu	83	18	122	49	18	24
Zn	111	81	157	74	84	161
Sr	49	59	118	215	218	248
Rb	0	0	4	3	31	42
Zr	71	79	84	122	71	74
Nb	4	4	4	8	3	4
Ba	31	38	51	40	51	68
Pb	6	4	5	2	3	2
Th	2	2	2	3	2	1
La	4	5	5	7	15	11
Ce	21	15	27	9	5	6
Nd	12	12	15	10	10	13
Y	26	37	43	30	19	18

Frontal Imbricates

IGNEOUS

	527	<u>528</u>	533	<u>679</u>	<u>723</u>	<u>733</u>	739	<u>760</u>	<u>761</u>	<u>764</u>	<u>765</u>
SiO2	33.89	47.09	50.66	27.34	72.23	63.4	48.08	66.93	76.65	73.44	74.64
Al2O3	13.06	15.93	15.55	7.32	9.61	11.98	14.49	11.29	10.12	12.51	2.81
Fe2O3	6.23	4.98	8.27	3.04	3.01	5.8	7.52	5.58	3.4	4.29	0.24
MgO	4.14	1.77	5.36	0.54	0.59	1.52	2.44	1.72	0.99	1	0.16
CaO	20.91	12.42	10.58	29.82	5.07	5.79	8.77	4.58	2.31	0.35	7.72
Na2O	2.74	5.17	3.21	4.1	4.51	5.38	4.03	3.86	3.71	5.9	0.085
K2O	0.71	1.82	0.87	0.03	0.323	0.405	3.75	1.017	0.5	0.87	0.37
TiO2	0.74	0.94	0.89	0.3	0.27	0.424	0.66	0.307	0.29	0.36	0.01
Mno	0.21	0.27	0.12	0.16	0.056	0.117	0.01	0.092	0.012	0.01	0.11
P2O5	0.91	0.35	0.22	1.21	0.158	0.132	0.21	0.103	0.086	0.105	0.11
LOI	16.34	8.33	4.59	23.72	4.76	5.42	9.22	4.52	1.99	1.44	0.47
Total	99.87	99.07	100.32	97.58	100.59	100.36	100.17	99.99	100.05	100.28	100.03
Ni	53	25	172	5	4	33	56	17	5	3	4
Cr	80	34	296	1	-1	6	360	3	-1	3	0
V	164	321	183	33	4	64	80	17	3	2	1
Sc	25	25	30	9	12	11	27	12	10	22	28
Cu	13	10	10	9	0	7	47	9	6	4	8
Zn	145	66	56	18	72	79	138	176	138	95	102
Sr	250	362	283	113	149	175	98	109	171	66	47
Rb	10	15	16	0	10	7	72	22	8	20	2
Zr	9	190	126	50	79	109	79	73	83	98	101
Nb	4	5	4	2	3	4	4	3	4	4	4
Ba	207	2710	142	1	284	258	40	121	1497	125	64
Pb	2	1	1	4	2	7	7	10	4	4	8
Th	0	3	3	1	3	2	4	4	3	4	3
La	13	19	15	14	15	11	21	39	9	5	17
Ce	40	53	35	33	30	21	21	81	25	18	27
Nd	27	30	18	27	18	19	12	57	17	15	14
Y	48	36	29	72	55	32	21	40	37	32	30

## Median Imbricates

## IGNEOUS

	12	17	<u>45</u>	<u>46</u>	<u>47</u>	<u>142</u>	<u>497</u>	<u>513</u>	<u>514</u>
SiO2	53.46	51.41	64.89	64.19	59.79	74.81	36.76	50.31	58.84
Al2O3	17.21	19.16	13.51	15.6	15.56	13	10.28	12.72	15.43
Fe2O3	8.04	9.73	2.88	5.35	3.99	2.21	5.29	10.81	5.46
MgO	2.4	4.41	0.18	0.72	0.6	0.54	0.77	1.86	1.75
CaO	7.31	2.25	0.3	2.69	6.6	1.02	22.04	7.64	5.54
Na2O	4.84	6.35	7.89	7.18	7.13	5.94	4.52	5.79	6.06
K2O	0.92	0.54	0.04	0.12	0.12	1.14	0.98	0.22	1.48
TiO2	1.3	1.17	0.48	0.58	0.58	0.14	0.6	2.64	0.43
Mno	0.31	0.17	0.03	0.05	0.15	0.02	0.11	1.17	0.08
P2O5	0.3	0.17	0.15	0.16	0.15	0.03	0.26	0.68	0.19
LOI	N/A	N/A	N/A	N/A	N/A	N/A	18.4	6.52	5.42
<b>Total</b>	<b>96.09</b>	<b>95.36</b>	<b>90.35</b>	<b>96.64</b>	<b>94.67</b>	<b>98.85</b>	<b>100.01</b>	<b>100.36</b>	<b>100.67</b>
Ni	26	15	6	10	11	6	45	88	58
Cr	14	5	0	1	0	0	256	47	35
V	170	130	9	9	5	18	62	171	75
Sc	26	22	12	19	21	4	16	24	11
Cu	9	8	0	0	0	0	24	62	26
Zn	334	132	93	142	145	28	54	139	98
Sr	337	342	116	195	592	83	165	207	199
Rb	22	12	0	0	0	10	17	4	33
Zr	161	170	158	209	245	198	44	328	126
Nb	3	3	5	5	5	4	3	14	7
Ba	209	153	789	135	1679	263	39	267	96
Pb	6	10	6	6	6	7	0	0	0
Th	2	2	3	3	0	11	0	0	0
La	19	21	20	14	14	35	5	16	11
Ce	46	53	31	38	36	72	11	51	28
Nd	28	32	27	30	29	29	12	27	14
Y	43	49	51	54	61	33	25	50	18

## GTZ

## IGNEOUS

	323	324	325	717	718A	718B	718C	719	721
SiO2	55.06	44.89	50.32	52.17	48.14	52.62	78.42	55.17	53.71
Al2O3	15.84	20.4	18.02	17.31	19.28	16.83	8.16	16.6	16.88
Fe2O3	8.96	9.72	9.73	8.93	8.93	8.56	7.13	8.49	10.93
MgO	5.39	5.5	5.57	4.64	4.63	3.26	2.06	3.73	5.15
CaO	7.69	11.13	9.11	10.07	10.91	12.67	0.2	8.17	6.51
Na2O	2.14	2.43	2.21	1.91	2.22	0.1	0.33	2.9	0.34
K2O	0.31	0.15	0.18	0.15	0.447	0.46	0.72	0.21	2.417
TiO2	0.56 <sup>.34</sup>	0.57 <sup>.34</sup>	0.62 <sup>.37</sup>	0.55 <sup>.34</sup>	0.655 <sup>.39</sup>	0.63 <sup>.38</sup>	0.48 <sup>.29</sup>	0.72 <sup>.43</sup>	0.837 <sup>.5</sup>
MnO	0.15	0.2	0.18	0.15	0.16	0.17	0.04	0.15	0.168
P2O5	0.05	0.08	0.05	0.08	0.08	0.06	0.1	0.07	0.09
LOI	3.93	5.3	4.74	4.35	4.61	4.63	2.2	3.78	3.9
Total	100.09	100.37	100.72	100.33	100.06	100	99.84	100	100.92
Ni	24	25	22	15	17	12	41	14	40
Cr	61	61	53	56	73	39	46	57	193
V	220	305	251	214	272	206	70	207	229
Sc	39	36	38	31	34	24	8	28	34
Cu	20	0	11	16	66	22	70	26	40
Zn	88	98	94	90	90	90	119	86	109
Sr	61	43	36	60	88	17	26	40	554
Rb	9	5	6	5	14	14	27	6	84
Zr	50	46	55	51	58	65	166	70	108
Nb	4	3	4	4	4	5	11	5	8
Ba	53	5	34	31	61	60	201	35	475
Pb	1	3	1	4	4	3	5	8	11
Th	2	2	3	3	2	3	7	3	5
La	6	3	4	8	9	9	22	-4	11
Ce	8	11	5	16	10	9	35	6	27
Nd	4	4	3	7	2	6	21	8	14
Y	16	18	18	18	21	24	20	27	30

## Jurassic Chert Association

## IGNEOUS

	31	305	305B	307	310	434	435	508	509
SiO2	59.82	46.03	46.17	46.46	46.14	54.66	53.76	43.69	33.73
Al2O3	10.34	17.42	17.52	16.89	16.69	17.66	17.87	14.5	10.46
Fe2O3	18.52	8.44	8.33	6.82	7.85	5.58	5.72	7.08	5.25
MgO	3.3	3	3.06	5.64	5.23	1.25	1.46	3.62	3.76
CaO	1.08	7.66	7.89	8.78	8.91	6.16	6.24	12.55	21.97
Na2O	0.97	0.35	0.28	1.78	2.05	5.97	5.56	3.65	2.65
K2O	1.81	6.95	6.87	3.88	3.4	1.94	2.42	2.3	1.88
TiO2	0.43	0.97	0.98	0.94	1.01	0.74	0.75	0.76	0.54
Mno	0.54	0.12	0.12	0.11	0.12	0.22	0.22	0.11	0.13
P2O5	0.11	0.35	0.33	0.21	0.23	0.33	0.33	0.41	0.25
LOI	N/A	9.46	9.73	8.99	8.43	5.06	5.66	10.96	19.18
<b>Total</b>	<b>96.93</b>	<b>100.74</b>	<b>101.28</b>	<b>100.5</b>	<b>100.05</b>	<b>99.56</b>	<b>99.99</b>	<b>99.63</b>	<b>99.8</b>
Ni	124	97	99	119	98	38	35	128	91
Cr	109	222	204	215	187	6	5	298	54
V	345	125	116	171	217	86	114	58	65
Sc	12	39	38	38	40	18	18	31	1
Cu	82	49	55	24	15	11	11	23	10
Zn	146	91	94	101	87	61	61	135	104
Sr	73	132	128	159	171	346	337	264	176
Rb	6	66	67	57	50	23	32	48	36
Zr	105	95	96	97	101	130	131	81	67
Nb	9	3	4	4	3	8	8	7	4
Ba	131	191	190	201	182	88	90	54	41
Pb	73	0	0	0	0	0	0	0	0
Th	34	0	0	0	0	0	0	0	0
La	33	20	18	14	14	15	15	19	10
Ce	38	37	35	32	29	30	33	40	26
Nd	17	21	22	16	15	17	17	20	17
Y	28	30	33	22	23	24	22	24	18

## APPENDIX 6

### THIN-SECTION CATALOG

#### APPENDIX 6a. BY STRATIGRAPHIC POSITION

##### PRIOLITHOS FORMATION

29 112 114 217 442 744 745 746 747 749 (443) (749)

##### DRIMOS FORMATION

35 36 74 75 76 77 78 79 80 87 109 115 116 117 118 119 120 121 207 394 397 419  
620 624 626 627 628 630 639 676 677 680 724 725 728a 728b 738 740 741 742 743  
761 762 763 764 768 (185) (738) (762) (769)

##### KASTELLI MUDSTONE MEMBER

83 84

##### AROANIA CHERT MEMBER

19 20 21 22 23 25 26 30 40 41 43 53 55 85 86 88 89 90 91 92 93 102 104 105 106  
124 126 127 129 130 131 133 215 223 225 233 307 309 347 349 376 439 440 449  
453 491 494 497 499 500 503 609 681 683 704 767 (230) (310) (494)

##### PAOS LIMESTONE MEMBER

71 134 380 381 382 598 649 650 652 663 667 701 733 759

##### KLITORIA SANDSTONE MEMBER

57 61 62 63 64 70 351 446 661 (350) (445) (660)

##### ERYMANTHOS LIMESTONE MEMBER

14 15 16 94 95 97 98 99 100 101 107 108 110 135 136 137a 375 379 383 598 618  
653 757 773 774 775 776 (775)

##### KATARAKTIS PASSAGE MEMBER

69 137b 138 139 140 615 675 735

##### PINDOS FLYSCH FORMATION

24 590 645 732 (317) (370) (495) (590)

##### TECTONO-SEDIMENTARY MELANGE LITHOLOGIES

1 2 3 4 5 6 7 8 9 10 11 12 13 17 44 45 46 47 48 49 50 51 52 286 294 295 331 335  
336 339 361 390 391 392 398 403 405 420 423 429 431 433 434 435 454 455 456  
457 458 460 462 463a 463b 464 465 479 473 474 479 481 482 485 486 508 513 514  
517 521 526 529 531 556 557 562 588 594 595 596 700 711 713b 715 733 758 770  
(404) (433) (472) (484)

##### GAVROVO-TRIPOLITZA ZONE LITHOLOGIES

31 38 241 242 243 324 414 487 558 597 613 616 687 691 693 695 709 717 721 750  
751 753 755 (709)

Numbers in parenthesis represent polished thin-sections for CL analysis.



APPENDIX 6b, BY LOCATION

**DRAKOVOUNI**

1 2 3 4 5 6 7 8 9 10 11 12 13 14 15 16 17 19 20 21 22 23 24 25 26 286 294 295 453  
454 455 456 457 458 460 462 463a 463b 464 465 470 472 473 474 479 481 482 484  
485 486 487 556 557 558 562 709a 709b

**ERYMANTHOS**

29 30 31 35 36 38 39 40 41 42 43 44 45 46 47 48 52 69 70 71 74 75 76 77a 77b 78  
79 80 83 84 85 86 87 88a 88b 89 90 91a 91b 92 93 94 95 97 98 99 100 101 449 491  
494a 494b 495 497 505 675 676 677 680 681 683 687 691 693 701a 701b 704 724  
725 728a 728b 732 733a 733b 735 738a 738b 740 741 742 743 744 745 746 747  
749a 749b 750 751 753 755 757 758 759 761 762 763 764 767 768 769

**CHELMOS**

55 102 104 105 106 107 241 242 243 324 588 590a 590b 594 595 596 597 598a  
598b 609 613 615 616 618 620 695 700 711 713b 715 717 721

**DENDRA**

108 109 110 112 114 115 116 117 118 119 120 121 124 126 127 129 130 131 133  
134 135 136 137a 137b 138 139 140 307 309 310 773 774 775a 775b 776

**AROANIA**

185 429 431 433a 433b 434 435 499 500 503 508 513 514

**LIVARDZI**

207 215 217 223 225 230 233 317 649 650 652 653

**KLITORIA**

57 61 62 63 64 624 626 627 628 630 639 645 660 661 663 667

**METHIDRIO/PALAEOHOUNI**

331 335 336 339 398 403 404 405 439 440 442 443 445 446

**TRIPOLIS**

53 414 419 420 423

**LESTEENA/SELLAS/KOKINO**

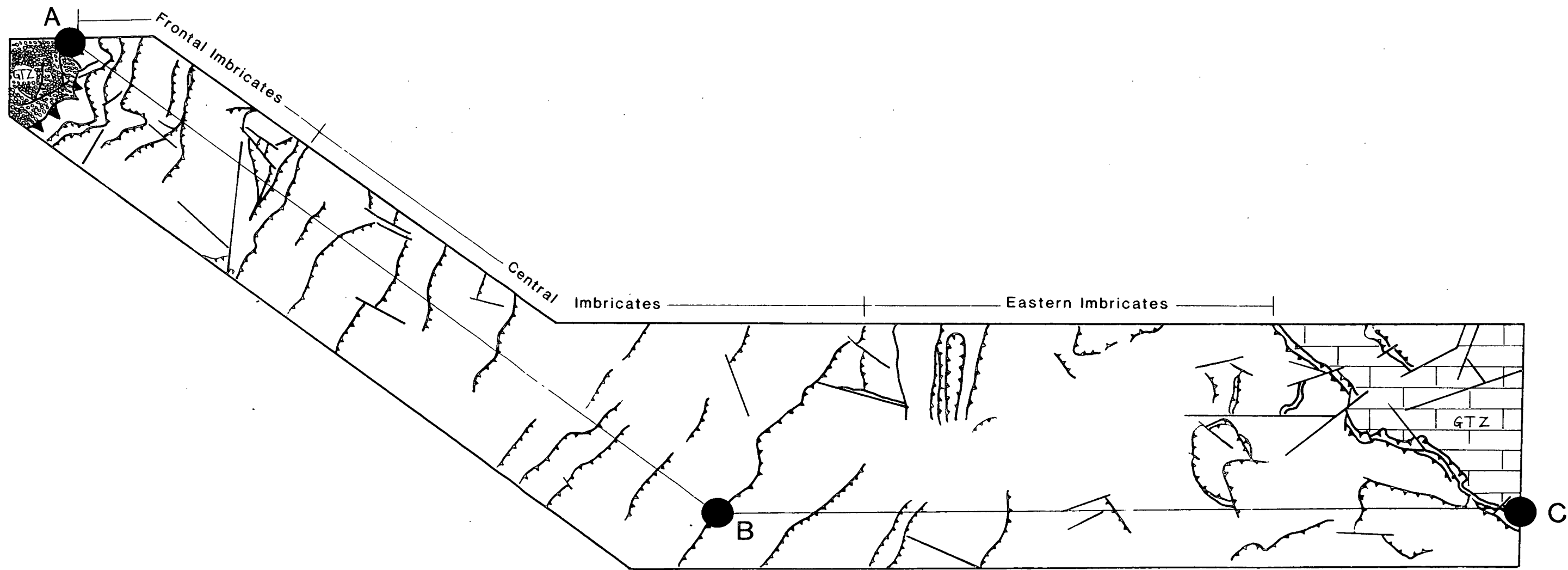
347 349 350 351 361 370 390 391 392 394 397  
770

**SOLINARI**

375 376 379 380 381 382 383

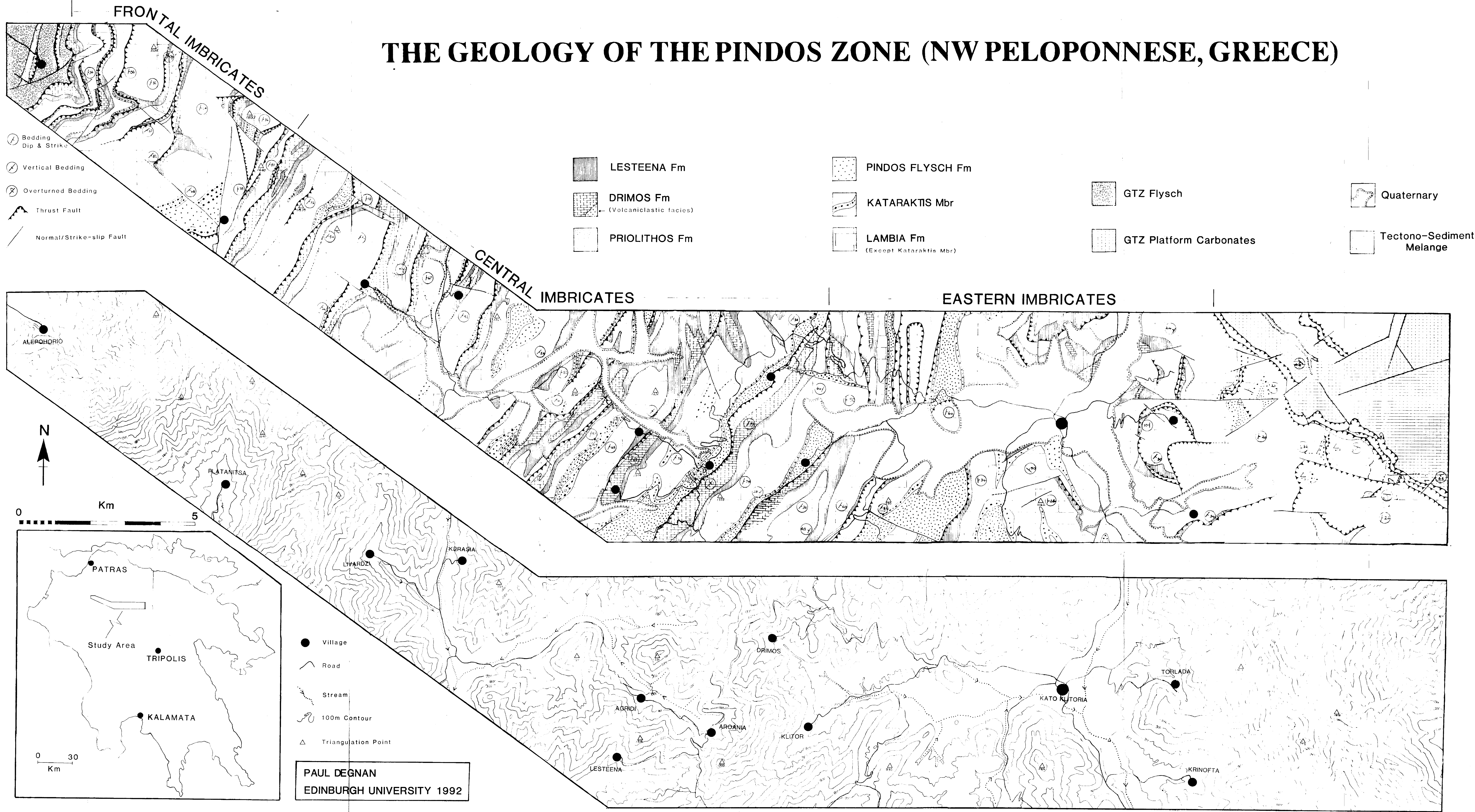
**GLAFKOS**

517 521 526 529 531



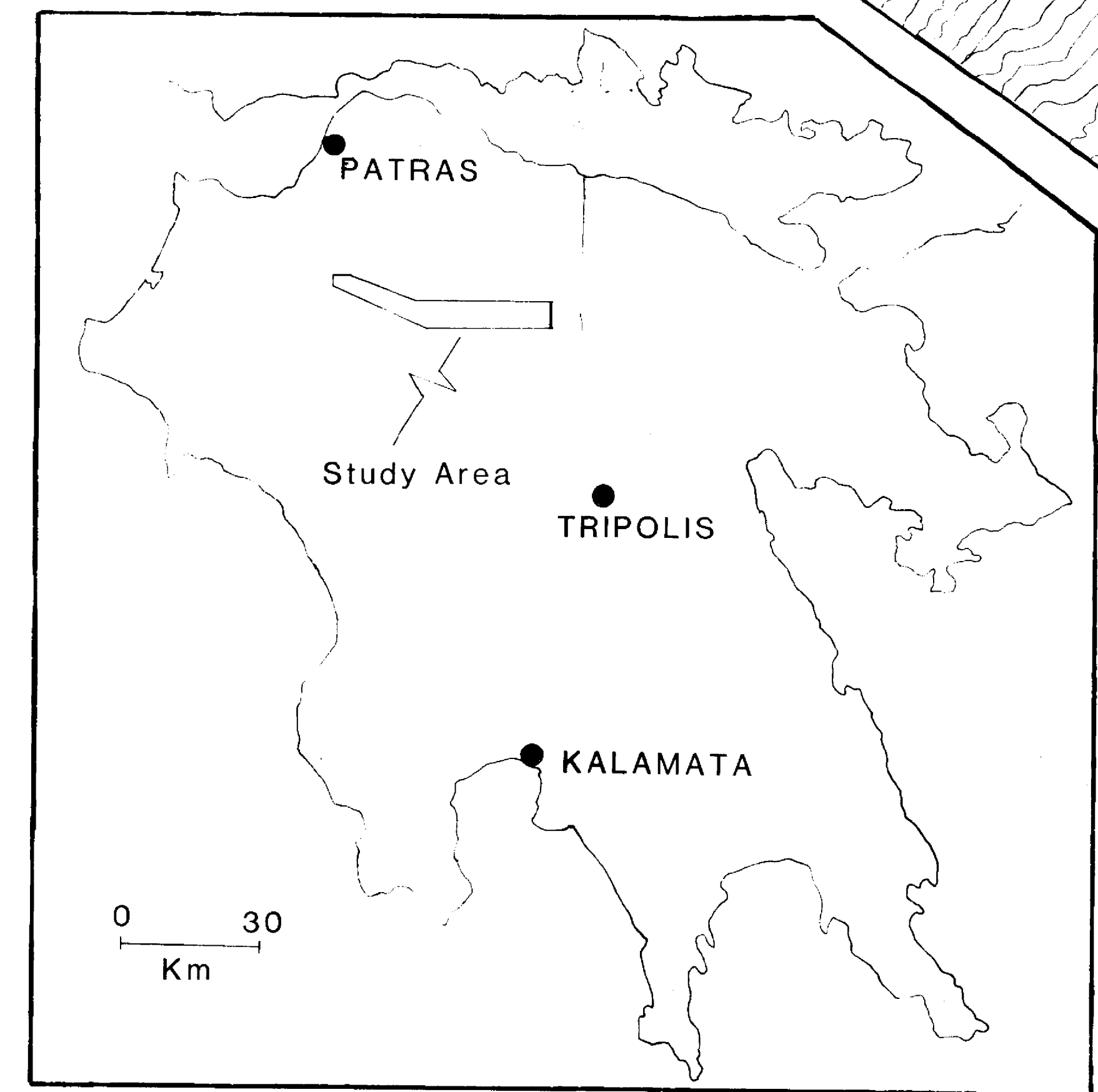
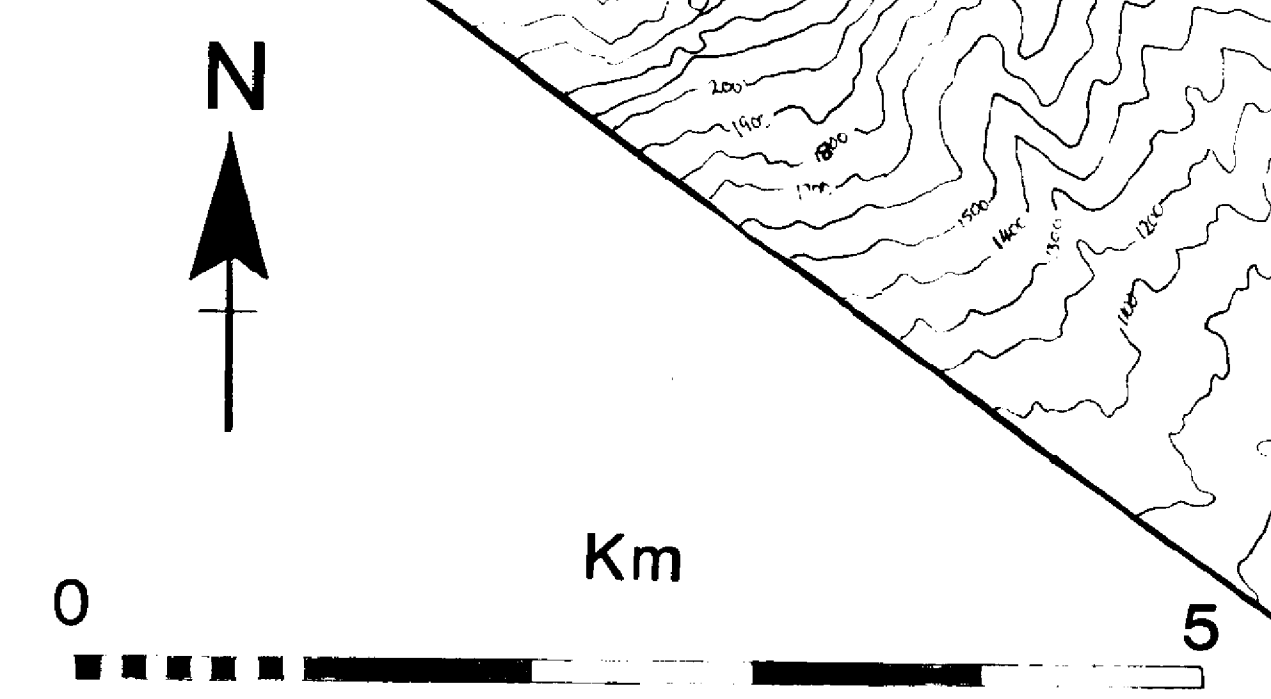
Outline of Enclosure 1 (Geological Map) with the line of section indicated.

# THE GEOLOGY OF THE PINDOS ZONE (NW PELOPONNESE, GREECE)



- Bedding Dip & Strike
- Vertical Bedding
- Overturned Bedding
- Thrust Fault
- Normal/Strike-slip Fault

- LESTEENA Fm
- DRIMOS Fm (Volcaniclastic facies)
- PRIOLITHOS Fm
- PINDOS FLYSCH Fm
- KATARAKTIS Mbr
- LAMBIA Fm (Except Kataraktis Mbr)
- GTZ Flysch
- GTZ Platform Carbonates
- Quaternary
- Tectono-Sedimentary Melange



- Village
- Road
- Stream
- 100m Contour
- Triangulation Point

PAUL DEGNAN  
EDINBURGH UNIVERSITY 1992

